Université du Québec

Institut National de la Recherche Scientifique

Centre Armand-Frappier Santé Biotechnologie

Early control of mRNA abundance and translation efficiency in macrophages infected with the protozoan parasite *Leishmania donovani*

By

Visnu Deva Chaparro Urbina

A dissertation submitted in partial fulfillment of the requirements for the degree of Philosophiae Doctor (PhD) in the Virology and Immunology Program

Evaluation Committee

Committee president and internal examiner	Simona Stäger INRS - CAFSB
External examiners	Barbara Papadopoulou CHU de Québec Research Center - Laval University
	Reza Salavati Institute of Parasitology – McGill University
Thesis advisor	Maritza Jaramillo Patiño INRS - CAFSB

August 4th, 2022

ACKNOWLEDGEMENTS

ABSTRACT

Macrophages are professional phagocytes and first responders of the innate immune system against infectious organisms. Armed with a battery of antimicrobial tools and numerous pathogen- and damage-recognition receptors, macrophages exhibit high plasticity and stress-tailored responses that rely (among others) on regulation of mRNA abundance and translation. Paradoxically, macrophages represent the replicative niche for different pathogens including sandfly-transmitted protozoan parasites of the genus *Leishmania*, which are causative agents of an array of diseases collectively known as leishmaniases. *L. donovani* infection leads to development of visceral leishmaniasis (VL), with an estimation of 200,000 to 400,000 cases and 20,000 - 40,000 fatalities globally per year. Following sandfly inoculation, macrophage-phagocytized promastigotes transform into the non-motile amastigote form, which disseminates to internal organs and tissues such as lymph nodes, liver, spleen, and bone marrow with concomitant development of fatal clinical symptoms when untreated. To favor its own survival, *L. donovani* parasites subvert macrophage immune and cellular processes including modulation of gene expression. Modulation of mRNA abundance has been extensively reported in macrophages infected with viruses, bacteria and parasites. However, the role of translation in the course of infections remains poorly explored especially for protozoan parasitic infections. High throughput *in vitro* studies indicate *L. donovani* infection induces widespread perturbation of mRNA and protein abundance, although the majority of these changes have been documented over 12 hours post infection non accounting for early events that could affect infection progress (i.e., modulation of parasitophorous vacuole formation, oxidative burst, transcription factor activity, apoptosis initiation) or they have been performed using the promastigote form instead of the clinically relevant amastigote. Additionally, the role of macrophage translational control during *L. donovani* infection is yet to be determined.

Herein, by using polysome profiling coupled with RNAseq quantification we generated host profiles of mRNA abundance and translation from macrophages infected or not with *L. donovani* amastigotes and promastigotes 6 hours post infection. Using a combination of bio-informatic and biochemical tools we identified a stage-specific regulation of macrophage mRNA abundance. Amastigote-driven changes where enriched in upregulated transcripts encoding proteins associated with DNA repair mechanisms, while those encoding antigen-presenting and macrophage activation factors were markedly downregulated. In parallel, upregulation of immune inhibitors as well as an antioxidant transcriptional signature associated with NRF2 activity were identified in promastigote infected datasets. Additionally, hierarchical clustering of mRNAs associated with IRF3 and IRF7 transcriptional activity suggests that macrophages activate antimicrobial pathways upon *L. donovani* promastigote infection. Conversely, translational efficiency changes were found to be similar in amastigote- and promastigote-infected datasets when compared to uninfected controls. Gene ontology analyses on translationally regulated transcripts showed an enrichment of upregulated categories associated with RNA metabolism (i.e., chromatin remodeling, transcription, splicing, transport, silencing, and translation) and -similarly to analysis of mRNA abundance- downregulation of macrophage immune activators. Notably, subsets of mTORC1- and eIF4A-sensitive transcripts were identified including

ii

63 PABPC1 and EIF2AK2, the expression of which was inhibited by rapamycin treatment and TGFB1, which

64 it was found to be affected after incubation with the rocaglate silvestrol. Furthermore, the biological

65 significance of mTORC1 and eIF4A activities during *L. donovani* infection was highlighted via *in vitro*

66 intracellular survival analysis indicating parasite survival is favored or compromised in the presence of

67 rapamycin or silvestrol respectively. In sum, *L. donovani* promastigote and amastigote infection leads to

68 the early widespread yet selective alterations of macrophage gene expression including mRNA abundance

69 and translation efficiency that can tailor protective and harmful responses to the host underscoring the

70 therapeutic potential of the molecular mechanisms regulating these events.

71

72

73

TABLE OF CONTENTS

75

76

LIST OF FIGURES AND TABLES

LIST OF ABBREVIATIONS

4E-BP:	eIF4E-binding protein
ADN:	Acide désoxyribonucléique
AKT:	Protein kinase B
AMA:	Amastigote
AME:	Analysis of Motif Enrichment
ANOVA:	Analysis of variance
ARE:	AU-rich element
ARN:	Acide ribonucléique
ARNm:	ARN messager
ATP:	Adenosine-5'-triphosphate
BMDM:	Bone marrow-derived macrophages
C3:	Complement component 3
CCL:	CC-containing chemokine ligand
CCR:	CC-containing chemokine receptor
cDNA:	Complementary DNA
CL:	Cutaneous leishmaniasis
CR3:	Complement component 3 receptor
CTR:	Non-infected/Non-treated control
CXCL:	CXC-containing chemokine ligand
CXCR:	CXC-containing chemokine receptor
DMSO:	Dimethyl sulfoxide
eIF1:	Eukaryotic translation initiation factor 1
eIF1A:	Eukaryotic translation initiation factor 1A
eIF2:	Eukaryotic translation initiation factor 2
EIF2AK1:	Eukaryotic translation initiation factor 2 subunit alpha kinase 1
EIF2AK2:	Eukaryotic translation initiation factor 2 subunit alpha kinase 2
EIF2AK3:	Eukaryotic translation initiation factor 2 subunit alpha kinase 3

EIF2AK4:	Eukaryotic translation initiation factor 2 subunit alpha kinase 4
EIF2α:	Eukaryotic translation initiation factor 2 subunit alpha
eIF3:	Eukaryotic translation initiation factor 3
eIF4A:	Eukaryotic translation initiation factor 4A
EIF4B:	Eukaryotic translation initiation factor 4B
eIF4E:	Eukaryotic translation initiation factor 4E
eIF4F:	Eukaryotic translation initiation factor 4F
eIF4G:	Eukaryotic translation initiation factor 4G
eIF5:	Eukaryotic translation initiation factor 5
ER:	Endoplasmic reticulum
FDR:	False discovery rate
G3BP1:	Ras-GTPase-activating protein-binding protein 1
GCN2:	General control nonderepressible 2
GO:	Gene ontology
GP63:	Glycoprotein 63, Leishmanolysin
GTP:	Guanosine-5'-triphosphate
HO-1:	Heme oxygenase 1
HRI:	Heme-regulated inhibitor
HRP:	Horseradish peroxidase
HSC:	Hematopoietic stem cells
HSP:	Heat shock protein
iC3b:	Cleaved inactive complement component 3
IFN:	Interferon
Ig:	Immunoglobulin
IL:	Interleukin
iNOS:	Inducible nitric oxide synthase
IPA:	Ingenuity pathway analysis
IRF:	Interferon regulatory factor

LARP1: La-related protein 1

LCCM: L929 fibroblast-conditioned medium

LCF: *Leishmania* chemotactic factor

lncRNA: Long non-coding RNA

LPG: Lipophosphoglycan

LPS: Lipopolysaccharide

LRV: *Leishmania* RNA virus

LV: leishmaniose viscérale

MAPK: Mitogen-activated protein kinase

MCL: Mucocutaneous leishmaniasis

MCL-1: Myeloid cell leukemia 1 Bcl-2 related

MDM: Monocyte-derived macrophage

MHC: Major histocompatibility complex

miRNA: micro-RNA

MNK: MAPK-interacting serine/threonine kinase

mRNA: Messenger RNA

mTOR: Mechanistic target of rapamycin

mTORC: Mechanistic target of rapamycin complex

MYD88: Myeloid differentiation primary response 88

NADPH: Reduced nicotinamide adenine dinucleotide phosphate

NF-κB: Nuclear factor kappa B

NLR: NOD-like receptor

NRF2: NFE2-Related Factor 2

ORF: Open reading frame

PABPC1: Poly(a)-binding protein C1

PB: Processing body

PD-1: Programmed cell death 1

PDCD4: Programmed-cell-death 4

PDL-1:	Programmed cell death 1 ligand 1
PDL-2:	Programmed cell death 1 ligand2
PERK:	PKR-like endoplasmic reticulum kinase
PI3K:	Phosphoinositide 3-kinase
PKDL:	Post-Kala-Azar dermal leishmaniasis
PKR:	Protein kinase RNA-activated
PM:	Peritoneal macrophages
PRO:	Promastigote
PRR:	Pathogen-associated recognition receptor
PSG:	Promastigote secretory gel
PV:	Parasitophorous vacuole
RBP:	RNA-binding protein
RIG-I:	Retinoic acid inducible gene 1
RISC:	RNA-induced silencing complex
RNAseq:	RNA sequencing
RNP:	Ribonucleoprotein
rpS6:	Ribosomal protein S6
rpS6K	Ribosomal protein S6 kinase
RSK:	90KDa ribosomal S6 kinase
SDS-PAGE:	SDS polyacrylamide gel electrophoresis
SG:	Stress granule
shRNA:	Short hairpin RNA
SMAD:	Sma- and Mad-related protein
STAT:	Signal transducer and activator of transcription
TAM:	Tumor-associated macrophage
TGFB1:	Transforming growth factor beta 1
TLR:	Toll-like receptor
TNF:	Tumor necrosis factor

TOP:	Tract of polypyrimidine
tRNA:	Transfer RNA
uORF:	Upstream open reading frame
UTR:	Untranslated region
VL:	Visceral leishmaniasis
ZFP36:	Zinc finger protein 36
ZFP36L1:	Zinc finger protein 36-like 1

82

83

84

85

86

87

88

89

90

91

92

93

94

95

96

97

CHAPTER 1

Introduction

1. Macrophage: The Host

Macrophages are avid phagocytes ubiquitous in body tissues and essential for numerous metabolic, immunological, and inflammatory processes in physiological and pathological conditions (Naito 2008). Expression of numerous pathogen-associated recognition receptors (PRRs) such as Toll-like receptors (TLRs), scavenger receptors (SRs), C-type lectin receptors (CLRs), NOD-like receptors (NLRs), double stranded RNA-sensing receptors (i.e., PKR, RIG-I) and β_2-integrins make of macrophages front line responders of the innate immune system during infectious and inflammatory processes (Areschoug and Gordon 2008). Of note, most tissue-resident macrophages are established prenatally and are considered self-sufficient, independent of hematopoietic input for renewal and pivotal for tissue homeostasis (Hoeffel and Ginhoux 2018). Primitive macrophages originate in blood islands of the yolk sac, which after migration give rise to microglia, resident macrophages in the nervous system (Ginhoux, Greter et al. 2010). In parallel, erythro-myeloid progenitors (EMPs) from the yolk-sac hemogenic endothelium will differentiate into pre-macrophages that colonize different tissues before birth and develop into alveolar (lung), Kupffer (liver), Langerhan (skin epidermis), and kidney-resident macrophages (Mass, Ballesteros et al. 2016). Additionally, postnatal bone marrow hematopoietic stem cells (HSC) can differentiate into circulating Ly6C+ monocytes that can infiltrate inflamed tissues and differentiate into monocyte-derived macrophages (MDM) (Menezes, Melandri et al. 2016), although at steady state levels, Ly6C+ monocytes also differentiate into resident intestinal and skin dermis macrophages (Tamoutounour, Guilliams et al. 2013, Bain, Bravo-Blas et al. 2014) (**Figure 1.1**). In consequence, the term macrophage refers to a heterogenous population highly influenced by their microenvironment (Gautier and Yvan-Charvet 2014), where modulation of mRNA metabolism (including transcriptional, posttranscriptional and translational mechanisms) stands as a core element in determining macrophage cellular and immune functions (Fu, Yang et al. 2012, Graff, Dickson et al. 2012, Gosselin, Link et al. 2014, Schultze, Freeman et al. 2015, Leroux, Lorent et al. 2018, Zhihua, Yulin et al. 2019).

126
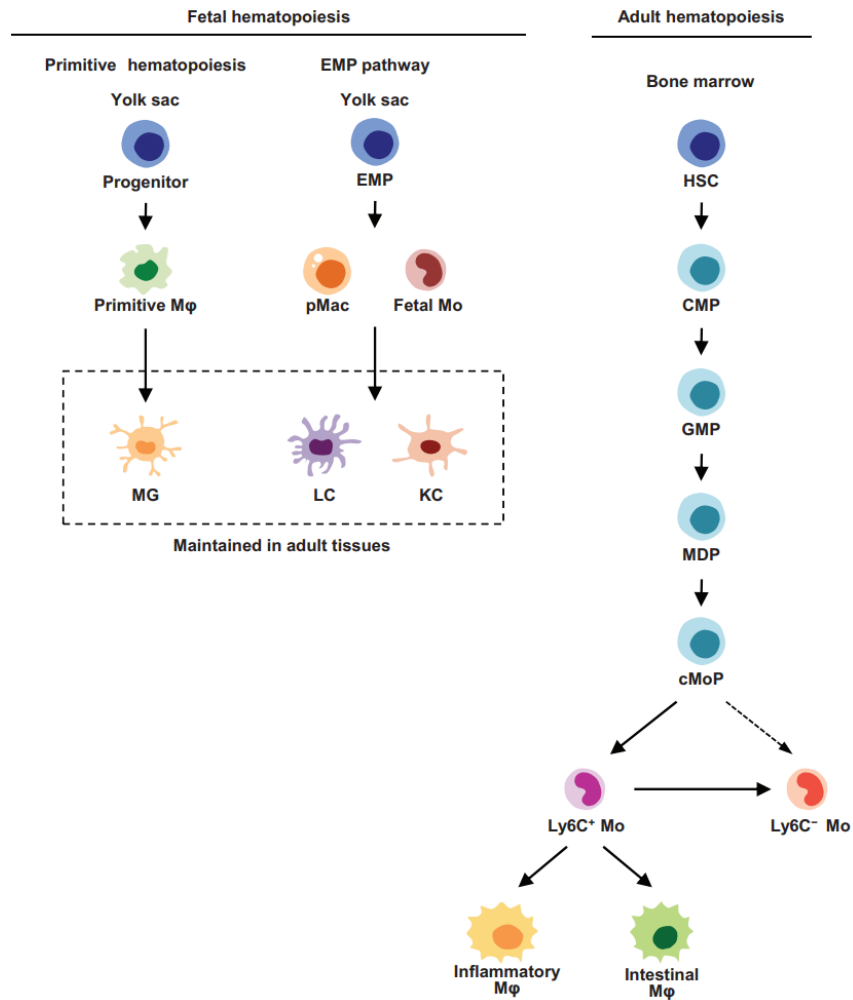
Figure 1.1. Macrophage and monocyte differentiation pathways. Tissue-resident macrophages are derived from fetal progenitors or circulating Ly6C+ monocytes. In adults, monocytes are generated from bone marrow HSCs via intermediate progenitors, including CMPs, GMPs, MDPs and cMoPs. Some tissue-resident macrophage subsets such as intestinal macrophages are replenished by circulating monocytes. KC, Kupffer cell; LC, Langerhans cell; Mφ, macrophage; MG, microglia; Mo, monocyte (Kurotaki, Sasaki et al. 2017)

1.1 Regulation of gene expression and macrophage functioning

1.1.1 Chromatin remodelling

As part of the myeloid lineage, epigenetic control of macrophage ontogeny is associated with a global decrease in DNA methylation as evidenced by CpG methylation mapping and lymphoid-skewed differentiation of multipotent progenitors incubated with DNA methylase inhibitors (Ji, Ehrlich et al. 2010). Gosselin *et al*, showed that microglia and peritoneal resident macrophages exhibit differences in histone modifications correlated with cell-type specific transcriptional patterns (Gosselin, Link et al. 2014). Similarly, Lavin *et al* reported distinctive landscapes of availability to transcriptional enhancers depending on epigenetic modifications in seven different tissue resident macrophages highlighting the role of local

141 environment in macrophage shaping (Lavin, Winter et al. 2014). Furthermore, IFNγ stimulation promotes

142 histone 3 lysine 27 methylation (H3K27me3) and subsequent upregulation of inflammatory TNF, IL6 and

143 IL12B expression following TLR4 stimulation (Qiao, Giannopoulou et al. 2013). Conversely, in response to

144 helminth infection or chitin incubation JMJD3 demethylase targets H3K27me3 sites to promote pathogen

145 controlling M2 macrophage polarization as evidenced by favored expression of *Arg1*, *Ym1*, *Fizz1*, and *Mr*

146 markers (Satoh, Takeuchi et al. 2010, Schultze, Freeman et al. 2015). Certainly, macrophage chromatin

147 remodeling is a target of intracellular pathogens such as *Mycobacterium tuberculosis*, which prevents IFNγ-

148 dependent upregulation of CIITA (Pennini, Pai et al. 2006), the master transcriptional regulator of members

149 of the major histocompatibility (MHC) class II complex (LeibundGut-Landmann, Waldburger et al. 2004).

150 This phenotype was found to be dependent on histone deacetylation and inhibited recruitment of the

151 chromatin-remodeling complex SWI/SNF as a mechanism of immune evasion by *M. tuberculosis* to hamper

152 IFNγ transcriptional response of the host (Pennini, Pai et al. 2006). In a similar way, the protozoan parasite

153 *Toxoplasma gondii* represses histone acetylation and BRG-1 (syn. SMARCA4, a member of the SWI/SNF

154 complex) recruitment to the CIITA promoter in macrophages upon IFNγ stimulation with histone acetylase

155 inhibitors being able to restore the original phenotype similar to uninfected cells (Lang, Hildebrandt et al.

156 2012). Thus, chromatin remodeling is a critical gene expression regulatory element in macrophage

157 development and functioning in physiological and pathogenic contexts.

158   **1.1.2 Transcription**

159   Macrophage heterogeneity is accompanied by tailored developmental gene expression programs

160 (Bonnardel and Guilliams 2018). For example, macrophage colony stimulating factor receptor (M-CSFR)

161 signaling by M-CSF and interleukin 34 (IL34) stimulation in parallel to TGFβ-dependent SMAD2/3 activation

162 are necessary for microglia development and maintenance (Sasaki, Yokoo et al. 2000, Wang, Szretter et

163 al. 2012, Butovsky, Jedrychowski et al. 2014). IL34 and TGFβ are also indispensable for Langerhans cell

164 differentiation through induction of the transcription factors RUNX3 and ID2 (Kurotaki, Sasaki et al. 2017).

165 On the other hand, it was recently reported that mice deficient for the nuclear liver X receptor-α (LXR- α)

166 transcription factor lack splenic marginal zone (SIGN-R1+) and marginal zone metallophillic (CD169+)

167 macrophages, although the molecular mechanism behind this observation remains to be characterized (N,

168 Guillen et al. 2013). In addition to these developmental programs of gene expression, fully differentiated

169 macrophages can undergo profound transcriptome remodelling upon activation and give rise to

170 subpopulations that have been historically identified as M1 (inflammatory) or M2 (wound healing) (Murray

171 2017). However, a thorough transcriptome-wide characterization of human monocyte-derived

172 macrophages confronted with various stimuli revealed that macrophages can assume different activation

173 states that fall into to a spectrum of responses rather than a rigid dichotomy (Xue, Schmidt et al. 2014),

174 which indicates transcriptional regulation is pivotal for macrophage functioning.

175   RNAseq data show that when confronted with fasting-refeeding metabolic stress, adipose tissue

176 macrophages upregulate transcription dependent on nuclear factor kappa (NF-κB) to drive proinflammatory

177   IL1 production in contrast to other tissue resident macrophages (e.g. pancreas, peritoneum, brain, liver,

178   colon macrophages) (Brykczynska, Geigges et al. 2020). Interestingly, in the same study Brykczynska *et*

179   *al* showed that under the same conditions, increased mRNA abundance of transcripts associated with

180   phagosome and antigen processing and presentation was common among the different macrophage types

181   (Brykczynska, Geigges et al. 2020). In parallel, macrophage response to infection by the Gram-positive

182   bacteria *Streptococcus pyogenes* is characterized by the induction of transcripts encoding inflammatory

183   (i.e., *Tnf*, *Il1α*, *Il1β*, *Il6*) and anti-inflammatory (i.e., *Arg1*, *Il10*) mediators (Goldmann, von Kockritz-

184   Blickwede et al. 2007). Furthermore, the high throughput data identified the incremented expression of

185   *p47hox*, an mRNA encoding for a subunit of NAPDH oxidase associated with pathogen clearance

186   (Goldmann, von Kockritz-Blickwede et al. 2007). However, transcriptional responses of macrophages to

187   infection are not universal. For example, microarray data obtained from human CD14^{+} monocyte-derived

188   macrophages and dendritic cells (DCs) confronted with phylogenetically diverse pathogens (e.g. *M.*

189   *tuberculosis*, *T. gondii*, *Leishmania major*, *L. donovani*, *Brugia malayi*) indicates that, although common

190   elements exist, macrophage response to infection is tailored to specific pathogens (Chaussabel, Semnani

191   et al. 2003). Furthermore, Koo *et al* showed how macrophage infection with two different strains of *M.*

192   *tuberculosis* (proinflammatory CDC1551 and hypervirulent HN878) can result in contrasting expression of

193   transcriptional regulators belonging to the early immune activation network (i.e., *Stat3*, *Stat5a*, *Atf3*) in one

194   (CDC1551) but not the other (HN878) (Koo, Subbian et al. 2012). Hence, transcriptome-wide analysis of

195   mRNA abundance represents a powerful tool that can be used to identify key elements of macrophage

196   response to sterile and infectious stress.

197   **1.1.3 miRNA regulation**

198   In 1993, the discovery made by Lee, Feinbaum and Ambros of a short RNA with antisense

199   complementarity to *Caenorhabditis elegans Lin14* transcript went almost unnoticed by the scientific

200   community (Lee, Feinbaum et al. 1993). Almost a decade later, Reinhart *et al* showed that a similar short

201   antisense RNA targeting the 3'-untranslated region (UTR) of *Lin41* was capable of regulating *C. elegans*

202   development, which ignited the interest on these non-coding regulatory microRNAs (miRNAs) (Reinhart,

203   Slack et al. 2000). Mature miRNAs are 18-24 nucleotide base long enzymatic products of longer (up to

204   thousands of nucleotide bases) RNA precursors, which in conjunction with the RNA-induced silencing

205   complex (RISC) modulate suppression of gene expression through mRNA degradation (Bartel 2004).

206   Commitment of HSCs to the monocyte/macrophage lineage is promoted by PU.1-dependent expression of

207   a subset of miRNAs (miR-146a, miR-342, miR-338, and miR-155) (Ghani, Riemke et al. 2011).

208   Furthermore, characterization of M1(stimulated with IFNγ + LPS)- and M2b (stimulated with IgG + LPS)-

209   polarized human MDMs identified distinctive patterns of miRNA expression with THP1 macrophage cells

210   phenocopying polarization features (increased *Il6*, *Tnf*, *Cxcl9* levels) upon transfection   with M1-

211   responsive(miR-29b, miR-155) miRNA mimics (Graff, Dickson et al. 2012). Liu *et al* described the

212   differential expression of miRNAs targeting transcripts associated with macrophage mobility, immune

213 response and metabolic activity in porcine macrophages infected with porcine cytomegalovirus (Liu, Liao
214 et al. 2016). In parallel, murine macrophages infected with *Listeria monocytogenes* showed an early (e.g.
215 3, 6 hours post infection) upregulation of miRNAs associated with favored inflammatory activation (i.e., miR-
216 155, miR-125a-3p, miR-125a-5p, miR-146a) in a MYD88-, TLR2- or NF-κB-dependent manner (Schnitger,
217 Machova et al. 2011). Additionally, protozoan parasite *T. gondii* inhibits macrophage apoptosis by targeting
218 expression of BIM, a known cell death promoter, through miR-17-92 upregulation (Cai, Chen et al. 2014).
219 Collectively, these data highlight the importance of miRNA post-transcriptional regulation in macrophage
220 polarization and functioning.

221 ### 1.1.4 RNA-binding proteins

222 Being styled as 'RNA clothes', RNA-binding proteins (RBPs) are essential regulatory components
223 of gene expression (transcription-dependent and transcription-independent) by participating in every step
224 of RNA biogenesis, maturation, and activity (Glisovic, Bachorik et al. 2008, Turner and Diaz-Munoz 2018).
225 In parallel, characterization of a number of long non-coding RNAs (lncRNAs) has proven that RNAs can
226 also affect and guide RBP recruitment and functioning (Cech and Steitz 2014). It has been reported that
227 macrophage differentiation is accompanied by fluctuations in RBP expression (Fu, Yang et al. 2012, Chen,
228 Dong et al. 2015). For example, the RBP ZFP36L1 targeted degradation of CDK6-encoding transcripts was
229 shown to contribute to HSC and monocytic THP1 cell line differentiation to macrophages (Chen, Dong et
230 al. 2015). Conversely, repression of RBP QKI5 is observed during macrophage differentiation of HSC and
231 HL-60 promyelocytic cells, which is associated with increased CSF1R expression (Fu, Yang et al. 2012).
232 Recently, Kübler et al showed that mice deficient for cold-inducible RBP (CIRP) expression presented a
233 decrease in total leukocyte (CD45^{+}) count in an experimental model of tissue ischemia (Kubler, Beck et al.
234 2021). Interestingly, tissues from *Cirp*^{-/-} mice showed decreased damage, improved vascularization, and
235 augmented number of wound-healing M2-like macrophages (CD68+/MRC1^{+}), which suggests CIRP activity
236 could be playing a role in macrophage polarization (Kubler, Beck et al. 2021). Furthermore, RNA-
237 interactome-capture (RIC, **Figure 1.2**) performed on LPS-treated RAW 264.7 murine macrophages
238 identified a proteome of 34 RBPs differentially associated to poly(A)+ RNAs (Liepelt, Naarmann-de Vries
239 et al. 2016), which might be related to LPS macrophage activation as previously described (Liepelt,
240 Mossanen et al. 2014). In parallel, it was reported that tristetraprolin (ZFP36) interacts with the poly-(A)-
241 binding protein 1 (PABPC1) upon TLR4 stimulation and target mRNAs (mostly inflammatory) bearing 3'
242 AU-rich element motifs (AREs) for degradation (Zhang, Chen et al. 2017) in murine macrophages.
243 Conversely, it was recently reported that CPEB4 acts in opposing manner to ZFP36 to stabilize anti-
244 inflammatory transcripts with 3' AREs or cytoplasmic polyadenylation element motifs (CPEs) as a fine-
245 tuning mechanism of inflammatory transcript expression (Suner, Sibilio et al. 2022).

246

UV irradiation   **Oligo(dT) capture**   **RNase treatment**   **Mass spectrometry**
                 (denaturing conditions)   **and data analysis**

Key: ⬭ Cell   ◯ RBP   ★ Protein-RNA crosslink   poly(A)⁺ RNA   TTTT● Oligo(dT) magnetic beads   Denatured RBP
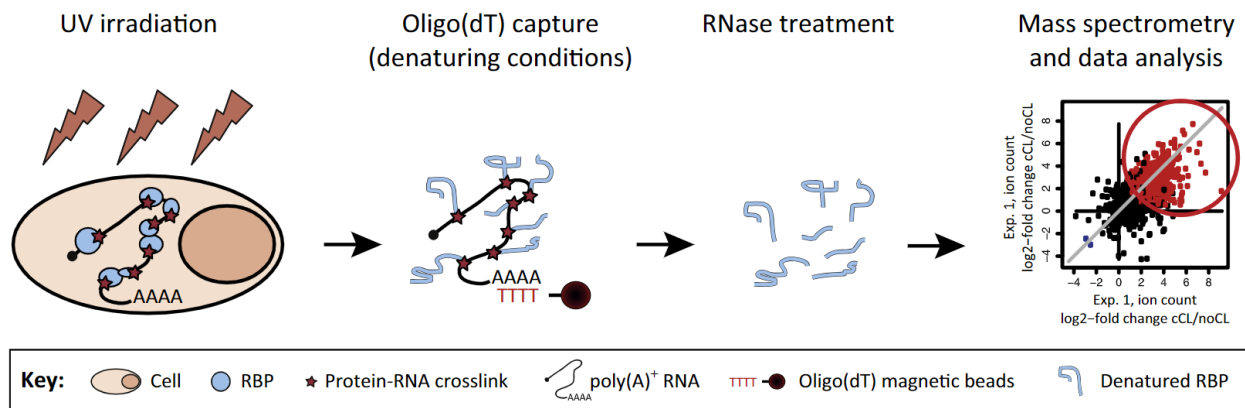
247

248   **Figure 1.2. Schematic Representation of RNA Interactome Capture.** Direct RNA-protein interactions are covalently linked through
249   UV radiation on living cells. Polyadenylated RNA and covalently bound protein partners are isolated by oligo(dT) pull-down under
250   denaturing conditions. After RNase treatment, the RBP repertoire is determined by quantitative mass spectrometry, comparing
251   proteins isolated from crosslinked cells (cCL) with those present in a mock pull-down (noCL). Only proteins with consistent enrichment
252   across replicates (encircled in red) are considered as the RNA interactome (Castello, Hentze et al. 2015).

253

254   In addition to this, RBPs can further modulate gene expression post-transcriptionally by forming
255 ribonucleoprotein (RNP) condensates typically known as granules (Anderson and Kedersha 2009). Multiple
256 nuclear and cytoplasmic granules have been characterized including Cajal bodies, paraspeckles, stress
257 granules (SGs) and processing bodies (PBs) (Lloyd 2013). SGs are enriched in translationally stalled
258 mRNAs and translation initiation factors, although they can also recruit immune-related proteins such as
259 the RNA sensors RIG-I and PKR associated with antiviral responses (Onomoto, Jogi et al. 2012, Reineke,
260 Kedersha et al. 2015). In turn, PBs contain translational repressors and elements of the mRNA decay
261 machinery responsible for decapping and degradation of target mRNAs (Luo, Na et al. 2018). Poliovirus
262 3C protease is known to prevent SG formation by cleaving G3BP1, a known SG marker. Interestingly, 3C
263 cleavage-resistant G3BP1-expressing cells show reduced viral replication, which indicates SG could act as
264 a host defense response during infection (White, Cardenas et al. 2007). Recently, Xiao *et al* showed that
265 porcine alveolar macrophages infected with porcine and respiratory syndrome virus upregulate
266 inflammatory expression and localization of the RBP CIRBP to SGs; Interestingly, CIRBP upregulation was
267 associated with NF-κB activation and increased levels of *Il6*, *Tnf*, *Il1b* (Xiao, Zhang et al. 2020). In parallel,
268 expression of the RNA uridyl transferase ZCCHC6 was shown to be associated with macrophage immune
269 response to *Streptococcus pneumoniae* since macrophages extracted from ZCCHC6 deficient mice
270 showed increased expression of CXCL1 at mRNA and protein levels, although the molecular mechanism
271 behind this observation remains to be elucidated (Kozlowski, Wasserman et al. 2017). Collectively, these
272 data indicate that macrophage biology and macrophage responses can be tailored in response to different
273 stimuli and that RBP activity is integral during infectious processes.

274

7

1.1.5 Translation

Protein synthesis is one of the most energy-consuming cellular processes (Buttgereit and Brand 1995) and nucleotide, amino acid pulse labelling analysis of gene expression places mRNA translation as a central proteome-defining mechanism (Schwanhausser, Busse et al. 2011). In eukaryotes, mRNA translation occurs in multiple steps including ribosome recruitment (initiation), peptide elongation, synthesis termination and ribosome recycling (**Figure 1.3**) (Jackson, Hellen et al. 2010, Dever and Green 2012). Of these, translation initiation is considered the rate limiting step due to number of components required for ribosome assembly on the cognate mRNA (Jackson, Hellen et al. 2010). During transcript maturation, an N7-methylated guanosine residue (termed cap) is linked to the 5' UTR end of cellular mRNAs and in the cytosol this residue is recognized by the translation initiation factor 4F (eIF4F), a trimeric complex comprised of the cap-binding protein 4E (eIF4E), the RNA helicase 4A (eIF4A) and the scaffold protein 4G (eIF4G) (Van Der Kelen, Beyaert et al. 2009). The eIF4F complex can subsequently recruit the 43S preinitiation complex (40S ribosomal subunit loaded with eIF1, eIF1A, eIF3, eIF5, and the ternary complex eIF2/^{Met}tRNA/GTP) through eIF4G/eIF3 interaction to position the small ribosomal subunit at the 5' UTR of cognate mRNA and initiate eIF4A-assisted scanning of the translation initiation codon (e.g., ATG). Once the first ATG is aligned with ^{Met}tRNA, the 60S (large) ribosomal subunit is loaded, translation initiation factors detach and peptide elongation can begin (Van Der Kelen, Beyaert et al. 2009) (**Figure 1.4**). Thus, without the need for *de novo* transcription, translational control allows for quick proteome remodeling in response to different intracellular and environmental cues (i.e., nutritional status, hypoxia, cell receptor engagement, infection) (Piccirillo, Bjur et al. 2014).

1.1.5.1 Translational regulation by mTORC1

The mechanistic target of rapamycin (mTOR) is a serine/threonine kinase, which along with RAPTOR, DEPTOR and mLST8 form the multimeric mTOR complex 1 (mTORC1) associated with cell growth modulation (Huang and Fingar 2014) and phospho-inactivation of members of the eIF4E-binding protein family (4E-BPs) (Hara, Yonezawa et al. 1997). 4E-BPs are translational repressors that compete with eIF4G for eIF4E binding through a shared eIF4E-binding motif thus preventing eIF4F complex assembly (Mader, Lee et al. 1995) (**Figure 1.5**). However, 4E-BPs dissociate from eIF4E upon mTORC1-dependent hierarchical phosphorylation in key residues (e.g., Thr37, Thr46, Thr70, and Ser65) (Gingras, Raught et al. 2001).

306
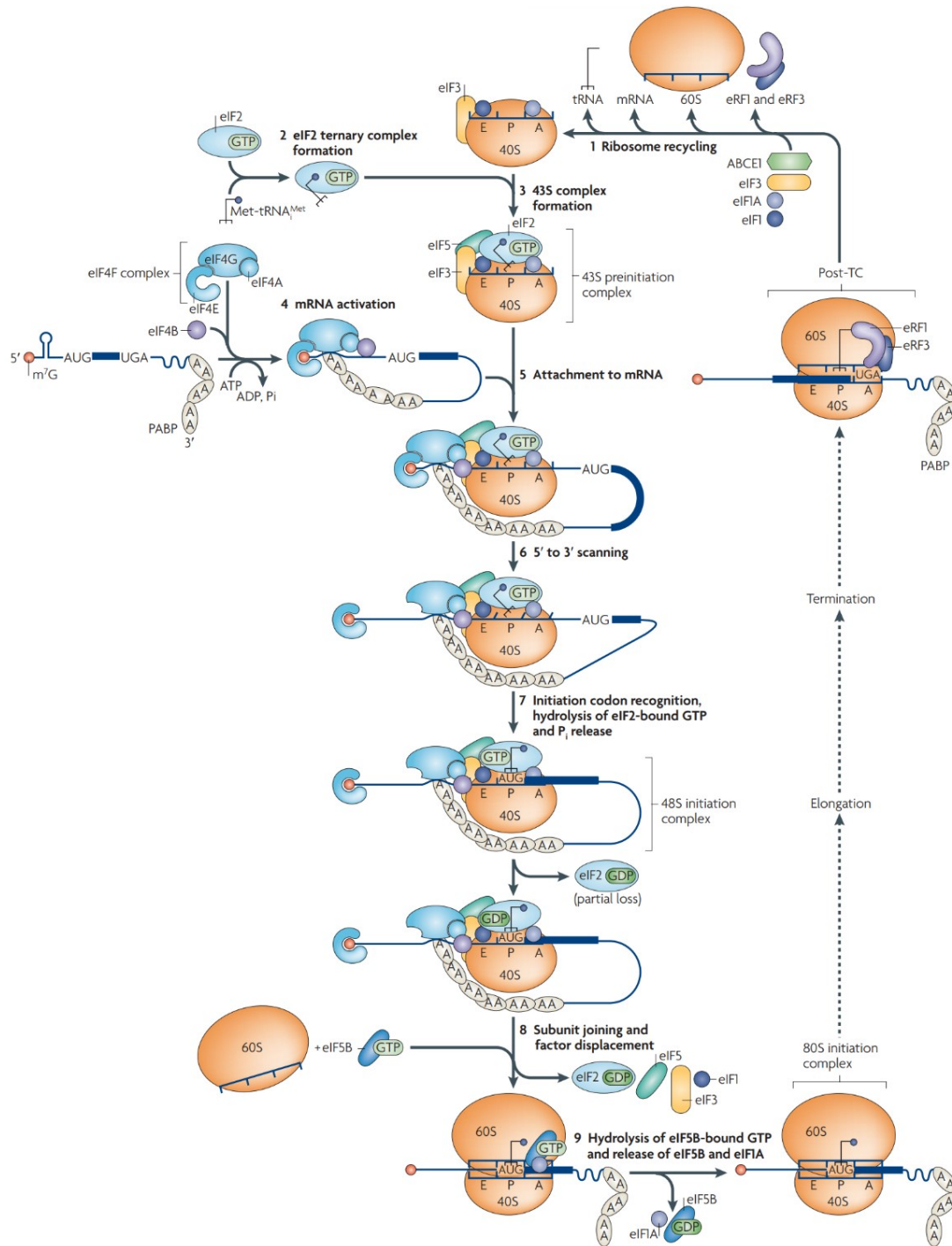
Figure 1.3. Model of the canonical pathway of eukaryotic mRNA translation. The canonical pathway of eukaryotic translation
initiation is divided into eight stages (2–9) followed by elongation of the polypeptidic chain and protein synthesis termination followed
by recycling of ribosomal subunits(1) (Jackson, Hellen et al. 2010).

In parallel, mTORC1 phosphorylates the La related protein 1 (LARP1), which is responsible for the
translational repression of mRNAs bearing a tract of polypyrimidine track (TOP) motif on their 5'UTRs
including mRNAs encoding numerous RBPs associated with the translational machinery (i.e., ribosomal

9

proteins and translational initiation, elongation factors) (Fonseca, Zakaria et al. 2015, Meyuhas and Kahan 2015). LARP1 binding to TOP sequence prevents eIF4F scanning activity and positioning of the small ribosomal subunit on the translation initiation codon. Phosphorylation by mTORC1 promotes the dissociation of LARP1 with its cognate sequence favoring TOP mRNA translation (Jia, Lahr et al. 2021) (**Figure 1.5**).
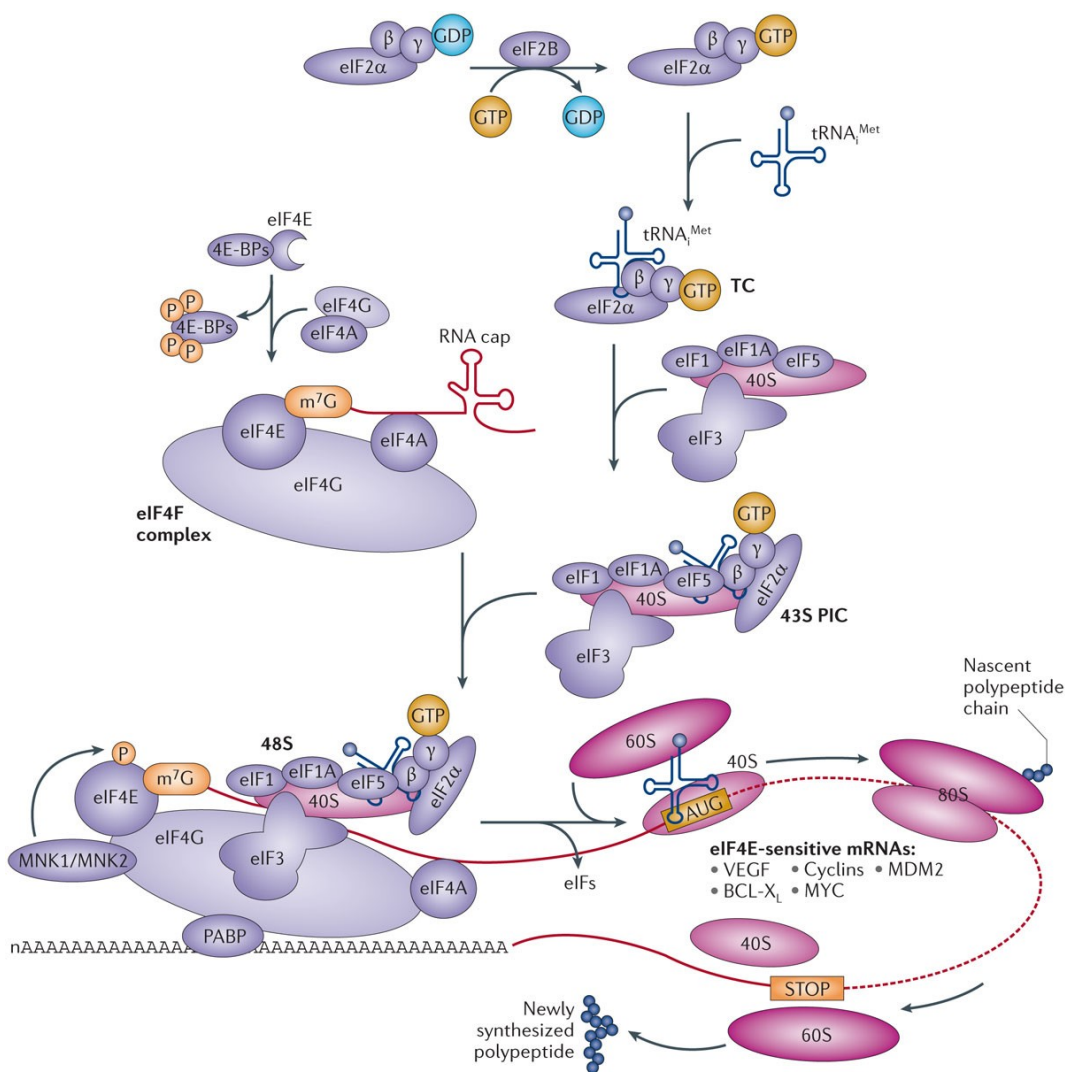
Figure 1.4. **Cap-dependent translation initiation**. The two best-characterized and most prominent mechanisms that regulate translation take place at the rate-limiting phase of initiation and involve controlling the assembly of a functional 40S subunit with its associated factors (43S pre-initiation complex (43S PIC)) or altering the access of PICs to the mRNA template. The 43S PIC is a large multifactorial complex formed by the association of the 40S ribosomal subunit with eukaryotic translation initiation factors (eIFs) eIF1, eIF1A, eIF3, eIF5 and the ternary complex (TC). The TC consists of a trimeric complex involving eIF2 (containing α-, β- and γ-subunits), initiator methionyl tRNA (tRNAiMet) and GTP. The recruitment of the 43S PIC to the mRNA template is facilitated by eIF4F, a complex consisting of the mRNA 5′-cap-binding subunit (eIF4E), a large scaffolding protein (eIF4G) and the DEAD box RNA helicase

327 (eIF4A), leading to 48S PIC assembly. eIF4F recruits ribosomes to mRNA through eIF4E–mRNA cap and eIF4G–eIF3 interactions,
328 resulting in the formation of a 48S initiation complex. eIF4G also interacts with the poly(A)-binding protein (PABP), which associates
329 with the mRNA 3′ poly(A) tail, to cause mRNA circularization to stabilize mRNAs and bolster translation. The eIF4A helicase
330 participates in the initial interactions of eIF4F with the mRNA 5′ end and may also facilitate scanning of the 40S ribosomal subunit
331 towards the initiation codon by resolving the secondary structure in the 5′ untranslated region (UTR). Recognition of the initiation
332 codon by the 43S PIC leads to the release of eIFs and joining of the 60S ribosomal subunit. The formation of a translation-competent
333 80S ribosome marks the end of initiation and the beginning of elongation. BCL-XL, B-cell lymphoma extra large; 4E-BP, 4E-binding
334 protein; m^{7}G, 7-methylguanosine 5′-cap; MNK, MAPK-interacting kinase; VEGF, vascular endothelial growth factor (Bhat, Robichaud
335 et al. 2015).

336   Additionally, mTORC1 activates the ribosomal protein S6 kinase (rpS6K), which subsequently
337 phosphorylates the ribosomal protein S6 (rpS6) contributing to different biological processes including
338 ribosome biogenesis, cell size regulation, and muscle functioning (Chauvin, Koka et al. 2014, Meyuhas
339 2015). mTORC1 activity is sensitive to different intra- and extracellular cues such as amino acid levels,
340 energy stress and receptor-mediated signaling (**Figure 1.6**). For example, PI3K/AKT activation leads to
341 increased mTORC1-dependent translation as shown by macrophage stimulation with different TLR
342 agonists (e.g., LPS, zymosan, poly I:C) (Lopez-Pelaez, Fumagalli et al. 2012). Additionally, by analyzing
343 the role of hypoxia for macrophage functioning in human gastric cancer, Zhihua et al described how TOP
344 mRNA translation was inhibited on tumor-associated macrophages (TAMs) with a parallel decrease in both
345 glycolytic rates and M1 polarization (Zhihua, Yulin et al. 2019). The molecular mechanism behind this
346 observation was associated with the hypoxia-sensitive expression of miR-30c, a miRNA targeting stability
347 of *Ddit4*, a transcript encoding the mTORC1 inhibitor REDD1 (Zhihua, Yulin et al. 2019).

348
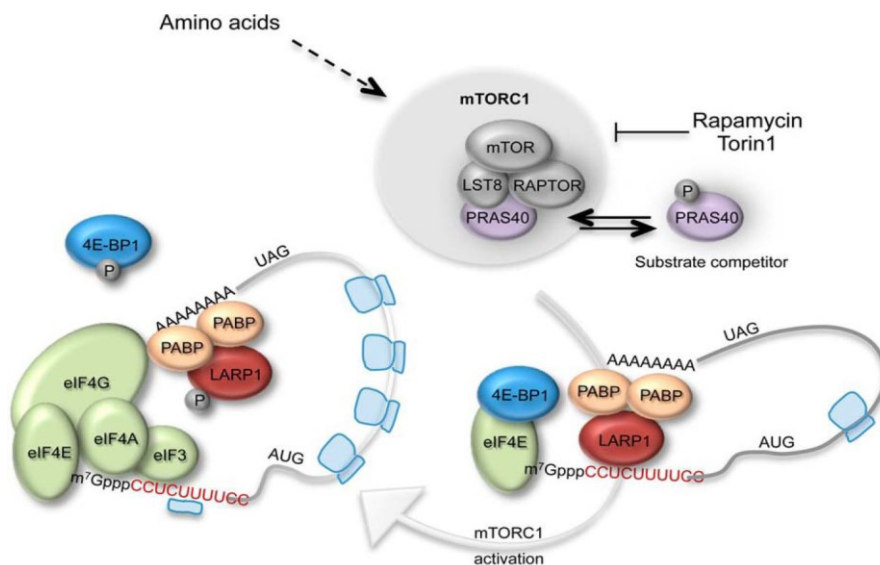
349

350 **Figure 1.5. Proposed model for LARP1-mediated repression of TOP mRNA translation downstream of mTORC1.** mTORC1
351 phosphorylates LARP1 at multiple residues (Yu, Yoon et al. 2011), effectively releasing LARP1 from the TOP motif. mTORC1 also
352 controls the phosphorylation of 4E-BP1, releasing it from eIF4E thus allowing for eIF4G to bind eIF4E and recruit the pre-initiation
353 complex to the mRNA, and translation ensues (Fonseca, Zakaria et al. 2015).

354   Modulation of mTORC1 activity has been reported to introduce translatome changes upon infection
355   by virus and bacteria in other cell types (Spangle and Munger 2010, Clippinger, Maguire et al. 2011,
356   Sokolova, Vieth et al. 2014). Of note, our group recently showed that infection with the protozoan parasite
357   *T. gondii* leads to the differential translation of over nine hundred transcripts in murine macrophages with
358   an enrichment of upregulated TOP mRNAs that mirrors increased mTORC1 phosphorylating activity on 4E-
359   BP1/2 and rpS6K (Leroux, Lorent et al. 2018). Furthermore, pharmacological mTORC1 inhibition with
360   rapamycin and torin-1 decreased parasite burden *in vitro*, which suggests mTORC1 activity is a host factor
361   that favors parasite survival (Leroux, Lorent et al. 2018). These data indicate that translation is a pivotal
362   process in macrophage responses to different triggers and, although its role during infection has been
363   explored for a number of pathogens, its involvement and that of mTORC1 in macrophage immune and
364   cellular functions during protozoan parasitic infections remains largely uncharacterized.
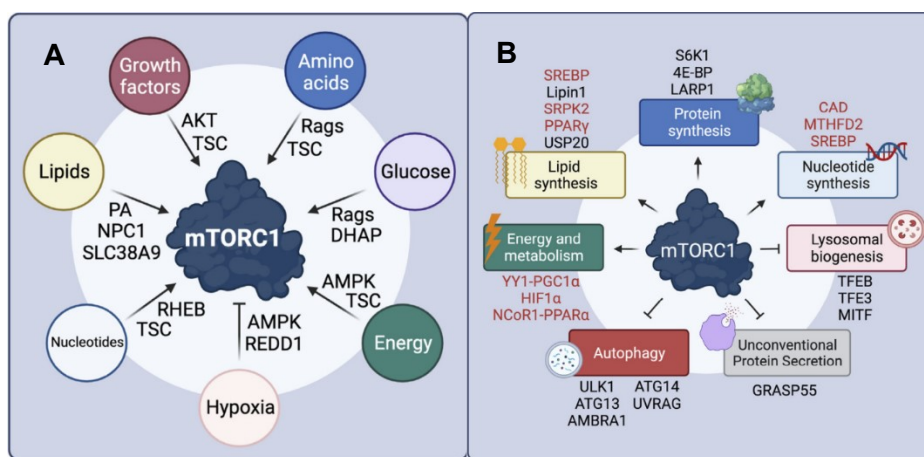
365

366   **Figure 1.6. Inputs and outputs of mTORC1 regulation. (A)** mTORC1 responds to regulation by nutritional, energy and oxygen
367   levels as well as receptor-mediated signaling (i.e., triggered by Growth factors). **(B)** In turn, mTORC1 promotes anabolic metabolism
368   including lipid, nucleotide and protein synthesis, while repressing autophagy and lysosome biogenesis. Proteins directly regulated by
369   mTORC1 are shown in black and indirect targets are shown in red (Fernandes and Demetriades 2021).

370   **1.1.5.2 Translational regulation by EIF4E/4E-BPs**

371   Activity of the cap-binding activity can be regulated by inhibitory binding of 4E-BPs and by direct
372   MAPK MNK-dependent phosphorylation (Raught and Gingras 1999). It has been shown that
373   overexpression of eIF4E in microglia leads to altered macrophage phagocytic capacity, motility, and a
374   systemic autism-like behavior in genetically modified male mice (Xu, Kim et al. 2020). Additionally,
375   macrophage stimulation with recombinant bacterial Shiga-1 toxin leads to MAPK activation and eIF4E
376   phosphorylation that was associated with increased expression of inflammatory cytokines IL8 and IL1β
377   (Cherla, Lee et al. 2006). In parallel, 4E-BP expression was reported to modulate inflammation on a murine
378   model of obesity. Macrophages isolated from mice deficient for 4E-BP1/2/3 expression showed enhanced
379   inflammatory responses along with upregulated IRF8 translation. Additionally, *Eif4ebp1/2/3*[-/-] mice fed with

12

380 high fat diet show proclivity to develop obesity and to accumulate inflammatory macrophages in adipose
381 tissue (Pearl, Katsumura et al. 2020).

382 Of note, our group described that 4E-BP translational repression activity contributed to the
383 regulation of macrophage anti-inflammatory response and capacity to induce T cell migration since
384 macrophages derived from 4E-BP1/2 knockout mice expressed higher levels of the immune-repressors
385 IL10, COX-2 and the chemokines CCL5, CXCL10 (William, Leroux et al. 2018, William, Leroux et al. 2019)
386 (**See Appendix 1 and 2**). Furthermore, we reported *T. gondii* infection-reduced macrophage
387 phosphorylation of MNK1/2 and eIF4E *in vitro* with parasite burden markedly increased in macrophages
388 and tissues from transgenic mice expressing a non-phosphorylatable mutant form of eIF4E (EIF4E^{S209A})
389 with a concomitant exacerbation of IFNγ serum levels during infection when compared to wild type controls
390 (Leroux, Chaparro et al. 2020) (**See Appendix 3**). In sum, eIF4E activity participates in different aspects of
391 macrophage biology and regulation through 4E-BPs or through MNK-mediated phosphorylation can affect
392 inflammatory and antimicrobial responses.

393   **1.1.5.3 Translational regulation by EIF4A**

394 Secondary structures present in the 5'UTR across different mRNA transcripts can hamper scanning
395 progression of the eIF4F complex if not for the activity of RNA helicases such as EIF4A (Svitkin, Pause et
396 al. 2001, Parsyan, Svitkin et al. 2011). By itself, EIF4A is an enzyme that exhibits modest ATPase and
397 helicase activities but interaction with translation initiation factors such as EIF4G and EIF4B notably
398 increase (over 13-fold) both activities (Andreou and Klostermeier 2014) (**Figure 1.7**), while binding to the
399 repressor programmed-cell-death-4 (PDCD4) results in the opposite effect thereby inhibiting protein
400 synthesis (Dennis, Jefferson et al. 2012). EIF4B phosphorylation by mTORC1/RPS6K (Raught, Peiretti et
401 al. 2004) and/or MAPK/RSK (Shahbazian, Roux et al. 2006) favors its recruitment to the translation
402 preinitiation complex, which facilitates its interaction with EIF4A (Dennis, Jefferson et al. 2012).
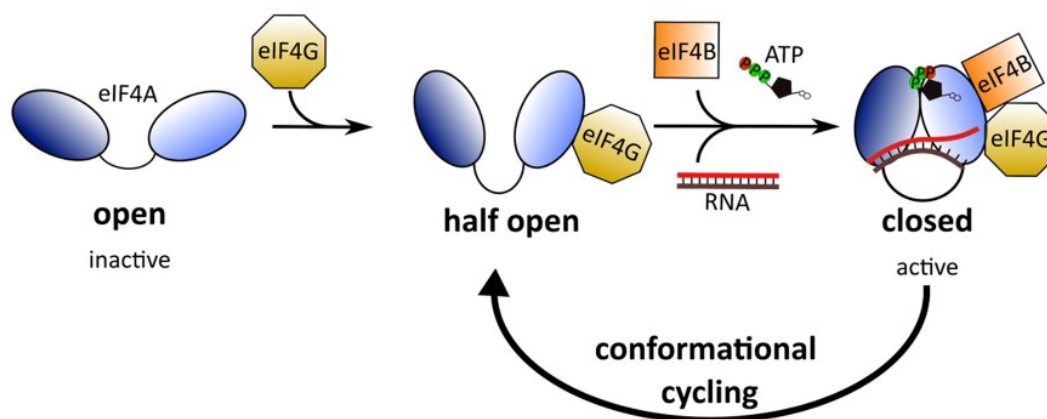
403

404 **Figure 1.7. Conformational cycling of eIF4A.** Binding of eIF4G enables eIF4A to switch from the open to the half-open state. In
405 the presence of eIF4B, ATP and an RNA substrate, eIF4A can undergo conformational cycling and alternate between the active-
406 closed and half-open state to enable helicase and ATPase activity (Taroncher-Oldenburg, Muller et al. 2021).

13

407   In parallel, inhibitory effect of PDCD4 on eIF4A can be relaxed by RPS6K- or AKT-mediated
408   phosphorylation, which targets PDCD4 for proteasomal degradation or nuclear translocation respectively
409   (Palamarchuk, Efanov et al. 2005, Dorrello, Peschiaroli et al. 2006). Interestingly, multiple natural
410   compounds isolated from algae, plants and animals have been reported to inhibit eIF4A activity through
411   different mechanisms including RNA clamping (i.e., rocaglates), inhibition ATPase activity (i.e., elatol,
412   allolaurinterol, elisabatin A), and inhibition of eIF4G (i.e., pateamine A, 15d-PGJ2) or RNA (i.e.,
413   hippuristanol) binding (**Figure 1.8**) (Taroncher-Oldenburg, Muller et al. 2021). Dysregulated EIF4A activity
414   is a hallmark of different types of cancer including T-cell acute lymphoblastic for, which translation of
415   transcripts containing guanine-quadruplexes in their 5'UTRs was differentially inhibited by silvestrol, a
416   rocaglate EIF4A inhibitor isolated from the plant *Aglaia foveolate* (Pan, Kardono et al. 2010, Wolfe, Singh
417   et al. 2014). BFL1, a toxin produced by the bacteria *Burkholderia pseudomallei* proved to be lethal *in vivo*
418   and *in vitro* against mice and macrophages through deaminating inhibition of eIF4A helicase activity, which
419   highlights the essential character of EIF4A for survival (Cruz-Migoni, Hautbergue et al. 2011). Furthermore,
420   silvestrol proved effective in macrophage control of Ebola virus infection attributed to the virus requirement
421   of host translational machinery to process highly structured viral 5'UTRs (Biedenkopf, Lange-Grunweller et
422   al. 2017).

423   The importance of EIF4A in macrophage immune functioning was further underscored by treatment
424   with synthetic rocaglates, which promote M1 polarization and increased IRF1 expression with a concomitant
425   enhancement in bactericidal capacity against *Franscicella tularensis* and *M. tuberculosis* infection
426   (Bhattacharya, Chatterjee et al. 2016, Chatterjee, Yabaji et al. 2021). In addition to targeting mammalian
427   host eIF4A, the synthetic rocaglate CR-1-31B showed antimalarial activity against *Plasmodium berghei*
428   EIF4A homologue thus positioning this family of compounds as potential dual-targeting therapeutical drugs
429   preventing development of cerebral malaria in a murine model (Langlais, Cencic et al. 2018).

430   **1.1.5.4 Translational regulation by EIF2A**

431   Similar to mTORC1 sensing activity, phosphorylation of the translation initiation factor 2 alpha
432   (EIF2α) greatly inhibits mRNA translation in response to different stimuli (Van Der Kelen, Beyaert et al.
433   2009). The upstream kinases heme-controlled repressor (HRI or EIF2AK1), interferon induced, double-
434   stranded RNA-activated kinase (PKR or EIF2AK2), PKR-like endoplasmic reticulum (ER) kinase (PERK or
435   EIF2AK3) and general control nonderepressible 2 (GCN2 or EIF2AK4) are respectively activated by heme
436   deficiency, viral infection/inflammation, ER stress (i.e., accumulation of unfolded proteins), and amino acid
437   starvation collectively constituting the integrated stress response (Pakos-Zebrucka, Koryga et al. 2016).
438   Phosphorylation of EIF2α impairs the formation of the eIF2/^{Met}tRNA/GTP trimeric complex, which is
439   essential for translation initiation thus turning EIF2α as pivotal sensor for cell homeostasis (Van Der Kelen,
440   Beyaert et al. 2009). Interestingly, translation of the transcription factor ATF4 is favored in stress conditions
441   that lead to EIF2α phosphorylation through a use of upstream open reading frames (uORFs) from *Atf4*
442   coding sequence (Vattem and Wek 2004). ATF4 is a transcription factor associated with upregulation of

14

stress response genes, which can promote (Ye, Kumanova et al. 2010) or inhibit cell survival (Teng, Gao et al. 2014). Notably, in macrophages eIF2α phosphorylation can affect the development of immune responses. For example, NLR stimulation increases EIF2α phosphorylation through HRI activation, which was reported to be essential for inflammasome assembly through ATF4-sustained expression of chaperone HSPB8 leading to increased levels of *Cxcl1* (Abdel-Nour, Carneiro et al. 2019). Additionally, Hsu *et al* showed that following TLR4 stimulation or infection with *Salmonella typhimurium*, *Yersinia pseudotuberculosis* or *Bacillus antracis*, PKR is promptly activated and subsequent eIF2α phosphorylation is critical for macrophage apoptosis. Notably, macrophages developed from EIF2α^{S51A}(defective for EIF2α phosphorylation) fetal precursors showed residual levels of apoptosis upon TLR4 stimulation, which the authors suggest might be associated with PKR-dependent and EIF2α-independent mechanisms (Hsu, Park et al. 2004).
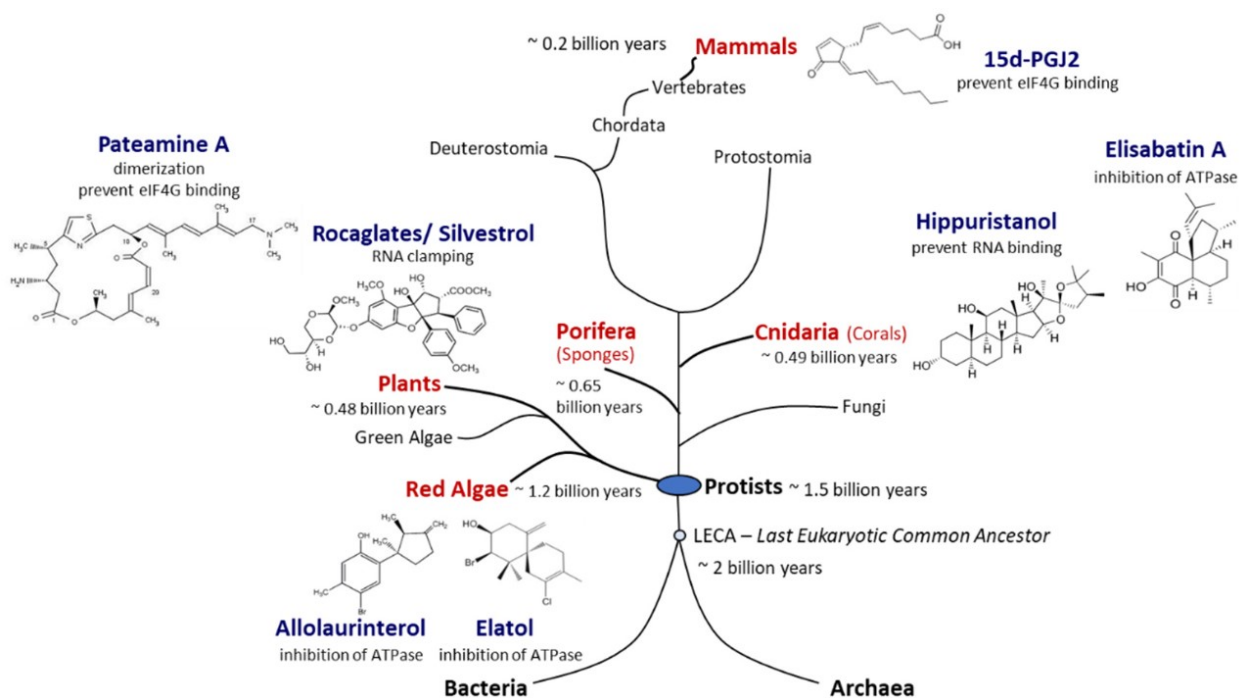
Figure 1.8. Natural producers of molecules with eIF4A inhibitory activity. (Taroncher-Oldenburg, Muller et al. 2021).

In synthesis, by expressing a wide array of sensors, macrophages can quickly respond to external cues and participate in multiple processes such as nutrient (i.e., iron, bilirubin, calcium, lipids, amino acids) homeostasis, dead cell removal (efferocytosis), cardiac conduction, tissue integrity and immune defense (Mosser, Hamidzadeh et al. 2021). Armed with a battery of antimicrobial effectors, macrophages are front line defenders for *in situ* pathogen control; Paradoxically, numerous pathogens evade host immune responses and use the macrophage as their main replication niche (Price and Vance 2014). Unsurprisingly, several pathogens target the macrophage gene expression response to their advantage (Chaussabel,

464 Semnani et al. 2003, Goldmann, von Kockritz-Blickwede et al. 2007, Rabhi, Rabhi et al. 2016, Leroux,

465 Lorent et al. 2018). However, the existence of tissue-specific phenotypes coupled to their natural low

466 frequency hampers efforts of macrophage characterization (Gordon, Pluddemann et al. 2014). Hence,

467 generating more homogeneous populations of macrophages is considered a necessary prerequisite for *in*

468 *vitro* research of macrophage biology (Davis 2013). Peritoneal macrophages (PMs) can be obtained in

469 large numbers via thioglycolate eliciting, however, PMs are usually activated upon thioglycolate stimulation,

470 which might introduce bias in subsequent experimentation (Davis 2013). In parallel, virus-transformed or

471 cancerous monocyte/macrophage cell lines such as RAW264.7 (mouse) and THP-1 (human) represent

472 practical alternatives to analyze macrophage responses in different biological settings, although

473 phenotypical differences with primary cells (Andreu, Phelan et al. 2017, Tedesco, De Majo et al. 2018) or

474 passage-associated loss of macrophage functions have been reported (Taciak, Bialasek et al. 2018). In

475 this scenario, primary mouse bone marrow-derived macrophages (BMDMs) and human monocyte-derived

476 macrophages (hMDM) represent robust alternatives with increased physiological relevance that can be

477 expanded in large numbers and additionally be differentiated from genetically modified hosts (e.g., mice)

478 (Andreu, Phelan et al. 2017). In this work it is studied the extent to which infection by the intracellular

479 protozoan parasite *Leishmania donovani* remodels mRNA translation and abundance programs of murine

480 BMDMs.

481

482

483

484

485

2. Leishmania: The parasite

Intracellular parasitism stands as an effective strategy to dampen notorious antimicrobial defense mechanisms such as complement and antibody opsonization. Additionally, it offers an otherwise unrestricted source of nutrients, while reducing the probability of cohabiting with competing microorganisms (Thakur, Mikkelsen et al. 2019). However, in order to successfully establish this lifestyle an organism must circumvent different barriers to allow invasion, survival and transmission between hosts. Certainly, a series of environmental and genetic constraints limit the array of combinations that make this shift from extracellular forms possible (Poulin and Randhawa 2015). Interestingly, emergence of intracellular parasitism in the Eukarya domain has been a rare event (Sibley 2011). Nonetheless, although eukaryote intracellular parasites (i.e., Apicomplexa, Trypanosomatida and Microsporidia) represent but a minute fraction of nucleated organisms, they also display some of the most successful species on earth (Sibley 2011). Their ample worldwide distribution and the high number of circulating genome copies indicate that transition from extracellular organisms (although a rare event) can render profitable results by overcoming heavy selective pressures.

In doing so, this process led to the appearance of some of the most lethal and morbid transmissible diseases known to humanity. Collectively, the causative agents of malaria (*Plasmodium* spp.), Chagas disease (*Trypanosoma cruzi*) and Leishmaniasis (*Leishmania* spp.) are responsible for thousands of deaths every year in regions, where hundreds of millions of individuals are at risk of infection (Andrews, Fisher et al. 2014). Furthermore, the lack of commercially available vaccines, the emergence of drug resistance as well as demographic mobilization from endemic areas (derived from war, civil conflict, military or commercial travel, and climate change) have contributed with variations in incidence and dispersion of these parasites (Cardenas, Sandoval et al. 2006, Beyrer, Villar et al. 2007, Gonzalez, Wang et al. 2010). Hence, understanding the biology of their infection is of paramount importance in order to better design cost-effective strategies against human intracellular parasitosis.

2.1 Leishmaniasis

Protozoan parasites of the genus *Leishmania* are the causative agents of a collective of diseases known as leishmaniases. Over 19 species are reported to infect humans, giving origin to an array of clinical manifestations that range from self-healing skin sores and deforming mucocutaneous lesions to potentially fatal visceral infections (Burza, Croft et al. 2018). *Leishmania* parasites are among the most geographically spread pathogens spanning across 98 tropical and subtropical countries around the world (Alvar, Velez et al. 2012). Being part of the Trypanosomatidae family (restricted to obligate parasites), *Leishmania* spp. are related to other pathogens with clinical, veterinary and economical importance for humans (i.e., *T. cruzi, T. brucei*), animals (i.e., *T. evansi*, Sauroleishmania) and plants (i.e., *Phytomonas staheli, P. leptovasorum*) (Birhanu, Fikru et al. 2015, Jaskowska, Butler et al. 2015, Lukes, Butenko et al. 2018).

17

520   Leishmaniases are vector-borne diseases transmitted by phlebotomine sandflies. There are more
521   than 800 reported sandfly species to date, 60% of which are present in the new world (America), while the
522   rest can be found in the old world (Africa and Eurasia) (Akhoundi, Kuhls et al. 2016). In the course of
523   evolution, females of the taxon Phlebotominae (Diptera, Psychodidae) developed hematophagous habits
524   in order to reach sexual maturity (Tuon, Neto et al. 2008). This process facilitated their subsequent
525   transformation into vectors for various pathogens including *Leishmania* spp., *Bartornella* spp., and different
526   arboviruses (Galati, Galvis-Ovallos et al. 2017). Flagellated *Leishmania* promastigotes proliferate in the
527   digestive tract of female sandflies and develop into infective metacyclic parasites that are inoculated into
528   mammal or reptile hosts during blood intake. Next, metacyclic promastigotes are internalized by
529   professional phagocytes of the immune system being the macrophage the definitive replicative niche, where
530   the parasites transform into the non-motile amastigote form, responsible for the different clinical
531   manifestations of the disease in mammals. Finally, female sandflies ingest blood from infected individuals
532   and amastigotes then transform into promastigotes keeping the chain of transmission (**Figure 1.5**) (Burza,
533   Croft et al. 2018).

534
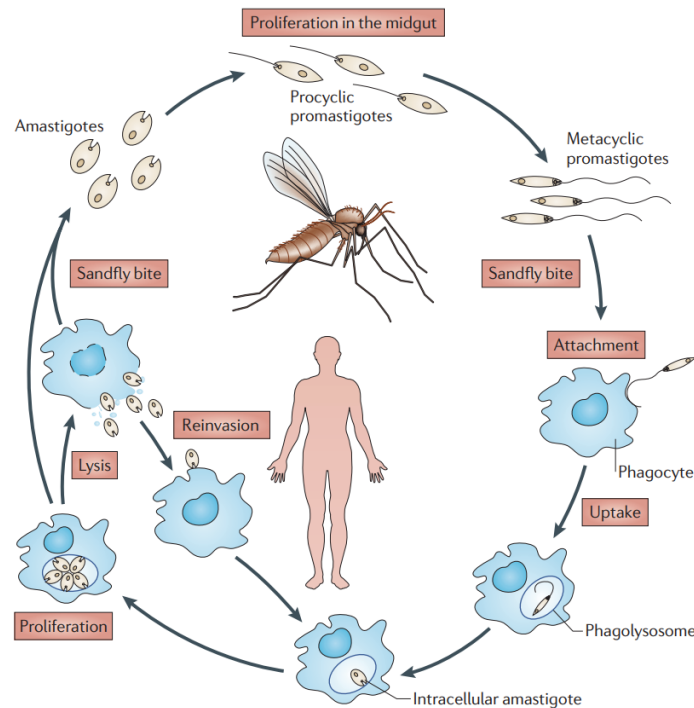
535

536   **Figure 1.9. Life cycle of *Leishmania* sp.** Promastigote-infected female sandflies transmit metacyclic parasites to mammalian hosts
537   (i.e., human). Professional phagocytes ingest the invading pathogens with the macrophage being the definitive niche for amastigote
538   differentiation and replication. Amastigotes are transmitted to a new female sandfly during a bloodmeal and the cycle starts again
539   (Kaye and Scott 2011).

540   **2.1.1 Cutaneous leishmaniasis**

541   Cutaneous leishmaniasis (CL) is the most common form of the disease with an estimate of 700,000

542   to 1,200,000 cases annually. Approximately, 75% of the cases originate in 10 countries from Africa (Algeria,

543   Ethiopia, North Sudan), America (Colombia, Brazil, Costa Rica, Peru) and the Greater Middle East

544   (Afghanistan, Iran, Syria) (Alvar, Velez et al. 2012). CL is caused by a gamma of *Leishmania* parasites (i.e.,

545   *L. major, L. tropica* and *L. aethiopica* in the old world and *L. mexicana, L. amazonensis, L. guyanensis, L.*

546   *panamensis, L. braziliensis* in the new world) and it presents itself as self-healing skin ulcers that may leave

547   permanent scars. Poverty and inadequate housing or sanitary conditions are among the most important

548   risk factors for contracting CL and, although rodents and hyraxes are considered the main reservoirs of

549   these parasites in the old world (Gholamrezaei, Mohebali et al. 2016, Pareyn, Van den Bosch et al. 2019);

550   reports of infected dogs, marsupials and bats in the new world point towards a complex network of

551   transmission involving domestic and sylvatic mammals (Quaresma, Rego et al. 2011, Berzunza-Cruz,

552   Rodriguez-Moreno et al. 2015).

553   Even though CL is considered non lethal, immunocompromised patients can develop more severe

554   manifestations (Choi and Lerner 2002). Reported CL complications in pregnant women (Morgan,

555   Guimaraes et al. 2007), patients with history of autoimmune disorders (Bardazzi, Giacomini et al. 2010,

556   Asgari, Gholizadeh et al. 2019) or during co-infection with human immunodeficiency virus (HIV) (Guerra,

557   Coelho et al. 2011) have prompted HIV testing on CL patients as a mandatory practice in territories such

558   as French Guyana, where dermal phenotypic diversity and antileishmanial therapeutic failures are a public

559   health problem (Couppie, Clyti et al. 2004). On the other hand, severe psychological sequalae related with

560   the visibility of the scars have been associated with depression, social stigmatization and self-depreciation

561   (Bennis, De Brouwere et al. 2018). Furthermore, the period of 1990 to 2013 saw and increase of 174.2%

562   in the global prevalence of CL (Aronson and Joya 2019), a fact that was recently aggravated by the military

563   conflict and the refugee crisis in Syria, where a severe epidemic of CL is currently ongoing and affecting

564   different regions of the Mediterranean basin (Du, Hotez et al. 2016, Kanani, Amr et al. 2019). As a result,

565   there is a critical need for improved mechanisms of surveillance and control of CL, a disease catalogued

566   by the WHO as one of numerous neglected tropical diseases (Molyneux, Savioli et al. 2017).

567   **2.1.2 Mucocutaneous leishmaniasis**

568   Tropism towards the oro-nasopharyngeal cavity during *Leishmania* infection represents between

569   5-20% of CL cases in countries like Bolivia, Brazil, Ethiopia and Peru, which register most (ca.90%) of the

570   reports of mucocutaneous leishmaniasis (MCL) (Handler, Patel et al. 2015, Carvalho, Llanos-Cuentas et

571   al. 2018). This pathology can range from mild lesions in the oral or nasal cavities to severe destruction of

572   the nasal septum and perturbation of the epiglottis or the vocal cords, which can progress to a potentially

573   fatal respiratory disfunction (David and Craft 2009). It remains unclear what are the determinant factors that

574   lead to the onset of this clinical manifestation, however, in most patients there is a history of previous

19

575 leishmaniasis episodes (Handler, Patel et al. 2015). Additionally, a strong correlation between MCL
576 pathogenesis and presence of *Leishmania* RNA virus (LRV) on clinical isolates has been documented
577 (Cantanhede, da Silva Junior et al. 2015). Furthermore, prognosis can be aggravated in cases where the
578 immune system is compromised (Padovese, Terranova et al. 2009, Darcis, Van der Auwera et al. 2017).
579 The most common causative agent is *L. braziliensis*, although *L. guyanensis*, *L. panamensis* and *L.*
580 *amazonensis* have been reported to lead to MCL manifestations in the new world and *L. major, L.*
581 *aethiopica,* and *L. infantum* in the old world (David and Craft 2009, Padovese, Terranova et al. 2009, Darcis,
582 Van der Auwera et al. 2017).

2.1.3 Visceral leishmaniasis

584 The most severe form of leishmaniasis is caused by members of the *Leishmania donovani*
585 complex, which includes both *L. donovani* and *L. infantum* (syn. *L. chagasi*). It is estimated that between
586 200,000 to 400,000 cases and 20,000 to 40,000 associated fatalities occur every year due to visceral
587 leishmaniasis (VL), also known as Kala Azar (Alvar, Velez et al. 2012). Over 90% of the global cases of VL
588 come from Brazil, Ethiopia, Kenya, Somalia, Sudan, South Sudan and India. Infection by *L. infantum* spans
589 throughout China and different countries in Latin America and the Mediterranean basin; maintained in a
590 zoonotic cycle through dogs as its main reservoir. On the other hand, infection by *L donovani* is considered
591 an anthroponosis mostly present in East Africa and the Indian subcontinent (van Griensven and Diro 2019).

592 Following sandfly inoculation, the parasites proliferate in macrophages and disseminate to internal
593 organs and tissues such as lymph nodes, liver, spleen, and bone marrow. The incubation period can range
594 between 2 weeks to 8 months and some of its signs and symptoms include irregular fever, weight loss,
595 splenomegaly, anemia and hypergammaglobulinemia (Burza, Croft et al. 2018). It has been reported that
596 bone marrow dysfunction favors parasite persistence in murine models (Abidin, Hammami et al. 2017).
597 Furthermore, subsequent immune suppression preludes susceptibility to secondary infections, which
598 together with bleeding proclivity and severe anemia make of VL a lethal infection if not treated (Chappuis,
599 Sundar et al. 2007). In consequence, the WHO strongly encourages surveillance in all continents for
600 coinfection with HIV given the immuno-debilitating outcome of both pathologies (Lindoso, Cota et al. 2014).

601 Of note, the global incidence of VL highly decreased after the second world war as a secondary
602 outcome on sandfly populations from the intense malaria eradication campaign carried out against
603 *Anopheles* spp. vectors by different nations (Joshi, Sharma et al. 2006). However, resurgence of VL was
604 noticeable during the 1990s, particularly in south western Europe were it was associated with the spread
605 of the HIV pandemic (Oryan and Akbari 2016). Currently, a decrease in the worldwide number of VL cases
606 can be attributed to the elimination initiative started by India, Nepal and Bangladesh to bring VL incidence
607 to less than 1 case per every 10,000 inhabitants (Singh, Hasker et al. 2016). However, it is acknowledged
608 that the distribution of the disease is growing southwards in Brazil and an increasing risk for a similar trend
609 is present to the north of the Mediterranean basin (Ready 2010, Pasquali, Baggio et al. 2019). Hence,

610 surveillance, treatment, and research on the biology of the disease is of the upmost importance in order to
611 control it.

2.1.4 Post-Kala-Azar Dermal Leishmaniasis

613 One of the features of VL caused by *L. donovani* is the persistence of parasites after clinical cure
614 is achieved. This becomes evident weeks to years after cure of the original infection when parasite-
615 containing dermal lesions manifest in the form of macules, nodules or papules (Burza, Croft et al. 2018)
616 referred to as Post-Kala-Azar Dermal leishmaniasis (PKDL). PKDL is more frequent in Sudan (observed in
617 50-60% of cured VL patients, being the papulonodular form predominant) than in south east Asia (10-20%
618 of cured VL patients, mostly macular) (Zijlstra, Musa et al. 2003). It is still not clear the factors that determine
619 the onset of PKDL after clinical cure of VL but associations have been noted with different parasite strains,
620 ultraviolet light exposure of the skin, antileishmanial drug scheme or dosing and failure of tissue-specific T
621 cell memory response (Mukhopadhyay, Dalton et al. 2014).

622 Most of the reported cases of PKDL self-heal within a year in Sudan and no treatment is prescribed
623 unless further complications emerge. On the contrary, treatment is mandatory in southeast Asia but since
624 its course warrants a long period of 4-12 months to be completed, reluctance and non-compliance are
625 common in the population (Gedda, Singh et al. 2020). Additionally, the potential of the lesions to act as
626 parasite reservoir is yet under debate. A recent study found that nodular lesions harbor a greater parasite
627 load than macules and are hence more infective to sandflies (Mondal, Bern et al. 2019). However, the
628 contribution of this observation to the dynamics of VL transmission and the threat it poses to elimination
629 programs remains to be established.

2.2 Leishmania and the host

2.2.1 Tissue disruption and host cells recruitment

632 During a blood meal, female sand fly bites create an insult to tissue and capillaries of the epidermal
633 layer of the skin. This event triggers a localized inflammatory response characterized by a rapid (within
634 hours) influx of neutrophils (Simpson and Ross 1972). This initial infiltration seems to be parasite-
635 independent since sterile needle puncture or sham inoculation with uninfected sand flies showed similar
636 recruitment levels (Peters, Egen et al. 2008). Nonetheless, further neutrophil mobilization can be enhanced
637 by components of the sandfly saliva (de Moura, Oliveira et al. 2010), gut microbiota (Dey, Joshi et al. 2018)
638 or from parasite-derived molecules such as the promastigote secretory gel (PSG) and the *Leishmania*
639 chemotactic factor (LCF) (van Zandbergen, Hermann et al. 2002). Different reports show that *Leishmania*
640 spp. are capable of subverting neutrophil functions such as phagosome maturation (Mollinedo, Janssen et
641 al. 2010). What is more, replication of *L. mexicana* promastigotes was observed in murine neutrophils,
642 although amastigote differentiation remains exclusive to the macrophage phagolysosome (Hurrell,

21

643   Beaumann et al. 2017). It has been proposed that neutrophils serve as intermediate hosts that promote
644   safe parasite internalization in macrophages through 2 different models. The *Trojan horse* model stipulates
645   that phagocytosis of infected apoptotic neutrophils prevents macrophage activation and favors parasite
646   survival (Laskay, van Zandbergen et al. 2003). On the other hand, two-photon-intravital-microscopy
647   suggests that viable parasites can "hop" to macrophages when released from apoptotic neutrophils (Peters,
648   Egen et al. 2008). Thus, the *Trojan rabbit* model postulates that free parasites derived from apoptotic
649   neutrophils might be better adapted to survive inside macrophages, however, this hypothesis is yet to be
650   tested (Kupani, Pandey et al. 2021). Interestingly, in experimental models of chronic visceral leishmaniasis,
651   myelocytic-skewed emergency hematopoiesis has proven to provide an influx of monocytes and monocyte-
652   like intermediates that become permissive host cells to *L. donovani* infection *in vivo* when macrophage
653   populations show a marked decrease in total numbers (Abidin, Hammami et al. 2017, Hammami, Abidin et
654   al. 2017).

655   **2.2.2 Leishmania and the macrophage**

656   After the initial wave of neutrophil infiltration macrophages are recruited to the wound site and the
657   majority of promastigotes are found in mononuclear phagocytes 24 hours post infection (Wilson, Innes et
658   al. 1987). *Leishmania* parasites rely on the interaction of some of their membrane-bound virulence factors
659   such as lipophosphoglycan (LPG) and leishmanolysin (GP63) with surface macrophage receptors for
660   molecules such as complement proteins, mannose residues, fibronectin fibers and Fcγ chains
661   (Podinovskaia and Descoteaux 2015). The physical contact between *Leishmania* and the macrophage is
662   enough to modulate different biological processes in the host cell (Podinovskaia and Descoteaux 2015).
663   For example, *Leishmania* promastigotes are known to inhibit lysis by the complement membrane attack
664   complex by cleaving C3 into the inactive iC3b form that is deposited on the parasite surface and through
665   which it can initialize phagocytosis using the C3 receptor (CR3) on the macrophage surface (Brittingham,
666   Morrison et al. 1995). By engaging CR3-dependent phagocytosis, the parasite can prevent macrophage
667   activation features such as oxidative burst, IL12 production and IFNγ responsiveness (Marth and Kelsall
668   1997). In contrast, amastigotes exhibit low levels of LPG and GP63 expression; hence, IgG opsonization
669   seems to be a preferred mechanism to induce macrophage phagocytosis via Fcγ receptors for this parasite
670   stage (Guy and Belosevic 1993).

671   Phagocytosis of particulate targets (including invading microorganisms) occurs through
672   invagination of vacuoles, which end up recruiting an arsenal of oxidative, acidifying and hydrolytic enzymes
673   through assembly of NAPDH oxidase and lysosome fusion in order to degrade their luminal contents (Fairn
674   and Grinstein 2012). *Leishmania p*arasites are quickly phagocytosed (10-20min) and parasitophorous
675   vacuoles (PVs) rapidly lose their fusogenic capabilities toward lysosomal compartments promoted by a
676   circumscribed polymerization of F-actin around the PV in an LPG-dependent manner (Lodge and
677   Descoteaux 2005, Forestier, Machu et al. 2011). This delayed maturation allows for the transition from the

678　promastigote to the amastigote form within 24 hours post infection (Frank, Marcu et al. 2015, Wheeler,
679　Gluenz et al. 2015), which is critical for infection since LPG-deficient *L. donovani* promastigotes form PVs
680　that become enriched on lysosomal markers (Matte, Arango Duque et al. 2021) and additionally show
681　reduced intracellular survival (McNeely and Turco 1990).

682　　　　Promptly after infection by *L. donovani* promastigotes, macrophages phosphorylate P38 -a MAPK
683　that has been associated with activation of NADPH oxidase and to increased expression of the inducible
684　nitric oxide synthase (iNOS)-, which could evoke the induction of a parasite-killing oxidative burst that could
685　end in macrophage apoptosis (Junghae and Raynes 2002). However, early upregulation of antiapoptotic
686　genes such as MCL-1 was also detected in macrophages infected with *L. donovani* promastigotes through
687　a mechanism relying on the activating phosphorylation of the transcriptional factor CREB (Giri, Srivastav et
688　al. 2016). Furthermore, recently Giri *et* al showed how *L. donovani* prevents MCL-1 degradation through
689　binding with translationally controlled tumor protein (TCTP) in both primary and transformed murine
690　macrophages up to 48 hours post infection (Giri, Basu et al. 2022). Additionally, RAW264.7 macrophage
691　infection with *L. donovani* promastigotes led to the induction of heme oxigenase-1 (HO-1) as an anti-
692　inflammatory mechanism preventing early oxidative burst and subsequent activation of inflammatory
693　transcription factors (NF-κB, IRF3) and cytokine expression (IL12, TNF) (Saha, Basu et al. 2019). In the
694　same report, Saha *et al* indicate that treatment of cells or mice with HO-1 shRNA or pharmacological HO-
695　1 antagonists decreased parasite persistence *in vitro* and *in vivo* (Saha, Basu et al. 2019). In line with
696　subversion of macrophage immune responses during *L. donovani* infection, Mattheoud *et al*, described how
697　antigen presentation is quickly compromised during promastigote infection through cleavage of the vesicle
698　trafficking protein VAMP8 mediated by the parasite virulence factor GP63 (Matheoud, Moradin et al. 2013).
699　Interestingly, although GP63 expression is heavily decreased in the amastigote form, the capacity of
700　amastigote-infected macrophages to activate T cells in an antigen-dependent manner is still reduced
701　(Meier, Svensson et al. 2003). In a similar way to their flagellate counterpart, altered activity of a
702　transcription factor (STAT1) was reported on amastigote-infected macrophages (Matte and Descoteaux
703　2010), while a report by Moore *et al*, showed that amastigote infection also increases macrophage viability
704　(Moore, Turco et al. 1994).

705　　　　High throughput analyses have provided evidence of global scale responses in macrophages at
706　the mRNA and protein abundance levels during *L. donovani* infection (Gregory, Sladek et al. 2008, Espitia,
707　Saldarriaga et al. 2014, Geraci, Tan et al. 2015, Singh, Pandey et al. 2015, Kong, Saldarriaga et al. 2017,
708　Medina-Colorado, Osorio et al. 2017, Shadab, Das et al. 2019, Ferreira, Mesquita et al. 2020, Mesquita,
709　Ferreira et al. 2020, Smirlis, Dingli et al. 2020). Microarray data of BMDM collected from BALB/c mice 24
710　hours post infection with *L. donovani* promastigotes revealed a "hybrid" gene expression profile non-
711　conforming to either classical (M1) or alternative (M2) macrophage polarization with expression of
712　immunomodulatory genes being upregulated (i.e., COX2) or inhibited (i.e., CCR5) (Gregory, Sladek et al.
713　2008). In parallel, through long term passaging, Shadab *et al* generated avirulent promastigotes, which

23

were used to infect BALB/c peritoneal macrophages and by RNA sequencing they showed that host genes associated with immune stimulation and infection control were highly upregulated when compared to infection with virulent counterparts (Shadab, Das et al. 2019). This observation might be related to differential levels of expression of virulence factors (i.e., LPG and GP63) between virulent strains in contrast to avirulent strains as previously reported (Chakrabarty, Mukherjee et al. 1996). Recently, two RNAseq-based reports from the groups of Ricardo Silvestre and Jérôme Estaquier recently described the early (6 hours post infection) changes in transcript abundance associated with host cell lipid and glutamine metabolism in macrophages infected with *L. donovani*, although the global transcriptional response was not analyzed in depth (Ferreira, Mesquita et al. 2020, Mesquita, Ferreira et al. 2020). Furthermore, the group of Peter Melby working with an experimental model of visceral leishmaniasis in hamsters described global splenic changes in mRNA abundance during acute and chronic infection by *L. donovani* (Espitia, Saldarriaga et al. 2014, Kong, Saldarriaga et al. 2017, Medina-Colorado, Osorio et al. 2017). For example, they showed that the first 2 weeks of infection (e.g., 7, 14 days) are relatively silent, while a profound effect is observed during the chronic phase (28 days post infection) with over 700 transcripts being differentially expressed with a distinctive enrichment in mRNAs associated with IFNγ and IL4 signaling pathways (Espitia, Saldarriaga et al. 2014). Interestingly, although high expression of type I and type II interferon response genes was identified in the splenic tissue, this was insufficient to induce a parasite killing M1 macrophage polarization. Paradoxically, IFNγ promoted amastigote growth by inducing a STAT3-dependent signature of parasite promoting transcripts (i.e., *Il10, Arg1*, *Ido1*, *Irg1*) (Kong, Saldarriaga et al. 2017). This observation was extended to CD4^{+} T cells, which also presented hybrid expression profiles of Th1 and Th2 cytokines with a particular upregulation of the inhibitory receptor PD-1 on CD4^{+} T cells and its corresponding ligands PDL-1 and PDL-2 in macrophages during chronic infection by *L. donovani* (Medina-Colorado, Osorio et al. 2017).

Conversely, Geraci *et al* described the effect of *L. major* or *L. donovani* infection on the post-transcriptional regulation of human phagocytes by small RNA sequencing and mature miRNA expression assessment (Geraci, Tan et al. 2015). Accordingly, they showed a species-specific upregulation (greater in *L. donovani* than *L. major*) of miRNAs (i.e., miR-155, miR-146b, miR2-6) targeting members of the MAPK, STAT1 and TGF-β pathways (Geraci, Tan et al. 2015), suggesting that mechanisms of post-transcriptional regulation are also elicited during infection by *L. donovani* affecting host cell defense responses. Interestingly, proteome analyses of human and murine macrophages identified components of the mRNA translation machinery as differentially regulated over 12 hours post infection, which indicates this process could also be affected during *L. donovani* infection (Shadab, Das et al. 2019, Smirlis, Dingli et al. 2020). However, the study of host translational control during infection by protozoan parasites remains largely unexplored. Previous reports indicate *L. donovani* infection induces an early activation of the PI3K/Akt and/or mTOR signaling pathways (Cheekatla, Aggarwal et al. 2012, Nandan, Camargo de Oliveira et al. 2012, Zhang, Prasad et al. 2018), which -as previously stated- can act as central regulators of cellular mRNA translation (Fonseca, Smith et al. 2014). In parallel, accumulating data has shown that the eIF2α

751   kinase PKR is induced in macrophages in response to *Leishmania* sp in a TLR-dependent manner and this

752   can have a parasite promoting or parasite-controlling effect depending on the pathogen species (Pereira,

753   Teixeira et al. 2010, Vivarini Ade, Pereira Rde et al. 2011, Faria, Calegari-Silva et al. 2014, Dias, Goundry

754   et al. 2022). Curiously, most high throuput analysis of macrophage gene expression in response to *L.*

755   *donovani* infection have been done 1) with promastigotes and not the clinically relevant amastigote, 2)

756   overlooking the contribution of mRNA translation as a pivotal component defining the cellular proteome, 3)

757   at least 12 hours post infection, leaving a time window where multiple physiological and immune changes

758   are taking place inside the host cell that could trigger or be elicited by changes in mRNA abundance or

759   translation. Thus, this works is oriented toward shedding light on unresolved aspects of the early

760   macrophage response to *L. donovani* promastigote and amastigote infection through mechanisms that

761   regulate mRNA translation and abundance.

762

763

764

765

766

767

768

769

770

771

772

773

774

775

CHAPTER 2

Hypothesis and Objectives

778

779

780

781

782

783

784

785   *L. donovani* is an obligate intracellular parasite in mammals using macrophages as their replicative

786   niche where the promastigote flagellated from transforms into the non-motile amastigote form (Burza, Croft

787   et al. 2018). Macrophages are professional phagocytes with central roles in homeostasis and disease and

788   as members of the innate immune system, they count with a battery of immune and microbicidal tools to

789   eliminate invading pathogens (Naito 2008). Thus, to survive in such a hostile environment *Leishmania*

790   parasites have evolved different subversive mechanisms to evade killing by the macrophage host including

791   modulation of gene expression (Kaye and Scott 2011). Much attention has been focused on describing

792   changes in macrophage mRNA abundance during *L. donovani* promastigote infection *in vitro* past time

793   frames where critical processes define infection progress (i.e., phagolysosome formation, oxidative burst

794   development, apoptosis initiation) (Chaussabel, Semnani et al. 2003, Gregory, Sladek et al. 2008, Shadab,

795   Das et al. 2019). Accumulating evidence indicates early *L. donovani* infection can affect discreet

796   components that lead to modulation of mRNA abundance (i.e., transcriptional factors, miRNAs) (Matte and

797   Descoteaux 2010, Geraci, Tan et al. 2015, Giri, Srivastav et al. 2016, Saha, Basu et al. 2019) and

798   translation (i.e., protein levels of translational components, PI3K/AKT/mTOR and eIF2α signaling)

799   (Cheekatla, Aggarwal et al. 2012, Nandan, Camargo de Oliveira et al. 2012, Singh, Pandey et al. 2015,

800   Zhang, Prasad et al. 2018, Smirlis, Dingli et al. 2020, Dias, Goundry et al. 2022) but a characterization of

801   the global response encircling both aspects of gene expression during the early infection by promastigotes

802   and amastigotes is yet lacking. Thus, the working hypothesis of this research is that widespread regulation

803   of early macrophage mRNA translation and abundance constitutes an integral component of the host

804   response that modulates *L. donovani* intracellular survival by selective expression of functional groups of

805   transcripts in a stage-specific manner upon infection.

806   To test this hypothesis, the first objective will be to generate datasets of total cytosolic and highly

807   translated (polysomal) RNA sequences of BMDM infected or not with *L. donovani* promastigotes or

808   amastigotes. To accomplish this, polysome profiling (Masek, Valasek et al. 2011) quantified by RNAseq

809   will be used to identify the different mRNA species expressed in control and *L. donovani*-infected BMDM.

810   The second objective will be to evaluate the role of changes in the translational landscape of BMDM

811   infected by promastigotes or amastigotes of *L. donovani*. To achieve this objective, we will employ the

812   bioinformatic tool *anota2seq* (Oertlin, Lorent et al. 2019), which allows for evaluation of differential

813   translational levels calculated as changes in polysomal RNA (e.g., mRNA transcripts loaded with ≥ 3

814   ribosomal subunits) factored along with variations in total cytosolic RNA to exclude false positives derived

815   from congruent variations in mRNA abundance. Functional transcript subsets will be identified using

816   hierarchical clustering software and biochemical and pharmacological approaches will be used to validate

817   selected targets.

818   The third objective will be to evaluate the role of changes in mRNA abundance of BMDM infected

819   by promastigotes or amastigotes of *L. donovani*. We will perform *anota2seq* differential expression analysis

820   on the total cytosolic RNA subsets generated in the first objective coupled with hierarchical clustering

821   software to identify functional subsets of mRNA transcripts as well as potential upstream transcriptional

822   regulators. Selected targets will be validated by RT-qPCR assays.

823

824

825

826

827

828

829

830

831

CHAPTER 3

Publication No.1

834

835 **Translational profiling of macrophages infected with *Leishmania donovani***

836 **identifies mTOR- and eIF4A-sensitive immune-related transcripts**

837 Visnu Chaparro[a,1], Louis-Philippe Leroux[a,1], Laia Masvidal[b], Julie Lorent[b], Tyson E. Graber[c], Aude

838 Zimmermann[a], Guillermo Arango Duque[a], Albert Descoteaux[a], Tommy Alain[c,d], Ola Larsson[b], Maritza

839 Jaramillo[a,2]

840 [a]Institut National de la Recherche Scientifique (INRS) – Centre Armand-Frappier Santé Biotechnologie

841 (CAFSB), Laval, Quebec, Canada

842 [b]Department of Oncology-Pathology, Science for Life Laboratory, Karolinska Institutet, Stockholm, Sweden

843 [c]Children's Hospital of Eastern Ontario Research Institute, Ottawa, Ontario, Canada

844 [d]Department of Biochemistry, Microbiology and Immunology, University of Ottawa, Ottawa, Ontario,

845 Canada

846 [1]Equal contribution

847 [2]Correspondence should be addressed to: maritza.jaramillo@iaf.inrs.ca

848 INRS – CAFSB, 531 boul. des Prairies, Laval, Québec, H7V 1B7, Canada

849 Tel.: +1 (450) 687-5010 ext. 8872; fax: +1 (450) 686-5566

852 Short Title: Dysregulation of host mRNA translation by *L. donovani*

853 Keywords: mRNA translation, *Leishmania donovani*, macrophage, mTOR, eIF4A, TOP, polysome-profiling

854 Author Contributions

855 Conceived and designed the experiments: VC, LPL, LM, AZ, OL, MJ. Performed the experiments: VC, LPL,

856 LM AZ, GAD. Analyzed data: VC, LPL, LM, JL, TEG, AZ, TA, OL, MJ. Contributed materials, methods,

857 and/or technology: GAD, AD, TA, OL. Wrote the manuscript: VC, LPL, OL, MJ

858 **3.1   Abstract**

859 The protozoan parasite *Leishmania donovani* (*L. donovani*) causes visceral Leishmaniasis, a chronic

860 infection which is fatal when untreated. Herein, we investigated whether in addition to altering transcription,

861 *L. donovani* modulates host mRNA translation to establish a successful infection. Polysome-profiling

862 revealed that one third of protein-coding mRNAs expressed in primary mouse macrophages are

863 differentially translated upon infection with *L. donovani* promastigotes or amastigotes. Gene ontology

864 analysis identified key biological processes enriched for translationally regulated mRNAs and were

865 predicted to be either activated (i.e., chromatin remodeling and RNA metabolism) or inhibited (i.e.,

866 intracellular trafficking and antigen presentation) upon infection. Mechanistic *in silico* and biochemical

867 analyses showed selective activation mTOR- and eIF4A-dependent mRNA translation, including transcripts

868 encoding central regulators of mRNA turnover and inflammation (i.e., PABPC1, EIF2AK2, and TGF-β). *L.*

869 *donovani* survival within macrophages was favored under mTOR inhibition but was dampened by

870 pharmacological blockade of eIF4A. Overall, this study uncovers a vast yet selective reprogramming of the

871 host cell translational landscape early during *L. donovani* infection, and suggests that some of these

872 changes are involved in host defense mechanisms, while others are part of parasite-driven survival

873 strategies. Further *in vitro* and *in vivo* investigation will shed light on the contribution of mTOR- and eIF4A-

874 dependent translational programs to the outcome of visceral Leishmaniasis.

3.2   Introduction

Visceral Leishmaniasis (VL) is a vector-borne infection caused by protozoan parasites of the *Leishmania donovani* (*L. donovani*) complex. VL is endemic in more than 60 countries and is frequently lethal if untreated (Kaye and Scott 2011). The lack of efficient vaccines and the failure to control emerging parasite resistance reflect the urgent need to design safe and efficient therapeutics targeting host-encoded factors (Dayakar, Chandrasekaran et al. 2019). In mammalian hosts, *Leishmania* promastigotes preferentially colonize macrophages, where they transform into replicative amastigotes that proliferate within modified phagolysosomes (Kaye and Scott 2011). To establish a successful infection, the parasite dampens antimicrobial responses, alters vesicle trafficking, and subverts immunomodulatory functions and metabolic processes of the host cell (Podinovskaia and Descoteaux 2015).

At the molecular level, *L. donovani* modulates the activity of multiple host cell signaling pathways and transcription factors (Podinovskaia and Descoteaux 2015). Consistently, profiling of mRNA levels in *L. donovani*-infected macrophages revealed vast perturbation in host gene expression programs associated with parasite persistence (Buates and Matlashewski 2001, Chaussabel, Semnani et al. 2003, Gregory, Sladek et al. 2008, Kong, Saldarriaga et al. 2017, Shadab, Das et al. 2019). The pioneering data supporting widespread changes in host cell mRNA levels following *L. donovani* infection were obtained in bone marrow-derived macrophages (BMDMs) using cDNA-microarrays (Buates and Matlashewski 2001). This study showed that *L. donovani* axenic amastigotes downregulate expression of genes involved in apoptosis and NF-κB signaling, while stimulating those encoding monocyte chemo-attractants. Subsequently, DNA-microarray based studies of human and mouse monocyte-derived macrophages infected with *L. donovani* promastigotes identified increased levels of transcripts related to cell migration and repression of genes encoding MHC class II molecules (Chaussabel, Semnani et al. 2003, Gregory, Sladek et al. 2008). More recently, RNA sequencing (RNAseq) of mouse peritoneal macrophages infected with *L. donovani* showed a strong suppression of genes related to immune activation, signal transduction, phagosome, and endocytosis (Shadab, Das et al. 2019). Remarkably, combined analysis of RNAseq data from cells and tissues of infected hamsters provided evidence that despite a strong pro-inflammatory signature in the spleen, *L. donovani* induced a complex gene expression pattern in splenic macrophages characterized by M1- and M2-associated transcripts that skews their responses to IFN-γ, thereby rendering them more susceptible to the infection (Kong, Saldarriaga et al. 2017). Altogether, these studies support an important role of parasite-directed reprogramming of the host transcriptome in the immunopathogenesis of VL. However, discrepancies between transcriptomics and proteomics data of *L. donovani*-infected macrophages (Singh, Pandey et al. 2015) suggest that post-transcriptional and post-translational mechanisms may also modulate the host cell proteome during VL infection.

Among post-transcriptional mechanisms, transcript-selective changes in translational efficiencies enable cells to swiftly remodel their proteomes in response to environmental cues without requiring *de novo* mRNA synthesis (Piccirillo, Bjur et al. 2014, Su, Yu et al. 2015, Langlais, Cencic et al. 2018, William, Leroux et al.

911 2019). In eukaryotes, translational efficiency is mainly regulated at the initiation step when ribosomes are
912 recruited to the mRNA (Jackson, Hellen et al. 2010). This process is facilitated by the eukaryotic translation
913 initiation factor 4F (eIF4F) complex, consisting of eIF4E, the mRNA 5'-m7G-cap-binding subunit; eIF4G, a
914 scaffolding protein; and eIF4A, an RNA helicase (Jackson, Hellen et al. 2010). Activation of the mechanistic
915 target of rapamycin (mTOR) complex 1 stimulates formation of the eIF4F complex which promotes
916 translation of mRNAs that are particularly sensitive to changes in eIF4E levels and/or availability. These
917 include those containing a 5' terminal oligopyrimidine (5' TOP) motif (Meyuhas and Kahan 2015, Masvidal,
918 Hulea et al. 2017), those with highly structured 5' UTR sequences, which are largely dependent on the RNA
919 helicase activity of eIF4A for their (Sen, Zhou et al. 2016), and those with very short 5'UTRs (Gandin,
920 Masvidal et al. 2016, Masvidal, Hulea et al. 2017). Many mTOR- and eIF4A-sensitive mRNAs encode
921 proteins related to translation, cell survival, metabolism, proliferation, and growth (Chu and Pelletier 2015,
922 Gandin, Masvidal et al. 2016, Masvidal, Hulea et al. 2017). Interestingly, a number of innate immune
923 regulators are also under translational control via mTOR- or eIF4A-dependent mechanisms (Kaur, Sassano
924 et al. 2008, Cramer, Sadek et al. 2018), including several pro- and anti-inflammatory mediators in
925 macrophages (Su, Yu et al. 2015, Bhattacharya, Chatterjee et al. 2016, Langlais, Cencic et al. 2018,
926 William, Leroux et al. 2019). Thus, key immune cell functions may be hijacked by intracellular pathogens
927 via modulation of mRNA translation. Here we show that infection with promastigotes or amastigotes of *L.*
928 *donovani* leads to an early translational reprogramming in macrophages partially depending on mTOR and
929 eIF4A activity which appears to contribute to both parasite persistence and host cell defense.

930 **3.3   Results**

931 **3.3.1   *L. donovani* selectively modulates the macrophage translatome**

932 To investigate the impact of *L. donovani* infection on the host cell translatome (i.e., the pool of efficiently
933 translated mRNAs) at a transcriptome-wide level, BMDMs were incubated with *L. donovani* promastigotes
934 or amastigotes for 6 h and compared to uninfected cells using polysome-profiling quantified by RNAseq
935 (**Fig 3.1A**). Polysome-profiling determines levels of both efficiently translated mRNA and cytoplasmic
936 mRNA. Such data enables identification of bona fide changes in translation efficiencies (i.e., changes in
937 levels of polysome-associated mRNA which are not paralleled by corresponding changes in cytoplasmic
938 mRNA levels) using the anota2seq algorithm (Oertlin, Lorent et al. 2019). At a false discovery rate (FDR) ≤
939 0.15, anota2seq identified widespread mRNA-selective alterations in translational efficiencies upon
940 infection with either parasite life stage (**Fig 3.1B**). From a total of 9,442 host protein-encoding mRNAs
941 detected, 27% showed altered translational efficiency following infection with *L. donovani* amastigotes (13%
942 increased and 14% reduced) (**Fig 3.1C**, left panel; **Fig 3.1D** top panels, and **S3.1 Table**). Similarly, the
943 translational efficiency of 18% of the host cell transcripts was altered in response to *L. donovani*
944 promastigotes (9% increased and 9% decreased) (**Fig 3.1C**, right panel; **Fig 3.1D**, bottom panels, and **S3.1**
945 **Table**). Consistent with changes in translational efficiencies largely independent of parasite stage, only
946 1.5% of all mRNAs differed between host cells infected with *L. donovani* promastigotes as compared to

947 amastigotes (**S3.1 Fig** and **S3.1 Table**). In addition to detecting differences in translational efficiency
948 predicted to affect protein expression, anota2seq allows for identification of transcripts whose changes in
949 mRNA abundance are buffered at the level of translation such that their polysome-association remains
950 largely unaltered (Oertlin, Lorent et al. 2019). This is a mode for regulation of gene expression which offsets
951 the relationship between mRNA levels and protein levels to suppress changes in protein levels imposed by
952 altered transcription or mRNA stability (Lorent, Kusnadi et al. 2019). Interestingly, a large subset of
953 transcripts whose abundance changed upon infection with *L. donovani* amastigotes or promastigotes was
954 buffered at the level of translation (21% out of 1,051 and 29% out of 1,604 mRNAs, respectively) (**Fig 3.1D**
955 and **S3.1 Table**). In contrast, only a small number of transcripts (71 mRNAs) whose levels differed between
956 *L. donovani* promastigote- and amastigote-infected BMDMs (**S3.1B-C Figs**) were translationally buffered.
957 Thus, both life stages of *L. donovani* induce abundant and largely similar selective changes in translational
958 efficiency of host cell mRNAs that modulate or maintain protein levels.

959 Polysome tracings experiments indicated an increase in translation initiation rates in BMDM incubated with
960 live parasites, as evidenced by a shift in the proportion of mRNAs found in the monosomal fractions (i.e.,
961 containing mRNAs that are not translated or poorly translated) towards the heavy polysome fractions, which
962 contain mRNAs that are being efficiently translated (**S3.2A Fig**, left panel and **S3.2B Fig**). In contrast, no
963 apparent changes in polysome-to-monosome ratios were detected in BMDM incubated with heat-killed
964 parasites or latex beads (**S3.2A Fig**, middle and right panels, respectively, and **S3.2B Fig**). These data
965 provide evidence that modulation of host cell mRNA translation initiation is specific to BMDM infection with
966 live *L. donovani* parasites.

967 **3.3.2 Transcript-selective changes in translation upon *L. donovani* infection target a variety of**
968 **macrophage functions**

969 To assess how the host cell phenotype is potentially affected by mRNA-selective perturbation of translation
970 during *L. donovani* infection, we searched for enrichment of cellular functions defined by Gene Ontology
971 (GO) classifications (Mi, Huang et al. 2017) among proteins encoded by transcripts showing altered
972 translational efficiencies (**Fig 3.2A** and **S3.2 Table**). Enriched categories, among translationally activated
973 transcripts in BMDMs infected by either parasite life stage, included chromatin remodeling, regulation of
974 mRNA metabolism (i.e., splicing, export from the nucleus, stability and translation), regulation of type I IFN
975 production and protein deubiquitylation (**Fig 3.2A**, left panel; FDR ≤ 0.05). Accordingly, mRNAs encoding
976 histone modifying enzymes (i.e., *Ash1l*, *Ep300*, *Kmt2a*, *Kmt4c*), transcription factors (i.e., *Cebpb*, *Foxo4*,
977 *Ets2*, *Elk4*), translation initiation factors (i.e., *Eif3a/b/c*, *Eif4g3*), ribosomal proteins (i.e., *Rpl13a*, *Rpl38*,
978 *Rps12*), RNA-binding proteins (RBPs) (i.e., *Pabpc1*, *Eif2ak2*, *Larp1*, *Pum1*), and ubiquitin hydrolases (i.e.,
979 *Usp25*, *Fam63b*, *Usp36*) showed increased translational efficiency in *L. donovani*-infected macrophages
980 compared to uninfected controls (log$_2$ fold-change >1.0, FDR ≤ 0.15) (**Fig 3.2B**, top panels). In contrast,
981 proteins encoded by mRNAs whose translational efficiency was suppressed upon infection by either life
982 stage of *L. donovani* were enriched for categories related to protein trafficking (i.e., Rab protein signal

983 transduction, vesicle organization, and post-Golgi vesicle-mediated transport), cell metabolism (i.e.,
984 mitochondrial membrane organization, mitochondrial respiratory chain complex assembly, fatty acid beta-
985 oxidation, and peroxisomal membrane transport), protein ubiquitylation, and tRNA metabolism (**Fig 3.2A**,
986 right panel; FDR ≤ 0.05). Specifically, mRNAs translationally suppressed by promastigotes or amastigotes
987 of *L. donovani* encode proteins involved in antigen presentation (i.e., *Cd74*, *H2-Q1*), intracellular transport
988 (i.e., *Rab18*, *Sec22a*, *Vamp3*, *Vps37c*), organization of lysosome (i.e., *Bloc1s2*, *Laptm4b*), mitochondria
989 (i.e., *Cox18*, *Ndufa8*, *Timm21*, *Tomm22*), peroxisome (i.e., *Paox*, *Pex2*, *Pex7*) and Golgi apparatus (i.e.,
990 *Golga7*, *Tango2*), lipid metabolism (i.e., *Nr1h2*, *Pla2g6*, *Scp2*), protein ubiquitylation (i.e., *Trim68*, *Ube2g1*,
991 *Ube2w*), and tRNA modifications (i.e., *Trmo*, *Tsen15*, *Trmt12*) ($\log_2$ fold-change < -1.0, FDR ≤ 0.15) (**Fig
992 3.2B**, bottom panels). Interestingly, several mRNAs encoding innate immune sensors showed activated
993 translation (i.e., *Dhx9*, *Tlr9*, and *Zbtb20*), while others were translationally suppressed (i.e., *Clec7a*, *Mavs*,
994 *Tlr2*).

3.3.3 *L. donovani* infection enhances mTOR-sensitive mRNA translation in macrophages

996 We next sought to identify upstream mechanisms underlying observed changes in selective mRNA
997 translation. Activation of Akt and ribosomal protein kinase 1 (S6K1) has been reported in macrophages as
998 early as 30 min post-infection with *L. donovani* promastigotes (Cheekatla, Aggarwal et al. 2012). As altered
999 activity of the PI3K/AKT/mTOR pathway modulates mRNA translation in a selective fashion (Fonseca,
1000 Smith et al. 2014, Gandin, Masvidal et al. 2016, Masvidal, Hulea et al. 2017), we characterized the kinetics
1001 of mTOR activity upon *L. donovani* infection. To this end, we monitored the phosphorylation status of its
1002 downstream targets S6K1 and eIF4E-binding protein 1 (4E-BP1) in BMDMs. Transient phosphorylation of
1003 S6K1 at T389 was observed in BMDMs infected by either *L. donovani* promastigotes or amastigotes (**Fig
1004 3.3A**). Accordingly, phosphorylation of S6K1 substrate ribosomal protein S6 (RPS6) at S235, S236, S240,
1005 and S244 was augmented during infection (**Fig 3.3A**). In addition, early phosphorylation of 4E-BP1 at
1006 T37/46 was induced with similar kinetics by both parasite life stages (**Fig 3.3A**). To assess whether mTOR-
1007 sensitive translation was regulated in *L. donovani*-infected BMDMs, we focused on 5' TOP-containing
1008 mRNAs, whose translation is highly dependent on mTOR activity and encode for ribosomal proteins and
1009 translation initiation and elongation factors (Fonseca, Smith et al. 2014, Gandin, Masvidal et al. 2016,
1010 Masvidal, Hulea et al. 2017). Indeed, translation of previously described TOP-mRNAs (Fonseca, Smith et
1011 al. 2014) was selectively activated during infection independent of parasite stage (p < 0.001 for both stages)
1012 (**Figs 3.3B-C**, and **S3.3A Table**). Thus, PI3K/AKT/mTOR signalling and downstream mTOR-sensitive
1013 translation are activated in BMDMs early during infection by *L. donovani* amastigotes or promastigotes.

3.3.4 Translation of mRNAs encoding RNA-binding proteins PABPC1 and EIF2AK2 is activated during *L. donovani* infection in an mTOR-dependent fashion

1016 A number of studies point to a central role for RBPs in coordinating macrophage inflammatory responses
1017 and anti-microbial activity (Turner and Diaz-Munoz 2018), including poly(A)-binding protein cytoplasmic 1
1018 (PABPC1) (Zhang, Chen et al. 2017) and protein kinase dsRNA-activated (PKR, also known as EIF2AK2)

1019 (Pereira, Teixeira et al. 2010, Faria, Calegari-Silva et al. 2014). Remarkably, anota2seq detected increased
1020 translational efficiency of *Pabpc1* and *Eif2ak2* mRNAs in BMDMs infected with *L. donovani* promastigotes
1021 or amastigotes (**Fig 3.2B**, top-middle panel and **S3.1 Table**). Accordingly, expression of both proteins
1022 increased upon infection (**Fig 3.4A**) without significant changes in mRNA abundance (**Fig 3.4B**). Moreover,
1023 phosphorylation of EIF2AK2 at T451 was augmented in response to infection with either parasite stage
1024 (**S3.2 Fig**). Surprisingly, phosphorylation of eIF2α at S51, a main downstream target of EIF2AK2 (Bou-
1025 Nader, Gordon et al. 2019), decreased in *L. donovani*-infected BMDMs (**S3.3 Fig**). The *Pabpc1* mRNA was
1026 previously shown to contain a TOP-motif (Meyuhas and Kahan 2015) and, consistently, BMDM treatment
1027 with mTOR inhibitors rapamycin or torin-1 suppressed PABPC1 protein expression during *L. donovani*
1028 infection (**Fig 3.4C**) independently of mRNA levels (**Fig 3.4D**, top panel).

1029 Of note, neither host cell (William, Leroux et al. 2019) nor extracellular parasite viability (**S3.4 Fig**) were
1030 affected by mTOR inhibition. EIF2AK2 is induced by TLR stimuli such as LPS and poly (I:C) which also
1031 activate mTOR signaling (Weichhart, Hengstschlager et al. 2015, Gal-Ben-Ari, Barrera et al. 2018).
1032 Moreover, *L. donovani* activates TLR signaling (Dias, Dias-Teixeira et al. 2019). Interestingly, *L. donovani*-
1033 induced EIF2AK2 protein expression in BMDMs was reduced in presence of rapamycin or torin-1 (**Fig 3.4C**)
1034 independently of *Eif2ak2* mRNA levels (**Fig 3.4D**, bottom panel). In sum, this set of experiments indicates
1035 that *L. donovani* infection activates translation of Pabpc1 and *Eif2ak2* mRNAs to increase PABPC1 and
1036 EIF2AK2 protein levels in BMDM by stimulating mTOR activity.

1037 **3.3.5   Translation of eIF4A-sensitive mRNAs is activated upon *L. donovani* infection**

1038 The RNA helicase eIF4A facilitates translation of transcripts harboring long and highly structured 5' UTR
1039 sequences. Some such encoded proteins are involved in tumor immune evasion (Cerezo, Guemiri et al.
1040 2018) and progression of viral (Muller, Schulte et al. 2018) and protozoan parasitic infections (Langlais,
1041 Cencic et al. 2018), suggesting that eIF4A-dependent translation may contribute to herein observed
1042 changes in translational efficiencies (**Fig 3.1**). In addition to eIF4F-complex formation, the unwinding activity
1043 of eIF4A is enhanced by the translation initiation factor eIF4B (Jackson, Hellen et al. 2010). Consistent with
1044 eIF4B-dependent modulation of eIF4A activity, levels of phosphorylated and total eIF4B protein were
1045 increased in BMDMs infected with *L. donovani* amastigotes or promastigotes (**Fig 3.5A**). To test whether
1046 this may contribute to selective regulation of mRNA translation following parasite infection, we assessed
1047 translational efficiencies of a compilation of previously described eIF4A-sensitive transcripts (Rubio,
1048 Weisburd et al. 2014, Wolfe, Singh et al. 2014, Modelska, Turro et al. 2015, Cerezo, Guemiri et al. 2018).
1049 Indeed, following infection independently of parasite stage, the translational efficiencies of such mRNAs
1050 were elevated as compared to background transcripts (p < 0.001) (**Fig 3.5B**). From a total of 1198
1051 previously described eIF4A-sensitive mRNAs, 149 were translationally activated, whereas 80 were
1052 translationally suppressed upon infection with promastigotes or amastigotes of *L. donovani* (**S3.3B Table**).
1053 The presence of a 5' UTR G-quadruplex-forming guanine quartet (CGG)$_4$ motif is an indirect approach to

assess whether transcripts are expected to be more dependent of eIF4A for their translation (Waldron, Raza et al. 2018).

Indeed, analysis of Motif Enrichment (AME) revealed a significant enrichment of the (CGG)$_4$ motif in 5' UTRs of transcripts with highly activated translation (≥ 4-fold increase in translational efficiency upon infection) as compared to 5' UTRs from transcripts with unaltered translational efficiency (p = 0.0036) (**Fig 3.5C**). TGF-β is a key cytokine implicated in the distinctive immune suppression that follows *L. donovani* infection (Bhattacharya, Chatterjee et al. 2016, Asad, Sabur et al. 2019). Upon infection with *L. donovani* amastigotes or promastigotes, anota2seq analysis identified augmented translational efficiency of the tumor growth factor-β 1 (*Tgfb1*) mRNA (**Fig. 3.2B**, top-right panel and **S3.1 Table**), which is highly dependent of eIF4A for its translation (Wolfe, Singh et al. 2014). Accordingly, production of TGF-β increased in BMDMs upon infection (**Fig 3.5D**) without changes in *Tgfb1* mRNA abundance (**Fig 3.5E**). Remarkably, inhibition of eIF4A activity using silvestrol abrogated TGF-β induction in *L. donovani*-infected BMDMs (**Fig 3.5D**) without affecting *Tgfb1* mRNA levels (**Fig 3.5E**). Of note, no acute toxicity was detected in BMDMs and extracellular parasites exposed to silvestrol (**S3.5 Fig**). Thus, these data indicate that, in addition to mTOR-dependent translation, *L. donovani* infection also bolsters eIF4A-sensitive translation of selected host cell transcripts, including the one encoding the immunomodulatory cytokine TGF-β.

3.3.6 *L. donovani* survival within macrophages is differentially modulated through mTOR and eIF4A activity

During the course of infectious diseases, translational control acts as a host defense mechanism but can also be exploited by the invading pathogen as a survival strategy (Mohr and Sonenberg 2012). In regard to infections caused by protozoan parasites, augmented mTOR-sensitive translation was associated with parasite persistence during *Toxoplasma gondii* infection in macrophages (Leroux, Lorent et al. 2018), whereas eIF4A inhibition suppressed progression of cerebral malaria (Langlais, Cencic et al. 2018). These findings in combination with activation of mTOR- and eIF4A-sensitive translation in BMDMs upon parasite infection (**Fig 3.3** and **Fig 3.5**, respectively), prompted us to investigate the role of these translational regulators for *L. donovani* survival within the host cell. To address this, BMDMs were pre-treated with either rapamycin or silvestrol and infected with *L. donovani* promastigotes. Interestingly, parasite numbers increased in presence of rapamycin at 24 h post-infection (~92% increase compared to DMSO control) (**Fig 3.6A**), whereas the opposite effect was observed upon cell exposure to silvestrol (~57% reduction compared to DMSO control) (**Fig 3.6B**). These data indicate that mTOR limits *L. donovani* persistence within the host cell, while eIF4A promotes it.

3.4   Discussion

Transcriptome-wide analyses of mRNA translation in infected cells and tissues have revealed profound yet selective perturbation of the host translatome during infections caused by intracellular pathogens, including viruses and the protozoan parasite *Toxoplasma gondii* (Araki, Morita et al. 2017, Leroux, Lorent et al. 2018, Holmes, Shah et al. 2019). *L. donovani* infection causes widespread changes in host gene expression (Buates and Matlashewski 2001, Chaussabel, Semnani et al. 2003, Gregory, Sladek et al. 2008, Kong, Saldarriaga et al. 2017, Asad, Sabur et al. 2019). Yet, differences between the transcriptome and the proteome of infected cells suggested that post-transcriptional mechanisms may also contribute to establishing the post-infection proteome (Singh, Pandey et al. 2015). Herein, using polysome-profiling, we demonstrate early translational reprogramming in macrophages following infection by *L. donovani* amastigotes and promastigotes. The majority of the changes in the translatome of the host cell were induced in a similar fashion by the two life stages of the parasite, including activation of both mTOR- and eIF4A-sensitive translation programs encoding central regulators of inflammation and mRNA metabolism. Inhibition of mTOR promoted parasite survival within the host cell, whereas blockade of eIF4A activity had the opposite effect. These data suggest that some of the changes detected in host mRNA translation during *L. donovani* infection could be involved in host defense mechanisms, while others might be part of parasite-driven survival strategies.

Previous high-throughput studies identified numerous biological processes affected in macrophages during *L. donovani* infection (Chaussabel, Semnani et al. 2003, Gregory, Sladek et al. 2008, Singh, Pandey et al. 2015, Shadab, Das et al. 2019). Translational profiling of infected macrophages indicates that in addition to altered mRNA levels, *L. donovani* selectively adjusts the proteome of the host cell to its own benefit by modulating the translational efficiencies of subsets of mRNAs. In line with dysregulated antigen presentation during *L. donovani* infection (Matheoud, Moradin et al. 2013), transcripts encoding several MHC class I components were translationally suppressed in *L. donovani*-infected macrophages. In contrast, translation of mRNAs related to chromatin remodeling (i.e., histones and DNA- and histone-modifying enzymes) was augmented in cells infected with *L. donovani*. This suggests translational control of parasite-directed epigenetic changes known to inhibit innate immune responses of the host cell (Marr, MacIsaac et al. 2014). Supporting this notion, a proteomics study identified several histones and chromatin remodelling proteins induced in macrophages during *L. donovani* infection which correlated with greater transcriptional activity (Singh, Pandey et al. 2015).

Additional biological processes targeted during VL are related to host mRNA metabolism (i.e., stability, splicing and translation) (Singh, Pandey et al. 2015, Gardinassi, Garcia et al. 2016). Consistently, we identified numerous macrophage transcripts encoding translation initiation factors, splicing factors and RBPs with altered translational efficiencies during *L. donovani* infection. The mouse genome encodes more than a thousand of RBPs (Hentze, Castello et al. 2018), including a subset we identified as translationally activated upon *L. donovani* infection. Regulation of RBPs is of particular interest during VL as they play a

1124 central role during immune responses (Turner and Diaz-Munoz 2018). Further investigation is required to

1125 assess the impact of translational control of host RBP and mRNA metabolism for the outcome of *L.*

1126 *donovani* infections.

1127 Consistent with reports on early activation of PI3K/Akt and/or mTOR signaling during *L. donovani* infection

1128 in human monocyte-derived macrophages as well as human monocytic-like THP-1 and mouse macrophage

1129 RAW 264.7 cell lines (Cheekatla, Aggarwal et al. 2012, Nandan, Camargo de Oliveira et al. 2012, Zhang,

1130 Prasad et al. 2018), we observed increased phosphorylation of mTOR downstream targets in BMDM as

1131 early as 2 h and up to 8 h post-infection. Moreover, our data showing no change in the phosphorylation

1132 status of S6K1 and 4E-BP1 between 12 and 24 h post-infection are in line with a study carried out in THP-

1133 1 infected with *L. donovani* for 24 h (Thomas, Nandan et al. 2018). Thus, rapid and transient activation of

1134 the mTOR pathway appears to be a hallmark of *L. donovani* infection in mouse and human macrophages.

1135 Herein, this event was paralleled by a significant increase in translational efficiencies of a large number of

1136 mTOR-sensitive transcripts characterized by the presence of a 5' TOP motif. In particular, we found that

1137 PABPC1, an RBP whose encoding mRNA harbors a TOP-motif (Meyuhas and Kahan 2015), is induced

1138 during infection in an mTOR-dependent fashion. PABPC1 regulates stability and translation of mRNAs

1139 (Gray, Hrabalkova et al. 2015). Notably, PABPC1 is part of an inhibitory translational complex along with

1140 the zing finger protein 36 (*Zfp36*) that prevents overexpression of pro-inflammatory mediators in activated

1141 macrophages (Zhang, Chen et al. 2017). Therefore, it is plausible that PABPC1 binds to specific host

1142 mRNAs to dampen macrophage inflammatory responses during *L. donovani* infection.

1143 In addition to PABPC1, our data indicate that EIF2AK2 is upregulated in *L. donovani*-infected macrophages

1144 through mTOR-dependent mechanisms. Given that *L. donovani* triggers TLR signaling in macrophages

1145 (Dias, Dias-Teixeira et al. 2019) and that both mTOR signaling and EIF2AK2 expression are augmented in

1146 response to TLR stimulation (Weichhart, Hengstschlager et al. 2015, Yu, Wang et al. 2019), TLR-dependent

1147 mTOR activation might account for increased EIF2AK2 synthesis in *L. donovani*-infected macrophages.

1148 Accumulating evidence suggests that the role of EIF2AK2 during *Leishmania* spp. infection varies between

1149 parasite species. For example, EIF2AK2 activity is induced during *L. amazonensis* infection and promotes

1150 parasite survival within macrophages through induction of an Nrf2-dependent antioxidant response

1151 (Pereira, Teixeira et al. 2010, Weber and Henikoff 2014, Vivarini, Calegari-Silva et al. 2017). Conversely,

1152 *L. major* prevents the activation of EIF2AK2 to avoid parasite clearance via EIF2AK2-inducible TNF

1153 production (Pereira, Teixeira et al. 2010, Faria, Calegari-Silva et al. 2014). We observed that eIF2α

1154 phosphorylation decreases upon infection despite upregulation in EIF2AK2 expression and

1155 phosphorylation. This may be explained by the concomitant increase in mTOR activity which can recruit

1156 NCK1 to eIF2α and thereby reduce eIF2α phosphorylation to bolster ternary complex formation (Gandin,

1157 Masvidal et al. 2016). Thus, the relative activity of eIF2α kinases and phosphatases may determine eIF2α

1158 phosphorylation-status and thereby downstream effects on gene expression and biology. Herein,

1159 regardless of the precise mechanism, the increased level of EIF2AK2 does not appear activate the
1160 integrated stress response (Guan, van Hoef et al. 2017).

1161 Our data showing that rapamycin favors parasite survival within macrophages suggest that mTOR-
1162 activation is part of a host defense mechanism against *L. donovani*. These observations are in agreement
1163 with a report in which macrophage exposure to rapamycin enhanced intracellular survival of another
1164 *Leishmania* sp. (i.e., *L. major*) (Jaramillo, Gomez et al. 2011). In contrast, rapamycin treatment has been
1165 shown to prevent parasite replication within macrophages infected with various *Leishmania* spp. (Khadir,
1166 Shaler et al. 2018, Khadir, Taheri et al. 2019), including *L. donovani* (Thomas, Nandan et al. 2018).
1167 However, this apparent discrepancy might stem from the fact that much higher concentrations of rapamycin
1168 (IC50 ≥ 8μM) were used in the studies reporting a leishmanicidal effect for this compound (i.e., at least 400-
1169 fold difference).

1170 Early phosphorylation of eIF4B and enrichment of reported eIF4A-sensitive mRNAs among translationally
1171 activated transcripts support that eIF4A also affects the translatome of *L. donovani*-infected macrophages.
1172 The activity of eIF4A facilitates translation of transcripts encoding immune modulators (i.e., CXCL10, IRF1,
1173 IRF7, iNOS, STAT3, TGF-β, etc.) in various cell types (Di Marco, Cammas et al. 2012, Wolfe, Singh et al.
1174 2014, Modelska, Turro et al. 2015, Gandin, Masvidal et al. 2016, Cramer, Sadek et al. 2018) including
1175 macrophages (Bhattacharya, Chatterjee et al. 2016, Langlais, Cencic et al. 2018). Similarly, we observed
1176 that translation of eIF4A-sensitive transcript *Tgfb* and subsequent TGF-β production were upregulated in
1177 *L. donovani*-infected in macrophages. TGF-β is a cytokine associated with immune suppression and
1178 resistance to treatment during human and experimental VL (Bhattacharya, Chatterjee et al. 2016, Asad,
1179 Sabur et al. 2019). In view of these previous studies and our present findings, it is conceivable that eIF4A-
1180 sensitive translation contributes to the immuno-pathogenesis of *L. donovani* infection. Further
1181 characterization of eIF4A translational outputs in *L. donovani* infected cells and tissues will shed light on
1182 this matter.

1183 We observed that silvestrol-mediated inhibition of eIF4A dampened *L. donovani* survival within
1184 macrophages. Interestingly, eIF4A inhibitors have been shown to act as dual-targeting therapeutic agents
1185 by interfering with both pathogen and host eIF4A activity during malaria, an infection caused by protozoan
1186 parasites of the genus *Plasmodium* (Langlais, Cencic et al. 2018). Of note, a strain of *L. donovani* resistant
1187 to miltefosine had increased levels of eIF4A (Singh, Chavan et al. 2008) and high-throughput screenings
1188 identified *Leishmania* eIF4A as a potential druggable target (Abdelkrim, Harigua-Souiai et al. 2018, Harigua-
1189 Souiai, Abdelkrim et al. 2018, Capelli-Peixoto, Mule et al. 2019, Naineni, Itoua Maiga et al. 2020).
1190 Collectively, our data along with previous studies warrant further investigation on the potential of targeting
1191 eIF4A-dependent host and parasite mRNA translation to treat *L. donovani* infections.

1192 The outcome of VL is defined by a complex network of converging molecular events at the interface
1193 between the parasite and the host (Kaye and Scott 2011). Herein, we have uncovered vast reprogrammed
1194 translation of protein-coding mRNAs expressed in macrophages upon infection by *L. donovani* amastigotes

1195   or promastigotes. Accordingly, numerous host transcripts critical during infection, including regulators of

1196   mRNA metabolism and inflammation, were found to be under translational control. Notably, our data

1197   indicate that some of these changes contribute to parasite clearance, whereas others favor parasite

1198   persistence within the host cell, hinting at the therapeutic potential of perturbing specific host translation

1199   programs to control the infection.

1200

1201

3.5   Materials and Methods

3.5.1   Reagents

Culture media and supplements were purchased from Wisent, Gibco, and Sigma-Aldrich; rapamycin was obtained from LC Laboratories; torin-1 was provided by Cayman; 10-phenanthroline monohydrate was acquired from Sigma-Aldrich; silvestrol was purchased from Biovision.

3.5.2   Parasites

L. donovani (LV9 strain) amastigotes were isolated from the spleen of infected female Golden Syrian hamsters (Harlan Laboratories) as previously described (Matte and Descoteaux 2010). *L. donovani* (LV9 strain) promastigotes were differentiated from freshly isolated amastigotes and were cultured at 26°C in M199 medium supplemented with 10% heat-inactivated FBS, 100 µM hypoxanthine, 5 µM hemin, 3 µM biopterin, 1 µM biotin, 100 U/mL penicillin, and 100 µg/mL streptomycin. Early passage stationary phase promastigotes were used for macrophage infections.

3.5.3   Ethics Statement

Housing and experiments were carried out under protocols approved by the Comité Institutionnel de Protection des Animaux (CIPA) of the INRS – Centre Armand-Frappier Santé Biotechnologie (CIPA 1308-04 and 1710-02). These protocols respect procedures on good animal practice provided by the Canadian Council on animal care.

3.5.4   Differentiation of bone marrow-derived macrophages

Bone marrow-derived macrophages (BMDM) were generated from precursor cells from murine bone marrow, as previously described (Leroux, Lorent et al. 2018). Briefly, marrow was extracted from bones of the hind legs, red blood cells were lysed, and progenitor cells were resuspended in BMDM culture medium supplemented with 15% L929 fibroblast-conditioned culture medium (LCCM). Non-adherent cells were collected the following day and were cultured for 7 days in BMDM culture medium supplemented with 30% LCCM with fresh medium replenishment at day 3 of incubation.

3.5.5   Infection of bone marrow-derived macrophages

BMDM cultures were inoculated with *L. donovani* promastigotes or amastigotes at a multiplicity of infection (MOI) of 10:1, as previously described (Atayde, da Silva Lira Filho et al. 2019). Prior to infection, cells were serum-starved for 2 h and treated with inhibitors, when applicable.

3.5.6   Viability assays

Viability of BMDM and extracellular *L. donovani* parasites was determined by the resazurin assay as described (William, Leroux et al. 2019). Briefly, cells were treated with increasing concentrations of rapamycin (2.5 – 160 nM), torin-1 (12.5 – 800 nM), silvestrol (0.8 – 100 nM) or an equivalent volume of

42

1234 DMSO (vehicle) for 24 h at 37°C, 5% CO2. Medium was removed and replaced with fresh culture medium

1235 supplemented with 0.025% resazurin. Cultures were incubated for 4 h in presence of the inhibitors or DMSO

1236 at 37°C, 5% CO2. Optical density was measured using a Multiskan GO (Thermo-Fisher) at 600 and 570

1237 nm. Absorbance at 600 nm was subtracted from readings at 570 nm. Experiments were performed in

1238 biological replicates (n =2); each sample was analyzed in a technical triplicate, the average of which was

1239 plotted against increasing concentrations of the respective inhibitor.

1240 **3.5.7   Quantification of intracellular parasites**

1241 BMDM cultures were treated with 20 nM rapamycin, 25 nM silvestrol or an equivalent volume of DMSO

1242 (vehicle) for 2 h, then inoculated with *L. donovani* parasites (MOI 10:1) for 6 and 24 h. Relative quantification

1243 of intracellular parasites was performed by RT-qPCR measuring the expression of *Leishmania* kmp11 gene

1244 as described (Zangger, Ronet et al. 2013). Primer sequences are listed in **S3.4 Table**. Primer efficiency

1245 was calculated using ThermoFisher's online qPCR Efficiency Calculator software (**S3.6 Figure**).

1246 **3.5.8   Quantitative RT-PCR**

1247 Purified RNA (500 ng) was reverse transcribed using the Superscript IV VILO Master Mix (Invitrogen).

1248 Quantitative PCR was performed with PowerUp™ SYBR® Green Master Mix (Applied Biosystems).

1249 Relative quantification was calculated using the comparative Ct method (ΔΔCt) (Taylor, Wakem et al. 2010)

1250 and relative expression was normalized to mouse *Actb*. Experiments were performed in independent

1251 biological replicates (n=3); each sample was analyzed in a technical triplicate, the average of which was

1252 plotted against the respective conditions used. Primers were designed using NCBI Primer-BLAST

1253 (http://www.ncbi.nlm.nih.gov/tools/primer-blast/) (**S3.4 Table**).

1254 **3.5.9   Western blot analysis**

1255 Following infection and other treatments, total cell lysates were prepared for SDS-PAGE and Western

1256 blotting as described (Chaparro, Leroux et al. 2019). Primary antibodies anti-mTOR (#2983), anti-phospho-

1257 S6K1 (T389; #9234), anti-phospho-RPS6 (S235/236; #2211), anti-phospho-RPS6 (S240/244; #5364), anti-

1258 phospho-eIF4B (S422, #3591), anti-eIF4B (#3591), anti-phospho-4E-BP1 (T37/46; #2855), anti-4E-BP1

1259 (#9644), anti-phospho-eIF2α (S51; #3398), anti-eIF2α (#2103), anti-PABCP1 (#4992), and β-actin (#3700)

1260 were purchased from Cell Signaling Technologies; anti-phospho-PKR (EIF2AK2) (T451; #07-886) was

1261 obtained from Millipore; anti-RPS6 (#sc-74459), anti-S6K1 (#sc-230), and anti-PKR (EIF2AK2) (#sc-6282)

1262 were acquired from Santa Cruz Biotechnology. Horseradish peroxidase (HRP)-linked goat anti-rabbit and

1263 goat anti-mouse IgG secondary antibodies were purchased from Sigma-Aldrich.

1264 **3.5.10   RNA fractionation and purification from polysome fractions**

1265 Cytosolic lysates of infected and control BMDM were prepared for RNA fractionation as described (Leroux,

1266 Lorent et al. 2018). Lysates were layered over 5 to 50% sucrose density gradients and sedimented using a

1267 Beckman SW41 rotor at 36,000 rpm (= 221,830.9 × g) for 2 h at 4°C. Gradients were fractionated and

1268 collected (30 s, 500 μL/fraction), and the absorbance at 254 nm was recorded continuously using a Brandel
1269 BR-188 density gradient fractionation system. Input material (total cytoplasmic mRNA) and efficiently
1270 translated mRNA (heavy polysome-associated, > 3 ribosomes) were extracted with QIAzol (Qiagen) and
1271 purified using RNeasy MinElute Cleanup Kit (Qiagen). Purity and integrity of RNA was assessed using a
1272 Bioanalyzer 2100 with a Eukaryote Total RNA Nano chip (Agilent Technologies).

1273 **3.5.11   RNAseq data processing**

1274 RNAseq libraries were generated using the Smart-seq2 method (Ramskold, Wang et al. 2009) to enable
1275 polysome-profiling of small samples as described previously (Liang, Bellato et al. 2018). Libraries were
1276 sequenced by using an Illumina HiSeq2500 instrument with a single-end 51-base sequencing setup for
1277 both total cytoplasmic and polysome-associated mRNAs (mRNAs associated with > 3 ribosomes) from
1278 three independent biological replicates for uninfected and *L. donovani* promastigote-infected BMDM, and
1279 five independent biological replicates for *L. donovani* amastigote-infected BMDM. First, RNAseq reads
1280 mapping to the reference genome of the Nepalese BPK282A1 strain of *L. donovani* were removed (12.7%
1281 and 1.4% mappings on average for promastigotes and amastigotes, respectively). The filtered reads were
1282 then aligned to the mouse genome mm10. HISAT2 was used for all alignments with default settings (Kim,
1283 Langmead et al. 2015). Gene expression was quantified using the RPKMforgenes.py script
1284 (http://sandberg.cmb.ki.se/media/data/rnaseq/rpkmforgenes.py) (Ramskold, Wang et al. 2009) with options
1285 -fulltranscript -readcount -onlycoding from which raw per gene RNAseq counts were obtained (version last
1286 modified 07.02.2014). Genes that had zero counts in all samples were discarded. Annotation of genes was
1287 obtained from RefSeq.

1288 **3.5.12   RNAseq data analysis using anota2seq**

1289 RNAseq counts were normalized within anota2seq using default TMM-log2 normalization (Oertlin, Lorent
1290 et al. 2019). Significant changes in translation, abundance and buffering were identified by anota2seq
1291 (Oertlin, Lorent et al. 2019) using default parameters with the following modifications:
1292 minSlopeTranslation=-0.5; maxSlopeTranslation=1.5; FDR ≤ 0.15; apvEff > $\log_2(2.0)$; deltaPT > $\log_2(1.25)$;
1293 and deltaP > $\log_2(1.5)$. In anota2seq model one, infections were compared to control (i.e., Ld PRO versus
1294 control and Ld AMA versus control); in model two, cells infected by different parasite stages were compared
1295 together with a contrast to complete the anota2seq model (i.e., Ld PRO vs Ld AMA and Ld PRO versus
1296 control). Identifiers for genes which cannot be distinguished based on their high sequence similarity (also
1297 reported by RPKMforgenes.py), were excluded from downstream analyses. For further analysis, we used
1298 a published list of TOP-containing mRNAs (Fonseca, Smith et al. 2014) and previously reported
1299 translational signatures of eIF4A-sensitive mRNAs (Rubio, Weisburd et al. 2014, Wolfe, Singh et al. 2014,
1300 Modelska, Turro et al. 2015, Cerezo, Guemiri et al. 2018). The difference in $\log_2$ fold-change of translational
1301 efficiency (i.e., apvEff) between the signatures and the background was assessed using Wilcoxon-Mann-
1302 Whitney tests.

1303 **3.5.13 Gene ontology analyses**

1304 Gene ontology analyses were performed using the panther tool (Mi, Huang et al. 2017) of the Gene
1305 Ontology Consortium (http://geneontology.org/) on the union of transcripts activated or inhibited in BMDMs
1306 infected by *L. donovani* amastigotes or promastigotes. Heatmaps of translational efficiencies of transcripts
1307 activated or inhibited in BMDMs infected by *L. donovani* amastigotes or promastigotes were generated
1308 using Morpheus.

1309 (https://software.broadinstitute.org/morpheus/index.html, Broad Institute)

1310 **3.5.14 RNA sequence motif analyses**

1311 Non-redundant RefSeq 5' UTRs were retrieved from genome build mm10 using the UCSC Table Browser
1312 (https://genome.ucsc.edu/cgi-bin/hgTables). Analysis of Motif Enrichment (AME) was performed on the
1313 RefSeq-annotated 5' UTR sequences from transcripts with ≥ 4-fold increases in TE in *L. donovani*-infected
1314 BMDM (402 5' UTRs) compared to a control list of 228 randomly selected 5' UTRs from the set of non-
1315 translationally regulated transcripts. The presence of the previously described guanine quartet $(CGG)_4$ motif
1316 (Wolfe, Singh et al. 2014) in both lists was scored and a one-tailed Fisher's exact test was performed to
1317 determine significance of enrichment.

1318 **3.5.15 Statistical Analysis**

1319 Where applicable, data are presented as the mean ± standard deviation (SD) of the mean. Statistical
1320 significance was determined by using one-way ANOVA followed by a Tukey post-hoc test; calculations
1321 were performed by using Prism 7 software package (GraphPad). Differences were considered significant
1322 when $*p < 0.05$, $** p < 0.01$, $*** p < 0.001$.

1323 **3.6   Acknowledgements**

1326

1327

1328

1329

1330

1331

1332

1333

1334 **3.7 Figures**

1335

1336
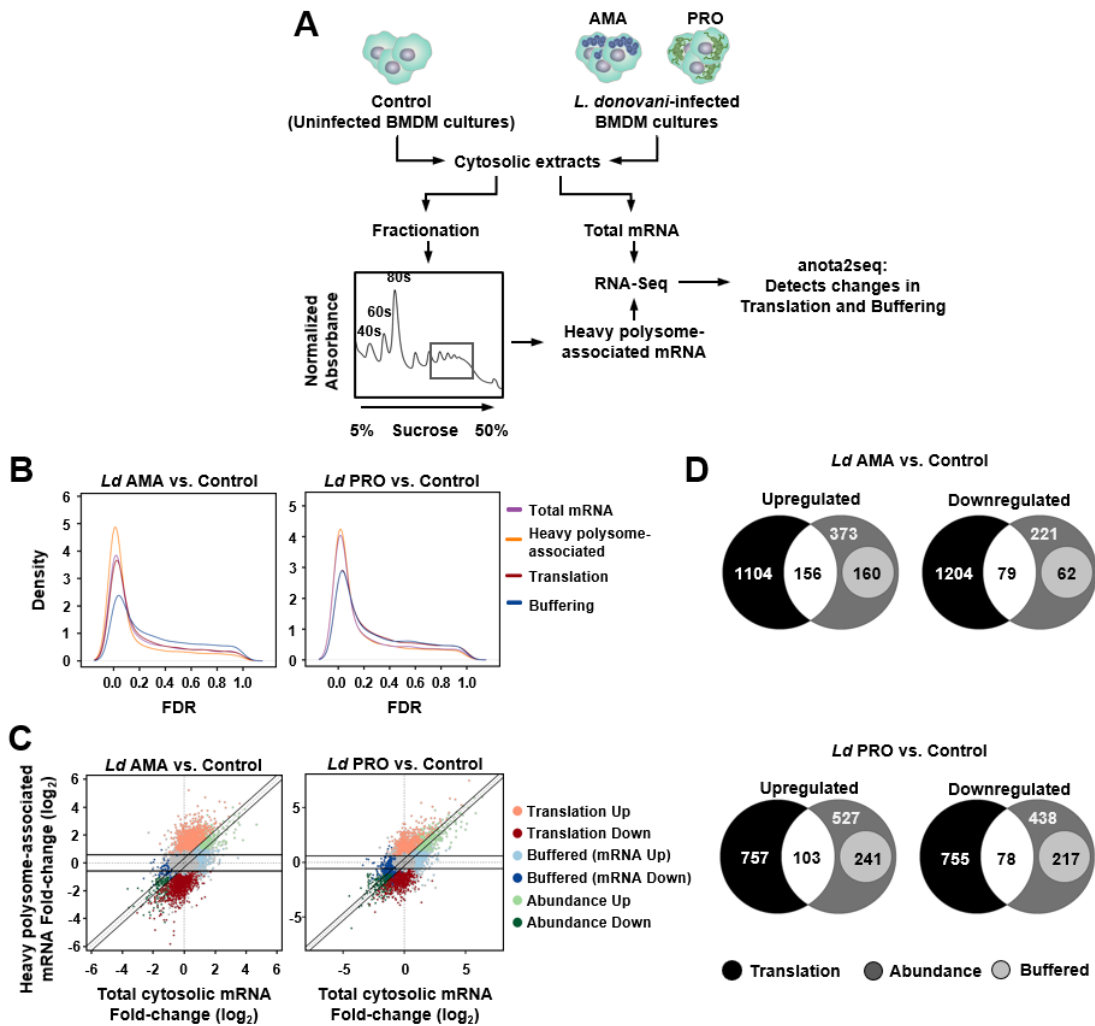
1337 **Figure 3.1.** ***L. donovani*** **infection causes widespread changes in mRNA translation in macrophages. (A)** Strategy to

1338 characterize the translatome of *L. donovani*-infected BMDMs. **(B)** Kernel densities of adjusted p values (FDRs) following anota2seq

1339 analysis of changes in total mRNA, heavy polysome-associated mRNA, translation (i.e., changes in polysome-associated mRNA not

1340 paralleled by changes in total mRNA) and translational buffering (i.e., changes in total mRNA buffered at the level of translation) for

1341 BMDMs infected with *L. donovani* amastigotes (*Ld* AMA) or promastigotes (*Ld* PRO) compared to uninfected cells (Control). **(C)**

1342 Scatter plots of $\log_2$ fold changes (for the same comparisons as in panel B) for heavy polysome-associated mRNA and total cytosolic

1343 mRNA. Differentially regulated transcripts through translation, abundance or buffering are indicated. Unchanged mRNAs are shown

1344 in grey. **(D)** Venn diagrams showing the number of mRNAs up- or down-regulated at the level of translation, abundance, and buffering

1345 for BMDMs infected with *Ld* AMA or *Ld* PRO compared to Control. **(B-D)** Data analyses were performed on samples generated from

1346 at least three biological replicates.
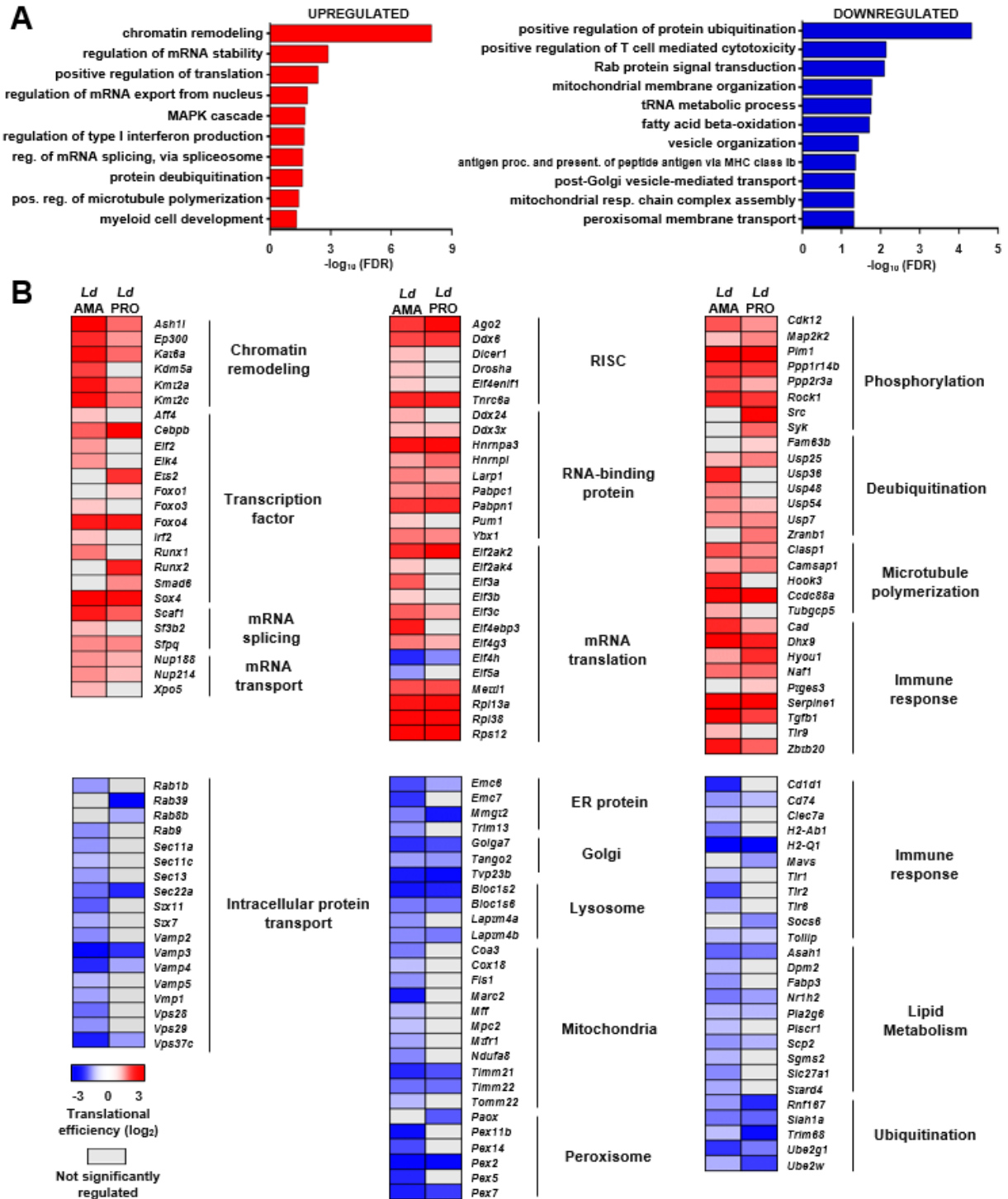
Figure 3.2. *L. donovani* infection-dependent translation targets core and immune cell functions. (A) FDR values (-log$_{10}$) for selected GO term enriched categories for translationally up- and down-regulated host mRNAs upon *L. donovani* infection. **(B)** Heatmaps showing changes in translational efficiencies for selected genes in enriched GO terms. Analyses were carried out on data generated from at least three biological replicates.
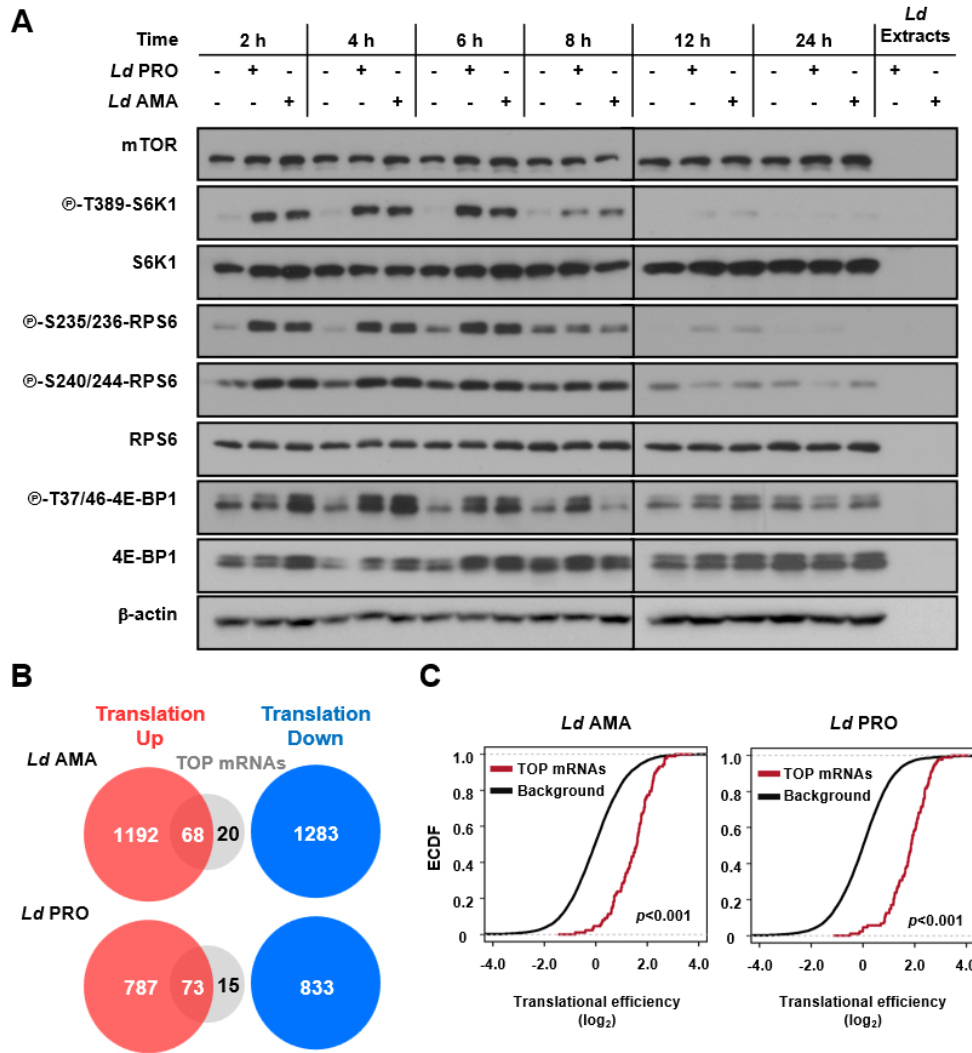
Figure 3.3. mTOR-sensitive host mRNA translation is activated during _L. donovani_ infection. (A) BMDM cultures were inoculated with either _Ld_ AMA or _Ld_ PRO or left uninfected for the indicated times. Phosphorylation and expression levels of indicated proteins were monitored by Western blotting. Total amounts of _β-actin_ were used as a loading control. Total protein extracts from _Ld_ cultures were used to control for any cross-reactivity of the antibodies against parasite antigens. **(B)** Venn diagrams indicating the numbers of transcripts harboring a TOP-motif among translationally activated vs. suppressed transcripts following Ld AMA or Ld PRO infection as compared to control BMDMs. **(C)** Empirical cumulative distribution function (ECDF) of translational efficiencies for TOP mRNAs as compared to those of all detected transcripts (background). Differences in translational efficiencies between transcripts with TOP-motifs vs control transcripts were assessed per parasite stage. **(A)** Results are representative of at least three independent experiments. **(B-C)** Data analyses were performed on samples generated from at least three biological replicates.

1363
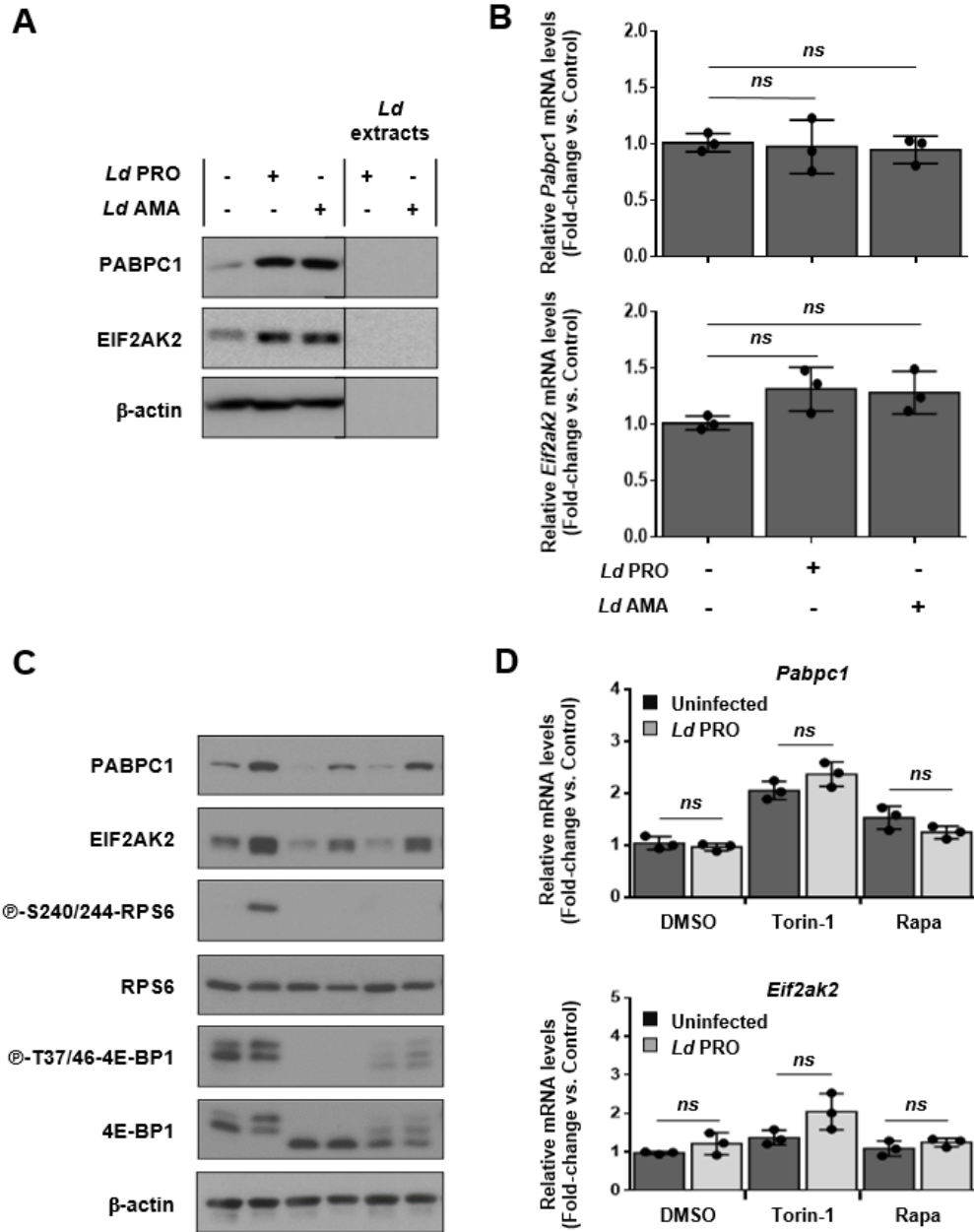
Figure 3.4. Upregulation of PABPC1 and EIF2AK2 in macrophages infected with *L. donovani* is mTOR-dependent. **(A-B)** BMDM cultures were inoculated with *Ld* AMA, *Ld* PRO or left uninfected for 6 h. **(C-D)** Cells were pre-treated with 200 nM of torin-1, 20 nM rapamycin (Rapa) or DMSO for 2 hours before infection. **(A, C)** Total levels of PABPC1 and EIF2AK2 were monitored by Western blotting. **(C)** Phosphorylation status of mTOR downstream targets RPS6 and 4E-BP1. **(B, D)** Relative mRNA amounts of *Pabpc1* and *Eif2ak2* (normalized to *Actb*) were measured by RT-qPCR. **(A, C)** Results are representative of three independent experiments. **(B, D)** Data are presented as mean ± SD (biological replicates, n=3). **p < 0.01, ***p < 0.001 (for the indicated comparisons), ns = non-significant. Protein extracts for Western blot analyses **(A and C)** originate from one of the three biological replicates employed to isolate RNA samples for RT-qPCR experiments **(B and D, respectively)**.
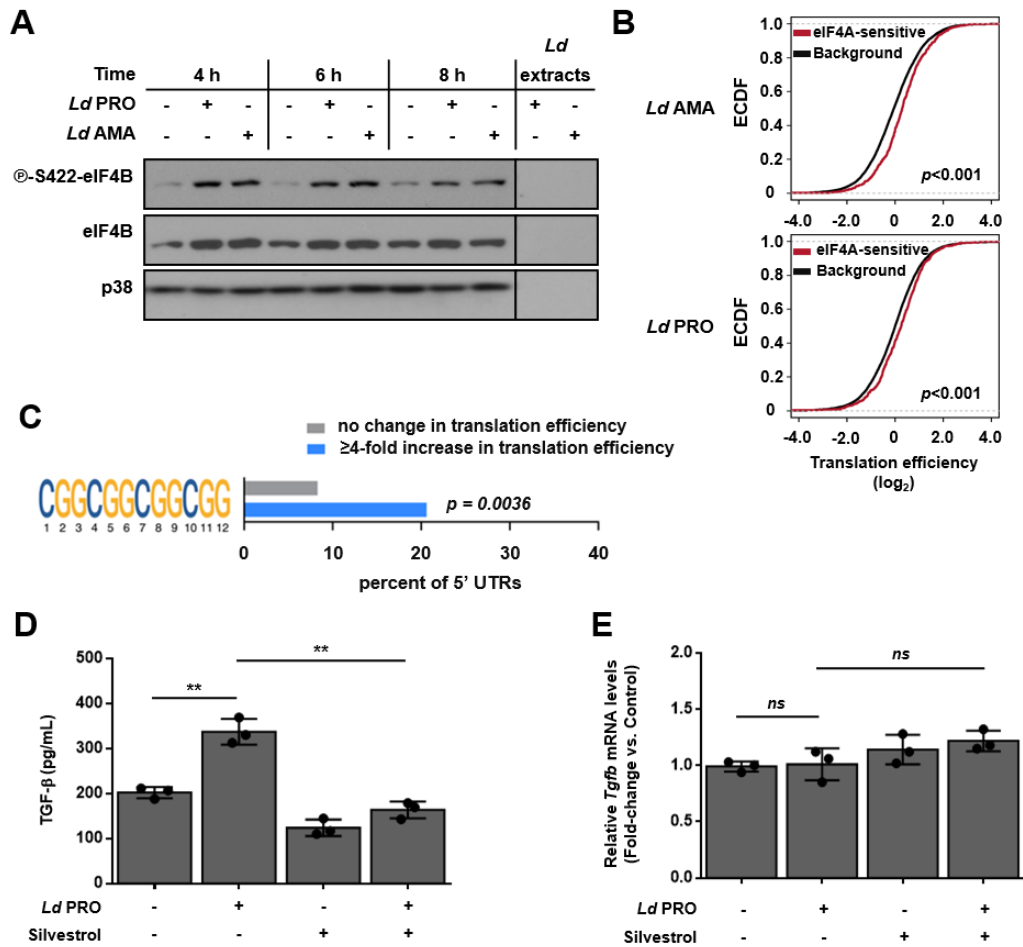
Figure 3.5. *L. donovani* **infection activates eIF4A-sensitive mRNA translation in macrophages. (A)** BMDM cultures were inoculated with *Ld* AMA, *Ld* PRO or left uninfected for the indicated times. Phosphorylation status and expression levels of eIF4B were monitored by Western blotting. Total levels of p38 MAPK were used as a loading control. **(B)** Empirical cumulative distribution function (ECDF) of translational efficiencies (infection vs. control) for the compilation of previously reported eIF4A-sensitive transcripts as compared to those of all detected transcripts (background). Differences in translational efficiencies between eIF4A-sensitive vs control transcripts were assessed per parasite stage. **(C)** Percentages of infection-associated translationally activated mRNAs (≥ 4-fold increase) with at least one $(CGG)_4$ motif in their 5' UTR as compared to a random set of unchanged mRNAs. Fisher's exact test was used to compare frequencies of the $(CGG)_4$ motif between the transcript subsets and the resulting p-value is indicated. **(D-E)** BMDM cultures were pre-treated with 25 nM silvestrol or vehicle for 2 h, then were inoculated with Ld PRO or left uninfected for 6 h. **(D)** Secreted levels of TGF-β were measured by sandwich ELISA. **(E)** Relative amount of *Tgfb1* mRNA (normalized to *Actb*) was measured by RT-qPCR. **(A)** Results are representative of three independent experiments. **(B-C)** Data analyses were performed on samples generated from at least three biological replicates. **(D-E)** Data are presented as mean ± SD (biological replicates, n=3). *p < 0.05, **p < 0.01 (for the indicated comparisons), ns = non-significant. Cell culture supernatants for ELISA experiments **(D)** originate from one of the three biological replicates employed to isolate RNA samples for RT-qPCR analyses **(E)**.

50
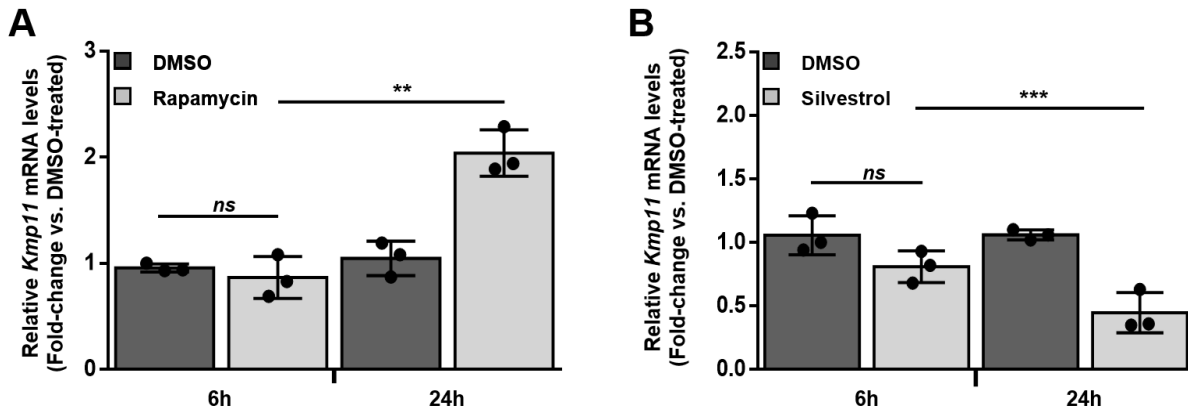
Figure 3.6. Host mTOR and eIF4A differentially regulate *L. donovani* persistence within macrophages. BMDM cultures were treated with **(A)** 20 nM rapamycin, **(B)** 25 nM silvestrol or an equivalent volume of DMSO (vehicle) for 2 h, then inoculated with *L. donovani* parasites (MOI 10) for 6 and 24 h. Quantification of intracellular parasites was performed by measuring the relative amount of *Leishmania Kmp11* mRNA (normalized to *Actb*) by RT-qPCR. Data are presented as mean ± SD (biological replicates, n=3). **p < 0.01, ***p < 0.001 (for the indicated comparisons), ns = non-significant.

3.8 Supplementary Information
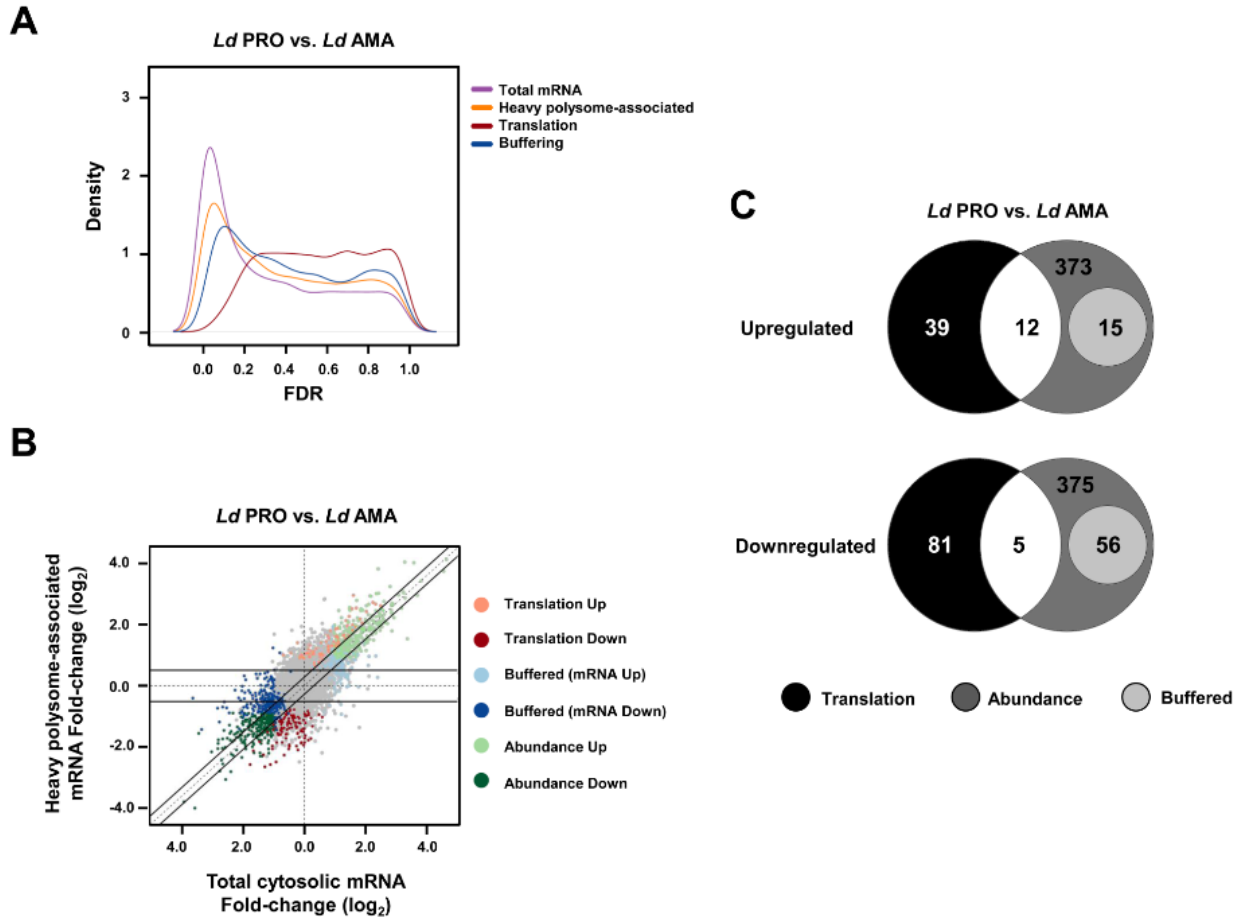
Supplementary Figure 3.1. Differential regulation of host mRNA translation between *L. donovani* promastigotes and
amastigotes. (A) Kernel densities of adjusted p values (FDRs) following anota2seq analysis on changes in total mRNA, heavy
polysome-associated mRNA, translational efficiency, and translational buffering comparing *Ld* PRO to *Ld* AMA-infected BMDM (n ≥
3). **(B)** Scatter plot of $\log_2$ fold changes (for the same comparisons as in panel A) for heavy polysome-associated mRNA and total
cytosolic mRNA. Differentially regulated transcripts through translation, abundance or buffering are indicated. Unchanged mRNAs are
shown in grey (n ≥ 3) **(C)** Venn diagrams indicating the number of mRNAs up- or down-regulated at the level of translation, abundance,
and buffering for *Ld* PRO-infected BMDM compared to *Ld* AMA-infected BMDM.

1421
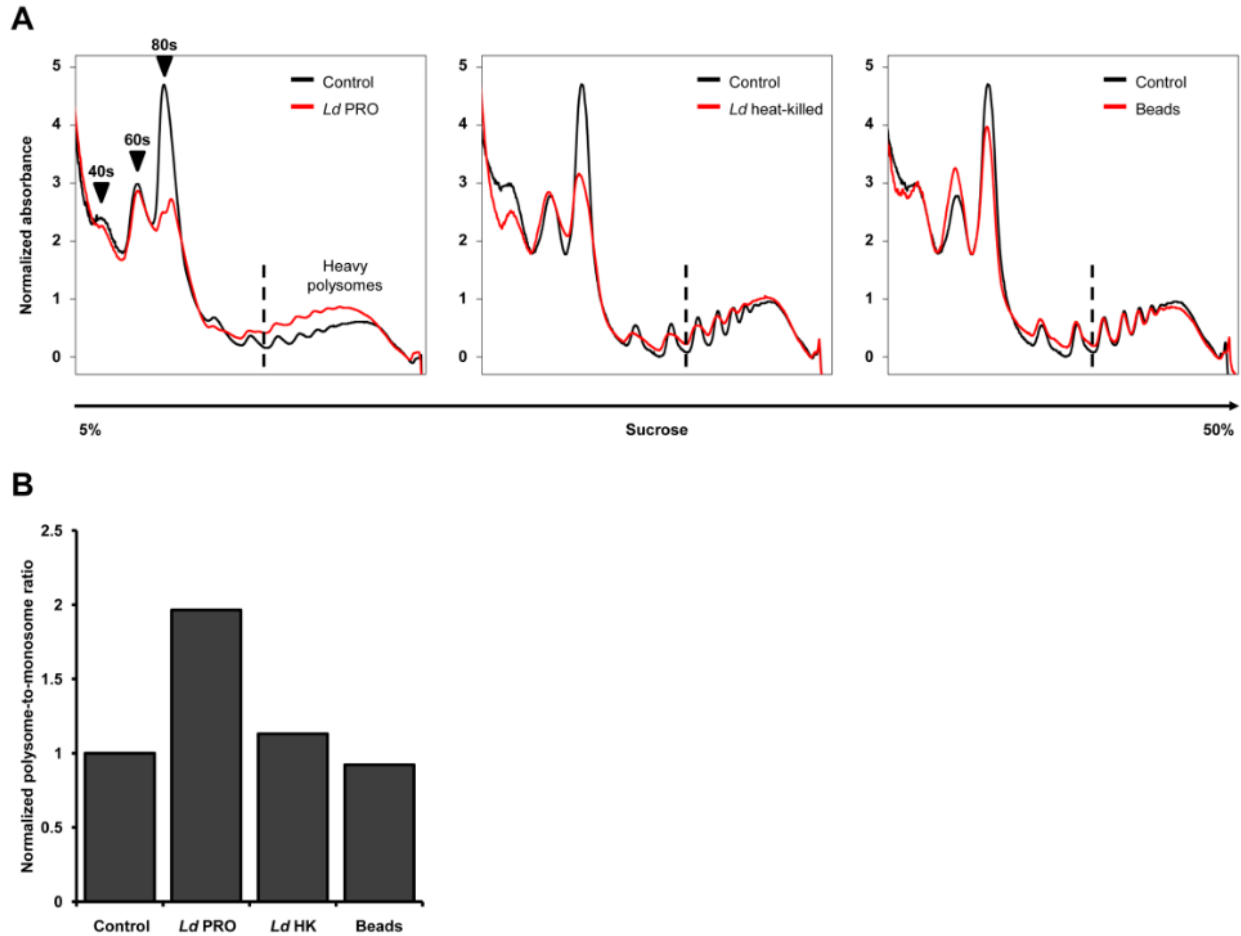
Supplementary Figure 3.2. Polysome tracings of BMDM infected with live or heat-killed *L. donovani* promastigotes or treated with latex beads. (A) BMDM cultures were inoculated with 10:1 live *L. donovani* promastigotes (*Ld* PRO) or heat-killed *Ld* PRO (*Ld* HK), latex beads, or left untreated (control) for 6 h. Cell lysates were sedimented on 5 to 50% sucrose gradients. Gradients were fractionated, and the absorbance at 254 nm was recorded continuously. Absorbance values were normalized. Arrows indicate the 40S and 60S ribosomal subunits and 80S (monosomes). The heavy polysome regions were identified as fractions containing mRNA associated with > 3 ribosomes (i.e., efficiently translated mRNAs). **(B)** The area under the curve of the monosome and heavy polysome regions was calculated, and the heavy polysome-to-monosome ratios were then normalized to values for control BMDM cultures. Data are representative of three independent experiments.

	Ld extracts	
Ld PRO	- + -	+ -
Ld AMA	- - +	- +

Ⓟ-T451-EIF2AK2

EIF2AK2

Ⓟ-S51-eIF2α

eIF2α

β-actin
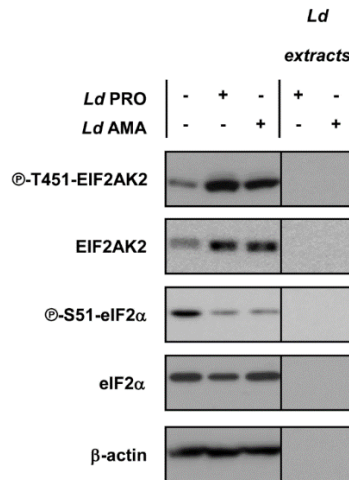
1433

1434 **Supplementary Figure 3.3. *L. donovani* infection promotes EIF2AK2 but not eIF2α phosphorylation.** BMDM cultures were

1435 inoculated with *Ld* AMA, *Ld* PRO or left uninfected for 6 h. Phosphorylation and expression levels of EIF2AK2 and eIF2α were

1436 monitored by Western blotting. Total amounts of β-actin were used as a loading control. Total protein extracts from *Ld* cultures were

1437 used to control for any cross-reactivity of the antibodies against parasite antigens. Data are representative of three independent

1438 experiments.

1439

1440

1441
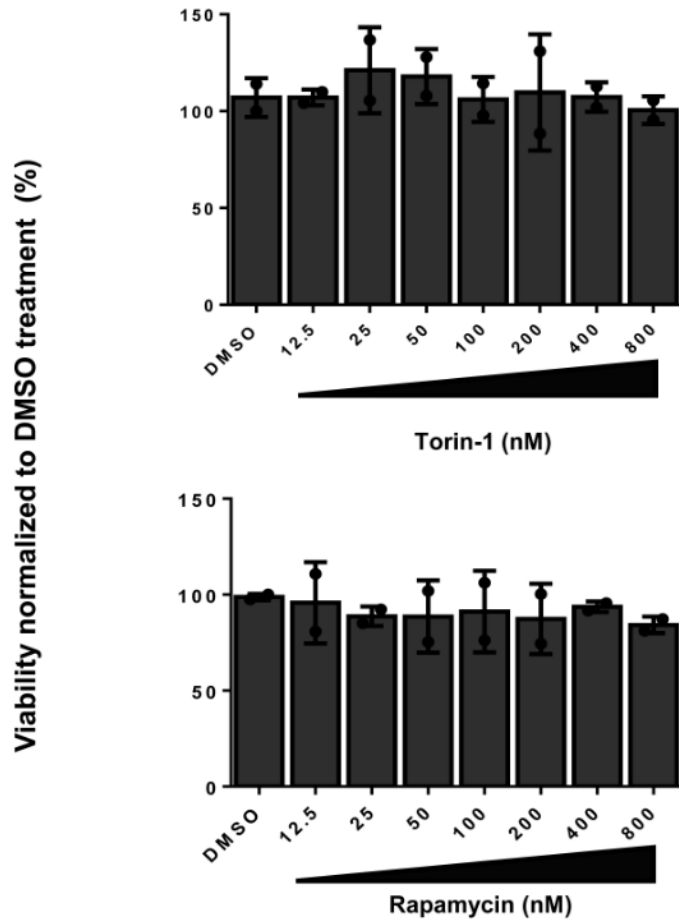
1442

Supplementary Figure 3.4. Measurement of acute toxicity of mTOR inhibitors on extracellular *L. donovani* promastigotes. *L. donovani* cultures were treated with increasing concentrations of rapamycin (2.5 – 160 nM), torin-1 (12.5 – 800 nM) or an equivalent volume of DMSO (vehicle) for 24 h. Acute toxicity of the inhibitors was measured by resazurin assays. Percent viability was normalized to DMSO-treated parasites. Data are representative of two independent experiments performed in technical triplicates.

1447

1448

1449

1450

1451

A

B
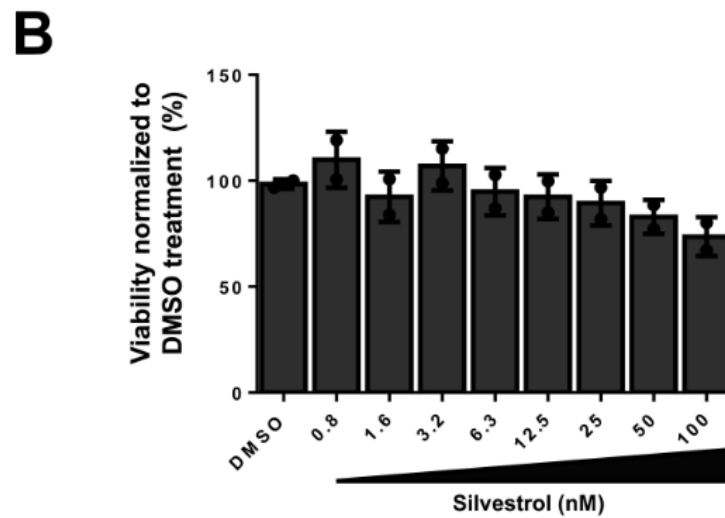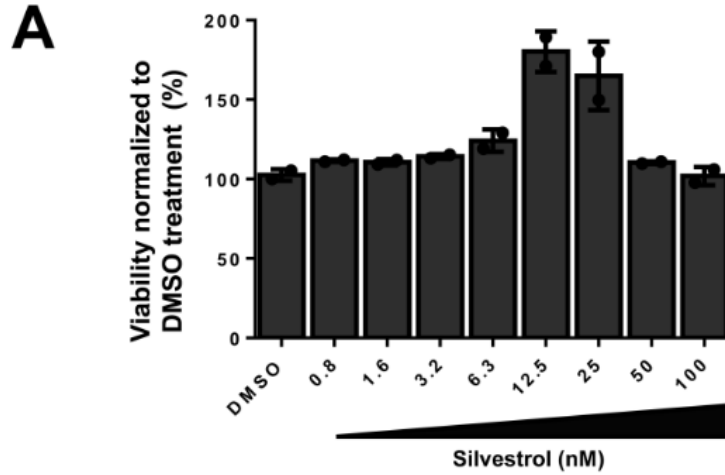
1452

Supplementary Figure 3.5. Measurement of acute toxicity of silvestrol on BMDMs and *L. donovani* promastigotes. (A) BMDM

and **(B)** *L. donovani* cultures were treated with increasing concentrations of silvestrol (0.8 – 100 nM) or an equivalent volume of DMSO

(vehicle) for 24 h. Acute toxicity of the inhibitor was measured by resazurin assays. Percent viability was normalized to DMSO-treated

parasites. Data are representative of two independent experiments performed in technical triplicates.

1453

1454

1455

1456

1457

1458

1459
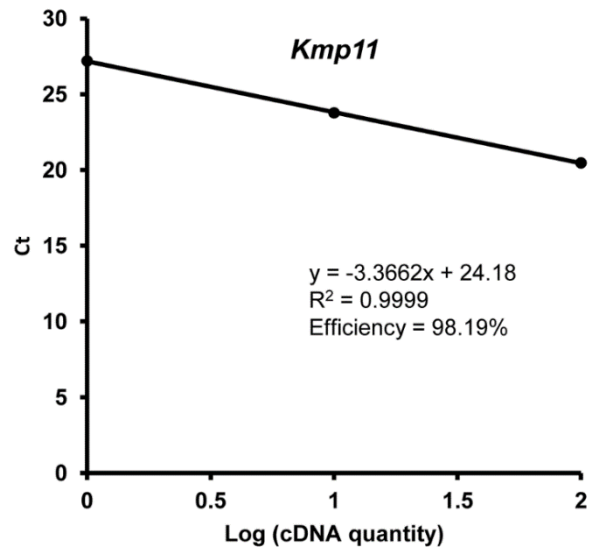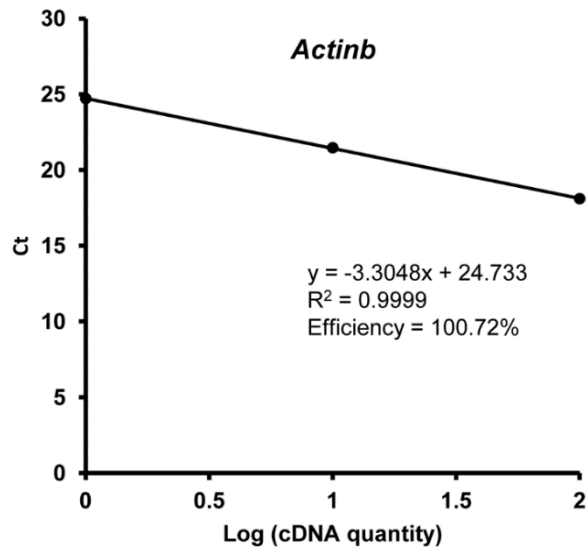
1460

1461 **Supplementary Figure 3.6. Primer efficiency for RT-qPCR analysis.** The efficiency of the primers used to amplify mouse *Actinb*

1462 and *Leishmania Kmp11* genes was verified by measuring Ct values along a serial dilution of cDNA (plotted as Log[cDNA amount]).

1463 Efficiency was calculated using ThermoFisher's online qPCR Efficiency Calculator software.

1464

1465

1466

1467

1468

1469

1470

1471

1472

1473

1474

1475

1476

1477

1478

1479

1480

1481 **CHAPTER 4**

1482 **Publication No. 2**

1483

1484

1485

1486 **Transcriptional profiling of macrophages reveals distinct parasite stage-driven**

1487 **signatures during early infection by *Leishmania donovani***

1488 Visnu Chaparro[a], Tyson E. Graber[b], Tommy Alain[b,c], Maritza Jaramillo[a,1]

1489 [a]Institut National de la Recherche Scientifique (INRS) – Centre Armand-Frappier Santé Biotechnologie

1490 (AFSB), Laval, Quebec, Canada

1491 [b]Children's Hospital of Eastern Ontario Research Institute, Ottawa, Ontario, Canada

1492 [c]Department of Biochemistry, Microbiology and Immunology, University of Ottawa, Ottawa, Ontario,

1493 Canada

1494 [1]Correspondence should be addressed to: maritza.jaramillo@inrs.ca

1495 INRS – Centre AFSB, 531 boul. des Prairies, Laval, Québec, H7V 1B7, Canada

1496 Tel.: +1 (450) 687-5010 ext. 8872; fax: +1 (450) 686-5566

1500 Conceived and designed the experiments: VC, MJ. Performed the experiments: VC. Analyzed data: VC,

1501 TG. Contributed materials, methods, and/or technology: TA. Wrote the manuscript: VC, TG, TA, MJ

1502

1503 **4.1   Abstract**

1504 Macrophages undergo swift changes in mRNA abundance upon pathogen invasion. Herein we describe

1505 early remodelling of the macrophage transcriptome during infection by amastigotes or promastigotes of

1506 *Leishmania donovani*. Approximately 10% - 16% of host mRNAs were differentially modulated in *L.*

1507 *donovani*-infected macrophages when compared to uninfected controls. This response was partially stage-

1508 specific as a third of changes in mRNA abundance were either exclusively driven by one of the parasite

1509 forms or significantly different between them. Gene ontology analyses identified categories associated with

1510 immune functions (i.e., antigen presentation and leukocyte activation) among significantly downregulated

1511 mRNAs during amastigote infection, while cytoprotective-related categories (i.e., DNA repair and apoptosis

1512 inhibition) were enriched in upregulated transcripts. Interestingly a combination of upregulated (i.e., cellular

1513 response to IFNβ) and repressed (i.e., leukocyte activation, chemotaxis) immune-related transcripts were

1514 overrepresented in the promastigote-infected dataset. In addition, INGENUITY PATHWAY ANALYSIS

1515 (IPA) associated specific mRNA subsets with a number of upstream transcriptional regulators predicted to

1516 be modulated in macrophages infected with *L. donovani* amastigotes (i.e., STAT1 inhibition) or

1517 promastigotes (i.e., NRF2, IRF3, and IRF7 activation). Overall, our results indicate that early parasite stage-

1518 driven transcriptional remodelling in macrophages contributes to orchestrate both protective and

1519 deleterious host cell responses during *L. donovani* infection.

1520

4.2 **Introduction**

1522 Macrophages are the main replicative niche of protozoan parasites of the genus *Leishmania*, the etiologic

1523 agents of a spectrum of vector-borne diseases known as *Leishmania*ses (Podinovskaia and Descoteaux

1524 2015). Within macrophages, sandfly-transmitted *Leishmania* promastigotes transform into amastigotes

1525 while subverting numerous host cell processes and immunological functions to ensure their proliferation

1526 (Podinovskaia and Descoteaux 2015). Visceral Leishmaniasis (VL) is a life-threatening disease that is

1527 caused by *L. donovani* and *L. infantum* (syn. *L. chagasi*) (Khadem and Uzonna 2014). VL is endemic in

1528 more than 60 countries where it represents a severe public health concern due to the lack of vaccines and

1529 the emergence of parasite drug resistance (Burza, Croft et al. 2018). Hence, a better understanding of the

1530 molecular events occurring at the host cell–parasite interface is critical to identify novel regulatory nodes

1531 for therapeutic intervention.

1532 Transcriptomic studies of macrophages infected with promastigotes of different *Leishmania* spp. (*L. major*,

1533 *L. amazonensis*, *L. chagasi*) indicate that the most distinctive changes occur in early stages after parasite

1534 internalization (i.e., 1-12 hours pos infection) (Rodriguez, Chang et al. 2004, Rabhi, Rabhi et al. 2012,

1535 Dillon, Suresh et al. 2015, Fernandes, Dillon et al. 2016). Even though *L. donovani* promastigotes elicit the

1536 activation of anti-parasitic intracellular signals in macrophages as early as 15 min post-infection (Junghae

1537 and Raynes 2002), they are able to dampen host cell responses involved in pathogen clearance within 6 h

1538 (i.e., phagolysosome maturation, antigen presentation, oxidative burst, and apoptosis) (Holm, Tejle et al.

1539 2001, Matheoud, Moradin et al. 2013, Giri, Srivastav et al. 2016, Saha, Basu et al. 2019). Consistent with

1540 this, rapid modulation of multiple transcription factors (i.e., STAT1, NRF2, IRF3 and IRF7) has been

1541 associated with either parasite persistence or host cell defense mechanisms against *L. donovani* (Matte

1542 and Descoteaux 2010, Phillips, Svensson et al. 2010, Saha, Basu et al. 2019, Saha, Roy et al. 2021). The

1543 first host cell gene expression profiles were performed in human and mouse primary macrophages infected

1544 with *L. donovani* amastigotes (Buates and Matlashewski 2001) or promastigotes (Chaussabel, Semnani et

1545 al. 2003, Gregory, Sladek et al. 2008) for 16 h to 96 h using DNA microarrays. However, this technique has

1546 several limitations (i.e., hybridization issues, limited probe availability, lower detection of splice junctions

1547 and rare or novel transcripts, etc.) (Rai, Tycksen et al. 2018). Subsequent transcriptional signatures of

1548 macrophages infected with *L. donovani* promastigotes were defined using RNAseq (Morimoto, Uchida et

1549 al. 2019, Shadab, Das et al. 2019), which outperforms earlier technologies by allowing transcriptome-wide

1550 direct sequencing (Rai, Tycksen et al. 2018). Two recent RNAseq-based studies carried out in murine

1551 macrophages infected with *L. donovani* promastigotes reported rapid changes in abundance of transcripts

1552 associated with host cell lipid and glutamine metabolic activity (6 h post-infection) (Ferreira, Mesquita et al.

1553 2020, Mesquita, Ferreira et al. 2020). Intriguingly, the global transcriptional response of macrophages to

1554 early infection was not analyzed in depth (Ferreira, Mesquita et al. 2020, Mesquita, Ferreira et al. 2020).

1555 In all, currently available datasets may not reflect the totality of changes in gene expression programs that

1556 trigger, or are elicited by, early macrophage responses during *L. donovani* infection. Of note, to the best of

1557   our knowledge, no high throughput comparative study of early transcriptional changes in macrophages

1558   driven by both stages of *L. donovani* is available to date. Herein, using RNAseq datasets from mouse

1559   primary macrophages infected with *L. donovani* amastigotes and promastigotes for 6 h, we describe broad

1560   yet selective changes in the transcriptome of the host cell that are likely to tailor key early cellular responses

1561   involved in host defense but also in disease progression during VL.

1562

4.3 Results

4.3.1 Infection with *L. donovani* amastigotes or promastigotes promotes early changes in the mRNA pool of the host cell

To compare the early effects of the two life stages *L. donovani* in the mature mRNA pool of the host cell, total cytosolic mRNA extracts from bone marrow-derived macrophage (BMDM) cultures infected with amastigote (AMA) or promastigote (PRO) parasites for 6 h were subjected to RNAseq and compared to non-infected controls (CTR) (**Fig 4.1A**). As shown by a projection of a principal component analysis, infection appears to be the main source of variation (PC1=37.4%) between the different datasets followed by a distinctive distribution of AMA samples along the second component (PC2 = 27.2%) (**Fig 4.1B**). Differentially regulated mRNAs were identified using the ANOTA2SEQ algorithm with a false discovery rate (FDR) ≤ 0.05 and a $\log_2$ expression fold-change ≥ 1.0. Out of 9442 mRNAs detected in BMDMs, 9.9% showed differential abundance during *L. donovani* amastigote infection (65.6% upregulated and 34.4% downregulated) (**Fig 4.1C** left panel and **Table S4.1**), while 15.8% were altered in BMDMs following infection with the promastigote stage (54.4% upregulated and 45.6% downregulated) (**Fig 4.1C** right panel and **Table S4.1**). These data indicate that infection by either amastigotes or promastigotes of *L. donovani* leads to early reprograming of the mRNA content of the host cell.

4.3.2 Early transcriptional changes in macrophages infected with *L. donovani* amastigotes are associated with the inhibition of cell death and immune functions

Gene Ontology (GO) hierarchical clustering analysis was carried out to determine whether subsets of mRNAs encoding functionally related proteins are selectively modulated in BMDMs upon infection with *L. donovani* amastigotes (**Fig 4.2A** and **Table S4.2**). Enrichment of functional categories related to regulation of gene expression, positive regulation of DNA repair, and negative regulation of apoptosis and protein modification was detected in the AMA-upregulated dataset (**Fig 4.2A** upper panel, and **Table S4.2**). Targets in these categories included transcripts that encode transcription (*Bdp1*, *Gtf3c6*, *Polr3f*, *Polr3g*), splicing (*Hnrnpa3*, *Hnrnpu*, *Sf3a2*, *Srsf1*) and translation (*Dhx29*, *Eif1a*, *Eif3a*, *Eif4g2*) factors, proteins involved in DNA repair (*Lig4*, *Mdc1*, *Nbn*, *Smc6*, *Topbp1*), and inhibitors of apoptosis (*Hdac2*, *Hsph1*, *Mdm2*) including *Bcl2* which was highly upregulated by both parasite stages (**Fig 4.2B**). In contrast, categories associated with immune response, cell adhesion, signal transduction, protein refolding, and cell cycle were enriched in the AMA-downregulated dataset (**Fig 4.2A** bottom panel and **Table S4.2**). Accordingly, lower levels of transcripts encoding innate and adaptive immune mediators (*Aif1*, *C1rb*, *Ccl5*, *Ifitm3*, *Il18bp*, *Irf7*, *Ly86*, *Lyz1*, *Nfil3*, *Ptger3*, *Tnfrsf14*), regulators of antigen presentation (*Cd74*, *H2-Aa*, *H2-Ab1*, *H2-Eb1*, *Unc93b1*), and adhesion molecules (*Icam1*, *Itgal*, *Itgb7*, *Rac2*) were detected in BMDMs infected with *L. donovani* amastigotes (**Fig 4.2B**). Thus, macrophages undergo widespread changes in the abundance of mRNA subsets associated with downregulation of immune cell functions and upregulation of host cell survival and RNA metabolism upon *L. donovani* amastigote infection.

4.3.3   Early transcriptional changes in macrophages infected with *L. donovani* promastigotes are indicative of both activation and inhibition of host defense responses

Enriched GO categories in upregulated transcripts of *L. donovani* promastigote-infected macrophages revealed contrasting groups of activating (i.e., *Cxcl10*, *Cxcl3*, *Gbp3*, *Ifit1*, *Ifit2*, *Irgm1*, *Tnf*) and inhibitory immune factors (*Cd200*, *Cd24a*, *Cd274*, *Cebpb*, *Nlrc5*, *Serpinb9*, *Socs1*) (**Fig 4.3A** upper panel, **Fig 4.3B** and **Table S4.2**). In parallel, mRNAs encoding proteins associated with cell survival (*Hmox1*, *Hsp90ab1*, *Optn*, *Wfs1*), iron transport (*Slc11a2*, *Slc25a37*, *Slc39a14*, *Slc40a1*) and redox homeostasis (*Cat*, *Gclm*, *Gsr*, *Prdx1*, *Sod2*, *Txnrd1*) were also overrepresented in the upregulated dataset (**Fig 4.3A** upper panel, **Fig 4.3B** and **Table S4.2**). In line with previous observations(Rabhi, Rabhi et al. 2012, Rabhi, Rabhi et al. 2016), an increase in the abundance of a group of transcripts associated with lipid metabolism was detected in the PRO data set (*Cd36*, *Lrp12*, *Lpl*, *Acsl1*, *Fabp4*) (**Table S4.1**).   In contrast, GO categories related to cell death (*Casp2*, *Casp6*, *Cradd*, *Dfna5*, *Dusp6*, *Mef2c*, *Rassf2*, *Sarm1*) and immune functions such as leukocyte activation (*Clec4a2*, *Dock8*, *Gpr183*, *Hdac5*, *Ifngr1*, *Notch1*), chemotaxis (*Ccr2*, *Cx3cr1*, *Cxcl14*, *Cxcr3*), and antigen presentation (*Fcgr3*, *H2-DMa*, *H2-DMb1*, *H2-DMb2*) were enriched in mRNAs with reduced abundance during infection by *L. donovani* promastigotes (**Fig 4.3A** lower panel, **Fig 4.3B** and **Table S4.2**). These data indicate that *L. donovani* promastigote infection elicits a transcriptome-wide response in macrophages that results in the upregulation of lipid metabolism, the concomitant expression of activating and inhibitory immune mediators, and the inhibition of cell death and antigen presentation.

4.3.4   Parasite stage-specific modulation of the host cell transcriptome during *L. donovani* infection

ANOTA2SEQ identified a subset of mRNAs (n=649) differentially regulated in the PRO- versus AMA-infected datasets (52.2% upregulated and 47.8% downregulated) (**Fig 4.4A** and **Table S4.1**). Comparison of this subset of transcripts with the AMA versus CTRL and PRO versus CTRL contrasts shown in **Fig. 4.1C** (**Table S4.1**) revealed a complex pattern of regulation with targets exhibiting a stage-exclusive (i.e., PRO only, AMA only), stage-enhanced (i.e., PRO enhanced, AMA enhanced) and stage-opposite (i.e., UP by PRO and DOWN by AMA, DOWN by PRO and UP by AMA) effects (**Fig 4.4B**, **Fig 4.5A** and **Table S4.1**). In the upregulated PRO versus AMA dataset (n=339), ANOTA2SEQ classified 70% of the transcripts as PRO only UP, 17% as AMA only DOWN, and 11% as PRO enhanced UP (i.e., UP by PRO and AMA but with a stronger effect in PRO) (**Fig 4.4B** and **Table S4.1**). In the downregulated PRO versus AMA dataset (n=310), ANOTA2SEQ classified 69% of the transcripts as PRO only DOWN, 23% as AMA only UP, and 6% as PRO enhanced DOWN (i.e., DOWN by PRO and AMA but with a stronger effect in PRO) (**Fig 4.4B** and **Table S4.1**). In addition, 7 transcripts showed an enhanced effect by amastigotes (i.e., AMA enhanced, 3 UP and 4 DOWN) (**Fig 4.4B**, **Fig 4.5A**, right panel, and **Table S4.1**), whereas 7 transcripts were oppositely regulated between both stages, including 3 that were classified as PRO UP and AMA

1633 DOWN (*Acss2*, *Slc16a3*, *Slpi*), and 4 as PRO DOWN and AMA UP (*Bcr*, *Fcrls*, *Gcnt1*, *Id1*) (**Fig 4.4B**, **Fig**

1634 **4.5A**, right panel, and **Table S4.1**).

1635 Hierarchical clustering of transcripts identified as exclusively regulated upon amastigote infection (i.e., AMA

1636 only) revealed an enrichment of GO categories among upregulated transcripts encoding proteins

1637 associated with Immune signaling (*Cad*, *Ccl2*, *Wnk1*), DNA repair (*Mcm2*, *Nucks1*, *Pds5v*, *Rif1*, *Smc2*),

1638 Transcription (*Etv1*, *Etv5*, *Myc*, *Rbl1*, *Sox4*), and Cell adhesion (*Icam1*, *Slfn1*) (**Fig 4.5A**, left panel, and

1639 **Table S4.2**), while downregulated targets exhibited an enrichment of GO categories associated with

1640 Immune response (*Ccl5*, *Cd14*, *H2-Aa*, *H2-Ab1*, *H2-Eb1*, *Il18bp*, *Irf7*, *Ly6c1*, *Ly6c2*, *Nfil3*) and Redox

1641 balance (*Folr1*, *Mgst1*, *Ppard*) (**Fig 4.5A**, left panel, and **Table S4.2**). The same type of analysis in the

1642 dataset of exclusively upregulated mRNAs upon promastigote infection (i.e., PRO only UP) identified GO

1643 categories related to Apoptosis regulation (i.e., *Bnip3*, *Cd274*, *Gclm*), Hydrogen peroxide metabolism (*Cat*,

1644 *Prdx1*, *Prdx6*, *Txnrd1*), Response to protozoan (*Cd40*, *Gbp2*, *Gbp3*, *Slc11a1*), and Response to type I IFN

1645 (I*fit1*, *Ifit2*, *Igtp*, *Irgm1*, *Mnda*) (**Fig 4.5A**, middle panel, and **Table S4.2**). By contrast, transcripts exclusively

1646 downregulated by promastigotes (i.e., PRO only DOWN) were enriched in GO categories linked to Cell

1647 activation (*Ajuba*, *Gpr183*, *Hdac5*, *Tcf4*), Chemotaxis (*Arap3*, *Dab2*, *Dock1*, *Itga6*) and Cell signaling

1648 (*Btbd11*, *Nfatc2*, *Pak1*, *Pram1*) (**Fig 4.5A**, middle panel, and **Table S4.2**). The PRO enhanced UP subset

1649 showed an overrepresentation of apoptosis inhibitors (*Bcl2a1d*, *Gbe1*, *Gclc*, *Hmox1*, *Il1rn*, *Plk2*, *Serpinb9*)

1650 (**Fig 4.5A**, right panel, and **Table S4.2**). Consistent with this, the activation of a transcriptional regulatory

1651 network leading to the inhibition of cell death was identified by INGENUITY PATHWAY ANALYSIS (IPA) in

1652 the PRO upregulated subset (**Fig S4.1**). Unlike the PRO enhanced transcripts, no GO categories were

1653 enriched in the AMA enhanced subset (**Fig 4.5A**, right panel). Changes in expression levels of three

1654 different transcripts regulated during infection by *L. donovani* amastigotes (*Ccl5*), promastigotes (*Cd274*)

1655 or both (*Hmox1*) was confirmed by RT-qPCR experiments (**Fig 4.5B**). Altogether, these results indicate that

1656 early infection by amastigotes or promastigotes of *L. donovani* elicits a selective and stage-specific

1657 transcriptional signature in macrophages involving mRNAs related to key cellular functions in disease

1658 progression.

1659 **4.3.5   Changes in host mRNA abundance upon *L. donovani* infection are associated with a**

1660 **network of upstream transcriptional regulators in macrophages**

1661 In order to identify potential upstream regulatory networks responsible for the changes in mRNA levels

1662 observed in BMDMs infected by the two life stages of *L. donovani*, we used IPA. With an activation score

1663 |Z| ≥ 2.0 and an FDR ≤ 0.01, IPA identified subsets of transcripts with a regulatory trend predicted to be

1664 dependent on the activation or inhibition of different transcriptional modulators in BMDMs infected with *L.*

1665 *donovani* amastigotes or promastigotes (**Table S4.3**). Some upstream regulators were common between

1666 both parasite stages (MYC, KLF4, and SMAD3) albeit with variations in the number and/or identity of

1667 downstream targets in each type of infection (**Fig 4.6A** left panel and **Table S4.3**). Others were predicted

1668 to be activated only by amastigotes (YY1, WDR5, and TP73) or promastigotes (NFE2L2, IRF7, IRF3,

1669   EPAS1, SPI1, NFATC2, ATF4, IFI16, CEBPB, CREB1, SP1, FOXO1, and FOS) (**Fig 4.6A** left panel and

1670   **Table S3**). As expected, transcriptional regulators predicted to be activated upon *L. donovani* infection

1671   showed high percentages of associated upregulated mRNAs (**Fig 4.6B**). In agreement with predicted

1672   induction of NFE2L2 (a.k.a. NRF2)-dependent transcriptional programs in BMDMs infected with *L. donovani*

1673   promastigotes (i.e., 63 genes) (**Fig 4.6B** right panel, **Fig S4.2A** and **Table S4.3**), NRF2-mediated Oxidative

1674   Stress Response was identified by IPA as one of the top networks to be activated by the promastigote

1675   stage (**Fig S4.2B**). In addition, a small group of transcription factors was predicted to be inhibited only upon

1676   infection with amastigotes (SOX6, RUNX3, and STAT1) or promastigotes (TRIM24, SIRT1, and FOXP3)

1677   (**Fig 4.6A** right panel and **Table S4.3**). Of note, SIRT1 was predicted to be activated in the amastigote-

1678   infected dataset (**Fig 4.6A** left panel and **Table S4.3**), whereas the opposite was observed during infection

1679   with the promastigote stage (**Fig 4.6A** right panel and **Table S4.3**), as previously reported(Moreira,

1680   Rodrigues et al. 2015). These data hint at the involvement of a complex regulatory network affecting the

1681   abundance of functional subsets of mRNAs in BMDMs infected with *L. donovani* amastigotes or

1682   promastigotes.

1683

4.4   Discussion

Early remodelling of the macrophage transcriptome has been reported to be pathogen-specific during bacterial and parasitic infections (Chaussabel, Semnani et al. 2003, Goldmann, von Kockritz-Blickwede et al. 2007, Bhatt, Pandya-Jones et al. 2012, Li, Shah-Simpson et al. 2016, Rabhi, Rabhi et al. 2016). Transcriptome-wide analyses of macrophages infected with *L. donovani* have mainly been described at ≥ 12 h post-infection (Gregory, Sladek et al. 2008, Espitia, Saldarriaga et al. 2014, Kong, Saldarriaga et al. 2017, Medina-Colorado, Osorio et al. 2017, Morimoto, Uchida et al. 2019, Shadab, Das et al. 2019), thereby omitting an earlier timeframe during which numerous molecular and cellular changes occurring within infected macrophages (Junghae and Raynes 2002, Forestier, Machu et al. 2011, Matheoud, Moradin et al. 2013, Giri, Srivastav et al. 2016) could trigger, or be elicited by, selective reprogramming of the host transcriptome. Herein, using RNAseq, we describe rapid changes in the levels of mRNAs of primary murine macrophages infected with *L. donovani* amastigotes and promastigotes. Distinct transcriptional signatures were identified in macrophages infected with each parasite stage. A marked inhibition of mRNAs encoding proteins related to different immune functions was found in the amastigote-infected dataset, whereas a combination of activating and inhibitory immune modulators was observed in promastigote-infected macrophages. Additionally, our *in silico* analyses identified host mRNA signatures in the up- and downregulated datasets that appear to be under the control of parasite-stage driven networks of transcription factors. These observations indicate that amastigotes and promastigotes of *L. donovani* elicit a complex transcriptome-wide reprogramming in infected macrophages that includes both parasite stage-specific and commonly regulated mRNA subsets.

L. donovani amastigote-driven changes in macrophage gene expression have been documented at ≥ 24 h post-infection (Gregory, Sladek et al. 2008, Kong, Saldarriaga et al. 2017, Smirlis, Dingli et al. 2020). Herein, we provide evidence that *L. donovani* amastigote infection leads to a vast remodelling of the macrophage transcriptome as early as 6 h post-infection. Among the downregulated targets, we found an enrichment in mRNAs encoding proteins related to several macrophage immune functions. IPA predicted that some of these changes are dependent on the inhibition of transcription factor STAT1. In this regard, Matte and Descoteaux previously reported that *L. donovani* amastigotes prevent STAT1 nuclear import and pro-inflammatory gene expression (i.e., *Nos2* and *Irf1*) in BMDMs stimulated with IFNγ (Matte and Descoteaux 2010). In addition, a transcriptomic study carried out in splenic macrophages revealed that these cells become insensitive to IFNγ during experimental VL despite a strong pro-inflammatory environment in the spleen (Kong, Saldarriaga et al. 2017). Hence, it is plausible that early blockade of STAT1-dependent transcriptional programs in macrophages infected by *L. donovani* amastigotes has a negative effect in IFNγ-mediated microbicidal and immune host responses at later stages of the disease. Further investigation is required to shed light on this matter.

Infection of macrophages results in an oxidative burst response that involves the production of potent microbicidal effectors such as reactive oxygen and nitrogen species (Rendra, Riabov et al. 2019). However,

67

1720   the antimicrobial oxidative stress response can also compromise macrophage DNA integrity and lead to

1721   the activation of apoptotic signals (Slupphaug, Kavli et al. 2003). Our GO analyses showed an enrichment

1722   in mRNAs encoding DNA repair enzymes and inhibitors of apoptosis in the upregulated dataset of *L.*

1723   *donovani* amastigote-infected BMDMs at 6 h post-infection. Similarly, a proteome-based analysis of human

1724   macrophages infected with *L. donovani* identified DNA repair as an enriched ontology category reaching

1725   maximal values at 24 h post-infection (Singh, Pandey et al. 2015). Moreover, among *L. donovani*

1726   promastigote- and amastigote-upregulated transcripts, we detected *Nbn*, which encodes a key member of

1727   the MRE11 DNA-damage-sensing complex (Pereira-Lopes, Tur et al. 2015). Interestingly, *Nbn* is also

1728   induced in macrophages upon LPS-induced oxidative damage and serves as a modulator of macrophage

1729   homeostasis preventing attrition (Lopez-Sanz, Bernal et al. 2018). These reports along with our RNAseq

1730   data indicate *L. donovani* amastigotes elicit a cytoprotective transcriptional program to prevent oxidative-

1731   driven macrophage apoptosis at early stages of infection. Future studies are necessary to fully understand

1732   the molecular underpinnings of parasite-driven activation of the host DNA repair machinery and its role in

1733   the establishment and progression of *L. donovani* infection within macrophages.

1734   *Leishmania* parasites inhibit macrophage oxidative burst in order to survive (Podinovskaia and Descoteaux

1735   2015). Recently, Reverte et al. showed that expression of the transcription factor NRF2, a master regulator

1736   of the antioxidant response (Vomund, Schafer et al. 2017), is augmented during *Leishmania* spp. infection,

1737   including *L. donovani* (Reverte, Eren et al. 2021). Furthermore, upregulation of NRF2 activity contributed

1738   to promote parasite persistence during *L. guyanensis* infection by limiting inflammation (Reverte, Eren et

1739   al. 2021). In addition, NRF2-dependent increase in heme oxygenase 1 (HO-1) and ATF3 upon *L. donovani*

1740   infection was critical in dampening macrophage oxidative burst and proinflammatory cytokine expression

1741   as part of a parasite survival strategy (Saha, Roy et al. 2021). Thus, our data showing an enrichment of

1742   transcripts associated with the activation of an NRF2-dependent antioxidant response in promastigote-

1743   infected BMDMs suggest that targeting this regulatory node could be a therapeutic approach to combat VL.

1744   Mounting evidence indicates that specific and abundant changes in the transcriptional landscape of

1745   macrophages occur with 1 – 4 h post-infection with promastigotes of different *Leishmania* species (*L. major*,

1746   *L. amazonensis*, *L. chagasi*) (Rodriguez, Chang et al. 2004, Rabhi, Rabhi et al. 2012, Dillon, Suresh et al.

1747   2015, Fernandes, Dillon et al. 2016). For example, microarray data from BMDMs infected with *L. infantum*

1748   (syn. *chagasi*) promastigotes for 4 h revealed a marked inhibition of inflammatory transcripts that was

1749   concomitant with the upregulation of multiple anti-inflammatory mediators such as *Tgfb1* (Rodriguez, Chang

1750   et al. 2004), a disease severity marker during VL (Khadem and Uzonna 2014). Even though we did not

1751   identify *Tgfb1* in the subset of transcripts upregulated in response to early infection with *L. donovani*

1752   promastigotes, we recently described eIF4A-dependent increase in *Tgfb1* mRNA translation efficiency in

1753   BMDMs infected with *L. donovani* promastigotes and amastigotes for 6 h (Chaparro, Leroux et al. 2020).

1754   Thus, different VL-causing *Leishmania* spp. (*L. infantum* and *L. donovani*) can lead to similar phenotypes

in macrophages, such as rapid production of TGF-β, through different regulatory mechanisms of gene expression.

Our IPA and GO analyses identified a transcriptional signature characterized by early induction of pro- and anti-inflammatory genes in macrophages infected with *L. donovani* promastigotes. These data are in line with previous reports on early reprogramming of the host cell transcriptome by promastigotes of *L. major* and *L. amazonensis*, two *Leishmania* species that cause cutaneous Leishmaniasis (CL). A common feature of this type of signature appears to be the upregulation of the pro-inflammatory gene *Tnf* (**Fig. 3**) (Rabhi, Rabhi et al. 2012, Dillon, Suresh et al. 2015, Fernandes, Dillon et al. 2016). TNF levels have been associated with early recruitment of immune cells, including potential host cells, at the site of infection (Arango Duque, Fukuda et al. 2014). Thus, it is conceivable that both VL- and CL-causing *Leishmania* species drive rapid *Tnf* transcription and TNF production by macrophages to favor their own replication.

Global-scale profiling of macrophages identified a transcriptional signature associated with the modulation of lipid metabolism during early infection with *L. major* promastigotes (Rabhi, Rabhi et al. 2012). This was further characterized by showing cholesterol accumulation and the dynamics of lipid droplet formation in infected macrophages (Rabhi, Rabhi et al. 2016). Our *in silico* analyses identified a subset of lipid metabolism-related mRNAs upregulated in the *L. donovani* promastigote-infected data set. Consistent with this, alterations in lipid metabolism have been reported in patients diagnosed with VL (Martínez and Ruiz 2019). Hence, our data along previous studies indicate that early transcriptional changes triggered by CL- and VL-causing *Leishmania* species contribute to reprogramming lipid metabolism of infected macrophages.

Recently, a transcriptomic analysis of macrophages infected with *L. donovani* promastigotes identified HIF-1α as a negative regulator of the parasite-promoting BNIP3/mTOR/SREBP-1c lipogenesis axis (Mesquita, Ferreira et al. 2020). In parallel, the induction of a transcriptional signature associated with glutamine metabolism was found to be pivotal in VL pathogenesis with a therapeutic potential in synergy with miltefosine treatment (Ferreira, Mesquita et al. 2020). Both studies performed RNAseq on macrophages infected with *L. donovani* promastigotes for 6 h and, although identified transcripts were validated *in vivo* and *in vitro*, the global transcriptional response of infected macrophages compared to uninfected controls was not analyzed (Ferreira, Mesquita et al. 2020, Mesquita, Ferreira et al. 2020). Even though we did not find an enrichment of HIF-1α-dependent transcripts in our dataset, we detected an increase in *Bnip3*, a transcriptional target of HIF-1α, as previously reported (Mesquita, Ferreira et al. 2020). Similarly, our IPA and GO analyses did not find an enrichment of transcripts associated with glutamine metabolism; however, mRNAs encoding subunits of glutamate-cysteine ligase, a key enzyme in glutathione synthesis and glutamine usage (Liu, Hyde et al. 2014), were upregulated in infected datasets when compared to uninfected controls (i.e., *Gclm* in PRO upregulated, and *Gclc* in PRO and AMA upregulated). In sum, data generated by others and by us indicate that regulation of host cell metabolism is at least in part dependent on parasite-driven transcriptional changes induced by both life stages of *L. donovani* early during infection.

In line with subversion of macrophage immune functions by *L. donovani* promastigotes (Podinovskaia and Descoteaux 2015), we identified a number of mRNAs encoding immune inhibitors in the upregulated promastigote-infected dataset, including *Cd274* (a.k.a. PDL1), *Socs1*, and *Cd200*. PDL1 and its receptor PD1 constitute an important inhibitory axis for T cell activity, and antibody therapy against PD1 has proven successful against numerous malignancies (Sun, Mezzadra et al. 2018). Notably, the PD1/PDL1 axis was recently identified to play an important role *in vivo* during VL and immunotherapy against PD1 was effective in hampering parasite burden and pathogenesis (Medina-Colorado, Osorio et al. 2017). In addition, early induction of SOCS1, a known antagonist of the proinflammatory JAK1/STAT1 pathway (Wei, Wang et al. 2014, Lopez-Sanz, Bernal et al. 2018), was identified as part of a cellular program to prevent oxidative burst-mediated apoptosis in macrophages infected with *L. donovani* (Srivastav, Basu Ball et al. 2014). Similarly, a swift increase of CD200 in macrophages exposed to *L. amazonensis* or *L. donovani* infection was described as a strategy to favor parasite proliferation (Cortez, Huynh et al. 2011, Sauter, Madrid et al. 2019, Rawat, Pal et al. 2020). Interestingly, immune blockade of CD200 led to an increase in proinflammatory mediators and parasite elimination capacity of macrophages and T cells, showing its potential as a therapeutic target (Rawat, Pal et al. 2020). Taken together, these reports and our transcriptomic study highlight the early ability of *L. donovani* promastigotes to limit macrophage antimicrobial responses through the modulation of host mRNA abundance.

IPA identified a transcriptional signature associated with type I interferon responses predicted to be activated via the transcription factors IRF3 and IRF7 in the promastigote-upregulated dataset. By contrast, downregulation of *Irf7* mRNA abundance was detected in the transcriptome of amastigote-infected BMDMs. IRF7-dependent parasite elimination was reported in macrophages of the splenic marginal zone during the acute phase of *L. donovani* amastigote infection *in vivo* (i.e., 5 to 48 h post-infection) and by a cell line of stromal macrophages *in vitro*. Although the expression of IRF7 was not modulated in hepatic macrophages during VL, IRF7-defficient mice showed a decreased ability to control parasite burden in the liver (Beattie, Phillips et al. 2011). These observations along with transcriptomic data and our *in silico* analysis suggest that the ability of macrophages to elicit IRF7-dependent antimicrobial transcriptional programs upon *L. donovani* infection is tissue- and/or parasite-stage specific.

Our group recently described rapid remodeling of the translatome of macrophages infected by promastigotes and amastigotes of *L. donovani* (Chaparro, Leroux et al. 2020). Herein, we expanded our findings by analyzing early changes in the abundance of host mRNAs during infection. Comparison of the transcriptome and the translatome of *L. donovani*-infected BMDMs at 6 h post-infection indicates that in contrast to changes in translation efficiency (Chaparro, Leroux et al. 2020), modulation of mRNA abundance is, at least in part, parasite stage-specific. It is plausible that differences in lipid composition (Bouazizi-Ben Messaoud, Guichard et al. 2017) and protein expression (Biyani and Madhubala 2012) between promastigotes and amastigotes can account for these stage-specific profiles. For example, *L.*

1827 *donovani* promastigotes exhibit a dense glycocalyx comprised of a variety of potent virulence factors (i.e.,
1828 lipophosphoglycan (LPG), the protease GP63, etc.) that are mostly absent in amastigotes (Matheoud,
1829 Moradin et al. 2013, Arango Duque, Fukuda et al. 2014). This in turn can affect the process of parasite
1830 internalization due to differential usage of macrophage receptors for phagocytosis (Ueno and Wilson 2012)
1831 leading to distinctive host signaling pathways and transcriptional changes upon infection (Podinovskaia and
1832 Descoteaux 2015).

1833 Amastigote-driven changes included the upregulation of transcripts encoding DNA repair modulators while
1834 inhibiting those encoding antigen-presenting and macrophage activation factors. Alternatively,
1835 promastigote-infected macrophages showed the upregulation of immune inhibitors as well as an antioxidant
1836 transcriptional signature associated to NRF2 activity. However, enrichment of transcripts associated with
1837 IRF3 and IRF7 suggests that macrophages activate antimicrobial pathways upon *L. donovani* promastigote
1838 infection. Interestingly, mRNAs encoding proteins associated with DNA damage-sensing or DNA repair,
1839 apoptosis inhibition and mRNA metabolism were upregulated via changes in abundance (**Figs 3.2 – 3.4**)
1840 and translation efficiency (Chaparro, Leroux et al. 2020). A similar dual effect was observed on a number
1841 of downregulated immune-related transcripts (i.e., antigen presentation, leukocyte activation, etc.) (**Figs
1842 3.2 – 3.4**) (Chaparro, Leroux et al. 2020). In all, previous studies, along with our current findings support
1843 the notion that early parasite-driven changes in macrophage gene expression programs are under the
1844 control of transcriptional and post-transcriptional regulatory mechanisms that tailor both protective and
1845 harmful host cell responses during *L. donovani* infection.

1846 **4.5   Materials and Methods**

1847 **4.5.1   Reagents and Parasites**

1848 Culture media and supplements were purchased from Wisent, Gibco, and Sigma-Aldrich. *L. donovani* (LV9
1849 strain) amastigotes were isolated from the spleen of infected female Golden Syrian hamsters (Harlan
1850 Laboratories) as previously described (Matte and Descoteaux 2010). *L. donovani* (LV9 strain)
1851 promastigotes were differentiated from freshly isolated amastigotes and were cultured at 26°C in M199
1852 medium supplemented with FBS (10%), hypoxanthine (100 μM), hemin (5 μM), biopterin (3 μM), biotin (1
1853 μM), penicillin (100 U/mL), and streptomycin (100 μg/mL). Early passage stationary phase promastigotes
1854 were used for macrophage infections.

1855 **4.5.2   Ethics Statement**

1856 Housing and experiments were carried out under protocols approved by the Comité Institutionnel de
1857 Protection des Animaux (CIPA) of the INRS – Centre Armand-Frappier Santé Biotechnologie (CIPA 1308-
1858 04 and 1710-02). All methods were performed in accordance with relevant guidelines and regulations.
1859 These protocols respect procedures on good animal practice provided by the Canadian Council on animal
1860 care. The study is reported in accordance with ARRIVE guidelines.

4.5.3   Differentiation and infection of bone marrow-derived macrophages

1862   Bone marrow-derived macrophages (BMDMs) were differentiated from bone marrow precursor cells
1863   isolated from C57BL/6 mice, as previously described (Leroux, Lorent et al. 2018). Briefly, marrow was
1864   extracted from bones of the hind legs, red blood cells were lysed, and progenitor cells were resuspended
1865   in BMDM culture medium supplemented with 15% L929 fibroblast-conditioned culture medium (LCCM).
1866   Non-adherent cells were collected the following day and were cultured for 7 days in BMDM culture medium
1867   supplemented with 30% LCCM with fresh medium replenishment at day 3 of incubation. BMDMs were then
1868   collected, viable cells were counted by trypan blue exclusion and plated in 150 mm petri dishes at a density
1869   of 2×10^5cells/cm^2 overnight. BMDM cultures were inoculated with *L. donovani* promastigotes or
1870   amastigotes at a multiplicity of infection (MOI) of 10:1 for 6 h, as previously described (Atayde, da Silva Lira
1871   Filho et al. 2019). Glass coverslips were prepared in parallel and stained with HEMA 3 PROTOCOL to
1872   assess the rate of infection according to the manufacturer instructions. Promastigote- and amastigote-
1873   infected samples averaged at 92.3% ± 2.5% and 86.8% ± 1.9% of infection respectively. Prior to infection,
1874   cells were serum-starved for 2 h.

1875   **4.5.4   Cytosolic mRNA extraction**

1876   Cytosolic lysates of infected and control BMDMs were prepared for RNA extraction as described (Leroux,
1877   Lorent et al. 2018). RNA was extracted with QIAzol (Qiagen) and purified using RNeasy MinElute Cleanup
1878   Kit (Qiagen) according to specifications of the manufacturer. Purity and integrity of RNA was assessed
1879   using a Bioanalyzer 2100 with a Eukaryote Total RNA Nano chip (Agilent Technologies).

1880   **4.5.5   RNAseq and data processing**

1881   RNAseq libraries were generated using the Smart-seq2 method (Picelli, Faridani et al. 2014) and
1882   sequenced by using an Illumina HiSeq2500 instrument with a single-end 51-base sequencing setup from
1883   three independent biological replicates for uninfected and *L. donovani* promastigote-infected BMDMs, and
1884   five independent biological replicates for *L. donovani* amastigote-infected BMDMs. First, RNAseq reads
1885   mapping to the reference genome of the Nepalese BPK282A1 strain of *L. donovani* (txid: 981087) were
1886   removed (12.7% and 1.4% mappings on average for promastigotes and amastigotes, respectively). The
1887   filtered reads were then mapped to the mouse genome assembly GRCm38 (mm10) using HISAT2 with
1888   default settings (Kim, Langmead et al. 2015). Gene expression was quantified using the RPKMforgenes.py
1889   script (Ramskold, Wang et al. 2009) with -fulltranscript -readcount -onlycoding flags from which raw per-
1890   gene RNAseq counts were obtained (version last modified 07.02.2014). Genes that had zero counts in all
1891   samples were discarded. Annotation of genes was obtained from RefSeq.

1892   **4.5.6   RNAseq data analysis using anota2seq**

1893   RNAseq counts were normalized within anota2seq using the default TMM-log$_2$ method (Oertlin, Lorent et
1894   al. 2019). Significant changes in mRNA abundance were identified by anota2seq (Oertlin, Lorent et al.

2019) using the default parameters with the following modifications: FDR ≤ 0.05; apvEff > $\log_2(2.0)$. In anota2seq, the number of contrasts per analysis equals n-1 being n the number of conditions (i.e., CTR, Ld AMA, Ld PRO). In analysis one, infections were contrasted to the uninfected control (i.e., Ld PRO versus CTR and Ld AMA versus CTR); in analysis two, cells infected by different parasite stages were compared together and an additional contrast was included to complete the anota2seq parameters (i.e., Ld PRO versus Ld AMA and Ld PRO versus CTR). Identifiers for genes which cannot be distinguished based on their high sequence similarity (also reported by RPKMforgenes.py), were excluded from downstream analyses.

4.5.7 Gene ontology analyses

Gene ontology analyses were performed using the PANTHER tool (Mi, Huang et al. 2017) of the Gene Ontology Consortium (http://geneontology.org/) on the union of transcripts activated or inhibited in BMDMs infected by *L. donovani* amastigotes or promastigotes. Heatmaps of abundance of transcripts activated or inhibited in BMDMs infected by *L. donovani* amastigotes or promastigotes were generated using MORPHEUS.

(https://software.broadinstitute.org/morpheus/index.html, Broad Institute).

4.5.8 Ingenuity Pathway Analysis

Enrichment of transcripts showing differential abundance in specific functional networks was determined using Ingenuity Pathway Analysis (IPA; Qiagen) by comparing ANOTA2SEQ-regulated gene sets against the entire sequenced datasets (Kramer, Green et al. 2014). Within the IPA application, statistical significance was calculated using a right-tailed Fisher Exact test and p-values were adjusted for multiple hypothesis testing using the Benjamini-Hochberg method to arrive at a FDR.

4.5.9 Quantitative RT-PCR

Purified RNA (500 ng) was reverse transcribed using the LunaScript RT SuperMix Kit (New England Biolabs, cat#E3010L). Quantitative PCR was performed with Luna Universal qPCR Master Mix (New England Biolabs, cat#M3003L). Relative quantification was calculated using the comparative Ct method (ΔΔCt) (Taylor, Wakem et al. 2010) and relative expression was normalized to mouse β-actin. Experiments were performed in independent biological replicates (n=3); each sample was analyzed in a technical triplicate, the average of which was plotted against the respective conditions used. Primers were designed using NCBI Primer-BLAST (http://www.ncbi.nlm.nih.gov/tools/primer-blast/) (**Table S4.4**).

73

4.6 Figures
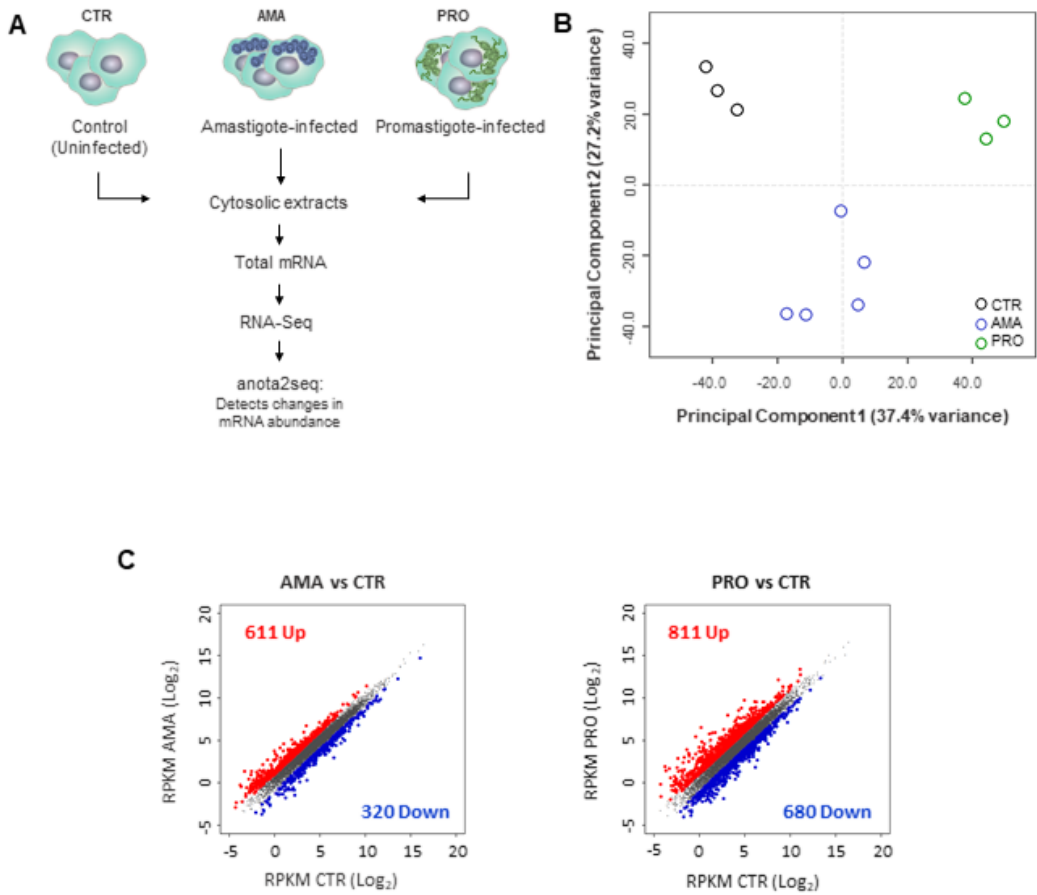
Figure 4.1. *L. donovani* **infection promotes early transcriptome-wide changes in macrophage mRNA abundance. (A)** Strategy to identify cytosolic mRNAs that are regulated in *L. donovani* amastigote (AMA)- or promastigote (PRO)-infected BMDMs. RNAseq experiments were carried out in three to five biological replicates per condition. **(B)** Cytosolic mRNA datasets of BMDMs infected or not with *L. donovani* AMA or PRO were projected on the first two components of a principal component analysis. **(C)** Scatter plots of gene expression as RPKM (log$_2$) values for total cytosolic mRNA. Differentially regulated transcripts are indicated in red (upregulated) or blue (downregulated). Unchanged mRNAs are shown in grey.

1937
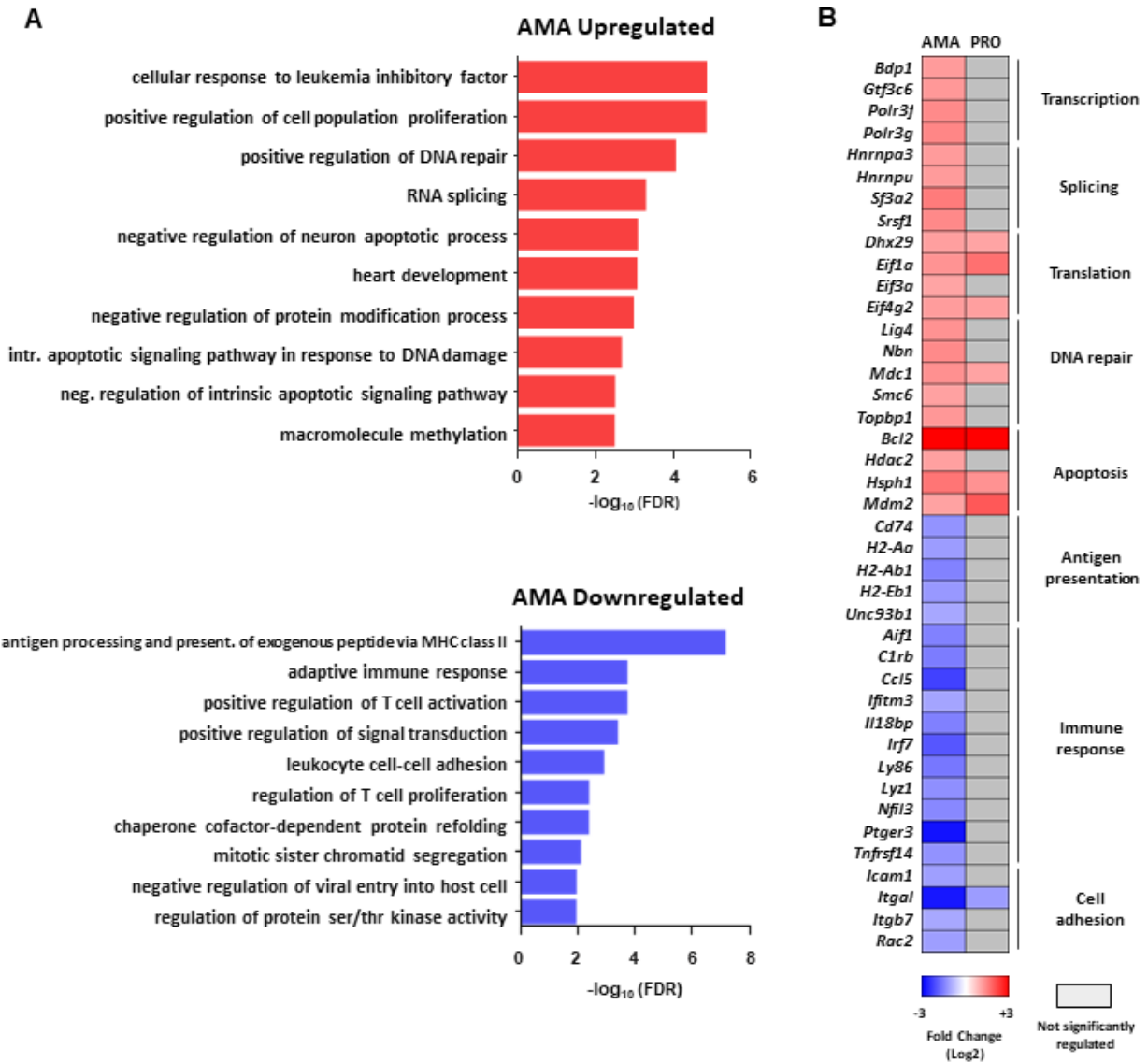
Figure 4.2. Selective changes in mRNA abundance predict amastigote-specific modulation of cell death and immune functions in macrophages during *L. donovani* infection. (A) FDR values (-log$_{10}$) for selected GO term enriched categories of differentially up- or downregulated mRNAs upon *L. donovani* AMA infection. **(B)** Changes in mRNA abundance for selected genes in enriched GO terms. Analyses were carried out on data generated from at least three biological replicates.

1942
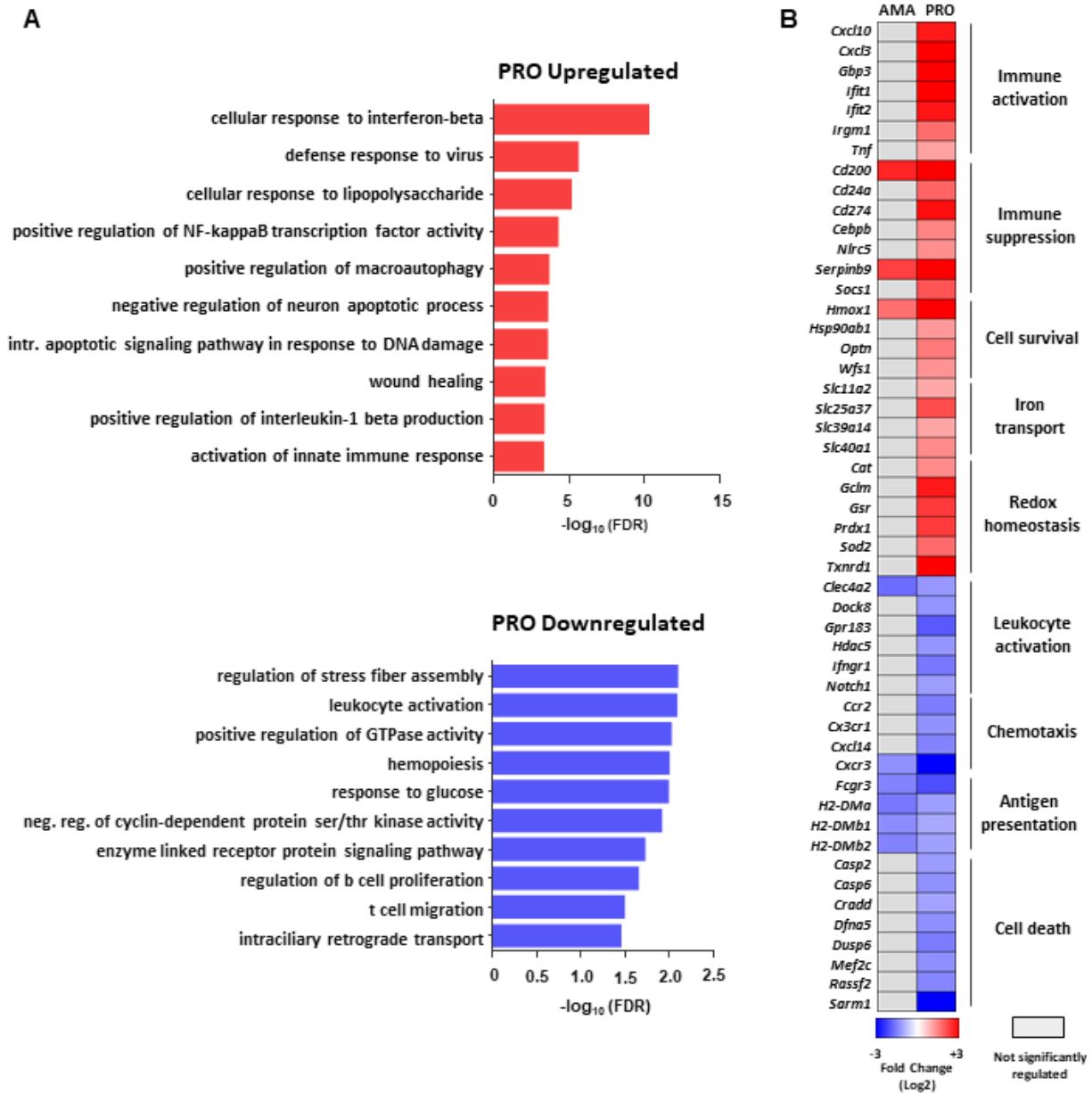
1943

Figure 4.3. Selective changes in mRNA abundance predict promastigote-specific activation and inhibition of macrophages defense responses during *L. donovani* infection. (A) FDR values (-log$_{10}$) for selected GO term enriched categories of differentially up- or downregulated mRNAs upon *L. donovani* PRO infection. **(B)** Changes in mRNA abundance for selected genes in enriched GO terms. Analyses were carried out on data generated from at least three biological replicates.

1948

1949

1950

1951

1952

1953
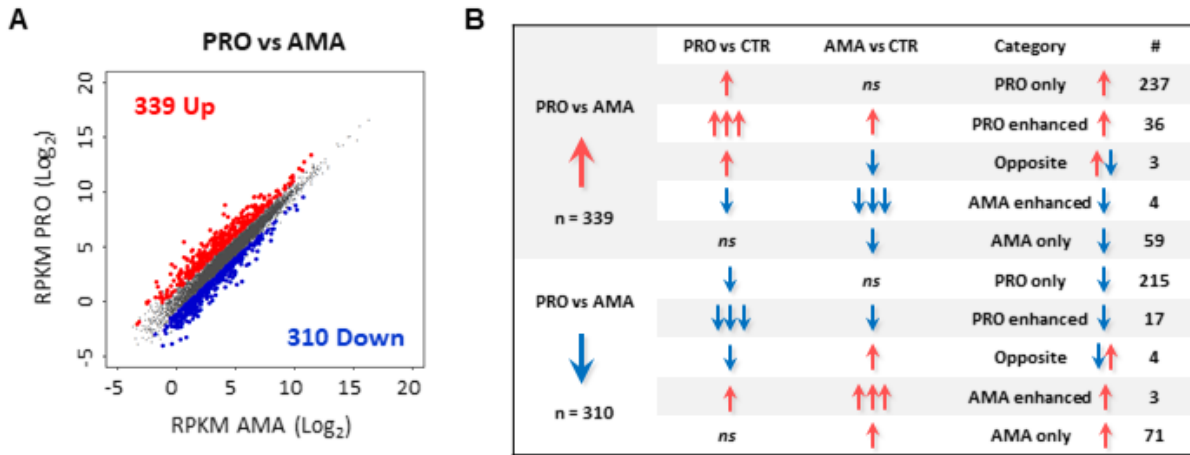
1954

Figure 4.4. Parasite stage-driven changes in macrophage mRNA abundance during *L. donovani* infection. (A) Scatter plot of gene expression as RPKM (log$_2$) values for total mRNA between PRO and AMA datasets. Differentially regulated transcripts are indicated in red (upregulated) or blue (downregulated). Unchanged mRNAs are shown in grey. **(B)** Category distribution of transcripts differentially regulated in macrophages upon *L. donovani* PRO versus AMA infection.

1959
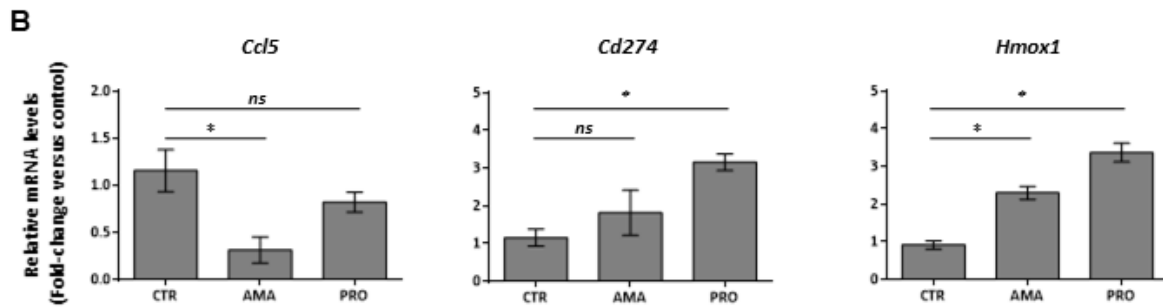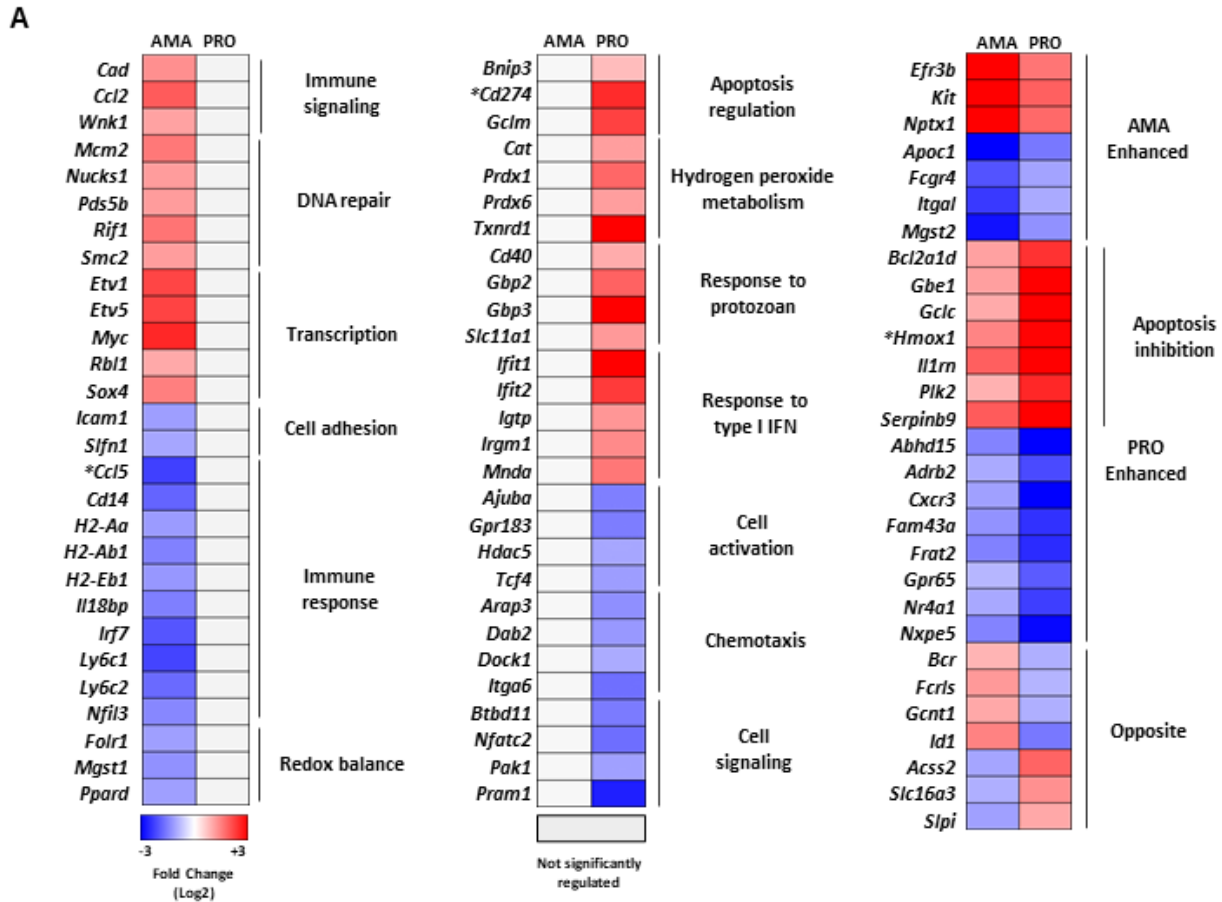
Figure 4.5. Parasite stage-driven modulation of macrophage transcripts encoding functionally related proteins during *L. donovani* infection. **(A)** Heatmaps of selected transcripts differentially regulated only by amastigotes (left panel), promastigotes (middle panel) or both (right panel). Manually curated ontology groups are shown for stage-specific regulated transcripts (left and middle panels). Analyses were carried out on data generated from at least three biological replicates. **(B)** Relative mRNA amounts of *Ccl5*, *Cd274*, and *Hmox1* (normalized to *Actb*) were measured by RT-qPCR. Data are presented as mean ± SD (biological replicates, n=3). *p < 0.05 (for the indicated comparisons), ns = non-significant.
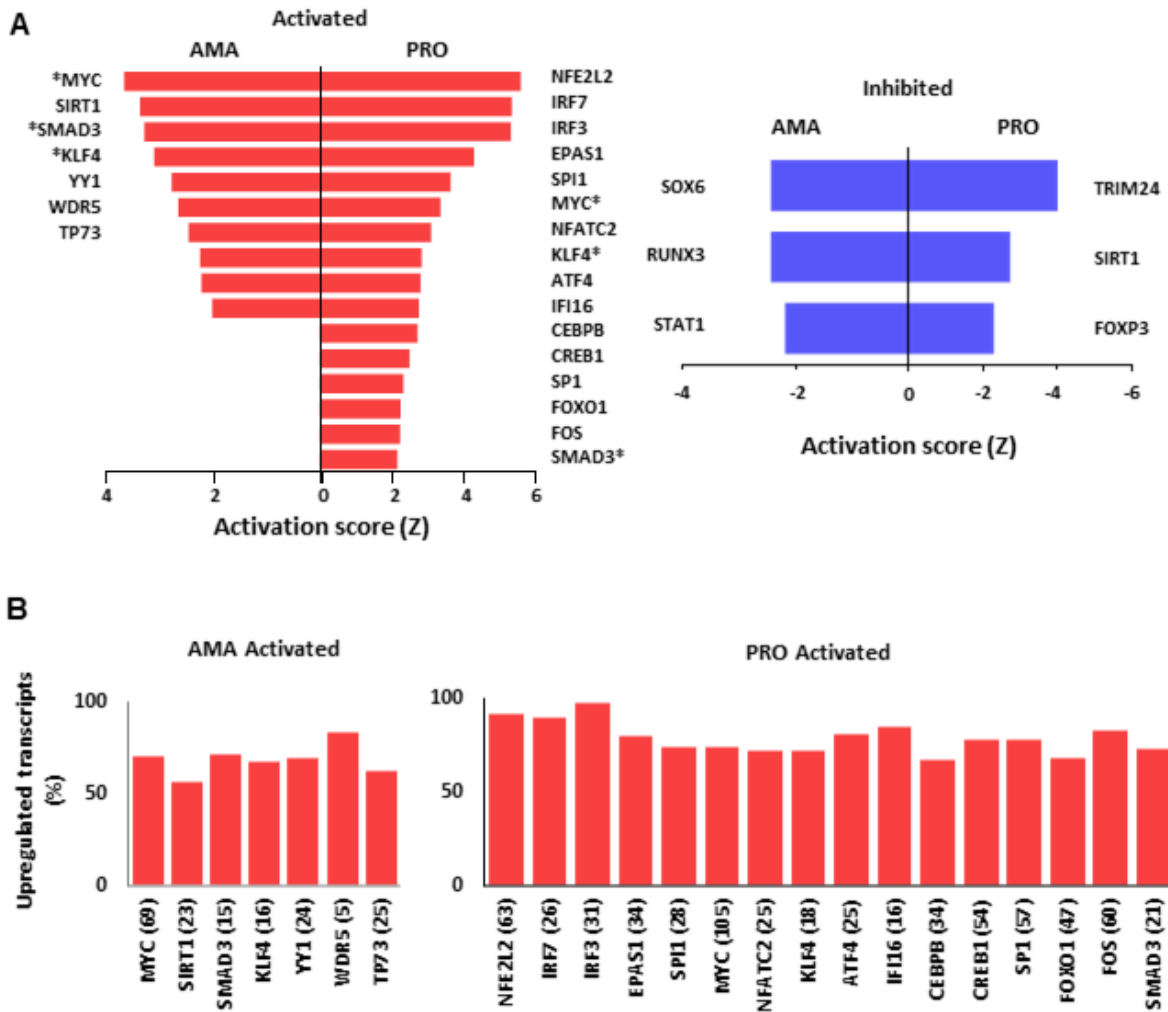
Figure 4.6. IPA predicts parasite stage-specific modulation of transcriptional regulators in macrophages infected _L. donovani_. (A) Activation score (Z) of transcriptional regulators predicted to be involved in the changes of mRNA abundance in macrophages upon _L. donovani_ AMA and PRO infection. *Common upstream regulators identified in PRO, AMA datasets by IPA. **(B)** Percentage distribution of upregulated mRNAs associated with upstream transcriptional regulators predicted to be activated in macrophages upon _L. donovani_ AMA and PRO infection. Total number of genes regulated by each transcription factor are shown in brackets. Analyses were carried out on data generated from at least three biological replicates.

4.7 Supplementary Information
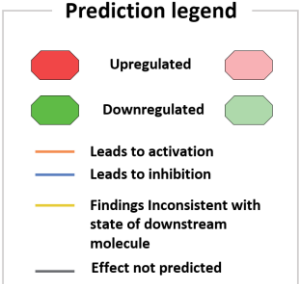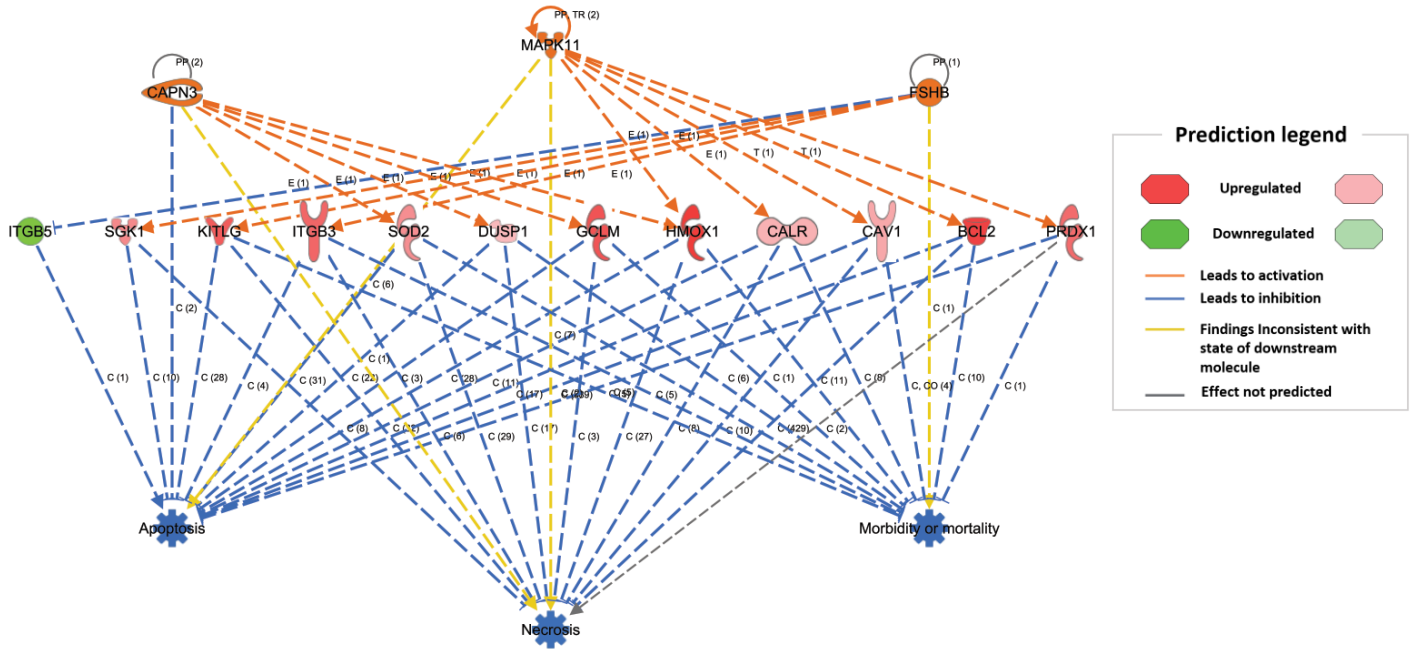
Supplementary Figure 4.1. *L. donovani* **promastigote infection favors the expression of cell death inhibitors**. RNAseq data
from PRO versus CTR datasets were subjected to IPA. A repressive regulatory network node comprised of 12 transcripts associated
with the inhibition of Apoptosis, Necrosis and Morbidity or Mortality is shown.
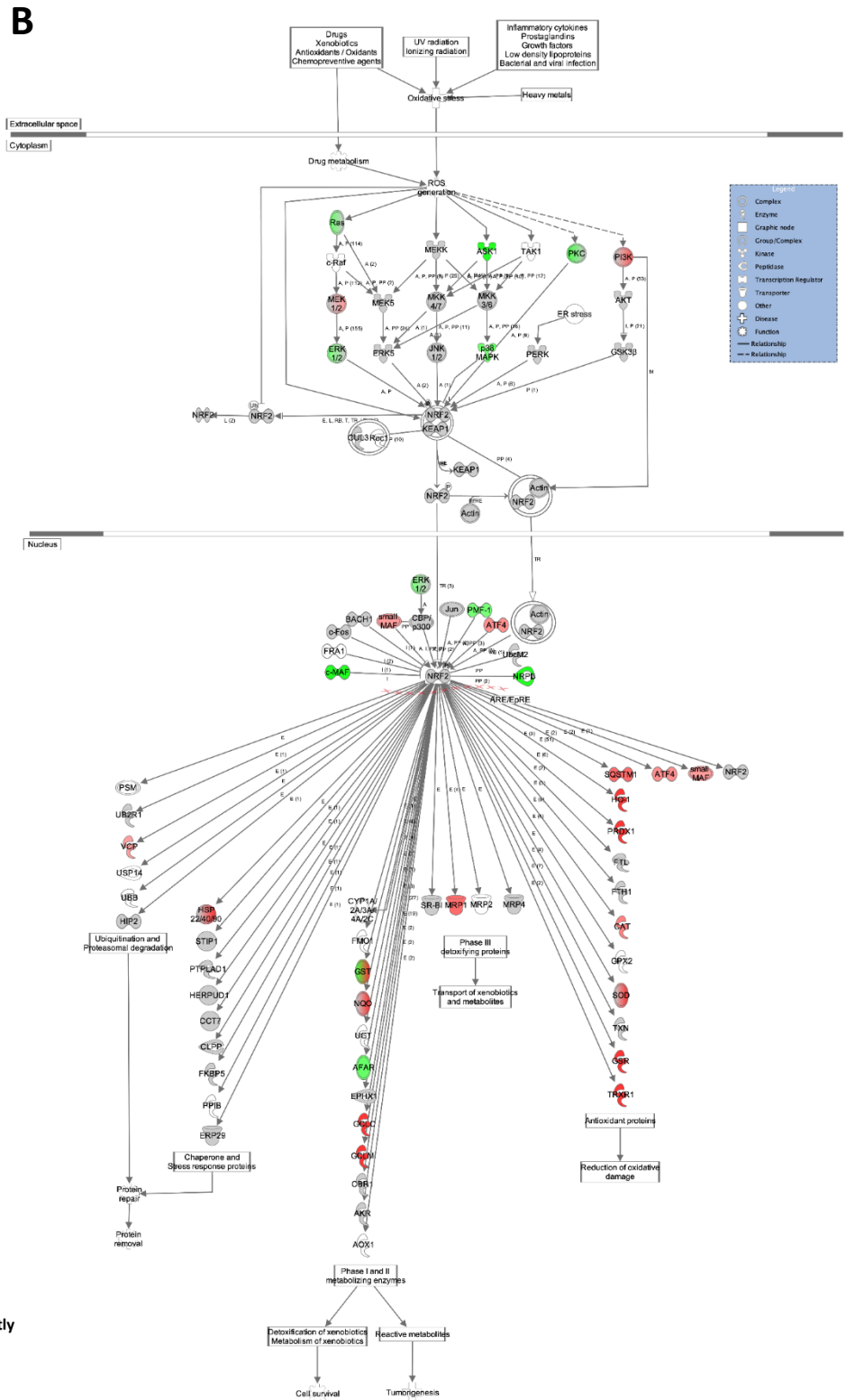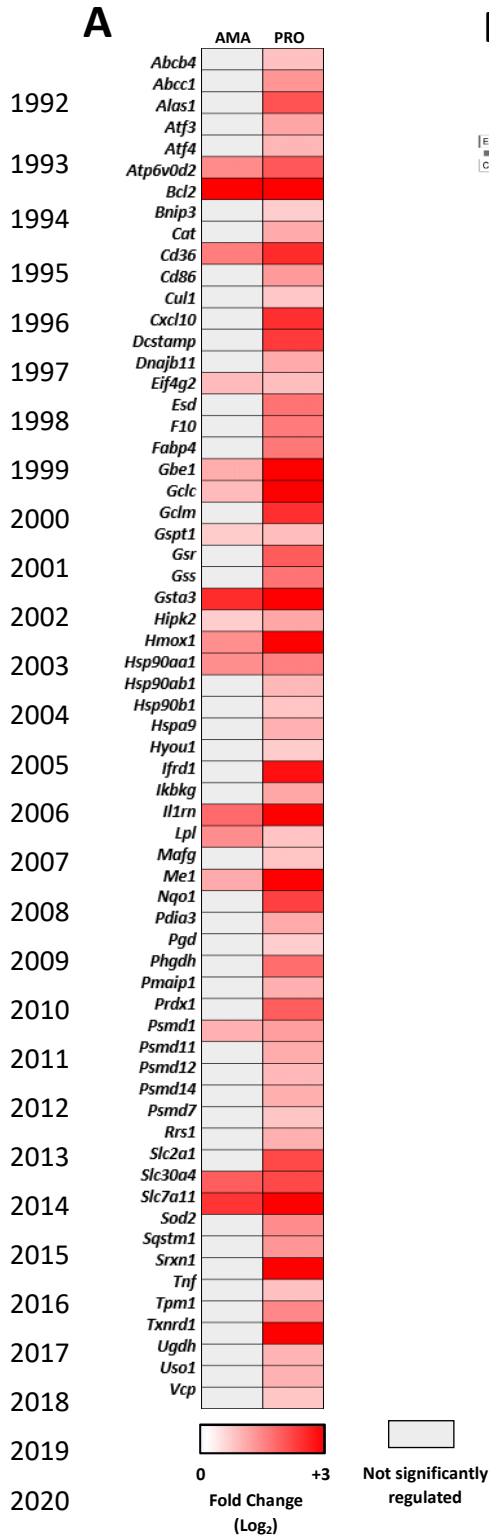
Supplementary Figure 4.2. NRF2-dependent oxidative stress response is predicted to be activated during *L. donovani* **promastigote infection**. **(A)** Expression levels of transcripts associated with NRF2 as an upstream transcriptional regulator identified by IPA in the PRO versus CTR dataset. **(B)** NRF2-dependent oxidative stress response was identified by IPA as one of the top induced regulatory networks in the PRO versus CTR dataset.

2027

2028

2029

2030

2031

2032

2033

2034

2035

2036

2037

2038

2039

2040

CHAPTER 5

Discussion

2041   Characterized with a remarkable plasticity, macrophages exhibit an ample array of molecular

2042   mechanisms to detect and eliminate invading organisms (Stout and Suttles 2004). Not surprisingly,

2043   macrophages undergo global remodeling of gene expression at the translational and transcriptional levels

2044   during infection (Chaussabel, Semnani et al. 2003, Goldmann, von Kockritz-Blickwede et al. 2007, Rabhi,

2045   Rabhi et al. 2016, Leroux, Lorent et al. 2018). Paradoxically, numerous pathogens evade host immune

2046   responses and use the macrophage as their main replication niche including vector-born protozoans of the

2047   genus *Leishmania* (Ren, Khan et al. 2017). *L. donovani*, the causative agent of visceral leishmaniasis -a

2048   chronic illness with an estimate of 50,000 annual deaths worldwide (van Griensven and Diro 2019)- induces

2049   widespread changes in host mRNA abundance (Gregory, Sladek et al. 2008, Kong, Saldarriaga et al. 2017,

2050   Medina-Colorado, Osorio et al. 2017, Morimoto, Uchida et al. 2019, Shadab, Das et al. 2019). However,

2051   most of these studies have been performed ≥ 12 hours post infection with the sandfly-transmitted

2052   promastigote stage of the parasite instead of the clinically relevant amastigote. In parallel, although various

2053   studies indicate mRNA translation is selectively targeted during infection by different pathogens (Hoang,

2054   Graber et al. 2019, Besic, Habibolahi et al. 2020, Etna, Severa et al. 2021, Kim, Kim et al. 2021) -including

2055   our work on macrophages infected by *Toxoplasma gondii* (Leroux, Lorent et al. 2018) (**See Appendix 4**)-

2056   the role of host translation for most protozoan parasite infections (e.g., *L. donovani*) remains largely

2057   unexplored. Moreover, discrepancies between reported transcriptome and proteome datasets of *L.*

2058   *donovani*-infected cells suggests post-transcriptional mechanisms such as mRNA translation could

2059   influence the macrophage response (Singh, Pandey et al. 2015, Smirlis, Dingli et al. 2020). Hence, an

2060   integrative characterization of the macrophage translational and transcriptional landscape during early

2061   infection -where critical processes could determine disease progression (Junghae and Raynes 2002,

2062   Forestier, Machu et al. 2011, Matheoud, Moradin et al. 2013, Giri, Srivastav et al. 2016)- by both parasite

2063   stages is yet lacking.

2064   Thus, by means of polysome profiling quantified by RNAseq we describe here the swift

2065   reprogramming of mRNA translation and abundance in primary murine macrophages infected with

2066   promastigotes or amastigotes of *L. donovani*. In chapter three, we identify an extensive translational

2067   reprogramming with similar dataset profiles of macrophages infected by either life stage of the parasite.

2068   Our results highlight functional categories (i.e., RNA metabolism, immune response, organelle organization

2069   and protein ubiquitylation) of translationally regulated mRNAs with a significant enrichment of mTORC1-

2070   and eIF4A-sensitive transcripts. Further, intracellular parasite survival was favored or compromised when

2071   mTORC1 or eIF4A activity was inhibited, respectively. Notably, in contrast to similar translational patterns

2072   in macrophages infected with promastigotes or amastigotes, our results in chapter four indicate that *L.*

2073   *donovani* infection is followed by parasite stage-driven host transcriptional signatures. Amastigote-infected

2074   datasets were enriched for upregulated DNA repair-associated transcripts and downregulated mRNAs

2075   encoding immune-related proteins whilst a combination of activating and inhibitory immune modulators as

2076   well as an anti-apoptotic transcriptional program was favored in promastigote-infected macrophages. These

2077   gene expression profiles were correlated to a network of upstream transcription factors as predicted by *in*

2078   *silico* analyses in a parasite stage-specific manner. In consequence, our data suggest mRNA translation
2079   constitutes an aspect of the early host response to infection with some of the changes oriented towards
2080   pathogen control and others favoring parasite survival. Conversely, widespread transcriptional changes in
2081   infected macrophages show the establishment of functional and selective gene expression programs that
2082   could tailor a stage-specific host response during infection.

2083   **5.1   *L. donovani* infection downregulates abundance and translational efficiency of mRNAs**
2084   **encoding components of the macrophage antigen presentation system**

2085   As evidenced by previous studies, translational changes can affect an ample array of immune-
2086   related processes (Mohr and Sonenberg 2012). For example, antigen presentation, a hallmark of the
2087   immune response, relies on the loading of endogenous and exogenous antigens on the *major*
2088   histocompatibility complex class I (MHC-I) and II (MHC-II) respectively (Kelly and Trowsdale 2019). In mice,
2089   MHC is encoded by different subtypes of the H2 antigen with MHC-I composed of a glycosylated heavy
2090   chain (comprised by H2-D, H2-K, H2-L, H2-Q, H2-M or H2-T subtypes) non-covalently associated with β2-
2091   microglobulin, while MHC-II constitutes dimer chains of H2-A or H2-E subtypes (Kotsias, Cebrian et al.
2092   2019). Translational modulation of MHC-II-encoding mRNAs has been observed upon IFNγ stimulation in
2093   both BMDM and B cells (Gonalons, Barrachina et al. 1998), while co-translational inhibition of MHC-I
2094   nascent peptides was observed in fibroblasts infected with rhesus cytomegalovirus (Powers and Fruh
2095   2008). Indications of impaired antigen presentation in monocytes of patients with visceral Leishmaniasis
2096   has been reported (Roy, Mukhopadhyay et al. 2015). In addition, GP63-dependent cleavage of VAMP8
2097   affected the antigen presentation capacity of macrophages and DCs infected with *L. donovani* and *L. major*
2098   *in vitro* (Matheoud, Moradin et al. 2013). Surprisingly, a combination of up (i.e., *H2-q4*, *H2-q6*, *H2-17*) and
2099   downregulated (i.e., *H2-aa*, *H2-oa*, *H2-ob*, *H2-dmb2*, *H2-dma*) MHC-encoding transcripts was detected on
2100   a transcriptome-wide analysis of *L. amazonensis*-infected dendritic cells (Lecoeur, Rosazza et al. 2020).

2101   Our data show a marked inhibition in translation and/or abundance of transcripts encoding MHC-
2102   associated proteins including β2-microglobulin (*B2m*) and CD74 (*Cd74*), a pivotal chaperone for MHC-II
2103   chains (Su, Na et al. 2017). Additionally, we found a translational repression of mRNAs that encode H2
2104   members of the MHC-I upon *L. donovani* infection, such as H2-T23, a molecule highly overexpressed upon
2105   IFNγ stimulation and associated with allograft rejection (Famulski, Einecke et al. 2006). In contrast to
2106   Lecoeur *et al*, our data show a translational downregulation of the *H2-q4* transcript, which encodes the α-
2107   chain of MHC-I, although a similar decrease in the abundance of MHC-II-encoding mRNAs (i.e., *H2-aa*,
2108   *H2-dmb2*, *H2-dma*) (Lecoeur, Rosazza et al. 2020) was also found in our dataset as shown in chapter four.
2109   Furthermore, proteomic analysis of cutaneous lesions from *L. major* or *L. amazonensis* infections displayed
2110   upregulation of different antigen presenting molecules such as the MHC-II member H2-AB1 (Negrao,
2111   Fernandez-Costa et al. 2019), however the corresponding transcript was found to be translationally
2112   inhibited in our data. This regulatory spectrum in the expression of molecules associated with antigen
2113   presentation suggests that different cell-, tissue-, and *Leishmania* species-specific mechanisms could be

elicited during infection to modulate this macrophage function. Interestingly, proteins of the CD1 family are antigen-presenting molecules expressed on the surface of APCs and a previous report showed that *L. donovani* inhibits transcription of *Cd1a-c* in human DCs (Amprey, Spath et al. 2004). The mouse genome only encodes for the *Cd1d1* and *Cd1d2* orthologs of the CD1 family (Seshadri, Shenoy et al. 2013) and our data indicates translation of *Cd1d1* was repressed in amastigote-infected macrophages. In consequence, as the main APCs of the immune system, it would be worth investigating if MHC mRNA translation is also targeted in *L. donovani*-infected DCs. Taken together, our data indicate *L. donovani* infection inhibits the expression and translation of macrophage mRNAs encoding MHC components *in vitro* and this might be part of the subversion mechanisms of host antigen presentation.

5.2 Protein ubiquitylation process as a transcriptional and translational target in macrophages infected with *L. donovani* amastigotes and promastigotes

Ubiquitylation represents one of the most common regulatory processes in eukaryote cells (Ben-Neriah 2002) and, although it is commonly considered as a marker for proteasome-mediated degradation, it can also participate in signal transduction of pathogen-recognition receptors (PRRs), endocytosis and protein synthesis (O'Neill 2009). A close association between ribosome engagement and the expression of ubiquitylating enzymes was found to be critical for neuron development (Rodrigues, Mufteev et al. 2020). Furthermore, ubiquitome analysis of mouse brain tissue infected with rabies virus identified enriched subsets of proteins associated with immune response and inflammation at late stages of the disease (Cai, Su et al. 2020). A classical example of non-degradative ubiquitylation signaling is represented by the ubiquitin-dependent activation of TRAF6, a mediator of PRR signaling (Heaton, Borg et al. 2016). The ubiquitylation status and activity of TRAF6 can be regulated by different proteins including A20 deubiquitylase (syn. TNFAIP3) (Boone, Turer et al. 2004) and ubiquitin ligase UBE2N (syn. UBC13) (Keating and Bowie 2009), which in turn can be affected by association with UBE2V1 (Deng, Wang et al. 2000) and UBE2V2 (Hofmann and Pickart 1999) enzymes. TRAF6 activation is crucial for NF-kB and MAPK activation in immune cells (Hu and Sun 2016). A previous report by Srivastav et al (Srivastav, Kar et al. 2012) showed that *L. donovani* promastigote infection leads to increased expression of A20 (both at the mRNA and protein level) with a concomitant decrease in TRAF6 ubiquitylation, which is determinant in supressing TLR signaling and the host immune response. In accordance with this observation, we found increased mRNA abundance of the A20 deubiquitylase in macrophages infected by *L. donovani* promastigotes. Interestingly, translation of *Ube2n* and *Ube2v1* (E2 ubiquitin conjugating enzymes) was found to be repressed during infection, which might further contribute to TRAF6 decreased ubiquitylation. These data suggest parasites target mRNA translation and abundance of ubiquitin-editing enzymes as a potential strategy to impair macrophage immune functions.

Interestingly, and in contrast to non-degradative ubiquitylation, in recent years parasite proteasome inhibition has been studied for treatment of different trypanosomiasis (Khare, Nagle et al. 2016) and a pre-clinical candidate was recently reported effective against visceral leishmaniasis (Wyllie, Brand et al. 2019).

2150 Although these drugs have been selected for non-mammalian proteasomes, it would be interesting to
2151 evaluate if alternative compounds can exhibit a dual host/parasite effect in a similar way as eIF4A inhibitors
2152 have in the case of malarial infections (Langlais, Cencic et al. 2018). Conversely, in 2003, the proteasome
2153 inhibitor Bortezomib was approved by the FDA for treatment of multiple myeloma, and multiple E1-3
2154 ubiquitin ligase inhibitors have been under scrutiny ever since (Landre, Rotblat et al. 2014). This could
2155 represent an additional avenue in the study of antileishmanial chemotherapies by analyzing the role of host
2156 degradative ubiquitylation in *Leishmania* parasite survival.

5.3 Differential expression of histones and chromatin-modifying enzymes during *L. donovani* infection

2159 Early infection by *L. donovani* favored the translation of transcripts encoding chromatin remodeling
2160 proteins such as histones and histone-modifying enzymes. In accordance with this finding, proteome
2161 analyses have shown similar enrichment patterns in macrophages infected by *L. donovani* and other
2162 *Leishmania* species (Isnard, Christian et al. 2015, Singh, Pandey et al. 2015). Regulation of histone-
2163 encoding mRNA metabolism is multitiered, including mechanisms of mRNA transcription, processing,
2164 nuclear export, translation, and decay (Rattray and Muller 2012). A group of histone-encoding transcripts
2165 are notorious for their lack of introns and a poly(A) tail; Instead, a secondary RNA structure near their 3'
2166 end is recognized by the hairpin binding protein (*Slbp*), which associates with multiple partners to modulate
2167 posttranscriptional RNA processing, translation and decay (Muller and Schumperli 1997). Our data indicate
2168 that *L. donovani* infection is followed by a translational repression of *Slbp* and also *Lsm10*, (*Slbp* interacting
2169 protein involved in histone mRNA maturation) (Rattray and Muller 2012). Interestingly, 31 transcripts
2170 encoding different histone variants were found to be translationally regulated (70% upregulated), whereas
2171 6 showed a modulation in abundance (all of them downregulated). Variations in the existing pool of histones
2172 can introduce substitutions in the nucleosome composition, affecting transcription via DNA sequence
2173 availability (Weber and Henikoff 2014). However, dysregulated expression of histones can lead to the
2174 formation of protein aggregates that are cytotoxic unless chaperones are available to facilitate the process
2175 of histone exchange, stabilization, or degradation (Mendiratta, Gatto et al. 2019).

2176 Coincidentally our data show that nucleophosmin 1 (*Npm1*), one of the most common histone
2177 chaperones (Box, Paquet et al. 2016), exhibits a high translational increase in macrophages upon infection
2178 by *L. donovani* amastigotes and promastigotes. Additionally, a recent report by Roy *et al* shows that histone
2179 deacetylase 1 (HDAC1) is transiently upregulated in human macrophages during the early infection (i.e., 6
2180 hours) by *L. donovani* leading to the transcriptional silencing of mRNAs encoding defensins (Roy, Brar et
2181 al. 2020). Although we did not find a modulation in *Hdac1* expression, other deacetylases associated with
2182 defensin expression (Andresen, Gunther et al. 2011, Yin and Chung 2011) showed increased (*Hdac2*) or
2183 decreased (*Hdac5*, *Hdac8*) levels of translation or abundance. Recently, the group of Späth reported that
2184 targeting of macrophage histone H3 acetylation by *L. amazonensis* prevents NF-κB/NLRP3-mediated
2185 inflammation, although the molecular mechanism behind this phenotype remains to be characterized

2186 (Lecoeur, Prina et al. 2020). It would be interesting to evaluate if the differential translation or transcription
2187 of chromatin-modifying proteins found in macrophages infected with *L. donovani* parasites affects
2188 inflammatory responses such as defensin production and NLRP3 inflammasome activation. Taken
2189 together, these data indicate *L. donovani* infection can introduce chromatin rearrangements and that
2190 differential translation and transcription of specific mRNA species could play a role in modulating this
2191 process.

2192 **5.4   Translation of RNA-binding proteins is significantly upregulated during infection**

2193   Remarkably, a significant enrichment of gene ontologies associated with RNA metabolism
2194 (transcription, splicing, transport, decay, and translation) was accompanied by translational modulation of
2195 numerous RBPs during *L. donovani* infection. Accumulating data from RNA interactome studies have
2196 allowed the annotation of over 1900 RBPs in the mouse genome (Hentze, Castello et al. 2018), 582 of
2197 which were identified in our data as translational targets (77% upregulated) during amastigote and
2198 promastigote infection (**Fig 5.1**). Being styled as RNA "clothes", RBPs can affect the functioning,
2199 localization, stability and availability of cognate RNA species by associating with sequence and
2200 conformational RNA-binding motifs in different transcript regions (i.e., UTRs, introns, exons) (Singh, Pratt
2201 et al. 2015). In consequence, RBPs are pivotal elements of the post-transcriptional regulation of gene
2202 expression (Glisovic, Bachorik et al. 2008) in homeostasis and disease affecting gastrointestinal epithelial
2203 functioning (Xiao and Wang 2014), muscle and neural development (Brinegar and Cooper 2016),
2204 cardiovascular pathologies (de Bruin, Rabelink et al. 2017), immunometabolism (Salem, Vonberg et al.
2205 2019) and inflammation (Kim 2020). For instance, mRNAs encoding inflammatory mediators (e.g.,
2206 chemokines and cytokines) are notoriously unstable due to the presence of RNA-binding motifs such as
2207 AU-rich elements (AREs) in their 3'-UTRs (Caput, Beutler et al. 1986, Datta, Biswas et al. 2008). Recently,
2208 Suñer *et al* described the role of the RBP CPEB4 upon macrophage LPS stimulation in stabilizing anti-
2209 inflammatory transcripts (i.e., *Il1rn*, *Socs1*) bearing ARE and cytoplasmic-polyadenylation element (CPE)
2210 motifs counteracting the role of tristetraprolin (ZFP36), an RBP that is known to promote the turnover of
2211 ARE-containing transcripts (Zhang, Chen et al. 2017, Suner, Sibilio et al. 2022).

2212   Our data indicates *Cpeb4* abundance is increased upon *L. donovani* promastigote or amastigote
2213 infection, while its translational efficiency is increased during amastigote infection. Concomitantly, mRNA
2214 abundance levels of *Socs1* is increased in the PRO dataset, while *Il1rn* is increased by *L. donovani* infection
2215 with either stage, which might be part of a parasite-promoted strategy of survival since SOCS1 upregulation
2216 has been reported to be protective for *Leishmania* parasites (Srivastav, Kar et al. 2012). Another example
2217 of mRNA stability regulation by RBPs is represented by the mRNAs encoding IFNγ, TNF and DUSP1, which
2218 are recognized by ZFP36L2, a CCCH zinc-finger protein known to promote the turnover of ARE-containing
2219 transcripts (Wang, Wang et al. 2015, Salerno, Engels et al. 2018). ZFP36L2 has been reported to localize
2220 in p-bodies (Franks and Lykke-Andersen 2007), which are ribonucleoprotein (RNP) granules enriched with
2221 decapping and exonucleolytic enzymes that participate in the mRNA decay pathway (Luo, Na et al. 2018).

2222 Our data indicate translation of ZFP32L2 was favored during *L. donovani* infection, which might contribute
2223 to the disruption of the inflammatory response in the host cell. Although the role of ZFP36L2 has been
2224 studied in the regulation and development of T cells (Hodson, Janas et al. 2010, Makita, Takatori et al.
2225 2020), its involvement during infective processes remains to be determined. Further studies are required
2226 to evaluate the contribution of ZFP36L2 and CPEB4 in the pathogenesis of visceral leishmaniasis.

2227
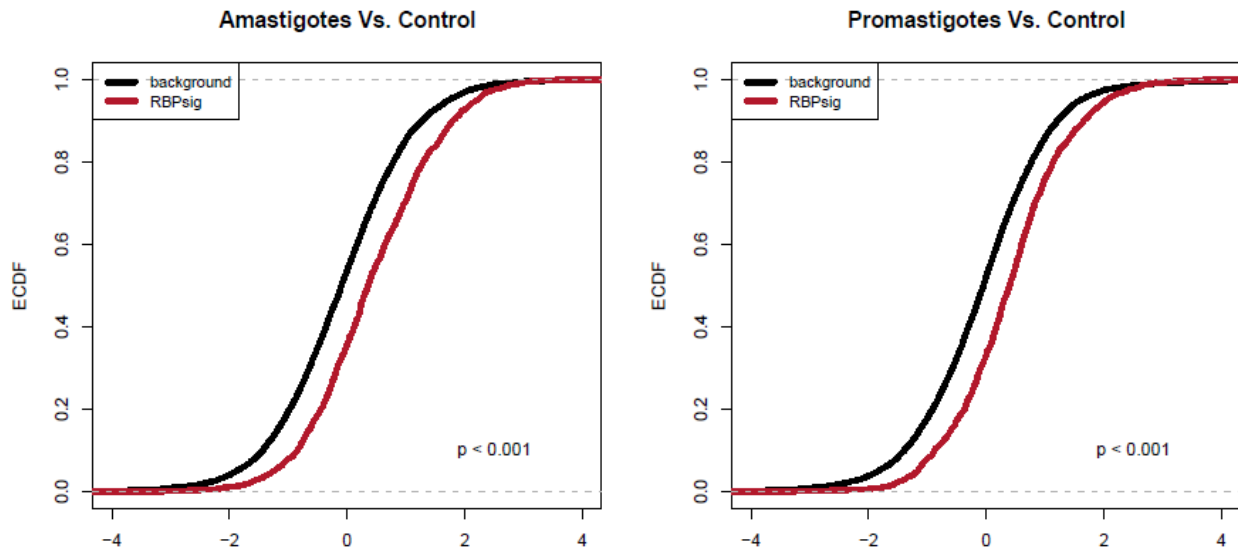
2228
2229

2230 **Figure 5.1. *L. donovani* infection increases translation efficiency of RBP encoding transcripts in murine macrophages.**
2231 Empirical cumulative distribution function (ECDF) of translational efficiencies (infection vs. control) for the compilation of transcripts
2232 encoding annotated RPBs as compared to those of all detected transcripts (background). Differences in translational efficiencies
2233 between RBP transcripts vs control transcripts were assessed per parasite stage.

2234 **5.5   *L. donovani* infection favors expression of transcripts encoding members of the IFNγ**
2235 **antagonist GAIT complex**

2236   In addition to canonical RBPs, alternative ("moonlight") RNA-binding partnerships have been found
2237 for numerous metabolic enzymes (Castello, Hentze et al. 2015). For example, upon IFNγ stimulation,
2238 glutamyl-prolyl tRNA synthetase (EPRS) is phosphorylated and subsequently associates with
2239 glyceraldehyde-3-phosphate dehydrogenase (GAPDH), ribosomal protein L13 (RPL13) and
2240 heterogeneous nuclear ribonucleoprotein Q (SYNCRIP) to form the interferon-γ-activated inhibitor of
2241 translation (GAIT) complex (Sampath, Mazumder et al. 2004). This heterotetramer binds mRNAs containing
2242 a secondary structure in their 3'-UTR called the GAIT element (Sampath, Mazumder et al. 2003). Once
2243 activated, the RNA-loaded GAIT complex interacts with the translation machinery of the cell to prevent the
2244 expression of numerous transcripts including ceruloplamisn, VEGFA and several chemokines and
2245 chemokine receptors as part of a negative feedback loop preventing excessive inflammation

2246 (Mukhopadhyay, Jia et al. 2009). During *L. donovani* infection, the IFNγ-driven Th1 response is a hallmark

2247 of host resistance (Ghalib, Whittle et al. 1995). However, contrary to the marked inflammatory signature of

2248 the splenic environment *in vivo*, spleen macrophages show insensitivity to IFNγ at chronic stages of

2249 experimental visceral Leishmaniasis using a hamster model (Kong, Saldarriaga et al. 2017), although the

2250 molecular basis for this impaired response remains to be fully elucidated. Interestingly, decreased levels of

2251 IFNγ receptor in human macrophages upon *L. donovani* infection correlates with *in vitro* observations of

2252 IFNγ-insensitivity (Ray, Gam et al. 2000, Matte and Descoteaux 2010). In this regard, we identified

2253 decreased translation efficiency of *Ifngr1* and *Ifngr2*, the transcripts encoding for IFNγ receptor subunits.

2254 Additionally, our RNAseq data showed increased levels in mRNA abundance or translation of *Eprs*, *Gapdh*,

2255 *Rpl13* and *Syncrip*. Remarkably, the mRNA of the ZIP kinase (*Dapk3*), one of the upstream activators in

2256 the assembly of the GAIT complex (Mukhopadhyay, Jia et al. 2009), was also translationally upregulated

2257 in *L. donovani* amastigote-infected macrophages. Although upregulation of these proteins is not indicative

2258 of a spontaneous activation of the GAIT system, *L. donovani* infection might be conducing macrophages

2259 toward a primed state were the formation or abundance of a functional GAIT complex is favored to counter

2260 a potential Th1 response elicited by the host. Translation levels of GAIT-sensitive mRNAs as well as

2261 immunoprecipitation analysis of GAIT complex assembly could be evaluated in *L. donovani*-infected

2262 macrophages subject to IFNγ stimulation compared to uninfected controls in order to validate this

2263 hypothesis.

5.6 Early mTORC1 activation promotes translation of TOP mRNAs including *Pabpc1* during infection

2266 As aforementioned, our data indicate that translation of the transcripts encoding *Npm1* and *Rpl13*

2267 is increased in macrophages during *L. donovani* infection. These mRNAs belong to a group of transcripts

2268 with a characteristic TOP motif in their 5' UTR. TOP mRNAs encode proteins associated with different cell

2269 functions and compartments such as cytoskeleton (*Vim*, *Tpt1*), cell signaling (*Rack1*), chromatin

2270 remodelling (*Npm1*, *Nap1l1*) and numerous RBPs of the translational machinery including ribosomal

2271 proteins and translation initiation and elongation factors (Meyuhas and Kahan 2015). Accumulating

2272 evidence indicates translational control of TOP mRNAs occurs via repression by the protein LARP1, which

2273 recognizes and binds to the TOP motif present in the 5' UTR of the corresponding mRNAs preventing the

2274 assembly of the translation initiation complex (Hong, Freeberg et al. 2017). Activation of mTORC1 leads to

2275 LARP1 phosphorylation and its dissociation of the cognate sequence, promoting the translation of a

2276 multitude of transcripts including TOP mRNAs (Jia, Lahr et al. 2021).

2277 Upon closer examination, we found an enrichment of translationally upregulated TOP mRNAs in

2278 macrophages infected with amastigotes or promastigotes of *L. donovani*, which goes in accordance with

2279 the early phosphorylation of mTORC1 downstream targets in our samples. For example, our RNAseq data

2280 revealed upregulation of the eukaryotic elongation factors 1α1 (*Eef1a1*) and 1β2 (*Eef1b2*), two TOP mRNAs

2281 involved in polypeptide synthesis elongation (Meyuhas and Kahan 2015). Although initiation is considered

2282   the rate-limiting step in mRNA translation (Jackson, Hellen et al. 2010), elongation has proven essential in
2283   embryonic development and neuron plasticity though ribosome stalling (Richter and Coller 2015). Of note,
2284   polysome profiling is unable to discern between co-sedimentation of active versus stalled ribosomes unless
2285   coupled with inhibitory treatments (i.e., puromycin) or through *in vitro* translation validation which are
2286   required to further elucidate the role of translation elongation on transcripts of interest (Richter and Coller
2287   2015).

2288   Among the group of translationally regulated TOP mRNAs we found the transcript encoding for the
2289   poly(A)-binding protein (PABPC1), a pivotal RBP that modulates translation and stability of numerous
2290   mRNA species (Wang, Day et al. 1999). PABPC1 has been reported to play different roles in the immune
2291   system; For example, by associating with hnRNPLL it regulates the switch in expression from membrane
2292   bound to secreted immunoglobulin forms in plasma cells (Peng, Yuan et al. 2017). In a similar way, the
2293   PABPC1/TTP interaction constitutes an inhibitory translational complex in activated macrophages that
2294   hinders the expression of pro-inflammatory mediators (Zhang, Chen et al. 2017). Contrasting evidence on
2295   the role of PABPC1 during infection shows that its cleavage by different picornavirus proteases favors viral
2296   replication by inhibiting host translation (Kuyumcu-Martinez, Joachims et al. 2002, Xue, Liu et al. 2020),
2297   whereas for Dengue virus, PABPC1 constitutes a virus-promoting host factor, although the precise
2298   mechanism behind this observation remains to be elucidated (Suzuki, Chin et al. 2016). Additionally,
2299   PABPC1 was reported to be required to contribute to cytomegalovirus (CMV) replication and that host cells
2300   can induce expression of the repressor PABP-interacting-protein 2 (PAIP2) as a strategy to control CMV
2301   infection (McKinney, Yu et al. 2013). Similarly, PABPC1 inhibition through repressed mRNA abundance
2302   and translation showed increased levels of bacterial elimination on human epithelial cells (Besic, Habibolahi
2303   et al. 2020). Notably, under mTORC1 decreased activity, LARP1 association with cognate mRNAs was
2304   reported to be guided by interaction with PABPC1 (Smith, Benbahouche et al. 2021). This becomes of
2305   relevance in the context of macrophage *L. donovani* infection since mTORC1 activity peaks at 6h.p.i. with
2306   a subsequent reduction after 8h.p.i. Thus, increased PABPC1 levels might affect LARP1 activity and gene
2307   expression at later time points following parasite inoculation when mTORC1 activity decreases. It would be
2308   interesting to generate genetically modified macrophages deficient for PABPC1 expression to evaluate
2309   parasite persistence *in vitro*. Additionally, it would be worth to follow a kinetics of PABPC1/LARP1
2310   interaction on infected cells versus uninfected controls and characterize their associated transcripts in the
2311   presence or absence of mTORC1 inducers (i.e., insulin) or inhibitors (i.e., rapamycin) to evaluate if
2312   mTORC1 activity levels can differentially affect translation of mRNAs that favor parasite survival or
2313   clearance.

2314   **5.7   Early mTORC1 activation promotes translation of *Eif2ak2, a* non-TOP mRNA during infection**

2315   Although the role of mTORC1 in regulating translation of TOP mRNAs is well stablished, mTORC1-
2316   driven translation of non-TOP RNAs has also been reported (Gandin, Masvidal et al. 2016). This diversity
2317   in target transcripts might derive from the conflating exogenous (i.e., growth factors, hormones, cytokines,

2318 TLR ligands) and endogenous (i.e., energy and nutritional status) stimuli that position mTORC1 as a nodal

2319 regulator of numerous cellular processes (Saxton and Sabatini 2017). During *L. donovani* infection,

2320 macrophage TLR signaling (one of mTORC1 upstream inducers) can be activated (Bhattacharjee,

2321 Majumder et al. 2016), which could lead in turn to increased expression of the double-stranded RNA-

2322 dependent protein kinase (PKR, syn. EIF2AK2) (Dias, Dias-Teixeira et al. 2019). The RBP EIF2AK2 is

2323 associated with the integrative stress response during viral infections through phosphorylation of the subunit

2324 α of the eukaryote translation initiation factor 2 (eIF2α), which results in a generalized inhibition of protein

2325 synthesis (Sheikh and Fornace 1999). Additionally, EIF2AK2 participates in the activation of MAPKs,

2326 cytokine expression (TNF, IL6, IL10) and modulation of NF-κB activity downstream TLR4 stimulation

2327 through direct interaction with TIRAP and TRAF proteins (Horng, Barton et al. 2001, Gil, Garcia et al. 2004).

2328 Previous reports show that *L. amazonensis* infection leads to increased levels of the total and

2329 phosphorylated forms of EIF2AK2 in a TLR2-dependent manner, which favors a parasite-promoting

2330 phenotype involving increased levels of IFNβ, IL10 and SOD1 (Pereira, Teixeira et al. 2010, Vivarini Ade,

2331 Pereira Rde et al. 2011). In sharp contrast, the inhibitor of serine protease 2 (ISP2), a virulence factor of *L.*

2332 *major*, prevents neutrophil elastase activation of EIF2AK2, which otherwise could lead to an NF-κB-

2333 dependent upregulation of TNF expression and subsequent parasite elimination (Faria, Calegari-Silva et

2334 al. 2014). Recently, it was shown that macrophages infected with *L. donovani*, similarly as with *L.*

2335 *amazonensis*, exhibit increased levels of total and phosphorylated EIF2AK2, which is associated with the

2336 upregulated expression of IFNβ, IL10 and SOD1 (Dias, Goundry et al. 2022). Our RNAseq data along with

2337 western blot protein measures and RT-qPCR determination of *eif2ak2* (a non-TOP mRNA) expression

2338 suggest that its translational efficiency is upregulated on *L. donovani*-infected datasets in a partially

2339 mTORC1-dependent manner. Certainly, neither rapamycin nor Torin-1 treatment fully inhibited EIF2AK2

2340 expression, which suggests mTORC1-independent mechanisms could contribute to its regulation in

2341 macrophages during infection by *L. donovani*. Notably, we found an increment in total *eif2ak2* levels in the

2342 promastigote-infected macrophages by RNAseq. Additionally, as shown in chapter 4, IPA identified IRF3

2343 as one of different upstream transcriptional regulators predicted to be activated during *L. donovani*

2344 promastigotes infection and *eif2ak2* is depicted as one of its associated targets in accordance with the

2345 presence of an interferon-sensitive response element in its promoter (Tanaka and Samuel 1994). Although

2346 we did see an upward trend in total *eif2ak2* levels by RT-qPCR, it did not reach statistical significance in *L.*

2347 *donovani*-infected samples versus uninfected controls. A thorough kinetics of *Eif2ak2*/EIF2AK2 expression

2348 would be necessary to better comprehend its pattern of regulation. In sum, our results indicate that *L.*

2349 *donovani* infection favors macrophage EIF2AK2 expression via -at least partially- mTORC1-dependent

2350 translation and potentially via IRF3-dependent transcription, which might affect parasite viability inside the

2351 macrophage.

2352

5.8　Host mTORC1 activation is detrimental for intracellular *L. donovani* survival as suggested by rapamycin pharmacological inhibition

The role of mTORC1 activity is commonly evaluated using chemical inhibitors such as rapamycin, a cell growth repressor and immunomodulator in numerous biological settings (Janes and Fruman 2009, Blagosklonny 2010). Rapamycin has been documented to be beneficial or detrimental in the resolution of viral, bacterial, and protozoan infections (Ozaki, Camara et al. 2005, Zhao, Liu et al. 2016, Huang, Hung et al. 2017, Rojas Marquez, Ana et al. 2018). In the case of *Leishmania* sp. infection, rapamycin effect has proven to be species- and context-specific with favorable (Pinheiro, Nunes et al. 2009, Jaramillo, Gomez et al. 2011, Dias, de Souza et al. 2018), negative (Cheekatla, Aggarwal et al. 2012, Franco, Fleuri et al. 2017, Kumar, Das et al. 2018, Duque, Serrao et al. 2021), or non-significant changes (Cyrino, Araujo et al. 2012, Phan, Baek et al. 2020) in parasite burden upon treatment. In our experimental model, rapamycin treatment leads to increased parasite burden *in vitro* (as measured by RT-qPCR and microscopical assessment, **Figs 3.6A and 5.2**), which suggests mTORC1 activation represents a host mechanism of parasite control during the early infection, although it is subsequently inhibited at approximately 8 hours post infection. Previous reports show how mTORC1 activity can promote translation of mitochondrial proteins (Morita, Gravel et al. 2013, Morita, Gravel et al. 2015), although this does not seem to be the case in our datasets since mitochondrial-associated mRNAs were found to be mostly downregulated. Notably, most of them have not been reported as mTORC1-dependent and those that have been documented as mTORC1-sensitive show no translational enrichment (**Fig 5.3**). Thus, in addition to translational repression of TOP mRNAs, rapamycin effect could be related to a yet undefined set of translationally mTORC1-regulated transcripts and/or to mTORC1 non-translational roles (Malik, Urbanska et al. 2013). In parallel, Moreira *et al* described how *L. infantum* -another VL causative *Leishmania* species- activates AMPK/SIRT1 signaling 10 hours post infection in response to increased AMP/ATP levels in primary murine macrophages to promote its own survival (Moreira, Rodrigues et al. 2015). AMPK and mTORC1 reciprocal inhibition is a determinant check point in response to changes in energy status (Gonzalez, Hall et al. 2020). Concomitantly, rapamycin has been reported to induce AMPK activation both *in vivo* (Hennig, Fiedler et al. 2017) and *in vitro* (Campos, Ziehe et al. 2016). Thus, rapamycin could be working synergistically with parasite-driven mechanisms for AMPK activation to counter mTORC1 as a nodal regulator in the host-parasite interaction during *L. donovani* infection.
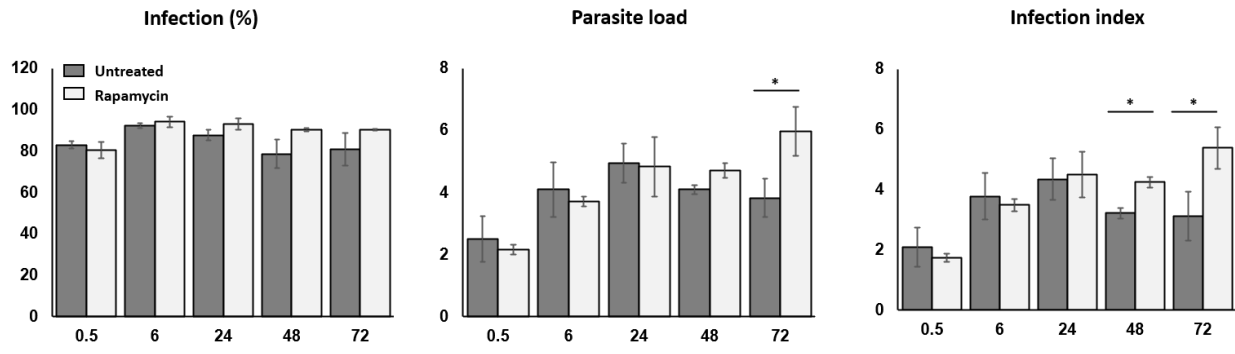
Infection (%) — {Infected macrophages (IM) / Total macrophages (M)}*100

Parasite load — Parasites (P) / Infected macrophages (IM)

Infection index — (IM/M) * (P/IM)

Figure 5.2. mTORC1 inhibition promotes *L. donovani* persistence *in vitro*. BMDM cultures were plated in glass coverslip-containing culture plates and treated with 20 nM rapamycin or an equivalent volume of DMSO (vehicle) for 2 h, then inoculated with *L. donovani* promastigotes (MOI=10). At the indicated time points glass coverslips were recovered, washed with PBS and stained with HEMA3 PROTOCOL as per the manufacturer indications. Non-phagocytized parasites were washed 6 hours post infection. Data are presented as mean ± SD (biological replicates, n=3). *$p < 0.05$ significance in a Student's t-test.
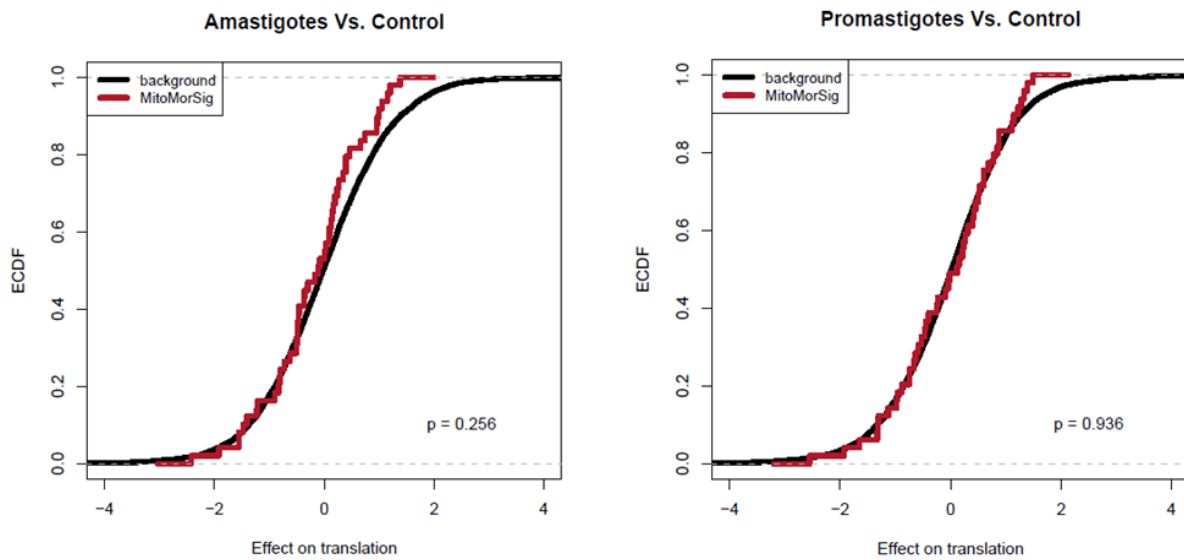
Figure 5.3. *L. donovani* infection does not affect mTORC1-driven translation of mitochondria-related transcripts. Empirical cumulative distribution function (ECDF) of translational efficiencies (infection vs. control) for the compilation of previously reported mTORC1-sensitive mitochondrial associated transcripts as compared to those of all detected transcripts (background). Differences in translational efficiencies between mTORC1-sensitive vs control transcripts were assessed per parasite stage.

5.9 eIF4A-dependent TGF translational upregulation concurrently with increased SMAD3 transcriptional activity suggests *L. donovani* infection triggers an autocrine signaling loop

In eukaryotes, scanning of 5' UTRs during translation initiation is an essential process that requires resolution of secondary RNA structures via eIF4A, a pivotal RNA helicase part of the trimeric eIF4F complex (Marintchev, Edmonds et al. 2009). G-quadruplexes (G-quads) are planar and stackable arrangements of

guanine tetrads in guanine-rich DNA and RNA sequences that have been associated with telomer stability, DNA transcription, replication, and eIF4A-dependent RNA translation (Rhodes and Lipps 2015). In a previous report, Wolfe *et al* described the role of G-quads and eIF4A in promoting translation of oncogenic markers including the cytokine TGFB1 (Wolfe, Singh et al. 2014). Furthermore, Modelska *et al* provided evidence that in addition to modulating *Tgfb1* translation, eIF4A inhibition was related to decreased TGFB1 signaling (Modelska, Turro et al. 2015). Our data indicate macrophages infected with *L. donovani* promastigotes or amastigotes favor translation of eIF4A-dependent transcripts (particularly with G-quad-containing 5' UTRs) including *Tgfb1*, which goes in accordance with increased phosphorylation of eIF4B, an important eIF4A activator (Holz, Ballif et al. 2021). TGFB1 expression has been reported as beneficial to *L. donovani* parasites through inhibition of IFNγ production and hampering of TLR4 signaling (Wilson, Young et al. 1998, Das, Pandey et al. 2012). Notably, in chapter 4 we show that part of the transcriptional signature of macrophages infected with promastigotes or amastigotes of *L. donovani* includes the upregulation of mRNAs associated to SMAD3 activation (e.g., *Atf4*, *Bcl2*, *Ccl2*, *Ccnd1*, *Ccnd2*, *Ctnnb1*, *Cxcl10*, *Dusp4*, *Gadd45b*, *Hmox1*, *Hsp90b1*, *Hspa5*, *Id2*, *Jag1*, *Jun*, *Lpar1*, *Mmp12*, *Mmp13*, *Myc*, *Net1*, *Pcna*, *Pmepa1*, *Por*, *Runx2*, *Spp1*, *Tnf*, and *Vim*), one of the main effectors in TGFB1 signaling (Abdel Mouti and Pauklin 2021). Additionally, we also found augmented translation levels of *Ep300*, an eIF4A-sensitive transcript encoding a SMAD2-4-interacting protein that facilitates TGFB1 transcriptional response by increasing chromatin accessibility (Abdel Mouti and Pauklin 2021). Furthermore, *L. donovani* cathepsin B-like cysteine proteases contribute to TGFB1 activating cleavage (Somanna, Mundodi et al. 2002), which could accentuate the cellular response to this cytokine. These observations suggest that *L. donovani* employs regulatory mechanisms of mRNA translation and abundance to induce the expression of an autocrine loop involving enhanced TGFB1 signaling placing eIF4A as a critical element of the host response to *L. donovani* infection.

5.10   Macrophage increased eIF4A activity is beneficial for *L. donovani* intracellular survival as suggested by silvestrol pharmacological inhibition

Rocaglates are cyclopenta[*b*]benzofuran flavaglines extracted form plants of the *Aglaia* genus (Pan, Woodard et al. 2014) and they also are among the most potent and better characterized eIF4A inhibitors (Chu and Pelletier 2015). Initially described for their insecticide properties (Janprasert, Satasook et al. 1992), rocaglates are also known for their antifungal (Harneti and Supratman 2021), antitumor (Cencic, Carrier et al. 2009) and anti-inflammatory activity (Baumann, Bohnenstengel et al. 2002, Proksch, Giaisi et al. 2005). Accumulating data strongly suggest eIF4A activity is essential in the progression of infectious processes. Their potential as antimalarials was reported by Langlais *et al* (Langlais, Cencic et al. 2018) with the synthetic rocaglate CR-1-31B targeting of both host and parasite eIF4A resulting in protection from cerebral malaria and decreased pathogen replication. This observation can be extended to bacterial infections since rocaglamide derivates were shown to affect macrophage polarization in synergy with IFNγ stimulation, which led to an increase in macrophage killing capacity against *Mycobacterium tuberculosis*

2435 (Bhattacharya, Chatterjee et al. 2016, Chatterjee, Yabaji et al. 2021). Additionally, silvestrol -a natural

2436 occurring rocaglate- has been documented to inhibit chikungunya virus replication in 293T and 3T3 cell

2437 lines (Henss, Scholz et al. 2018). Our results show that silvestrol -treatment of macrophages before *L.*

2438 *donovani* promastigote infection leads to a decreased intracellular parasite persistence (as measured by

2439 RT-qPCR and microscopical assessment, **Figs 3.6B and 5.4**). This could be related to a modulation of host

2440 eIF4A-driven translation including sensitive targes such as *Tgfb1* as aforementioned. In accordance with

2441 high homology (74-85.9%) between human/mouse and *Leishmania* eIF4A (Dhalia, Reis et al. 2005,

2442 Barhoumi, Tanner et al. 2006), silvestrol might be influencing *Leishmania* 4A since previous studies have

2443 shown the toxicity of eIF4A inhibitors against both extra- and intra-cellular parasite forms (Astelbauer,

2444 Obwaller et al. 2011, Harigua-Souiai, Abdelkrim et al. 2018). In sum, our results indicate *L. donovani*

2445 infection leads to an early activation of an eIF4A-driven translational program that is beneficial for parasite

2446 replication. PDCD4 is a natural interacting partner and eIF4A inhibitor (Yang, Jansen et al. 2003), it has

2447 been reported that mice deficient for PDCD4 expression show proclivity to develop B cell lymphomas,

2448 although they are resistant to inflammatory diseases such a diabetes as well as LPS insensitivity (Hilliard,

2449 Hilliard et al. 2006). Additionally, *Pdcd4*^{-/-} mice show reduced bacterial lung proliferation, which is

2450 associated with decreased inflammation (Cohen and Prince 2013). Thus, it would be interesting to evaluate

2451 expression levels of PDCD4 in *L. donovani*-infected macrophages as well as intracellular parasite burden

2452 in macrophages from *Pdcd4*^{-/-} mice compared with wild type counterparts. Additionally, we could use

2453 pharmacological treatment (i.e., eIF4A inhibitors) or genetic approaches (IF4A deficient or heterozygote

2454 mutant mice) to evaluate progression of visceral leishmaniasis when compared to wild type or untreated

2455 controls.
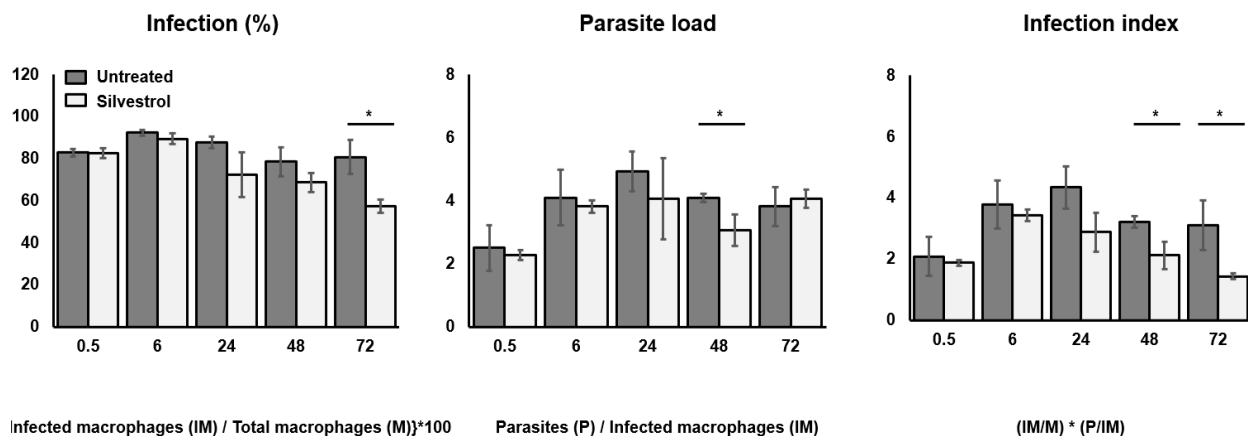
2456 Infected macrophages (IM) / Total macrophages (M)}*100   Parasites (P) / Infected macrophages (IM)   (IM/M) * (P/IM)

2457 **Figure 5.4. eIF4A inhibition dampens *L. donovani* persistence *in vitro*.** BMDM cultures were plated in glass coverslip-containing

2458 culture plates and treated with 25 nM silvestrol or an equivalent volume of DMSO (vehicle) for 2 h, then inoculated with *L. donovani*

2459 promastigotes (MOI=10). At the indicated time points glass coverslips were recovered, washed with PBS and stained with HEMA3

2460 PROTOCOL as per the manufacturer indications. Non-phagocytized parasites were washed 6 hours post infection. Data are presented

2461 as mean ± SD (biological replicates, n=3). *p < 0.05 significance in a Student's t-test.

5.11 *L. donovani* **amastigote infection favors increased abundance and translation of transcripts encoding cytoprotective regulators associated to DNA-repair**

L. donovani amastigotes exhibit tropism for internal organs (e.g., liver, bone marrow and spleen), where they can initiate a chronic inflammatory response characterized by increased TNF and IFNγ expression, which results in substantial tissue remodeling (i.e., splenomegaly) (Stanley and Engwerda 2007, Yurdakul, Dalton et al. 2011, Kong, Saldarriaga et al. 2017). Under these conditions, host DNA integrity can be compromised as a result of oxidative stress, a common antimicrobial strategy, leading to apoptosis activation (Slupphaug, Kavli et al. 2003). Concomitantly, DNA repair mechanisms can prove essential in the modulation of immune responses (Bednarski and Sleckman 2019). For example, knockout mice for the DNA repair kinase ATM show enhanced antibacterial and antiviral responses associated with increased DNA damage-sensing STING activity (Hartlova, Erttmann et al. 2015). In parallel, NBS1 (syn. NBN), a key member of the MRE11 DNA-damage-sensing complex (Pereira-Lopes, Tur et al. 2015), prevents macrophage attrition upon LPS-induced oxidative damage (Lopez-Sanz, Bernal et al. 2018). Similarly, Annexin 1 (ANXA1), a protein associated with DNA integrity protection (Nair, Hande et al. 2010), inhibits inflammation and promotes macrophage M2 polarization (Li, Cai et al. 2011, Cooray, Gobbetti et al. 2013). Our results indicate that upon *L. donovani* amastigote infection, transcripts encoding proteins associated with DNA repair and apoptosis inhibition show an increase in total levels (i.e., *Anxa1*, *Atm*, *Nbn*) and as shown in chapter three some showed favored translation (i.e., *Ercc6*, *Prkdc*, *Rif1*). This observation goes in agreement with proteomic data on *L. donovani*-infected human macrophages (Singh, Pandey et al. 2015) showing a similar upregulation of proteins associated with cytoprotective functions, which potentially affect disease progression. Certainly, although mice deficient for ANXA1 are equally able to control parasite infection as their wild type counterparts, they also develop significantly larger cutaneous lesions after *L. braziliensis* inoculation with a concurrent increase in TNF, IFNγ and nitric oxide production (Oliveira, Souza-Testasicca et al. 2017). Further studies evaluating parasite survival or immune markers on cells and tissues from mice deficient for members of the DNA-repair response including ANXA1 (Oliveira, Souza-Testasicca et al. 2017), ATM (Hartlova, Erttmann et al. 2015) and NBN (Difilippantonio, Celeste et al. 2005) might shed some light on the role of this pathway in the pathogenesis of *L. donovani* visceral leishmaniasis.

5.12 **Macrophage transcriptional and translational response to** *L. donovani* **amastigote infection highlights the potential role of phosphodiesterase 4B during infection**

L. donovani amastigote infection also featured the downregulation of different transcripts encoding signal transduction mediators. For example, cyclic-AMP (cAMP) was the first molecule described to act as a secondary messenger for different hormones (Sutherland, Robison et al. 1968), although it has proven to be central regulator of multiple processes such as learning, brain memory, heart muscle contraction and water uptake in the kidney (Cheng, Ji et al. 2008). Certainly, cAMP signaling is recognized as a notorious anti-inflammatory mechanism regulating nonphlogistic recruitment of monocytes/macrophages and inflammation resolution (Tavares, Negreiros-Lima et al. 2020). Intracellularly, cAMP levels are determined

2498   by the enzymatic equilibrium between its synthesis (i.e., adenylyl cyclases as the main source) and

2499   degradation (i.e., hydrolysis by phosphodiesterases) (Aslam and Ladilov 2022). Notably, it has been

2500   reported that in response to *L. donovani* infection, macrophage cAMP levels are increased in a mechanism

2501   dependent on PGE$_2$, which results in increased intracellular parasite survival (Saha, Biswas et al. 2014).

2502   Signaling through cAMP activates a number of effectors including PKA and EPAC, which in turn can also

2503   activate the energy sensor AMPK (Aslam and Ladilov 2022). Interestingly, activation of the AMPK/SIRT1

2504   axis was responsible for promoting parasite survival in macrophages infected with *L. infantum* (Moreira,

2505   Rodrigues et al. 2015). Our data indicate that the transcript encoding phosphodiesterase 4B (*Pde4b*), a

2506   member of the largest family of cAMP-hydrolyzing enzymes (Fertig and Baillie 2018), shows a significant

2507   decrease of both abundance and translation in macrophages upon *L. donovani* amastigote infection.

2508   Multiple pharmacological inhibitors of PDE4 have been developed and approved for the treatment of

2509   autoimmune diseases such as chronic obstructive pulmonary disease, psoriasis and psoriasis arthritis

2510   (Raker, Becker et al. 2016). Notably, chemical inhibition of PDE4B was reported to activate AMPK and

2511   promote mitochondrial synthesis (Park, Ahmad et al. 2021). Furthermore, cAMP signaling has proven to be

2512   pivotal for *L. donovani* since PDE4 inhibitors are able to hamper parasite survival both *in vivo* and *in vitro*

2513   (Saha, Bhattacharjee et al. 2020). Thus, PDE4B inhibitors might exert a dual function against the cAMP

2514   signaling pathway in both *L. donovani* parasites and its host in detriment of the former. Remarkably, the

2515   role of differential PDE4B expression during *L. donovani* infection and visceral leishmaniasis pathogenesis

2516   has not been explored, which places it as an ideal target for evaluating intracellular parasite survival.

2517   **5.13   Decreased *Icosl* mRNA abundance in *L. donovani* amastigote-infected macrophages could**

2518   **potentially affect splenic responses**

2519   Disruption of splenic functions is a hallmark of chronic VL as evidenced by splenomegaly and

2520   tissular microarchitecture loss (Yurdakul, Dalton et al. 2011). Concomitant with spleen remodeling, germinal

2521   center dysfunction has been reported for visceral leishmaniasis *in vivo* (Smelt, Engwerda et al. 1997, Silva,

2522   Andrade et al. 2012). For example, follicular CD4$^+$ T helper (Tfh) cells are a key component of the splenic

2523   white pulp providing signals for survival and differentiation to maturing B cells to ensure appropriate humoral

2524   responses (Crotty 2011). Similar to other specialized T helper subtypes, Tfh differentiation is controlled by

2525   a master transcriptional regulator (e.g., BCL6) (Hatzi, Nance et al. 2015), which can be activated via

2526   stimulation of the inducible T cell costimulator (ICOS) (Stone, Pepper et al. 2015). A link between

2527   macrophage expression of ICOS ligand (ICOSL) and Tfh production has been reported in mice infected

2528   with *Schistosoma japonicum* (Chen, Yang et al. 2014). ICOSL/ICOS physical interaction has been shown

2529   to inhibit FOXO1 and consequently activate the BCL6 transcriptional program leading to Tfh differentiation

2530   (Stone, Pepper et al. 2015). Thus, ICOSL expression in macrophages could be a determinant factor in B

2531   cell response through Tfh cell regulation. In a model of experimental VL it was reported that rhesus

2532   macaques failed to maintain Tfh cell population in the chronic stages of the disease, which was postulated

2533   to be associated with abnormal immune humoral responses (Rodrigues, Cordeiro-da-Silva et al. 2016). In

parallel, Perez-Cabezas *et al* showed that this phenomenon might be partially strain-specific in mice since a marked decrease of Tfh cells was observed in *L. infantum*-infected C57Bl/6 but not BALB/c nor Sv/129 mice (Perez-Cabezas, Cecilio et al. 2019). Our data indicates *Icosl* abundance was promptly inhibited in macrophages during *L. donovani* amastigote infection. It would be interesting to evaluate ICOSL expression levels on splenic macrophages in a model of experimental leishmaniasis. Additionally, the role of macrophage ICOSL expression in the promotion of Tfh cell differentiation *in vivo* and the onset of VL pathogenesis upon *L. donovani* infection of *Icosl*^{-/-} versus wild type mice remains to be defined.

5.14   Increased abundance of defense GTPases is elicited during *L. donovani* promastigote infection

Accumulating evidence show that in contrast to amastigote infection, promastigote-infected macrophages are capable of inducing various transcripts encoding different proinflammatory molecules (Rabhi, Rabhi et al. 2012, Dillon, Suresh et al. 2015, Fernandes, Dillon et al. 2016), including our report showing that *Leishmania* spp. promastigotes induce the expression of the membrane-bound CXCL16 chemokine (Chaparro, Leroux et al. 2019) (**See Appendix 5**). Certainly, our data indicate promastigote infection led to the upregulation of different immune defense activators. For example, immune-related GTPases including guanylate-binding proteins (GBPs) have been reported to form multimers of up to 6,000 units, which deposit on and destabilize *T. gondii*-containing PV membranes and *T. gondii* membrane itself leading to parasite killing (Degrandi, Konermann et al. 2007). In parallel, GBP-dependent disruption of actin polymerization has been shown to prevent intracellular Kaposi's sarcoma herpes virus delivery to the host cell nucleus (Zou, Meng et al. 2017) and *Burkholderia thailandensis* motility and proliferation (Place, Briard et al. 2020). In accordance with our results, previous reports identified a transcriptional upregulation of different GBPs following *L. major* infection *in vitro* (Frank, Marcu et al. 2015) and *in vivo* (Sohrabi, Volkova et al. 2018). Furthermore, Haldar *et al* showed that in murine fibroblasts, GBP2-dependent lysosomal recruitment to *L. donovani*-containing PVs constitutes an important parasite killing mechanism, however, while GBP2 expression was also shown to be induced in peritoneal macrophages, *L. donovani* survival was not affected by GBP2 activity (Haldar, Nigam et al. 2020). Certainly, GBP2 activity facilitated lysosomal fusion with *L. donovani* PVs in infected fibroblasts, while the authors argue that the capacity of *L. donovani* to modulate the macrophage autophagic machinery to promote its own survival might account for the cell type specific effect of GBP2 activity (Thomas, Nandan et al. 2018, Haldar, Nigam et al. 2020). Thus, our results indicating increased abundance levels of defense GTPases (i.e., *Gbp2*, *Gbp3*, *Gbp6*, *Gbp10*, *Igtp*, *Irgm1*, *Mx1*, *Tgtp1* and *Tgtp2*) following incubation with *L. donovani* promastigotes suggests macrophages are able to detect *L. donovani* infection and initiate microbicidal responses oriented to control pathogen proliferation despite parasite-driven mechanisms of self-preservation.

5.15 *L. donovani* **promastigotes promote macrophage mRNA abundance and translation efficiency of members of the ISGylation system**

These GTPases belong to a superfamily of Interferon-stimulated genes(ISGs) (Kim, Shenoy et al. 2012) and IPA predicted the transcriptional factors IRF3 and IRF7 as potential upstream regulators in accordance with a previous report of IFN-driven responses in leprosy patients (Teles, Lu et al. 2019). Among other ISGs, infection with *L. donovani* promastigotes led to transcriptional and translational upregulation of ISG15, a small ubiquitin-like modulator that can be covalently linked and thus affect the activity of different proteins in a process called ISGylation (Villarroya-Beltri, Guerra et al. 2017). This system depends on different activating E1 (e.g., UBA7), conjugating E2 (e.g., UBE2H) and E3 ligase enzymes (e.g., HERC6, ARIH1, TRIM25) in conjunction with different ubiquitin proteases (i.e., USP18) to modulate levels of ISG15 conjugation (Campbell and Lenschow 2013). For example, ISG15 can suppress NF-κB activation through association to PP2Cβ (Takeuchi, Kobayashi et al. 2006). Additionally, ISGylation can inhibit RIG-1 signaling and promote PKR activation independently of viral RNA stimulation (Kim, Hwang et al. 2008, Okumura, Okumura et al. 2013). Furthermore, activity of free (non-covalently bound) ISG15 has proven to be essential in the production of IFNγ as a mechanism conferring protection against mycobacterial infection (Bogunovic, Byun et al. 2012). Interestingly, the role of ISG15 in dampening inflammation was reported by Werneke *et al* during Chikungunya viral infection *in vivo* by showing that *Isg15*^{-/-} mice exhibit deregulated expression of multiple cytokines and chemokines leading to decreased host survival (Werneke, Schilte et al. 2011). Moreover, members of the ISGylation system were found to be downregulated in bovine macrophages infected with the protozoan parasite *Theileria annulate*, while treatment with the anti-theilerial drug buparvaquone led to ISG15, USP18 upregulation and parasite control (Oura, McKellar et al. 2006). In parallel, through ATG5 interactome analysis ISG15 was recently identified as a molecular bridge connecting IFNγ-driven induction of autophagy with *T. gondii* growth arrest in lung epithelial cells (Bhushan, Radke et al. 2020). Notably, ISG15 was reported to be upregulated in DCs upon infection by *L. braziliensis* (but not *L. amazonensis*) promastigotes and axenic amastigotes, although the role of this protein in leishmaniasis pathogenesis remains to be characterized (Vargas-Inchaustegui, Xin et al. 2008). In addition to favored *Isg15* abundance by both parasite stages and upregulated translation in the promastigote-infected dataset, our data showed increased abundance of *Herc6*, *Arih1* and *Usp18* in macrophages infected with *L. donovani* promastigotes, which suggests ISG15 signaling might be altered during infection. A previous report by *Villarroya-Beltri et al*, showed that ISGylation was determinant in exosome release on IFN-I-treated murine macrophages derived from *Isg15*^{-/-} or *Usp18*^{-/-} mice (Villarroya-Beltri, Baixauli et al. 2016). It has been reported that macrophage-derived exosomes exhibit antitumor activity and promote inflammation following infection by *M. avium*, *Salmonella typhimurium* and *T. gondii* (Bhatnagar and Schorey 2007, Bhatnagar, Shinagawa et al. 2007). Extensive work has been dedicated to the role of *Leishmania* sp-secreted exosomes during infection (Dong, Filho et al. 2019) but the role of macrophage-derived vesicles and the potential role of early ISGylation activation remains to be

2605 characterized. It would be worth evaluating if ISG15-modified targets are altered during infection as well as

2606 investigating VL progression in *Isg15*^{-/-} or *Usp18*^{-/-} mice upon *L. donovani* infection.

5.16 ***L. donovani* promastigote infection represses the abundance of transcripts encoding macrophage activating effectors**

2609 As discussed in chapter four and as described before, in addition to promoting the abundance of

2610 immune activators *L. donovani* promastigote infection induced the abundance of immune repressors (i.e.,

2611 *Cd274*, *Cd200*, and *Socs1*), with blockade of *Cd274* being beneficial for control of splenic parasite burden

2612 (Joshi, Rodriguez et al. 2009, Medina-Colorado, Osorio et al. 2017). Concomitantly, transcripts encoding

2613 various activators of macrophage immune functions were inhibited during infection. For example, NFAT

2614 activating protein with ITAM motif 1 mRNA (*Nfam1*) showed reduced levels in the PRO dataset. NFAM1

2615 was originally described as an activator of the transcriptional factor NFAT1 in the regulation of B cell

2616 development (Ohtsuka, Arase et al. 2004), although recently it has been shown to play a role in osteoclast

2617 formation (Sambandam, Sundaram et al. 2017) and proinflammatory cytokine production in monocytes

2618 (Juchem, Gounder et al. 2021). Interestingly, splenocytes from NFAT1 knockout mice showed augmented

2619 immune responses compared to wild type controls upon incubation with *L. major* promastigotes as

2620 measured by splenocyte proliferation through 3H-Thymidine incorporation (Xanthoudakis, Viola et al.

2621 1996). Furthermore, NFAM1 activity has been correlated to CCR2 expression (Long, Chen et al. 2020), the

2622 transcript of which (*Ccr2*) is coincidentally downregulated in the PRO dataset. Notably, CCR2 is reported

2623 to contribute to the protective response against *L. braziliensis* (Costa, Lima-Junior et al. 2016), while CCR2

2624 knockout mice showed decreased IFNγ expression (acute) and hepatic granuloma organization (acute and

2625 chronic) during an experimental model of *L. donovani* visceral leishmaniasis when compared to wild type

2626 counterparts (Sato, Kuziel et al. 1999). Nonetheless, the role of NFAM1 in the regulation of CCR2 and

2627 NFAT1 activity in the macrophage response to *L. donovani* infection or in the pathogenesis of visceral

2628 leishmaniasis remains to be established.

2629 In parallel, expression of the purinergic receptor P2X7 (*P2rx7*), a ubiquitous inducer of

2630 inflammasome and immune cell activation (Young and Gorecki 2018), was also repressed in macrophages

2631 infected with *L. donovani* promastigotes. P2RX7 is a ligand-gated cation channel that favors Ca^{2+} import in

2632 response to different stimuli including increased extracellular ATP levels (Li, Campbell et al. 2002), TLR

2633 activation (Babelova, Moreth et al. 2009), and ROS production (Munoz, Gao et al. 2017). The nematode

2634 *Trichuris suis* is known to inhibit P2RX7 to skew TLR4-driven inflammatory responses (Ottow, Klaver et al.

2635 2014). Additionally, this receptor plays an active role in mediating the intracellular killing of pathogens such

2636 as *M. marinum* (Matty, Knudsen et al. 2019) and *T. gondii* (Lees, Fuller et al. 2010). Moreover,

2637 macrophages infected with promastigotes of *L. amazonensis* increase P2XR7 expression as part of a host

2638 mechanism for infection control dependent on the production of leukotriene B4 (Chaves, Torres-Santos et

2639 al. 2009, Chaves, Sinflorio et al. 2019). In stark contrast, macrophages infected with *L. donovani* show

2640 decreased sensitivity to extracellular ATP, preventing caspase1 activation and macrophage cytolysis

2641 (Kushawaha, Pati Tripathi et al. 2022), which might be associated with a decrease in P2RX7 expression,
2642 although this remains to be validated.

2643   In sum, by means of RNAseq analysis of the early response of macrophages to infection with *L.*
2644 *donovani* promastigotes or amastigotes we identified a widespread yet selective reshaping of the host
2645 transcriptome and translatome through modulation of both mRNA abundance and translation, respectively.
2646 Accordingly, stage-specific transcriptional profiles pointed to the marked capacity of *L. donovani* amastigote
2647 infection to inhibit immune activation (i.e., *Icosl*, *Pde4b* modulation), whereas a distinctive ambivalence in
2648 this regard was highlighted in macrophages infected with *L. donovani* promastigotes (i.e., differential
2649 abundance levels of *Gbps*, *Isg15*, *Nfam1*, *P2rx7*). In contrast, similar translational patterns between
2650 amastigote- and promastigote-infected macrophages exhibited an enrichment of up- and downregulated
2651 transcripts associated with host immune (i.e., antigen presentation, GAIT complex assembly) and cellular
2652 processes (i.e., protein ubiquitylation, chromatin remodeling, RNA metabolism) with particular subsets with
2653 reported dependency on mTORC1 (i.e., *Pabpc1*, *Eif2ak2*) and eIF4A (i.e., *Tgfb1*) activities. Furthermore,
2654 pharmacological inhibition of mTORC1 and eIF4A proved effective in hampering or promoting intracellular
2655 parasite survival *in vitro* respectively. Thus, our data indicate that early regulation of macrophage gene
2656 expression identifies numerous targets that exhibit a significant therapeutic potential, which opens research
2657 avenues that would allow for a better understanding of the intricate network of effectors that tailor the host
2658 response to control or promote infection by *L. donovani* developmental stages.

2659

Chapter 6
Synthèse en français

6.1 Résumé

2661

2662   Les macrophages sont des phagocytes professionnels et ils font partie du premier mécanisme de
2663 défense du système immunitaire inné contre les organismes infectieux. Armés d'une batterie d'outils
2664 antimicrobiens et de nombreux récepteurs de reconnaissance des agents pathogènes et des dommages,
2665 les macrophages présentent une grande plasticité et des réponses adaptées au stress qui reposent (entre
2666 autres) sur la régulation de l'abondance et de la traduction de l'ARNm. Paradoxalement, les macrophages
2667 représentent la niche réplicative de différents agents pathogènes, y compris les parasites protozoaires du
2668 genre *Leishmania* (transmis par les phlébotomes), qui sont des agents responsables d'un éventail de
2669 maladies collectivement appelées leishmanioses. L'infection à *Leishmania donovani* conduit au
2670 développement de la leishmaniose viscérale (LV), avec une estimation de 200 000 à 400 000 cas et 20
2671 000 à 40 000 décès par année dans le monde. Suite à l'inoculation par des phlébotomes, les promastigotes
2672 phagocytés par les macrophages se transforment en la forme amastigote qui se propage aux organes et
2673 tissus internes tels que les ganglions lymphatiques, le foie, la rate et la moelle osseuse avec le
2674 développement concomitant de symptômes cliniques mortels lorsqu'ils ne sont pas traités. Pour favoriser
2675 leur propre survie, *L. donovani* subvertit les processus immunitaires et cellulaires des macrophages, y
2676 compris la modulation de l'expression des gènes. La modulation de l'abondance de l'ARNm a été largement
2677 rapportée dans les macrophages infectés par des virus, des bactéries et des parasites. Cependant, le rôle
2678 de la traduction au cours des infections reste peu exploré notamment pour les infections parasitaires
2679 protozoaires. Des études *in vitro* à haut débit indiquent que l'infection à *L. donovani* induit une perturbation
2680 généralisée de l'abondance de l'ARNm et des protéines, bien que la majorité de ces changements aient
2681 été documentés plus de 12 heures après l'infection, sans tenir compte des événements précoces qui
2682 pourraient affecter la progression de l'infection (c.-à-d. la modulation de la formation de vacuoles
2683 parasitophores, stress oxydant, activité des facteurs de transcription, initiation de l'apoptose) ou elles ont
2684 été réalisées en utilisant le promastigote au lieu de l'amastigote qui est la forme plus cliniquement pertinent.
2685 De plus, le rôle du contrôle de la traduction des macrophages au cours de l'infection à *L. donovani* reste à
2686 déterminer.

2687   Ici, en utilisant le « Polysome profiling » couplé à la quantification de le RNAseq, nous avons généré
2688 des profils de l'abondance et de la traduction de l'ARNm à partir de macrophages infectés ou non par des
2689 amastigotes et des promastigotes de *L. donovani* 6 heures après l'infection. En utilisant une combinaison
2690 d'outils bio-informatiques et biochimiques, nous avons identifié une régulation stade spécifique de
2691 l'abondance de l'ARNm des macrophages. Les modifications induites par les amastigotes étaient enrichies
2692 de transcrits régulés à la hausse codant pour des protéines associées aux mécanismes de réparation de
2693 l'ADN, tandis que ceux codant pour les facteurs de présentation d'antigène et d'activation des macrophages
2694 étaient nettement régulés à la baisse. En parallèle, une régulation positive des inhibiteurs immunitaires
2695 ainsi qu'une signature transcriptionnelle antioxydante associée à l'activité de NRF2 ont été identifiées dans
2696 des ensembles de données des macrophages infectés par des promastigotes. De plus, le regroupement
2697 hiérarchique des ARNm associés à l'activité transcriptionnelle de l'IRF3 et de l'IRF7 suggère que les

2698 macrophages activent des voies antimicrobiennes lors de l'infection par les promastigotes de *L. donovani*.

2699 À l'inverse, les modifications de l'efficacité de la traduction se sont avérées similaires dans les ensembles

2700 de données des macrophages infectés par les amastigotes et les promastigotes par rapport aux témoins

2701 non infectés. Les analyses d'ontologie génique sur les transcrits régulés traductionnellement ont montré un

2702 enrichissement des catégories régulées à la hausse associées au métabolisme de l'ARN (c.-à-d. le

2703 remodelage de la chromatine, la transcription, l'épissage, le transport, la stabilité et la traduction) et - de la

2704 même manière que l'analyse de l'abondance de l'ARNm - la régulation à la baisse des activateurs

2705 immunitaires des macrophages. Notamment, des sous-ensembles de transcrits sensibles à mTORC1 et

2706 eIF4A ont été identifiés, notamment PABPC1 et EIF2AK2, dont l'expression a été inhibée par le traitement

2707 à la rapamycine et TGFB1, qui s'est avéré affecté après incubation avec le rocaglate silvestrol. De plus, la

2708 signification biologique des activités mTORC1 et eIF4A au cours de l'infection à *L. donovani* a été mise en

2709 évidence via une analyse de survie intracellulaire in vitro indiquant que la survie du parasite est favorisée

2710 ou compromise en présence de rapamycine ou de silvestrol respectivement. En somme, l'infection par des

2711 promastigotes et des amastigotes de *L. donovani* entraîne des altérations précoces généralisées mais

2712 sélectives de l'expression des gènes des macrophages, notamment l'abondance de l'ARNm et l'efficacité

2713 de la traduction, qui peuvent adapter les réponses protectrices et nocives pour l'hôte, soulignant le potentiel

2714 thérapeutique des mécanismes moléculaires régulant ces événements.

2715

6.2 Sommaire du premier article : Le profilage translationnel des macrophages infectés par *Leishmania donovani* identifie des transcrits liés au système immunitaire sensibles à mTOR et eIF4A.

La leishmaniose viscérale (LV) est une maladie transmise par les phlébotomes et causée par des parasites protozoaires du complexe *Leishmania donovani* (par exemple *L. donovani*, *L. infantum*) (Alvar, Velez et al. 2012). La LV est endémique dans les régions tropicales et subtropicales du monde et se caractérise par fièvre irrégulière, perte de poids, splénomégalie, anémie et hypergammaglobulinémie (Burza, Croft et al. 2018). Entre 200 000 et 400 000 cas de LV se produisent chaque année et la maladie est généralement mortelle si non traitée (Alvar, Velez et al. 2012). Après la piqûre de phlébotome, les promastigotes sont phagocytés par les macrophages où ils résident dans des compartiments vacuolaires ou phagolysosomes. Ensuite, les promastigotes se différencient en la forme non mobile ou amastigote qui est responsable des symptômes cliniques chez l'humain (Burza, Croft et al. 2018). Dans le cadre du système immunitaire, les macrophages sont armés d'un large éventail d'outils microbicides qui peuvent cibler et éliminer les agents pathogènes envahisseurs ainsi que moduler la réponse immunitaire (Areschoug and Gordon 2008). Pour survivre dans cet environnement hostile, les parasites du genre *Leishmania* détournent de nombreux processus cellulaires et immunologiques des macrophages à leur avantage, y compris les profils d'expression génique (Podinovskaia and Descoteaux 2015). Une vaste documentation recueillie au cours de l'infection des macrophages par différentes espèces de *Leishmania* indique que l'abondance de l'ARNm est fortement affectée par ce parasite protozoaire (Gregory, Sladek et al. 2008, Rabhi, Rabhi et al. 2012, Rabhi, Rabhi et al. 2016, Shadab, Das et al. 2019, Mesquita, Ferreira et al. 2020). Cependant, il reste à savoir si cela est aussi le cas pour la traduction de l'ARNm.

Dans ce travail, nous avons utilisé le profilage des polysomes quantifié par RNAseq pour évaluer les changements de traduction des ARNm dans les macrophages primaires (dérivés de la moelle osseuse de souris) infectées par des promastigotes ou des amastigotes de *L. donovani* pendant 6 heures *in vitro*. Nous avons identifié 9 442 transcrits codant pour des protéines dans des échantillons infectés et des témoins non infectés et environ un tiers d'entre eux (32,9 %, 3 108 au total) ont été affectés de façon traductionnelle pendant l'infection. Notamment, la plupart des ARNm (95%) présentant des niveaux différentiels de traduction étaient courants parmi les ensembles de données provenant des macrophages infectés par des promastigotes ou des amastigotes. De plus, des analyses *in silico* d'ontologie de gènes (GO) ont identifié des sous-ensembles fonctionnels de transcrits régulés par la traduction soit régulés positivement (c.-à-d. associés au métabolisme de l'ARNm, au remodelage de la chromatine, à la déubiquitination) soit régulés négativement (c.-à-d. associés à la présentation de l'antigène, à l'organisation des organites, au transport intracellulaire). De plus, nous avons trouvé un enrichissement des ARNm avec des motifs 5' UTR associés à la régulation par l'activité du mTORC1 et d'eIF4A, deux régulateurs centraux de la traduction des ARNm. En lien avec ces résultats, l'analyse biochimique a montré que la phosphorylation des cibles en aval de l'activité mTORC1 (c.-à-d. rpS6K1, rpS6 et 4E-BP1) ainsi que de

l'agoniste d'eIF4A, eIF4B, était augmentée dans les macrophages au début de l'infection par les promastigotes ou les amastigotes de *L. donovani*. Des transcrits sélectionnés associés à l'activité mTORC1 (PABPC1, EIF2AK2) ou eIF4A (TGFB1) ont été validés au niveau de l'ARNm et des protéines. De plus, l'inhibition pharmacologique de mTORC1 avec du Torin-1 (inhibiteur du site actif) ou de la rapamycine (inhibiteur allostérique) et d'eIF4A avec du silvestrol (rocaglate naturel) a diminué la régulation à la hausse des protéines dépendantes de l'infection par *L. donovani* (PABPC1, EIF2AK2 et TGFB1) sans effet global sur l'abondance d'ARNm. Enfin, le prétraitement des macrophages avec de la rapamycine ou du silvestrol entraîne respectivement une augmentation ou une diminution de la survie intracellulaire de *L. donovani*, ce qui indique l'importance de l'activité des régulateurs de traduction mTORC1 et eIF4A dans la réponse de l'hôte contre le pathogène. En conclusion, l'infection par *L. donovani* provoque un remodelage sélectif du translatome des macrophages de sorte que certains de ces changements favorisent ou antagonisent la survie du parasite. Ainsi, ces résultats ouvrent la voie à l'étude du contrôle traductionnel de l'hôte comme potentielle cible de développement thérapeutique.

6.3 Sommaire du deuxième article : Le profilage transcriptionnel des macrophages révèle des signatures distinctives liées au stade du parasite au cours de l'infection précoce par *Leishmania donovani*.

La modulation de l'expression des gènes fait partie intégrale de la réponse des macrophages lors de l'infection par différents agents pathogènes (Chaussabel, Semnani et al. 2003). Les parasites du genre *Leishmania* sont des agents responsables d'un éventail de maladies connues collectivement sous le nom de leishmanioses avec des manifestations cliniques allant de lésions dermiques légères à des infections viscérales potentiellement mortelles (Burza, Croft et al. 2018). L'accumulation de données indique que différentes espèces de *Leishmania* introduisent des changements généralisés dans les niveaux d'abondance de l'ARNm des macrophages pour favoriser sa propre survie, affectant de nombreux processus cellulaires et immunologiques (Gregory, Sladek et al. 2008, Rabhi, Rabhi et al. 2012, Rabhi, Rabhi et al. 2016, Shadab, Das et al. 2019). Cependant, la plupart des données transcriptomiques des macrophages infectés par *L. donovani* (l'un des agents responsables de la LV mortelle) ont été réalisées plus de 12 heures après l'infection, laissant une fenêtre où des réponses clés de l'hôte peuvent affecter ou être provoquées par des modifications de l'expression de l'ARNm. Au moyen du séquençage de l'ARN, nous avons caractérisé les changements précoces (6 h) d'abondance de l'ARNm des macrophages au cours de l'infection par les amastigotes et promastigotes de *L. donovani*. Un total de 10 à 16 % des ARNm de macrophages présentaient des niveaux d'abondance différentiels lorsqu'ils étaient infectés par *L. donovani* et environ un tiers de ces changements étaient spécifiques au stade du parasite. Des analyses *in silico* ont identifié des catégories associées aux fonctions immunitaires (par exemple, la présentation de l'antigène et l'activation des leucocytes) parmi les ARNm significativement régulés négativement au cours de l'infection par les amastigotes, tandis que les catégories liées à la cytoprotection (par exemple, la réparation de l'ADN et l'inhibition de l'apoptose) étaient enrichies en transcrits régulés positivement. Notamment, l'ensemble de données provenant des macrophages infectés par les promastigotes présentaient une combinaison de transcrits liés à l'immunité régulés positivement (par exemple, réponse cellulaire à l'IFNβ) et réprimés (par exemple, activation des leucocytes, chimiotaxie). De plus, nous avons utilisé IPA pour identifier les modèles de régulation associés aux régulateurs transcriptionnels en amont dans nos ensembles de données, identifiant avec succès des signatures enrichies d'ARNm associées à l'inhibition de STAT1 dans les macrophages infectés par les amastigotes de *L. donovani* et l'activation de NRF2, IRF3, IRF7 dans les cellules infectées par les promastigotes. Puis, en plus des résultats présentés au chapitre trois décrivant le remodelage du translatome des macrophages au cours de l'infection par amastigotes et promastigotes de *L. donovani* (Chaparro, Leroux et al. 2020), nous avons constaté ici que les macrophages infectés présentent aussi des changements spécifiques au stade de vie du parasite dans les niveaux totaux d'ARNm codant pour des protéines qui pourraient adapter à la fois les réponses protectrices et délétères lors d'une infection parasitaire.

REFERENCES

Abdel-Nour, M., L. A. M. Carneiro, J. Downey, J. Tsalikis, A. Outlioua, D. Prescott, L. S. Da Costa, E. S. Hovingh, A. Farahvash, R. G. Gaudet, R. Molinaro, R. van Dalen, C. C. Y. Lau, F. C. Azimi, N. K. Escalante, A. Trotman-Grant, J. E. Lee, S. D. Gray-Owen, M. Divangahi, J. J. Chen, D. J. Philpott, D. Arnoult and S. E. Girardin (2019). "The heme-regulated inhibitor is a cytosolic sensor of protein misfolding that controls innate immune signaling." Science **365**(6448).

Abdel Mouti, M. and S. Pauklin (2021). "TGFB1/INHBA Homodimer/Nodal-SMAD2/3 Signaling Network: A Pivotal Molecular Target in PDAC Treatment." Mol Ther **29**(3): 920-936.

Abdelkrim, Y. Z., E. Harigua-Souiai, M. Barhoumi, J. Banroques, A. Blondel, I. Guizani and N. K. Tanner (2018). "The steroid derivative 6-aminocholestanol inhibits the DEAD-box helicase eIF4A (LieIF4A) from the Trypanosomatid parasite Leishmania by perturbing the RNA and ATP binding sites." Mol Biochem Parasitol **226**: 9-19.

Abidin, B. M., A. Hammami, S. Stager and K. M. Heinonen (2017). "Infection-adapted emergency hematopoiesis promotes visceral leishmaniasis." PLoS Pathog **13**(8): e1006422.

Akhoundi, M., K. Kuhls, A. Cannet, J. Votypka, P. Marty, P. Delaunay and D. Sereno (2016). "A Historical Overview of the Classification, Evolution, and Dispersion of Leishmania Parasites and Sandflies." PLoS Negl Trop Dis **10**(3): e0004349.

Alvar, J., I. D. Velez, C. Bern, M. Herrero, P. Desjeux, J. Cano, J. Jannin and M. den Boer (2012). "Leishmaniasis worldwide and global estimates of its incidence." PLoS One **7**(5): e35671.

Amprey, J. L., G. F. Spath and S. A. Porcelli (2004). "Inhibition of CD1 expression in human dendritic cells during intracellular infection with Leishmania donovani." Infect Immun **72**(1): 589-592.

Anderson, P. and N. Kedersha (2009). "RNA granules: post-transcriptional and epigenetic modulators of gene expression." Nat Rev Mol Cell Biol **10**(6): 430-436.

Andreou, A. Z. and D. Klostermeier (2014). "eIF4B and eIF4G jointly stimulate eIF4A ATPase and unwinding activities by modulation of the eIF4A conformational cycle." J Mol Biol **426**(1): 51-61.

Andresen, E., G. Gunther, J. Bullwinkel, C. Lange and H. Heine (2011). "Increased expression of beta-defensin 1 (DEFB1) in chronic obstructive pulmonary disease." PLoS One **6**(7): e21898.

Andreu, N., J. Phelan, P. F. de Sessions, J. M. Cliff, T. G. Clark and M. L. Hibberd (2017). "Primary macrophages and J774 cells respond differently to infection with Mycobacterium tuberculosis." Sci Rep **7**: 42225.

Andrews, K. T., G. Fisher and T. S. Skinner-Adams (2014). "Drug repurposing and human parasitic protozoan diseases." Int J Parasitol Drugs Drug Resist **4**(2): 95-111.

2833   Araki, K., M. Morita, A. G. Bederman, B. T. Konieczny, H. T. Kissick, N. Sonenberg and R. Ahmed (2017).

2834   "Translation is actively regulated during the differentiation of CD8(+) effector T cells." Nat

2835   Immunol **18**(9): 1046-1057.

2836   Arango Duque, G., M. Fukuda, S. J. Turco, S. Stager and A. Descoteaux (2014). "Leishmania promastigotes

2837   induce cytokine secretion in macrophages through the degradation of synaptotagmin XI." J

2838   Immunol **193**(5): 2363-2372.

2839   Areschoug, T. and S. Gordon (2008). "Pattern recognition receptors and their role in innate immunity:

2840   focus on microbial protein ligands." Contrib Microbiol **15**: 45-60.

2841   Aronson, N. E. and C. A. Joya (2019). "Cutaneous Leishmaniasis: Updates in Diagnosis and Management."

2842   Infect Dis Clin North Am **33**(1): 101-117.

2843   Asad, M., A. Sabur, M. Shadab, S. Das, M. Kamran, N. Didwania and N. Ali (2019). "EB1-3 Chain of IL-35

2844   Along With TGF-beta Synergistically Regulate Anti-leishmanial Immunity." Front Immunol **10**: 616.

2845   Asgari, Q., F. Gholizadeh, M. Nohtani, M. Mirzaeipour, M. Zare and M. S. Bahreini (2019). "Cutaneous

2846   leishmaniasis associated with Systemic Lupus Erythematosus (SLE)." Infez Med **27**(3): 345-349.

2847   Aslam, M. and Y. Ladilov (2022). "Emerging Role of cAMP/AMPK Signaling." Cells **11**(2).

2848   Astelbauer, F., A. Obwaller, A. Raninger, B. Brem, H. Greger, M. Duchene, W. Wernsdorfer and J.

2849   Walochnik (2011). "Anti-leishmanial activity of plant-derived acridones, flavaglines, and sulfur-

2850   containing amides." Vector Borne Zoonotic Dis **11**(7): 793-798.

2851   Atayde, V. D., A. da Silva Lira Filho, V. Chaparro, A. Zimmermann, C. Martel, M. Jaramillo and M. Olivier

2852   (2019). "Exploitation of the Leishmania exosomal pathway by Leishmania RNA virus 1." Nat

2853   Microbiol **4**(4): 714-723.

2854   Babelova, A., K. Moreth, W. Tsalastra-Greul, J. Zeng-Brouwers, O. Eickelberg, M. F. Young, P. Bruckner, J.

2855   Pfeilschifter, R. M. Schaefer, H. J. Grone and L. Schaefer (2009). "Biglycan, a danger signal that

2856   activates the NLRP3 inflammasome via toll-like and P2X receptors." J Biol Chem **284**(36): 24035-

2857   24048.

2858   Bain, C. C., A. Bravo-Blas, C. L. Scott, E. G. Perdiguero, F. Geissmann, S. Henri, B. Malissen, L. C. Osborne,

2859   D. Artis and A. M. Mowat (2014). "Constant replenishment from circulating monocytes maintains

2860   the macrophage pool in the intestine of adult mice." Nat Immunol **15**(10): 929-937.

2861   Bardazzi, F., F. Giacomini, F. Savoia, C. Misciali and A. Patrizi (2010). "Discoid chronic lupus erythematosus

2862   at the site of a previously healed cutaneous leishmaniasis: an example of isotopic response."

2863   Dermatol Ther **23 Suppl 2**: S44-46.

Barhoumi, M., N. K. Tanner, J. Banroques, P. Linder and I. Guizani (2006). "Leishmania infantum LeIF protein is an ATP-dependent RNA helicase and an eIF4A-like factor that inhibits translation in yeast." FEBS J **273**(22): 5086-5100.

Bartel, D. P. (2004). "MicroRNAs: genomics, biogenesis, mechanism, and function." Cell **116**(2): 281-297.

Baumann, B., F. Bohnenstengel, D. Siegmund, H. Wajant, C. Weber, I. Herr, K. M. Debatin, P. Proksch and T. Wirth (2002). "Rocaglamide derivatives are potent inhibitors of NF-kappa B activation in T-cells." J Biol Chem **277**(47): 44791-44800.

Beattie, L., R. Phillips, N. Brown, B. M. Owens, N. Chauhan, J. E. Dalton and P. M. Kaye (2011). "Interferon regulatory factor 7 contributes to the control of Leishmania donovani in the mouse liver." Infect Immun **79**(3): 1057-1066.

Bednarski, J. J. and B. P. Sleckman (2019). "At the intersection of DNA damage and immune responses." Nat Rev Immunol **19**(4): 231-242.

Ben-Neriah, Y. (2002). "Regulatory functions of ubiquitination in the immune system." Nat Immunol **3**(1): 20-26.

Bennis, I., V. De Brouwere, Z. Belrhiti, H. Sahibi and M. Boelaert (2018). "Psychosocial burden of localised cutaneous Leishmaniasis: a scoping review." BMC Public Health **18**(1): 358.

Berzunza-Cruz, M., A. Rodriguez-Moreno, G. Gutierrez-Granados, C. Gonzalez-Salazar, C. R. Stephens, M. Hidalgo-Mihart, C. F. Marina, E. A. Rebollar-Tellez, D. Bailon-Martinez, C. D. Balcells, C. N. Ibarra-Cerdena, V. Sanchez-Cordero and I. Becker (2015). "Leishmania (L.) mexicana infected bats in Mexico: novel potential reservoirs." PLoS Negl Trop Dis **9**(1): e0003438.

Besic, V., F. Habibolahi, B. Noel, S. Rupp, A. Genovesio and A. Lebreton (2020). "Coordination of transcriptional and translational regulations in human epithelial cells infected by Listeria monocytogenes." RNA Biol **17**(10): 1492-1507.

Beyrer, C., J. C. Villar, V. Suwanvanichkij, S. Singh, S. D. Baral and E. J. Mills (2007). "Neglected diseases, civil conflicts, and the right to health." Lancet **370**(9587): 619-627.

Bhat, M., N. Robichaud, L. Hulea, N. Sonenberg, J. Pelletier and I. Topisirovic (2015). "Targeting the translation machinery in cancer." Nat Rev Drug Discov **14**(4): 261-278.

Bhatnagar, S. and J. S. Schorey (2007). "Exosomes released from infected macrophages contain Mycobacterium avium glycopeptidolipids and are proinflammatory." J Biol Chem **282**(35): 25779-25789.

Bhatnagar, S., K. Shinagawa, F. J. Castellino and J. S. Schorey (2007). "Exosomes released from macrophages infected with intracellular pathogens stimulate a proinflammatory response in vitro and in vivo." Blood **110**(9): 3234-3244.

Bhatt, D. M., A. Pandya-Jones, A. J. Tong, I. Barozzi, M. M. Lissner, G. Natoli, D. L. Black and S. T. Smale (2012). "Transcript dynamics of proinflammatory genes revealed by sequence analysis of subcellular RNA fractions." Cell **150**(2): 279-290.

Bhattacharjee, A., S. Majumder, S. Das, S. Ghosh, S. Biswas and S. Majumdar (2016). "Leishmania donovani-Induced Prostaglandin E2 Generation Is Critically Dependent on Host Toll-Like Receptor 2-Cytosolic Phospholipase A2 Signaling." Infect Immun **84**(10): 2963-2973.

Bhattacharya, B., S. Chatterjee, W. G. Devine, L. Kobzik, A. B. Beeler, J. A. Porco, Jr. and I. Kramnik (2016). "Fine-tuning of macrophage activation using synthetic rocaglate derivatives." Sci Rep **6**: 24409.

Bhushan, J., J. B. Radke, Y. C. Perng, M. McAllaster, D. J. Lenschow, H. W. Virgin and L. D. Sibley (2020). "ISG15 Connects Autophagy and IFN-gamma-Dependent Control of Toxoplasma gondii Infection in Human Cells." mBio **11**(5).

Biedenkopf, N., K. Lange-Grunweller, F. W. Schulte, A. Weisser, C. Muller, D. Becker, S. Becker, R. K. Hartmann and A. Grunweller (2017). "The natural compound silvestrol is a potent inhibitor of Ebola virus replication." Antiviral Res **137**: 76-81.

Birhanu, H., R. Fikru, M. Said, W. Kidane, T. Gebrehiwot, A. Hagos, T. Alemu, T. Dawit, D. Berkvens, B. M. Goddeeris and P. Buscher (2015). "Epidemiology of Trypanosoma evansi and Trypanosoma vivax in domestic animals from selected districts of Tigray and Afar regions, Northern Ethiopia." Parasit Vectors **8**: 212.

Biyani, N. and R. Madhubala (2012). "Quantitative proteomic profiling of the promastigotes and the intracellular amastigotes of Leishmania donovani isolates identifies novel proteins having a role in Leishmania differentiation and intracellular survival." Biochim Biophys Acta **1824**(12): 1342-1350.

Blagosklonny, M. V. (2010). "Revisiting the antagonistic pleiotropy theory of aging: TOR-driven program and quasi-program." Cell Cycle **9**(16): 3151-3156.

Bogunovic, D., M. Byun, L. A. Durfee, A. Abhyankar, O. Sanal, D. Mansouri, S. Salem, I. Radovanovic, A. V. Grant, P. Adimi, N. Mansouri, S. Okada, V. L. Bryant, X. F. Kong, A. Kreins, M. M. Velez, B. Boisson, S. Khalilzadeh, U. Ozcelik, I. A. Darazam, J. W. Schoggins, C. M. Rice, S. Al-Muhsen, M. Behr, G. Vogt, A. Puel, J. Bustamante, P. Gros, J. M. Huibregtse, L. Abel, S. Boisson-Dupuis and J. L. Casanova

2925   (2012). "Mycobacterial disease and impaired IFN-gamma immunity in humans with inherited
2926   ISG15 deficiency." <u>Science</u> **337**(6102): 1684-1688.
2927 Bonnardel, J. and M. Guilliams (2018). "Developmental control of macrophage function." <u>Curr Opin</u>
2928   <u>Immunol</u> **50**: 64-74.
2929 Boone, D. L., E. E. Turer, E. G. Lee, R. C. Ahmad, M. T. Wheeler, C. Tsui, P. Hurley, M. Chien, S. Chai, O.
2930   Hitotsumatsu, E. McNally, C. Pickart and A. Ma (2004). "The ubiquitin-modifying enzyme A20 is
2931   required for termination of Toll-like receptor responses." <u>Nat Immunol</u> **5**(10): 1052-1060.
2932 Bou-Nader, C., J. M. Gordon, F. E. Henderson and J. Zhang (2019). "The search for a PKR code-differential
2933   regulation of protein kinase R activity by diverse RNA and protein regulators." <u>RNA</u> **25**(5): 539-
2934   556.
2935 Bouazizi-Ben Messaoud, H., M. Guichard, P. Lawton, I. Delton and S. Azzouz-Maache (2017). "Changes in
2936   Lipid and Fatty Acid Composition During Intramacrophagic Transformation of Leishmania
2937   donovani Complex Promastigotes into Amastigotes." <u>Lipids</u> **52**(5): 433-441.
2938 Box, J. K., N. Paquet, M. N. Adams, D. Boucher, E. Bolderson, K. J. O'Byrne and D. J. Richard (2016).
2939   "Nucleophosmin: from structure and function to disease development." <u>BMC Mol Biol</u> **17**(1): 19.
2940 Brinegar, A. E. and T. A. Cooper (2016). "Roles for RNA-binding proteins in development and disease."
2941   <u>Brain Res</u> **1647**: 1-8.
2942 Brittingham, A., C. J. Morrison, W. R. McMaster, B. S. McGwire, K. P. Chang and D. M. Mosser (1995). "Role
2943   of the Leishmania surface protease gp63 in complement fixation, cell adhesion, and resistance to
2944   complement-mediated lysis." <u>J Immunol</u> **155**(6): 3102-3111.
2945 Brykczynska, U., M. Geigges, S. J. Wiedemann, E. Dror, M. Boni-Schnetzler, C. Hess, M. Y. Donath and R.
2946   Paro (2020). "Distinct Transcriptional Responses across Tissue-Resident Macrophages to Short-
2947   Term and Long-Term Metabolic Challenge." <u>Cell Rep</u> **30**(5): 1627-1643 e1627.
2948 Buates, S. and G. Matlashewski (2001). "General suppression of macrophage gene expression during
2949   Leishmania donovani infection." <u>J Immunol</u> **166**(5): 3416-3422.
2950 Burza, S., S. L. Croft and M. Boelaert (2018). "Leishmaniasis." <u>Lancet</u> **392**(10151): 951-970.
2951 Butovsky, O., M. P. Jedrychowski, C. S. Moore, R. Cialic, A. J. Lanser, G. Gabriely, T. Koeglsperger, B. Dake,
2952   P. M. Wu, C. E. Doykan, Z. Fanek, L. Liu, Z. Chen, J. D. Rothstein, R. M. Ransohoff, S. P. Gygi, J. P.
2953   Antel and H. L. Weiner (2014). "Identification of a unique TGF-beta-dependent molecular and
2954   functional signature in microglia." <u>Nat Neurosci</u> **17**(1): 131-143.
2955 Buttgereit, F. and M. D. Brand (1995). "A hierarchy of ATP-consuming processes in mammalian cells."
2956   <u>Biochem J</u> **312 (Pt 1)**: 163-167.

2957 Cai, Y., H. Chen, X. Mo, Y. Tang, X. Xu, A. Zhang, Z. Lun, F. Lu, Y. Wang and J. Shen (2014). "Toxoplasma
2958   gondii inhibits apoptosis via a novel STAT3-miR-17-92-Bim pathway in macrophages." <u>Cell Signal</u>
2959   **26**(6): 1204-1212.

2960 Cai, Y., J. Su, N. Wang, W. Zhao, M. Zhu and S. Su (2020). "Comprehensive analysis of the ubiquitome in
2961   rabies virus-infected brain tissue of Mus musculus." <u>Vet Microbiol</u> **241**: 108552.

2962 Campbell, J. A. and D. J. Lenschow (2013). "Emerging roles for immunomodulatory functions of free
2963   ISG15." <u>J Interferon Cytokine Res</u> **33**(12): 728-738.

2964 Campos, T., J. Ziehe, F. Fuentes-Villalobos, O. Riquelme, D. Pena, R. Troncoso, S. Lavandero, V. Morin, R.
2965   Pincheira and A. F. Castro (2016). "Rapamycin requires AMPK activity and p27 expression for
2966   promoting autophagy-dependent Tsc2-null cell survival." <u>Biochim Biophys Acta</u> **1863**(6 Pt A):
2967   1200-1207.

2968 Cantanhede, L. M., C. F. da Silva Junior, M. M. Ito, K. P. Felipin, R. Nicolete, J. M. Salcedo, R. Porrozzi, E.
2969   Cupolillo and G. Ferreira Rde (2015). "Further Evidence of an Association between the Presence
2970   of Leishmania RNA Virus 1 and the Mucosal Manifestations in Tegumentary Leishmaniasis
2971   Patients." <u>PLoS Negl Trop Dis</u> **9**(9): e0004079.

2972 Capelli-Peixoto, J., S. N. Mule, F. T. Tano, G. Palmisano and B. S. Stolf (2019). "Proteomics and
2973   Leishmaniasis: Potential Clinical Applications." <u>Proteomics Clin Appl</u> **13**(6): e1800136.

2974 Caput, D., B. Beutler, K. Hartog, R. Thayer, S. Brown-Shimer and A. Cerami (1986). "Identification of a
2975   common nucleotide sequence in the 3'-untranslated region of mRNA molecules specifying
2976   inflammatory mediators." <u>Proc Natl Acad Sci U S A</u> **83**(6): 1670-1674.

2977 Cardenas, R., C. M. Sandoval, A. J. Rodriguez-Morales and C. Franco-Paredes (2006). "Impact of climate
2978   variability in the occurrence of leishmaniasis in northeastern Colombia." <u>Am J Trop Med Hyg</u> **75**(2):
2979   273-277.

2980 Carvalho, E. M., A. Llanos-Cuentas and G. A. S. Romero (2018). "Mucosal leishmaniasis: urgent need for
2981   more research." <u>Rev Soc Bras Med Trop</u> **51**(1): 120-121.

2982 Castello, A., M. W. Hentze and T. Preiss (2015). "Metabolic Enzymes Enjoying New Partnerships as RNA-
2983   Binding Proteins." <u>Trends Endocrinol Metab</u> **26**(12): 746-757.

2984 Cech, T. R. and J. A. Steitz (2014). "The noncoding RNA revolution-trashing old rules to forge new ones."
2985   <u>Cell</u> **157**(1): 77-94.

2986 Cencic, R., M. Carrier, G. Galicia-Vazquez, M. E. Bordeleau, R. Sukarieh, A. Bourdeau, B. Brem, J. G.
2987   Teodoro, H. Greger, M. L. Tremblay, J. A. Porco, Jr. and J. Pelletier (2009). "Antitumor activity and
2988   mechanism of action of the cyclopenta[b]benzofuran, silvestrol." <u>PLoS One</u> **4**(4): e5223.

2989   Cerezo, M., R. Guemiri, S. Druillennec, I. Girault, H. Malka-Mahieu, S. Shen, D. Allard, S. Martineau, C. Welsch, S. Agoussi, C. Estrada, J. Adam, C. Libenciuc, E. Routier, S. Roy, L. Desaubry, A. M. Eggermont, N. Sonenberg, J. Y. Scoazec, A. Eychene, S. Vagner and C. Robert (2018). "Translational control of tumor immune escape via the eIF4F-STAT1-PD-L1 axis in melanoma." <u>Nat Med</u> **24**(12): 1877-1886.

2994   Chakrabarty, R., S. Mukherjee, H. G. Lu, B. S. McGwire, K. P. Chang and M. K. Basu (1996). "Kinetics of entry of virulent and avirulent strains of Leishmania donovani into macrophages: a possible role of virulence molecules (gp63 and LPG)." <u>J Parasitol</u> **82**(4): 632-635.

2997   Chaparro, V., L. P. Leroux, L. Masvidal, J. Lorent, T. E. Graber, A. Zimmermann, G. Arango Duque, A. Descoteaux, T. Alain, O. Larsson and M. Jaramillo (2020). "Translational profiling of macrophages infected with Leishmania donovani identifies mTOR- and eIF4A-sensitive immune-related transcripts." <u>PLoS Pathog</u> **16**(6): e1008291.

3001   Chaparro, V., L. P. Leroux, A. Zimmermann, A. Jardim, B. Johnston, A. Descoteaux and M. Jaramillo (2019). "Leishmania donovani Lipophosphoglycan Increases Macrophage-Dependent Chemotaxis of CXCR6-Expressing Cells via CXCL16 Induction." <u>Infect Immun</u> **87**(5).

3004   Chappuis, F., S. Sundar, A. Hailu, H. Ghalib, S. Rijal, R. W. Peeling, J. Alvar and M. Boelaert (2007). "Visceral leishmaniasis: what are the needs for diagnosis, treatment and control?" <u>Nat Rev Microbiol</u> **5**(11): 873-882.

3007   Chatterjee, S., S. M. Yabaji, O. S. Rukhlenko, B. Bhattacharya, E. Waligurski, N. Vallavoju, S. Ray, B. N. Kholodenko, L. E. Brown, A. B. Beeler, A. R. Ivanov, L. Kobzik, J. A. Porco, Jr. and I. Kramnik (2021). "Channeling macrophage polarization by rocaglates increases macrophage resistance to Mycobacterium tuberculosis." <u>iScience</u> **24**(8): 102845.

3011   Chaussabel, D., R. T. Semnani, M. A. McDowell, D. Sacks, A. Sher and T. B. Nutman (2003). "Unique gene expression profiles of human macrophages and dendritic cells to phylogenetically distinct parasites." <u>Blood</u> **102**(2): 672-681.

3014   Chauvin, C., V. Koka, A. Nouschi, V. Mieulet, C. Hoareau-Aveilla, A. Dreazen, N. Cagnard, W. Carpentier, T. Kiss, O. Meyuhas and M. Pende (2014). "Ribosomal protein S6 kinase activity controls the ribosome biogenesis transcriptional program." <u>Oncogene</u> **33**(4): 474-483.

3017   Chaves, M. M., D. A. Sinflorio, M. L. Thorstenberg, M. D. A. Martins, A. C. A. Moreira-Souza, T. P. Rangel, C. L. M. Silva, M. Bellio, C. Canetti and R. Coutinho-Silva (2019). "Non-canonical NLRP3 inflammasome activation and IL-1beta signaling are necessary to L. amazonensis control mediated by P2X7 receptor and leukotriene B4." <u>PLoS Pathog</u> **15**(6): e1007887.

3021 Chaves, S. P., E. C. Torres-Santos, C. Marques, V. R. Figliuolo, P. M. Persechini, R. Coutinho-Silva and B.
3022   Rossi-Bergmann (2009). "Modulation of P2X(7) purinergic receptor in macrophages by Leishmania
3023   amazonensis and its role in parasite elimination." Microbes Infect **11**(10-11): 842-849.

3024 Cheekatla, S. S., A. Aggarwal and S. Naik (2012). "mTOR signaling pathway regulates the IL-12/IL-10 axis in
3025   Leishmania donovani infection." Med Microbiol Immunol **201**(1): 37-46.

3026 Chen, M. T., L. Dong, X. H. Zhang, X. L. Yin, H. M. Ning, C. Shen, R. Su, F. Li, L. Song, Y. N. Ma, F. Wang, H.
3027   L. Zhao, J. Yu and J. W. Zhang (2015). "ZFP36L1 promotes monocyte/macrophage differentiation
3028   by repressing CDK6." Sci Rep **5**: 16229.

3029 Chen, X., X. Yang, Y. Li, J. Zhu, S. Zhou, Z. Xu, L. He, X. Xue, W. Zhang, X. Dong, H. Wu, C. J. Li, H. T. Hsu, W.
3030   Kong, F. Liu, P. B. Tripathi, M. S. Yu, J. Chang, L. Zhou and C. Su (2014). "Follicular helper T cells
3031   promote liver pathology in mice during Schistosoma japonicum infection." PLoS Pathog **10**(5):
3032   e1004097.

3033 Cheng, X., Z. Ji, T. Tsalkova and F. Mei (2008). "Epac and PKA: a tale of two intracellular cAMP receptors."
3034   Acta Biochim Biophys Sin (Shanghai) **40**(7): 651-662.

3035 Cherla, R. P., S. Y. Lee, P. L. Mees and V. L. Tesh (2006). "Shiga toxin 1-induced cytokine production is
3036   mediated by MAP kinase pathways and translation initiation factor eIF4E in the macrophage-like
3037   THP-1 cell line." J Leukoc Biol **79**(2): 397-407.

3038 Choi, C. M. and E. A. Lerner (2002). "Leishmaniasis: recognition and management with a focus on the
3039   immunocompromised patient." Am J Clin Dermatol **3**(2): 91-105.

3040 Chu, J. and J. Pelletier (2015). "Targeting the eIF4A RNA helicase as an anti-neoplastic approach." Biochim
3041   Biophys Acta **1849**(7): 781-791.

3042 Clippinger, A. J., T. G. Maguire and J. C. Alwine (2011). "The changing role of mTOR kinase in the
3043   maintenance of protein synthesis during human cytomegalovirus infection." J Virol **85**(8): 3930-
3044   3939.

3045 Cohen, T. S. and A. S. Prince (2013). "Bacterial pathogens activate a common inflammatory pathway
3046   through IFNlambda regulation of PDCD4." PLoS Pathog **9**(10): e1003682.

3047 Cooray, S. N., T. Gobbetti, T. Montero-Melendez, S. McArthur, D. Thompson, A. J. Clark, R. J. Flower and
3048   M. Perretti (2013). "Ligand-specific conformational change of the G-protein-coupled receptor
3049   ALX/FPR2 determines proresolving functional responses." Proc Natl Acad Sci U S A **110**(45): 18232-
3050   18237.

3051   Cortez, M., C. Huynh, M. C. Fernandes, K. A. Kennedy, A. Aderem and N. W. Andrews (2011). "Leishmania
3052   promotes its own virulence by inducing expression of the host immune inhibitory ligand CD200."
3053   Cell Host Microbe **9**(6): 463-471.

3054   Costa, D. L., D. S. Lima-Junior, M. S. Nascimento, L. A. Sacramento, R. P. Almeida, V. Carregaro and J. S.
3055   Silva (2016). "CCR2 signaling contributes to the differentiation of protective inflammatory
3056   dendritic cells in Leishmania braziliensis infection." J Leukoc Biol **100**(2): 423-432.

3057   Couppie, P., E. Clyti, M. Sobesky, F. Bissuel, P. Del Giudice, D. Sainte-Marie, J. P. Dedet, B. Carme and R.
3058   Pradinaud (2004). "Comparative study of cutaneous leishmaniasis in human immunodeficiency
3059   virus (HIV)-infected patients and non-HIV-infected patients in French Guiana." Br J Dermatol
3060   **151**(6): 1165-1171.

3061   Cramer, Z., J. Sadek, G. G. Vazquez, S. Di Marco, A. Pause, J. Pelletier and I. E. Gallouzi (2018). "eIF4A
3062   inhibition prevents the onset of cytokine-induced muscle wasting by blocking the STAT3 and iNOS
3063   pathways." Sci Rep **8**(1): 8414.

3064   Crotty, S. (2011). "Follicular helper CD4 T cells (TFH)." Annu Rev Immunol **29**: 621-663.

3065   Cruz-Migoni, A., G. M. Hautbergue, P. J. Artymiuk, P. J. Baker, M. Bokori-Brown, C. T. Chang, M. J. Dickman,
3066   A. Essex-Lopresti, S. V. Harding, N. M. Mahadi, L. E. Marshall, G. W. Mobbs, R. Mohamed, S.
3067   Nathan, S. A. Ngugi, C. Ong, W. F. Ooi, L. J. Partridge, H. L. Phillips, M. F. Raih, S. Ruzheinikov, M.
3068   Sarkar-Tyson, S. E. Sedelnikova, S. J. Smither, P. Tan, R. W. Titball, S. A. Wilson and D. W. Rice
3069   (2011). "A Burkholderia pseudomallei toxin inhibits helicase activity of translation factor eIF4A."
3070   Science **334**(6057): 821-824.

3071   Cyrino, L. T., A. P. Araujo, P. P. Joazeiro, C. P. Vicente and S. Giorgio (2012). "In vivo and in vitro Leishmania
3072   amazonensis infection induces autophagy in macrophages." Tissue Cell **44**(6): 401-408.

3073   Darcis, G., G. Van der Auwera, J. B. Giot, M. P. Hayette, F. Tassin, J. Arrese Estrada, L. Cnops, M.
3074   Moutschen, L. de Leval and P. Leonard (2017). "Recurrence of visceral and muco-cutaneous
3075   leishmaniasis in a patient under immunosuppressive therapy." BMC Infect Dis **17**(1): 478.

3076   Das, S., K. Pandey, A. Kumar, A. H. Sardar, B. Purkait, M. Kumar, S. Kumar, V. N. Ravidas, S. Roy, D. Singh
3077   and P. Das (2012). "TGF-beta1 re-programs TLR4 signaling in L. donovani infection: enhancement
3078   of SHP-1 and ubiquitin-editing enzyme A20." Immunol Cell Biol **90**(6): 640-654.

3079   Datta, S., R. Biswas, M. Novotny, P. G. Pavicic, Jr., T. Herjan, P. Mandal and T. A. Hamilton (2008).
3080   "Tristetraprolin regulates CXCL1 (KC) mRNA stability." J Immunol **180**(4): 2545-2552.

3081   David, C. V. and N. Craft (2009). "Cutaneous and mucocutaneous leishmaniasis." Dermatol Ther **22**(6):
3082   491-502.

3083 Davis, B. K. (2013). "Isolation, culture, and functional evaluation of bone marrow-derived macrophages."
3084 Methods Mol Biol **1031**: 27-35.

3085 Dayakar, A., S. Chandrasekaran, S. V. Kuchipudi and S. K. Kalangi (2019). "Cytokines: Key Determinants of
3086 Resistance or Disease Progression in Visceral Leishmaniasis: Opportunities for Novel Diagnostics
3087 and Immunotherapy." Front Immunol **10**: 670.

3088 de Bruin, R. G., T. J. Rabelink, A. J. van Zonneveld and E. P. van der Veer (2017). "Emerging roles for RNA-
3089 binding proteins as effectors and regulators of cardiovascular disease." Eur Heart J **38**(18): 1380-
3090 1388.

3091 de Moura, T. R., F. Oliveira, G. C. Rodrigues, M. W. Carneiro, K. F. Fukutani, F. O. Novais, J. C. Miranda, M.
3092 Barral-Netto, C. Brodskyn, A. Barral and C. I. de Oliveira (2010). "Immunity to Lutzomyia
3093 intermedia saliva modulates the inflammatory environment induced by Leishmania braziliensis."
3094 PLoS Negl Trop Dis **4**(6): e712.

3095 Degrandi, D., C. Konermann, C. Beuter-Gunia, A. Kresse, J. Wurthner, S. Kurig, S. Beer and K. Pfeffer (2007).
3096 "Extensive characterization of IFN-induced GTPases mGBP1 to mGBP10 involved in host defense."
3097 J Immunol **179**(11): 7729-7740.

3098 Deng, L., C. Wang, E. Spencer, L. Yang, A. Braun, J. You, C. Slaughter, C. Pickart and Z. J. Chen (2000).
3099 "Activation of the IkappaB kinase complex by TRAF6 requires a dimeric ubiquitin-conjugating
3100 enzyme complex and a unique polyubiquitin chain." Cell **103**(2): 351-361.

3101 Dennis, M. D., L. S. Jefferson and S. R. Kimball (2012). "Role of p70S6K1-mediated phosphorylation of
3102 eIF4B and PDCD4 proteins in the regulation of protein synthesis." J Biol Chem **287**(51): 42890-
3103 42899.

3104 Dever, T. E. and R. Green (2012). "The elongation, termination, and recycling phases of translation in
3105 eukaryotes." Cold Spring Harb Perspect Biol **4**(7): a013706.

3106 Dey, R., A. B. Joshi, F. Oliveira, L. Pereira, A. B. Guimaraes-Costa, T. D. Serafim, W. de Castro, I. V. Coutinho-
3107 Abreu, P. Bhattacharya, S. Townsend, H. Aslan, A. Perkins, S. Karmakar, N. Ismail, M. Karetnick, C.
3108 Meneses, R. Duncan, H. L. Nakhasi, J. G. Valenzuela and S. Kamhawi (2018). "Gut Microbes Egested
3109 during Bites of Infected Sand Flies Augment Severity of Leishmaniasis via Inflammasome-Derived
3110 IL-1beta." Cell Host Microbe **23**(1): 134-143 e136.

3111 Dhalia, R., C. R. Reis, E. R. Freire, P. O. Rocha, R. Katz, J. R. Muniz, N. Standart and O. P. de Melo Neto
3112 (2005). "Translation initiation in Leishmania major: characterisation of multiple eIF4F subunit
3113 homologues." Mol Biochem Parasitol **140**(1): 23-41.

3114   Di Marco, S., A. Cammas, X. J. Lian, E. N. Kovacs, J. F. Ma, D. T. Hall, R. Mazroui, J. Richardson, J. Pelletier
3115   and I. E. Gallouzi (2012). "The translation inhibitor pateamine A prevents cachexia-induced muscle
3116   wasting in mice." Nat Commun **3**: 896.

3117   Dias, B. R. S., C. S. de Souza, N. J. Almeida, J. G. B. Lima, K. F. Fukutani, T. B. S. Dos Santos, J. Franca-Cost,
3118   C. I. Brodskyn, J. P. B. de Menezes, M. I. Colombo and P. S. T. Veras (2018). "Autophagic Induction
3119   Greatly Enhances Leishmania major Intracellular Survival Compared to Leishmania amazonensis
3120   in CBA/j-Infected Macrophages." Front Microbiol **9**: 1890.

3121   Dias, B. T., K. L. Dias-Teixeira, J. P. Godinho, M. S. Faria, T. Calegari-Silva, M. M. Mukhtar, U. Lopes, J. C.
3122   Mottram and A. Lima (2019). "Neutrophil elastase promotes Leishmania donovani infection via
3123   interferon-beta." FASEB J **33**(10): 10794-10807.

3124   Dias, B. T., A. Goundry, A. C. Vivarini, T. F. R. Costa, J. C. Mottram, U. G. Lopes and A. Lima (2022). "Toll-
3125   Like Receptor- and Protein Kinase R-Induced Type I Interferon Sustains Infection of Leishmania
3126   donovani in Macrophages." Front Immunol **13**: 801182.

3127   Difilippantonio, S., A. Celeste, O. Fernandez-Capetillo, H. T. Chen, B. Reina San Martin, F. Van Laethem, Y.
3128   P. Yang, G. V. Petukhova, M. Eckhaus, L. Feigenbaum, K. Manova, M. Kruhlak, R. D. Camerini-
3129   Otero, S. Sharan, M. Nussenzweig and A. Nussenzweig (2005). "Role of Nbs1 in the activation of
3130   the Atm kinase revealed in humanized mouse models." Nat Cell Biol **7**(7): 675-685.

3131   Dillon, L. A., R. Suresh, K. Okrah, H. Corrada Bravo, D. M. Mosser and N. M. El-Sayed (2015). "Simultaneous
3132   transcriptional profiling of Leishmania major and its murine macrophage host cell reveals insights
3133   into host-pathogen interactions." BMC Genomics **16**: 1108.

3134   Dong, G., A. L. Filho and M. Olivier (2019). "Modulation of Host-Pathogen Communication by Extracellular
3135   Vesicles (EVs) of the Protozoan Parasite Leishmania." Front Cell Infect Microbiol **9**: 100.

3136   Dorrello, N. V., A. Peschiaroli, D. Guardavaccaro, N. H. Colburn, N. E. Sherman and M. Pagano (2006).
3137   "S6K1- and betaTRCP-mediated degradation of PDCD4 promotes protein translation and cell
3138   growth." Science **314**(5798): 467-471.

3139   Du, R., P. J. Hotez, W. S. Al-Salem and A. Acosta-Serrano (2016). "Old World Cutaneous Leishmaniasis and
3140   Refugee Crises in the Middle East and North Africa." PLoS Negl Trop Dis **10**(5): e0004545.

3141   Duque, T. L. A., T. Serrao, A. Goncalves, E. F. Pinto, M. P. Oliveira-Neto, C. Pirmez, L. O. R. Pereira and R. F.
3142   S. Menna-Barreto (2021). "Leishmania (V.) braziliensis infection promotes macrophage autophagy
3143   by a LC3B-dependent and BECLIN1-independent mechanism." Acta Trop **218**: 105890.

3144   Espitia, C. M., O. A. Saldarriaga, B. L. Travi, E. Y. Osorio, A. Hernandez, M. Band, M. J. Patel, A. A. Medina,
3145   M. Cappello, A. Pekosz and P. C. Melby (2014). "Transcriptional profiling of the spleen in

progressive visceral leishmaniasis reveals mixed expression of type 1 and type 2 cytokine-responsive genes." BMC Immunol **15**: 38.

Etna, M. P., M. Severa, V. Licursi, M. Pardini, M. Cruciani, F. Rizzo, E. Giacomini, G. Macchia, O. Palumbo, R. Stallone, M. Carella, M. Livingstone, R. Negri, S. Pellegrini and E. M. Coccia (2021). "Genome-Wide Gene Expression Analysis of Mtb-Infected DC Highlights the Rapamycin-Driven Modulation of Regulatory Cytokines via the mTOR/GSK-3beta Axis." Front Immunol **12**: 649475.

Fairn, G. D. and S. Grinstein (2012). "How nascent phagosomes mature to become phagolysosomes." Trends Immunol **33**(8): 397-405.

Famulski, K. S., G. Einecke, J. Reeve, V. Ramassar, K. Allanach, T. Mueller, L. G. Hidalgo, L. F. Zhu and P. F. Halloran (2006). "Changes in the transcriptome in allograft rejection: IFN-gamma-induced transcripts in mouse kidney allografts." Am J Transplant **6**(6): 1342-1354.

Faria, M. S., T. C. Calegari-Silva, A. de Carvalho Vivarini, J. C. Mottram, U. G. Lopes and A. P. Lima (2014). "Role of protein kinase R in the killing of Leishmania major by macrophages in response to neutrophil elastase and TLR4 via TNFalpha and IFNbeta." FASEB J **28**(7): 3050-3063.

Fernandes, M. C., L. A. Dillon, A. T. Belew, H. C. Bravo, D. M. Mosser and N. M. El-Sayed (2016). "Dual Transcriptome Profiling of Leishmania-Infected Human Macrophages Reveals Distinct Reprogramming Signatures." mBio **7**(3).

Fernandes, S. A. and C. Demetriades (2021). "The Multifaceted Role of Nutrient Sensing and mTORC1 Signaling in Physiology and Aging." Frontiers in Aging **2**.

Ferreira, C., I. Mesquita, A. M. Barbosa, N. S. Osorio, E. Torrado, C. J. Beauparlant, A. Droit, C. Cunha, A. Carvalho, B. Saha, J. Estaquier and R. Silvestre (2020). "Glutamine supplementation improves the efficacy of miltefosine treatment for visceral leishmaniasis." PLoS Negl Trop Dis **14**(3): e0008125.

Fertig, B. A. and G. S. Baillie (2018). "PDE4-Mediated cAMP Signalling." J Cardiovasc Dev Dis **5**(1).

Fonseca, B. D., E. M. Smith, N. Yelle, T. Alain, M. Bushell and A. Pause (2014). "The ever-evolving role of mTOR in translation." Semin Cell Dev Biol **36**: 102-112.

Fonseca, B. D., C. Zakaria, J. J. Jia, T. E. Graber, Y. Svitkin, S. Tahmasebi, D. Healy, H. D. Hoang, J. M. Jensen, I. T. Diao, A. Lussier, C. Dajadian, N. Padmanabhan, W. Wang, E. Matta-Camacho, J. Hearnden, E. M. Smith, Y. Tsukumo, A. Yanagiya, M. Morita, E. Petroulakis, J. L. Gonzalez, G. Hernandez, T. Alain and C. K. Damgaard (2015). "La-related Protein 1 (LARP1) Represses Terminal Oligopyrimidine (TOP) mRNA Translation Downstream of mTOR Complex 1 (mTORC1)." J Biol Chem **290**(26): 15996-16020.

3177   Forestier, C. L., C. Machu, C. Loussert, P. Pescher and G. F. Spath (2011). "Imaging host cell-Leishmania
3178   interaction dynamics implicates parasite motility, lysosome recruitment, and host cell wounding
3179   in the infection process." <u>Cell Host Microbe</u> **9**(4): 319-330.

3180   Franco, L. H., A. K. A. Fleuri, N. C. Pellison, G. F. S. Quirino, C. V. Horta, R. V. H. de Carvalho, S. C. Oliveira
3181   and D. S. Zamboni (2017). "Autophagy downstream of endosomal Toll-like receptor signaling in
3182   macrophages is a key mechanism for resistance to Leishmania major infection." <u>J Biol Chem</u>
3183   **292**(32): 13087-13096.

3184   Frank, B., A. Marcu, A. L. de Oliveira Almeida Petersen, H. Weber, C. Stigloher, J. C. Mottram, C. J. Scholz
3185   and U. Schurigt (2015). "Autophagic digestion of Leishmania major by host macrophages is
3186   associated with differential expression of BNIP3, CTSE, and the miRNAs miR-101c, miR-129, and
3187   miR-210." <u>Parasit Vectors</u> **8**: 404.

3188   Franks, T. M. and J. Lykke-Andersen (2007). "TTP and BRF proteins nucleate processing body formation to
3189   silence mRNAs with AU-rich elements." <u>Genes Dev</u> **21**(6): 719-735.

3190   Fu, H., G. Yang, M. Wei, L. Liu, L. Jin, X. Lu, L. Wang, L. Shen, J. Zhang, H. Lu, L. Yao and Z. Lu (2012). "The
3191   RNA-binding protein QKI5 is a direct target of C/EBPalpha and delays macrophage differentiation."
3192   <u>Mol Biol Cell</u> **23**(9): 1628-1635.

3193   Gal-Ben-Ari, S., I. Barrera, M. Ehrlich and K. Rosenblum (2018). "PKR: A Kinase to Remember." <u>Front Mol</u>
3194   <u>Neurosci</u> **11**: 480.

3195   Galati, E. A. B., F. Galvis-Ovallos, P. Lawyer, N. Leger and J. Depaquit (2017). "An illustrated guide for
3196   characters and terminology used in descriptions of Phlebotominae (Diptera, Psychodidae)."
3197   <u>Parasite</u> **24**: 26.

3198   Gandin, V., L. Masvidal, M. Cargnello, L. Gyenis, S. McLaughlan, Y. Cai, C. Tenkerian, M. Morita, P.
3199   Balanathan, O. Jean-Jean, V. Stambolic, M. Trost, L. Furic, L. Larose, A. E. Koromilas, K. Asano, D.
3200   Litchfield, O. Larsson and I. Topisirovic (2016). "mTORC1 and CK2 coordinate ternary and eIF4F
3201   complex assembly." <u>Nat Commun</u> **7**: 11127.

3202   Gandin, V., L. Masvidal, L. Hulea, S. P. Gravel, M. Cargnello, S. McLaughlan, Y. Cai, P. Balanathan, M.
3203   Morita, A. Rajakumar, L. Furic, M. Pollak, J. A. Porco, Jr., J. St-Pierre, J. Pelletier, O. Larsson and I.
3204   Topisirovic (2016). "nanoCAGE reveals 5' UTR features that define specific modes of translation
3205   of functionally related MTOR-sensitive mRNAs." <u>Genome Res</u> **26**(5): 636-648.

3206   Gardinassi, L. G., G. R. Garcia, C. H. Costa, V. Costa Silva and I. K. de Miranda Santos (2016). "Blood
3207   Transcriptional Profiling Reveals Immunological Signatures of Distinct States of Infection of
3208   Humans with Leishmania infantum." <u>PLoS Negl Trop Dis</u> **10**(11): e0005123.

3209   Gautier, E. L. and L. Yvan-Charvet (2014). "Understanding macrophage diversity at the ontogenic and
3210   transcriptomic levels." Immunol Rev **262**(1): 85-95.

3211   Gedda, M. R., B. Singh, D. Kumar, A. K. Singh, P. Madhukar, S. Upadhyay, O. P. Singh and S. Sundar (2020).
3212   "Post kala-azar dermal leishmaniasis: A threat to elimination program." PLoS Negl Trop Dis **14**(7):
3213   e0008221.

3214   Geraci, N. S., J. C. Tan and M. A. McDowell (2015). "Characterization of microRNA expression profiles in
3215   Leishmania-infected human phagocytes." Parasite Immunol **37**(1): 43-51.

3216   Ghalib, H. W., J. A. Whittle, M. Kubin, F. A. Hashim, A. M. el-Hassan, K. H. Grabstein, G. Trinchieri and S. G.
3217   Reed (1995). "IL-12 enhances Th1-type responses in human Leishmania donovani infections." J
3218   Immunol **154**(9): 4623-4629.

3219   Ghani, S., P. Riemke, J. Schonheit, D. Lenze, J. Stumm, M. Hoogenkamp, A. Lagendijk, S. Heinz, C. Bonifer,
3220   J. Bakkers, S. Abdelilah-Seyfried, M. Hummel and F. Rosenbauer (2011). "Macrophage
3221   development from HSCs requires PU.1-coordinated microRNA expression." Blood **118**(8): 2275-
3222   2284.

3223   Gholamrezaei, M., M. Mohebali, A. A. Hanafi-Bojd, M. M. Sedaghat and M. R. Shirzadi (2016). "Ecological
3224   Niche Modeling of main reservoir hosts of zoonotic cutaneous leishmaniasis in Iran." Acta Trop
3225   **160**: 44-52.

3226   Gil, J., M. A. Garcia, P. Gomez-Puertas, S. Guerra, J. Rullas, H. Nakano, J. Alcami and M. Esteban (2004).
3227   "TRAF family proteins link PKR with NF-kappa B activation." Mol Cell Biol **24**(10): 4502-4512.

3228   Gingras, A. C., B. Raught, S. P. Gygi, A. Niedzwiecka, M. Miron, S. K. Burley, R. D. Polakiewicz, A. Wyslouch-
3229   Cieszynska, R. Aebersold and N. Sonenberg (2001). "Hierarchical phosphorylation of the
3230   translation inhibitor 4E-BP1." Genes Dev **15**(21): 2852-2864.

3231   Ginhoux, F., M. Greter, M. Leboeuf, S. Nandi, P. See, S. Gokhan, M. F. Mehler, S. J. Conway, L. G. Ng, E. R.
3232   Stanley, I. M. Samokhvalov and M. Merad (2010). "Fate mapping analysis reveals that adult
3233   microglia derive from primitive macrophages." Science **330**(6005): 841-845.

3234   Giri, J., M. Basu, S. Roy, T. Mishra, K. Jana, A. Chande and A. Ukil (2022). "Translationally Controlled Tumor
3235   Protein-Mediated Stabilization of Host Antiapoptotic Protein MCL-1 Is Critical for Establishment
3236   of Infection by Intramacrophage Parasite Leishmania donovani." J Immunol **208**(11): 2540-2548.

3237   Giri, J., S. Srivastav, M. Basu, S. Palit, P. Gupta and A. Ukil (2016). "Leishmania donovani Exploits Myeloid
3238   Cell Leukemia 1 (MCL-1) Protein to Prevent Mitochondria-dependent Host Cell Apoptosis." J Biol
3239   Chem **291**(7): 3496-3507.

3240 Glisovic, T., J. L. Bachorik, J. Yong and G. Dreyfuss (2008). "RNA-binding proteins and post-transcriptional
3241   gene regulation." FEBS Lett **582**(14): 1977-1986.

3242 Goldmann, O., M. von Kockritz-Blickwede, C. Holtje, G. S. Chhatwal, R. Geffers and E. Medina (2007).
3243   "Transcriptome analysis of murine macrophages in response to infection with Streptococcus
3244   pyogenes reveals an unusual activation program." Infect Immun **75**(8): 4148-4157.

3245 Gonalons, E., M. Barrachina, J. A. Garcia-Sanz and A. Celada (1998). "Translational control of MHC class II
3246   I-A molecules by IFN-gamma." J Immunol **161**(4): 1837-1843.

3247 Gonzalez, A., M. N. Hall, S. C. Lin and D. G. Hardie (2020). "AMPK and TOR: The Yin and Yang of Cellular
3248   Nutrient Sensing and Growth Control." Cell Metab **31**(3): 472-492.

3249 Gonzalez, C., O. Wang, S. E. Strutz, C. Gonzalez-Salazar, V. Sanchez-Cordero and S. Sarkar (2010). "Climate
3250   change and risk of leishmaniasis in north america: predictions from ecological niche models of
3251   vector and reservoir species." PLoS Negl Trop Dis **4**(1): e585.

3252 Gordon, S., A. Pluddemann and F. Martinez Estrada (2014). "Macrophage heterogeneity in tissues:
3253   phenotypic diversity and functions." Immunol Rev **262**(1): 36-55.

3254 Gosselin, D., V. M. Link, C. E. Romanoski, G. J. Fonseca, D. Z. Eichenfield, N. J. Spann, J. D. Stender, H. B.
3255   Chun, H. Garner, F. Geissmann and C. K. Glass (2014). "Environment drives selection and function
3256   of enhancers controlling tissue-specific macrophage identities." Cell **159**(6): 1327-1340.

3257 Graff, J. W., A. M. Dickson, G. Clay, A. P. McCaffrey and M. E. Wilson (2012). "Identifying functional
3258   microRNAs in macrophages with polarized phenotypes." J Biol Chem **287**(26): 21816-21825.

3259 Gray, N. K., L. Hrabalkova, J. P. Scanlon and R. W. Smith (2015). "Poly(A)-binding proteins and mRNA
3260   localization: who rules the roost?" Biochem Soc Trans **43**(6): 1277-1284.

3261 Gregory, D. J., R. Sladek, M. Olivier and G. Matlashewski (2008). "Comparison of the effects of Leishmania
3262   major or Leishmania donovani infection on macrophage gene expression." Infect Immun **76**(3):
3263   1186-1192.

3264 Guan, B. J., V. van Hoef, R. Jobava, O. Elroy-Stein, L. S. Valasek, M. Cargnello, X. H. Gao, D. Krokowski, W.
3265   C. Merrick, S. R. Kimball, A. A. Komar, A. E. Koromilas, A. Wynshaw-Boris, I. Topisirovic, O. Larsson
3266   and M. Hatzoglou (2017). "A Unique ISR Program Determines Cellular Responses to Chronic
3267   Stress." Mol Cell **68**(5): 885-900 e886.

3268 Guerra, J. A., L. I. Coelho, F. R. Pereira, A. M. Siqueira, R. L. Ribeiro, T. M. Almeida, M. V. Lacerda, M.
3269   Barbosa and S. Talhari (2011). "American tegumentary leishmaniasis and HIV-AIDS association in
3270   a tertiary care center in the Brazilian Amazon." Am J Trop Med Hyg **85**(3): 524-527.

3271   Guy, R. A. and M. Belosevic (1993). "Comparison of receptors required for entry of Leishmania major
3272   amastigotes into macrophages." Infect Immun **61**(4): 1553-1558.

3273   Haldar, A. K., U. Nigam, M. Yamamoto, J. Coers and N. Goyal (2020). "Guanylate Binding Proteins Restrict
3274   Leishmania donovani Growth in Nonphagocytic Cells Independent of Parasitophorous Vacuolar
3275   Targeting." mBio **11**(4).

3276   Hammami, A., B. M. Abidin, T. Charpentier, A. Fabie, A. P. Duguay, K. M. Heinonen and S. Stager (2017).
3277   "HIF-1alpha is a key regulator in potentiating suppressor activity and limiting the microbicidal
3278   capacity of MDSC-like cells during visceral leishmaniasis." PLoS Pathog **13**(9): e1006616.

3279   Handler, M. Z., P. A. Patel, R. Kapila, Y. Al-Qubati and R. A. Schwartz (2015). "Cutaneous and
3280   mucocutaneous leishmaniasis: Clinical perspectives." J Am Acad Dermatol **73**(6): 897-908; quiz
3281   909-810.

3282   Hara, K., K. Yonezawa, M. T. Kozlowski, T. Sugimoto, K. Andrabi, Q. P. Weng, M. Kasuga, I. Nishimoto and
3283   J. Avruch (1997). "Regulation of eIF-4E BP1 phosphorylation by mTOR." J Biol Chem **272**(42):
3284   26457-26463.

3285   Harigua-Souiai, E., Y. Z. Abdelkrim, I. Bassoumi-Jamoussi, O. Zakraoui, G. Bouvier, K. Essafi-Benkhadir, J.
3286   Banroques, N. Desdouits, H. Munier-Lehmann, M. Barhoumi, N. K. Tanner, M. Nilges, A. Blondel
3287   and I. Guizani (2018). "Identification of novel leishmanicidal molecules by virtual and biochemical
3288   screenings targeting Leishmania eukaryotic translation initiation factor 4A." PLoS Negl Trop Dis
3289   **12**(1): e0006160.

3290   Harneti, D. and U. Supratman (2021). "Phytochemistry and biological activities of Aglaia species."
3291   Phytochemistry **181**: 112540.

3292   Hartlova, A., S. F. Erttmann, F. A. Raffi, A. M. Schmalz, U. Resch, S. Anugula, S. Lienenklaus, L. M. Nilsson,
3293   A. Kroger, J. A. Nilsson, T. Ek, S. Weiss and N. O. Gekara (2015). "DNA damage primes the type I
3294   interferon system via the cytosolic DNA sensor STING to promote anti-microbial innate
3295   immunity." Immunity **42**(2): 332-343.

3296   Hatzi, K., J. P. Nance, M. A. Kroenke, M. Bothwell, E. K. Haddad, A. Melnick and S. Crotty (2015). "BCL6
3297   orchestrates Tfh cell differentiation via multiple distinct mechanisms." J Exp Med **212**(4): 539-553.

3298   Heaton, S. M., N. A. Borg and V. M. Dixit (2016). "Ubiquitin in the activation and attenuation of innate
3299   antiviral immunity." J Exp Med **213**(1): 1-13.

3300   Hennig, M., S. Fiedler, C. Jux, L. Thierfelder and J. D. Drenckhahn (2017). "Prenatal Mechanistic Target of
3301   Rapamycin Complex 1 (m TORC1) Inhibition by Rapamycin Treatment of Pregnant Mice Causes

Intrauterine Growth Restriction and Alters Postnatal Cardiac Growth, Morphology, and Function." J Am Heart Assoc **6**(8).

Henss, L., T. Scholz, A. Grunweller and B. S. Schnierle (2018). "Silvestrol Inhibits Chikungunya Virus Replication." Viruses **10**(11).

Hentze, M. W., A. Castello, T. Schwarzl and T. Preiss (2018). "A brave new world of RNA-binding proteins." Nat Rev Mol Cell Biol **19**(5): 327-341.

Hilliard, A., B. Hilliard, S. J. Zheng, H. Sun, T. Miwa, W. Song, R. Goke and Y. H. Chen (2006). "Translational regulation of autoimmune inflammation and lymphoma genesis by programmed cell death 4." J Immunol **177**(11): 8095-8102.

Hoang, H. D., T. E. Graber, J. J. Jia, N. Vaidya, V. H. Gilchrist, X. Xiang, W. Li, K. N. Cowan, C. G. Gkogkas, M. Jaramillo, S. M. Jafarnejad and T. Alain (2019). "Induction of an Alternative mRNA 5' Leader Enhances Translation of the Ciliopathy Gene Inpp5e and Resistance to Oncolytic Virus Infection." Cell Rep **29**(12): 4010-4023 e4015.

Hodson, D. J., M. L. Janas, A. Galloway, S. E. Bell, S. Andrews, C. M. Li, R. Pannell, C. W. Siebel, H. R. MacDonald, K. De Keersmaecker, A. A. Ferrando, G. Grutz and M. Turner (2010). "Deletion of the RNA-binding proteins ZFP36L1 and ZFP36L2 leads to perturbed thymic development and T lymphoblastic leukemia." Nat Immunol **11**(8): 717-724.

Hoeffel, G. and F. Ginhoux (2018). "Fetal monocytes and the origins of tissue-resident macrophages." Cell Immunol **330**: 5-15.

Hofmann, R. M. and C. M. Pickart (1999). "Noncanonical MMS2-encoded ubiquitin-conjugating enzyme functions in assembly of novel polyubiquitin chains for DNA repair." Cell **96**(5): 645-653.

Holm, A., K. Tejle, K. E. Magnusson, A. Descoteaux and B. Rasmusson (2001). "Leishmania donovani lipophosphoglycan causes periphagosomal actin accumulation: correlation with impaired translocation of PKCalpha and defective phagosome maturation." Cell Microbiol **3**(7): 439-447.

Holmes, M. J., P. Shah, R. C. Wek and W. J. Sullivan, Jr. (2019). "Simultaneous Ribosome Profiling of Human Host Cells Infected with Toxoplasma gondii." mSphere **4**(3).

Holz, M. K., B. A. Ballif, S. P. Gygi and J. Blenis (2021). "mTOR and S6K1 mediate assembly of the translation preinitiation complex through dynamic protein interchange and ordered phosphorylation events." Cell **184**(8): 2255.

Hong, S., M. A. Freeberg, T. Han, A. Kamath, Y. Yao, T. Fukuda, T. Suzuki, J. K. Kim and K. Inoki (2017). "LARP1 functions as a molecular switch for mTORC1-mediated translation of an essential class of mRNAs." Elife **6**.

3334 Horng, T., G. M. Barton and R. Medzhitov (2001). "TIRAP: an adapter molecule in the Toll signaling
3335   pathway." <u>Nat Immunol</u> **2**(9): 835-841.

3336 Hsu, L. C., J. M. Park, K. Zhang, J. L. Luo, S. Maeda, R. J. Kaufman, L. Eckmann, D. G. Guiney and M. Karin
3337   (2004). "The protein kinase PKR is required for macrophage apoptosis after activation of Toll-like
3338   receptor 4." <u>Nature</u> **428**(6980): 341-345.

3339 Hu, H. and S. C. Sun (2016). "Ubiquitin signaling in immune responses." <u>Cell Res</u> **26**(4): 457-483.

3340 Huang, C. T., C. Y. Hung, T. C. Chen, C. Y. Lin, Y. C. Lin, C. S. Chang, Y. C. He, Y. L. Huang and A. Dutta (2017).
3341   "Rapamycin adjuvant and exacerbation of severe influenza in an experimental mouse model." <u>Sci</u>
3342   <u>Rep</u> **7**(1): 4136.

3343 Huang, K. and D. C. Fingar (2014). "Growing knowledge of the mTOR signaling network." <u>Semin Cell Dev</u>
3344   <u>Biol</u> **36**: 79-90.

3345 Hurrell, B. P., M. Beaumann, S. Heyde, I. B. Regli, A. J. Muller and F. Tacchini-Cottier (2017). "Frontline
3346   Science: Leishmania mexicana amastigotes can replicate within neutrophils." <u>J Leukoc Biol</u> **102**(5):
3347   1187-1198.

3348 Isnard, A., J. G. Christian, M. Kodiha, U. Stochaj, W. R. McMaster and M. Olivier (2015). "Impact of
3349   Leishmania infection on host macrophage nuclear physiology and nucleopore complex integrity."
3350   <u>PLoS Pathog</u> **11**(3): e1004776.

3351 Jackson, R. J., C. U. Hellen and T. V. Pestova (2010). "The mechanism of eukaryotic translation initiation
3352   and principles of its regulation." <u>Nat Rev Mol Cell Biol</u> **11**(2): 113-127.

3353 Janes, M. R. and D. A. Fruman (2009). "Immune regulation by rapamycin: moving beyond T cells." <u>Sci Signal</u>
3354   **2**(67): pe25.

3355 Janprasert, J., C. Satasook, P. Sukumalanand, D. E. Champagne, M. B. Isman, P. Wiriyachitra and G. H. N.
3356   Towers (1992). "Rocaglamide, a natural benzofuran insecticide from Aglaia odorata."
3357   <u>Phytochemistry</u> **32**(1): 67-69.

3358 Jaramillo, M., M. A. Gomez, O. Larsson, M. T. Shio, I. Topisirovic, I. Contreras, R. Luxenburg, A. Rosenfeld,
3359   R. Colina, R. W. McMaster, M. Olivier, M. Costa-Mattioli and N. Sonenberg (2011). "Leishmania
3360   repression of host translation through mTOR cleavage is required for parasite survival and
3361   infection." <u>Cell Host Microbe</u> **9**(4): 331-341.

3362 Jaskowska, E., C. Butler, G. Preston and S. Kelly (2015). "Phytomonas: trypanosomatids adapted to plant
3363   environments." <u>PLoS Pathog</u> **11**(1): e1004484.

3364 Ji, H., L. I. Ehrlich, J. Seita, P. Murakami, A. Doi, P. Lindau, H. Lee, M. J. Aryee, R. A. Irizarry, K. Kim, D. J.
3365   Rossi, M. A. Inlay, T. Serwold, H. Karsunky, L. Ho, G. Q. Daley, I. L. Weissman and A. P. Feinberg

3366 (2010). "Comprehensive methylome map of lineage commitment from haematopoietic
3367   progenitors." Nature **467**(7313): 338-342.

3368 Jia, J. J., R. M. Lahr, M. T. Solgaard, B. J. Moraes, R. Pointet, A. D. Yang, G. Celucci, T. E. Graber, H. D. Hoang,
3369   M. R. Niklaus, I. A. Pena, A. K. Hollensen, E. M. Smith, M. Chaker-Margot, L. Anton, C. Dajadian,
3370   M. Livingstone, J. Hearnden, X. D. Wang, Y. Yu, T. Maier, C. K. Damgaard, A. J. Berman, T. Alain
3371   and B. D. Fonseca (2021). "mTORC1 promotes TOP mRNA translation through site-specific
3372   phosphorylation of LARP1." Nucleic Acids Res **49**(6): 3461-3489.

3373 Joshi, D. D., M. Sharma and S. Bhandari (2006). "Visceral leishmaniasis in Nepal during 1980-2006." J
3374   Commun Dis **38**(2): 139-148.

3375 Joshi, T., S. Rodriguez, V. Perovic, I. A. Cockburn and S. Stager (2009). "B7-H1 blockade increases survival
3376   of dysfunctional CD8(+) T cells and confers protection against Leishmania donovani infections."
3377   PLoS Pathog **5**(5): e1000431.

3378 Juchem, K. W., A. P. Gounder, J. P. Gao, E. Seccareccia, N. Yeddula, N. J. Huffmaster, A. Cote-Martin, S. E.
3379   Fogal, D. Souza, S. S. Wang, E. R. A. Glynn, I. Yung, J. Ritchie, L. Li, J. Zheng, M. L. Mbow, J. Li and
3380   S. K. Chanda (2021). "NFAM1 Promotes Pro-Inflammatory Cytokine Production in Mouse and
3381   Human Monocytes." Front Immunol **12**: 773445.

3382 Junghae, M. and J. G. Raynes (2002). "Activation of p38 mitogen-activated protein kinase attenuates
3383   Leishmania donovani infection in macrophages." Infect Immun **70**(9): 5026-5035.

3384 Kanani, K., Z. S. Amr, B. Shadfan, R. Khorma, G. Ro, M. Abid, A. F. Gabrielli and J. Haskew (2019).
3385   "Cutaneous leishmaniasis among Syrian refugees in Jordan." Acta Trop **194**: 169-171.

3386 Kaur, S., A. Sassano, B. Dolniak, S. Joshi, B. Majchrzak-Kita, D. P. Baker, N. Hay, E. N. Fish and L. C. Platanias
3387   (2008). "Role of the Akt pathway in mRNA translation of interferon-stimulated genes." Proc Natl
3388   Acad Sci U S A **105**(12): 4808-4813.

3389 Kaye, P. and P. Scott (2011). "Leishmaniasis: complexity at the host-pathogen interface." Nat Rev
3390   Microbiol **9**(8): 604-615.

3391 Keating, S. E. and A. G. Bowie (2009). "Role of non-degradative ubiquitination in interleukin-1 and toll-like
3392   receptor signaling." J Biol Chem **284**(13): 8211-8215.

3393 Kelly, A. and J. Trowsdale (2019). "Genetics of antigen processing and presentation." Immunogenetics
3394   **71**(3): 161-170.

3395 Khadem, F. and J. E. Uzonna (2014). "Immunity to visceral leishmaniasis: implications for
3396   immunotherapy." Future Microbiol **9**(7): 901-915.

3397   Khadir, F., C. R. Shaler, A. Oryan, P. T. Rudak, D. M. Mazzuca, T. Taheri, J. D. Dikeakos, S. M. M. Haeryfar
3398   and S. Rafati (2018). "Therapeutic control of leishmaniasis by inhibitors of the mammalian target
3399   of rapamycin." PLoS Negl Trop Dis **12**(8): e0006701.

3400   Khadir, F., T. Taheri, S. Habibzadeh, F. Zahedifard, E. Gholami, M. Heidari-Kharaji, A. Oryan and S. Rafati
3401   (2019). "Antileishmanial effect of rapamycin as an alternative approach to control Leishmania
3402   tropica infection." Vet Parasitol **276**: 108976.

3403   Khare, S., A. S. Nagle, A. Biggart, Y. H. Lai, F. Liang, L. C. Davis, S. W. Barnes, C. J. Mathison, E. Myburgh, M.
3404   Y. Gao, J. R. Gillespie, X. Liu, J. L. Tan, M. Stinson, I. C. Rivera, J. Ballard, V. Yeh, T. Groessl, G.
3405   Federe, H. X. Koh, J. D. Venable, B. Bursulaya, M. Shapiro, P. K. Mishra, G. Spraggon, A. Brock, J. C.
3406   Mottram, F. S. Buckner, S. P. Rao, B. G. Wen, J. R. Walker, T. Tuntland, V. Molteni, R. J. Glynne and
3407   F. Supek (2016). "Proteasome inhibition for treatment of leishmaniasis, Chagas disease and
3408   sleeping sickness." Nature **537**(7619): 229-233.

3409   Kim, B. H., A. R. Shenoy, P. Kumar, C. J. Bradfield and J. D. MacMicking (2012). "IFN-inducible GTPases in
3410   host cell defense." Cell Host Microbe **12**(4): 432-444.

3411   Kim, C. (2020). "How Z-DNA/RNA binding proteins shape homeostasis, inflammation, and immunity." BMB
3412   Rep **53**(9): 453-457.

3413   Kim, D., S. Kim, J. Park, H. R. Chang, J. Chang, J. Ahn, H. Park, J. Park, N. Son, G. Kang, J. Kim, K. Kim, M. S.
3414   Park, Y. K. Kim and D. Baek (2021). "A high-resolution temporal atlas of the SARS-CoV-2
3415   translatome and transcriptome." Nat Commun **12**(1): 5120.

3416   Kim, D., B. Langmead and S. L. Salzberg (2015). "HISAT: a fast spliced aligner with low memory
3417   requirements." Nat Methods **12**(4): 357-360.

3418   Kim, M. J., S. Y. Hwang, T. Imaizumi and J. Y. Yoo (2008). "Negative feedback regulation of RIG-I-mediated
3419   antiviral signaling by interferon-induced ISG15 conjugation." J Virol **82**(3): 1474-1483.

3420   Kong, F., O. A. Saldarriaga, H. Spratt, E. Y. Osorio, B. L. Travi, B. A. Luxon and P. C. Melby (2017).
3421   "Transcriptional Profiling in Experimental Visceral Leishmaniasis Reveals a Broad Splenic
3422   Inflammatory Environment that Conditions Macrophages toward a Disease-Promoting
3423   Phenotype." PLoS Pathog **13**(1): e1006165.

3424   Koo, M. S., S. Subbian and G. Kaplan (2012). "Strain specific transcriptional response in Mycobacterium
3425   tuberculosis infected macrophages." Cell Commun Signal **10**(1): 2.

3426   Kotsias, F., I. Cebrian and A. Alloatti (2019). "Antigen processing and presentation." Int Rev Cell Mol Biol
3427   **348**: 69-121.

3428　Kozlowski, E., G. A. Wasserman, M. Morgan, D. O'Carroll, N. P. Ramirez, S. Gummuluru, J. Y. Rah, A. C.
3429　　　　Gower, M. Ieong, L. J. Quinton, J. P. Mizgerd and M. R. Jones (2017). "The RNA uridyltransferase
3430　　　　Zcchc6 is expressed in macrophages and impacts innate immune responses." PLoS One **12**(6):
3431　　　　e0179797.

3432　Kramer, A., J. Green, J. Pollard, Jr. and S. Tugendreich (2014). "Causal analysis approaches in Ingenuity
3433　　　　Pathway Analysis." Bioinformatics **30**(4): 523-530.

3434　Kubler, M., S. Beck, S. Fischer, P. Gotz, K. Kumaraswami, H. Ishikawa-Ankerhold, M. Lasch and E. Deindl
3435　　　　(2021). "Absence of Cold-Inducible RNA-Binding Protein (CIRP) Promotes Angiogenesis and
3436　　　　Regeneration of Ischemic Tissue by Inducing M2-Like Macrophage Polarization." Biomedicines
3437　　　　**9**(4).

3438　Kumar, A., S. Das, A. Mandal, S. Verma, K. Abhishek, A. Kumar, V. Kumar, A. K. Ghosh and P. Das (2018).
3439　　　　"Leishmania infection activates host mTOR for its survival by M2 macrophage polarization."
3440　　　　Parasite Immunol **40**(11): e12586.

3441　Kupani, M., R. K. Pandey and S. Mehrotra (2021). "Neutrophils and Visceral Leishmaniasis: Impact on
3442　　　　innate immune response and cross-talks with macrophages and dendritic cells." J Cell Physiol
3443　　　　**236**(4): 2255-2267.

3444　Kurotaki, D., H. Sasaki and T. Tamura (2017). "Transcriptional control of monocyte and macrophage
3445　　　　development." Int Immunol **29**(3): 97-107.

3446　Kushawaha, P. K., C. D. Pati Tripathi and A. Dube (2022). "Leishmania donovani secretory protein
3447　　　　nucleoside diphosphate kinase b localizes in its nucleus and prevents ATP mediated cytolysis of
3448　　　　macrophages." Microb Pathog: 105457.

3449　Kuyumcu-Martinez, N. M., M. Joachims and R. E. Lloyd (2002). "Efficient cleavage of ribosome-associated
3450　　　　poly(A)-binding protein by enterovirus 3C protease." J Virol **76**(5): 2062-2074.

3451　Landre, V., B. Rotblat, S. Melino, F. Bernassola and G. Melino (2014). "Screening for E3-ubiquitin ligase
3452　　　　inhibitors: challenges and opportunities." Oncotarget **5**(18): 7988-8013.

3453　Lang, C., A. Hildebrandt, F. Brand, L. Opitz, H. Dihazi and C. G. Luder (2012). "Impaired chromatin
3454　　　　remodelling at STAT1-regulated promoters leads to global unresponsiveness of Toxoplasma
3455　　　　gondii-infected macrophages to IFN-gamma." PLoS Pathog **8**(1): e1002483.

3456　Langlais, D., R. Cencic, N. Moradin, J. M. Kennedy, K. Ayi, L. E. Brown, I. Crandall, M. J. Tarry, M. Schmeing,
3457　　　　K. C. Kain, J. A. Porco, Jr., J. Pelletier and P. Gros (2018). "Rocaglates as dual-targeting agents for
3458　　　　experimental cerebral malaria." Proc Natl Acad Sci U S A **115**(10): E2366-E2375.

3459   Laskay, T., G. van Zandbergen and W. Solbach (2003). "Neutrophil granulocytes--Trojan horses for
3460   Leishmania major and other intracellular microbes?" <u>Trends Microbiol</u> **11**(5): 210-214.

3461   Lavin, Y., D. Winter, R. Blecher-Gonen, E. David, H. Keren-Shaul, M. Merad, S. Jung and I. Amit (2014).
3462   "Tissue-resident macrophage enhancer landscapes are shaped by the local microenvironment."
3463   <u>Cell</u> **159**(6): 1312-1326.

3464   Lecoeur, H., E. Prina, T. Rosazza, K. Kokou, P. N'Diaye, N. Aulner, H. Varet, G. Bussotti, Y. Xing, G. Milon, R.
3465   Weil, G. Meng and G. F. Spath (2020). "Targeting Macrophage Histone H3 Modification as a
3466   Leishmania Strategy to Dampen the NF-kappaB/NLRP3-Mediated Inflammatory Response." <u>Cell</u>
3467   <u>Rep</u> **30**(6): 1870-1882 e1874.

3468   Lecoeur, H., T. Rosazza, K. Kokou, H. Varet, J. Y. Coppee, A. Lari, P. H. Commere, R. Weil, G. Meng, G. Milon,
3469   G. F. Spath and E. Prina (2020). "Leishmania amazonensis Subverts the Transcription Factor
3470   Landscape in Dendritic Cells to Avoid Inflammasome Activation and Stall Maturation." <u>Front</u>
3471   <u>Immunol</u> **11**: 1098.

3472   Lee, R. C., R. L. Feinbaum and V. Ambros (1993). "The C. elegans heterochronic gene lin-4 encodes small
3473   RNAs with antisense complementarity to lin-14." <u>Cell</u> **75**(5): 843-854.

3474   Lees, M. P., S. J. Fuller, R. McLeod, N. R. Boulter, C. M. Miller, A. M. Zakrzewski, E. J. Mui, W. H. Witola, J.
3475   J. Coyne, A. C. Hargrave, S. E. Jamieson, J. M. Blackwell, J. S. Wiley and N. C. Smith (2010). "P2X7
3476   receptor-mediated killing of an intracellular parasite, Toxoplasma gondii, by human and murine
3477   macrophages." <u>J Immunol</u> **184**(12): 7040-7046.

3478   LeibundGut-Landmann, S., J. M. Waldburger, M. Krawczyk, L. A. Otten, T. Suter, A. Fontana, H. Acha-Orbea
3479   and W. Reith (2004). "Mini-review: Specificity and expression of CIITA, the master regulator of
3480   MHC class II genes." <u>Eur J Immunol</u> **34**(6): 1513-1525.

3481   Leroux, L. P., V. Chaparro and M. Jaramillo (2020). "Infection by the Protozoan Parasite Toxoplasma gondii
3482   Inhibits Host MNK1/2-eIF4E Axis to Promote Its Survival." <u>Front Cell Infect Microbiol</u> **10**: 488.

3483   Leroux, L. P., J. Lorent, T. E. Graber, V. Chaparro, L. Masvidal, M. Aguirre, B. D. Fonseca, L. C. van Kempen,
3484   T. Alain, O. Larsson and M. Jaramillo (2018). "The Protozoan Parasite Toxoplasma gondii
3485   Selectively Reprograms the Host Cell Translatome." <u>Infect Immun</u> **86**(9).

3486   Li, C. M., S. J. Campbell, D. S. Kumararatne, A. V. Hill and D. A. Lammas (2002). "Response heterogeneity
3487   of human macrophages to ATP is associated with P2X7 receptor expression but not to
3488   polymorphisms in the P2RX7 promoter." <u>FEBS Lett</u> **531**(2): 127-131.

3489   Li, Y., L. Cai, H. Wang, P. Wu, W. Gu, Y. Chen, H. Hao, K. Tang, P. Yi, M. Liu, S. Miao and D. Ye (2011).
3490   "Pleiotropic regulation of macrophage polarization and tumorigenesis by formyl peptide
3491   receptor-2." Oncogene **30**(36): 3887-3899.

3492   Li, Y., S. Shah-Simpson, K. Okrah, A. T. Belew, J. Choi, K. L. Caradonna, P. Padmanabhan, D. M. Ndegwa, M.
3493   R. Temanni, H. Corrada Bravo, N. M. El-Sayed and B. A. Burleigh (2016). "Transcriptome
3494   Remodeling in Trypanosoma cruzi and Human Cells during Intracellular Infection." PLoS Pathog
3495   **12**(4): e1005511.

3496   Liang, S., H. M. Bellato, J. Lorent, F. C. S. Lupinacci, C. Oertlin, V. van Hoef, V. P. Andrade, M. Roffe, L.
3497   Masvidal, G. N. M. Hajj and O. Larsson (2018). "Polysome-profiling in small tissue samples."
3498   Nucleic Acids Res **46**(1): e3.

3499   Liepelt, A., J. C. Mossanen, B. Denecke, F. Heymann, R. De Santis, F. Tacke, G. Marx, D. H. Ostareck and A.
3500   Ostareck-Lederer (2014). "Translation control of TAK1 mRNA by hnRNP K modulates LPS-induced
3501   macrophage activation." RNA **20**(6): 899-911.

3502   Liepelt, A., I. S. Naarmann-de Vries, N. Simons, K. Eichelbaum, S. Fohr, S. K. Archer, A. Castello, B. Usadel,
3503   J. Krijgsveld, T. Preiss, G. Marx, M. W. Hentze, D. H. Ostareck and A. Ostareck-Lederer (2016).
3504   "Identification of RNA-binding Proteins in Macrophages by Interactome Capture." Mol Cell
3505   Proteomics **15**(8): 2699-2714.

3506   Lindoso, J. A., G. F. Cota, A. M. da Cruz, H. Goto, A. N. Maia-Elkhoury, G. A. Romero, M. L. de Sousa-Gomes,
3507   J. R. Santos-Oliveira and A. Rabello (2014). "Visceral leishmaniasis and HIV coinfection in Latin
3508   America." PLoS Negl Trop Dis **8**(9): e3136.

3509   Liu, X., S. Liao, Z. Xu, L. Zhu, F. Yang and W. Guo (2016). "Identification and Analysis of the Porcine
3510   MicroRNA in Porcine Cytomegalovirus-Infected Macrophages Using Deep Sequencing." PLoS One
3511   **11**(3): e0150971.

3512   Liu, Y., A. S. Hyde, M. A. Simpson and J. J. Barycki (2014). "Emerging regulatory paradigms in glutathione
3513   metabolism." Adv Cancer Res **122**: 69-101.

3514   Lloyd, R. E. (2013). "Regulation of stress granules and P-bodies during RNA virus infection." Wiley
3515   Interdiscip Rev RNA **4**(3): 317-331.

3516   Lodge, R. and A. Descoteaux (2005). "Modulation of phagolysosome biogenesis by the lipophosphoglycan
3517   of Leishmania." Clin Immunol **114**(3): 256-265.

3518   Long, J., J. Chen, Q. Wang, F. Gao, M. Lian, P. Zhang, Y. Yang and H. Zhu (2020). "NFAT activating protein
3519   with ITAM motif 1 (NFAM1) is upregulated on circulating monocytes in coronary artery disease
3520   and potentially correlated with monocyte chemotaxis." Atherosclerosis **307**: 39-51.

130

3521 Lopez-Pelaez, M., S. Fumagalli, C. Sanz, C. Herrero, S. Guerra, M. Fernandez and S. Alemany (2012).
3522   "Cot/tpl2-MKK1/2-Erk1/2 controls mTORC1-mediated mRNA translation in Toll-like receptor-
3523   activated macrophages." Mol Biol Cell **23**(15): 2982-2992.

3524 Lopez-Sanz, L., S. Bernal, C. Recio, I. Lazaro, A. Oguiza, A. Melgar, L. Jimenez-Castilla, J. Egido and C. Gomez-
3525   Guerrero (2018). "SOCS1-targeted therapy ameliorates renal and vascular oxidative stress in
3526   diabetes via STAT1 and PI3K inhibition." Lab Invest **98**(10): 1276-1290.

3527 Lorent, J., E. P. Kusnadi, V. van Hoef, R. J. Rebello, M. Leibovitch, J. Ristau, S. Chen, M. G. Lawrence, K. J.
3528   Szkop, B. Samreen, P. Balanathan, F. Rapino, P. Close, P. Bukczynska, K. Scharmann, I. Takizawa,
3529   G. P. Risbridger, L. A. Selth, S. A. Leidel, Q. Lin, I. Topisirovic, O. Larsson and L. Furic (2019).
3530   "Translational offsetting as a mode of estrogen receptor alpha-dependent regulation of gene
3531   expression." EMBO J **38**(23): e101323.

3532 Lukes, J., A. Butenko, H. Hashimi, D. A. Maslov, J. Votypka and V. Yurchenko (2018). "Trypanosomatids Are
3533   Much More than Just Trypanosomes: Clues from the Expanded Family Tree." Trends Parasitol
3534   **34**(6): 466-480.

3535 Luo, Y., Z. Na and S. A. Slavoff (2018). "P-Bodies: Composition, Properties, and Functions." Biochemistry
3536   **57**(17): 2424-2431.

3537 Mader, S., H. Lee, A. Pause and N. Sonenberg (1995). "The translation initiation factor eIF-4E binds to a
3538   common motif shared by the translation factor eIF-4 gamma and the translational repressors 4E-
3539   binding proteins." Mol Cell Biol **15**(9): 4990-4997.

3540 Makita, S., H. Takatori, A. Iwata, S. Tanaka, S. Furuta, K. Ikeda, A. Suto, K. Suzuki, S. B. V. Ramos and H.
3541   Nakajima (2020). "RNA-Binding Protein ZFP36L2 Downregulates Helios Expression and Suppresses
3542   the Function of Regulatory T Cells." Front Immunol **11**: 1291.

3543 Malik, A. R., M. Urbanska, M. Macias, A. Skalecka and J. Jaworski (2013). "Beyond control of protein
3544   translation: what we have learned about the non-canonical regulation and function of mammalian
3545   target of rapamycin (mTOR)." Biochim Biophys Acta **1834**(7): 1434-1448.

3546 Marintchev, A., K. A. Edmonds, B. Marintcheva, E. Hendrickson, M. Oberer, C. Suzuki, B. Herdy, N.
3547   Sonenberg and G. Wagner (2009). "Topology and regulation of the human eIF4A/4G/4H helicase
3548   complex in translation initiation." Cell **136**(3): 447-460.

3549 Marr, A. K., J. L. MacIsaac, R. Jiang, A. M. Airo, M. S. Kobor and W. R. McMaster (2014). "Leishmania
3550   donovani infection causes distinct epigenetic DNA methylation changes in host macrophages."
3551   PLoS Pathog **10**(10): e1004419.

3552	Marth, T. and B. L. Kelsall (1997). "Regulation of interleukin-12 by complement receptor 3 signaling." J Exp
3553	Med **185**(11): 1987-1995.

3554	Martínez, C. R. and C. J. Ruiz (2019). "Alterations in Host Lipid Metabolism Produced During Visceral
3555	Leishmaniasis Infections." Current Tropical Medicine Reports **6**(4): 250-255.

3556	Masek, T., L. Valasek and M. Pospisek (2011). "Polysome analysis and RNA purification from sucrose
3557	gradients." Methods Mol Biol **703**: 293-309.

3558	Mass, E., I. Ballesteros, M. Farlik, F. Halbritter, P. Gunther, L. Crozet, C. E. Jacome-Galarza, K. Handler, J.
3559	Klughammer, Y. Kobayashi, E. Gomez-Perdiguero, J. L. Schultze, M. Beyer, C. Bock and F.
3560	Geissmann (2016). "Specification of tissue-resident macrophages during organogenesis." Science
3561	**353**(6304).

3562	Masvidal, L., L. Hulea, L. Furic, I. Topisirovic and O. Larsson (2017). "mTOR-sensitive translation: Cleared
3563	fog reveals more trees." RNA Biol **14**(10): 1299-1305.

3564	Matheoud, D., N. Moradin, A. Bellemare-Pelletier, M. T. Shio, W. J. Hong, M. Olivier, E. Gagnon, M.
3565	Desjardins and A. Descoteaux (2013). "Leishmania evades host immunity by inhibiting antigen
3566	cross-presentation through direct cleavage of the SNARE VAMP8." Cell Host Microbe **14**(1): 15-
3567	25.

3568	Matte, C., G. Arango Duque and A. Descoteaux (2021). "Leishmania donovani Metacyclic Promastigotes
3569	Impair Phagosome Properties in Inflammatory Monocytes." Infect Immun **89**(7): e0000921.

3570	Matte, C. and A. Descoteaux (2010). "Leishmania donovani amastigotes impair gamma interferon-induced
3571	STAT1alpha nuclear translocation by blocking the interaction between STAT1alpha and importin-
3572	alpha5." Infect Immun **78**(9): 3736-3743.

3573	Matty, M. A., D. R. Knudsen, E. M. Walton, R. W. Beerman, M. R. Cronan, C. J. Pyle, R. E. Hernandez and
3574	D. M. Tobin (2019). "Potentiation of P2RX7 as a host-directed strategy for control of mycobacterial
3575	infection." Elife **8**.

3576	McKinney, C., D. Yu and I. Mohr (2013). "A new role for the cellular PABP repressor Paip2 as an innate
3577	restriction factor capable of limiting productive cytomegalovirus replication." Genes Dev **27**(16):
3578	1809-1820.

3579	McNeely, T. B. and S. J. Turco (1990). "Requirement of lipophosphoglycan for intracellular survival of
3580	Leishmania donovani within human monocytes." J Immunol **144**(7): 2745-2750.

3581	Medina-Colorado, A. A., E. Y. Osorio, O. A. Saldarriaga, B. L. Travi, F. Kong, H. Spratt, L. Soong and P. C.
3582	Melby (2017). "Splenic CD4+ T Cells in Progressive Visceral Leishmaniasis Show a Mixed Effector-

3583 Regulatory Phenotype and Impair Macrophage Effector Function through Inhibitory Receptor

3584 Expression." <u>PLoS One</u> **12**(1): e0169496.

3585 Meier, C. L., M. Svensson and P. M. Kaye (2003). "Leishmania-induced inhibition of macrophage antigen

3586 presentation analyzed at the single-cell level." <u>J Immunol</u> **171**(12): 6706-6713.

3587 Mendiratta, S., A. Gatto and G. Almouzni (2019). "Histone supply: Multitiered regulation ensures

3588 chromatin dynamics throughout the cell cycle." <u>J Cell Biol</u> **218**(1): 39-54.

3589 Menezes, S., D. Melandri, G. Anselmi, T. Perchet, J. Loschko, J. Dubrot, R. Patel, E. L. Gautier, S. Hugues,

3590 M. P. Longhi, J. Y. Henry, S. A. Quezada, G. Lauvau, A. M. Lennon-Dumenil, E. Gutierrez-Martinez,

3591 A. Bessis, E. Gomez-Perdiguero, C. E. Jacome-Galarza, H. Garner, F. Geissmann, R. Golub, M. C.

3592 Nussenzweig and P. Guermonprez (2016). "The Heterogeneity of Ly6C(hi) Monocytes Controls

3593 Their Differentiation into iNOS(+) Macrophages or Monocyte-Derived Dendritic Cells." <u>Immunity</u>

3594 **45**(6): 1205-1218.

3595 Mesquita, I., C. Ferreira, D. Moreira, G. E. G. Kluck, A. M. Barbosa, E. Torrado, R. J. Dinis-Oliveira, L. G.

3596 Goncalves, C. J. Beauparlant, A. Droit, L. Berod, T. Sparwasser, N. Bodhale, B. Saha, F. Rodrigues,

3597 C. Cunha, A. Carvalho, A. G. Castro, J. Estaquier and R. Silvestre (2020). "The Absence of HIF-1alpha

3598 Increases Susceptibility to Leishmania donovani Infection via Activation of BNIP3/mTOR/SREBP-

3599 1c Axis." <u>Cell Rep</u> **30**(12): 4052-4064 e4057.

3600 Meyuhas, O. (2015). "Ribosomal Protein S6 Phosphorylation: Four Decades of Research." <u>Int Rev Cell Mol</u>

3601 <u>Biol</u> **320**: 41-73.

3602 Meyuhas, O. and T. Kahan (2015). "The race to decipher the top secrets of TOP mRNAs." <u>Biochim Biophys</u>

3603 <u>Acta</u> **1849**(7): 801-811.

3604 Mi, H., X. Huang, A. Muruganujan, H. Tang, C. Mills, D. Kang and P. D. Thomas (2017). "PANTHER version

3605 11: expanded annotation data from Gene Ontology and Reactome pathways, and data analysis

3606 tool enhancements." <u>Nucleic Acids Res</u> **45**(D1): D183-D189.

3607 Modelska, A., E. Turro, R. Russell, J. Beaton, T. Sbarrato, K. Spriggs, J. Miller, S. Graf, E. Provenzano, F.

3608 Blows, P. Pharoah, C. Caldas and J. Le Quesne (2015). "The malignant phenotype in breast cancer

3609 is driven by eIF4A1-mediated changes in the translational landscape." <u>Cell Death Dis</u> **6**: e1603.

3610 Mohr, I. and N. Sonenberg (2012). "Host translation at the nexus of infection and immunity." <u>Cell Host</u>

3611 <u>Microbe</u> **12**(4): 470-483.

3612 Mollinedo, F., H. Janssen, J. de la Iglesia-Vicente, J. A. Villa-Pulgarin and J. Calafat (2010). "Selective fusion

3613 of azurophilic granules with Leishmania-containing phagosomes in human neutrophils." <u>J Biol</u>

3614 <u>Chem</u> **285**(45): 34528-34536.

3615   Molyneux, D. H., L. Savioli and D. Engels (2017). "Neglected tropical diseases: progress towards addressing
3616   the chronic pandemic." <u>Lancet</u> **389**(10066): 312-325.

3617   Mondal, D., C. Bern, D. Ghosh, M. Rashid, R. Molina, R. Chowdhury, R. Nath, P. Ghosh, L. A. C. Chapman,
3618   A. Alim, G. Bilbe and J. Alvar (2019). "Quantifying the Infectiousness of Post-Kala-Azar Dermal
3619   Leishmaniasis Toward Sand Flies." <u>Clin Infect Dis</u> **69**(2): 251-258.

3620   Moore, K. J., S. J. Turco and G. Matlashewski (1994). "Leishmania donovani infection enhances
3621   macrophage viability in the absence of exogenous growth factor." <u>J Leukoc Biol</u> **55**(1): 91-98.

3622   Moreira, D., V. Rodrigues, M. Abengozar, L. Rivas, E. Rial, M. Laforge, X. Li, M. Foretz, B. Viollet, J. Estaquier,
3623   A. Cordeiro da Silva and R. Silvestre (2015). "Leishmania infantum modulates host macrophage
3624   mitochondrial metabolism by hijacking the SIRT1-AMPK axis." <u>PLoS Pathog</u> **11**(3): e1004684.

3625   Morgan, D. J., L. H. Guimaraes, P. R. Machado, A. D'Oliveira, Jr., R. P. Almeida, E. L. Lago, D. R. Faria, W. L.
3626   Tafuri, W. O. Dutra and E. M. Carvalho (2007). "Cutaneous leishmaniasis during pregnancy:
3627   exuberant lesions and potential fetal complications." <u>Clin Infect Dis</u> **45**(4): 478-482.

3628   Morimoto, A., K. Uchida, J. K. Chambers, K. Sato, J. Hong, C. Sanjoba, Y. Matsumoto, J. Yamagishi and Y.
3629   Goto (2019). "Hemophagocytosis induced by Leishmania donovani infection is beneficial to
3630   parasite survival within macrophages." <u>PLoS Negl Trop Dis</u> **13**(11): e0007816.

3631   Morita, M., S. P. Gravel, V. Chenard, K. Sikstrom, L. Zheng, T. Alain, V. Gandin, D. Avizonis, M. Arguello, C.
3632   Zakaria, S. McLaughlan, Y. Nouet, A. Pause, M. Pollak, E. Gottlieb, O. Larsson, J. St-Pierre, I.
3633   Topisirovic and N. Sonenberg (2013). "mTORC1 controls mitochondrial activity and biogenesis
3634   through 4E-BP-dependent translational regulation." <u>Cell Metab</u> **18**(5): 698-711.

3635   Morita, M., S. P. Gravel, L. Hulea, O. Larsson, M. Pollak, J. St-Pierre and I. Topisirovic (2015). "mTOR
3636   coordinates protein synthesis, mitochondrial activity and proliferation." <u>Cell Cycle</u> **14**(4): 473-480.

3637   Mosser, D. M., K. Hamidzadeh and R. Goncalves (2021). "Macrophages and the maintenance of
3638   homeostasis." <u>Cell Mol Immunol</u> **18**(3): 579-587.

3639   Mukhopadhyay, D., J. E. Dalton, P. M. Kaye and M. Chatterjee (2014). "Post kala-azar dermal leishmaniasis:
3640   an unresolved mystery." <u>Trends Parasitol</u> **30**(2): 65-74.

3641   Mukhopadhyay, R., J. Jia, A. Arif, P. S. Ray and P. L. Fox (2009). "The GAIT system: a gatekeeper of
3642   inflammatory gene expression." <u>Trends Biochem Sci</u> **34**(7): 324-331.

3643   Muller, B. and D. Schumperli (1997). "The U7 snRNP and the hairpin binding protein: Key players in histone
3644   mRNA metabolism." <u>Semin Cell Dev Biol</u> **8**(6): 567-576.

3645 Muller, C., F. W. Schulte, K. Lange-Grunweller, W. Obermann, R. Madhugiri, S. Pleschka, J. Ziebuhr, R. K.
3646   Hartmann and A. Grunweller (2018). "Broad-spectrum antiviral activity of the eIF4A inhibitor
3647   silvestrol against corona- and picornaviruses." Antiviral Res **150**: 123-129.

3648 Munoz, F. M., R. Gao, Y. Tian, B. A. Henstenburg, J. E. Barrett and H. Hu (2017). "Neuronal P2X7 receptor-
3649   induced reactive oxygen species production contributes to nociceptive behavior in mice." Sci Rep
3650   **7**(1): 3539.

3651 Murray, P. J. (2017). "Macrophage Polarization." Annu Rev Physiol **79**: 541-566.

3652 N, A. G., J. A. Guillen, G. Gallardo, M. Diaz, J. V. de la Rosa, I. H. Hernandez, M. Casanova-Acebes, F. Lopez,
3653   C. Tabraue, S. Beceiro, C. Hong, P. C. Lara, M. Andujar, S. Arai, T. Miyazaki, S. Li, A. L. Corbi, P.
3654   Tontonoz, A. Hidalgo and A. Castrillo (2013). "The nuclear receptor LXRalpha controls the
3655   functional specialization of splenic macrophages." Nat Immunol **14**(8): 831-839.

3656 Naineni, S. K., R. Itoua Maiga, R. Cencic, A. A. Putnam, L. A. Amador, A. D. Rodriguez, E. Jankowsky and J.
3657   Pelletier (2020). "A comparative study of small molecules targeting eIF4A." RNA **26**(5): 541-549.

3658 Nair, S., M. P. Hande and L. H. Lim (2010). "Annexin-1 protects MCF7 breast cancer cells against heat-
3659   induced growth arrest and DNA damage." Cancer Lett **294**(1): 111-117.

3660 Naito, M. (2008). "Macrophage differentiation and function in health and disease." Pathol Int **58**(3): 143-
3661   155.

3662 Nandan, D., C. Camargo de Oliveira, A. Moeenrezakhanlou, M. Lopez, J. M. Silverman, J. Subek and N. E.
3663   Reiner (2012). "Myeloid cell IL-10 production in response to leishmania involves inactivation of
3664   glycogen synthase kinase-3beta downstream of phosphatidylinositol-3 kinase." J Immunol **188**(1):
3665   367-378.

3666 Negrao, F., C. Fernandez-Costa, N. Zorgi, S. Giorgio, M. Nogueira Eberlin and J. R. Yates, 3rd (2019). "Label-
3667   Free Proteomic Analysis Reveals Parasite-Specific Protein Alterations in Macrophages Following
3668   Leishmania amazonensis, Leishmania major, or Leishmania infantum Infection." ACS Infect Dis
3669   **5**(6): 851-862.

3670 O'Neill, L. A. (2009). "Regulation of signaling by non-degradative ubiquitination." J Biol Chem **284**(13):
3671   8209.

3672 Oertlin, C., J. Lorent, C. Murie, L. Furic, I. Topisirovic and O. Larsson (2019). "Generally applicable
3673   transcriptome-wide analysis of translation using anota2seq." Nucleic Acids Res **47**(12): e70.

3674 Ohtsuka, M., H. Arase, A. Takeuchi, S. Yamasaki, R. Shiina, T. Suenaga, D. Sakurai, T. Yokosuka, N. Arase,
3675   M. Iwashima, T. Kitamura, H. Moriya and T. Saito (2004). "NFAM1, an immunoreceptor tyrosine-

3676   based activation motif-bearing molecule that regulates B cell development and signaling." <u>Proc</u>

3677   <u>Natl Acad Sci U S A</u> **101**(21): 8126-8131.

3678   Okumura, F., A. J. Okumura, K. Uematsu, S. Hatakeyama, D. E. Zhang and T. Kamura (2013). "Activation of

3679   double-stranded RNA-activated protein kinase (PKR) by interferon-stimulated gene 15 (ISG15)

3680   modification down-regulates protein translation." <u>J Biol Chem</u> **288**(4): 2839-2847.

3681   Oliveira, L. G., M. C. Souza-Testasicca, J. P. Vago, A. B. Figueiredo, A. M. Canavaci, L. O. Perucci, T. P.

3682   Ferreira, E. A. Coelho, D. U. Goncalves, M. O. Rocha, E. S. PM, C. N. Ferreira, C. Queiroz-Junior, L.

3683   P. Sousa and A. P. Fernandes (2017). "Annexin A1 Is Involved in the Resolution of Inflammatory

3684   Responses during Leishmania braziliensis Infection." <u>J Immunol</u> **198**(8): 3227-3236.

3685   Onomoto, K., M. Jogi, J. S. Yoo, R. Narita, S. Morimoto, A. Takemura, S. Sambhara, A. Kawaguchi, S. Osari,

3686   K. Nagata, T. Matsumiya, H. Namiki, M. Yoneyama and T. Fujita (2012). "Critical role of an antiviral

3687   stress granule containing RIG-I and PKR in viral detection and innate immunity." <u>PLoS One</u> **7**(8):

3688   e43031.

3689   Oryan, A. and M. Akbari (2016). "Worldwide risk factors in leishmaniasis." <u>Asian Pac J Trop Med</u> **9**(10):

3690   925-932.

3691   Ottow, M. K., E. J. Klaver, T. C. van der Pouw Kraan, P. D. Heijnen, L. C. Laan, H. Kringel, D. Y. Vogel, C. D.

3692   Dijkstra, G. Kooij and I. van Die (2014). "The helminth Trichuris suis suppresses TLR4-induced

3693   inflammatory responses in human macrophages." <u>Genes Immun</u> **15**(7): 477-486.

3694   Oura, C. A., S. McKellar, D. G. Swan, E. Okan and B. R. Shiels (2006). "Infection of bovine cells by the

3695   protozoan parasite Theileria annulata modulates expression of the ISGylation system." <u>Cell</u>

3696   <u>Microbiol</u> **8**(2): 276-288.

3697   Ozaki, K. S., N. O. Camara, N. Z. Galante, L. F. Camargo and A. Pacheco-Silva (2005). "Decreased

3698   Cytomegalovirus infection after antilymphocyte therapy in sirolimus-treated renal transplant

3699   patients." <u>Int Immunopharmacol</u> **5**(1): 103-106.

3700   Padovese, V., M. Terranova, L. Toma, G. A. Barnabas and A. Morrone (2009). "Cutaneous and

3701   mucocutaneous leishmaniasis in Tigray, northern Ethiopia: clinical aspects and therapeutic

3702   concerns." <u>Trans R Soc Trop Med Hyg</u> **103**(7): 707-711.

3703   Pakos-Zebrucka, K., I. Koryga, K. Mnich, M. Ljujic, A. Samali and A. M. Gorman (2016). "The integrated

3704   stress response." <u>EMBO Rep</u> **17**(10): 1374-1395.

3705   Palamarchuk, A., A. Efanov, V. Maximov, R. I. Aqeilan, C. M. Croce and Y. Pekarsky (2005). "Akt

3706   phosphorylates and regulates Pdcd4 tumor suppressor protein." <u>Cancer Res</u> **65**(24): 11282-11286.

3707   Pan, L., L. B. Kardono, S. Riswan, H. Chai, E. J. Carcache de Blanco, C. M. Pannell, D. D. Soejarto, T. G.
3708   McCloud, D. J. Newman and A. D. Kinghorn (2010). "Isolation and characterization of minor
3709   analogues of silvestrol and other constituents from a large-scale re-collection of Aglaia foveolata."
3710   J Nat Prod **73**(11): 1873-1878.

3711   Pan, L., J. L. Woodard, D. M. Lucas, J. R. Fuchs and A. D. Kinghorn (2014). "Rocaglamide, silvestrol and
3712   structurally related bioactive compounds from Aglaia species." Nat Prod Rep **31**(7): 924-939.

3713   Pareyn, M., E. Van den Bosch, N. Girma, N. van Houtte, S. Van Dongen, G. Van der Auwera, F. Massebo, S.
3714   Shibru and H. Leirs (2019). "Ecology and seasonality of sandflies and potential reservoirs of
3715   cutaneous leishmaniasis in Ochollo, a hotspot in southern Ethiopia." PLoS Negl Trop Dis **13**(8):
3716   e0007667.

3717   Park, S. J., F. Ahmad, R. J. Bahde, A. Philp, J. Kim, T. Huang, M. K. Kim, W. C. Trenkle and J. H. Chung (2021).
3718   "Potent PDE4 inhibitor activates AMPK and Sirt1 to induce mitochondrial biogenesis." PLoS One
3719   **16**(6): e0253269.

3720   Parsyan, A., Y. Svitkin, D. Shahbazian, C. Gkogkas, P. Lasko, W. C. Merrick and N. Sonenberg (2011). "mRNA
3721   helicases: the tacticians of translational control." Nat Rev Mol Cell Biol **12**(4): 235-245.

3722   Pasquali, A. K. S., R. A. Baggio, W. A. Boeger, N. Gonzalez-Britez, D. C. Guedes, E. C. Chaves and V. Thomaz-
3723   Soccol (2019). "Dispersion of Leishmania (Leishmania) infantum in central-southern Brazil:
3724   Evidence from an integrative approach." PLoS Negl Trop Dis **13**(8): e0007639.

3725   Pearl, D., S. Katsumura, M. Amiri, N. Tabatabaei, X. Zhang, V. Vinette, X. Pang, S. T. Beug, S. H. Kim, L. M.
3726   Jones, N. Robichaud, S. G. Ong, J. J. Jia, H. Ali, M. L. Tremblay, M. Jaramillo, T. Alain, M. Morita, N.
3727   Sonenberg and S. Tahmasebi (2020). "4E-BP-Dependent Translational Control of Irf8 Mediates
3728   Adipose Tissue Macrophage Inflammatory Response." J Immunol **204**(9): 2392-2400.

3729   Peng, Y., J. Yuan, Z. Zhang and X. Chang (2017). "Cytoplasmic poly(A)-binding protein 1 (PABPC1) interacts
3730   with the RNA-binding protein hnRNPLL and thereby regulates immunoglobulin secretion in
3731   plasma cells." J Biol Chem **292**(29): 12285-12295.

3732   Pennini, M. E., R. K. Pai, D. C. Schultz, W. H. Boom and C. V. Harding (2006). "Mycobacterium tuberculosis
3733   19-kDa lipoprotein inhibits IFN-gamma-induced chromatin remodeling of MHC2TA by TLR2 and
3734   MAPK signaling." J Immunol **176**(7): 4323-4330.

3735   Pereira-Lopes, S., J. Tur, J. A. Calatayud-Subias, J. Lloberas, T. H. Stracker and A. Celada (2015). "NBS1 is
3736   required for macrophage homeostasis and functional activity in mice." Blood **126**(22): 2502-2510.

3737   Pereira, R. M., K. L. Teixeira, V. Barreto-de-Souza, T. C. Calegari-Silva, L. D. De-Melo, D. C. Soares, D. C.
3738   Bou-Habib, A. M. Silva, E. M. Saraiva and U. G. Lopes (2010). "Novel role for the double-stranded

RNA-activated protein kinase PKR: modulation of macrophage infection by the protozoan parasite Leishmania." FASEB J **24**(2): 617-626.

Perez-Cabezas, B., P. Cecilio, T. B. Gaspar, F. Gartner, R. Vasconcellos and A. Cordeiro-da-Silva (2019). "Understanding Resistance vs. Susceptibility in Visceral Leishmaniasis Using Mouse Models of Leishmania infantum Infection." Front Cell Infect Microbiol **9**: 30.

Peters, N. C., J. G. Egen, N. Secundino, A. Debrabant, N. Kimblin, S. Kamhawi, P. Lawyer, M. P. Fay, R. N. Germain and D. Sacks (2008). "In vivo imaging reveals an essential role for neutrophils in leishmaniasis transmitted by sand flies." Science **321**(5891): 970-974.

Phan, T. N., K. H. Baek, N. Lee, S. Y. Byun, D. Shum and J. H. No (2020). "In Vitro and in Vivo Activity of mTOR Kinase and PI3K Inhibitors Against Leishmania donovani and Trypanosoma brucei." Molecules **25**(8).

Phillips, R., M. Svensson, N. Aziz, A. Maroof, N. Brown, L. Beattie, N. Signoret and P. M. Kaye (2010). "Innate killing of Leishmania donovani by macrophages of the splenic marginal zone requires IRF-7." PLoS Pathog **6**(3): e1000813.

Piccirillo, C. A., E. Bjur, I. Topisirovic, N. Sonenberg and O. Larsson (2014). "Translational control of immune responses: from transcripts to translatomes." Nat Immunol **15**(6): 503-511.

Picelli, S., O. R. Faridani, A. K. Bjorklund, G. Winberg, S. Sagasser and R. Sandberg (2014). "Full-length RNA-seq from single cells using Smart-seq2." Nat Protoc **9**(1): 171-181.

Pinheiro, R. O., M. P. Nunes, C. S. Pinheiro, H. D'Avila, P. T. Bozza, C. M. Takiya, S. Corte-Real, C. G. Freire-de-Lima and G. A. DosReis (2009). "Induction of autophagy correlates with increased parasite load of Leishmania amazonensis in BALB/c but not C57BL/6 macrophages." Microbes Infect **11**(2): 181-190.

Place, D. E., B. Briard, P. Samir, R. Karki, A. Bhattacharya, C. S. Guy, J. L. Peters, S. Frase, P. Vogel, G. Neale, M. Yamamoto and T. D. Kanneganti (2020). "Interferon inducible GBPs restrict Burkholderia thailandensis motility induced cell-cell fusion." PLoS Pathog **16**(3): e1008364.

Podinovskaia, M. and A. Descoteaux (2015). "Leishmania and the macrophage: a multifaceted interaction." Future Microbiol **10**(1): 111-129.

Poulin, R. and H. S. Randhawa (2015). "Evolution of parasitism along convergent lines: from ecology to genomics." Parasitology **142 Suppl 1**: S6-S15.

Powers, C. J. and K. Fruh (2008). "Signal peptide-dependent inhibition of MHC class I heavy chain translation by rhesus cytomegalovirus." PLoS Pathog **4**(10): e1000150.

Price, J. V. and R. E. Vance (2014). "The macrophage paradox." Immunity **41**(5): 685-693.

Proksch, P., M. Giaisi, M. K. Treiber, K. Palfi, A. Merling, H. Spring, P. H. Krammer and M. Li-Weber (2005). "Rocaglamide derivatives are immunosuppressive phytochemicals that target NF-AT activity in T cells." J Immunol **174**(11): 7075-7084.

Qiao, Y., E. G. Giannopoulou, C. H. Chan, S. H. Park, S. Gong, J. Chen, X. Hu, O. Elemento and L. B. Ivashkiv (2013). "Synergistic activation of inflammatory cytokine genes by interferon-gamma-induced chromatin remodeling and toll-like receptor signaling." Immunity **39**(3): 454-469.

Quaresma, P. F., F. D. Rego, H. A. Botelho, S. R. da Silva, A. J. Moura Junior, R. G. Teixeira Neto, F. M. Madeira, M. B. Carvalho, A. P. Paglia, M. N. Melo and C. M. Gontijo (2011). "Wild, synanthropic and domestic hosts of Leishmania in an endemic area of cutaneous leishmaniasis in Minas Gerais State, Brazil." Trans R Soc Trop Med Hyg **105**(10): 579-585.

Rabhi, I., S. Rabhi, R. Ben-Othman, A. Rasche, A. Daskalaki, B. Trentin, D. Piquemal, B. Regnault, A. Descoteaux, L. Guizani-Tabbane and C. Sysco (2012). "Transcriptomic signature of Leishmania infected mice macrophages: a metabolic point of view." PLoS Negl Trop Dis **6**(8): e1763.

Rabhi, S., I. Rabhi, B. Trentin, D. Piquemal, B. Regnault, S. Goyard, T. Lang, A. Descoteaux, J. Enninga and L. Guizani-Tabbane (2016). "Lipid Droplet Formation, Their Localization and Dynamics during Leishmania major Macrophage Infection." PLoS One **11**(2): e0148640.

Rai, M. F., E. D. Tycksen, L. J. Sandell and R. H. Brophy (2018). "Advantages of RNA-seq compared to RNA microarrays for transcriptome profiling of anterior cruciate ligament tears." J Orthop Res **36**(1): 484-497.

Raker, V. K., C. Becker and K. Steinbrink (2016). "The cAMP Pathway as Therapeutic Target in Autoimmune and Inflammatory Diseases." Front Immunol **7**: 123.

Ramskold, D., E. T. Wang, C. B. Burge and R. Sandberg (2009). "An abundance of ubiquitously expressed genes revealed by tissue transcriptome sequence data." PLoS Comput Biol **5**(12): e1000598.

Rattray, A. M. and B. Muller (2012). "The control of histone gene expression." Biochem Soc Trans **40**(4): 880-885.

Raught, B. and A. C. Gingras (1999). "eIF4E activity is regulated at multiple levels." Int J Biochem Cell Biol **31**(1): 43-57.

Raught, B., F. Peiretti, A. C. Gingras, M. Livingstone, D. Shahbazian, G. L. Mayeur, R. D. Polakiewicz, N. Sonenberg and J. W. Hershey (2004). "Phosphorylation of eucaryotic translation initiation factor 4B Ser422 is modulated by S6 kinases." EMBO J **23**(8): 1761-1769.

Rawat, A. K., K. Pal, R. Singh, A. Anand, S. Gupta, D. Kishore, S. Singh and R. K. Singh (2020). "The CD200-CD200R cross-talk helps Leishmania donovani to down regulate macrophage and CD4(+)CD44(+)

3803   T cells effector functions in an NFkappaB independent manner." <u>Int J Biol Macromol</u> **151**: 394-
3804   401.

3805   Ray, M., A. A. Gam, R. A. Boykins and R. T. Kenney (2000). "Inhibition of interferon-gamma signaling by
3806   Leishmania donovani." <u>J Infect Dis</u> **181**(3): 1121-1128.

3807   Ready, P. D. (2010). "Leishmaniasis emergence in Europe." <u>Euro Surveill</u> **15**(10): 19505.

3808   Reineke, L. C., N. Kedersha, M. A. Langereis, F. J. van Kuppeveld and R. E. Lloyd (2015). "Stress granules
3809   regulate double-stranded RNA-dependent protein kinase activation through a complex containing
3810   G3BP1 and Caprin1." <u>mBio</u> **6**(2): e02486.

3811   Reinhart, B. J., F. J. Slack, M. Basson, A. E. Pasquinelli, J. C. Bettinger, A. E. Rougvie, H. R. Horvitz and G.
3812   Ruvkun (2000). "The 21-nucleotide let-7 RNA regulates developmental timing in Caenorhabditis
3813   elegans." <u>Nature</u> **403**(6772): 901-906.

3814   Ren, Y., F. A. Khan, N. S. Pandupuspitasari and S. Zhang (2017). "Immune Evasion Strategies of Pathogens
3815   in Macrophages: the Potential for Limiting Pathogen Transmission." <u>Curr Issues Mol Biol</u> **21**: 21-
3816   40.

3817   Rendra, E., V. Riabov, D. M. Mossel, T. Sevastyanova, M. C. Harmsen and J. Kzhyshkowska (2019).
3818   "Reactive oxygen species (ROS) in macrophage activation and function in diabetes."
3819   <u>Immunobiology</u> **224**(2): 242-253.

3820   Reverte, M., R. O. Eren, B. Jha, C. Desponds, T. Snaka, F. Prevel, N. Isorce, L. F. Lye, K. L. Owens, U. Gazos
3821   Lopes, S. M. Beverley and N. Fasel (2021). "The antioxidant response favors Leishmania parasites
3822   survival, limits inflammation and reprograms the host cell metabolism." <u>PLoS Pathog</u> **17**(3):
3823   e1009422.

3824   Rhodes, D. and H. J. Lipps (2015). "G-quadruplexes and their regulatory roles in biology." <u>Nucleic Acids</u>
3825   <u>Res</u> **43**(18): 8627-8637.

3826   Richter, J. D. and J. Coller (2015). "Pausing on Polyribosomes: Make Way for Elongation in Translational
3827   Control." <u>Cell</u> **163**(2): 292-300.

3828   Rodrigues, D. C., M. Mufteev, R. J. Weatheritt, U. Djuric, K. C. H. Ha, P. J. Ross, W. Wei, A. Piekna, M. A.
3829   Sartori, L. Byres, R. S. F. Mok, K. Zaslavsky, P. Pasceri, P. Diamandis, Q. Morris, B. J. Blencowe and
3830   J. Ellis (2020). "Shifts in Ribosome Engagement Impact Key Gene Sets in Neurodevelopment and
3831   Ubiquitination in Rett Syndrome." <u>Cell Rep</u> **30**(12): 4179-4196 e4111.

3832   Rodrigues, V., A. Cordeiro-da-Silva, M. Laforge, R. Silvestre and J. Estaquier (2016). "Regulation of
3833   immunity during visceral Leishmania infection." <u>Parasit Vectors</u> **9**: 118.

Rodriguez, N. E., H. K. Chang and M. E. Wilson (2004). "Novel program of macrophage gene expression induced by phagocytosis of Leishmania chagasi." Infect Immun **72**(4): 2111-2122.

Rojas Marquez, J. D., Y. Ana, R. E. Baigorri, C. C. Stempin and F. M. Cerban (2018). "Mammalian Target of Rapamycin Inhibition in Trypanosoma cruzi-Infected Macrophages Leads to an Intracellular Profile That Is Detrimental for Infection." Front Immunol **9**: 313.

Roy, G., H. K. Brar, R. Muthuswami and R. Madhubala (2020). "Epigenetic regulation of defense genes by histone deacetylase1 in human cell line-derived macrophages promotes intracellular survival of Leishmania donovani." PLoS Negl Trop Dis **14**(4): e0008167.

Roy, S., D. Mukhopadhyay, S. Mukherjee, S. Ghosh, S. Kumar, K. Sarkar, D. Pal, P. Bhowmik, K. Mandal, D. Modak, S. K. Guha, N. Pramanik, R. P. Goswami, B. Saha and M. Chatterjee (2015). "A Defective Oxidative Burst and Impaired Antigen Presentation are Hallmarks of Human Visceral Leishmaniasis." J Clin Immunol **35**(1): 56-67.

Rubio, C. A., B. Weisburd, M. Holderfield, C. Arias, E. Fang, J. L. DeRisi and A. Fanidi (2014). "Transcriptome-wide characterization of the eIF4A signature highlights plasticity in translation regulation." Genome Biol **15**(10): 476.

Saha, A., A. Bhattacharjee, A. Vij, P. K. Das, A. Bhattacharya and A. Biswas (2020). "Evaluation of Modulators of cAMP-Response in Terms of Their Impact on Cell Cycle and Mitochondrial Activity of Leishmania donovani." Front Pharmacol **11**: 782.

Saha, A., A. Biswas, S. Srivastav, M. Mukherjee, P. K. Das and A. Ukil (2014). "Prostaglandin E2 negatively regulates the production of inflammatory cytokines/chemokines and IL-17 in visceral leishmaniasis." J Immunol **193**(5): 2330-2339.

Saha, S., M. Basu, S. Guin, P. Gupta, A. M. Mitterstiller, G. Weiss, K. Jana and A. Ukil (2019). "Leishmania donovani Exploits Macrophage Heme Oxygenase-1 To Neutralize Oxidative Burst and TLR Signaling-Dependent Host Defense." J Immunol **202**(3): 827-840.

Saha, S., S. Roy, A. Dutta, K. Jana and A. Ukil (2021). "Leishmania donovani Targets Host Transcription Factor NRF2 To Activate Antioxidant Enzyme HO-1 and Transcriptional Repressor ATF3 for Establishing Infection." Infect Immun **89**(7): e0076420.

Salem, E. S. B., A. D. Vonberg, V. J. Borra, R. K. Gill and T. Nakamura (2019). "RNAs and RNA-Binding Proteins in Immuno-Metabolic Homeostasis and Diseases." Front Cardiovasc Med **6**: 106.

Salerno, F., S. Engels, M. van den Biggelaar, F. P. J. van Alphen, A. Guislain, W. Zhao, D. L. Hodge, S. E. Bell, J. P. Medema, M. von Lindern, M. Turner, H. A. Young and M. C. Wolkers (2018). "Translational

3865   repression of pre-formed cytokine-encoding mRNA prevents chronic activation of memory T
3866   cells." <u>Nat Immunol</u> **19**(8): 828-837.

3867 Sambandam, Y., K. Sundaram, T. Saigusa, S. Balasubramanian and S. V. Reddy (2017). "NFAM1 signaling
3868   enhances osteoclast formation and bone resorption activity in Paget's disease of bone." <u>Bone</u> **101**:
3869   236-244.

3870 Sampath, P., B. Mazumder, V. Seshadri and P. L. Fox (2003). "Transcript-selective translational silencing
3871   by gamma interferon is directed by a novel structural element in the ceruloplasmin mRNA 3'
3872   untranslated region." <u>Mol Cell Biol</u> **23**(5): 1509-1519.

3873 Sampath, P., B. Mazumder, V. Seshadri, C. A. Gerber, L. Chavatte, M. Kinter, S. M. Ting, J. D. Dignam, S.
3874   Kim, D. M. Driscoll and P. L. Fox (2004). "Noncanonical function of glutamyl-prolyl-tRNA
3875   synthetase: gene-specific silencing of translation." <u>Cell</u> **119**(2): 195-208.

3876 Sasaki, A., H. Yokoo, M. Naito, C. Kaizu, L. D. Shultz and Y. Nakazato (2000). "Effects of macrophage-colony-
3877   stimulating factor deficiency on the maturation of microglia and brain macrophages and on their
3878   expression of scavenger receptor." <u>Neuropathology</u> **20**(2): 134-142.

3879 Sato, N., W. A. Kuziel, P. C. Melby, R. L. Reddick, V. Kostecki, W. Zhao, N. Maeda, S. K. Ahuja and S. S. Ahuja
3880   (1999). "Defects in the generation of IFN-gamma are overcome to control infection with
3881   Leishmania donovani in CC chemokine receptor (CCR) 5-, macrophage inflammatory protein-1
3882   alpha-, or CCR2-deficient mice." <u>J Immunol</u> **163**(10): 5519-5525.

3883 Satoh, T., O. Takeuchi, A. Vandenbon, K. Yasuda, Y. Tanaka, Y. Kumagai, T. Miyake, K. Matsushita, T.
3884   Okazaki, T. Saitoh, K. Honma, T. Matsuyama, K. Yui, T. Tsujimura, D. M. Standley, K. Nakanishi, K.
3885   Nakai and S. Akira (2010). "The Jmjd3-Irf4 axis regulates M2 macrophage polarization and host
3886   responses against helminth infection." <u>Nat Immunol</u> **11**(10): 936-944.

3887 Sauter, I. P., K. G. Madrid, J. B. de Assis, A. Sa-Nunes, A. C. Torrecilhas, D. I. Staquicini, R. Pasqualini, W.
3888   Arap and M. Cortez (2019). "TLR9/MyD88/TRIF signaling activates host immune inhibitory CD200
3889   in Leishmania infection." <u>JCI Insight</u> **4**(10).

3890 Saxton, R. A. and D. M. Sabatini (2017). "mTOR Signaling in Growth, Metabolism, and Disease." <u>Cell</u> **168**(6):
3891   960-976.

3892 Schnitger, A. K., A. Machova, R. U. Mueller, A. Androulidaki, B. Schermer, M. Pasparakis, M. Kronke and
3893   N. Papadopoulou (2011). "Listeria monocytogenes infection in macrophages induces vacuolar-
3894   dependent host miRNA response." <u>PLoS One</u> **6**(11): e27435.

3895 Schultze, J. L., T. Freeman, D. A. Hume and E. Latz (2015). "A transcriptional perspective on human
3896   macrophage biology." <u>Semin Immunol</u> **27**(1): 44-50.

142

3897   Schwanhausser, B., D. Busse, N. Li, G. Dittmar, J. Schuchhardt, J. Wolf, W. Chen and M. Selbach (2011).
3898   "Global quantification of mammalian gene expression control." <u>Nature</u> **473**(7347): 337-342.
3899   Sen, N. D., F. Zhou, M. S. Harris, N. T. Ingolia and A. G. Hinnebusch (2016). "eIF4B stimulates translation
3900   of long mRNAs with structured 5' UTRs and low closed-loop potential but weak dependence on
3901   eIF4G." <u>Proc Natl Acad Sci U S A</u> **113**(38): 10464-10472.
3902   Seshadri, C., M. Shenoy, R. D. Wells, T. Hensley-McBain, E. Andersen-Nissen, M. J. McElrath, T. Y. Cheng,
3903   D. B. Moody and T. R. Hawn (2013). "Human CD1a deficiency is common and genetically
3904   regulated." <u>J Immunol</u> **191**(4): 1586-1593.
3905   Shadab, M., S. Das, A. Banerjee, R. Sinha, M. Asad, M. Kamran, M. Maji, B. Jha, M. Deepthi, M. Kumar, A.
3906   Tripathi, B. Kumar, S. Chakrabarti and N. Ali (2019). "RNA-Seq Revealed Expression of Many Novel
3907   Genes Associated With Leishmania donovani Persistence and Clearance in the Host Macrophage."
3908   <u>Front Cell Infect Microbiol</u> **9**: 17.
3909   Shahbazian, D., P. P. Roux, V. Mieulet, M. S. Cohen, B. Raught, J. Taunton, J. W. Hershey, J. Blenis, M.
3910   Pende and N. Sonenberg (2006). "The mTOR/PI3K and MAPK pathways converge on eIF4B to
3911   control its phosphorylation and activity." <u>EMBO J</u> **25**(12): 2781-2791.
3912   Sheikh, M. S. and A. J. Fornace, Jr. (1999). "Regulation of translation initiation following stress." <u>Oncogene</u>
3913   **18**(45): 6121-6128.
3914   Sibley, L. D. (2011). "Invasion and intracellular survival by protozoan parasites." <u>Immunol Rev</u> **240**(1): 72-
3915   91.
3916   Silva, J. S., A. C. Andrade, C. C. Santana, L. Q. Santos, C. I. Oliveira, P. S. Veras, J. Vassallo and W. L. dos-
3917   Santos (2012). "Low CXCL13 expression, splenic lymphoid tissue atrophy and germinal center
3918   disruption in severe canine visceral leishmaniasis." <u>PLoS One</u> **7**(1): e29103.
3919   Simpson, D. M. and R. Ross (1972). "The neutrophilic leukocyte in wound repair a study with
3920   antineutrophil serum." <u>J Clin Invest</u> **51**(8): 2009-2023.
3921   Singh, A. K., R. K. Pandey, J. L. Siqueira-Neto, Y. J. Kwon, L. H. Freitas-Junior, C. Shaha and R. Madhubala
3922   (2015). "Proteomic-based approach to gain insight into reprogramming of THP-1 cells exposed to
3923   Leishmania donovani over an early temporal window." <u>Infect Immun</u> **83**(5): 1853-1868.
3924   Singh, G., H. D. Chavan and C. S. Dey (2008). "Proteomic analysis of miltefosine-resistant Leishmania
3925   reveals the possible involvement of eukaryotic initiation factor 4A (eIF4A)." <u>Int J Antimicrob</u>
3926   <u>Agents</u> **31**(6): 584-586.
3927   Singh, G., G. Pratt, G. W. Yeo and M. J. Moore (2015). "The Clothes Make the mRNA: Past and Present
3928   Trends in mRNP Fashion." <u>Annu Rev Biochem</u> **84**: 325-354.

3929 Singh, O. P., E. Hasker, M. Boelaert and S. Sundar (2016). "Elimination of visceral leishmaniasis on the
3930   Indian subcontinent." Lancet Infect Dis **16**(12): e304-e309.

3931 Slupphaug, G., B. Kavli and H. E. Krokan (2003). "The interacting pathways for prevention and repair of
3932   oxidative DNA damage." Mutat Res **531**(1-2): 231-251.

3933 Smelt, S. C., C. R. Engwerda, M. McCrossen and P. M. Kaye (1997). "Destruction of follicular dendritic cells
3934   during chronic visceral leishmaniasis." J Immunol **158**(8): 3813-3821.

3935 Smirlis, D., F. Dingli, P. Pescher, E. Prina, D. Loew, N. Rachidi and G. F. Spath (2020). "SILAC-based
3936   quantitative proteomics reveals pleiotropic, phenotypic modulation in primary murine
3937   macrophages infected with the protozoan pathogen Leishmania donovani." J Proteomics **213**:
3938   103617.

3939 Smith, E. M., N. E. H. Benbahouche, K. Morris, A. Wilczynska, S. Gillen, T. Schmidt, H. A. Meijer, R. Jukes-
3940   Jones, K. Cain, C. Jones, M. Stoneley, J. A. Waldron, C. Bell, B. D. Fonseca, S. Blagden, A. E. Willis
3941   and M. Bushell (2021). "The mTOR regulated RNA-binding protein LARP1 requires PABPC1 for
3942   guided mRNA interaction." Nucleic Acids Res **49**(1): 458-478.

3943 Sohrabi, Y., V. Volkova, T. Kobets, H. Havelkova, I. Krayem, M. Slapnickova, P. Demant and M. Lipoldova
3944   (2018). "Genetic Regulation of Guanylate-Binding Proteins 2b and 5 during Leishmaniasis in Mice."
3945   Front Immunol **9**: 130.

3946 Sokolova, O., M. Vieth, T. Gnad, P. M. Bozko and M. Naumann (2014). "Helicobacter pylori promotes
3947   eukaryotic protein translation by activating phosphatidylinositol 3 kinase/mTOR." Int J Biochem
3948   Cell Biol **55**: 157-163.

3949 Somanna, A., V. Mundodi and L. Gedamu (2002). "Functional analysis of cathepsin B-like cysteine
3950   proteases from Leishmania donovani complex. Evidence for the activation of latent transforming
3951   growth factor beta." J Biol Chem **277**(28): 25305-25312.

3952 Spangle, J. M. and K. Munger (2010). "The human papillomavirus type 16 E6 oncoprotein activates
3953   mTORC1 signaling and increases protein synthesis." J Virol **84**(18): 9398-9407.

3954 Srivastav, S., W. Basu Ball, P. Gupta, J. Giri, A. Ukil and P. K. Das (2014). "Leishmania donovani prevents
3955   oxidative burst-mediated apoptosis of host macrophages through selective induction of
3956   suppressors of cytokine signaling (SOCS) proteins." J Biol Chem **289**(2): 1092-1105.

3957 Srivastav, S., S. Kar, A. G. Chande, R. Mukhopadhyaya and P. K. Das (2012). "Leishmania donovani exploits
3958   host deubiquitinating enzyme A20, a negative regulator of TLR signaling, to subvert host immune
3959   response." J Immunol **189**(2): 924-934.

144

3960 Stanley, A. C. and C. R. Engwerda (2007). "Balancing immunity and pathology in visceral leishmaniasis."
3961   Immunol Cell Biol **85**(2): 138-147.

3962 Stone, E. L., M. Pepper, C. D. Katayama, Y. M. Kerdiles, C. Y. Lai, E. Emslie, Y. C. Lin, E. Yang, A. W. Goldrath,
3963   M. O. Li, D. A. Cantrell and S. M. Hedrick (2015). "ICOS coreceptor signaling inactivates the
3964   transcription factor FOXO1 to promote Tfh cell differentiation." Immunity **42**(2): 239-251.

3965 Stout, R. D. and J. Suttles (2004). "Functional plasticity of macrophages: reversible adaptation to changing
3966   microenvironments." J Leukoc Biol **76**(3): 509-513.

3967 Su, H., N. Na, X. Zhang and Y. Zhao (2017). "The biological function and significance of CD74 in immune
3968   diseases." Inflamm Res **66**(3): 209-216.

3969 Su, X., Y. Yu, Y. Zhong, E. G. Giannopoulou, X. Hu, H. Liu, J. R. Cross, G. Ratsch, C. M. Rice and L. B. Ivashkiv
3970   (2015). "Interferon-gamma regulates cellular metabolism and mRNA translation to potentiate
3971   macrophage activation." Nat Immunol **16**(8): 838-849.

3972 Sun, C., R. Mezzadra and T. N. Schumacher (2018). "Regulation and Function of the PD-L1 Checkpoint."
3973   Immunity **48**(3): 434-452.

3974 Suner, C., A. Sibilio, J. Martin, C. L. Castellazzi, O. Reina, I. Dotu, A. Caballe, E. Rivas, V. Calderone, J. Diez,
3975   A. R. Nebreda and R. Mendez (2022). "Macrophage inflammation resolution requires CPEB4-
3976   directed offsetting of mRNA degradation." Elife **11**.

3977 Sutherland, E. W., G. A. Robison and R. W. Butcher (1968). "Some Aspects of the Biological Role of
3978   Adenosine 3',5'-monophosphate (Cyclic AMP)." Circulation **37**(2): 279-306.

3979 Suzuki, Y., W. X. Chin, Q. Han, K. Ichiyama, C. H. Lee, Z. W. Eyo, H. Ebina, H. Takahashi, C. Takahashi, B. H.
3980   Tan, T. Hishiki, K. Ohba, T. Matsuyama, Y. Koyanagi, Y. J. Tan, T. Sawasaki, J. J. Chu, S. G.
3981   Vasudevan, K. Sano and N. Yamamoto (2016). "Characterization of RyDEN (C19orf66) as an
3982   Interferon-Stimulated Cellular Inhibitor against Dengue Virus Replication." PLoS Pathog **12**(1):
3983   e1005357.

3984 Svitkin, Y. V., A. Pause, A. Haghighat, S. Pyronnet, G. Witherell, G. J. Belsham and N. Sonenberg (2001).
3985   "The requirement for eukaryotic initiation factor 4A (eIF4A) in translation is in direct proportion
3986   to the degree of mRNA 5' secondary structure." RNA **7**(3): 382-394.

3987 Taciak, B., M. Bialasek, A. Braniewska, Z. Sas, P. Sawicka, L. Kiraga, T. Rygiel and M. Krol (2018). "Evaluation
3988   of phenotypic and functional stability of RAW 264.7 cell line through serial passages." PLoS One
3989   **13**(6): e0198943.

3990 Takeuchi, T., T. Kobayashi, S. Tamura and H. Yokosawa (2006). "Negative regulation of protein
3991   phosphatase 2Cbeta by ISG15 conjugation." FEBS Lett **580**(18): 4521-4526.

3992   Tamoutounour, S., M. Guilliams, F. Montanana Sanchis, H. Liu, D. Terhorst, C. Malosse, E. Pollet, L.
3993   Ardouin, H. Luche, C. Sanchez, M. Dalod, B. Malissen and S. Henri (2013). "Origins and functional
3994   specialization of macrophages and of conventional and monocyte-derived dendritic cells in mouse
3995   skin." Immunity **39**(5): 925-938.

3996   Tanaka, H. and C. E. Samuel (1994). "Mechanism of interferon action: structure of the mouse PKR gene
3997   encoding the interferon-inducible RNA-dependent protein kinase." Proc Natl Acad Sci U S A
3998   **91**(17): 7995-7999.

3999   Taroncher-Oldenburg, G., C. Muller, W. Obermann, J. Ziebuhr, R. K. Hartmann and A. Grunweller (2021).
4000   "Targeting the DEAD-Box RNA Helicase eIF4A with Rocaglates-A Pan-Antiviral Strategy for
4001   Minimizing the Impact of Future RNA Virus Pandemics." Microorganisms **9**(3).

4002   Tavares, L. P., G. L. Negreiros-Lima, K. M. Lima, E. S. PMR, V. Pinho, M. M. Teixeira and L. P. Sousa (2020).
4003   "Blame the signaling: Role of cAMP for the resolution of inflammation." Pharmacol Res **159**:
4004   105030.

4005   Taylor, S., M. Wakem, G. Dijkman, M. Alsarraj and M. Nguyen (2010). "A practical approach to RT-qPCR-
4006   Publishing data that conform to the MIQE guidelines." Methods **50**(4): S1-5.

4007   Tedesco, S., F. De Majo, J. Kim, A. Trenti, L. Trevisi, G. P. Fadini, C. Bolego, P. W. Zandstra, A. Cignarella
4008   and L. Vitiello (2018). "Convenience versus Biological Significance: Are PMA-Differentiated THP-1
4009   Cells a Reliable Substitute for Blood-Derived Macrophages When Studying in Vitro Polarization?"
4010   Front Pharmacol **9**: 71.

4011   Teles, R. M. B., J. Lu, M. Tio-Coma, I. M. B. Goulart, S. Banu, D. Hagge, K. Bobosha, T. H. M. Ottenhoff, M.
4012   Pellegrini, A. Geluk and R. L. Modlin (2019). "Identification of a systemic interferon-gamma
4013   inducible antimicrobial gene signature in leprosy patients undergoing reversal reaction." PLoS
4014   Negl Trop Dis **13**(10): e0007764.

4015   Teng, Y., M. Gao, J. Wang, Q. Kong, H. Hua, T. Luo and Y. Jiang (2014). "Inhibition of eIF2alpha
4016   dephosphorylation enhances TRAIL-induced apoptosis in hepatoma cells." Cell Death Dis **5**: e1060.

4017   Thakur, A., H. Mikkelsen and G. Jungersen (2019). "Intracellular Pathogens: Host Immunity and Microbial
4018   Persistence Strategies." J Immunol Res **2019**: 1356540.

4019   Thomas, S. A., D. Nandan, J. Kass and N. E. Reiner (2018). "Countervailing, time-dependent effects on host
4020   autophagy promotes intracellular survival of Leishmania." J Biol Chem **293**(7): 2617-2630.

4021   Tuon, F. F., V. A. Neto and V. S. Amato (2008). "Leishmania: origin, evolution and future since the
4022   Precambrian." FEMS Immunol Med Microbiol **54**(2): 158-166.

4023   Turner, M. and M. D. Diaz-Munoz (2018). "RNA-binding proteins control gene expression and cell fate in
4024   the immune system." <u>Nat Immunol</u> **19**(2): 120-129.

4025   Ueno, N. and M. E. Wilson (2012). "Receptor-mediated phagocytosis of Leishmania: implications for
4026   intracellular survival." <u>Trends Parasitol</u> **28**(8): 335-344.

4027   Van Der Kelen, K., R. Beyaert, D. Inze and L. De Veylder (2009). "Translational control of eukaryotic gene
4028   expression." <u>Crit Rev Biochem Mol Biol</u> **44**(4): 143-168.

4029   van Griensven, J. and E. Diro (2019). "Visceral Leishmaniasis: Recent Advances in Diagnostics and
4030   Treatment Regimens." <u>Infect Dis Clin North Am</u> **33**(1): 79-99.

4031   van Zandbergen, G., N. Hermann, H. Laufs, W. Solbach and T. Laskay (2002). "Leishmania promastigotes
4032   release a granulocyte chemotactic factor and induce interleukin-8 release but inhibit gamma
4033   interferon-inducible protein 10 production by neutrophil granulocytes." <u>Infect Immun</u> **70**(8):
4034   4177-4184.

4035   Vargas-Inchaustegui, D. A., L. Xin and L. Soong (2008). "Leishmania braziliensis infection induces dendritic
4036   cell activation, ISG15 transcription, and the generation of protective immune responses." <u>J
4037   Immunol</u> **180**(11): 7537-7545.

4038   Vattem, K. M. and R. C. Wek (2004). "Reinitiation involving upstream ORFs regulates ATF4 mRNA
4039   translation in mammalian cells." <u>Proc Natl Acad Sci U S A</u> **101**(31): 11269-11274.

4040   Villarroya-Beltri, C., F. Baixauli, M. Mittelbrunn, I. Fernandez-Delgado, D. Torralba, O. Moreno-Gonzalo, S.
4041   Baldanta, C. Enrich, S. Guerra and F. Sanchez-Madrid (2016). "ISGylation controls exosome
4042   secretion by promoting lysosomal degradation of MVB proteins." <u>Nat Commun</u> **7**: 13588.

4043   Villarroya-Beltri, C., S. Guerra and F. Sanchez-Madrid (2017). "ISGylation - a key to lock the cell gates for
4044   preventing the spread of threats." <u>J Cell Sci</u> **130**(18): 2961-2969.

4045   Vivarini, A. C., T. C. Calegari-Silva, A. M. Saliba, V. S. Boaventura, J. Franca-Costa, R. Khouri, T. Dierckx, K.
4046   L. Dias-Teixeira, N. Fasel, A. M. P. Barral, V. M. Borges, J. Van Weyenbergh and U. G. Lopes (2017).
4047   "Systems Approach Reveals Nuclear Factor Erythroid 2-Related Factor 2/Protein Kinase R
4048   Crosstalk in Human Cutaneous Leishmaniasis." <u>Front Immunol</u> **8**: 1127.

4049   Vivarini Ade, C., M. Pereira Rde, K. L. Teixeira, T. C. Calegari-Silva, M. Bellio, M. D. Laurenti, C. E. Corbett,
4050   C. M. Gomes, R. P. Soares, A. M. Silva, F. T. Silveira and U. G. Lopes (2011). "Human cutaneous
4051   leishmaniasis: interferon-dependent expression of double-stranded RNA-dependent protein
4052   kinase (PKR) via TLR2." <u>FASEB J</u> **25**(12): 4162-4173.

4053   Vomund, S., A. Schafer, M. J. Parnham, B. Brune and A. von Knethen (2017). "Nrf2, the Master Regulator
4054   of Anti-Oxidative Responses." <u>Int J Mol Sci</u> **18**(12).

4055   Waldron, J. A., F. Raza and J. Le Quesne (2018). "eIF4A alleviates the translational repression mediated by
4056   classical secondary structures more than by G-quadruplexes." <u>Nucleic Acids Res</u> **46**(6): 3075-3087.
4057   Wang, K. T., H. H. Wang, Y. Y. Wu, Y. L. Su, P. Y. Chiang, N. Y. Lin, S. C. Wang, G. D. Chang and C. J. Chang
4058   (2015). "Functional regulation of Zfp36l1 and Zfp36l2 in response to lipopolysaccharide in mouse
4059   RAW264.7 macrophages." <u>J Inflamm (Lond)</u> **12**: 42.
4060   Wang, Y., K. J. Szretter, W. Vermi, S. Gilfillan, C. Rossini, M. Cella, A. D. Barrow, M. S. Diamond and M.
4061   Colonna (2012). "IL-34 is a tissue-restricted ligand of CSF1R required for the development of
4062   Langerhans cells and microglia." <u>Nat Immunol</u> **13**(8): 753-760.
4063   Wang, Z., N. Day, P. Trifillis and M. Kiledjian (1999). "An mRNA stability complex functions with poly(A)-
4064   binding protein to stabilize mRNA in vitro." <u>Mol Cell Biol</u> **19**(7): 4552-4560.
4065   Weber, C. M. and S. Henikoff (2014). "Histone variants: dynamic punctuation in transcription." <u>Genes Dev</u>
4066   **28**(7): 672-682.
4067   Wei, H., S. Wang, Q. Chen, Y. Chen, X. Chi, L. Zhang, S. Huang, G. F. Gao and J. L. Chen (2014). "Suppression
4068   of interferon lambda signaling by SOCS-1 results in their excessive production during influenza
4069   virus infection." <u>PLoS Pathog</u> **10**(1): e1003845.
4070   Weichhart, T., M. Hengstschlager and M. Linke (2015). "Regulation of innate immune cell function by
4071   mTOR." <u>Nat Rev Immunol</u> **15**(10): 599-614.
4072   Werneke, S. W., C. Schilte, A. Rohatgi, K. J. Monte, A. Michault, F. Arenzana-Seisdedos, D. L.
4073   Vanlandingham, S. Higgs, A. Fontanet, M. L. Albert and D. J. Lenschow (2011). "ISG15 is critical in
4074   the control of Chikungunya virus infection independent of UbE1L mediated conjugation." <u>PLoS</u>
4075   <u>Pathog</u> **7**(10): e1002322.
4076   Wheeler, R. J., E. Gluenz and K. Gull (2015). "Basal body multipotency and axonemal remodelling are two
4077   pathways to a 9+0 flagellum." <u>Nat Commun</u> **6**: 8964.
4078   White, J. P., A. M. Cardenas, W. E. Marissen and R. E. Lloyd (2007). "Inhibition of cytoplasmic mRNA stress
4079   granule formation by a viral proteinase." <u>Cell Host Microbe</u> **2**(5): 295-305.
4080   William, M., L. P. Leroux, V. Chaparro, T. E. Graber, T. Alain and M. Jaramillo (2019). "Translational
4081   repression of Ccl5 and Cxcl10 by 4E-BP1 and 4E-BP2 restrains the ability of mouse macrophages
4082   to induce migration of activated T cells." <u>Eur J Immunol</u> **49**(8): 1200-1212.
4083   William, M., L. P. Leroux, V. Chaparro, J. Lorent, T. E. Graber, M. N. M'Boutchou, T. Charpentier, A. Fabie,
4084   C. M. Dozois, S. Stager, L. C. van Kempen, T. Alain, O. Larsson and M. Jaramillo (2018). "eIF4E-
4085   Binding Proteins 1 and 2 Limit Macrophage Anti-Inflammatory Responses through Translational
4086   Repression of IL-10 and Cyclooxygenase-2." <u>J Immunol</u> **200**(12): 4102-4116.

4087   Wilson, M. E., D. J. Innes, A. D. Sousa and R. D. Pearson (1987). "Early histopathology of experimental
4088   infection with Leishmania donovani in hamsters." J Parasitol **73**(1): 55-63.

4089   Wilson, M. E., B. M. Young, B. L. Davidson, K. A. Mente and S. E. McGowan (1998). "The importance of
4090   TGF-beta in murine visceral leishmaniasis." J Immunol **161**(11): 6148-6155.

4091   Wolfe, A. L., K. Singh, Y. Zhong, P. Drewe, V. K. Rajasekhar, V. R. Sanghvi, K. J. Mavrakis, M. Jiang, J. E.
4092   Roderick, J. Van der Meulen, J. H. Schatz, C. M. Rodrigo, C. Zhao, P. Rondou, E. de Stanchina, J.
4093   Teruya-Feldstein, M. A. Kelliher, F. Speleman, J. A. Porco, Jr., J. Pelletier, G. Ratsch and H. G.
4094   Wendel (2014). "RNA G-quadruplexes cause eIF4A-dependent oncogene translation in cancer."
4095   Nature **513**(7516): 65-70.

4096   Wyllie, S., S. Brand, M. Thomas, M. De Rycker, C. W. Chung, I. Pena, R. P. Bingham, J. A. Bueren-Calabuig,
4097   J. Cantizani, D. Cebrian, P. D. Craggs, L. Ferguson, P. Goswami, J. Hobrath, J. Howe, L. Jeacock, E.
4098   J. Ko, J. Korczynska, L. MacLean, S. Manthri, M. S. Martinez, L. Mata-Cantero, S. Moniz, A. Nuhs,
4099   M. Osuna-Cabello, E. Pinto, J. Riley, S. Robinson, P. Rowland, F. R. C. Simeons, Y. Shishikura, D.
4100   Spinks, L. Stojanovski, J. Thomas, S. Thompson, E. Viayna Gaza, R. J. Wall, F. Zuccotto, D. Horn, M.
4101   A. J. Ferguson, A. H. Fairlamb, J. M. Fiandor, J. Martin, D. W. Gray, T. J. Miles, I. H. Gilbert, K. D.
4102   Read, M. Marco and P. G. Wyatt (2019). "Preclinical candidate for the treatment of visceral
4103   leishmaniasis that acts through proteasome inhibition." Proc Natl Acad Sci U S A **116**(19): 9318-
4104   9323.

4105   Xanthoudakis, S., J. P. Viola, K. T. Shaw, C. Luo, J. D. Wallace, P. T. Bozza, D. C. Luk, T. Curran and A. Rao
4106   (1996). "An enhanced immune response in mice lacking the transcription factor NFAT1." Science
4107   **272**(5263): 892-895.

4108   Xiao, L. and J. Y. Wang (2014). "RNA-binding proteins and microRNAs in gastrointestinal epithelial
4109   homeostasis and diseases." Curr Opin Pharmacol **19**: 46-53.

4110   Xiao, X., W. Zhang, D. Hua, L. Zhang, W. Meng, J. Huang and L. Zhang (2020). "Cold-inducible RNA-binding
4111   protein (CIRBP) promotes porcine reproductive and respiratory syndrome virus (PRRSV)-induced
4112   inflammatory response." Int Immunopharmacol **86**: 106728.

4113   Xu, Z. X., G. H. Kim, J. W. Tan, A. E. Riso, Y. Sun, E. Y. Xu, G. Y. Liao, H. Xu, S. H. Lee, N. Y. Do, C. H. Lee, A.
4114   E. Clipperton-Allen, S. Kwon, D. T. Page, K. J. Lee and B. Xu (2020). "Elevated protein synthesis in
4115   microglia causes autism-like synaptic and behavioral aberrations." Nat Commun **11**(1): 1797.

4116   Xue, J., S. V. Schmidt, J. Sander, A. Draffehn, W. Krebs, I. Quester, D. De Nardo, T. D. Gohel, M. Emde, L.
4117   Schmidleithner, H. Ganesan, A. Nino-Castro, M. R. Mallmann, L. Labzin, H. Theis, M. Kraut, M.

Beyer, E. Latz, T. C. Freeman, T. Ulas and J. L. Schultze (2014). "Transcriptome-based network analysis reveals a spectrum model of human macrophage activation." Immunity **40**(2): 274-288.

Xue, Q., H. Liu, Z. Zhu, Z. Xue, X. Liu and H. Zheng (2020). "Seneca Valley Virus 3C(pro) Cleaves PABPC1 to Promote Viral Replication." Pathogens **9**(6).

Yang, H. S., A. P. Jansen, A. A. Komar, X. Zheng, W. C. Merrick, S. Costes, S. J. Lockett, N. Sonenberg and N. H. Colburn (2003). "The transformation suppressor Pdcd4 is a novel eukaryotic translation initiation factor 4A binding protein that inhibits translation." Mol Cell Biol **23**(1): 26-37.

Ye, J., M. Kumanova, L. S. Hart, K. Sloane, H. Zhang, D. N. De Panis, E. Bobrovnikova-Marjon, J. A. Diehl, D. Ron and C. Koumenis (2010). "The GCN2-ATF4 pathway is critical for tumour cell survival and proliferation in response to nutrient deprivation." EMBO J **29**(12): 2082-2096.

Yin, L. and W. O. Chung (2011). "Epigenetic regulation of human beta-defensin 2 and CC chemokine ligand 20 expression in gingival epithelial cells in response to oral bacteria." Mucosal Immunol **4**(4): 409-419.

Young, C. N. J. and D. C. Gorecki (2018). "P2RX7 Purinoceptor as a Therapeutic Target-The Second Coming?" Front Chem **6**: 248.

Yu, S., D. Wang, L. Huang, Y. Zhang, R. Luo, D. Adah, Y. Tang, K. Zhao and B. Lu (2019). "The complement receptor C5aR2 promotes protein kinase R expression and contributes to NLRP3 inflammasome activation and HMGB1 release from macrophages." J Biol Chem **294**(21): 8384-8394.

Yu, Y., S. O. Yoon, G. Poulogiannis, Q. Yang, X. M. Ma, J. Villen, N. Kubica, G. R. Hoffman, L. C. Cantley, S. P. Gygi and J. Blenis (2011). "Phosphoproteomic analysis identifies Grb10 as an mTORC1 substrate that negatively regulates insulin signaling." Science **332**(6035): 1322-1326.

Yurdakul, P., J. Dalton, L. Beattie, N. Brown, S. Erguven, A. Maroof and P. M. Kaye (2011). "Compartment-specific remodeling of splenic micro-architecture during experimental visceral leishmaniasis." Am J Pathol **179**(1): 23-29.

Zangger, H., C. Ronet, C. Desponds, F. M. Kuhlmann, J. Robinson, M. A. Hartley, F. Prevel, P. Castiglioni, F. Pratlong, P. Bastien, N. Muller, L. Parmentier, N. G. Saravia, S. M. Beverley and N. Fasel (2013). "Detection of Leishmania RNA virus in Leishmania parasites." PLoS Negl Trop Dis **7**(1): e2006.

Zhang, N., S. Prasad, C. E. Huyghues Despointes, J. Young and P. E. Kima (2018). "Leishmania parasitophorous vacuole membranes display phosphoinositides that create conditions for continuous Akt activation and a target for miltefosine in Leishmania infections." Cell Microbiol **20**(11): e12889.

4149　Zhang, X., X. Chen, Q. Liu, S. Zhang and W. Hu (2017). "Translation repression via modulation of the

4150　　　cytoplasmic poly(A)-binding protein in the inflammatory response." Elife **6**.

4151　Zhao, C., T. Liu, T. Zhou, Y. Fu, H. Zheng, Y. Ding, K. Zhang and W. Xu (2016). "The rodent malaria liver stage

4152　　　survives in the rapamycin-induced autophagosome of infected Hepa1-6 cells." Sci Rep **6**: 38170.

4153　Zhihua, Y., T. Yulin, W. Yibo, D. Wei, C. Yin, X. Jiahao, J. Runqiu and X. Xuezhong (2019). "Hypoxia decreases

4154　　　macrophage glycolysis and M1 percentage by targeting microRNA-30c and mTOR in human gastric

4155　　　cancer." Cancer Sci **110**(8): 2368-2377.

4156　Zijlstra, E. E., A. M. Musa, E. A. Khalil, I. M. el-Hassan and A. M. el-Hassan (2003). "Post-kala-azar dermal

4157　　　leishmaniasis." Lancet Infect Dis **3**(2): 87-98.

4158　Zou, Z., Z. Meng, C. Ma, D. Liang, R. Sun and K. Lan (2017). "Guanylate-Binding Protein 1 Inhibits Nuclear

4159　　　Delivery of Kaposi's Sarcoma-Associated Herpesvirus Virions by Disrupting Formation of Actin

4160　　　Filament." J Virol **91**(16).

Appendix 1

4162

eIF4E-binding proteins 1 and 2 limit macrophage anti-inflammatory responses

through translational repression of Interleukin-10 and Cyclooxygenase-2

4165

4166 Mirtha William[*], Louis-Philippe Leroux[*], Visnu Chaparro[*], Julie Lorent[†], Tyson E. Graber[¶], Marie-Noël

4167 M'Boutchou[‡,§], Tania Charpentier[*], Aymeric Fabié[*], Charles M. Dozois[*], Simona Stäger[*], Léon C. van

4168 Kempen[‡,§], Tommy Alain[¶], Ola Larsson[†] and Maritza Jaramillo[*, 1]

4169

4170 [*]INRS - Institut Armand Frappier and Centre for Host-Parasite Interactions, Laval, QC, Canada;

4171 [†]Department of Oncology-Pathology, Science for Life Laboratory, Karolinska Institutet, Stockholm, Sweden;

4172 [‡]Department of Pathology, McGill University, Lady Davis Institute, Jewish General Hospital, Montreal, QC,

4173 Canada; [§]Department of Pathology and Medical Biology, University Medical Centre Groningen, The

4174 Netherlands; [¶]Children's Hospital of Eastern Ontario Research Institute, Department of Biochemistry,

4175 Microbiology and Immunology, University of Ottawa, Ottawa, ON, Canada

4176

4177 [1]To whom correspondence and requests for materials should be addressed: Maritza Jaramillo, INRS -

4178 Institut Armand Frappier and Centre for Host-Parasite Interactions, 531 boulevard des Prairies, Laval, QC,

4179 Canada H7V 1B7; Phone number (1)-450-687-5010, Ext 8872; Fax number (1) 450-686-5389; E-mail:

4180 maritza.jaramillo@iaf.inrs.ca

4181

4182 **Short title**: 4E-BP1/2 repress macrophage *Il-10* and *Cox-2* mRNA translation

4185

4186

Abstract

Macrophages represent one of the first lines of defense during infections and are essential for resolution of inflammation following pathogen clearance. Rapid activation or suppression of protein synthesis via changes in translational efficiency allows cells of the immune system, including macrophages, to quickly respond to external triggers or cues without *de novo* mRNA synthesis. The translational repressors eIF4E-binding proteins 1 and 2 (4E-BP1/2) are central regulators of pro-inflammatory cytokine synthesis during viral and parasitic infections. However, it remains to be established whether 4E-BP1/2 play a role in translational control of anti-inflammatory responses. By comparing translational efficiencies of immune-related transcripts in macrophages from wild-type (WT) and 4E-BP1/2 double knockout (DKO) mice, we found that translation of mRNAs encoding two major regulators of inflammation, interleukin-10 (IL-10) and prostaglandin-endoperoxide synthase 2/cyclooxygenase-2 (PTGS2/COX-2), is controlled by 4E-BP1/2. Genetic deletion of 4E-BP1/2 in macrophages increased endogenous IL-10 and prostaglandin E_2 (PGE_2) protein synthesis in response to TLR4 stimulation and reduced their bactericidal capacity. The molecular mechanism involves enhanced anti-inflammatory gene expression (s*Il1ra*, *Nfil3*, *Arg1*, *Serpinb2*) owing to up-regulation of IL-10-STAT3 and PGE_2-C/EBPβ signaling. These data provide evidence that 4E-BP1/2 limit anti-inflammatory responses in macrophages, and suggest that dysregulated activity of 4E-BP1/2 might be involved in reprogramming of the translational and downstream transcriptional landscape of macrophages during pathological conditions, such as infections and cancer.

Introduction

In eukaryotes, translational control (i.e., regulation of the efficiency of mRNA translation) mostly occurs at the rate-limiting initiation step during which the ribosome is recruited to the mRNA (1). This process is facilitated by the eukaryotic translation initiation factor 4F (eIF4F), a heterotrimeric complex consisting of eIF4E, the mRNA 5'-m^{7}G-cap-binding subunit; eIF4A, an RNA helicase; and eIF4G, a scaffolding protein. Assembly of eIF4F is blocked by a reversible association between eIF4E and eIF4E-binding proteins (4E-BPs), a family of repressor proteins that, in mammals, comprises 4E-BP1, 4E-BP2 and 4E-BP3 (2). The mechanistic target of rapamycin (mTOR) complex 1 (mTORC1) phosphorylates 4E-BP1 and 4E-BP2 (4E-BP1/2), promotes their dissociation from eIF4E, and thereby enables the assembly of a functional eIF4F complex. Conversely, in conditions of mTORC1 inhibition, hypophosphorylated 4E-BP1/2 and inducible 4E-BP3 bind with high affinity to eIF4E, prevent the formation of the eIF4F complex and thereby inhibit initiation of translation (3, 4).

Translational control enables cells to rapidly adjust their proteomes in response to stress without the requirement of *de novo* mRNA synthesis (5). The ability to quickly modulate gene expression is a key feature of the immune system; therefore, several innate immune regulators are under translational control. For example, analysis of the translatome (i.e., the transcriptome-wide pools of efficiently translated mRNA) in mouse embryonic fibroblasts (MEFs) from *Eif4ebp1$^{-/-}$/Eif4ebp2$^{-/-}$* double knockout (4E-BP1/2 DKO) mice identified *Irf7* as an mRNA translated in a 4E-BP1/2-sensitive fashion (6). Moreover, similar studies on MEFs from mice mutated at the residue where eIF4E is phosphorylated (i.e., eIF4E S209A knock-in (KI)) demonstrated that translational efficiency of *IκBα*, the inhibitor of NF-κB, is controlled by the MNK-eIF4E axis (7, 8). The transcription factors IRF-7 and NF-κB promote the activation of *Ifnα* and *Ifnβ* genes (9, 10). Accordingly, 4E-BP1/2 DKO and eIF4E KI MEFs and mice are resistant to viral infections owing to enhanced type I IFN responses (6-8). These findings support the notion that eIF4E-dependent translational control constitutes an important regulatory mechanism of innate immune responses. Yet, these studies used MEFs and therefore, may not reflect the entire transcript repertoire under translational control in immune cells.

Macrophages are sentinels of the innate immune system that alter their phenotype, ranging from inflammatory to regulatory and anti-inflammatory depending on the environmental cues (11). Selective changes in translational efficiency direct macrophage differentiation (12) and activation (13-17). This includes the response to cytokines and TLR ligands, where regulation of mTORC1 and MNK signaling modulates translational efficiency of immune-related transcripts (13, 14, 17). Moreover, previous studies conducted in MEFs demonstrated that 4E-BP1/2 play a crucial role in translational control of antiviral innate immunity (6, 18). Consistently, 4E-BP1/2 are involved in macrophage resistance to infection by a protozoan parasite through type I interferon- and nitric oxide-mediated mechanisms (19). These findings indicate that 4E-BP1/2 regulate macrophage pro-inflammatory and microbicidal functions via selective changes in translational efficiencies; however, the identity of such transcripts remains unknown. Notably, the impact of

4243   4E-BP1/2-dependent translational control in macrophage anti-inflammatory responses is yet to be

4244   investigated. Here we show that translational efficiency of mRNAs encoding anti-inflammatory mediators,

4245   interleukin-10 (IL-10) and cyclooxygenase-2 (COX-2), is regulated through 4E-BP1/2, which thereby

4246   modulate the anti-inflammatory phenotype of macrophages.

Materials and Methods

Reagents

Lipopolysaccharide (LPS, *Escherichia coli* serotype 0111:B4) and cycloheximide were purchased from Sigma-Aldrich. NS-398 was provided by Cayman Chemical. Rat monoclonal antibody against mouse IL-10 (#MAB417) and rat IgG1 isotype control (#MAB005) were obtained from R&D Systems. BP-1-102 was purchased from Selleck Chemicals. Dulbecco's Modified Eagle Medium (DMEM), fetal bovine serum (FBS), Hank's Balanced Salt Solution (HBSS), 0.05% EDTA-Trypsin, penicillin and streptomycin were provided by Wisent.

Differentiation of bone marrow-derived macrophages

Hind legs from *Eif4ebp1⁻/⁻/Eif4ebp2⁻/⁻* C57BL/6 mice (6, 19) and their wild-type C57BL/6 littermates, originally purchased from The Jackson Laboratories, were kindly provided by Dr. Nahum Sonenberg (McGill University, Montreal, QC, Canada). All procedures were in compliance with the Canadian Council on Animal Care guidelines and approved by the Comité institutionnel de protection des animaux of the INRS (CIPA #1611-10). Bone marrow precursor cells were extracted from the femurs and tibias for differentiation into bone marrow-derived macrophages (BMDM). Briefly, marrow was flushed from femurs and tibias maintained in HBSS (100 U/ml penicillin, 100 µg/ml streptomycin, 4.2 mM sodium bicarbonate, 20 mM HEPES) at 4°C. Precursor cells were resuspended in BMDM culture medium (DMEM, 10% heat-inactivated FBS, 2 mM L-glutamate, 1 mM sodium pyruvate, 100 U/ml penicillin, 100 µg/ml streptomycin) supplemented with 15% L929 fibroblast-conditioned culture medium (LCCM). Cells were seeded in 10 cm-diameter tissue culture-treated dishes, and incubated overnight at 37°C, 5% CO_2. The following day, non-adherent cells were collected, resuspended in BMDM culture medium supplemented with 15% LCCM, and plated in 10 cm-diameter non-treated Petri dishes (~5 dishes/mouse). LCCM was added every 2 days (~1.5 ml/dish) and differentiated BMDM were collected at 8 days after marrow extraction. Differentiation of precursor cells into macrophages was routinely assessed by monitoring for CD11b and F4/80 co-expression by flow cytometry using APC anti-mouse/human CD11b antibody #101211 and PE anti-mouse F4/80 antibody # 123109 (Biolegend), as previously described (20).

Polysome-Profiling and RNA extraction

Samples were processed for polysome-profiling and RNA fractionation as previously described (19). BMDM were seeded in 15 cm-diameter culture dishes (3×10^7 cells/plate) in DMEM containing 100 U/ml penicillin, 100 µg/ml streptomycin, and supplemented with 10% FBS and 1% LCCM. A total of 9×10^7 cells per genotype were used to generate each polysome profile. Cells were treated with 100 µg/ml cycloheximide for 5 min and were washed three times with cold PBS containing 100 µg/ml cycloheximide. Cells were centrifuged at 200 x g for 10 min at 4°C and lysed in hypotonic lysis buffer containing 5 mM Tris-HCl pH 7.5, 2.5 mM $MgCl_2$, 1.5 mM KCl, 100 µg/ml cycloheximide, 2 mM DTT, 0.5% Triton-X-100, 0.5% sodium deoxycholate and 200 U RNasin (Promega). Lysates were cleared by centrifugation (20,000 x g, 2

157

min at 4°C). A 50 µl sample was collected (10% of the lysate) to isolate cytoplamsic RNA using TRIzol (Invitrogen). Five to 50% (w/v) sucrose density gradients (20 mM HEPES-KOH pH 7.6, 100 mM KCl, 5mM $MgCl_2$) were generated using a Gradient Master 108 (Biocomp). Samples were loaded onto the sucrose gradients and subjected to ultracentrifugation at 221, 830.9 *x g* (SW 41 rotor, Beckman Coulter) for 2 h at 4°C. Sucrose gradients were fractionated (35 s for each fraction = 750 µl per fraction) by displacement by 60% sucrose/0.01 % bromophenol blue. The optical density at 254 nm was continuously recorded using a BR-188 Density Gradient Fractionation System (Brandel). Fractions were flash-frozen immediately after fractionation and stored at -80°C. RNA from each fraction was isolated using TRIzol and purified using the RNeasy Kit (Qiagen). Fractions with mRNA associated to > 3 ribosomes were pooled (polysome-associated mRNA).

NanoString nCounter Assays and Data Analysis

RNA samples from three independent biological replicas were prepared for NanoString nCounter assays and analyzed as previously described (21). In addition to polysome-associated mRNA samples described above, a parallel sample was collected from the lysates loaded onto the sucrose gradient (total cytoplasmic mRNA) and RNA was isolated using TRIzol and purified using the RNeasy Kit. RNA quality was assessed using an Agilent 2100 Bioanalyzer (Agilent Technologies). Next, 150 ng RNA was used as input for the NanoString nCounter assays using the nCounter® Mouse Immunology Panel (NanoString). Data were generated as previously described (22). For NanoString data analysis, the obtained counts were log_2-transformed. Per sample normalization was performed using geometric means from three housekeeping genes (*Rpl19, Eef1g,* and *Gapdh*). Differential translation (FDR < 0.25) was identified using anota (23, 24), which corrects changes in polysome-associated mRNA for changes in cytoplasmic total mRNA, applies variance-shrinkage (the random variance model [RVM]) and adjusts the *P* values for multiple testing using the Benjamini and Hochberg's false-discovery rate (FDR) method. The translational activity in 4E-BP1/2 DKO cells (i.e., the intercepts from analysis of partial variance [APV]) were obtained for those mRNAs that are translationally up-regulated and compared to WT control cells to obtain relative changes in translational efficiency.

5' UTR Analysis

5'UTRs of transcripts from the top 11 gene hits were retrieved from the mm10 genome build using the UCSC Table Browser (https://genome.ucsc.edu). Minimum free energy (MFE) and secondary structures were obtained from the "foldUtr5" table which contains MFE structures computed using RNAfold (25). Secondary structures were plotted using VARNA (26).

Quantitative RT-PCR

Pools of efficiently translated mRNAs (i.e., mRNAs associated to > 3 ribosomes) and total cytoplasmic RNA were isolated using TRIzol (Invitrogen). RNA (1 µg) was reverse transcribed with

Superscript III reverse transcriptase and oligo(dT) (both from Invitrogen). Quantitative PCR was performed with PowerUp™ SYBR® Green Master Mix (Applied Biosystems), according to the manufacturer's instructions using a QuantStudio 3 Real-Time PCR System (Applied Biosciences). Analysis was carried out by relative quantification using the Comparative CT method ($\Delta\Delta$Ct) (27). Experiments were performed in independent biological replicates (n=3), whereby each sample was analyzed in a technical triplicate. Relative mRNA expression was normalized to *Gapdh* and *Rpl19*. Primers were designed using NCBI Primer-BLAST (http://www.ncbi.nlm.nih.gov/tools/primer-blast/). The list of primers is provided in Supplemental Table I.

Western blot analysis

BMDM were seeded in 6-well plates (2×10^6 cells/well). After stimulation, cells were scraped in cold PBS pH 7.4, collected by centrifugation and lysed in cold RIPA buffer containing 25 mM Tris-HCl pH 7.6, 150 mM NaCl, 1% Triton-X-100, 0.5% sodium deoxycholate, 0.1% SDS, supplemented with phosphatase and EDTA-free protease inhibitor cocktails (Roche). Cell debris was removed by centrifugation at 20,000 *x g* for 15 min at 4°C and total protein content was determined using the BCA Protein Assay kit (Pierce). Whole-cell protein extracts were subjected to SDS-PAGE and the separated proteins were transferred onto a PVDF membrane (Bio-Rad). Membranes were blocked for 1 h in 5% skim milk TBS-T (0.1 % Tween 20) and incubated with specific primary antibodies O/N at 4°C. Proteins were then detected with IgG horseradish peroxidase (HRP)-linked antibodies by chemiluminescence using Clarity Western ECL substrate (Bio-Rad). Antibodies detecting phospho-4E-BP1 (T37/46) (#2855), phospho-4E-BP1 (T70) (#9455), phospho-4E-BP1 (S65) (#9451), 4E-BP1 (#9452), 4E-BP2 (#2845), COX-2 (#4842), CEBP/β (NO. 3087), eIF4G (#2498), phospho-STAT3 (Y705) (#9145), STAT3 (#9139), and β-actin (#3700) were obtained from Cell Signaling Technology. The antibody detecting sIL-1Ra (#MAB4801) was purchased from R&D Systems. The anti-NFIL-3 antibody (#685402) was provided by Biolegend. The following secondary HRP-conjugated antibodies were used in this study: anti-rabbit IgG (#A0545) and anti-mouse IgG (#A4416) from Sigma-Aldrich, and anti-rat IgG (#HAF005) from R&D Systems.

m^{7}GTP-agarose pull down assays

BMDM were plated in 10 cm-diameter plates (1.5×10^7 cells/plate). Cell treatment was followed by lysis in ice-cold Buffer A (lysis buffer; 50 mM MOPS pH 7.4, 100 mM NaCl, 2 mM EDTA, 2 mM EGTA, 1% IGEPAL CA-630, 1% sodium deoxycholate, 7 mM β-mercaptoethanol) supplemented with phosphatase and EDTA-free protease inhibitor cocktails. Samples were incubated 15 min on ice and regularly mixed gently, and the crude lysates were cleared by centrifugation. About 0.5 mg of proteins of each sample were mixed with 50% slurry of 2'/3'-EDA-m^{7}GTP immobilized on agarose beads (#AC-142S, Jena Bioscience) and diluted up to 1 ml with Buffer B (wash buffer; 50 mM MOPS pH 7.4, 100 mM NaCl, 0.5 mM EDTA, 0.5 mM EGTA, 7 mM β-mercaptoethanol, 0.1 mM GTP) supplemented with phosphatase and EDTA-free protease inhibitor cocktails. Samples were mixed for 1 h at 4°C with end-over-end mixing and beads were

4358   pelleted by centrifugation. The supernatants (i.e., flow-through, FT) were kept, while the beads were

4359   washed in Buffer B and finally resuspended in Laemmli loading buffer for further analysis by western

4360   blotting.

4361

4362   **ELISA**

4363   Cells were seeded in 96-well plates (2×10^5 cells/well) and stimulated with 1-10 ng/ml *E. coli* LPS

4364   for 6, 12 or 24 h. Cell culture supernatant samples were collected and the concentration of secreted IL-10

4365   and PGE_2 were assessed by ELISA using the mouse IL-10 ELISA MAX™ Deluxe kit (Biolegend) and the

4366   Prostaglandin E_2 ELISA Kit (Cayman Chemical), according to the manufacturer's instructions.

4367

4368   **Image flow cytometry**

4369   BMDM were seeded in 6 cm-diameter non-treated plates (5×10^6 cells/plate) and were stimulated

4370   with 10 ng/ml LPS for 4, 6 or 10 h. After cell fixation and staining, samples were acquired on the

4371   ImageStreamX MarkII imaging cytometer (Amnis), as described (28). Briefly, BMDM were collected by

4372   trypsinization (0.05% EDTA-Trypsin) and fixed in 1.5% PFA. Cells were permeabilized in ice-cold methanol

4373   and were washed twice with staining buffer (1% BSA-PBS). Supernatants were discarded and cells were

4374   incubated with an anti-CD16/32 antibody (BioLegend, #101302) for 15 minutes on ice. Cell staining was

4375   performed by a 25 min incubation on ice using the following fluorescent reagents and antibodies: 4',6-

4376   diamidino-2-phenylindole (DAPI) (Sigma), A488-coupled anti-Y705-STAT3 (BD Bioscience, #557814),

4377   A488-coupled isotype control (BD Bioscience, #558055), A647-coupled anti-β-actin (Cell Signaling, #8584),

4378   A647-coupled isotype control (Cell Signaling, #3452). Next, cells were washed twice with staining buffer

4379   and samples were acquired on the ImageStreamX MarkII imaging cytometer (Amnis). Bright field and

4380   fluorescent images were collected at 40X magnification. Ten- to thirty-thousand cell singlets were gated

4381   from each sample. The analysis was performed using the IDEAS software (Amnis).

4382   **Bacterial Infection**

4383   BMDM were seeded in 24-well plates (5×10^5 cells/well) and treated with 10 ng/ml LPS with or

4384   without 2 μg/ml anti-IL-10 antibody and 50 μM NS-398 for 24h before infection. Conditioned media was

4385   present throughout the entire experiment. Bacterial infection was carried out as previously described (29).

4386   Briefly, *E. coli* MG 1655 (non-pathogenic strain) was grown overnight at 37 °C and then sub-cultured at a

4387   dilution of 1:4 in fresh Luria-Bertani (LB) broth without antibiotics to mid-logarithmic phase (OD_{600} ~ 0.1).

4388   BMDM were infected with 2.5×10^6 bacteria (5:1 ratio) and centrifuged for 10 min at 500 *x g* to synchronize

4389   phagocytosis. BMDM were cultured in 1% FBS DMEM without antibiotics at 37 °C for 2 h and after three

4390   washes in PBS treated with 100 μg/ml gentamicin for 1 h to eliminate extracellular bacteria. The infected

4391   cells were either lysed in 1% Triton X-100 to assess bacterial invasion (t=0) or further incubated for a total

4392   of 6, 8 or 24 h in presence of 12 μg/ml gentamicin. When indicated, 10 ng/ml LPS with or without 2 μg/ml

4393   anti-IL-10 antibody and 50 μM NS-398 were added to cells 24 h before infection and were also present

4394   during the subsequent steps of infection. Surviving bacteria were determined as colony-forming-units (CFU)

4395   by plating serial dilutions (1/10) of whole cell lysates in LB agar.

4396

Statistical Analysis

4398   nCounter data were analyzed using the anota "R" package to identify mRNAs under translational

4399   control between WT and 4E-BP1/2 DKO BMDM (23, 24). Statistical differences were calculated using two-

4400   way ANOVA embedded in GraphPad Prism 7 software package. Results are presented as the mean ±

4401   standard deviation (SD) of the mean. Differences were considered to be statistically significant when * $P <$

4402   0.05, ** $P < 0.01$, *** $P < 0.001$.

4403

Results

The eIF4E-binding proteins 1 and 2 control translational efficiency of *Interleukin-10* and
***Cyclooxygenase-2* mRNAs in macrophages**

4407   mTORC1 orchestrates effective immune responses through a number of effectors including the
4408 translational repressors 4E-BP1/2 (6, 18, 30). However, the impact of 4E-BP1/2 on selective translational
4409 control in macrophages and the effects on anti-inflammatory responses remain largely unexplored. To begin
4410 addressing this issue, cytosolic RNA from WT and 4E-BP1/2 DKO bone marrow-derived macrophages
4411 (BMDM) at steady-state was subjected to polysome-profiling (19). Polysome-profiling generated a pool of
4412 efficiently translated mRNA that was quantified in parallel with total cytosolic mRNA (input) using targeted
4413 nCounter® assays (mouse immunology panel) (**Fig. 1A**). Herein, translational efficiency is defined as the
4414 proportion of the mRNA copies transcribed from a gene that are in heavy polysomes (in this case associated
4415 with > 3 ribosomes) and hence efficiently translated. Changes in polysome-associated mRNA levels can
4416 be due to altered translational efficiency or to changes in mRNA levels (e.g., via altered transcription or
4417 mRNA stability) (5). To identify mRNAs whose translation depends on 4E-BP1/2 in BMDM, we employed
4418 the "anota" algorithm, which specifically captures differences in translational efficiency of individual
4419 transcripts independent of changes in total mRNA levels, i.e., changes in the amount of mRNA copies
4420 associated with heavy polysomes after adjusting for changes in total cytosolic mRNA (24). We thereby
4421 identified 11 mRNAs more efficiently translated in 4E-BP1/2 DKO as compared to WT BMDM
4422 (**Supplemental Table II**). Among the most regulated transcripts were *Il-10* and *Cox-2*/*Ptgs2*, which encode
4423 proteins involved in macrophage anti-inflammatory responses. The graphical representation of anota
4424 analysis illustrates that *Il-10* mRNA was more abundant in the pool of polysome-associated mRNA in 4E-
4425 BP1/2 DKO than in WT BMDM despite having similar total cytosolic mRNA levels (2.48 fold-change in
4426 translational efficiency) (**Fig. 1B).** Similarly, translational efficiency of *Cox-2* mRNA was up-regulated in the
4427 absence of 4E-BP1/2 (4.20 fold-change) (**Fig. 1C**). In Figs. 1B-C, each biological replicate is represented
4428 by an "X" and the lines correspond to regressions used by anota to adjust changes in polysome-associated
4429 mRNA levels (y-axis) for changes in total cytosolic mRNA levels (x-axis). A difference in intercepts of the
4430 regression lines on the y-axis (i.e., when total cytosolic mRNA is set to 0) indicates changes in translational
4431 efficiency (when there is no change in translational efficiency, there is no difference in intercept). In
4432 summary, this analysis demonstrates that *Il-10* and *Cox-2* mRNAs are under the control of the translational
4433 repressors 4E-BP1/2 DKO in BMDM at steady state.

4434   Select translational control through the mTORC1-4E-BP1/2-eIF4E axis is associated with distinct
4435 features in the 5' UTRs of mRNAs (5, 31, 32). To assess whether the identified immune-related transcripts
4436 under translational control contain such features, we conducted 5' UTR analysis. Eight of these mRNAs
4437 (*Il1a*, *Il1b*, *Il10*, *Il12b*, *Ccl5*, *Ccl12*, *Cd40*, and *Cxcl10*) harbor relatively short 5' UTRs (between 50 and 90
4438 nucleotides (nt)) with minimum free energy (MFE) ranging from -5 to -30 kcal/mol (**Fig. 1D** and
4439 **Supplemental Table III**). In addition, we identified 4 mRNAs (*Cox-2*, *Ifit2*, *Il1b*, and *Mx-1*) that contain
4440 longer 5' UTRs (up to ~1300 nt) with MFE as low as -487.3 kcal/mol. Exceptionally, several 5' UTR

4441   sequences are annotated for and *Il1b* and *Mx1* (3 and 5, respectively), which differ in length and structure.

4442   Interestingly, the 5' UTR of *Il-10* is relatively short (67 nt and MEF = -12.3 kcal/mol) whereas that of *Cox-2*

4443   is longer and more structured (193 nt and MEF = -48.92 kcal/mol) (**Fig. 1E**), indicating that these may be

4444   regulated by distinct mechanisms. Thus, selective 4E-BP1/2-dependent translational control of immune-

4445   related mRNAs in macrophages could at least partially be linked to the length and structure of their 5' UTRs,

4446   as previously reported for transcripts that are highly sensitive to eIF4E levels and / or availability (5, 31, 32).

4447

4448   **LPS promotes *Interleukin-10* mRNA translation by limiting the activity of 4E-BP1 and 4E-BP2**

4449   After having identified *Il-10* and *Cox-2* as targets of translational control downstream of 4E-BP1/2,

4450   we set out to elucidate the biological impact of such regulation in macrophage anti-inflammatory responses.

4451   The bacterial endotoxin lipopolysaccharide (LPS), a TLR4 ligand, regulates a large number of immune cell

4452   functions by controlling gene expression at the levels of transcription, mRNA stability, and mRNA translation

4453   (33). Activation of mTORC1 signaling is required for IL-10 production in LPS-stimulated macrophages (34).

4454   However, it remains unclear whether this increase is, at least in part, dependent on regulation of *Il-10*

4455   translational efficiency via the mTORC1-4E-BP1/2 axis. To address this, WT and 4E-BP1/2 DKO BMDM

4456   were stimulated with 10 ng/ml *Escherichia coli* (*E. coli*) LPS for 4 h and cytoplasmic RNA was fractionated

4457   by polysome-profiling (**Fig. 2A**). RT-qPCR analyses for *Il-10* were conducted in total cytosolic and heavy

4458   polysome-associated RNA isolated from control (unstimulated) and LPS-treated cells. Consistent with

4459   selective modulation of IL-10 via changes in translational efficiency, the amount of heavy polysome-

4460   associated mRNA encoding *Il-10* was higher in 4E-BP1/2 DKO than in WT control cells (2.8 fold-increase)

4461   (**Fig. 2B**), while total cytosolic *Il-10* mRNA, although slightly higher (1.5 fold-change) did not fully explain

4462   this difference. Notably, we also observed greater accumulation of *Il-10* mRNA associated to heavy

4463   polysomes in 4E-BP1/2 DKO than in WT cells after LPS treatment (7.6 fold-change), which was only partly

4464   explained by changes in total cytosolic mRNA levels (3.6 fold-change), and therefore is consistent with

4465   activated translation of *Il-10* mRNA in 4E-BP1/2 DKO macrophages as compared to WT counterparts

4466   following LPS exposure (**Fig. 2B**). To further assess differences in translational efficiency of *Il-10* between

4467   WT and 4E-BP1/2 DKO cells, we monitored *Il-10* mRNA distribution in subpolysomal, light polysome and

4468   heavy polysome fractions. Note that subpolysomal fractions contain mRNAs that are not efficiently

4469   translated (i.e., free mRNAs or associated with 1 ribosome). In light polysome fractions, mRNAs are

4470   associated with > 1 and ≤ 3 ribosomes and therefore are not translated as efficiently as those found in

4471   heavy polysome fractions (mRNAs associated with > 3 ribosomes). In control WT cells, 60.1% of *Il-10*

4472   mRNA was found in subpolysomal fractions and the remaining 39.9% was equally distributed in the light

4473   and heavy polysome fractions (19.9% and 20%, respectively) (**Fig. 2C**, left top panel). In contrast, only

4474   29.5% of *Il-10* mRNA was present in subpolysomal fractions of 4E-BP1/2 DKO BMDM (30.6% less in DKO

4475   than WT), which resulted in greater *Il-10* mRNA amount in light and heavy polysome fractions (37.6% and

4476   32.9%, respectively). Further supporting that LPS promotes *Il-10* translation by inactivating 4E-BP1/2, we

4477   observed a significant shift in the distribution of *Il-10* mRNA from subpolysomal to light polysome fractions

4478   of LPS-treated WT cells as compared to control (~25.7% increase in *Il-10* accumulation in light polysomes)

4479   (**Fig. 2C**, left vs right top panels, WT).

4480   Conversely, no apparent differences were detected between control and stimulated 4E-BP1/2 DKO

4481   BMDM (**Fig. 2C**, left vs right top panels, DKO). Distribution of *Gapdh* across polysome profiles indicated

4482   that, in contrast to *Il-10*, this mRNA is efficiently translated in both WT and 4E-BP1/2-deficient cells (**Fig.**

4483   **2C**, bottom panels). These observations are in line with the notion that 4E-BP1/2 control translational

4484   efficiency of select transcripts. In keeping with greater *Il-10* mRNA translational efficiency, we detected a

4485   significant up-regulation of IL-10 protein secretion by 4E-BP1/2 DKO BMDM stimulated with LPS as

4486   compared to WT cells (3078 vs 1762 pg/ml) (**Fig. 2D**). Consistent with the involvement of the mTORC1-

4487   4E-BP1/2 axis in the regulation of IL-10 production, active site mTOR inhibitor (asTORi) PP242 reduced IL-

4488   10 induction by LPS in WT BMDM (35% reduction) but had no effect in 4E-BP1/2 DKO counterparts

4489   (**Supplemental Fig. 1A**). In support of the role of 4E-BP1/2 in modulating translation in response to LPS,

4490   a substantial increase in 4E-BP1/2 phosphorylation at T37/46, T70 and S65 (**Fig. 2E**), and a dramatic

4491   reduction in the interaction of 4E-BP1/2 with eIF4E (**Fig. 2F)** were detected in LPS-stimulated as compared

4492   to untreated BMDM. Accordingly, the amount of eIF4G bound to eIF4E augmented upon LPS exposure.

4493   Thus, LPS leads to 4E-BP1/2 inactivation and thereby promotes eIF4F complex formation in macrophages.

4494   Note that similar total cytosolic and heavy polysome-associated *Tlr4* mRNA levels were found in WT and

4495   4E-BP1/2 DKO BMDM (**Supplemental Fig. 1B**), ruling out the possibility that enhanced responses to LPS

4496   in 4E-BP1/2 deficient cells were caused by higher *Tlr4* transcription and/or translation. Overall, these data

4497   provide evidence that, in addition to activating *Il-10* transcription, LPS promotes *Il-10* mRNA translation in

4498   macrophages by dampening the activity of the inhibitory proteins 4E-BP1/2.

4499

4500   **4E-BP1 and 4E-BP2 control the activity of the transcription factor STAT3 via translational repression**

4501   **of IL-10**

4502   IL-10 induces expression of anti-inflammatory genes via the signal transducer and activator of

4503   transcription 3 (STAT3) (35, 36). Therefore, in the absence of 4E-BP1/2, enhanced translational efficiency

4504   of *Il-10* and elevated IL-10 secretion may promote STAT3 activity. To test this hypothesis, WT and 4E-

4505   BP1/2 DKO BMDM were stimulated with LPS for various time periods and the phosphorylation status of

4506   STAT3 was assessed by western blotting. As previously reported (37), LPS treatment induced STAT3

4507   phosphorylation at Y705 (Y705-STAT3) in WT BMDM. Notably, this response was markedly amplified in

4508   the absence of 4E-BP1/2 (**Fig. 3A**, top panel), reaching maximal differences between 4 and 6 h post-

4509   stimulation (~3 fold-change DKO/WT) (**Fig. 3A**, bottom panel). In parallel, culture supernatants were

4510   collected from the same cells to quantify the amount of IL-10 by ELISA. As predicted, greater secretion of

4511   IL-10 in 4E-BP1/2 DKO cells followed a similar kinetics to that of Y705-STAT3 phosphorylation

4512   (**Supplemental Fig. 1C**). Accordingly, when the activity of IL-10 was blocked using a neutralizing antibody

4513   (**Supplemental Fig. 1D**), Y705-STAT3 phosphorylation was abrogated in both WT and BP1/2 DKO cells

4514   (**Fig. 3B**). This set of experiments indicates that higher endogenous production of IL-10 is responsible for

4515 the increase in Y705-STAT3 phosphorylation in LPS-stimulated 4E-BP1/2 DKO as compared to WT BMDM.

4516 Further supporting this notion, WT and 4E-BP1/2 DKO BMDM expressed the same levels of total cytosolic

4517 and heavy polysome-associated *Il-10r1* and *Il-10r2* mRNA (**Supplemental Fig. 1E**), confirming that up-

4518 regulated IL-10 signaling in 4E-BP1/2 DKO over WT cells is not caused by differential transcription and/or

4519 translation of the IL-10 receptor.

4520 Phosphorylation of STAT3 at Y705 is a requirement for its dimerization and translocation to the

4521 nucleus (37). In agreement with our western blot data, time course experiments analyzed by image flow

4522 cytometry revealed that STAT3 nuclear translocation is enhanced in 4E-BP1/2 DKO BMDM. Differential

4523 nuclear levels of STAT3 were observed as early as 4 h following LPS stimulation and were sustained up to

4524 10 h (**Figs. 3C-D**). Nuclear STAT3 was found in 75.7% of Y705-STAT3$^+$ 4E-BP1/2 DKO BMDM at 4 h post-

4525 treatment (**Fig. 3D**, right panel). By contrast, nuclear translocation of STAT3 was detected in only 45% of

4526 Y705-STAT3$^+$ WT cells. Notably, nuclear levels of STAT3 remained higher in 4E-BP1/2 DKO BMDM for a

4527 longer period of time, as evidenced by the presence of nuclear STAT3 in 29% Y705-STAT3$^+$ 4E-BP1/2

4528 DKO versus 15.5% WT cells at 10 h post-stimulation. Altogether, these data provide evidence that elevated

4529 STAT3 activity in 4E-BP1/2 DKO cells is triggered by translational derepression of *Il-10*, which enhances

4530 the secretion and the autocrine effect of IL-10.

4531

4532 **4E-BP1 and 4E-BP2 regulate the expression of IL-10-STAT3-dependent anti-inflammatory genes**

4533 ***Nfil3*** **and s***Il1ra*** **in macrophages**

4534 Activation of the transcription factor STAT3 is required for anti-inflammatory responses induced by

4535 IL-10 (38). ChIP-seq for STAT3 identified a large repertoire of anti-inflammatory factors that are controlled

4536 by STAT3 in IL-10-stimulated macrophages (36). Our data showing elevated STAT3 nuclear translocation

4537 in 4E-BP1/2 DKO BMDM prompted us to investigate whether the expression of IL-10-STAT3-responsive

4538 genes was altered in the absence of 4E-BP1/2. We focused on two genes that are transcriptionally

4539 controlled by LPS via IL-10-STAT3 signaling, *Nfil3* and s*Il1ra*. Nuclear factor interleukin-3 regulated (NFIL-

4540 3) is a key component of a negative feedback loop that suppresses pro-inflammatory responses in myeloid

4541 cells by inhibiting *Il12b* transcription (39). Secreted interleukin-1 receptor antagonist (sIL-1Ra) is a naturally

4542 occurring inhibitor of the pro-inflammatory action of IL-1 since it binds to the IL-1 receptor with high affinity

4543 but lacks IL-1-like activity (40). In keeping with previous reports (37, 39), LPS up-regulated *Nfil3* and s*Il1ra*

4544 mRNA expression in WT BMDM. This effect was substantially enhanced in 4E-BP1/2 DKO over WT cells,

4545 as evidenced by a 3.2 and a 1.8 fold-change in *Nfil3* and s*Il1ra* mRNA levels, respectively (**Figs. 4A-B**).

4546 Accordingly, western blot analyses revealed that NFIL-3 and sIL-1Ra protein levels are higher in 4E-BP1/2

4547 deficient cells treated with LPS than WT counterparts (~4 and ~2.5 fold-change DKO/WT, respectively)

4548 (**Fig. 4C**). BP-1-102, a small-molecule inhibitor of STAT3 activation (41), repressed Y705-STAT3

4549 phosphorylation in LPS-stimulated BMDM in a dose-dependent manner (**Supplemental Fig. 1F**).

4550 Consistent with that *Nfil3* transcription is regulated by STAT3, BP-1-102 reduced *Nfil3* mRNA expression

4551 in WT and 4E-BP1/2 DKO BMDM (51% and 65%, respectively). Similarly, a decrease in s*Il1ra* mRNA levels

165

4552 was detected in BP-1-102-treated cells (34% in WT and 39% in DKO) (**Fig. 4A**). Specific blockade of IL-10

4553 activity with a neutralizing antibody reduced the expression of *Nfil3* and *sIl1ra* to the same extent in WT and

4554 4E-BP1/2 DKO BMDM (~40% decrease in *Nfil3* and ~30% in *sIl1ra*) (**Fig. 4B**). Note that induction of *Nfil3*

4555 and *sIl1ra* was significantly down-regulated but not completely abrogated by blocking either STAT3 or IL-

4556 10 activity in WT and 4E-BP1/2 DKO cells (**Figs. 4A-B**). Interestingly, augmented expression of *Nfil3* and

4557 *sIl1ra* in 4E-BP1/2 DKO BMDM was markedly reduced by BP-1-102 or anti-IL-10 antibody but remained

4558 higher than in WT cells (**Figs. 4A-B**). Collectively, these results indicate that transcriptional activation of the

4559 anti-inflammatory genes encoding NFIL-3 and sIL-1Ra is reduced by the translational repressors 4E-BP1/2

4560 mainly through the control of IL-10-STAT3-dependent signaling.

4561

4562 **4E-BP1 and 4E-BP2 negatively regulate *Cox-2* mRNA translation and Prostaglandin E$_2$ synthesis**

4563 COX-2 is a rate-limiting enzyme in the production of prostaglandin E$_2$ (PGE$_2$), a lipid mediator

4564 involved in numerous physiological and pathological processes including inflammation (42). We found that

4565 translation efficiency of *Cox-2* mRNA is amplified in 4E-BP1/2 DKO as compared to WT BMDM at steady

4566 state (**Fig. 1C**). Therefore, we set out to investigate the impact of *Cox-2* translational control by 4E-BP1/2

4567 in macrophage anti-inflammatory responses. To address this, we treated WT and 4E-BP1/2 DKO BMDM

4568 with LPS, isolated heavy polysome-associated mRNA and total cytosolic mRNA, and quantified *Cox-2*

4569 mRNA levels by RT-qPCR. In keeping with anota analysis of translational efficiency of *Cox-2* mRNA (**Fig.**

4570 **1C**), there was a substantial increase in the amount of efficiently translated *Cox-2* mRNA in 4E-BP1/2 DKO

4571 cells as compared to WT at steady state (7.4 fold-change) without any detectable change in total cytosolic

4572 mRNA (1.03 fold-change) (**Fig. 5A**). The relative amount of *Cox-2* mRNA associated to heavy polysomes

4573 was also augmented after LPS stimulation in 4E-BP1/2 DKO as compared to WT BMDM (3.10 fold-change),

4574 without changes in total cytosolic mRNA levels (1.15 fold-change) (**Fig. 5A**). Confirming and extending

4575 these data, mRNA fractionation and quantification across polysome profiles showed a 30.3% reduction in

4576 *Cox-2* mRNA isolated from subpolysomal fractions of 4E-BP1/2 DKO BMDM DKO as compared to WT

4577 cells, which resulted in higher accumulation of *Cox-2* mRNA in light and heavy polysomal fractions (37.7%

4578 and 32% in DKO vs. 20 and 19.5% in WT) (**Fig. 5B**, top panel). Notably, LPS treatment led to a remarkable

4579 shift in the distribution of *Cox-2* mRNA from subpolysomal to light polysome fractions in WT BMDM, as

4580 indicated by an 18.8% reduction in subpolysomal *Cox-2* mRNA concomitant with a 24.4% increase in light

4581 polysome fractions (**Fig. 5B**, left vs right top panels, WT). By contrast, no significant differences were

4582 detected in the distribution of *Cox-2* mRNA across polysome profiles of LPS-treated vs. control 4E-BP1/2

4583 DKO BMDM (**Fig. 5B**, left vs right top panels, DKO). These results provide evidence that LPS stimulates

4584 *Cox-2* mRNA translation through the inactivation of the repressors 4E-BP1/2. Accordingly, a more rapid

4585 kinetics and a greater induction of COX-2 protein expression was detected in 4E-BP1/2 DKO than in WT

4586 BMDM after LPS stimulation (~13 fold-change at 4 h and ~6 fold-change up to 8 h post-treatment) (**Fig.**

4587 **5C**). Notably, PP242 blocked LPS-inducible COX-2 expression in WT BMDM while exerting only a mild

4588 effect in 4E-BP1/2 DKO counterparts (**Supplemental Fig. 1G**), a clear indicative that mTORC1-mediated

4589   4E-BP1/2 inactivation contributes to the regulation of COX-2 production. In keeping with higher COX-2

4590   levels, PGE$_2$ synthesis in response to LPS was amplified in absence of 4E-BP1/2, as evidenced by a 1.74-

4591   fold-change in the accumulation of PGE$_2$ in cell culture supernatants of 4E-BP1/2 DKO BMDM as compared

4592   to WT (**Fig. 5D**). Collectively, these results support the notion that translational activity of *Cox-2* mRNA and

4593   subsequent PGE$_2$ induction are controlled by the translational repressors 4E-BP1/2.

4594

4595   **4E-BP1 and 4E-BP2 limit PGE$_2$-C/EBP-β-mediated macrophage anti-inflammatory gene expression**

4596   Prostaglandins are autocrine and paracrine lipid mediators that maintain local homeostasis.

4597   Endogenous PGE$_2$ production potentiates macrophage anti-inflammatory responses via activation of

4598   CCAAT/enhancer-binding protein β (C/EBP-β) signaling (42). Our data indicated that induction of PGE$_2$

4599   synthesis in LPS-stimulated cells is augmented in the absence of 4E-BP1/2. Thus, we sought to determine

4600   whether enhanced PGE$_2$ secretion amplified its autocrine effect and potentiated C/EBP-β-activity in 4E-

4601   BP1/2 DKO BMDM. RT-qPCR experiments showed that *C/ebpb* mRNA expression was substantially up-

4602   regulated in 4E-BP1/2 DKO BMDM after LPS stimulation (1.56 fold-change over WT) (**Fig. 6A**). Blockade

4603   of COX-2 activity with the selective NS-398 inhibitor (43) down-regulated but did not abolish the expression

4604   of *C/ebpb* mRNA in WT and 4E-BP1/2 DKO BMDM (36% and 66%, respectively) (**Fig. 6B**). Thus,

4605   transcriptional activation of *C/ebpb* appears to require COX-2-PGE$_2$-dependent and independent signals in

4606   macrophages. Remarkably, NS-389 reduced *C/ebpb* mRNA expression in 4E-BP1/2 DKO cells to WT

4607   levels (**Fig. 6B**). In keeping with the kinetics of *C/ebpb* accumulation, western blot analyses revealed that

4608   C/EBP-β□ protein levels augmented more rapidly and to a greater extent in LPS-treated 4E-BP1/2 DKO

4609   than WT BMDM (~2.5 fold-change DKO/WT at 4 - 6 h) (**Fig. 6C**). As expected, C/EBP-β-induction by LPS

4610   was reduced when cells were treated with NS-398 (**Supplemental Fig. 1H**). These data support the notion

4611   that enhanced PGE$_2$ secretion and autocrine action potentiates *C/ebpb* transcription and protein expression

4612   in 4E-BP1/2 DKO BMDM.

4613   C/EBP-β is required for transcriptional activation of anti-inflammatory genes in macrophages (42,

4614   44). We predicted that amplified PGE$_2$/C/EBP-β signaling would promote this cellular response in 4E-BP1/2

4615   DKO BMDM. We focused on *Arg1* and *SerpinB2* because these genes are transcriptionally activated via

4616   C/EBP-β□in LPS-stimulated macrophages and have central roles in local homeostasis (45, 46). Arginase-

4617   1 functions as an inhibitor of chronic inflammation in Th2-polarized immune responses (47) and SerpinB2

4618   suppresses Th1 responses during inflammatory processes (48). At first, we stimulated WT and 4E-BP1/2

4619   DKO BMDM with LPS over a 24-h period and monitored the expression of *Arg1* and *SerpinB2* by RT-qPCR.

4620   A dramatic increase in *Arg1* mRNA levels was detected in 4E-BP1/2 DKO over WT cells at 12 h (4.0 fold-

4621   change) and 24 h (10.5 fold-change) post-treatment (**Fig. 6D**). Accumulation of *SerpinB2* mRNA was also

4622   markedly amplified in absence of 4E-BP1/2. Significant differences were observed as early as 6 h after LPS

4623   stimulation (1.9 fold-change DKO/WT), were maximal at 8 h (2.48 fold-change) and remained detectable

4624   up to 24 h (**Fig. 6E**). Consistent with the requirement of COX-2 activity for *Arg1* transcription, NS-398

4625   prevented accumulation of *Arg1* mRNA in WT and 4E-BP1/2 DKO BMDM (~91 % decrease) (**Fig. 6F**).

4626   Similarly, *SerpinB2* mRNA levels were drastically down-regulated in NS-398-treated WT and DKO cells

4627   (~76 % decrease) (**Fig. 6G**). Notably, greater expression of *Arg1* and *SerpinB2* mRNA in 4E-BP1/2 DKO

4628   BMDM was reduced to WT levels by NS-398 treatment (**Figs. 6F-G**). Collectively, this set of experiments

4629   provides evidence that in the absence of 4E-BP1/2, translational derepression of *Cox-2* mRNA potentiates

4630   synthesis and autocrine action of endogenous PGE_2, which in turn promotes C/EBP-β-mediated

4631   transcriptional activation of anti-inflammatory genes.

4632

4633   4E-BP1 and 4E-BP2 regulate macrophage bactericidal capacity by repressing Interleukin-10 and

4634   Cyclooxygenase-2 anti-inflammatory effects

4635   Macrophage anti-inflammatory responses are essential for the resolution of inflammation and local

4636   tissue repair after elimination of invading pathogens; however, when dysregulated, host susceptibility to

4637   infection can emerge (11). IL-10-STAT3 and PGE_2-C/EBPβ signaling augment the expression of anti-

4638   inflammatory genes (36, 44, 45). In addition, IL-10 and PGE_2 exert a suppressive effect on pro-inflammatory

4639   and microbicidal mediator production (17, 49-51). Consistent with elevated levels of IL-10 and PGE_2 in 4E-

4640   BP1/2 DKO BMDM, transcriptional activation of several anti-inflammatory genes was enhanced in these

4641   cells. Conversely, LPS-inducible accumulation of pro-inflammatory transcripts *Tnf*, *Il-6* and *Nos2* declined

4642   more rapidly and to a greater extent in 4E-BP1/2 DKO than in WT BMDM (**Figs. 7A-C**). Collectively, these

4643   data suggested that in the absence of 4E-BP1/2, the bactericidal capacity of LPS-stimulated macrophages

4644   could be diminished. To test this hypothesis, WT and 4E-BP1/2 DKO BMDM were treated or not with 10

4645   ng/ml LPS for 24 h and subsequently infected with a non-pathogenic strain of *E .coli* (MG 1655).

4646   Unstimulated WT and 4E-BP1/2 DKO BMDM were able to control the infection. In stark contrast, bacteria

4647   survival increased in LPS-treated 4E-BP1/2 DKO over WT cells at 8 h post-infection (2.1 fold-change) and

4648   remained augmented up to 24 h (3.7 fold-change) (**Fig. 8A**). Bacterial numbers were equivalent in WT and

4649   4E-BP1/2 DKO cells at 6 h post-infection, confirming that differential bacterial survival observed at later

4650   time points was not due to changes in phagocytic activity in response to TLR4 stimulation. Notably,

4651   simultaneous blockade of IL-10 and PGE_2 activity with a neutralizing anti-IL-10 antibody and a specific

4652   inhibitor of COX-2 restored bacteria killing by ~82% in 4E-BP1/2 DKO BMDM, reaching similar levels to WT

4653   counterparts (**Fig. 8B**). By contrast, the same treatment had no significant effect in bactericidal activity of

4654   WT BMDM. These data support the notion that excess IL-10- and PGE_2-mediated anti-inflammatory

4655   responses hamper the bactericidal potential of LPS-stimulated 4E-BP1/2 DKO BMDM. In conclusion, our

4656   study uncovered a crucial role for 4E-BP1/2 in macrophage homeostasis by limiting the anti-inflammatory

4657   action of IL-10-STAT3 and PGE_2-C/EBPβ signaling (**Fig. 9**).

4658

Discussion

4659
4660   The mTORC1 downstream effectors 4E-BP1/2 play a crucial role in the regulation of pro-
4661   inflammatory mediators during viral and parasitic infections (6, 18, 19). Surprisingly, there are considerable
4662   gaps regarding the impact of 4E-BP1/2 in the control of anti-inflammatory responses. We identified the
4663   mTORC1-4E-BP1/2-eIF4E axis as a central regulator of macrophage homeostasis. In the absence of 4E-
4664   BP1/2, translational derepression of *Il-10* and *Cox-2* mRNAs triggered a transcriptional program that
4665   amplified anti-inflammatory gene expression and promoted bacteria survival in macrophages upon TLR4
4666   stimulation. These data provide evidence that 4E-BP1/2-dependent translational control of select mRNAs
4667   contributes to modify gene expression networks that orchestrate macrophage responses.

4668   Among 564 immune-related transcripts that were screened in this study, only 11 were identified as
4669   targets of translational control via 4E-BP1/2 in macrophages. These data are in line with numerous reports,
4670   including comparative analyses of the translatomes of WT and 4E-BP1/2 DKO mice and cells (6, 52),
4671   showing that 4E-BPs do not act as general translational repressors but rather target specific subsets of
4672   mRNAs (21, 53-59). Despite the fact that eIF4E is required for cap-dependent translation of all nuclear-
4673   encoded mRNAs, some of them are particularly sensitive to eIF4E levels and / or availability, and therefore
4674   are referred to as "eIF4E-sensitive" (5, 31, 32). Accordingly, their translational efficiency is repressed by
4675   genetic deletion of eIF4E (32) or increased cellular 4E-BP to eIF4E ratios (59). Two major subsets of
4676   transcripts have been identified as being targets of select translational control via eIF4E-dependent
4677   mechanisms. The first one comprises mRNAs known as "eIF4A-sensitive" (5, 31, 32), which harbor long
4678   and highly structured 5' UTRs and therefore depend on the RNA helicase activity of eIF4A to be efficiently
4679   translated (32, 60-62). eIF4E sensitivity of these mRNAs is thought to stem from eIF4E-dependent
4680   recruitment of eIF4A to the eIF4F complex and stimulation of eIF4A activity (5, 63). Consistent with a central
4681   role for 4E-BP1/2 as regulators of eIF4A-sensitive mRNAs, pharmacological inhibition of mTORC1 signaling
4682   represses translational efficiency of such transcripts in WT cells but not in 4E-BP1/2 DKO counterparts (21,
4683   53). Accumulating evidence indicates that eIF4A-sensitive mRNAs encode proteins related to specific
4684   cellular processes, namely cell proliferation and survival (21, 32, 53) but also immune responses (6, 32).
4685   Indeed, *Irf-7*, which encodes a central regulator of antiviral immunity (10), was identified as an eIF4A-
4686   sensitive mRNA (32). Accordingly, *Irf-7* mRNA harbors a long and highly structured 5' UTR and its
4687   translational efficiency is tightly controlled through 4E-BP1/2 (6). Note that *Irf-7* was not identified in our
4688   screening, which might be explained by differences in cell types employed (MEFs vs, BMDM) and treatment
4689   (serum stimulated vs. steady state). Indeed, selective changes in mRNA translation via mTORC1-mediated
4690   inactivation of 4E-BP1/2 appear to be dependent on the nature of the stimulus or type of stress to which
4691   the cell is exposed (5, 31, 57). In support of the notion that 4E-BP1/2 limit translation efficiency of immune-
4692   related transcripts containing long and structured 5'UTRs, our bioinformatic analysis indicated that *Cox-2*,
4693   *Ifit2*, *Il1b*, and *Mx-1* might fall into this category. Further investigation is required to determine whether
4694   selective translational control of these mRNAs via 4E-BP1/2 is dictated by their sensitivity to eIF4A activity.

A second subset of "eIF4E-sensitive" mRNAs is characterized by very short 5' UTRs (i.e., 30 nt) that some cases contain a Translation Initiator of Short 5 'UTR (TISU) element (32, 54, 56, 64). As such, their translational efficiency is less sensitive to eIF4A (32) and they are referred to as "eIF4A-insensitive" mRNAs (5, 31, 32). These transcripts encode proteins involved in mitochondrial-related functions (64) and their translational efficiency is limited by 4E-BP1/2 (54, 56). We identified several immune-related mRNAs (*Il1a*, *Il1b*, *Il10*, *Il12b*, *Ccl5*, *Ccl12*, *Cd40* and *Cxcl10*) that harbor relatively short 5' UTRs; however, none of them contains a TISU element and, with the exception of *Il1a*, their length exceeds 30 nucleotides. Thus, they do not seem to meet the criteria to be considered as short-5' UTR-containing "eIF4E-sensitive" transcripts. It is conceivable that these and other immune-related transcripts are subject to an alternative mechanism of 4E-BP1/2-dependent translational control, which might involve yet to be discovered sequence and/or structural features in their 5' UTRs. Alternatively, these mRNAs might be expressed in macrophages with 5'UTRs differing from those reported in data bases. Further investigation is needed to resolve these possibilities.

An additional explanation that could account for the small amount of selective translational control of immune-related transcripts through 4E-BP1/2 is that our comparative analysis was performed in macrophages at steady-state. Since we employed an immunology panel, it seems reasonable that changes in translational activity for many of these transcripts cannot be detected without cell activation. Further support for this hypothesis was obtained from our data showing that TLR4 stimulation was required to detect IL-10 and COX-2 at the protein level, despite the fact that *Il-10* and *Cox-2* mRNAs were translated more efficiently in 4E-BP1/2 DKO than WT BMDM at steady-state. These observations are in line with a study showing that even though *Il-10* is transcribed in macrophages at basal level, IL-10 secretion can only be detected in stimulated cells. The authors presented experimental evidence indicating that macrophages are poised to secrete IL-10 and will do so if they receive appropriate signals (65). Thus, our data along with this previous report suggest that in the absence of 4E-BP1/2, select mRNAs might be "primed" to be more efficiently translated in response to triggers or cues, a phenomenon recently described in NK cells (66).

Consistent with the central role of IL-10 and COX-2 in anti-inflammatory responses (35, 36, 42, 44), their expression is tightly regulated through transcriptional and post-transcriptional mechanisms, including RNA stability and translational control via RNA-binding proteins, such as T cell intracellular antigen 1 (TIA-1) and tristetraprolin (TTP) (reviewed in (67, 68)). The adenosine A2B receptor activates translation of *Il-10* mRNA in macrophages by relieving the translational repressive effect of RNA-binding protein elements in its 3' UTR (69). In regards to COX-2, different mechanisms of translational control have been reported. The translational silencer and RNA-binding protein TIA-1 represses *Cox-2* mRNA translation (70). Moreover, COX-2 protein synthesis was shown to be dependent on mTORC1 signaling in neutrophils (71); however, the underlying mechanism remained unclear. Confirming and extending previous reports, we found that the inhibitors of cap-dependent translation, 4E-BP1/2, limit *Il-10* and *Cox-2* mRNA translation efficiency in macrophages. Because the activity of 4E-BP1/2 is altered by a number of pathogens (reviewed

4731 in (72)), it is plausible that dysregulated translational control of *Il-10* and *Cox-2* may contribute to the
4732 pathogenesis of infections by skewing anti-inflammatory responses in macrophages.

4733 Our results indicate that translational control of mRNAs encoding select immunomodulatory factors,
4734 such as IL-10 and COX-2, is required for fine tuning of macrophage responses to the bacterial toxin and
4735 TLR4 ligand LPS. In keeping with this reasoning, several reports showed that LPS-inducible expression of
4736 activators and suppressors of inflammation is, at least part, controlled at the level of mRNA translation in
4737 macrophages. For instance, TLR4 stimulation with LPS activates mRNA translation of several pro-
4738 inflammatory mediators including the transcription factor IRF-8 (14) and the transforming growth factor-
4739 activated kinase (TAK1) (15). In stark contrast, a previous study showed that LPS promotes translation of
4740 macrophage mRNAs encoding negative feedback regulators of the inflammatory response, such as
4741 inhibitors of NF-kB (e.g., IER3, NFKBID) and RNA-binding proteins that prevent the expression of cytokines
4742 at the post-transcriptional level (e.g., TTP) (16). These reports, along with our data, suggest that microbial
4743 components, such as LPS, trigger antagonistic translational control programs during infection (i.e pro- and
4744 anti-inflammatory), which might contribute to pathogen clearance while helping to maintain macrophage
4745 homeostasis.

4746 We found that 4E-BP1/2-dependent mTORC1 signaling is necessary to control *Il-10* and *Cox-2*
4747 mRNA translation and subsequent IL-10 and COX-2 production. These data are in agreement with previous
4748 studies that have linked translational control via eIF4E availability or activity to changes in translation of
4749 mRNAs encoding regulators of inflammation in macrophages. Indeed, IFN-γ enhances TLR2-stimulated
4750 M1 macrophage activation by suppressing mRNA translation of the transcriptional repressor HES-1 via
4751 MNK1/2 and mTORC1 inhibition (13). Similarly, IL-10 was shown to disrupt MNK signaling and thereby
4752 repress mRNA translation of the pro-inflammatory cytokine TNF (17). Conversely, LPS was found to
4753 activate the MNK pathway and induce protein synthesis of IRF-8. Notably, MNK-dependent regulation of
4754 IRF-8 promoted pro-inflammatory gene expression and M1 macrophage polarization (14). In view of these
4755 studies and our current findings, selective translational control through eIF4E-dependent mechanisms
4756 appears to regulate transcriptional programs that coordinate the onset and the resolution of inflammatory
4757 responses in macrophages.

4758 Macrophages deficient in 4E-BP1/2 displayed a defect in their bactericidal capacity. We postulate
4759 that this phenotype is associated with translational derepression of *Il-10* and *Cox-2* and the amplified
4760 autocrine action of endogenous IL-10 and PGE_2 produced in response to LPS. Further supporting our
4761 model, the anti-inflammatory and immunosuppressive effects of IL-10 and PGE_2 are well documented and
4762 have been linked to their ability to inversely regulate anti- and pro- inflammatory gene expression (17, 36,
4763 37, 42). Importantly, IL-10 and PGE_2 are negative regulators of LPS-mediated inflammatory responses (49,
4764 51). However, we cannot rule out the possibility that in addition to IL-10 and COX-2, 4E-BP1/2 control other
4765 immunomodulatory factors that impact anti-inflammatory responses and bacterial survival in macrophages.
4766 In contrast to our observations, 4E-BP1/2 DKO MEFs were resistant to viral infections (6) and 4E-BP1/2
4767 DKO peritoneal macrophages were less susceptible to a protozoan parasite (19). This discrepancy might

171

4768 be related to distinct translational programs triggered by specific stimulus or stressors in different cell types.
4769 Further characterization of the molecular mechanisms of 4E-BP1/2-dependent translational control during
4770 infections will shed light on this matter.

4771 Collectively, this work provides evidence that the mTORC1-4E-BP1/2 axis orchestrates
4772 translational and thereby transcriptional programs that limit anti-inflammatory responses in macrophages.
4773 Notably, our data suggest that dysregulated activity of 4E-BP1/2 during pathological conditions, such as
4774 infections and cancer, might contribute to reprogram the translational and transcriptional landscape of
4775 macrophages and thereby favor disease progression. Targeted sequencing and transcriptome-wide
4776 analyses of the translatome of pathology-associated macrophages will generate a more complete repertoire
4777 of the mRNAs that are translationally controlled through 4E-BP1/2-dependent mechanisms, and will provide
4778 insight on the regulation of gene expression networks in health and disease.

4779

4785
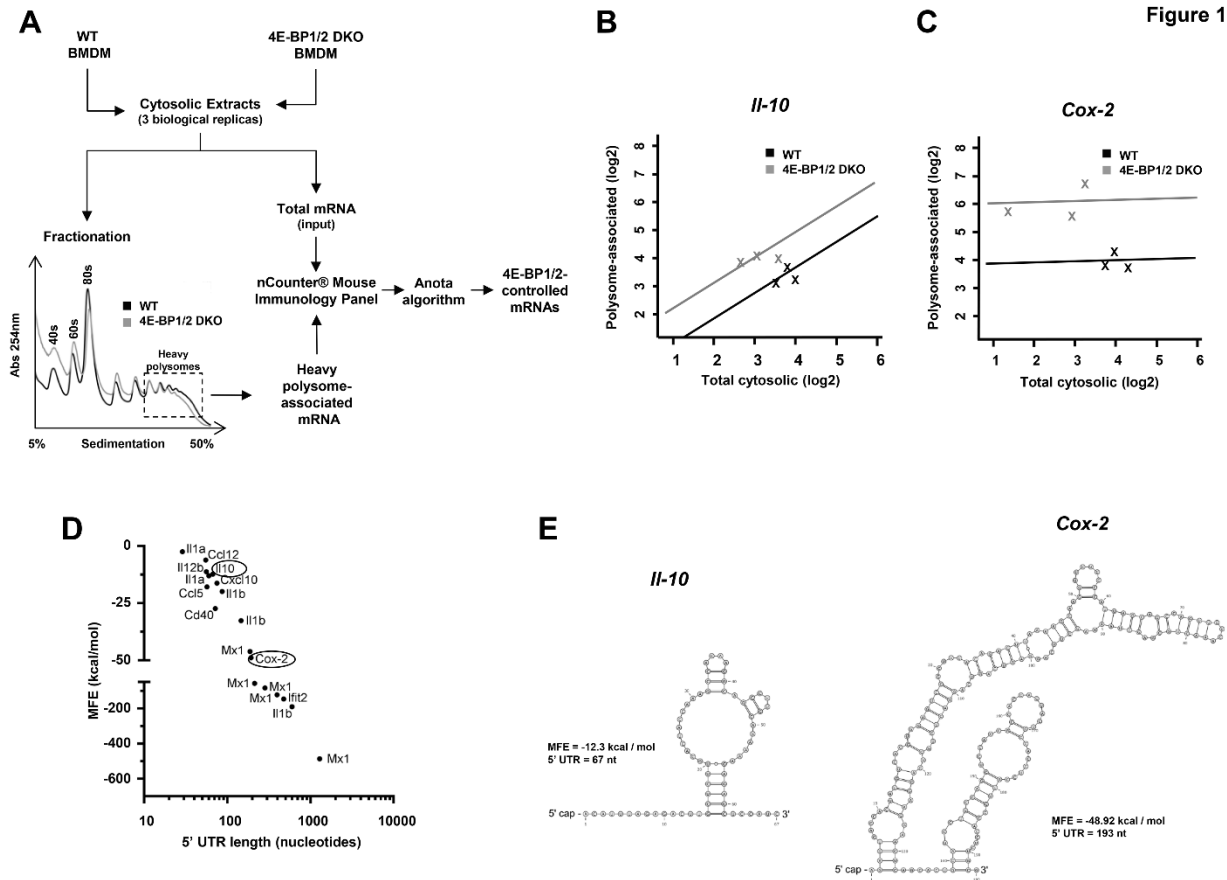
4786

4787 **Figure 1. 4E-BP1/2 limit translational efficiency of *Il-10*, *Cox-2* and other immune-related mRNAs in**

4788 **macrophages.** (**A**) Cytosolic extracts from WT and 4E-BP1/2 DKO BMDM were sedimented on a sucrose

4789 gradient. Heavy polysome fractions (i.e., with mRNA associated to > 3 ribosomes) were pooled (referred to

4790 as polysome-associated mRNA) and quantified in parallel with total mRNA using targeted nCounter assays

4791 (towards mRNAs encoding immune related proteins) (n=3). Translational efficiency of *Il-10* (**B**) and *Cox-2*

4792 (**C**) in 4E-BP1/2 DKO cells as compared to WT cells. Shown is the fold-increase (log2) in total cytosolic

4793 mRNAs levels (x-axis) vs. heavy polysome-associated mRNAs levels (y-axis) for each genotype. The lines

4794 indicate the regressions used by anota to adjust changes in polysome-associated mRNA levels for changes

4795 in cytosolic mRNA levels. (**D**) Minimum free energy (MFE) and 5' UTR length of top 11 immune-related

4796 mRNAs identified by anota as targets of 4E-BP1/2-dependent translational control in macrophages

4797 (translational efficiency $\geq$ 2, FDR $<$ 0.25). (**E**) Secondary structures of mouse *Il-10* and *Cox-2* 5' UTRs as

4798 predicted by RNAfold.

4799
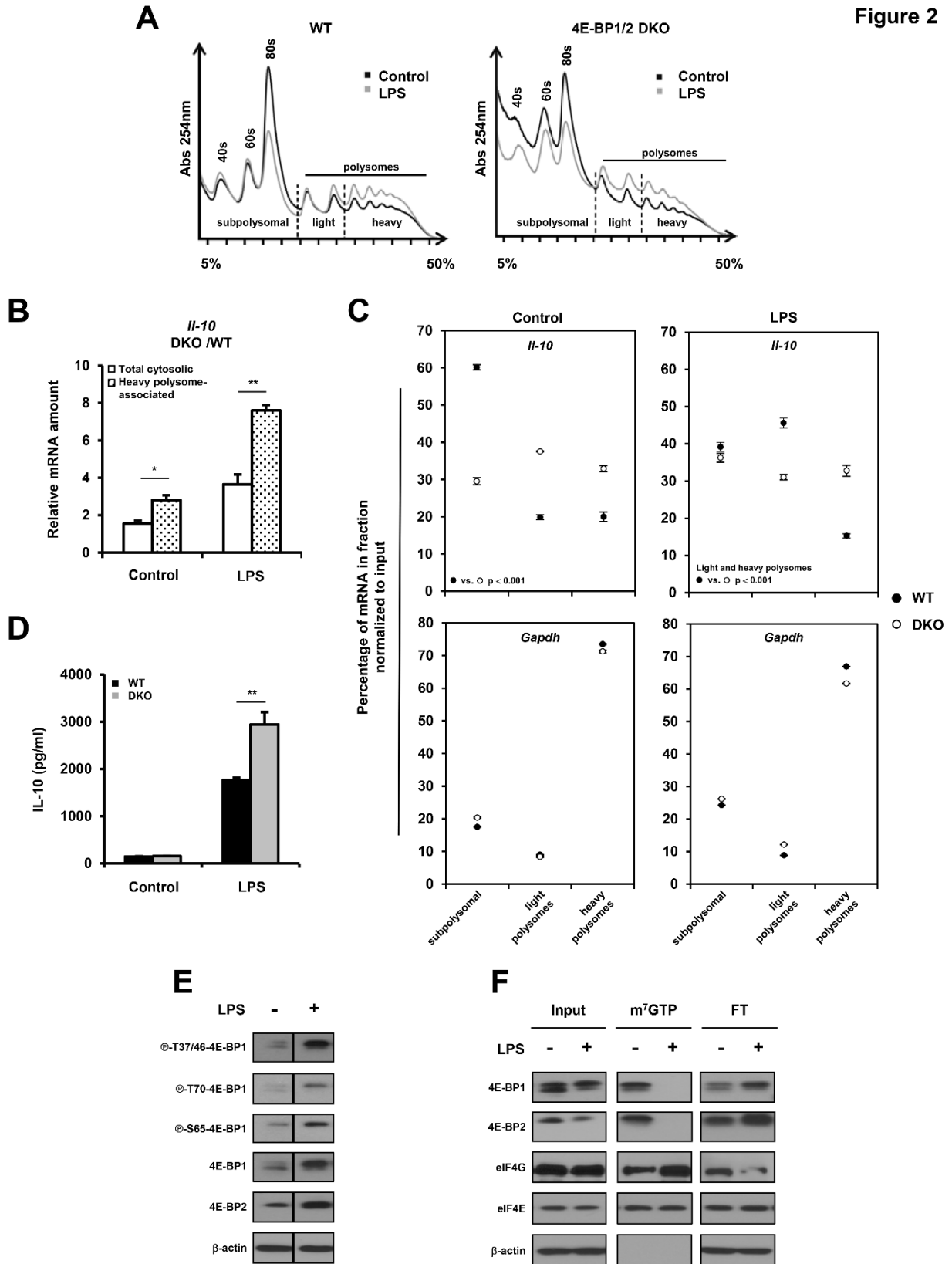
Figure 2

Figure 2. LPS-induced *Il-10* mRNA translation is under the control of 4E-BP1/2. (**A**) WT and 4E-BP1/2 DKO BMDM were left untreated (control) or stimulated with 10 ng/ml LPS for 4 h. Cytosolic extracts were loaded onto 5-50% sucrose gradients and sedimented by ultracentrifugation. Polysome tracings were generated by recording the UV absorbance at 254 nm. Subpolysomal, light and heavy polysome fractions were pooled for further mRNA isolation and quantification (n=3). (**B**) RT-qPCR of total cytosolic and heavy polysome-associated *Il-10* mRNA in control and LPS-stimulated WT and 4E-BP1/2 DKO BMDM. Results are shown as mean values ± SD of 4E-BP1/2 DKO/WT (fold increase in DKO over WT normalized to *Gapdh*) (n = 3). (**C**) Amount of *Il-10* (top panels) and *Gapdh* (bottom panels) mRNA in subpolysomal, light polysome and heavy polysome fractions isolated from cells described in A were determined by RT-qPCR. Experiments were carried out in independent duplicates, each consisting of a triplicate. Data are expressed as percentage of a given mRNA in each fraction. (**D**) IL-10 protein secreted by WT and 4E-BP1/2 DKO cells untreated (control) or stimulated with LPS for 12 h (mean values ± SD; n=3). (**E**) Total proteins were extracted and separated by SDS-PAGE. Phosphorylation status and expression levels of 4E-BP1 and 4E-BP2 were monitored by Western blotting using phospho-specific and total antibodies, respectively. β-actin was used as loading control. Note that images were obtained after the same time exposure of a single film in contact with one membrane. Scans were cropped to remove unrelated samples that were loaded on the same gel. (**F**) Cell lysates were processed for m^{7}GTP-agarose pull down assays to assess changes in the interaction between cap-bound eIF4E and 4E-BP1, 4E-BP2 or eIF4G (m^{7}GTP panels). The phosphorylation status of 4E-BP1/2 was monitored in total extracts (Input panels). Unbound 4E-BP1, 4E-BP2 and eIF4G levels were detected in flow-through (FT) samples. (**E** and **F**) Data are representative of at least two independent biological replicates.
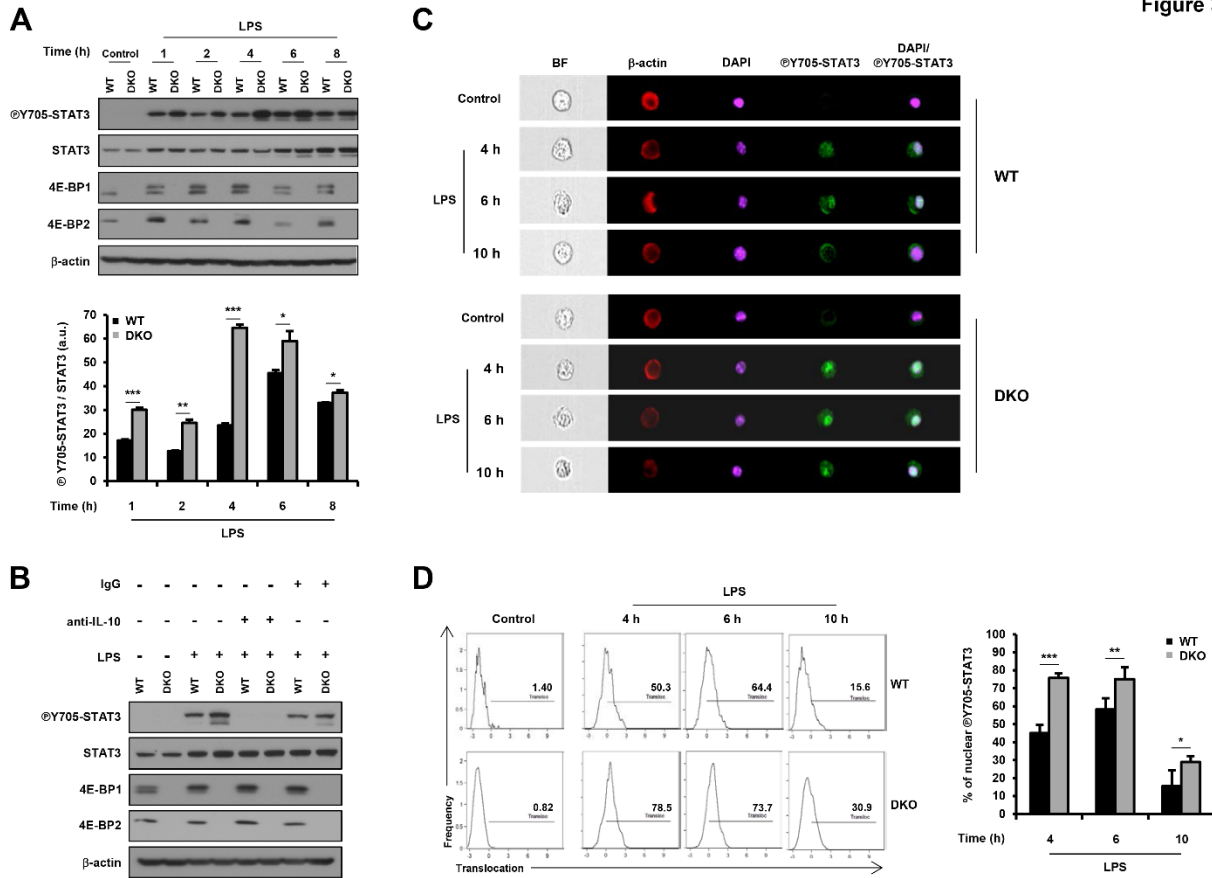
Figure 3. 4E-BP1/2 regulate STAT3 activity by limiting the autocrine effect of endogenous IL-10 in LPS-stimulated macrophages. (**A**) WT and 4E-BP1/2 DKO cells were treated with LPS for the indicated time. Phosphorylation status and STAT3 levels were monitored by western blotting using phospho-specific and total antibodies against STAT3, respectively. 4E-BP1 and 4E-BP2 antibodies were employed as controls for cell genotype. β-actin served as loading control (top panel). Quantification of Y705-STAT3 phosphorylation (normalized to total STAT3) in LPS-stimulated cells using Image J (mean ± SD; n= 3) (bottom panel). (**B**) Cells were stimulated with LPS with or without 2 μg/ml anti-IL-10 or anti-IgG1 isotype control for 4 h. STAT3 phosphorylation at Y705 was assessed by western blotting. (**C**) Representative images captured by image flow cytometry showing nuclear translocation of STAT3 in WT and 4E-BP1/2 DKO cells untreated (control) or stimulated with LPS at indicated time. Control samples were collected at 10 h. From left to right: Brightfield image (BF), β-actin (red, cytoplasm), DAPI (purple, nucleus), phospho-Y705-STAT3 (green), and DAPI/phospho-Y705-STAT3 merge (white, indicates nuclear co-localization). (**D**) Quantification of STAT3 nuclear translocation in phospho-Y705-STAT3+ cells. Representative histogram showing the percentage of phospho-Y705-STAT3 present in the nucleus after LPS exposure for the indicated time (left panel). Shown are mean values ± SD of three independent biological replicates (right panel). (**A** – **C**) Data are representative of three independent experiments.

176
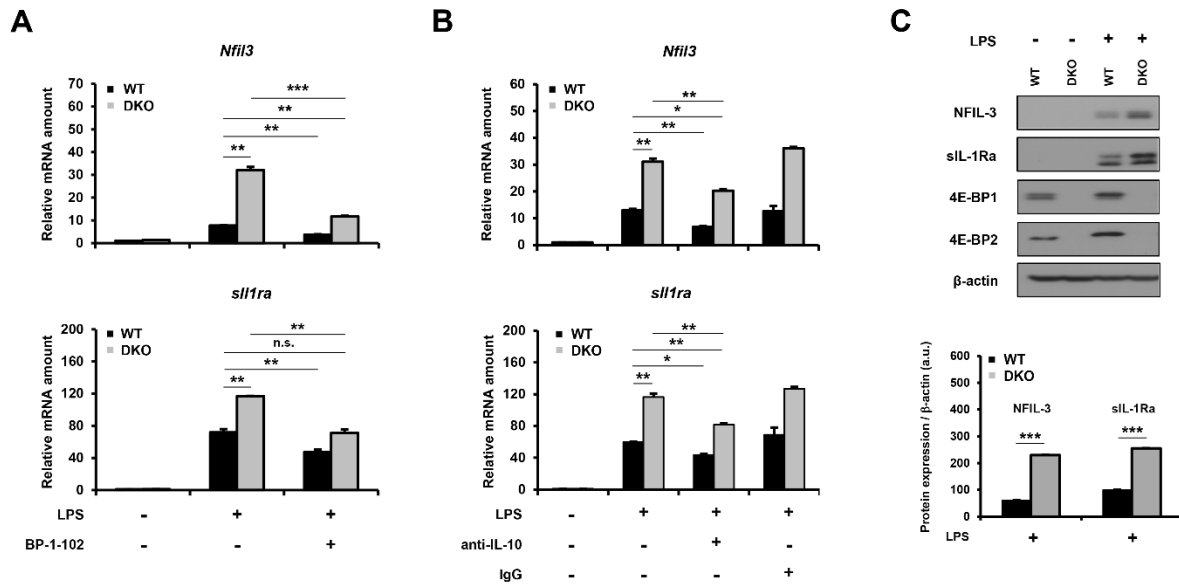
Figure 4

Figure 4. IL-10-STAT3-mediated anti-inflammatory responses are amplified in 4E-BP1/2 DKO macrophages. WT and 4E-BP1/2 DKO cells were treated for 4 h with 10 ng/ml LPS with or without 2 µM BP-1-102 (**A**) or with LPS with or without 2 µg/ml anti-IL-10 or anti-IgG1 isotype control (**B**) and relative amounts of *Nfil3* and s*Il1ra* mRNAs were quantified using RT-qPCR (normalized to *Rpl19*). (**C**) Western blots of NFIL-3 and sIL-1Ra were carried out in total protein extracts from control and LPS-treated cells (top panel). Quantification of western blot analyses on NFIL-3 and sIL-1Ra (normalized to β-actin) by Image J (bottom panel). Results are presented as mean ± SD (n = 3).

Figure 5

4852

4853

178
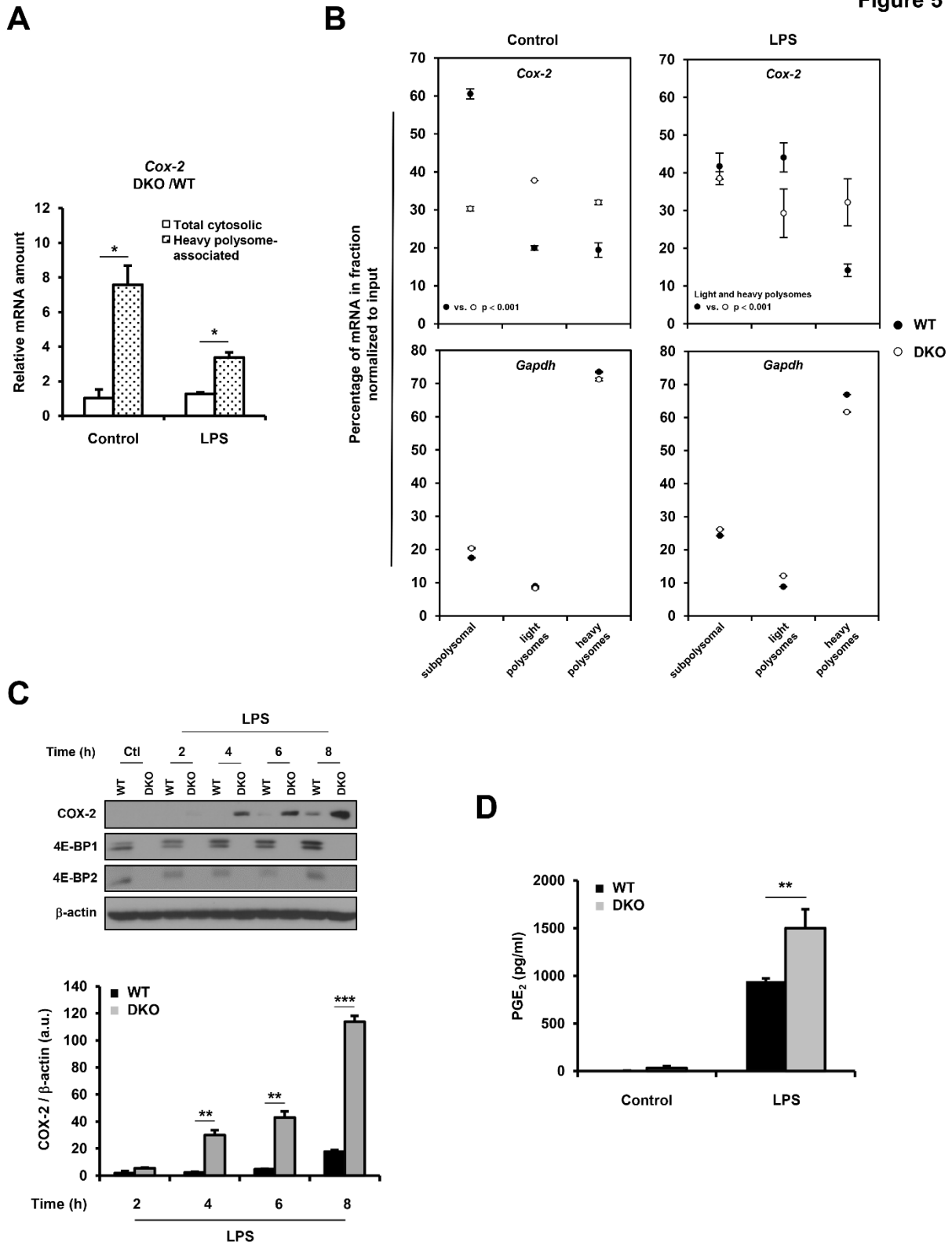
4854   **Figure 5. 4E-BP1/2 limit *Cox-2* translational efficiency and PGE$_2$ synthesis.** (**A**) RT-qPCR of total

4855   cytosolic and heavy polysome-associated *Cox-2* mRNA in control and LPS-stimulated 4E-BP1/2 DKO and

4856   WT cells (fold increase in 4E-BP1/2 DKO over WT normalized to *Gapdh*). (**B**) Amount of *Cox-2* (top panels)

4857   and *Gapdh* (bottom panels) mRNA in subpolysomal, light polysome and heavy polysome fractions isolated

4858   from control and LPS-stimulated 4E-BP1/2 DKO and WT cells quantified by RT-qPCR. Experiments were

4859   carried out in independent duplicates, each consisting of a triplicate. Data are expressed as percentage of

4860   a given mRNA in each fraction. (**C**) WT and 4E-BP1/2 DKO cells were treated with LPS for the indicated

4861   time and COX-2 expression was assessed by western blotting (top panel). Quantification of western blot

4862   analyses on COX-2 (normalized to β-actin) by Image J (bottom panel). (**D**) PGE$_2$ levels were quantified in

4863   the supernatants of WT and 4E-BP1/2 DKO cells untreated (control) or stimulated with LPS for 12 h. (**A**, **C**-

4864   **D**) Results are presented as mean ± SD (n = 3).

4865

Figure 6
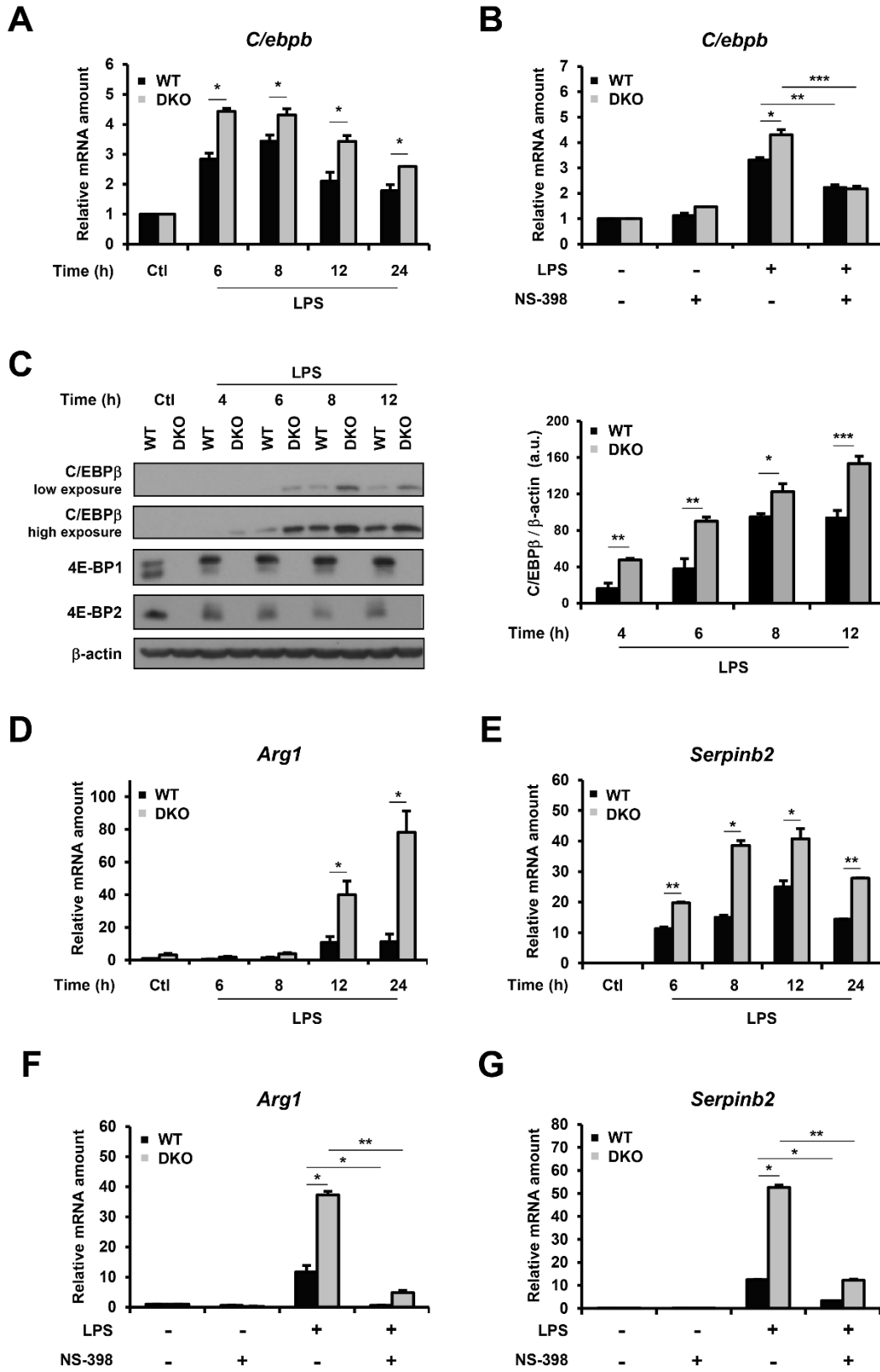
4868   **Figure 6. PGE$_2$-C/EBPβ-mediated anti-inflammatory responses are augmented in 4E-BP1/2 DKO**

4869   **macrophages.** Relative amounts of *C/ebpb* mRNA normalized to *Gapdh* were examined by RT-qPCR in

4870   WT and 4E-BP1/2 DKO cells stimulated with LPS for the indicated time (**A**) or treated with LPS with or

4871   without 50 µM NS-398 for 8 h (**B**). (**C**) Western blots of C/EBPβ in control and LPS-stimulated cells (left

4872   panel). Quantification of western blot analyses on C/EBPβ (normalized to β-actin) using Image J (right

4873   panel). Changes in *Arg1* and *Serpinb2* mRNA levels relative to *Gapdh* mRNA were determined by RT-

4874   qPCR in WT and 4E-BP1/2 DKO cells stimulated with LPS for the indicated time (**D** and **E**, respectively) or

4875   treated with LPS with or without 50 µM NS-398 for 8-12 h (**F** and **G**, respectively). Results are presented

4876   as mean ± SD (n = 3).

4877

Figure 7

A

B

C
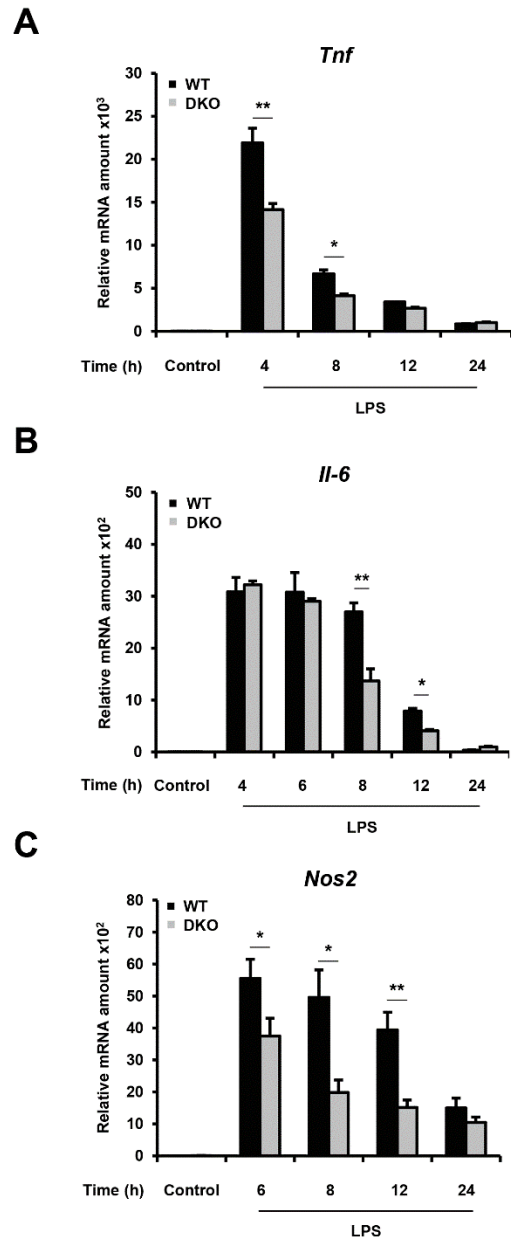
4878

4879 **Figure 7.   LPS-inducible pro-inflammatory gene expression is reduced in 4E-BP1/2 DKO**

4880 **macrophages.** Relative amounts of *Tnf* (**A**), *Il-6* (**B**) and *Nos2* (**C**) mRNA normalized to *Gapdh* were

4881 quantified in control and LPS-treated WT and 4E-BP1/2 DKO BMDM by RT-qPCR Results are presented

4882 as mean ± SD (n = 3).

4883

Figure 8
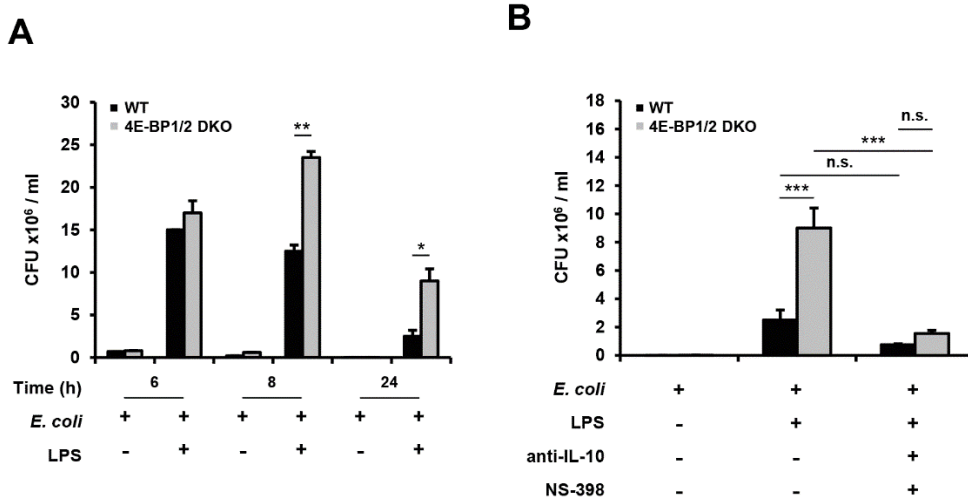
4884

4885

4886 **Figure 8. 4E-BP1/2 regulate macrophage bactericidal capacity through the control of IL-10 and PGE$_2$**

4887 **signaling.** (**A**) WT and 4E-BP1/2 DKO BMDM untreated or pre-treated with 10 ng/ml LPS for 24 h were

4888 subsequently infected with *E. coli* MG 1655 (10:1 ratio) for 6, 8 or 24 h. Surviving bacteria were quantified

4889 as colony forming units (CFU) / ml. (**B**) Cells untreated or stimulated with LPS with or without 2 µg/ml anti-

4890 IL-10 antibody and 50 µM NS-398, were infected for 24 h. Results are presented as mean ± SD (n = 3).

4891

Figure 9
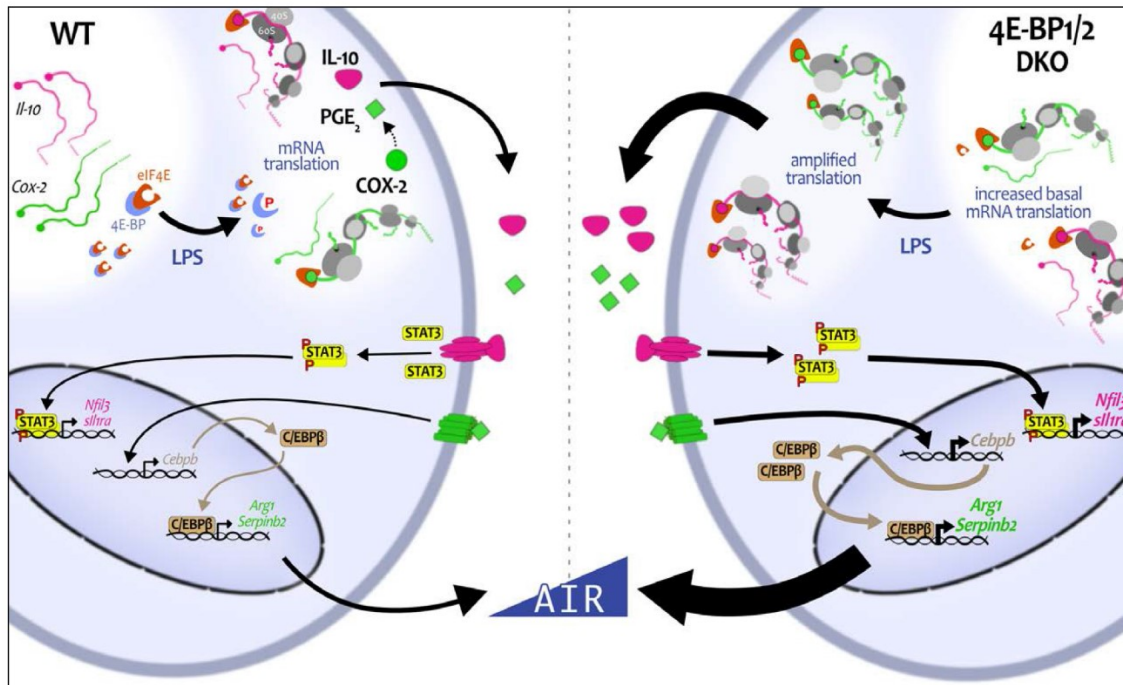
Figure 9. Proposed mechanism of 4E-BP1/2-mediated regulation of anti-inflammatory responses in macrophages. In WT macrophages, LPS stimulation induces *Il-10* and *Cox-2* mRNA translation, IL-10 production and COX-2-dependent PGE_2 synthesis. IL-10 signaling activates STAT3, which promotes *Nfil3* and s*Il1ra* transcription. PGE_2 signaling activates *C/ebpb* transcription and C/EBPβ-dependent *Arg1* and *Serpinb2* gene expression. In 4E-BP1/2 DKO macrophages, *Il-10* and *Cox-2* mRNA translational efficiency is augmented at basal level and is further enhanced upon LPS treatment. Amplification of IL-10-STAT3 and PGE_2-C/EBPβ signaling results in exacerbated anti-inflammatory gene expression.

4902   **Supplemental Table I.** List of primers used for RT-qPCR

Gene	Primer Sequence (5' - 3')
mouse *Arg1*	Forward 5' -GGTCTGTGGGGAAAGCCAAT-3'
	Reverse 5' -TGGTTGTCAGGGGAGTGTTG-3'
mouse *Cebpb*	Forward 5' -CGTTTCGGGACTTGATGCAATC-3'
	Reverse 5' -CAACAACCCCGCAGGAACAT-3'
mouse *Cox-2*	Forward 5' -TTGGAGGCGAAGTGGGTTTT-3'
	Reverse 5' -TGGCTGTTTTGGTAGGCTGT-3'
mouse *Gapdh*	Forward 5' -TTCTTGTGCAGTGCCAGCCTC-3'
	Reverse 5' -CAAATGGCAGCCCTGGTGAC-3'
mouse *Il-6*	Forward 5' -CAACGATGATGCACTTGCAGA-3'
	Reverse 5' -GGTACTCCAGAAGACCAGAGGA-3'
mouse *Il-10*	Forward 5' -AGTGGAGCAGGTGAAGAGTG-3'
	Reverse 5' -TCATCATGTATGCTTCTATGCAGT-3'
mouse *Il-10ra*	Forward 5' -CGTTTGCTCCCATTCCTCGT-3'
	Reverse 5' -GAAGGGCTTGGCAGTTCGTA-3'
mouse Il-10rb	Forward 5' -TTCTGGTGCCAGCTCTAGG-3'
	Reverse 5' -AGTCAGGTTCGTTTTGGGGAA-3'
mouse *Nfil3*	Forward 5' -AGCTCTTTTGTGGACGAGCA-3'
	Reverse 5' -CCTCTGACACATCGGAGAGC-3'
mouse *Nos2*	Forward 5' -GGACCCAGAGACAAGCCTAC-3'
	Reverse 5' -CAGAGTGAGCTGGTAGGTTCC-3'
mouse *Rpl19*	Forward 5' -GCTGCGGGAAAAAGAAGGTC-3'
	Reverse 5' -AGCTTCCTGATCTGCTGACG-3'
mouse *Serpinb2*	Forward 5' -GTTAGAAAGTGCAAACAAGCTG-3'
	Reverse 5' -GGATTTCACCTTTGGTTTGAG-3'
mouse *sil1ra*	Forward 5' -AAATCTGCTGGGGACCCTAC-3'
	Reverse 5' -TCCCAGATTCTGAAGGCTTG
mouse *Tlr4*	Forward 5' -TGGGAGGACAATCCTCTGGG
	Reverse 5' -CAGGTCCAAGTTGCCGTTTC
mouse *Tnf*	Forward 5' -ACTCCAGGCGGTGCCTATGA
	Reverse 5' -AGTGTGAGGGTCTGGGCCAT

4903

4904

4905 **Supplemental Table II. Immune-related mRNAs translationally controlled by 4E-BP1/2 in mouse**

4906 **macrophages**

4907

4908

Gene Symbol	4E-BP1/2 DKO vs. WT	
	Fold-change (log2)	FDR
Ccl5	4.42	0.001
Ccl12	1.37	0.136
Cd40	1.42	0.045
Cox-2	2.10	0.034
Cxcl10	3.79	0.002
Il1a	1.55	0.156
Il1b	2.54	0.029
Ifit2	1.28	0.064
Il10	1.24	0.072
Il12b	1.41	0.127
Mx1	0.91	0.156

4909
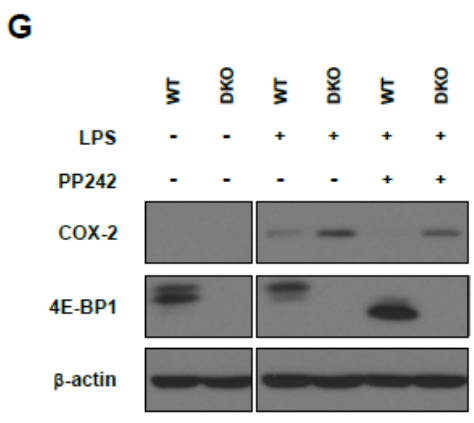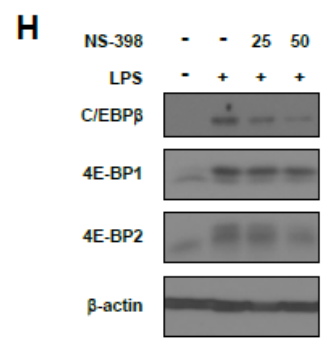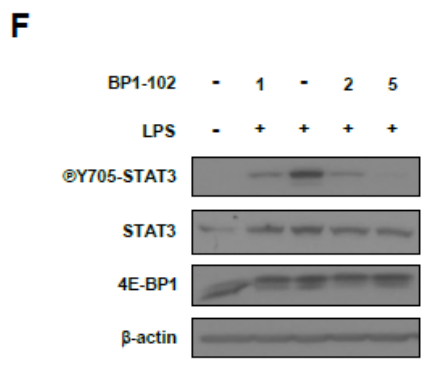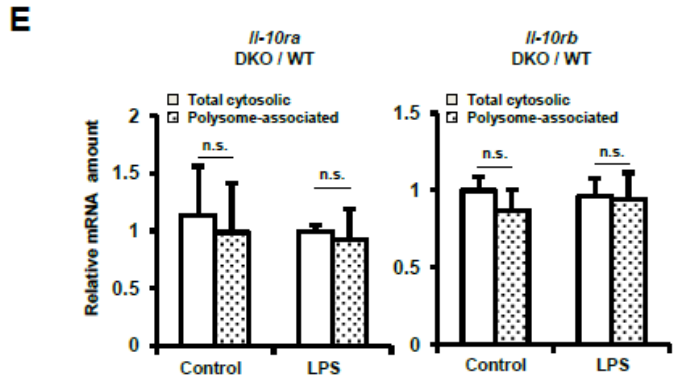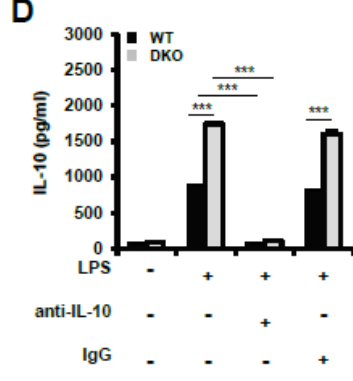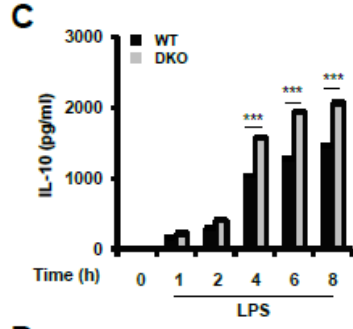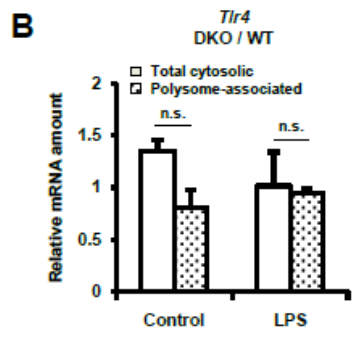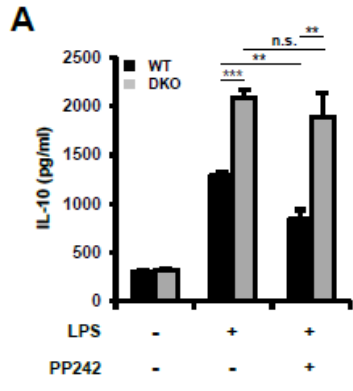
4915 **Supplemental Figure 1. The mTORC1-4E-BP1/2 axis contributes to regulate IL-10 and COX-2**
4916 **production in LPS-stimulated macrophages**. (**A**, **C-D**) IL-10 was quantified by ELISA in WT and 4E-
4917 BP1/2 DKO BMDM treated as follows: (**A**) LPS ± 2.5 µM PP242 for 6 h; (**C**) LPS for 1 - 8 h; (**D**) LPS ± 2
4918 mg/ml anti-IL-10 or isotype control for 6 h. (**B**, **E**) RT-qPCR of total cytosolic and heavy polysome-
4919 associated mRNA in WT and 4E-BP1/2 DKO cells (normalized to *Gapdh*). (**B**) *Tlr4* mRNA; (**E**) *Il10ra* and
4920 *Il10rb* mRNA. (**F-H**) Western blot analyses. (**F**) Phosphorylation status of STAT3 at Y705 in WT BMDM
4921 treated with LPS ± BP-1-102 (µM) for 4 h. (**G**) Total COX-2 protein levels in WT and DKO cells treated as
4922 indicated in A. (**H**) C/EBPβ protein expression in WT BMDM treated with LPS ± NS-398 (mM) for 4 h. (A-
4923 E) Experiments were carried out in independent duplicates, each consisting of a triplicate. Data are
4924 expressed as mean ± SD. (F-H) Data are representative of two independent biological replicates.
4925

References

4926

4927 1. Jackson, R. J., C. U. T. Hellen, and T. V. Pestova. 2010. The mechanism of eukaryotic translation

4928 initiation and principles of its regulation. *Nat Rev Mol Cell Biol* 11: 113-127.

4929 2. Siddiqui, N., and N. Sonenberg. 2015. Signalling to eIF4E in cancer. *Biochem Soc Trans* 43: 763-

4930 772.

4931 3. Gingras, A. C., B. Raught, S. P. Gygi, A. Niedzwiecka, M. Miron, S. K. Burley, R. D. Polakiewicz,

4932 A. Wyslouch-Cieszynska, R. Aebersold, and N. Sonenberg. 2001. Hierarchical phosphorylation of

4933 the translation inhibitor 4E-BP1. *Genes Dev* 15: 2852-2864.

4934 4. Tsukumo, Y., T. Alain, B. D. Fonseca, R. Nadon, and N. Sonenberg. 2016. Translation control

4935 during prolonged mTORC1 inhibition mediated by 4E-BP3. *Nat Commun* 7: 11776.

4936 5. Masvidal, L., L. Hulea, L. Furic, I. Topisirovic, and O. Larsson. 2017. mTOR-sensitive translation:

4937 Cleared fog reveals more trees. *RNA Biol*: 1-7.

4938 6. Colina, R., M. Costa-Mattioli, R. J. Dowling, M. Jaramillo, L. H. Tai, C. J. Breitbach, Y. Martineau,

4939 O. Larsson, L. Rong, Y. V. Svitkin, A. P. Makrigiannis, J. C. Bell, and N. Sonenberg. 2008.

4940 Translational control of the innate immune response through IRF-7. *Nature* 452: 323-328.

4941 7. Furic, L., L. Rong, O. Larsson, I. H. Koumakpayi, K. Yoshida, A. Brueschke, E. Petroulakis, N.

4942 Robichaud, M. Pollak, L. A. Gaboury, P. P. Pandolfi, F. Saad, and N. Sonenberg. 2010. eIF4E

4943 phosphorylation promotes tumorigenesis and is associated with prostate cancer progression. *Proc*

4944 *Natl Acad Sci U S A* 107: 14134-14139.

4945 8. Herdy, B., M. Jaramillo, Y. V. Svitkin, A. B. Rosenfeld, M. Kobayashi, D. Walsh, T. Alain, P. Sean,

4946 N. Robichaud, I. Topisirovic, L. Furic, R. J. Dowling, A. Sylvestre, L. Rong, R. Colina, M. Costa-

4947 Mattioli, J. H. Fritz, M. Olivier, E. Brown, I. Mohr, and N. Sonenberg. 2012. Translational control of

4948 the activation of transcription factor NF-kappaB and production of type I interferon by

4949 phosphorylation of the translation factor eIF4E. *Nat Immunol* 13: 543-550.

4950 9. Visvanathan, K. V., and S. Goodbourn. 1989. Double-stranded RNA activates binding of NF-kappa

4951 B to an inducible element in the human beta-interferon promoter. *EMBO J* 8: 1129-1138.

4952   10.   Honda, K., H. Yanai, H. Negishi, M. Asagiri, M. Sato, T. Mizutani, N. Shimada, Y. Ohba, A. Takaoka,

4953   N. Yoshida, and T. Taniguchi. 2005. IRF-7 is the master regulator of type-I interferon-dependent

4954   immune responses. *Nature* 434: 772-777.

4955   11.   Murray, P. J., and T. A. Wynn. 2011. Protective and pathogenic functions of macrophage subsets.

4956   *Nat Rev Immunol* 11: 723-737.

4957   12.   Kristensen, A. R., J. Gsponer, and L. J. Foster. 2013. Protein synthesis rate is the predominant

4958   regulator of protein expression during differentiation. *Mol Sys Biol* 9.

4959   13.   Su, X., Y. Yu, Y. Zhong, E. G. Giannopoulou, X. Hu, H. Liu, J. R. Cross, G. Ratsch, C. M. Rice, and

4960   L. B. Ivashkiv. 2015. Interferon-gamma regulates cellular metabolism and mRNA translation to

4961   potentiate macrophage activation. *Nat Immunol* 16: 838-849.

4962   14.   Xu, H., J. Zhu, S. Smith, J. Foldi, B. Zhao, A. Y. Chung, H. Outtz, J. Kitajewski, C. Shi, S. Weber,

4963   P. Saftig, Y. Li, K. Ozato, C. P. Blobel, L. B. Ivashkiv, and X. Hu. 2012. Notch-RBP-J signaling

4964   regulates the transcription factor IRF8 to promote inflammatory macrophage polarization. *Nat*

4965   *Immunol* 13: 642-650.

4966   15.   Liepelt, A., J. C. Mossanen, B. Denecke, F. Heymann, R. De Santis, F. Tacke, G. Marx, D. H.

4967   Ostareck, and A. Ostareck-Lederer. 2014. Translation control of TAK1 mRNA by hnRNP K

4968   modulates LPS-induced macrophage activation. *RNA* 20: 899-911.

4969   16.   Schott, J., S. Reitter, J. Philipp, K. Haneke, H. Schafer, and G. Stoecklin. 2014. Translational

4970   regulation of specific mRNAs controls feedback inhibition and survival during macrophage

4971   activation. *PLoS Genet* 10: e1004368.

4972   17.   Chan, C. S., A. Ming-Lum, G. B. Golds, S. J. Lee, R. J. Anderson, and A. L. Mui. 2012. Interleukin-

4973   10 inhibits lipopolysaccharide-induced tumor necrosis factor-alpha translation through a SHIP1-

4974   dependent pathway. *J Biol Chem* 287: 38020-38027.

4975   18.   Nehdi, A., P. Sean, I. Linares, R. Colina, M. Jaramillo, and T. Alain. 2014. Deficiency in either 4E-

4976   BP1 or 4E-BP2 augments innate antiviral immune responses. *PLoS ONE* 9: e114854.

4977   19.   Jaramillo, M., M. A. Gomez, O. Larsson, M. T. Shio, I. Topisirovic, I. Contreras, R. Luxenburg, A.

4978   Rosenfeld, R. Colina, R. W. McMaster, M. Olivier, M. Costa-Mattioli, and N. Sonenberg. 2011.

Leishmania repression of host translation through mTOR cleavage is required for parasite survival and infection. *Cell Host Microbe* 9: 331-341.

20. Leroux, L. P., D. Dasanayake, L. M. Rommereim, B. A. Fox, D. J. Bzik, A. Jardim, and F. S. Dzierszinski. 2015. Secreted *Toxoplasma gondii* molecules interfere with expression of MHC-II in interferon gamma-activated macrophages. *Int J Parasitol* 45: 319-332.

21. Larsson, O., M. Morita, I. Topisirovic, T. Alain, M. J. Blouin, M. Pollak, and N. Sonenberg. 2012. Distinct perturbation of the translatome by the antidiabetic drug metformin. *Proc Natl Acad Sci U S A* 109: 8977-8982.

22. Geiss, G. K., R. E. Bumgarner, B. Birditt, T. Dahl, N. Dowidar, D. L. Dunaway, H. P. Fell, S. Ferree, R. D. George, T. Grogan, J. J. James, M. Maysuria, J. D. Mitton, P. Oliveri, J. L. Osborn, T. Peng, A. L. Ratcliffe, P. J. Webster, E. H. Davidson, L. Hood, and K. Dimitrov. 2008. Direct multiplexed measurement of gene expression with color-coded probe pairs. *Nat Biotechnol* 26: 317-325.

23. Larsson, O., N. Sonenberg, and R. Nadon. 2010. Identification of differential translation in genome wide studies. *Proc Natl Acad Sci U S A* 107: 21487-21492.

24. Larsson, O., N. Sonenberg, and R. Nadon. 2011. anota: Analysis of differential translation in genome-wide studies. *Bioinformatics* 27: 1440-1441.

25. Lorenz, R., S. H. Bernhart, C. Honer Zu Siederdissen, H. Tafer, C. Flamm, P. F. Stadler, and I. L. Hofacker. 2011. ViennaRNA Package 2.0. *Algorithms Mol Biol: AMB* 6: 26.

26. Darty, K., A. Denise, and Y. Ponty. 2009. VARNA: Interactive drawing and editing of the RNA secondary structure. *Bioinformatics* 25: 1974-1975.

27. Taylor, S., M. Wakem, G. Dijkman, M. Alsarraj, and M. Nguyen. 2010. A practical approach to RT-qPCR-Publishing data that conform to the MIQE guidelines. *Methods* 50: S1-5.

28. Hammami, A., B. M. Abidin, T. Charpentier, A. Fabié, A.-P. Duguay, K. M. Heinonen, and S. Stäger. 2017. HIF-1α is a key regulator in potentiating suppressor activity and limiting the microbicidal capacity of MDSC-like cells during visceral leishmaniasis. *PLOS Pathog* 13: e1006616.

29. Daigle, F., J. E. Graham, and R. Curtiss, 3rd. 2001. Identification of Salmonella typhi genes expressed within macrophages by selective capture of transcribed sequences (SCOTS). *Mol Microbiol* 41: 1211-1222.

5007   30.   Piccirillo, C. A., E. Bjur, I. Topisirovic, N. Sonenberg, and O. Larsson. 2014. Translational control

5008   of immune responses: from transcripts to translatomes. *Nat Immunol* 15: 503-511.

5009   31.   Morita, M., S. P. Gravel, L. Hulea, O. Larsson, M. Pollak, J. St-Pierre, and I. Topisirovic. 2015.

5010   mTOR coordinates protein synthesis, mitochondrial activity and proliferation. *Cell Cycle* 14: 473-

5011   480.

5012   32.   Gandin, V., L. Masvidal, L. Hulea, S. P. Gravel, M. Cargnello, S. McLaughlan, Y. Cai, P.

5013   Balanathan, M. Morita, A. Rajakumar, L. Furic, M. Pollak, J. A. Porco, Jr., J. St-Pierre, J. Pelletier,

5014   O. Larsson, and I. Topisirovic. 2016. nanoCAGE reveals 5' UTR features that define specific modes

5015   of translation of functionally related MTOR-sensitive mRNAs. *Genome Res* 26: 636-648.

5016   33.   Eichelbaum, K., and J. Krijgsveld. 2014. Rapid temporal dynamics of transcription, protein

5017   synthesis, and secretion during macrophage activation. *Mol Cell Proteomics:*13: 792-810.

5018   34.   Weichhart, T., M. Haidinger, K. Katholnig, C. Kopecky, M. Poglitsch, C. Lassnig, M. Rosner, G. J.

5019   Zlabinger, M. Hengstschlager, M. Muller, W. H. Horl, and M. D. Saemann. 2011. Inhibition of mTOR

5020   blocks the anti-inflammatory effects of glucocorticoids in myeloid immune cells. *Blood* 117: 4273-

5021   4283.

5022   35.   Saraiva, M., and A. O'Garra. 2010. The regulation of IL-10 production by immune cells. *Nat Rev*

5023   *Immunol* 10: 170-181.

5024   36.   Hutchins, A. P., S. Poulain, and D. Miranda-Saavedra. 2012. Genome-wide analysis of STAT3

5025   binding in vivo predicts effectors of the anti-inflammatory response in macrophages. *Blood* 119:

5026   e110-e119.

5027   37.   Carl, V. S., J. K. Gautam, L. D. Comeau, and M. F. Smith, Jr. 2004. Role of endogenous IL-10 in

5028   LPS-induced STAT3 activation and IL-1 receptor antagonist gene expression. *J Leukoc Biol* 76:

5029   735-742.

5030   38.   Hutchins, A. P., D. Diez, and D. Miranda-Saavedra. 2013. The IL-10/STAT3-mediated anti-

5031   inflammatory response: recent developments and future challenges. *Brief Funct Genomics* 12: 489-

5032   498.

5033   39.   Kobayashi, T., K. Matsuoka, S. Z. Sheikh, H. Z. Elloumi, N. Kamada, T. Hisamatsu, J. J. Hansen,

5034   K. R. Doty, S. D. Pope, S. T. Smale, T. Hibi, P. B. Rothman, M. Kashiwada, and S. E. Plevy. 2011.

5035 NFIL3 is a regulator of IL-12 p40 in macrophages and mucosal immunity. *J Immunol* 186: 4649-

5036 4655.

5037 40. Hannum, C. H., C. J. Wilcox, W. P. Arend, F. G. Joslin, D. J. Dripps, P. L. Heimdal, L. G. Armes,

5038 A. Sommer, S. P. Eisenberg, and R. C. Thompson. 1990. Interleukin-1 receptor antagonist activity

5039 of a human interleukin-1 inhibitor. *Nature* 343: 336-340.

5040 41. Zhang, X., P. Yue, B. D. Page, T. Li, W. Zhao, A. T. Namanja, D. Paladino, J. Zhao, Y. Chen, P. T.

5041 Gunning, and J. Turkson. 2012. Orally bioavailable small-molecule inhibitor of transcription factor

5042 Stat3 regresses human breast and lung cancer xenografts. *Proc Natl Acad Sci U S A* 109: 9623-

5043 9628.

5044 42. Na, Y. R., D. Jung, B. R. Yoon, W. W. Lee, and S. H. Seok. 2015. Endogenous prostaglandin E2

5045 potentiates anti-inflammatory phenotype of macrophage through the CREB-C/EBP-beta cascade.

5046 *Eur J Immunol* 45: 2661-2671.

5047 43. Futaki, N., S. Takahashi, M. Yokoyama, I. Arai, S. Higuchi, and S. Otomo. 1994. NS-398, a new

5048 anti-inflammatory agent, selectively inhibits prostaglandin G/H synthase/cyclooxygenase (COX-2)

5049 activity in vitro. *Prostaglandins* 47: 55-59.

5050 44. Ruffell, D., F. Mourkioti, A. Gambardella, P. Kirstetter, R. G. Lopez, N. Rosenthal, and C. Nerlov.

5051 2009. A CREB-C/EBPbeta cascade induces M2 macrophage-specific gene expression and

5052 promotes muscle injury repair. *Proc Natl Acad Sci U S A* 106: 17475-17480.

5053 45. Albina, J. E., E. J. Mahoney, J. M. Daley, D. E. Wesche, S. M. Morris, Jr., and J. S. Reichner. 2005.

5054 Macrophage arginase regulation by CCAAT/enhancer-binding protein beta. *Shock* 23: 168-172.

5055 46. Udofa, E. A., B. W. Stringer, P. Gade, D. Mahony, M. S. Buzza, D. V. Kalvakolanu, and T. M.

5056 Antalis. 2013. The transcription factor C/EBP-beta mediates constitutive and LPS-inducible

5057 transcription of murine SerpinB2. *PloS ONE* 8: e57855.

5058 47. Pesce, J. T., T. R. Ramalingam, M. M. Mentink-Kane, M. S. Wilson, K. C. El Kasmi, A. M. Smith,

5059 R. W. Thompson, A. W. Cheever, P. J. Murray, and T. A. Wynn. 2009. Arginase-1-expressing

5060 macrophages suppress Th2 cytokine-driven inflammation and fibrosis. *PLoS Pathog* 5: e1000371.

5061   48.   Schroder, W. A., T. T. Le, L. Major, S. Street, J. Gardner, E. Lambley, K. Markey, K. P. MacDonald,

5062   R. J. Fish, R. Thomas, and A. Suhrbier. 2010. A physiological function of inflammation-associated

5063   SerpinB2 is regulation of adaptive immunity. *J Immunol* 184: 2663-2670.

5064   49.   Lang, R., D. Patel, J. J. Morris, R. L. Rutschman, and P. J. Murray. 2002. Shaping Gene Expression

5065   in Activated and Resting Primary Macrophages by IL-10. *J Immunol* 169: 2253-2263.

5066   50.   Agard, M., S. Asakrah, and L. A. Morici. 2013. PGE(2) suppression of innate immunity during

5067   mucosal bacterial infection. *Front Cell Infect Microbiol* 3: 45.

5068   51.   Strassmann, G., V. Patil-Koota, F. Finkelman, M. Fong, and T. Kambayashi. 1994. Evidence for

5069   the involvement of interleukin 10 in the differential deactivation of murine peritoneal macrophages

5070   by prostaglandin E2. *J Exp Med* 180: 2365-2370.

5071   52.   Kim, Y. Y., L. Von Weymarn, O. Larsson, D. Fan, J. M. Underwood, M. S. Peterson, S. S. Hecht,

5072   V. A. Polunovsky, and P. B. Bitterman. 2009. Eukaryotic Initiation Factor 4E Binding Protein Family

5073   of Proteins: Sentinels at a Translational Control Checkpoint in Lung Tumor Defense. *Cancer Res*

5074   69: 8455-8462.

5075   53.   Dowling, R. J., I. Topisirovic, T. Alain, M. Bidinosti, B. D. Fonseca, E. Petroulakis, X. Wang, O.

5076   Larsson, A. Selvaraj, Y. Liu, S. C. Kozma, G. Thomas, and N. Sonenberg. 2010. mTORC1-

5077   mediated cell proliferation, but not cell growth, controlled by the 4E-BPs. *Science* 328: 1172-1176.

5078   54.   Morita, M., S. P. Gravel, V. Chenard, K. Sikstrom, L. Zheng, T. Alain, V. Gandin, D. Avizonis, M.

5079   Arguello, C. Zakaria, S. McLaughlan, Y. Nouet, A. Pause, M. Pollak, E. Gottlieb, O. Larsson, J. St-

5080   Pierre, I. Topisirovic, and N. Sonenberg. 2013. mTORC1 controls mitochondrial activity and

5081   biogenesis through 4E-BP-dependent translational regulation. *Cell Metab* 18: 698-711.

5082   55.   Gkogkas, C. G., A. Khoutorsky, I. Ran, E. Rampakakis, T. Nevarko, D. B. Weatherill, C. Vasuta, S.

5083   Yee, M. Truitt, P. Dallaire, F. Major, P. Lasko, D. Ruggero, K. Nader, J. C. Lacaille, and N.

5084   Sonenberg. 2013. Autism-related deficits via dysregulated eIF4E-dependent translational control.

5085   *Nature* 493: 371-377.

5086   56.   Morita, M., J. Prudent, K. Basu, V. Goyon, S. Katsumura, L. Hulea, D. Pearl, N. Siddiqui, S. Strack,

5087   S. McGuirk, J. St-Pierre, O. Larsson, I. Topisirovic, H. Vali, H. M. McBride, J. J. Bergeron, and N.

194

5088	Sonenberg. 2017. mTOR Controls Mitochondrial Dynamics and Cell Survival via MTFP1. *Molecular*

5089	*Cell* 67: 922-935

5090	57.	Miloslavski, R., E. Cohen, A. Avraham, Y. Iluz, Z. Hayouka, J. Kasir, R. Mudhasani, S. N. Jones,

5091	N. Cybulski, M. A. Ruegg, O. Larsson, V. Gandin, A. Rajakumar, I. Topisirovic, and O. Meyuhas.

5092	2014. Oxygen sufficiency controls TOP mRNA translation via the TSC-Rheb-mTOR pathway in a

5093	4E-BP-independent manner. *J Mol Cell Biol* 6: 255-266.

5094	58.	Yi, W., S. Gupta, E. Ricker, M. Manni, R. Jessberger, Y. Chinenov, H. Molina, and A. B. Pernis.

5095	2017. The mTORC1-4E-BP-eIF4E axis controls de novo Bcl6 protein synthesis in T cells and

5096	systemic autoimmunity. *Nat Commun* 8: 254.

5097	59.	Alain, T., M. Morita, B. D. Fonseca, A. Yanagiya, N. Siddiqui, M. Bhat, D. Zammit, V. Marcus, P.

5098	Metrakos, L.-A. Voyer, V. Gandin, Y. Liu, I. Topisirovic, and N. Sonenberg. 2012. eIF4E/4E-BP

5099	Ratio Predicts the Efficacy of mTOR Targeted Therapies. *Cancer Res* 72: 6468-6476.

5100	60.	Koromilas, A. E., A. Lazaris-Karatzas, and N. Sonenberg. 1992. mRNAs containing extensive

5101	secondary structure in their 5' non-coding region translate efficiently in cells overexpressing

5102	initiation factor eIF4E. *EMBO J* 11: 4153-4158.

5103	61.	Hinnebusch, A. G., I. P. Ivanov, and N. Sonenberg. 2016. Translational control by 5'-untranslated

5104	regions of eukaryotic mRNAs. *Science* 352: 1413-1416.

5105	62.	Svitkin, Y. V., A. Pause, A. Haghighat, S. Pyronnet, G. Witherell, G. J. Belsham, and N. Sonenberg.

5106	2001. The requirement for eukaryotic initiation factor 4A (eIF4A) in translation is in direct proportion

5107	to the degree of mRNA 5' secondary structure. *RNA* 7: 382-394.

5108	63.	Feoktistova, K., E. Tuvshintogs, A. Do, and C. S. Fraser. 2013. Human eIF4E promotes mRNA

5109	restructuring by stimulating eIF4A helicase activity. *Proc Natl Acad Sci U S A* 110: 13339-13344.

5110	64.	Sinvani, H., O. Haimov, Y. Svitkin, N. Sonenberg, A. Tamarkin-Ben-Harush, B. Viollet, and R.

5111	Dikstein. 2015. Translational tolerance of mitochondrial genes to metabolic energy stress involves

5112	TISU and eIF1-eIF4GI cooperation in start codon selection. *Cell Metab* 21: 479-492.

5113	65.	Powell, M. J., S. A. J. Thompson, Y. Tone, H. Waldmann, and M. Tone. 2000. Posttranscriptional

5114	Regulation of IL-10 Gene Expression Through Sequences in the 3′-Untranslated Region. *J*

5115	*Immunol* 165: 292-296.

5116   66.   Mao, Y., V. van Hoef, X. Zhang, E. Wennerberg, J. Lorent, K. Witt, L. Masvidal, S. Liang, S. Murray,

5117   O. Larsson, R. Kiessling, and A. Lundqvist. 2016. IL-15 activates mTOR and primes stress-

5118   activated gene expression leading to prolonged antitumor capacity of NK cells. *Blood* 128: 1475-

5119   1489.

5120   67.   Anderson, P. 2010. Post-transcriptional regulons coordinate the initiation and resolution of

5121   inflammation. *Nat Rev Immunol* 10: 24-35.

5122   68.   Mazumder, B., X. Li, and S. Barik. 2010. Translation control: a multifaceted regulator of

5123   inflammatory response. *J Immunol* 184: 3311-3319.

5124   69.   Nemeth, Z. H., C. S. Lutz, B. Csoka, E. A. Deitch, S. J. Leibovich, W. C. Gause, M. Tone, P. Pacher,

5125   E. S. Vizi, and G. Hasko. 2005. Adenosine augments IL-10 production by macrophages through

5126   an A2B receptor-mediated posttranscriptional mechanism. *J Immunol* 175: 8260-8270.

5127   70.   Dixon, D. A., G. C. Balch, N. Kedersha, P. Anderson, G. A. Zimmerman, R. D. Beauchamp, and S.

5128   M. Prescott. 2003. Regulation of cyclooxygenase-2 expression by the translational silencer TIA-1.

5129   *J Exp Med* 198: 475-481.

5130   71.   Fernandez, N., A. Gonzalez, I. Valera, S. Alonso, and M. S. Crespo. 2007. Mannan and

5131   peptidoglycan induce COX-2 protein in human PMN via the mammalian target of rapamycin. *Eur J*

5132   *Immunol* 37: 2572-2582.

5133   72.   Mohr, I., and N. Sonenberg. 2012. Host translation at the nexus of infection and immunity. *Cell*

5134   *Host Miicrobe* 12: 470-483.

5135

5136

Footnotes

Abbreviations

BMDM, bone marrow-derived macrophage; COX-2, cyclooxygenase-2; DKO, double knockout; eIF, eukaryotic translation initiation factor; 4E-BP, eIF4E binding protein; MFE, minimum free energy; mTOR, mechanistic target of rapamycin; mTORC1, mTOR complex 1; NFIL-3, nuclear factor interleukin-3 regulated; nt, nucleotide; PGE_2, prostaglandin E_2; sIL-1Ra, secreted interleukin-1 receptor antagonist; TISU, Translation Initiator of Short 5' UTR; UTR, untranslated region; WT, wild-type.

Author Contributions

Conceived and designed experiments: MW, L-PL, OL and MJ; performed experiments: MW, L-PL, VC, M-NM'B and TC; contributed new technology/analytic tools: TEG, CD, SS, TA, LCvK and OL; analyzed data: MW, L-PL, VC, JL, TEG, TC, AF, CD, SS, TA, LCvK, OL and MJ; wrote the manuscript: L-PL, OL and MJ.

Appendix 2

Translational repression of *Ccl5* and *Cxcl10* by 4E-BP1 and 4E-BP2 restrains the ability of macrophages to induce migration of activated T cells

Mirtha William[*,1], Louis-Philippe Leroux[*,1,2], Visnu Chaparro[*], Tyson E. Graber[†], Tommy Alain[†] and Maritza Jaramillo[*,2]

[*]INRS - Institut Armand-Frappier, Laval, QC, Canada; [†]Children's Hospital of Eastern Ontario Research Institute, Department of Biochemistry, Microbiology and Immunology, University of Ottawa, Ottawa, ON, Canada

[1]Equal contribution

[2]To whom correspondence should be addressed: Maritza Jaramillo and Louis-Philippe Leroux, INRS - Institut Armand-Frappier, 531 boulevard des Prairies, Laval, QC, Canada H7V 1B7; Phone number (1) 450-687-5010; Fax number (1) 450-686-5389; E-mail: maritza.jaramillo@iaf.inrs.ca or Louis-Philippe.Leroux@iaf.inrs.ca

Short Title: Translational control of *Ccl5* and *Cxcl10* mRNAs in macrophages

Keywords: macrophages, chemokines, mRNA translation, 4E-BP, mTOR

Abbreviations: BMDM, bone marrow-derived macrophage; DKO, double knockout; 4E-BP, eIF4E binding protein; eIF4F, eukaryotic translation initiation factor 4F; FDR, false discovery rate; IP-10, IFN-gamma-induced protein 10; KI, knock-in; LCCM, L929 fibroblast-conditioned culture medium; MEF, mouse embryonic fibroblast; MFE, minimum free energy; MNK, MAP kinase interacting serine/threonine kinase; mTOR, mechanistic target of rapamycin; mTORC1, mTOR complex 1; RT-qPCR, real-time quantitative PCR; UTR, untranslated region; WT, wild-type.

5189   **Abstract**

5190   Signaling through the mechanistic target of rapamycin complex 1 (mTORC1) is a major regulatory

5191   node of pro-inflammatory mediator production by macrophages. However, it is still unclear whether such

5192   regulation relies on selective translational control by two of the main mTORC1 effectors, the eIF4E-binding

5193   proteins 1 and 2 (4E-BP1/2). By comparing translational efficiencies of immune-related transcripts of wild-

5194   type (WT) and 4E-BP1/2 double-knockout (DKO) macrophages, we found that translation of mRNAs

5195   encoding the pro-inflammatory chemokines CCL5 and CXCL10 is controlled by 4E-BP1/2. Macrophages

5196   deficient in 4E-BP1/2 produced higher levels of CCL5 and CXCL10 upon LPS stimulation, which enhanced

5197   chemoattraction of activated T cells. Consistent with this, treatment of WT cells with mTORC1 inhibitors

5198   promoted the activation of 4E-BP1/2 and reduced CCL5 and CXCL10 secretion. In contrast, the

5199   phosphorylation status of eIF4E did not affect the synthesis of these chemokines since macrophages

5200   derived from mice harboring a non-phosphorylatable form of the protein produced similar levels of CCL5

5201   and CXCL10 to WT counterparts. These data provide evidence that the mTORC1-4E-BP1/2 axis

5202   contributes to regulate the production of chemoattractants by macrophages by limiting translation efficiency

5203   of *Ccl5* and *Cxcl10* mRNAs, and suggest that 4E-BP1/2 act as immunological safeguards by fine-tuning

5204   inflammatory responses in macrophages.

5205

Introduction

5206

5207	The inflammatory chemokines CCL5 and CXCL10 are major regulators of a variety of cellular

5208	processes including leukocyte migration, glucose metabolism, proliferation, cell growth, and apoptosis [1-

5209	3]. CCL5/RANTES is mainly produced by CD8$^+$ T cells, macrophages, platelets, fibroblasts, epithelial cells,

5210	and some types of tumor cells [3]. CCL5 activates the surface receptors CCR1, CCR2, CCR3, and CCR5

5211	present on T cells, monocytes, dendritic cells, NK cells, mast cells, eosinophils, and basophils [1].

5212	Moreover, CCL5 is one of the highest affinity ligands for the atypical chemokine receptor 1 (ACKR1) [4],

5213	which in addition to erythrocytes is constitutively expressed by venular endothelial cells and a subset of

5214	neurons [5, 6]. Similarly, CCL5 interacts with ACKR2 expressed on dendritic cells, B cells, and other

5215	leukocytes [5]. CXCL10/IFN-γ-induced protein 10 kDa (IP-10) is primarily secreted by monocytes,

5216	macrophages, neutrophils, eosinophils, fibroblasts, and endothelial cells [2]. CXCL10 specifically binds to

5217	CXCR3, which is predominantly expressed on activated T and B cells, natural killer cells, dendritic cells and

5218	macrophages [2]. Of note, these different chemokine receptors are promiscuous as they bind to several

5219	chemokines other than CCL5 and CXCL10 [5].

5220	In eukaryotes, translational control (i.e., regulation of mRNA translation efficiency) occurs mainly

5221	at the initiation step [7]. This process is largely dependent on the recruitment of the ribosome to the mRNA

5222	via the eukaryotic translation initiation factor 4F (eIF4F), a heterotrimeric complex formed by the m^{7}G-cap-

5223	binding subunit, eIF4E; the scaffold protein, eIF4G; and the RNA helicase, eIF4A [8]. The mechanistic

5224	target of rapamycin (mTOR) complex 1 (mTORC1) promotes the assembly of the eIF4F complex by

5225	inactivating the translational repressors eIF4E-binding proteins (4E-BPs) [9]. In addition, the activity of

5226	eIF4E is increased through direct phosphorylation at S209 by the MAP kinase interacting serine/threonine

5227	kinases 1 and 2 (MNK1/2) [10]. Consistent with the pivotal role of mTORC1 and MNK1/2 in translational

5228	control of immune responses (reviewed in [11]), emerging evidence points to their involvement in the

5229	regulation of CCL5 and CXCL10 protein synthesis [12-17]. Indeed, the use of rapamycin, an allosteric

5230	inhibitor of mTOR, blocks CCL5 secretion under pro-inflammatory conditions *in vitro* and *in vivo* [12, 13].

5231	Moreover, silencing of MNK1 reduces CCL5 and CXCL10 protein expression in response to TNF in smooth

5232	muscle cells [14]. Similarly, studies using mouse embryonic fibroblasts (MEFs) deficient in upstream

5233	regulators (Akt1/2) or downstream effectors (4E-BP1 or S6K1/2) of mTORC1 established a crucial role for

5234	this pathway in the induction of CXCL10 by IFN-γ [15-17]. However, none of these reports provided

5235	conclusive data demonstrating that *Ccl5* and *Cxcl10* mRNAs are direct targets of translational control via

5236	mTORC1 or MNK1/2 signaling. Of note, most of these works were carried out in nonimmune cells and

5237	therefore, they might not reflect the full scope of the molecular mechanisms that govern CCL5 and CXCL10

5238	protein synthesis during immune responses.

5239	Elevated CCL5 and CXCL10 production is a hallmark of inflammatory macrophages [18], and has

5240	been linked to either protective effects or negative outcomes in a wide range of pathological conditions,

5241	including infections, cancer, and immune-mediated disorders [2, 18-21]. It is well documented that selective

5242	changes in mRNA translation via mTORC1 and MNK1/2 signaling contribute to shape pro-and anti-

201

5243   inflammatory responses in macrophages [22, 23]. Notably, the translational repressors 4E-BP1/2 control

5244   macrophage type I IFN-dependent antiparasitic activity and LPS-inducible anti-inflammatory mediator

5245   production [24, 25]. Herein, we report that 4E-BP1/2 limit translation efficiency of mRNAs encoding the

5246   potent pro-inflammatory chemokines CCL5 and CXCL10 in macrophages and thereby hinder their ability

5247   to induce the migration of activated T cells.

5248

5249

Results

The mTORC1-4E-BP1/2 axis regulates LPS-induced translation initiation and CCL5 and CXCL10 production in macrophages

Signaling through mTORC1 regulates the production of numerous immune-related factors in myeloid cells [26], including the chemokine CCL5 [12]. However, it remains to be established whether such regulation is, at least in part, dependent on translational control via the mTORC1-4E-BP1/2 axis. To begin addressing this issue, we monitored the phosphorylation status of 4E-BP1 and 4E-BP2 in BMDM treated or not with canonical mTOR inhibitors prior to stimulation with *E. coli* LPS, a strong mTOR activator [26] and a potent inducer of CCL5 and CXCL10 production in macrophages [12, 27]. Exposure to LPS markedly increased the phosphorylation of 4E-BP1 at all four residues (T37/46, T70, and S65), as observed using phospho-specific antibodies, and by the predominance of the hyperphosphorylated gamma (γ) form over the beta (β, partially phosphorylated) and the alpha (α; hypophosphorylated) forms (**Fig. 1A**). LPS also augmented the phosphorylation of 4E-BP2, as evidenced by an upward shift in the migration pattern of the protein. In contrast, when cell lysates were treated with lambda (λ) phosphatase, only the hypophosphorylated forms of 4E-BP1 and 4E-BP2 (4E-BP1/2) were detected and the phosphorylation of 4E-BP1 at T37/46 was abrogated (**Supplemental Fig. 1A**). These data indicate that changes in the migration patterns of 4E-BP1/2 in LPS-stimulated BMDM are due to an increase in phosphorylation but not in protein expression. The phosphorylation of 4E-BP1 in LPS-treated and unstimulated cells was partially resistant to rapamycin but highly sensitive to active-site mTOR inhibitors (asTORi) PP242 and Torin-1 (**Fig. 1A**), as previously reported [28]. However, phosphorylation of 4E-BP2 appeared to be more sensitive than 4E-BP1 to rapamycin treatment as revealed by a downward band shift (corresponding to the hypophosphorylated form) (**Fig. 1A**). Consistent with this, rapamycin led to a greater binding of 4E-BP2 to m⁷GTP-bound eIF4E as compared to 4E-BP1 in LPS-stimulated BMDM (**Fig. 1B**). As expected, asTORi treatment led to a substantial increase in the binding of both 4E-BP1 and 4E-BP2 to eIF4E (**Fig. 1B**). Accordingly, eIF4G binding to eIF4E was abolished in the presence of PP242 or Torin-1. Although much less potent than asTORi, rapamycin also augmented 4E-BP1:eIF4E interaction, and reduced the amount of eIF4G bound to eIF4E. Consistent with our western blot and cap-pull down experiments, polysome tracings revealed that translation initiation in LPS-stimulated BMDM was down-regulated in the presence of rapamycin, and was disrupted by PP242 (**Figs. 1C-D**). Thus, LPS-inducible mTORC1 activity, eIF4F complex formation, and mRNA translation are hindered by mTOR inhibitors in macrophages.

To gain insight into the requirement of the mTORC1-4E-BP1/2 axis for CCL5 and CXCL10 production, we measured cytokine secretion by ELISA in the culture supernatant of cells treated with different mTOR inhibitors at the concentrations that blocked mTORC1 activity and translation initiation in BMDM. Neither CCL5 nor CXCL10 were detected in cultures that were not stimulated with LPS regardless of the presence of the inhibitors (**Figs. 1E-F**). Pre-treatment with rapamycin caused a moderate reduction of LPS-induced CCL5 production compared to levels measured in DMSO-treated cultures but had a greater inhibitory effect on CXCL10 (**Figs. 1E-F**). Exposure to asTORi led to a significant down-regulation of

5287   chemokine secretion. Of note, differential repression of CCL5 and CXCL10 production by rapamycin and

5288   asTORi reflected the greater potency of the latter to activate 4E-BP1/2 (**Figs. 1A-B**), as previously reported

5289   [28]. Importantly, reduced chemokine levels could not be attributed to potential toxic effects of the inhibitors,

5290   as indicated by cell viability assays (**Supplemental Fig. 1B**). Taken together, these data suggest that

5291   mTORC1 activity is required for LPS-mediated CCL5 and CXCL10 protein synthesis in macrophages.

5292

5293   **4E-BP1/2 dampen translational efficiency of *Ccl5* and *Cxcl10* mRNAs**

5294   The mTORC1-4E-BP1/2 axis contributes to coordinate efficient immune responses [11, 24, 29, 30],

5295   yet selective 4E-BP1/2-dependent translational control of macrophage functions remains incompletely

5296   defined. Polysome profiling of WT and 4E-BP1/2 DKO BMDM quantified by nCounter® assays (mouse

5297   immunology panel) (**Fig. 2A**) allowed us to identify several immune-related mRNAs whose translational

5298   efficiency is under the control of 4E-BP1/2 [25]. Of note, the top two transcripts identified in our screening

5299   were those encoding CCL5 and CXCL10. Target identification was achieved using the anota algorithm,

5300   which specifically captures differences in translational efficiency of individual transcripts independent of

5301   changes in total mRNA levels [31]. Indeed, the graphical representation of anota analysis showed that *Ccl5*

5302   (top panel) and *Cxcl10* (bottom panel) mRNAs were more abundant in polysome-associated mRNA pools

5303   in 4E-BP1/2 DKO than in WT BMDM (**Fig. 2B**). These differences were not attributable to changes in

5304   transcription since total cytosolic mRNA levels were similar between genotypes. In **Fig. 2B**, each biological

5305   replicate (i.e., independent experiment) is denoted by an "X", while the lines correspond to regressions

5306   used by anota to adjust changes in polysome-associated mRNA levels (*y*-axis) for changes in total cytosolic

5307   mRNA levels (*x*-axis). A difference in intercepts of the regression lines on the *y*-axis (i.e., when total

5308   cytosolic mRNA is set to 0) indicates changes in translational efficiency (when there is no change in

5309   translational efficiency, there is no difference in intercept). Thus, translational efficiency of *Ccl5* and *Cxcl10*

5310   mRNAs is regulated by 4E-BP1/2 in macrophages.

5311   The length and structure of 5' UTR has been linked to selective translational control through the

5312   mTORC1-4E-BP1/2-eIF4E axis [32]. Bioinformatic analysis of transcripts regulated via 4E-BP1/2 in

5313   macrophages indicated that *Ccl5* and *Cxcl10* fall into the category of those that harbor relatively short 5'

5314   UTRs (57 and 75 nt, respectively) with a minimum free energy (MFE) of -17.8 and -16.2 kcal/mol,

5315   respectively (**Supplemental Fig. 2**). Interestingly, *Ccl5* and *Cxcl10* share these features with *Il1a*, *Il1b*, *Il10*,

5316   *Il12b*, *Ccl12*, and *Cd40* [25]. These similarities suggest a common mechanism of 4E-BP1/2-dependent

5317   selective translational control of immune-related mRNAs in macrophages.

5318

5319   **LPS favors *Ccl5* and *Cxcl10* mRNA translation by limiting the activity of 4E-BP1/2**

5320   To validate the data obtained from the nCounter® analysis and to further delineate changes in

5321   translational efficiency of *Ccl5* and *Cxcl10* mRNA, we fractionated RNA from WT and 4E-BP1/2 DKO

5322   macrophages both at steady-state and following LPS stimulation by polysome-profiling (**Fig. 3A**).

5323   Subpolysomal (untranslated or poorly translated), and light (2-3 ribosomes; efficiently translated) and heavy

204

polysome (≥ 4 ribosomes; highly efficiently translated) fractions were pooled and RT-qPCR analyses were performed to measure mRNA distribution of *Ccl5* and *Cxcl10*. In steady-state WT cells, the highest amount of *Ccl5* mRNA was found in subpolysomal fractions while the remainder was detected at near equal amounts in light and heavy polysomes. In stark contrast, distribution of *Ccl5* was skewed towards light and heavy polysomes in 4E-BP1/2 DKO macrophages (**Fig. 3B**, top left panel). Exposure to LPS caused a substantial shift in the distribution of *Ccl5* mRNA from subpolysomal to light polysome fractions in WT cells. Conversely, no major changes were observed in LPS-treated cells compared to unstimulated 4E-BP1/2 DKO BMDM (**Fig. 3B**, top right panel). A similar trend was observed for *Cxcl10* mRNA distribution across polysome profiles. Subpolysomal fractions contained the greatest amount of *Cxcl10* mRNA in resting WT cells, while it was evenly distributed in 4E-BP1/2 DKO macrophages (**Fig. 3B**, middle left panel). Upon LPS treatment, light polysome fractions were enriched for *Cxcl10* mRNA in WT BMDM, yet no such changes were detected in 4E-BP1/2 DKO cells (**Fig. 3B**, middle right panel). In contrast to *Ccl5* and *Cxcl10*, *Gapdh* mRNA was mostly present in heavy polysome fractions regardless of genotype and activation status of the cells (**Fig. 3B**, bottom panels). Importantly, no significant differences were observed in total levels of *Ccl5* and *Cxcl10* mRNA between genotypes (**Figs. 3C-D**).These data, along with our previous observations regarding *Il-10* and *Cox-2/Ptgs2* [25], support the notion that LPS enhances translation efficiency of specific immune transcripts, including *Ccl5* and *Cxcl10*, by limiting the activity of 4E-BP1/2.

In line with increased translational efficiency of *Ccl5* and *Cxcl10* mRNAs in the absence of 4E-BP1/2 (i.e., higher levels of heavy polysome-associated mRNA), a significant up-regulation in CCL5 and CXCL10 secretion was observed in LPS-stimulated 4E-BP1/2 DKO BMDM as compared to WT counterparts (**Figs. 4A-B**). In addition to the modulation of 4E-BP1/2 activity, eIF4E-dependent translational control of select immune-related mRNAs occurs via the MNK1/2-eIF4E axis [22, 23, 33, 34]. Of note, inhibition of MNK1/2 signaling has been linked to a reduction in CCL5 and CXCL10 production [14]. Surprisingly, BMDM derived from mice mutated at the residue where eIF4E is phosphorylated (i.e., eIF4E S209A knock-in (KI)) [33] secreted similar levels of CCL5 and CXCL10 to their WT counterparts in response to LPS stimulation (**Figs. 4C-D).** This set of experiments provides evidence that LPS promotes *Ccl5* and *Cxcl10* mRNA translation in macrophages via mTORC1-4E-BP1/2-dependent and MNK1/2-eIF4E-independent mechanisms.

4E-BP1/2 control the production of CCL5- and CXCL10 by macrophages and limit their ability to attract activated T cells.

CCL5 and CXCL10 are potent chemoattractants and activators of CCR5$^+$ and CXCR3$^+$ T lymphocytes, respectively [2, 3]. Therefore, we hypothesized that elevated CCL5 and CXCL10 secretion by 4E-BP1/2 DKO BMDM would enhance their ability to favor the migration of activated T cells. Initially, we isolated murine splenic T cells (**Supplemental Fig. 3A)** and activated them *in vitro* with Concanavalin A (Con A) to induce the expression of CXCR3 and CCR5. Flow cytometric analysis determined that a large proportion of activated T lymphocytes were either CCR5$^+$ or CXCR3$^+$CCR5$^+$ (**Fig. 5A**, **Supplemental Fig.**

205

5361   **3B**). Activated T cells were then used as target cells in chemotaxis assays performed in the presence of

5362   conditioned medium (CM) from steady-state and LPS-treated WT and 4E-BP1/2 DKO BMDM (**Fig. 5B**).

5363   Greater numbers of activated T cells migrated towards CM from LPS-treated 4E-BP1/2 DKO cells

5364   compared to CM from WT macrophages (**Fig. 5C**). Moreover, incubation of CM with neutralizing antibodies

5365   against CCL5 and CXCL10 prior to chemotaxis assays impaired migration of T cells exposed to CM from

5366   LPS-stimulated WT and 4E-BP1/2 DKO BMDM. Conversely, no negative effect on T cell chemotaxis was

5367   detected following incubation of CM with isotype-matched control antibodies (**Fig. 5C**). Collectively our data

5368   indicate that 4E-BP1/2 contribute to regulate the migration of CCL5- and CXCL10-responsive T cells by

5369   limiting translational efficiency of *Ccl5* and *Cxcl10* mRNA and subsequent protein synthesis and secretion

5370   by macrophages.

5371

Discussion

Translational repression has emerged as a central regulatory mechanism of inflammatory responses [35, 36]. In this regard, a number of studies indicate that in addition to RNA-binding proteins and microRNAs (miRNAs) [37, 38], eIF4E inhibitory proteins 4E-BP1/2 coordinate the onset and resolution of inflammation via translational silencing [15, 24, 25, 29, 30]. Extending these previous findings, we demonstrate that 4E-BP1/2 act as negative regulators of the pro-inflammatory chemokines CCL5 and CXCL10. Indeed, genetic deletion of 4E-BP1/2 in primary mouse macrophages led to translational derepression of *Ccl5* and *Cxcl10* transcripts. As such, higher levels of heavy polysome-associated *Ccl5* and *Cxcl10* (i.e., highly efficient translated) mRNAs in 4E-BP1/2 DKO cells correlated with enhanced CCL5 and CXCL10 protein synthesis. Consequently, activated T cell chemotaxis was enhanced towards CM from TLR4-stimulated 4E-BP1/2 DKO macrophages. Thus, our data support the notion that selective 4E-BP1/2-dependent translational control of macrophage functions contributes to orchestrate T cell migration to inflammatory sites.

The pleiotropic chemokines CCL5 and CXCL10 regulate cell migration, proliferation, metabolism, and survival in response to stress (e.g., infection, injury, energy status, etc.) [1, 2]. As such, their expression must be quickly adjusted through a combination of transcriptional and post-transcriptional mechanisms to ensure efficient cell activation while preventing deleterious responses [27, 34, 39]. Various mechanisms of translational control have been described for *Ccl5*, including miRNAs and potentially the IFN-γ-activated inhibitor of translation (GAIT) complex [40, 41]. In regards to *Cxcl10*, previous works in MEFs deficient in 4E-BP1 or S6K1/2 pointed to a mechanism of mTORC1-dependent translational control triggered by IFN-γ [15, 17]. Indeed, differential CXCL10 protein expression between WT and 4E-BP1 KO or S6K1/2 DKO MEFs was not paralleled by altered *Cxcl10* mRNA transcription; however, experimental data on *Cxcl10* translation efficiency was lacking (i.e., distribution of *Cxcl10* mRNA across polysome profiles). Moreover, mRNA and protein levels of CXCL10 were assessed only after 48 h of IFN-γ treatment; thus, it is conceivable that early transcriptional changes and/or indirect mechanisms of translational control were at least in part responsible for the phenotype observed in 4E-BP1 and S6K1/2 deficient cells. Of note, the contribution of S6K1/2 and 4E-BP1 to such regulation was not resolved. In the current study, polysome-profiling quantified by two different methods (i.e., nCounter assays and RT-qPCR) confirmed that translation efficiency of *Cxcl10* mRNA is under the control of 4E-BP1/2 and demonstrated that this is also the case for *Ccl5*. Intriguingly, *Ccl5* and *Cxcl10* were not identified as mRNAs translated in a 4E-BP1/2-sensitive fashion in a comparative analysis of the translatome of WT and 4E-BP1/2 DKO MEFs (i.e., transcriptome-wide analysis pools of efficiently translated mRNA) [29]. Upon first consideration, these observations would seem inconsistent with our findings and those published in IFN-γ-stimulated 4E-BP1 KO MEFs [15]. However, these discrepancies could be attributed to specific translational programs triggered by different stimuli or stressors in immune versus nonimmune cells, as described by others and by us [24, 25, 32, 42].

In addition to mTORC1-mediated 4E-BP1/2 inactivation, eIF4E-dependent translational control of immune-related transcripts relies on the MNK1/2-eIF4E axis [11, 22, 23, 33, 34, 43]. In regards to CCL5

207

5409   and CXCL10, several lines of evidence indicate that MNK1/2 regulate their expression through different

5410   mechanisms [14, 33, 34, 44]. Activation of MNK1/2 was shown to be required for late transcription of *Ccl5*

5411   mRNA via translational control of the transcription factor RFLAT-1 in IL-2-treated T cells [34]. Similarly,

5412   inhibition of MNK1/2 abrogated *Cxcl10* transcription and CXCL10 secretion in TNF stimulated smooth

5413   muscle cells [14]. Interestingly, the authors also showed that CCL5 and CXCL10 protein expression was

5414   reduced in MNK1 knock-down cells compared to WT controls [14], yet no experimental evidence on

5415   differential transcription and/or mRNA translation was provided. Of note, polysome-profiling of WT and

5416   eIF4E S209A KI MEFs quantified by microarray did not identify *Ccl5* and *Cxcl10* as targets of translational

5417   control via the MNK1/2-eIF4E axis [33]. Moreover, a later study from the same group did not report any

5418   differences in CCL5 and CXCL10 serum levels between tumor-bearing WT and eIF4E S209A KI mice [44].

5419   In line with these data, we observed that LPS-stimulated WT and eIF4E S209A KI BMDM secrete similar

5420   levels of CCL5 and CXCL10. Thus, we conclude that the phosphorylation status of eIF4E does not affect

5421   the synthesis of these chemokines in our experimental setting. However, we cannot exclude the possibility

5422   that MNK1/2 regulate the expression of CCL5 and CXCL10 in an eIF4E-independent manner. Indeed,

5423   phosphorylation of the RNA-binding protein hnRNP A1 by MNK1/2 was shown to relieve *Tnf* mRNA from

5424   translational repression in activated T cells [45]. Thus, it is conceivable that other mRNAs coding pro-

5425   inflammatory factors are regulated through a similar mechanism. Further characterization of MNK1/2-

5426   dependent translational control in immune cells will shed light on this matter.

5427   In view of our findings, we postulate that the translational repressors 4E-BP1/2 might link innate

5428   and adaptive immune responses by acting as immunological "safeguards" to curtail excessive CCL5 and

5429   CXCL10 secretion by macrophages and to avoid subsequent exacerbated immune responses. Indeed,

5430   CCL5 and CXCL10 are implicated in the pathogenesis of a wide range of inflammatory, autoimmune, and

5431   degenerative diseases [3, 21], and their production is elevated in various cancers [1, 20, 46]. Hence, the

5432   regulatory node mTORC1-4E-BP1/2 might emerge as an attractive therapeutic target to fine-tune the

5433   expression of CCL5 and CXCL10. This consideration could be of particular interest in cancers with altered

5434   eIF4E/4E-BP ratios and/or elevated phosphorylation of 4E-BPs due to a hyperactivated mTORC1 pathway

5435   [47, 48]. Importantly, similar therapeutic applications might be relevant during infectious diseases in which

5436   the mTORC1-4E-BP1/2 axis is dysregulated [49]. Collectively, our findings highlight the key role of eIF4E-

5437   dependent translational control of immunological mediators produced by macrophages, and suggest that

5438   aberrant activity of mTORC1-4E-BP1/2 during diseased states could result in unchecked immune

5439   responses. Ultimately, a better understanding of how chemokine expression is regulated at the level of

5440   mRNA translation might contribute to identify mechanisms potentially targetable by macrophage-centered

5441   therapeutics.

5442

Materials and Methods

Reagents

Culture media and supplements were purchased from Wisent; LPS *Escherichia coli* serotype 0111:B4), concanavalin (Con) A, cycloheximide, and resazurin sodium salt were acquired from Sigma-Aldrich; RNasin was provided by Promega; rapamycin (sirolimus) was obtained from LC Laboratories; Torin-1 was purchased from Cayman; PP242 was acquired from Chemdea; PowerUp™ SYBR® Green Master Mix was obtained from Applied Biosystems; cOmplete EDTA-free protease inhibitor and PhosSTOP phosphatase inhibitor tablets were purchased from Roche; recombinant lambda (λ) phosphatase was purchased from New England Biolabs; Pan T cell Isolation Kit II, mouse and LD columns were acquired from Miltenyi Biotec.

Bone marrow-derived macrophage (BMDM) differentiation

Hind legs from *Eif4ebp1*$^{-/-}$/*Eif4ebp2*$^{-/-}$ and eIF4E$^{S209A/S209A}$ C57BL/6 mice [29, 33] and their wild-type (WT) littermates, originally purchased from The Jackson Laboratories, were kindly provided by Dr. Nahum Sonenberg (McGill University, Montreal, QC, Canada). All procedures were in compliance with the Canadian Council on Animal Care guidelines and approved by the *Comité institutionnel de protection des animaux* of the INRS (CIPA #1611-10). Murine bone marrow-derived macrophages (BMDM) were obtained by differentiating precursor cells, as previously described [25]. Differentiation of precursor cells into macrophages was routinely assessed by monitoring CD11b and F4/80 co-expression by flow cytometry (**Supplemental Fig. 4A**). Viability of WT and 4E-BP1/2 DKO cells was compared using the resazurin colorimetric assay (**Supplemental Fig. 4B**), as described below.

BMDM treatment and viability assays

Cells were plated one day prior to treatment in BMDM culture medium and allowed to adhere O/N at 37°C, 5% CO_2. When applicable, cells were pre-treated with 20 nM rapamycin, 2.5 µM PP242, 200 nM Torin-1, or an equivalent volume of vehicle (DMSO) for 1 h. Cells were either left unstimulated or stimulated with 100 ng/mL LPS for 4 to 24 h, as indicated. For viability experiments, cells were treated with the various inhibitors in the presence of LPS for 24 h. Medium was removed and replaced with fresh BMDM culture medium supplemented with 0.025% resazurin. Cultures were incubated for 6 h at 37°C, 5% CO_2, then optical density was measured using a Multiskan GO (Thermo-Fisher) at 600 and 570 nm. Absorbance at 600 nm was subtracted from readings at 570 nm, values from wells without any cells were used as blanks, and DMSO-treated cells were used to normalize values.

Western blot analysis

Cells were lysed in ice-cold RIPA buffer (25 mM Tris-HCl pH 7.6, 150 mM NaCl, 1% Triton-X-100, 0.5% sodium deoxycholate, 0.1% SDS), supplemented with phosphatase and EDTA-free protease inhibitor cocktails (Roche). Total protein samples were processed for SDS-PAGE and western blotting, as previously

209

5480 described [25]. Total and phospho-specific primary antibodies were purchased from BD Biosciences, anti-
5481 eIF4E (#610270), Santa Cruz Biotechnology, anti-RPS6 (#SC-74459), and Cell Signaling Technology: anti-
5482 phospho-4E-BP1 (T37/46) (#2855), anti-phospho-4E-BP1 (T70) (#9455), anti-phospho-4E-BP1 (S65)
5483 (#9451), anti-4E-BP1 (#9644), anti-4E-BP2 (#2845), anti-phospho-RPS6 (S240/244) (#5364), anti-eIF4G
5484 (#2498), and anti-β-actin (#3700). Secondary goat anti-rabbit and goat anti-mouse IgG horseradish
5485 peroxidase (HRP)-linked antibodies were obtained from Sigma-Aldrich.

5486

5487 **m^7GTP-agarose pull down assays**
5488 Following treatment, cultures were lysed in ice-cold Buffer A (lysis buffer; 50 mM MOPS pH 7.4,
5489 100 mM NaCl, 2 mM EDTA, 2 mM EGTA, 1% IGEPAL CA-630, 1% sodium deoxycholate, 7 mM β-
5490 mercaptoethanol) supplemented with phosphatase and EDTA-free protease inhibitor cocktails. Samples
5491 were processed for m^7GTP-agarose pull down assays, as described [25].

5492

5493 **ELISA**
5494 Cells were seeded in 96-well plates (2×10^5 cells/well). Following treatment, culture supernatants
5495 were collected, and the concentration of secreted CCL5 and CXCL10 was measured by sandwich ELISA
5496 using the mouse CCL5 (#DY478-05) and CXCL10 (#DY466-05) DuoSet ELISA kits (R&D Systems),
5497 according to the manufacturer's specifications.

5498

5499 **5' UTR analysis**
5500 5'UTRs of murine *Ccl5* and *Cxcl10* were retrieved from the mm10 genome build using the UCSC
5501 Table Browser (https://genome.ucsc.edu). Minimum free energy (MFE) and secondary structures were
5502 obtained from the "foldUtr5" table which contains MFE structures computed using RNAfold [50]. Secondary
5503 structures were plotted using VARNA [51].

5504

5505 **Polysome-tracing analysis and RNA fractionation**
5506 Samples were processed for polysome-tracing and RNA fractionation as previously described [25].
5507 Cells lysates were layered onto 5 to 50% (w/v) sucrose density gradients (20 mM HEPES pH 7.6, 100 mM
5508 KCl, 5 mM $MgCl_2$, 100 µg/mL CHX, and 200 U RNAsin) and subjected to ultracentrifugation at 221,830.9 $\times$
5509 *g* (SW 41 rotor, Beckman Coulter) for 2 h at 4°C. Gradients were fractionated and collected, and the
5510 absorbance at 254 nm was recorded continuously using a Brandel BR-188 density gradient fractionation
5511 system.

5512

5513 **RNA extraction and quantitative RT-PCR**
5514 Total and fractionated cytosolic RNA was isolated using QIAzol (Qiagen) and purified using the
5515 RNeasy kit (Qiagen), according to the manufacturer's recommendations. Approximately 1 µg of RNA was
5516 reverse transcribed using Superscript III reverse transcriptase and oligo(dT) (Invitrogen). Quantitative PCR

210

5517   was performed with PowerUp™ SYBR® Green Master Mix (Applied Biosystems) using a QuantStudio 3

5518   Real-Time PCR System (Applied Biosciences). Relative quantification was calculated using the

5519   comparative Ct method ($\Delta\Delta$Ct) [52] and relative expression was normalized to *Gapdh*. Experiments were

5520   performed in independent biological replicates (n = 3 independent experiments); each sample was analyzed

5521   in a technical triplicate. Primers were designed using NCBI Primer-BLAST

5522   (http://www.ncbi.nlm.nih.gov/tools/primer-blast/). The list of primers is provided in **Supplemental Table I**.

5523

5524   **T cell purification and activation, and flow cytometry**

5525   Spleens were collected from naïve WT C57BL/6 mice, ground, and passed through a 100 µm-nylon

5526   cell strainer. Red blood cells were lysed in ACK lysis buffer (150 mM NH_4Cl, 10 mM $KHCO_3$, 0.1 mM EDTA)

5527   for 7 min at RT. Cells were washed, pelleted, and resuspended in ice-cold MACS buffer (PBS [pH 7.2-7.4]

5528   supplemented with 0.5% BSA, 2 mM EDTA). T cells were purified by negative selection using a Pan T cell

5529   Isolation Kit II (Miltenyi Biotec #130-095-130) and LD columns (#130-042-901 fitted onto MidiMACS

5530   separators, as per manufacturer's specifications. T cell purity was assessed by flow cytometry by

5531   determining CD3$^+$ cell population (**Supplemental Fig. 3A**). Isolated T cells were resuspended in culture

5532   medium (RPMI, 10% heat-inactivated FBS, 2 mM L-glutamate, 1 mM sodium pyruvate, 100 U/mL penicillin,

5533   100 µg/mL streptomycin, 55 µM β-ME) supplemented with 2 µg/mL Con A, and plated in 24-well plates (2

5534 $\times 10^6$ cells/well) for 48-72 h. CCR5 and CXCR3 expression in Con A-activated CD3$^+$ T cells was assessed

5535   by flow cytometry. Briefly, cells were washed and resuspended in PBS (pH 7.2-7.4) and stained with Zombie

5536   Violet™ (BioLegend #423113) for 20 min at RT. Cells were washed in FACS buffer (PBS [pH 7.2-7.4], 0.1%

5537   BSA), then Fc receptors were blocked with a rat anti-mouse CD16/32 (clone 93; BioLegend #101301) for

5538   15 min on ice, then stained with the following fluorophore-conjugated antibodies (BioLegend) for 30 min on

5539   ice: FITC-anti-mouse-CXCR3 (clone CXCR3-173; #126535), PE-anti-mouse-CCR5 (clone HM-CCR5;

5540   #107005), and APC-anti-mouse-CD3□ (clone 17A2; #100235). Isotype-matched control antibodies were

5541   included to assess non-specific binding as follows: APC-rat IgG2b,κ (clone RTK4530; #4006211), and

5542   FITC- and PE-Armenian hamster IgG (clone HTK888; BioLegend #400905 and #400907). Cells were fixed

5543   with 1% PFA in PBS for 10 min on ice. Fixative solution was quenched by rinsing cells with 0.1 M glycine

5544   in PBS. Heat-killed cells (56°C, 10 min) stained with Zombie Violet™ only and BD CompBeads (BD

5545   Biosciences #552845) stained with each fluorophore in the panel of markers were used as compensation

5546   controls. Samples were acquired using a BD LSRFortessa™ (BD Biosciences), and data were analyzed

5547   using FlowJo software (Tree Star). Note that we have adhered to the *Guidelines for the use of flow*

5548   *cytometry and cell sorting in immunological studies*

5549   (http://onlinelibrary.wiley.com/doi/10.1002/eji.201646632/pdf) for data analysis and graphic representation.

5550

5551   **Chemotaxis assay**

5552   WT and 4E-BP1/2 DKO BMDM cultures were stimulated with 100 ng/mL LPS or left unstimulated

5553   for 24 h. Conditioned medium (CM) was collected and added to the lower chambers of transwell plates

5554   (Corning). Anti-CCL5 (1 µg/mL; #AF478) and anti-CXCL10 (5 µg/mL; #MAB466-100) neutralizing

5555   antibodies or isotype-matched control antibodies (R&D Systems) were added to the CM, as indicated, and

5556   incubated 1 h at 37°C before the start of the assay. Con A-activated T cells were added to 5 µm pore size

5557   transwell inserts (5 $\times$ 10^5 cells/insert) and were allowed to migrate for 2 h at 37°C, 5% CO_2. Cells in the

5558   lower chamber were enumerated using a hemocytometer.

5559

5560   **Statistical Analysis**

5561   nCounter data were analyzed using the anota "R" package to identify mRNAs under translational

5562   control between WT and 4E-BP1/2 DKO BMDM [31, 53]. Where applicable, statistical differences were

5563   calculated using one-way ANOVA followed by Tukey post-hoc test embedded in GraphPad Prism 7

5564   software package. Results are presented as the mean ± standard deviation (SD) of the mean. Differences

5565   were considered to be statistically significant when * $p < 0.05$, ** $p < 0.01$, *** $p < 0.001$.

5566

Conflict of Interest Disclosure

The authors declare no competing interests.
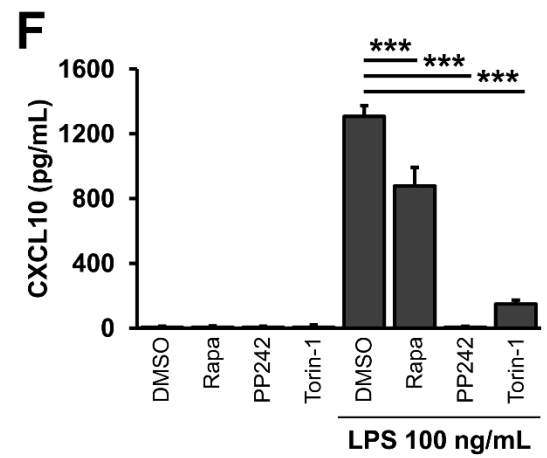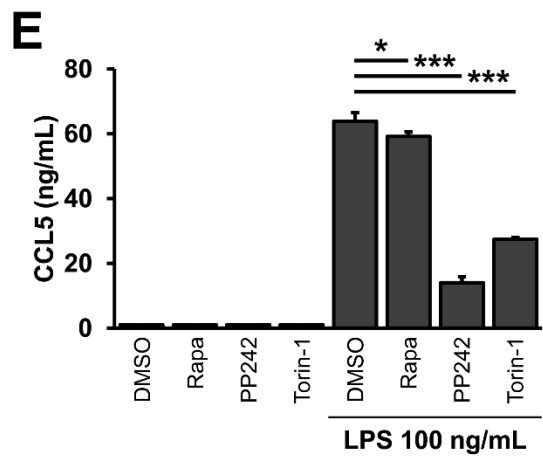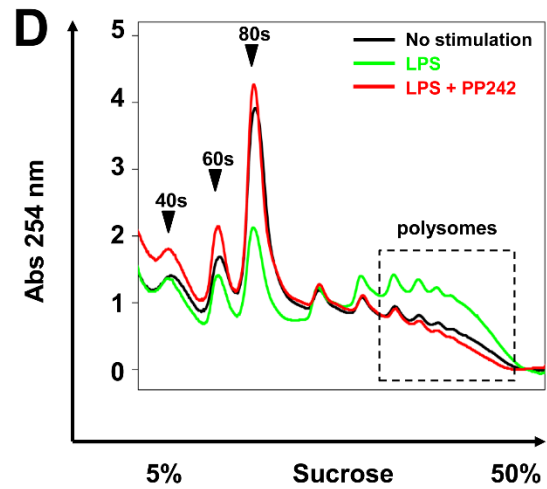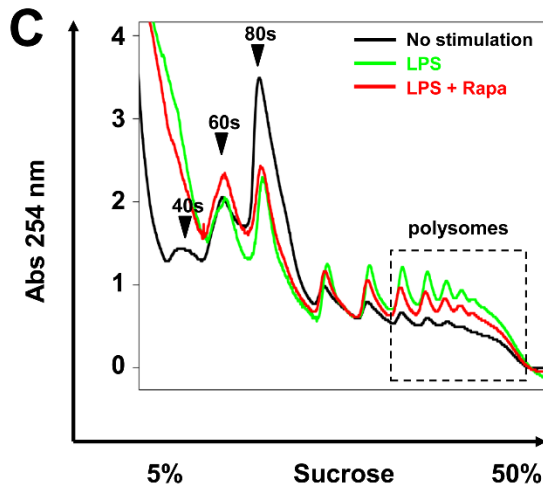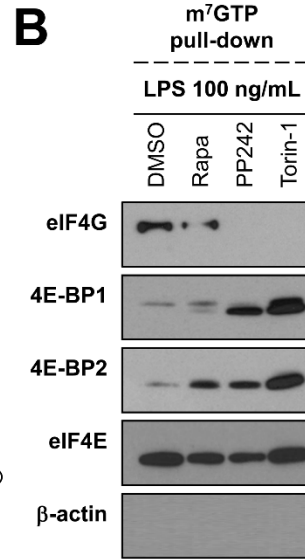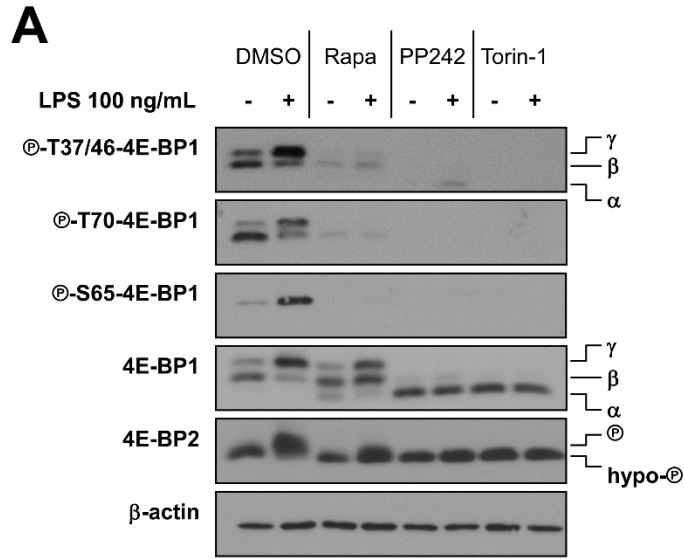
Figure 1. The mTORC1-4E-BP1/2 axis regulates cellular translation initiation and CCL5 and CXCL10

secretion by LPS-stimulated macrophages. BMDM cultures were pre-treated with 20 nM rapamycin, 2.5 µM PP242, 200 nM Torin-1, or an equivalent volume of vehicle (DMSO) for 1 h. **(A-B)** Cells were stimulated or not with 100 ng/mL LPS for 4 h. **(A)** Phosphorylation status and expression levels of 4E-BP1/2 were monitored by western blotting. Total amounts of β-actin were used as a loading control. The hyperphosphorylated gamma (γ), partially phosphorylated beta (β), and hypophosphorylated alpha (α) forms of 4E-BP1 are indicated as well as the higher migrating phosphorylated (Ⓟ) and hypophosphorylated (hypo-Ⓟ) forms of 4E-BP2 are indicated accordingly. **(B)** Total protein extracts were prepared for m^{7}GTP pull down assays, and levels of indicated proteins in pulled-down material were determined by western blotting. **(C-D)** Polysome tracings of BMDM stimulated with LPS with or without rapamycin **(C)** or PP242 **(D)** for 4 h. **(E-F)** Culture supernatants were collected after 24 h of no treatment or LPS stimulation with or without mTOR inhibitors, and CCL5 **(E)** and CXCL10 **(F)** levels were measured by sandwich ELISA. **(A-D)** Data are representative of at least two independent experiments. **(E-F)** Results are presented as mean [SD] (n = 3 independent experiments). Each independent experiment consisting of pools of BMDM isolated from different mice (pools of 2 to 3 mice per genotype). Statistical significance was assessed by one-way ANOVA followed by Tukey post-hoc test. * $p < 0.05$ and *** $p < 0.001$.

215
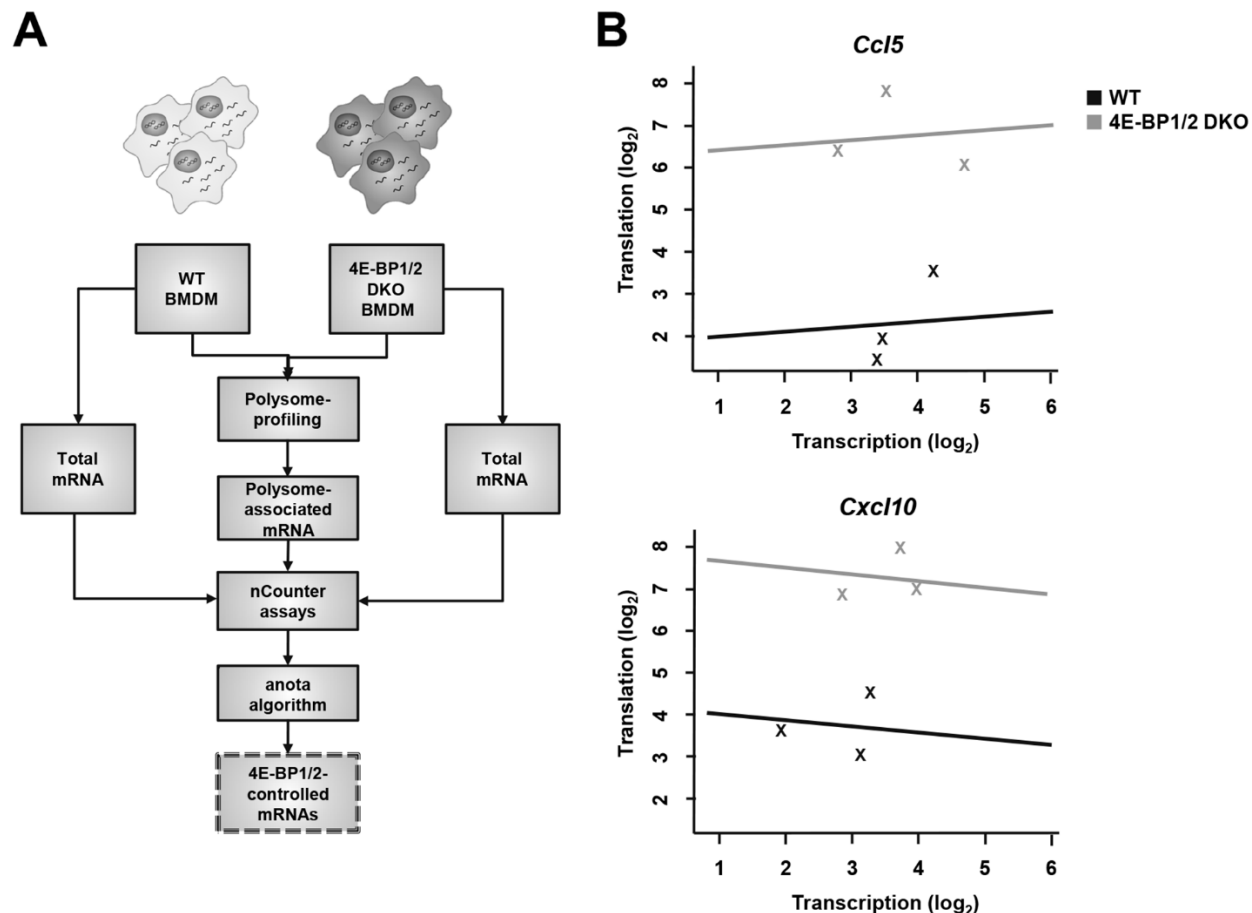
Figure 2. Translational efficiency of *Ccl5* and *Cxcl10* mRNAs is repressed by 4E-BP1/2 in macrophages. (A) Schematic diagram outlines the strategy employed to identify translationally-controlled mRNAs by 4E-BP1/2 in BMDM. Cytosolic extracts from WT and 4E-BP1/2 DKO primary macrophages were sedimented on a sucrose gradient. Heavy polysome fractions (i.e., with mRNA associated to $\geq$ 4 ribosomes) were pooled (referred to as polysome-associated mRNA) and quantified in parallel with total mRNA (input) using targeted nCounter assay (nCounter® Mouse Immunology Panel, Nanostring) (n = 3 independent experiments). Each independent experiment consisting of pools of BMDM isolated from different mice (pools of 5 mice per genotype). Data were analyzed by anota, and mRNAs differentially regulated were identified. **(B)** Translational efficiency of *Ccl5* (top panel) and *Cxcl10* (bottom panel) in 4E-BP1/2 DKO cells as compared to WT cells. Shown is the fold-increase ($\log_2$) in total cytosolic mRNAs levels ("Transcription", *x*-axis) vs. heavy polysome-associated mRNAs levels ("Translation", *y*-axis) for each genotype. Each independent experiment is denoted by an "X" (n = 3). Lines indicate regressions used by anota to adjust changes in polysome-associated mRNA levels for changes in cytosolic mRNA levels.
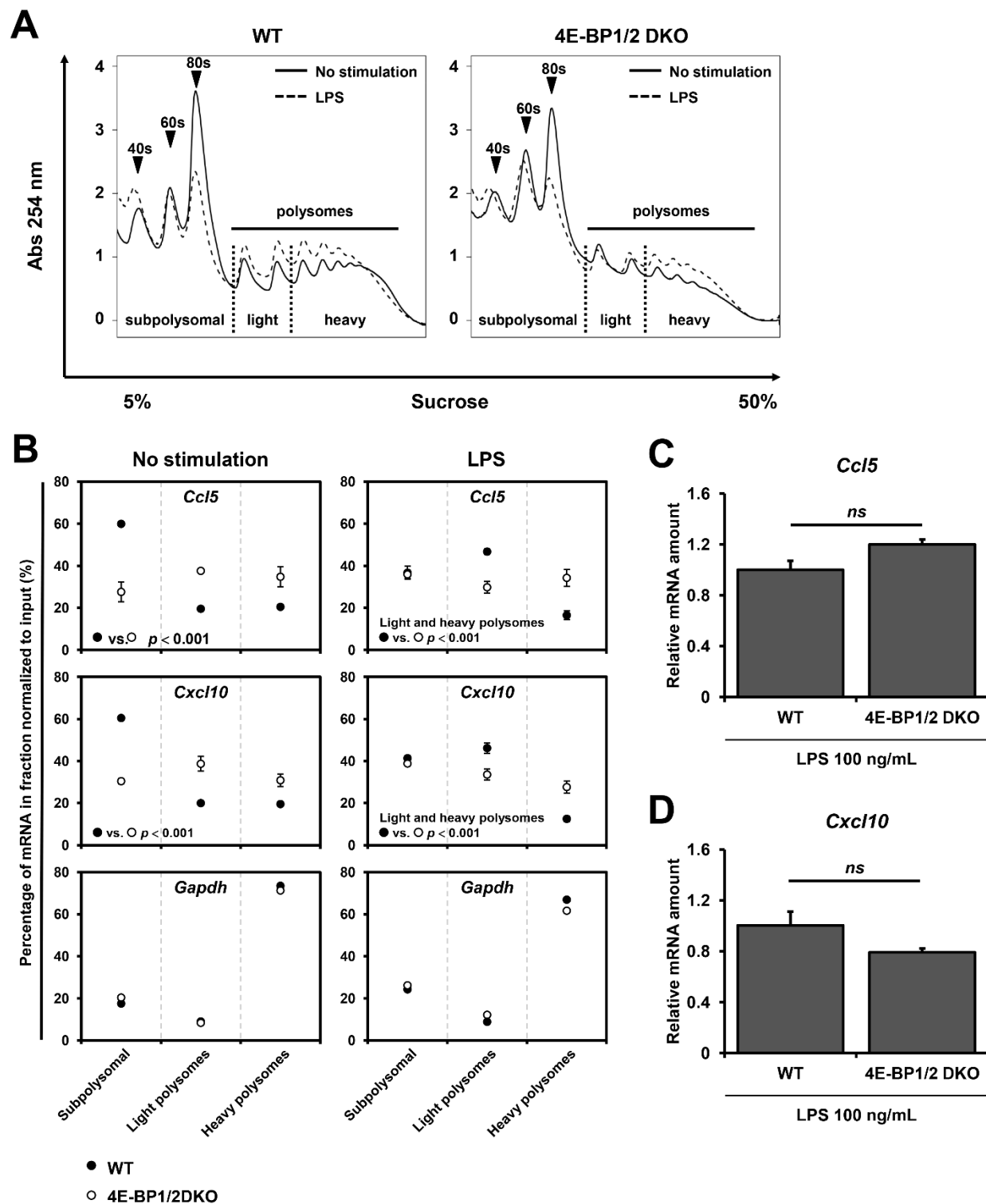
Figure 3. LPS-induced *Ccl5* and *Cxcl10* mRNA translation is regulated by 4E-BP1/2 in macrophages.

(A) WT (left panel) and 4E-BP1/2 DKO (right panel) BMDM cultures were stimulated with 100 ng/mL LPS

5622   (dashed line) or left untreated (solid line) for 4h. Cell lysates were sedimented onto 5 to 50% sucrose

5623   gradients. Gradients were fractionated and absorbance at 254 nm was recorded continuously. Arrows

5624   indicate the 40S and 60S ribosomal subunits, and 80S (monosomes). Regions corresponding to

5625   subpolysomal, and light 2 - 3 ribosomes) and heavy polysome ($\geq$ 4 ribosomes) fractions are indicated under

5626   the tracings. Polysome tracings are representative of three independent experiments. **(B)** Amount of *Ccl5*

5627   (top panels), *Cxcl10* (middle panels), and *Gapdh* (bottom panels) mRNA in subpolysomal, and light and

5628   heavy polysome fraction pools were determined by RT-qPCR. Analysis was performed in WT and 4E-BP1/2

5629   DKO macrophages at steady-state (no stimulation, left column) and after 4 h of LPS stimulation (right

5630   column). Results are expressed as percentage of a given mRNA in each fraction. **(C-D)** Relative mRNA

5631   amounts of total *Ccl5* **(C)** and *Cxcl10* **(D)** mRNAs in LPS-treated WT and 4E-BP1/2 DKO macrophages

5632   were measured by RT-qPCR. Relative expression was normalized to *Gapdh* and relative quantification was

5633   calculated using the comparative Ct method ($\Delta\Delta$Ct). **(B-D)** Data are represented as mean [SD] (n = 3

5634   independent experiments). Each independent experiment consisting of pools of BMDM isolated from

5635   different mice (pools of 5 mice per genotype). Statistical significance was assessed by one-way ANOVA

5636   followed by Tukey post-hoc test; *ns* = not significant.

5637
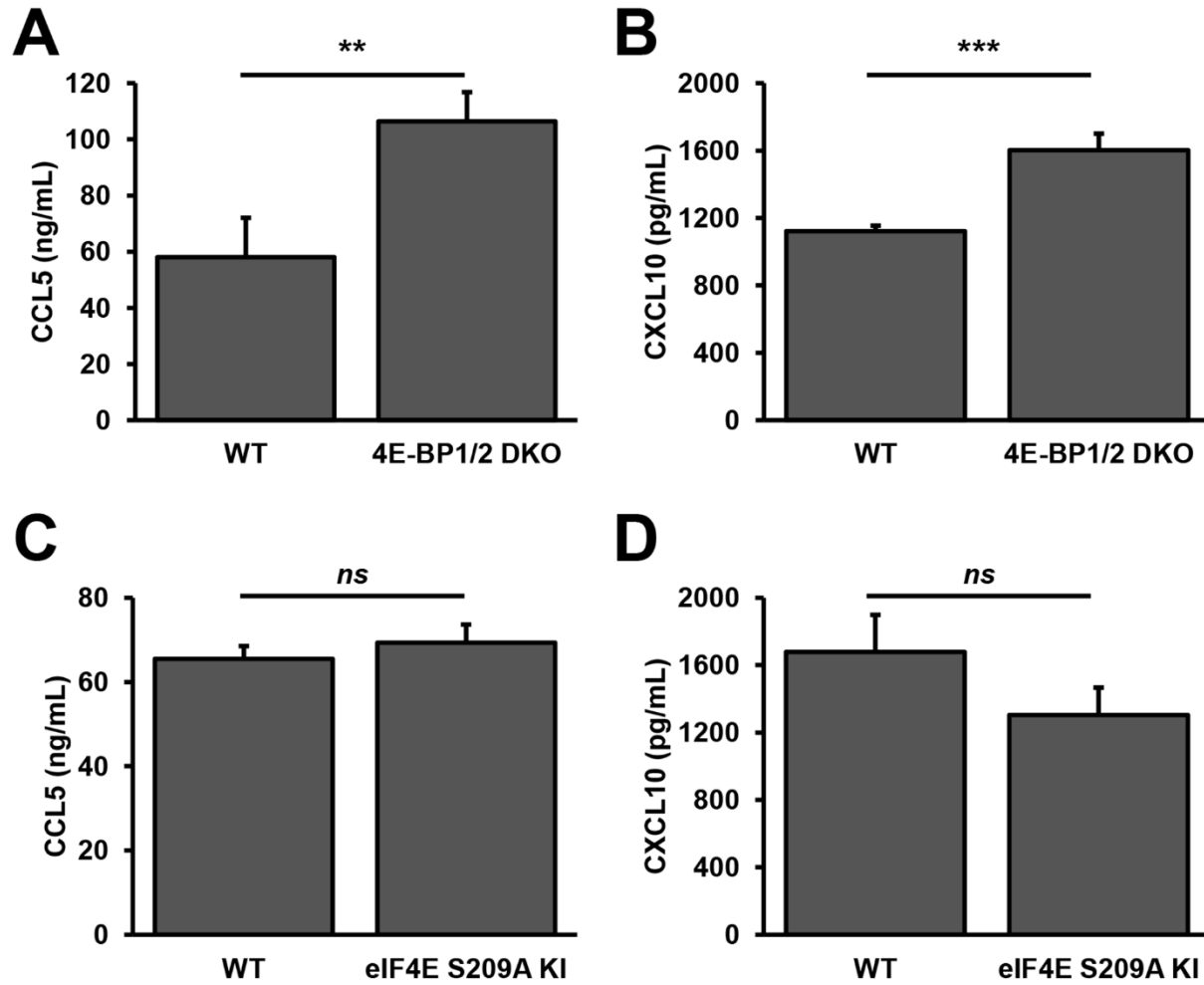
Figure 4. LPS induces CCL5 and CXCL10 protein synthesis via 4E-BP1/2-dependent and MNK-eIF4E-independent mechanisms in macrophages. WT and 4E-BP1/2 DKO **(A-B)** or eIF4E S209A KI **(C-D)** BMDM were stimulated with 100 ng/mL LPS or left unstimulated for 24 h. **(A, C)** CCL5 and **(B, D)** CXCL10 levels were measured by sandwich ELISA. Data are represented as mean [SD] (n = 3 independent experiments). Each independent experiment consisting of pools of BMDM isolated from different mice (pools of 2 to 3 mice per genotype). Statistical significance was assessed by one-way ANOVA followed by Tukey post-hoc test. ** $p < 0.01$; *** $p < 0.001$; *ns* = not significant.

5648
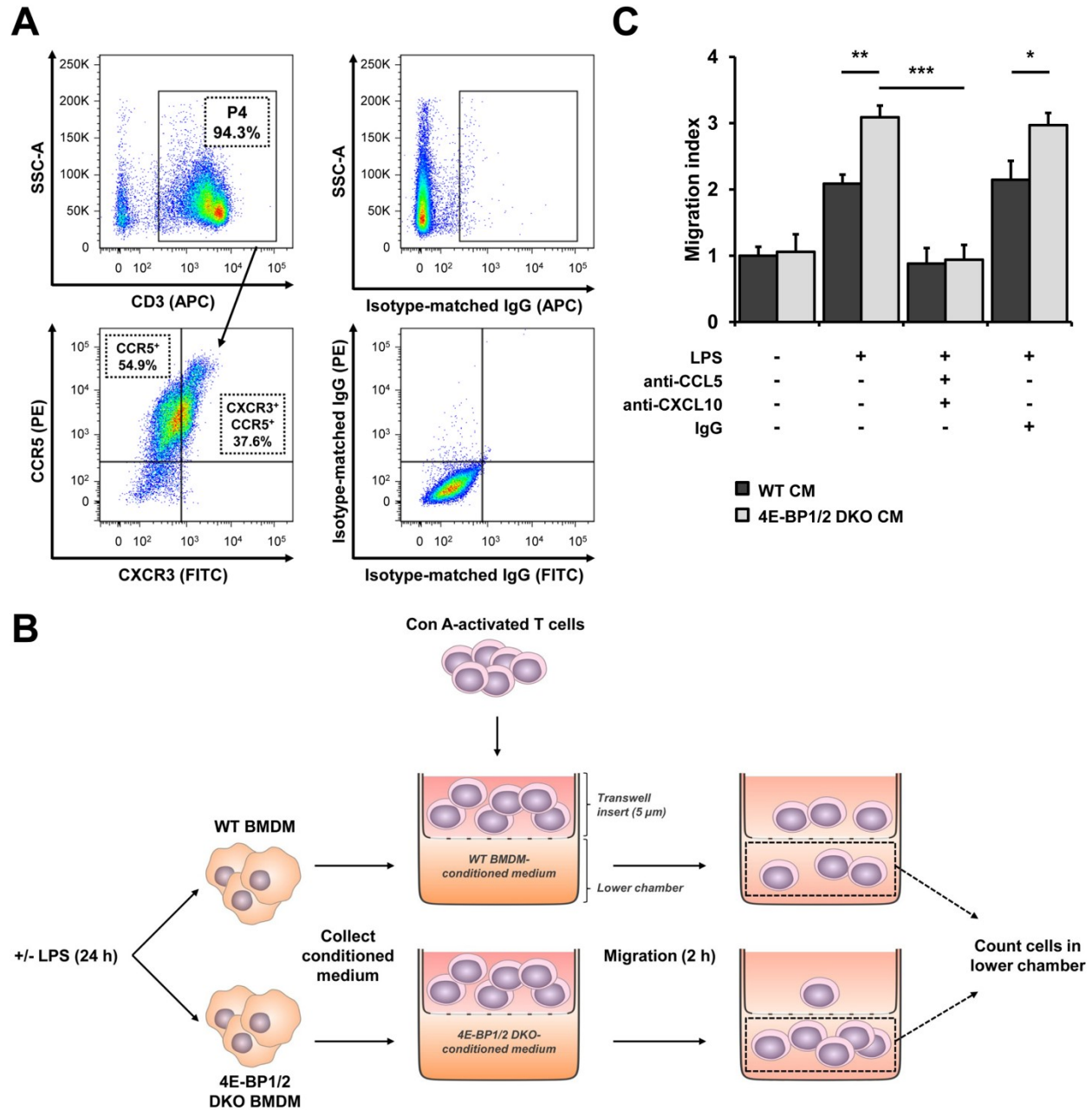
5649

Figure 5. 4E-BP1/2 restrain the ability of macrophages to attract activated T cells through translational repression of CCL5 and CXCL10 (A) Flow cytometry analysis was conducted to monitor CXCR3 and CCR5 expression in Con A-activated CD3$^+$ T cells. Isotype-matched antibodies were used to monitor non-specific binding. Shown here are representative data from three independent experiments. Full gating strategy is outlined in **Supplemental Fig. 3B**. **(B)** Schematic diagram of the procedure employed to measure migration of activated T cells exposed to conditioned medium from WT and 4E-BP1/2 DKO BMDM. Cells were stimulated with 100 ng/mL LPS or left untreated for 24 h. Conditioned medium (CM)

220

5657 was collected and added to the lower chambers of transwell plates. Con A-activated T cells, target cells for

5658 the chemokines of interest, were added to 5 μm pore size transwell inserts and allowed to migrate for 2 h

5659 at 37°C, 5% CO_2. Cells that had migrated towards the lower chamber were counted. **(C)** Migration index

5660 refers to the number of migrated T cells in each condition normalized to that observed with CM from

5661 unstimulated WT BMDM. Neutralizing antibodies against CCL5 (1 μg/mL) and CXCL10 (5 μg/mL) or

5662 isotype-matched control antibodies (IgG) were added to CM, as indicated, and incubated 1 h at 37°C before

5663 the start of the assay. Data are represented as mean [SD] (n = 3 independent experiments). Each

5664 independent experiment consisting of pools of BMDM isolated from different mice (pools of 2 to 3 mice per

5665 genotype). Statistical significance was assessed by one-way ANOVA followed by Tukey post-hoc test. * *p*

5666 < 0.05 ; ** *p* < 0.01; *** *p* < 0.001.

5667
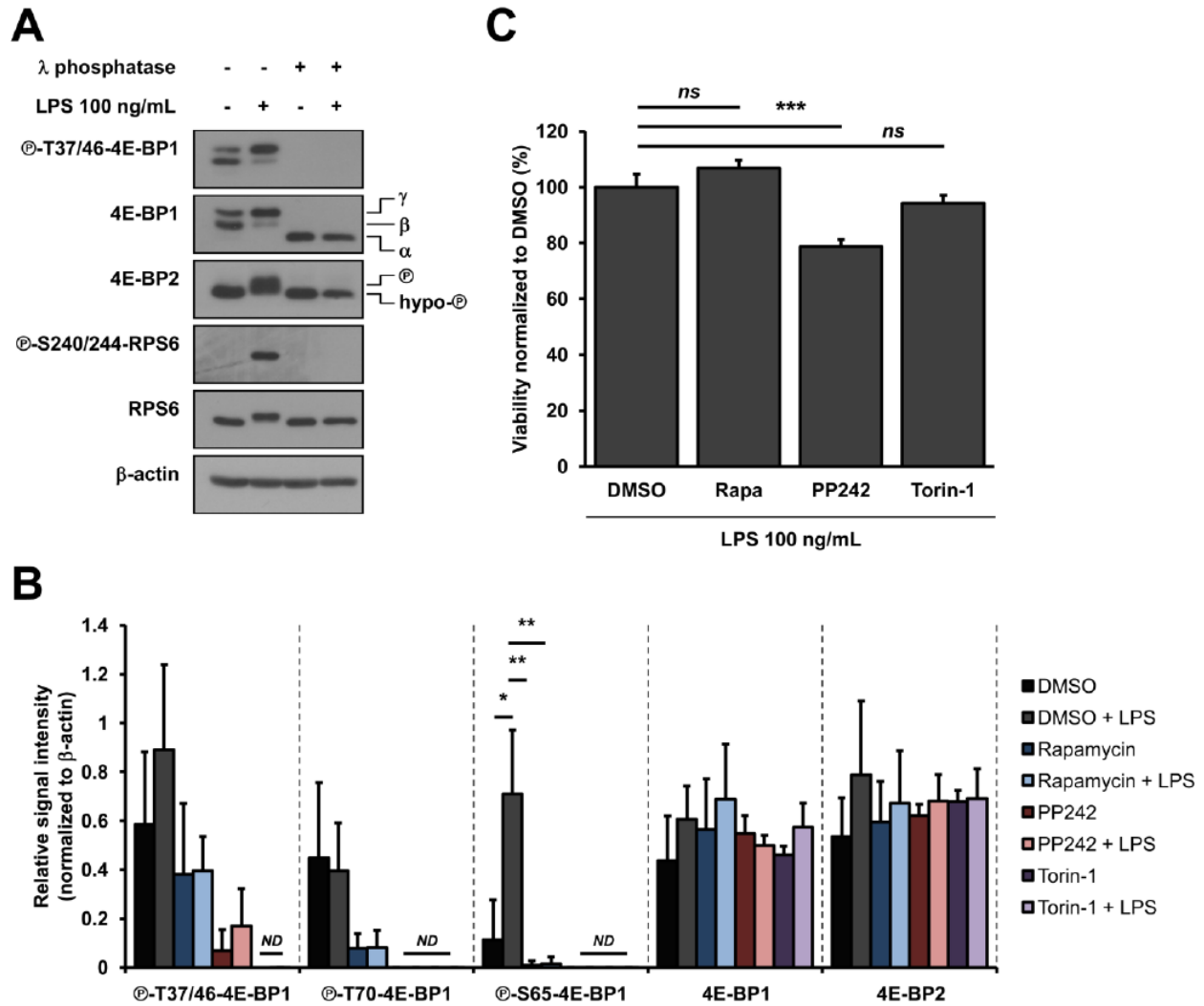
Supplemental Figure 1: **(A)** Changes in migration patterns of 4E-BP1/2 are due to phosphorylation. BMDM cultures were stimulated with 100 ng/mL LPS or left untreated for 4h. Cells were collected, resuspended in lambda (λ) phosphatase buffer supplemented with MnCl2 and protease inhibitor cocktail, and subjected to three freeze-thaw cycles. Recombinant λ phosphatase was added (400 units; NEB #P0753S) or not to lysates. Samples were incubated at 30°C for 45 min. Phosphorylation status of 4E-BP1/2 was monitored by the migration patterns observed by western blotting. Additionally, the phosphorylation of 4E-BP1 at residues T37/46 and of ribosomal protein (RP) S6 at S240/244 was determined with the use of phospho-specific antibodies to confirm phosphatase activity. Total amounts of β-actin were used as a loading control. Data are representative of two independent experiments. **(B)** Quantification of 4E-BP1 and 4E-BP2 blots presented in **Fig. 1A**. Data are represented as mean [SD] (n = 5 for phospho-T37/46 4E-BP1, total 4E-BP1, and total 4E-BP2; n =4 for phospho-T70 4E-BP1 and phospho-S65 4E-BP1). ND = not detected. Statistical significance was assessed by one-way ANOVA followed by Tukey post-hoc test; * $p < 0.05$ and ** $p < 0.01$. **(C)** Viability assessment of LPS-stimulated BMDM exposed to mTOR inhibitors. Macrophages were pre-

5683   treated with 20 nM rapamycin, 2.5 µM PP242, 200 nM Torin-1, or an equivalent volume of vehicle (DMSO)

5684   for 1 h. Cells were then stimulated with 100 ng/mL LPS for 24 h. Medium was removed and replaced with

5685   fresh BMDM culture medium supplemented with 0.025% resazurin. Cultures were incubated for 6 h, then

5686   optical density was measured at 600 and 570 nm. Absorbance at 600 nm was subtracted from readings at

5687   570 nm, values from wells without any cells were used as blanks, and DMSO-treated cells were

5688   used to normalize values. Data are represented as mean [SD] (n = 3 independent experiments). Each

5689   independent experiment consisting of pools of BMDM isolated from different mice (pools of 2 to 3 mice).

5690   Statistical significance assessed by one-way ANOVA followed by Tukey post-hoc test. *** $p < 0.01$; ns =

5691   not significant.

5692
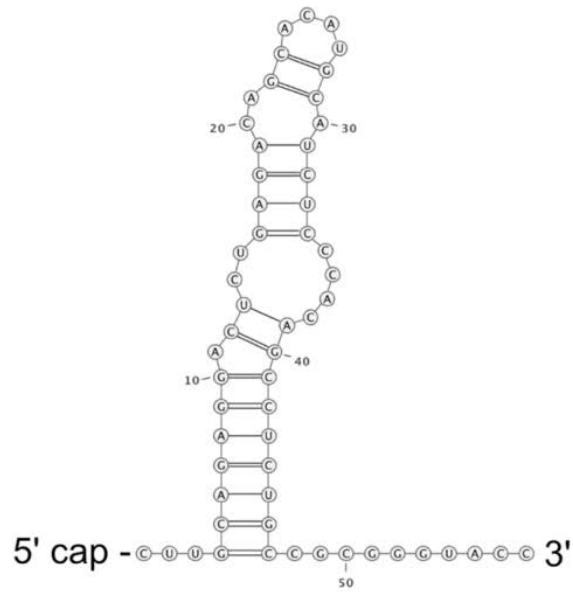
Ccl5

MFE = -17.8 kcal/mol

5' UTR = 57 nt
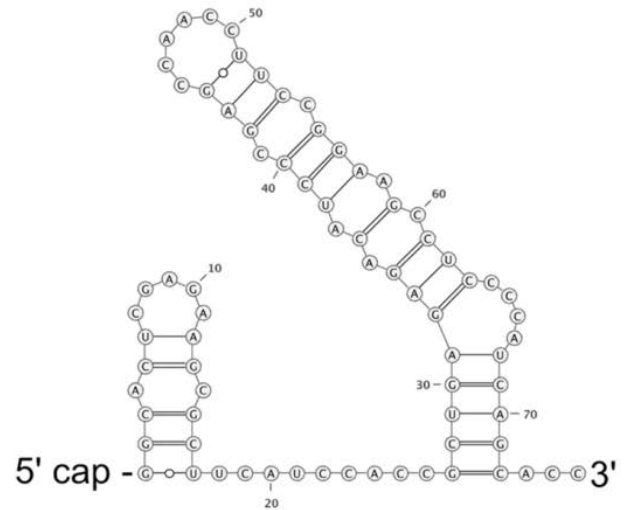
Cxcl10

MFE = -16.2 kcal/mol

5' UTR = 75 nt

Supplemental Figure 2. Secondary structures of murine *Ccl5* (left panel) and *Cxcl10* (right panel) 5' UTRs as predicted by RNAfold. Minimum free energy (MFE) and 5' UTR length corresponding to each mRNA are indicated under the respective structures. 5'UTRs of murine *Ccl5* and *Cxcl10* were retrieved from the mm10 genome build using the UCSC Table Browser (https://genome.ucsc.edu). Minimum free energy (MFE) and secondary structures were obtained from the "foldUtr5" table which contains MFE structures computed using RNAfold (50). Secondary structures were plotted using VARNA (51).
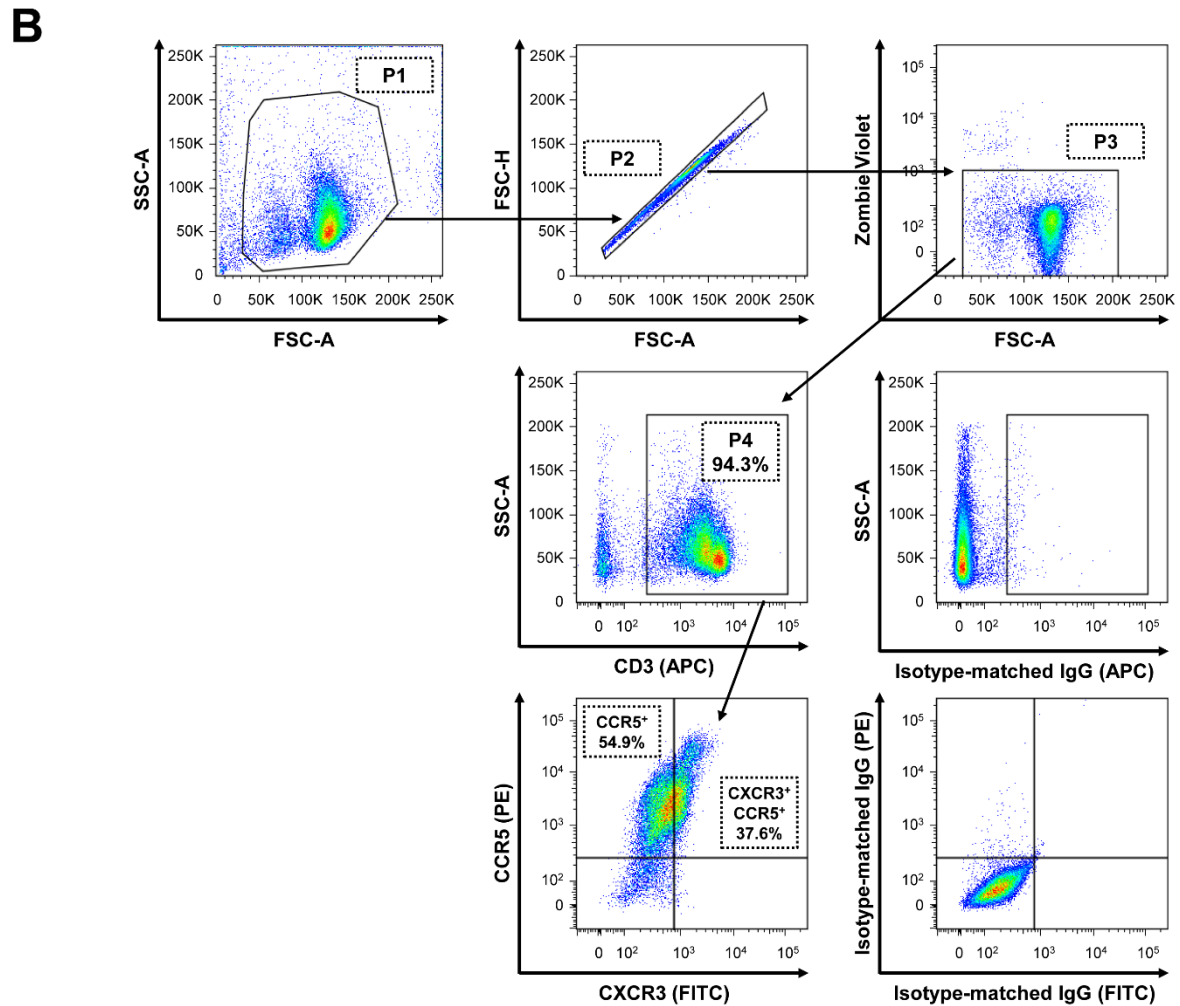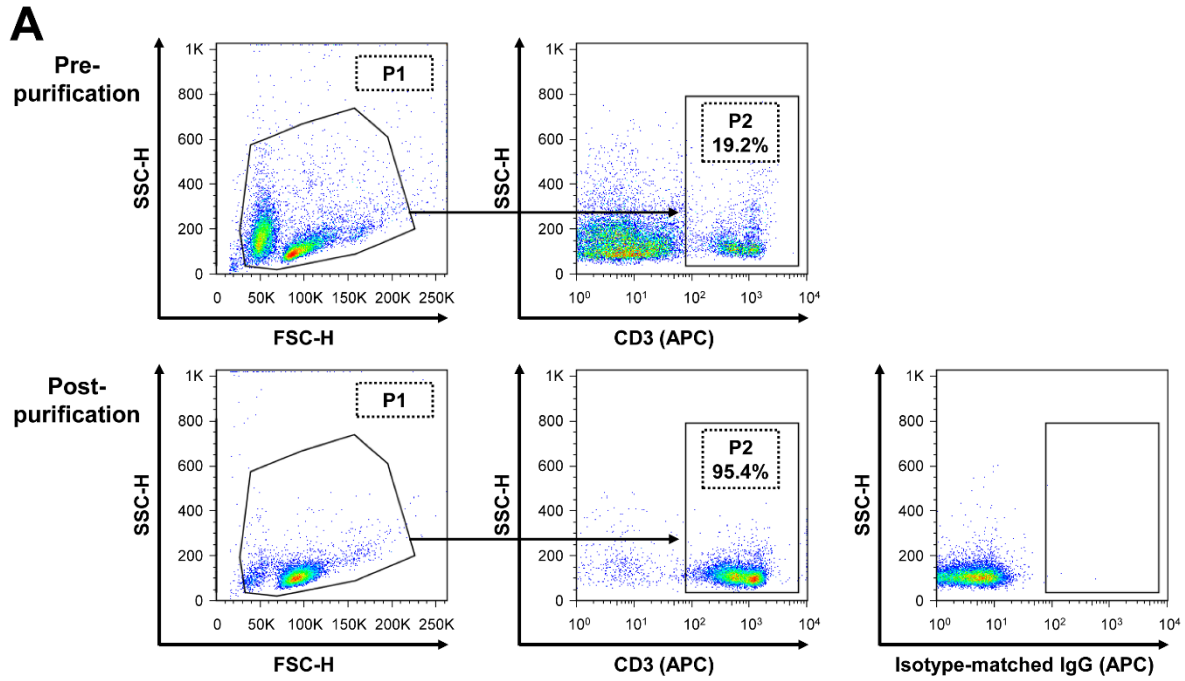
5702 **Supplemental Figure 3.** Splenic T cell isolation. CD3+ T cells were purified by negative selection using a
5703 Pan T cell Isolation Kit II and LD columns (Miltenyi Biotec). **(A)** Splenic cells prior to magnetic sorting ("pre-
5704 purification") and purified T cells (post-purification; following negative selection) were stained with APC-
5705 coupled anti-CD3ε and analyzed by flow cytometry to assess T cell enrichment. Isotype-matched control
5706 antibody was used to assess non-specific binding. **(B)** Con A-activated T cells were analyzed by flow
5707 cytometry to measure CXCR3 and CCR5 expression. Cells were stained with Zombie Violet™, then stained
5708 with APC-coupled anti-CD3ε, FITC-coupled anti-CXCR3, and PE-coupled anti-CCR5 antibodies. Isotype-
5709 matched control antibody was used to assess non-specific binding. Gating strategy was performed as
5710 follows: cells were identified according to FSC-A and SSCA profiles (P1 gate) excluding debris, singlets
5711 were determined according to FSC-A and FSCH profiles (P2) and doublets were excluded, live cells were
5712 gated according to low Zombie Violet™ staining (P3) and dead cells were excluded, and CD3 expression
5713 was determined (P4). Results are representative of three independent experiments.
5714

A

WT

4E-BP1/2 DKO

B
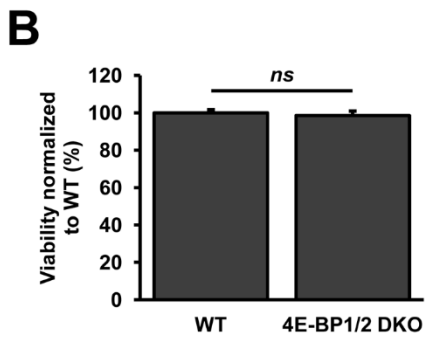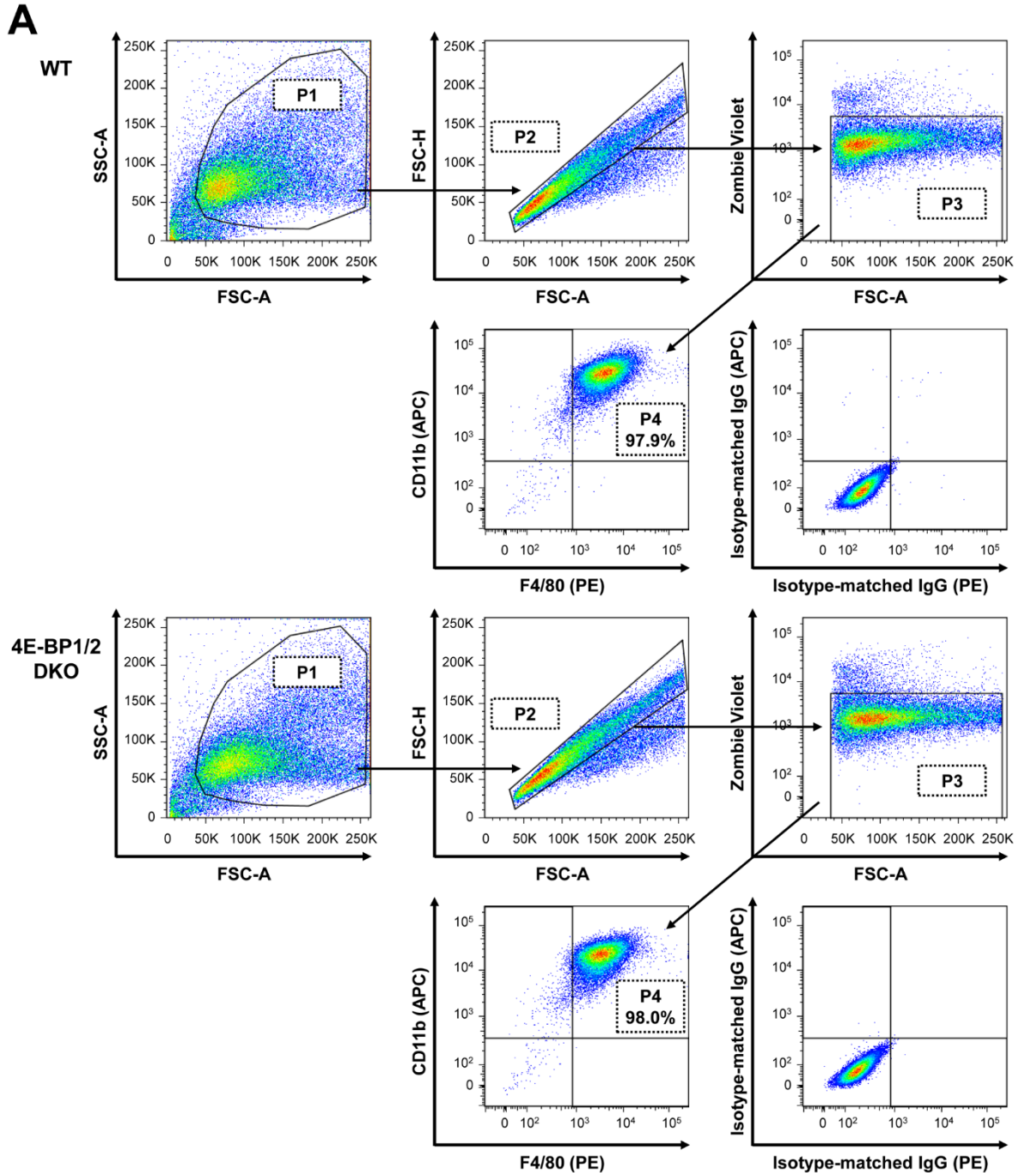
5716 **Supplemental Figure 4**: **(A)** Macrophage differentiation from WT and 4E-BP1/2 DKO bone marrow
5717 precursor cells was compared by flow cytometry. Differentiated BMDM cells were stained with Zombie
5718 Violet™ for 20 min at RT, then stained with APC-coupled anti-CD11b and PE-coupled anti-F4/80 antibodies
5719 and analyzed by flow cytometry. Isotype-matched control antibodies were used to assess non-specific
5720 binding. Gating strategy was performed as follows: cells were identified according to FSC-A and SSC-A
5721 profiles (P1 gate) excluding debris, singlets were determined according to FSC-A and FSC-H profiles (P2)
5722 and doublets were excluded, live cells were gated according to low Zombie Violet™ staining (P3) and dead
5723 cells were excluded, and F4/80 and CD11b co-expression was assessed (P4). Results are representative
5724 of two independent experiments. **(B)** Viability between WT and 4E-BP1/2 DKO BMDM was compared. Cells
5725 were incubated in culture medium supplemented with 0.025% resazurin for 6 h, then optical density was
5726 measured at 600 and 570 nm. Absorbance at 600 nm was subtracted from readings at 570 nm, values from
5727 wells without any cells were used as blanks, and WT cells were used to normalize values. Data are
5728 represented as mean [SD] (n = 3 independent experiments). Statistical significance was assessed by one-
5729 way ANOVA; ns = not significant. (**A-B**) Each independent experiment consisting of pools of BMDM isolated
5730 from different mice (pools of 2 to 3 mice).
5731

5732 **Supplemental Table I.** List of primers used for RT-qPCR

Gene	Primer Sequence (5' - 3')
mouse *Ccl5*	Forward 5' -TCACCATATGGCTCGGACACC-3'
	Reverse 5' -CACACTTGGCGGTTCCTTCG-3'
mouse *Cxcl10*	Forward 5' -CTGCCGTCATTTTCTGCCTC-3'
	Reverse 5' -ATGATCTCAACACGTGGGCA-3'
mouse *Gapdh*	Forward 5' -TTCTTGTGCAGTGCCAGCCTC-3'
	Reverse 5' -CAAATGGCAGCCCTGGTGAC-3'
mouse *Rpl19*	Forward 5' -GCTGCGGGAAAAAGAAGGTC-3'
	Reverse 5' -AGCTTCCTGATCTGCTGACG-3'

5733

5734

References

5736   1   **Khalid, A., Wolfram, J., Ferrari, I., Mu, C., Mai, J., Yang, Z., Zhao, Y. et al.,** Recent Advances in Discovering the Role of CCL5 in Metastatic Breast Cancer. *Mini Rev Med Chem* 2015. **15**: 1063-1072.

5739   2   **Liu, M., Guo, S., Hibbert, J. M., Jain, V., Singh, N., Wilson, N. O. and Stiles, J. K.,** CXCL10/IP-10 in infectious diseases pathogenesis and potential therapeutic implications. *Cytokine Growth Factor Rev* 2011. **22**: 121-130.

5742   3   **Appay, V. and Rowland-Jones, S. L.,** RANTES: a versatile and controversial chemokine. *Trends in Immunol* 2001. **22**: 83-87.

5744   4   **Gardner, L., Patterson, A. M., Ashton, B. A., Stone, M. A. and Middleton, J.,** The human Duffy antigen binds selected inflammatory but not homeostatic chemokines. *Biochem Biophys Res Commun* 2004. **321**: 306-312.

5747   5   **Bachelerie, F., Ben-Baruch, A., Burkhardt, A. M., Combadiere, C., Farber, J. M., Graham, G. J., Horuk, R. et al.,** International Union of Basic and Clinical Pharmacology. LXXXIX. Update on the extended family of chemokine receptors and introducing a new nomenclature for atypical chemokine receptors. *Pharmacol Rev* 2014. **66**: 1-79.

5751   6   **Pruenster, M., Mudde, L., Bombosi, P., Dimitrova, S., Zsak, M., Middleton, J., Richmond, A. et al.,** The Duffy antigen receptor for chemokines transports chemokines and supports their promigratory activity. *Nat Immunol* 2008. **10**: 101.

5754   7   **Jackson, R. J., Hellen, C. U. T. and Pestova, T. V.,** The mechanism of eukaryotic translation initiation and principles of its regulation. *Nat Rev Mol Cell Biol* 2010. **11**: 113-127.

5756   8   **Siddiqui, N. and Sonenberg, N.,** Signalling to eIF4E in cancer. *Biochem Soc Trans* 2015. **43**: 763-772.

5758   9   **Gingras, A. C., Raught, B., Gygi, S. P., Niedzwiecka, A., Miron, M., Burley, S. K., Polakiewicz, R. D. et al.,** Hierarchical phosphorylation of the translation inhibitor 4E-BP1. *Genes Dev* 2001. **15**: 2852-2864.

5761   10   **Waskiewicz, A. J., Flynn, A., Proud, C. G. and Cooper, J. A.,** Mitogen-activated protein kinases activate the serine/threonine kinases Mnk1 and Mnk2. *EMBO J* 1997. **16**: 1909-1920.

5763   11   **Piccirillo, C. A., Bjur, E., Topisirovic, I., Sonenberg, N. and Larsson, O.,** Translational control

5764   of immune responses: from transcripts to translatomes. *Nat Immunol* 2014. **15**: 503-511.

5765   12   **Lin, H. Y., Chang, K. T., Hung, C. C., Kuo, C. H., Hwang, S. J., Chen, H. C., Hung, C. H. and**

5766   **Lin, S. F.,** Effects of the mTOR inhibitor rapamycin on monocyte-secreted chemokines. *BMC*

5767   *Immunol* 2014. **15**: 37.

5768   13   **Lui, S. L., Tsang, R., Chan, K. W., Zhang, F., Tam, S., Yung, S. and Chan, T. M.,** Rapamycin

5769   attenuates the severity of established nephritis in lupus-prone NZB/W F1 mice. *Nephrol Dial*

5770   *Transplant* 2008. **23**: 2768-2776.

5771   14   **Seidel, P., Sun, Q., Costa, L., Lardinois, D., Tamm, M. and Roth, M.,** The MNK-1/eIF4E

5772   pathway as a new therapeutic pathway to target inflammation and remodelling in asthma. *Cell*

5773   *Signal* 2016. **28**: 1555-1562.

5774   15   **Kaur, S., Lal, L., Sassano, A., Majchrzak-Kita, B., Srikanth, M., Baker, D. P., Petroulakis, E.**

5775   **et al.,** Regulatory effects of mammalian target of rapamycin-activated pathways in type I and II

5776   interferon signaling. *J Biol Chem* 2007. **282**: 1757-1768.

5777   16   **Kaur, S., Sassano, A., Dolniak, B., Joshi, S., Majchrzak-Kita, B., Baker, D. P., Hay, N. et al.,**

5778   Role of the Akt pathway in mRNA translation of interferon-stimulated genes. *Proc Nat Acad Sci U*

5779   *S A* 2008. **105**: 4808-4813.

5780   17   **Kroczynska, B., Kaur, S., Katsoulidis, E., Majchrzak-Kita, B., Sassano, A., Kozma, S. C.,**

5781   **Fish, E. N. and Platanias, L. C.,** Interferon-dependent engagement of eukaryotic initiation factor

5782   4B via S6 kinase (S6K)- and ribosomal protein S6K-mediated signals. *Mol Cell Biol* 2009. **29**:

5783   2865-2875.

5784   18   **Mantovani, A., Sica, A., Sozzani, S., Allavena, P., Vecchi, A. and Locati, M.,** The chemokine

5785   system in diverse forms of macrophage activation and polarization. *Trends Immunol* 2004. **25**:

5786   677-686.

5787   19   **Qidwai, T. and Khan, M. Y.,** Impact of genetic variations in C-C chemokine receptors and

5788   ligands on infectious diseases. *Human Immunol* 2016. **77**: 961-971.

5789 20 **Ding, H., Zhao, L., Dai, S., Li, L., Wang, F. and Shan, B.,** CCL5 secreted by tumor associated

5790 macrophages may be a new target in treatment of gastric cancer. *Biomed Pharmacother* 2016.

5791 **77**: 142-149.

5792 21 **Antonelli, A., Ferrari, S. M., Giuggioli, D., Ferrannini, E., Ferri, C. and Fallahi, P.,** Chemokine

5793 (C–X–C motif) ligand (CXCL)10 in autoimmune diseases. *Autoimmun Rev* 2014. **13**: 272-280.

5794 22 **Su, X., Yu, Y., Zhong, Y., Giannopoulou, E. G., Hu, X., Liu, H., Cross, J. R. et al.,** Interferon-

5795 gamma regulates cellular metabolism and mRNA translation to potentiate macrophage activation.

5796 *Nat Immunol* 2015. **16**: 838-849.

5797 23 **Xu, H., Zhu, J., Smith, S., Foldi, J., Zhao, B., Chung, A. Y., Outtz, H. et al.,** Notch–RBP-J

5798 signaling regulates the transcription factor IRF8 to promote inflammatory macrophage

5799 polarization. *Nat Immunol* 2012. **13**: 642.

5800 24 **Jaramillo, M., Gomez, M. A., Larsson, O., Shio, M. T., Topisirovic, I., Contreras, I.,**

5801 **Luxenburg, R. et al.,** *Leishmania* repression of host translation through mTOR cleavage is

5802 required for parasite survival and infection. *Cell Host Microbe* 2011. **9**: 331-341.

5803 25 **William, M., Leroux, L.-P., Chaparro, V., Lorent, J., Graber, T. E., M'Boutchou, M.-N.,**

5804 **Charpentier, T. et al.,** eIF4E-Binding Proteins 1 and 2 Limit Macrophage Anti-Inflammatory

5805 Responses through Translational Repression of IL-10 and Cyclooxygenase-2. *J Immunol* 2018.

5806 **200**: 4102-4116.

5807 26 **Weichhart, T., Costantino, G., Poglitsch, M., Rosner, M., Zeyda, M., Stuhlmeier, K. M.,**

5808 **Kolbe, T. et al.,** The TSC-mTOR signaling pathway regulates the innate inflammatory response.

5809 *Immunity* 2008. **29**: 565-577.

5810 27 **Bandow, K., Kusuyama, J., Shamoto, M., Kakimoto, K., Ohnishi, T. and Matsuguchi, T.,**

5811 LPS-induced chemokine expression in both MyD88-dependent and -independent manners is

5812 regulated by Cot/Tpl2-ERK axis in macrophages. *FEBS Lett* 2012. **586**: 1540-1546.

5813 28 **Dowling, R. J., Topisirovic, I., Alain, T., Bidinosti, M., Fonseca, B. D., Petroulakis, E., Wang,**

5814 **X. et al.,** mTORC1-mediated cell proliferation, but not cell growth, controlled by the 4E-BPs.

5815 *Science* 2010. **328**: 1172-1176.

5816   29   **Colina, R., Costa-Mattioli, M., Dowling, R. J., Jaramillo, M., Tai, L. H., Breitbach, C. J.,**

5817   **Martineau, Y. et al.,** Translational control of the innate immune response through IRF-7. *Nature*

5818   2008. **452**: 323-328.

5819   30   **Nehdi, A., Sean, P., Linares, I., Colina, R., Jaramillo, M. and Alain, T.,** Deficiency in either 4E-

5820   BP1 or 4E-BP2 augments innate antiviral immune responses. *PLoS One* 2014. **9**: e114854.

5821   31   **Larsson, O., Sonenberg, N. and Nadon, R.,** anota: Analysis of differential translation in

5822   genome-wide studies. *Bioinformatics* 2011. **27**: 1440-1441.

5823   32   **Masvidal, L., Hulea, L., Furic, L., Topisirovic, I. and Larsson, O.,** mTOR-sensitive translation:

5824   Cleared fog reveals more trees. *RNA Biol* 2017: 1-7.

5825   33   **Furic, L., Rong, L., Larsson, O., Koumakpayi, I. H., Yoshida, K., Brueschke, A., Petroulakis,**

5826   **E. et al.,** eIF4E phosphorylation promotes tumorigenesis and is associated with prostate cancer

5827   progression. *Proc Natl Acad Sci U S A* 2010. **107**: 14134-14139.

5828   34   **Nikolcheva, T., Pyronnet, S., Chou, S. Y., Sonenberg, N., Song, A., Clayberger, C. and**

5829   **Krensky, A. M.,** A translational rheostat for RFLAT-1 regulates RANTES expression in T

5830   lymphocytes. *J Clin Invest* 2002. **110**: 119-126.

5831   35   **Schott, J., Reitter, S., Philipp, J., Haneke, K., Schafer, H. and Stoecklin, G.,** Translational

5832   regulation of specific mRNAs controls feedback inhibition and survival during macrophage

5833   activation. *PLoS Genet* 2014. **10**: e1004368.

5834   36   **Mazumder, B., Li, X. and Barik, S.,** Translation control: a multifaceted regulator of inflammatory

5835   response. *J Immunol* 2010. **184**: 3311-3319.

5836   37   **Johanna, S. and Georg, S.,** Networks controlling mRNA decay in the immune system. *Wiley*

5837   *Interdiscip Rev RNA* 2010. **1**: 432-456.

5838   38   **Anderson, P.,** Post-transcriptional regulons coordinate the initiation and resolution of

5839   inflammation. *Nat Rev Immunol* 2010. **10**: 24-35.

5840   39   **Carpenter, S., Aiello, D., Atianand, M. K., Ricci, E. P., Gandhi, P., Hall, L. L., Byron, M. et al.,**

5841   A Long Noncoding RNA Mediates Both Activation and Repression of Immune Response Genes.

5842   *Science* 2013. **341**: 789-792.

5843   40   **Perry, M. M., Moschos, S. A., Williams, A. E., Shepherd, N. J., Larner-Svensson, H. M. and**

5844   **Lindsay, M. A.,** Rapid changes in microRNA-146a expression negatively regulate the IL-1beta-

5845   induced inflammatory response in human lung alveolar epithelial cells. *J Immunol* 2008. **180**:

5846   5689-5698.

5847   41   **Poddar, D., Kaur, R., Baldwin Iii, W. M. and Mazumder, B.,** L13a-dependent translational

5848   control in macrophages limits the pathogenesis of colitis. *Cell Mol Immunol* 2015. **13**: 816.

5849   42   **Miloslavski, R., Cohen, E., Avraham, A., Iluz, Y., Hayouka, Z., Kasir, J., Mudhasani, R. et al.,**

5850   Oxygen sufficiency controls TOP mRNA translation via the TSC-Rheb-mTOR pathway in a 4E-

5851   BP-independent manner. *J Mol Cell Biol* 2014. **6**: 255-266.

5852   43   **Herdy, B., Jaramillo, M., Svitkin, Y. V., Rosenfeld, A. B., Kobayashi, M., Walsh, D., Alain, T.**

5853   **et al.,** Translational control of the activation of transcription factor NF-kappaB and production of

5854   type I interferon by phosphorylation of the translation factor eIF4E. *Nat Immunol* 2012. **13**: 543-

5855   550.

5856   44   **Robichaud, N., Hsu, B. E., Istomine, R., Alvarez, F., Blagih, J., Ma, E. H., Morales, S. V. et**

5857   **al.,** Translational control in the tumor microenvironment promotes lung metastasis:

5858   Phosphorylation of eIF4E in neutrophils. *Proc Natl Acad Sci U S A* 2018. **6**: E2202-2209.

5859   45   **Buxade, M., Parra, J. L., Rousseau, S., Shpiro, N., Marquez, R., Morrice, N., Bain, J. et al.,**

5860   The Mnks are novel components in the control of TNF alpha biosynthesis and phosphorylate and

5861   regulate hnRNP A1. *Immunity* 2005. **23**: 177-189.

5862   46   **Liu, J., Li, F., Ping, Y., Wang, L., Chen, X., Wang, D., Cao, L. et al.,** Local production of the

5863   chemokines CCL5 and CXCL10 attracts CD8+ T lymphocytes into esophageal squamous cell

5864   carcinoma. *Oncotarget* 2015. **6**: 24978-24989.

5865   47   **Alain, T., Morita, M., Fonseca, B. D., Yanagiya, A., Siddiqui, N., Bhat, M., Zammit, D. et al.,**

5866   eIF4E/4E-BP Ratio Predicts the Efficacy of mTOR Targeted Therapies. *Cancer Res* 2012. **72**:

5867   6468-6476.

5868   48   **Bhat, M., Robichaud, N., Hulea, L., Sonenberg, N., Pelletier, J. and Topisirovic, I.,** Targeting

5869   the translation machinery in cancer. *Nat Rev Drug Discov* 2015. **14**: 261-278.

5870   49   **Mohr, I. and Sonenberg, N.,** Host translation at the nexus of infection and immunity. *Cell Host*

5871   *Microbe* 2012. **12**: 470-483.

5872   50   **Lorenz, R., Bernhart, S. H., Honer Zu Siederdissen, C., Tafer, H., Flamm, C., Stadler, P. F.**

5873   **and Hofacker, I. L.,** ViennaRNA Package 2.0. *Algorithms Mol Biol* 2011. **6**: 26.

5874   51   **Darty, K., Denise, A. and Ponty, Y.,** VARNA: Interactive drawing and editing of the RNA

5875   secondary structure. *Bioinformatics* 2009. **25**: 1974-1975.

5876   52   **Taylor, S., Wakem, M., Dijkman, G., Alsarraj, M. and Nguyen, M.,** A practical approach to RT-

5877   qPCR-Publishing data that conform to the MIQE guidelines. *Methods* 2010. **50**: S1-5.

5878   53   **Larsson, O., Sonenberg, N. and Nadon, R.,** Identification of differential translation in genome

5879   wide studies. *Proc Natl Acad Sci U S A* 2010. **107**: 21487-21492.

5880

Appendix 3

5882 **Infection by the protozoan parasite *Toxoplasma gondii* inhibits host MNK1/2-eIF4E axis to**

5883 **promote its survival**

5884

5885 Louis-Philippe Leroux[1,*], Visnu Chaparro[1], Maritza Jaramillo[1,*]

5886

5887 [1]Institut National de la Recherche Scientifique (INRS)-Centre Armand-Frappier Santé Biotechnologie

5888 (CAFSB), Laval, Quebec, Canada

5889

5890 [*]Correspondence should be addressed to: maritza.jaramillo@iaf.inrs.ca or to louis-

5891 philippe.leroux@iaf.inrs.ca

5892 INRS-CAFSB, 531 boul. des Prairies, Laval, Québec, H7V 1B7, Canada

5893 Tel.: +1 (450) 687-5010 ext. 8872; fax: +1 (450) 686-5566

5894

5899   **Abstract**

5900   The obligate intracellular parasite *Toxoplasma gondii* reprograms host gene expression through

5901   multiple mechanisms that promote infection, including the up-regulation of mTOR-dependent host mRNA

5902   translation. In addition to the mTOR-4E-BP1/2 axis, MAPK-interacting kinases 1 and 2 (MNK1/2) control

5903   the activity of the mRNA cap-binding protein eIF4E. Herein, we show that *T. gondii* inhibits the

5904   phosphorylation of MNK1/2 and their downstream target eIF4E in murine and human macrophages.

5905   Exposure to soluble *T. gondii* antigens (STAg) failed to fully recapitulate this phenotype indicating the

5906   requirement of live infection. Treatment with okadaic acid, a potent phosphatase inhibitor, restored

5907   phosphorylation of MNK1/2 and eIF4E regardless of infection. *T. gondii* replication was higher in

5908   macrophages isolated from mice mutated at the residue where eIF4E is phosphorylated (eIF4E S209A

5909   knock-in) than in wild-type (WT) control cells despite no differences in infection rates. Similarly, parasitemia

5910   in the mesenteric lymph nodes and spleen, as well as brain cyst burden were significantly augmented in

5911   infected eIF4E S209A knock-in mice compared to their WT counterparts. Of note, mutant mice were more

5912   susceptible to acute toxoplasmosis and displayed exacerbated levels of IFNγ. In all, these data suggest

5913   that the MNK1/2-eIF4E axis is required to control *T. gondii* infection and that its inactivation represents a

5914   strategy exploited by the parasite to promote its survival.

5915

Introduction

Toxoplasma gondii (*T. gondii*), the etiologic agent of toxoplasmosis, is an intracellular protozoan parasite that infects a wide variety of vertebrate hosts, including humans and mice (Innes et al., 2019). It is estimated that about 30-50% of the world population is seropositive for *T. gondii* (Montazeri et al., 2017). Toxoplasmosis is generally asymptomatic yet reactivation of encysted parasites can lead to life-threatening consequences in immuno-compromised individuals (Luft and Remington, 1992), or cause abortions or birth defects if contracted during pregnancy (Montoya and Remington, 2008). *T. gondii* is able to invade any nucleated cell and usurps host cell organelles and nutrients in order to replicate within its parasitophorous vacuole (Clough and Frickel, 2017). The parasite targets signaling pathways and host gene expression to subvert immune responses and establish a favorable environment (Hakimi et al., 2017; Blume and Seeber, 2018; Delgado Betancourt et al., 2019). Among the different strategies employed by the parasite, it was shown that *T. gondii* is able to fine-tune host gene expression post-transcriptionally in part through perturbations in translational efficiency of host mRNAs (Leroux et al., 2018a).

Translational control enables cells to rapidly adapt their proteome to respond to stress or other metabolic cues without *de novo* mRNA synthesis (Gebauer and Hentze, 2004; Sonenberg and Hinnebusch, 2009; Leroux et al., 2018b). Changes in translational efficiency represent a fundamental mechanism in normal biological processes including cell differentiation, growth, metabolism, and proliferation (Gebauer and Hentze, 2004; Hershey et al., 2012). Translational control is also required for balanced immune functions (Piccirillo et al., 2014) and is observed during infectious diseases (Alain et al., 2010; Mohr and Sonenberg, 2012; Walsh et al., 2013; Nehdi et al., 2014; Leroux et al., 2018a; Hoang et al., 2019; Chaparro et al., 2020). In eukaryotic cells, translational efficiency is mainly regulated at the initiation step during which ribosomes are recruited to the mRNA, a process facilitated by recognition of the mRNA 5'-m^{7}G-cap structure by eukaryotic initiation factor 4E (eIF4E), which, together with scaffold protein eIF4G and RNA helicase eIF4A, form the eIF4F complex (Jackson et al., 2010). Assembly of the eIF4F complex is precluded by eIF4E-binding proteins (4E-BPs), which block eIF4E:eIF4G interaction and eIF4F formation (Pause et al., 1994; Lin and Lawrence, 1996). Hyper-phosphorylation of 4E-BPs by mechanistic target of rapamycin (mTOR) complex 1 (mTORC1) lowers 4E-BPs' affinity to eIF4E, thus favoring eIF4E:eIF4G interaction and initiation of translation (Gingras et al., 2001). Phosphorylation of eIF4E at residue S209 is an additional regulatory mechanism of translation initiation (Pelletier et al., 2015), and is mediated by MAP kinase-interacting serine/threonine-protein kinase 1 and 2 (MNK1/2) (Ueda et al., 2004). MNK1/2 are phosphorylated by upstream kinases, specifically p38 MAPK and ERK1/2, following various stimuli (ex: growth factors, cytokines, etc.) (Waskiewicz et al., 1997).

Some studies have reported an increase in translation upon eIF4E phosphorylation (Furic et al., 2010; Robichaud et al., 2015). In contrast, others have suggested that phosphorylation of eIF4E lowers its affinity for the mRNA cap structure (Scheper et al., 2002; Zuberek et al., 2003; Zuberek et al., 2004; Slepenkov et al., 2006). These seemingly contradictory observations could be reconciled by the possibility that reduced cap affinity favors eIF4E recycling and thus increases translation initiation rates (Scheper and

239

Proud, 2002). Translation of transcripts with highly structured 5' UTRs is facilitated through eIF4E activity, and RNA regulons controlling cell proliferation and survival are tightly regulated themselves by eIF4E (Volpon et al., 2019). In addition to its role in translation initiation, eIF4E carries out other functions including mRNA nuclear export, stability, and sequestration (Volpon et al., 2019). However, aberrant eIF4E activity is a determining factor in the development of various pathologies. Dysregulated MNK1/2 activity as well as elevated levels of phosphorylated and total amounts of eIF4E have been shown to promote oncogenesis and tumor growth (Proud, 2015). Phosphorylation of eIF4E was reported to increase translational efficiency of the mRNA encoding the NF-κB inhibitor IκBα. Hence, mice mutated at the residue where eIF4E is phosphorylated (S209A) were less susceptible to viral infections by virtue of enhanced NF-κB activity and type I interferon production (Herdy et al., 2012). In macrophages, efficient translation of HES-1 (Su et al., 2015), a transcriptional repressor of inflammatory genes, and IRF8 (Xu et al., 2012), a transcription factor that promotes M1 polarization, was shown to require MNK-mediated phosphorylation of eIF4E.

Modulation of eIF4E phosphorylation has been associated with enhanced viral replication (Kleijn et al., 1996; Walsh and Mohr, 2004). However, the role of the MNK1/2-eIF4E axis during infections caused by protozoan parasites has yet to be investigated. Here, we report that *T. gondii* reduces MNK1/2 and eIF4E phosphorylation levels and disrupts upstream signaling in infected macrophages. Importantly, we demonstrate that genetic ablation of eIF4E phosphorylation dramatically increases parasite replication *in vitro* as well as parasitemia and host susceptibility in an experimental toxoplasmosis model. These results highlight an important role for the MNK1/2-eIF4E axis in mitigating disease outcome during *T. gondii* infection.

Materials and Methods

Reagents

Culture media and supplements were purchased from Wisent; okadaic acid (*Prorocentrum* sp.) and phorbol-12-myristate-13-acetate (PMA) were acquired from Calbiochem; CellTracker Green (CMFDA) and DAPI were purchased from Invitrogen; Zombie Violet was supplied by BioLegend; resazurin sodium salt was acquired through Alfa Aesar; High Pure PCR Template Preparation Kit, and cOmplete EDTA-free protease inhibitor and PhosSTOP phosphatase inhibitor tablets were purchased from Roche; antibodies were acquired from Cell Signaling Technologies, R&D Systems, Sigma-Aldrich, and BD Biosciences.

Differentiation of murine bone marrow-derived macrophages

Bone marrow-derived macrophages (BMDMs) were generated from 6-8 week-old female C57BL/6 mice (Jackson Laboratory), as previously described (Leroux et al., 2018a; Zakaria et al., 2018; Chaparro et al., 2020). Briefly, marrow was extracted from bones of the hind legs, red blood cells were lysed, and progenitor cells were resuspended in BMDM culture medium supplemented with 15% L929 fibroblast-conditioned culture medium (LCCM). Non-adherent cells were collected the following day and were cultured for 7 days in BMDM culture medium supplemented with 30% LCCM with fresh medium replenishment at day 3 of incubation.

THP-1 culture and differentiation

The human monocytic cell line THP-1 (ATCC TIB-202) was maintained in suspension (DMEM, 10% heat-inactivated FBS, 2 mM L-glutamate, 1 mM sodium pyruvate, 100 U/mL penicillin, 100 μg/mL streptomycin, 20 mM HEPES, 55 μM β-mercaptoethanol). Cells were differentiated into macrophages by adding 20 ng/mL PMA for 24 h. The following day, spent medium was removed and fresh medium without PMA was added, and cells were allowed to rest for another 24 h prior to infection.

Parasite maintenance and harvest

T. gondii cultures (RH and ME49 strains) were maintained by serial passages in Vero cells, as previously described (Leroux et al., 2018a). For experimental infections, freshly egressed tachyzoites were harvested from Vero cultures, pelleted by centrifugation ($1,300 \times g$, 7 min, 4°C), resuspended in ice-cold PBS (pH 7.2-7.4), and passed through a syringe fitted with a 27 G needle. Large cellular debris and intact host cells were pelleted by low-speed centrifugation ($200 \times g$, 3 min, 4°C), and the supernatant containing parasites was filtered with a 3 μm-polycarbonate filter (Millipore). Tachyzoites were then washed twice in PBS and finally resuspended in the appropriate culture medium, according to the experiment.

Soluble *T. gondii* antigens (STAg)

STAg were prepared from freshly egressed tachyzoites, as previously described (Leroux et al., 2015a). Briefly, parasites were resuspended in ice-cold PBS, subjected to three 5-min cycles of

241

6012 freezing/thawing using liquid nitrogen and a 37°C water bath, then sonicated on ice for 5 min (1 sec on/off

6013 pulses, 30% duty cycle) using a Sonic Dismembrator FB505 (ThermoFisher). Lysates were cleared by

6014 centrifugation (21,000 $\times g$, 15 min, 4°C), and soluble material containing STAg was used for downstream

6015 experiments.

6016

6017 **Infection and treatments of BMDM and THP-1 cultures**

6018 Macrophages were plated one day before infection and allowed to adhere O/N at 37°C, 5% CO_2.

6019 Cultures were serum-starved for 2 h and then inoculated with *T. gondii* (MOI 6:1; unless otherwise

6020 specified), treated with 50 µg/mL STAg (where applicable), or left uninfected in fresh medium with 1% FBS.

6021 Any remaining extracellular parasites were rinsed away with warm PBS (pH 7.2-7.4) 1 h following

6022 inoculation, and fresh medium was added. Cells were treated with 10 nM okadaic acid or DMSO 1 h after

6023 infection (where applicable).

6024

6025 **Western blot analysis**

6026 Cells were lysed in RIPA buffer supplemented with protease and phosphatase inhibitors, and

6027 samples were prepared for western blotting as described (Leroux et al., 2018a; William et al., 2019). Primary

6028 antibodies anti-phospho-p38 (T180/Y182; #9216), anti-p38 (#8690), anti-phospho-ERK1/2 (T202/Y204;

6029 #9106), anti-ERK1/2 (#9102), anti-phospho-MNK1/2 (T197/202; #2111), anti-MNK1/2 (#2195), anti-

6030 phospho-eIF4E (S209; #9741), and anti-β-actin (#3700) were purchased from Cell Signaling Technologies;

6031 anti-eIF4E (#610269) was obtained from BD Biosciences; and anti-*T. gondii* profilin (#AF3860) was

6032 acquired from R&D Systems. Horseradish peroxidase (HRP)-linked goat anti-rabbit (#A0545) and goat anti-

6033 mouse IgG (#A4416) secondary antibodies were purchased from Sigma-Aldrich, and rabbit anti-goat

6034 (#HAF017) was acquired from R&D Systems. Densitometric analyses were performed with FIJI software.

6035

6036 **Experimental toxoplasmosis**

6037 Tachyzoites were harvested as described above and resuspended in sterile PBS. WT and eIF4E

6038 S209A KI mice in the C57BL/6 background (Furic et al., 2010) were infected intraperitoneally with either

6039 10^2 RH or 10^3 ME49 *T. gondii*, or mock infected with PBS. Serum, mesenteric lymph nodes (MLN), and

6040 spleens were collected 8 days post-infection (acute), while brains were harvested after 21 days (chronic)

6041 for downstream analyses. Mouse health status was monitored up to 21 days post-infection. At least 5 mice

6042 per genotype were monitored in each infection trial.

6043

6044 **Measurement of *in vitro* parasite replication, *in vivo* parasitemia, and cyst burden by qPCR**

6045 *In vitro* parasite replication was evaluated by epifluorescence microscopy. Briefly, infected BMDM

6046 cultures were fixed at the indicated times with PBS with 3.7% PFA (15 min, RT). Cells were permeabilized

6047 with PBS with 0.2% Triton X-100 (5 min, RT), stained with DAPI (5 min, RT), then mounted onto slides. The

6048 number of parasites in at least 50 vacuoles in different fields for each genotype and time point was counted

242

6049   by microscopy using a 60X oil-immersion objective. The observer was blinded as to which sample was

6050   being evaluated to avoid bias during enumeration of the parasites. *In vivo* parasitemia and cyst burden

6051   were quantified by amplification of the *T. gondii B1* gene, as previously described (Leroux et al., 2015b;

6052   Leroux et al., 2018a). Genomic DNA (gDNA) was extracted from MLN, spleen, and brain tissues using High

6053   Pure PCR Template Preparation Kit (Roche) as per manufacturer's guidelines. *T. gondii B1* gene was

6054   amplified by qPCR using the PowerUP SYBR Green PCR Master Mix (Applied Biosystems) with the

6055   following primers: forward (5'-TCCCCTCTGCTGGCGAAAAGT-3') and reverse (5'-

6056   AGCGTTCGTGGTCAACTATCGATTG-3') (Integrated DNA Technologies). Reaction was carried out in a

6057   QuantStudio 3 Real-Time PCR System (Applied Biosciences). Values were normalized using the mouse β-

6058   *actin* gene amplified with forward (5'-CACCCACACTGTGCCCATCTACGA-3') and reverse (5'-

6059   CAGCGGAACCGCTCATTGCCAATGG-3') primers. Analysis was carried out by relative quantification

6060   using the Comparative C_t method ($2^{-\Delta\Delta Ct}$) (Livak and Schmittgen, 2001).

6061

6062   **ELISA**

6063   Serum from acutely infected mice and mock-injected control mice was collected 8 days post-

6064   infection. IFNγ levels were measured by sandwich ELISA using a Mouse IFN-γ ELISA MAX Deluxe kit

6065   (Biolegend; #430804).

6066

6067   **Statistical analyses**

6068   Where applicable, data are presented as mean [SD]. Statistical significance was determined using

6069   unpaired T test followed by Welch's correction or paired T test (for *in vitro* replication assay); calculations

6070   were performed using Prism Software (GraphPad). For survival curves, log-rank test (Mantel-Cox) was

6071   used to determined significance. Differences were considered significant when * $P < 0.05$, ** $P < 0.01$, ***

6072 $P < 0.001$.

Results

T. gondii inhibits host MNK1/2 and eIF4E phosphorylation and disrupts upstream signaling in infected macrophages

As we and others have previously demonstrated, infection by *T. gondii* increases host mTOR signaling (Wang et al., 2010; Al-Bajalan et al., 2017) and mTOR-dependent mRNA translation (Leroux et al., 2018a). In addition to the mTOR-4E-BP1/2 axis, MAPK-interacting kinases 1 and 2 (MNK1/2) control the activity of the mRNA cap-binding protein eIF4E (Proud, 2015). We therefore sought to determine if the cap-binding initiation factor eIF4E and its upstream signaling intermediates were activated upon infection by monitoring their phosphorylation status. Of note, parasite extracts (i.e., devoid of any host cell; "*Tg* only") were probed in parallel to rule out the possibility that any observed changes in signaling were due to cross-reactivity of the antibodies against *T. gondii* proteins. We first assayed the phosphorylation status of the upstream kinases of MNK1/2, specifically p38 MAPK and ERK1/2 (Waskiewicz et al., 1997). Phosphorylation of p38 MAPK (T180/Y182) was severely compromised in infected BMDMs by both parasite strains (**Figures 1A, B**). As for ERK1/2, phosphorylation at residues T202/Y204 gradually increased over time in cells infected by ME49 only, revealing a strain-dependent modulation. Regardless of ERK1/2 activation, phosphorylation of MNK1/2 (T197/202) was reduced in BMDMs infected with either strain compared to uninfected control cells. Consistently, phosphorylation levels of eIF4E (S209) were readily abrogated and remained as such in infected BMDM cultures. The induction of ERK1/2 phosphorylation by ME49, and the inhibition of MNK1/2 and eIF4E phosphorylation by both RH and ME49 followed an MOI-dependent trend whereby the respective phenotypes were increasingly pronounced as the parasite-to-host ratio increased (**Supplementary Figure 1**). On the other hand, an MOI of 1:1 was enough to lead to the inhibition of p38 phosphorylation by both *T. gondii* strains. In addition, MNK1/2 and eIF4E phosphorylation levels were reduced in infected human THP-1 macrophages (**Figures 1C, D**). In summary, *T. gondii* infection inhibits the MNK1/2-eIF4E signaling axis in both murine and human macrophages.

Live parasites and phosphatase activity are required for inhibition of the MNK1/2-eIF4E axis during T. gondii infection in macrophages

We next sought to determine if live infection was required to disrupt the activation of the MNK1/2-eIF4E pathway. Unlike infection with live parasites, treatment of BMDM cultures with soluble *T. gondii* antigens (STAg) failed to inhibit eIF4E phosphorylation (**Figures 2A, B**). To begin deciphering the molecular mechanisms involved in the inhibition of MNK1/2-eIF4E phosphorylation, we first infected BMDM cultures and 1 h later treated them with 10 nM okadaic acid, a potent protein phosphatase type 1 and 2A inhibitor (Li et al., 2010). This approach helped avoid any effects of the inhibitor on the parasite's ability to infect host cells. Treatment with okadaic acid restored phosphorylation of MNK1/2 and eIF4E regardless of infection by *T. gondii* (**Figures 2C, D**). However, p38 phosphorylation levels remained markedly inhibited in infected cells suggesting that different mechanisms are responsible for the dephosphorylation of p38 and MNK1/2-eIF4E observed upon infection. Of note, treatment with 10 to 50 nM okadaic acid did not affect the

6110   viability of BMDM cultures and extracellular *T. gondii* parasites up to 12 and 24 h, respectively
6111   (**Supplementary Figures 2A, B**). Taking together, these results indicate a complex repression of the
6112   MNK1/2-eIF4E axis by *T. gondii* that is independent of p38 inactivation but implicates parasite- and/or host-
6113   derived phosphatases that remain to be identified.

6114

6115   **Parasite replication within eIF4E S209A KI BMDMs is increased while 4E KI mice are more**
6116   **susceptible to toxoplasmosis**

6117   To begin evaluating the impact of eIF4E phosphorylation on *T. gondii* replication, we infected
6118   BMDM cultures generated from WT mice or mutated at the residue where eIF4E is phosphorylated (eIF4E
6119   S209A knock-in [KI]; 4E KI) (Furic et al., 2010). *In vitro* parasite replication was enhanced in eIF4E S209A
6120   KI BMDMs compared to WT cells as measured by microscopic analyses (**Figure 3A**). The average number
6121   of parasite per vacuole appeared to increase at a slightly higher rate for both RH and ME49 in the mutant
6122   host cells at 16 h post-infection, a phenotype was statistically significant at 24 h and on following infection.
6123   These data suggest that the inhibition of eIF4E phosphorylation in BMDMSs represents a strategy that
6124   favors *T. gondii*. Importantly, the rate of infection (i.e., number of infected cells) did not differ between WT
6125   and 4E KI BMDMS cultures (**Supplementary Figures 3A, B**). Furthermore, up-regulation of ERK1/2
6126   phosphorylation, and inhibition of p38 and MNK1/2 phosphorylation by *T. gondii* were similar in WT and
6127   mutant macrophages (**Supplementary Figures 3C, D**).

6128   To further extent our *in vitro* observations and to determine the impact of eIF4E phosphorylation
6129   on the outcome of toxoplasmosis, we infected and compared WT and eIF4E S209A KI mice. We first
6130   measured parasitemia levels in the mesenteric lymph nodes (MLN) and spleens 8 days post-inoculation
6131   (i.e., acute phase). Analyses by qPCR revealed a substantial increase in parasite loads in both MLN and
6132   spleen tissues in 4E KI mice compared to WT counterparts (**Figure 3B**). Inflammation appeared to be
6133   exacerbated in the former group as revealed by a ~4-fold increase in serum IFNγ concentration (**Figure**
6134   **3C**). The observed phenotype in 4E KI mice did not appear to be due to an underlying basal inflammatory
6135   state since IFNγ was not detectable in mock-injected animals. In light of these results, we then compared
6136   survival rates between 4E KI and WT mice. While most WT animals survived past the acute phase into the
6137   chronic phase, 4E KI mice were significantly more susceptible to acute toxoplasmosis with a majority of
6138   mortality (~77%) occurring within two weeks post-infection (**Figure 4A**). This heighten susceptibility was
6139   reflected by a larger increase in the *T. gondii* cyst burden in the brain of 4E KI mice that survived until the
6140   chronic phase of infection in comparison to WT counterparts (**Figure 4B**). In summary, the absence of
6141   eIF4E phosphorylation appears to compromise host resistance against toxoplasmosis despite increased
6142   IFNγ production.

6143

6144

6145

6146

Discussion

     Disruption of host signaling pathways and gene expression through altered translation is a strategy employed by diverse pathogens (Mohr and Sonenberg, 2012; Walsh et al., 2013). In this study, our results suggest that *T. gondii* targets and disrupts the host MNK1/2-eIF4E signaling axis, an important translational control node. Both type I and II strains markedly inhibit p38, MNK1/2, and eIF4E phosphorylation in infected macrophages. Interestingly, we have observed a marked difference in the induction of ERK1/2 phosphorylation between the two parasite strains. ERK1/2 phosphorylation increased transiently 1 h after infection by both strains and decreased afterwards. At later time points, however, infection by ME49 led to a gradually increased and sustained phosphorylation of ERK1/2, an observation in line with a recent study that reported a similar trend in bone marrow-derived dendritic cells infected with Prugniaud, another type II strain (Olafsson et al., 2020). Meanwhile, phospho-ERK1/2 levels in RH-infected cells remained low and comparable to basal levels seen in uninfected cultures. Chemical inhibition of phosphatases PP1 and PP2A with okadaic acid restores MNK1/2 and eIF4E phosphorylation but not p38, revealing a disconnection between these signaling mediators following *T. gondii* infection. Seemingly conflicting reports about the regulation of p38 by *Toxoplasma* are found in the literature. A study by Kim and colleagues had reported a transient phosphorylation of p38 in BMDMSs between 10 to 20 min (RH) and 10 to 60 min (ME49) following infection, after which phospho-p38 levels return to levels comparable to uninfected controls (Kim et al., 2006). It has also been shown that dense granule protein 24 (GRA24) directly interacts with and activates p38 through autophosphorylation (Braun et al., 2013). As the authors of the latter study pointed out, GRA24 presents several alternative splice variants. Thus, under certain growth conditions (e.g., host cell type and/or species, high vs. reduced nutrient availability, time of infection, etc.), *T. gondii* may turn off GRA24-dependent p38 autophosphorylation by synthesizing different GRA24 isoforms (Braun et al., 2013). In contrast, ROP18 is predicted to bind to p38 and cause its degradation (Yang et al., 2017). In our model, we have consistently observed a rapid (i.e., within 15 min after inoculation) and robust inhibition of phosphorylation of p38 by both RH and ME49 strains in both WT and eIF4E S209A KI macrophages. Thus, the reasons for the disparities among the different reports regarding this signaling molecule remain unclear at this point.

     The data we obtained with okadaic acid treatment suggest that either parasite-derived phosphatases (devoid of function-altering strain polymorphisms) and/or host phosphatases are implicated in inactivation of the MNK1/2-eIF4E axis by *T. gondii*. To date, the mammalian PP2A phosphatase is the only enzyme shown to dephosphorylate both MNK1/2 and eIF4E (Li et al., 2010). Intriguingly, *T. gondii* GRA16 forms a complex with host PP2A and Herpesvirus-associated ubiquitin-specific protease (HAUSP) (Bougdour et al., 2013). Also, GRA18 binds to host GSK3/PP2A-B56 and to affect β-catenin-mediated gene expression (He et al., 2018). Whether these GRA16- and GRA18-containing complexes display phosphatase activity towards host MNK1/2 and eIF4E or that other host-parasite chimeric complexes are formed remains to be determined. For example, TgWIP, a rhoptry protein, interacts with host SHP2 phosphatase (Sangare et al., 2019). There are 52 predicted phosphatase genes in the *T. gondii* genome

246

6184 of which two encode for the PP2A catalytic subunits, referred to as PP2A1 and PP2A2 (Yang and

6185 Arrizabalaga, 2017). The PP2A1 protein sequence contains a signal peptide which raises the possibility

6186 that it is secreted into the host cells and targets host MNK1/2 and eIF4E. The fact that STAg failed to

6187 recapitulate the effects of live infection does not exclude that soluble factors are linked to MNK1/2-eIF4E

6188 dephosphorylation but rather that certain events are required for these factors to mediate their effects within

6189 the host cell (e.g., formation and presence of the parasitophorous vacuole membrane, specific route of

6190 entry of these molecules, etc.).

6191 The increased replication rate *in vitro*, and parasitemia and virulence in eIF4E S209A KI mice

6192 suggest that preventing eIF4E phosphorylation favors *T. gondii* persistence within its host. We observed a

6193 substantial increase in serum IFNγ levels eight days post-infection in 4E KI mice compared to their WT

6194 counterparts. Although IFNγ has long been identified as a critical cytokine to control toxoplasmosis (Denkers

6195 and Gazzinelli, 1998), it is possible that exacerbated inflammation leads to detrimental effects. Also, it is

6196 conceivable that complete absence of eIF4E phosphorylation in infected but also in uninfected 4E KI cells

6197 and mice precludes an appropriate immune response to develop against toxoplasmosis. Coincidentally,

6198 excessive inflammation has been linked to changes in eIF4E phosphorylation levels in other conditions. In

6199 a study by Amorim and colleagues, it was shown that LPS treatment leads to a greater production of

6200 inflammatory cytokines IL-2, TNFα, and IFNγ in the brain of 4E KI mice compared to WT animals (Amorim

6201 et al., 2018). Similarly, decreased synthesis of the NF-κB inhibitor IκBα has been reported in 4E KI

6202 fibroblasts infected with vesicular stomatitis virus (VSV), which leads to increased production of IFNβ (Herdy

6203 et al., 2012), and in the brain of 4E KI mice (Aguilar-Valles et al., 2018). Another recent study reported

6204 heighten levels of TNFα and IL-1β in 4E KI in old and young mice, respectively (Mody et al., 2020). Thus,

6205 higher IFNγ levels in 4E KI mice following *T. gondii* infection could be due to increased parasite burden

6206 and/or genetic predisposition to exacerbated inflammation in these mutant mice, which, according to our

6207 model, appears to be detrimental to the host. Future studies will be necessary to fully understand the

6208 underlying mechanisms linked to the increased susceptibility of 4E KI mice to toxoplasmosis.

6209 It has been reported that phosphorylation of eIF4E regulates translation of a subset of mRNAs

6210 including several containing a gamma interferon-activated inhibition of translation (GAIT) element in their

6211 3' UTR (Amorim et al., 2018), or a 5'-terminal cap and a hairpin structure (Korneeva et al., 2016). It remains

6212 to be determined if the translational efficiency of specific subsets of host transcripts is affected by the

6213 reduction of phosphorylated eIF4E levels in *T. gondii*-infected cells. Functions of eIF4E beyond translation

6214 initiation *per se* are yet to be investigated in the context of parasitic infections. Furthermore, eIF4E-

6215 independent effects mediated by MNK1/2 could also play a role during *T. gondii* infection. Other MNK1/2

6216 substrates identified to date include hnRNP A1, PSF, Sprouty2, and cPLA2 (Xie et al., 2019). One study

6217 showed that phosphorylation of hnRNP A1 by MNK1/2 decreases its affinity for *Tnfa* mRNA which, in turn,

6218 increases translation and synthesis of TNFα by T cells (Buxade et al., 2005). This evidence brings forth the

6219 possibility that immune responses mediated by MNK1/2 and its substrates could be dysregulated upon *T.*

6220 *gondii* and warrant future investigation.

6221   In summary, our study identifies the MNK1/2-eIF4E axis as another regulatory node targeted by *T.*

6222   *gondii* to subvert host cell functions and promote its replication. Future studies will allow identification of

6223   host- and parasite-derived factors linked to this molecular rewiring and will provide a better understanding

6224   of its biological consequences during toxoplasmosis.

6225

Data Availability Statement

6232   The datasets generated for this study are available upon request to the corresponding author.
6233

Ethics Statement

6235   Housing and experiments were carried out under protocols approved by the Comité Institutionnel
6236 de Protection des Animaux (CIPA) of the INRS-CAFSB (CIPA 1502-03 and 1611-10). These protocols
6237 respect procedures on good animal practice provided by the Canadian Council on animal care.
6238

Author Contributions

6240   LPL and MJ conceived and designed the experiments, and wrote the manuscript. LPL, VC, and MJ
6241 analyzed the data. LPL performed the experiments. All authors reviewed and edited the manuscript.
6242

Conflict of Interest

6251   The authors declare no competing interests.
6252

A

Time (h)	0.25			0.5			1			2			4			8			12			*Tg* only	
RH	-	+	-	-	+	-	-	+	-	-	+	-	-	+	-	-	+	-	-	+	-	+	-
ME49	-	-	+	-	-	+	-	-	+	-	-	+	-	-	+	-	-	+	-	-	+	-	+

Ⓟ-T180/Y182-p38

p38

Ⓟ-T202/Y204-ERK1/2

ERK1/2

Ⓟ-T197/202-MNK1/2

MNK1/2

Ⓟ-S209-eIF4E

eIF4E

β-actin

T. gondii profilin

B

C

RH - +

Ⓟ-T197/202-MNK1/2

MNK1/2

Ⓟ-S209-eIF4E

eIF4E

β-actin

T. gondii profilin

D

Time (h)   0.25 | 0.5 | 1 | 2 | 4 | 8 | 12

RH - +

6253
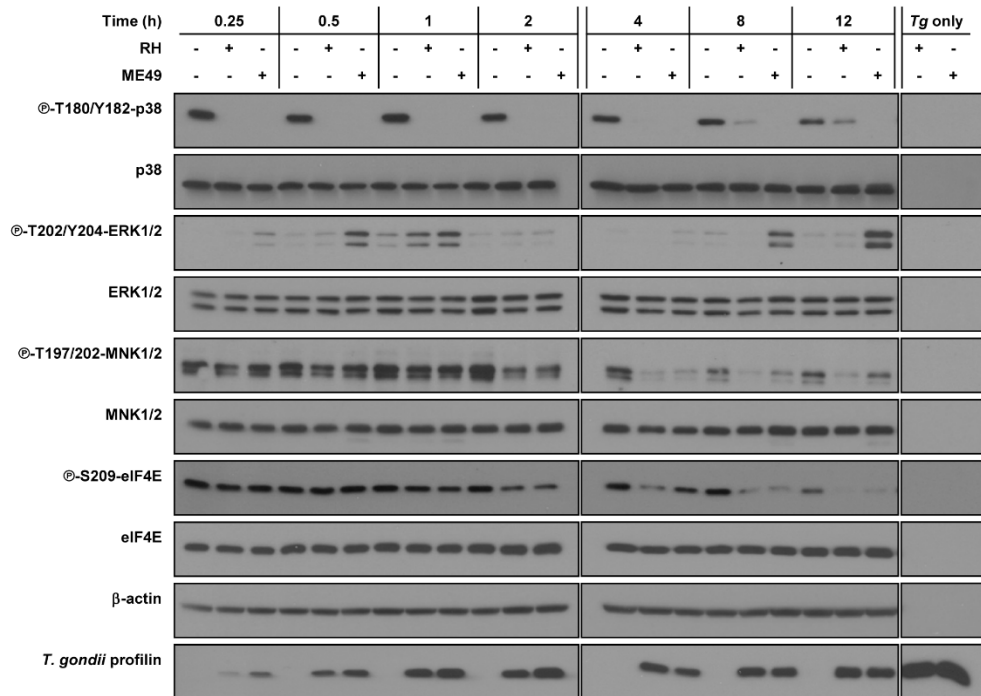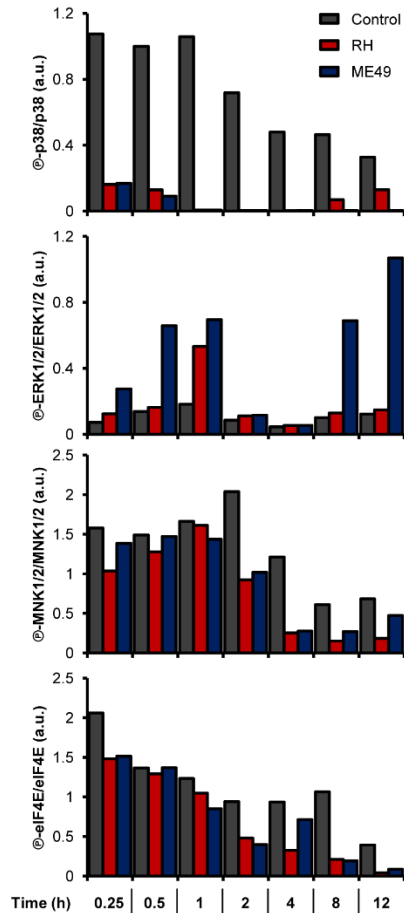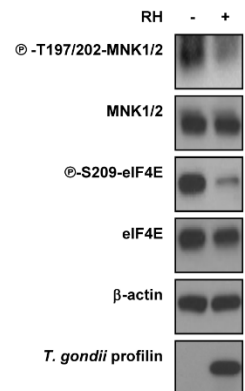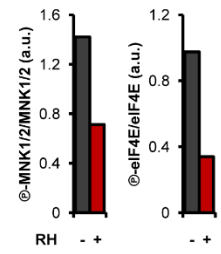
6254 **Figure 1: *T. gondii* represses MNK1/2-eIF4E signaling pathway in macrophages**. (**A-B**) BMDMS

6255 cultures were infected with either RH or ME49 for the indicated times or left uninfected. (**C-D**) PMA-

6256 differentiated THP-1 cells were infected with RH strain for 8 h or left uninfected. (**A**, **C**) Phosphorylation and

6257 expression levels of indicated proteins were monitored by western blotting. Total amounts of β-actin were

6258 used as a loading control and an antibody against *T. gondii* profilin-like protein was employed to assess the

6259 infection of the BMDMS cultures. Total protein extracts from extracellular tachyzoites (RH and ME49) (*Tg*

6260 only) were used to control for any cross-reactivity of the antibodies against *T. gondii* proteins. (**B, D**)

6261 Densitometric analysis of the phosphorylation status of indicated proteins in uninfected control cultures and

6262 infected cells using the FIJI software. Data and data analyses are representative of at least two biological

6263 replicates.

6264
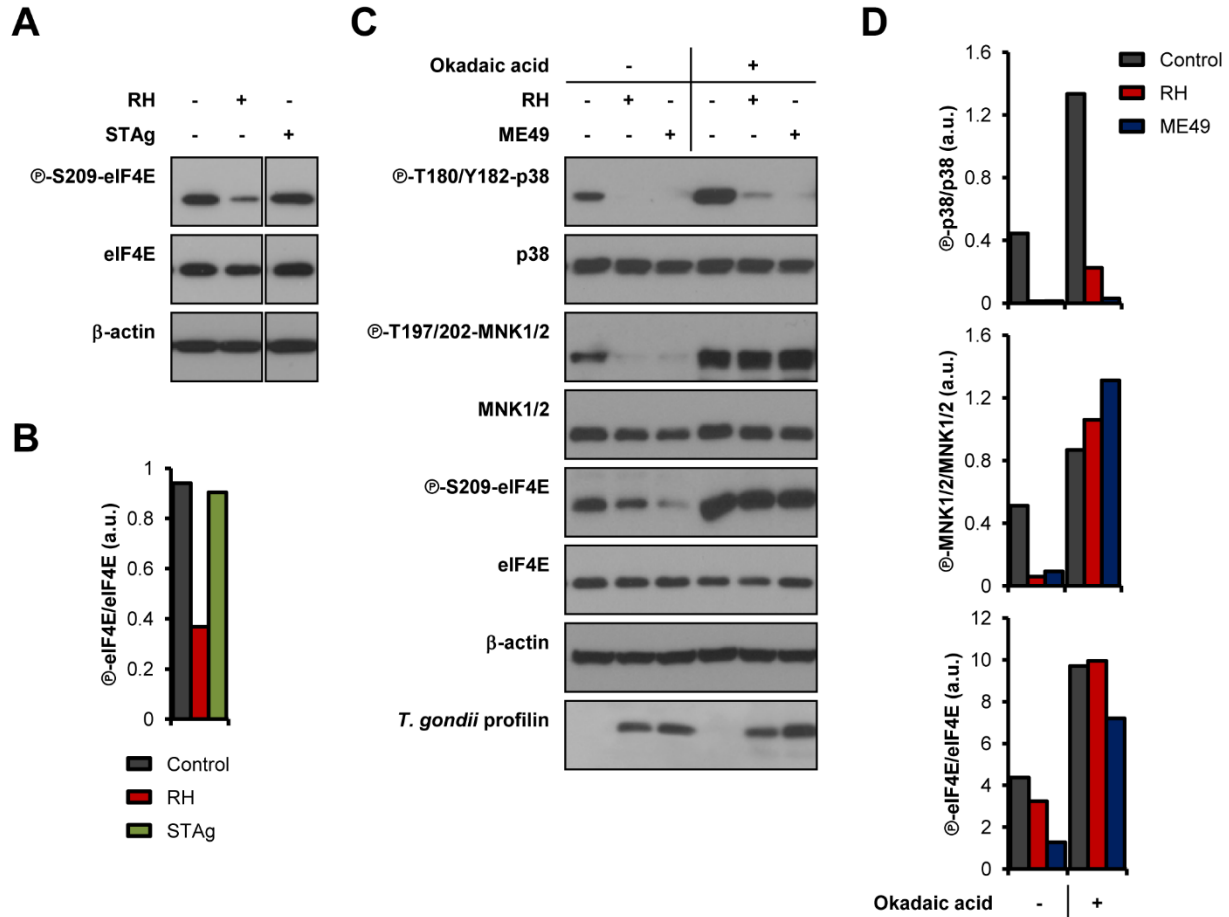
Figure 2: *T. gondii*-derived soluble antigens do not fully recapitulate inhibitory effects of live infection, while okadaic acid restores phosphorylation levels of MNK1/2-eIF4E. BMDMS cultures were infected with (**A-B**) RH strain or treated with 50 µg/mL of STAg, or (**C-D**) infected with either RH or ME49 strains then treated with DMSO (vehicle) or 10 nM okadaic acid for 8 h. In all cases, uninfected cultures were collected in parallel. (**A**, **C**) Phosphorylation and expression levels of indicated proteins were monitored by western blotting. Total amounts of β-actin were used as a loading control and an antibody against *T. gondii* profilin-like protein was employed to assess the infection of the BMDMS cultures. (**B, D**) Densitometric analysis of the phosphorylation status of indicated proteins in uninfected control cultures and infected cells using the FIJI software. Data and data analyses are representative of two biological replicates.
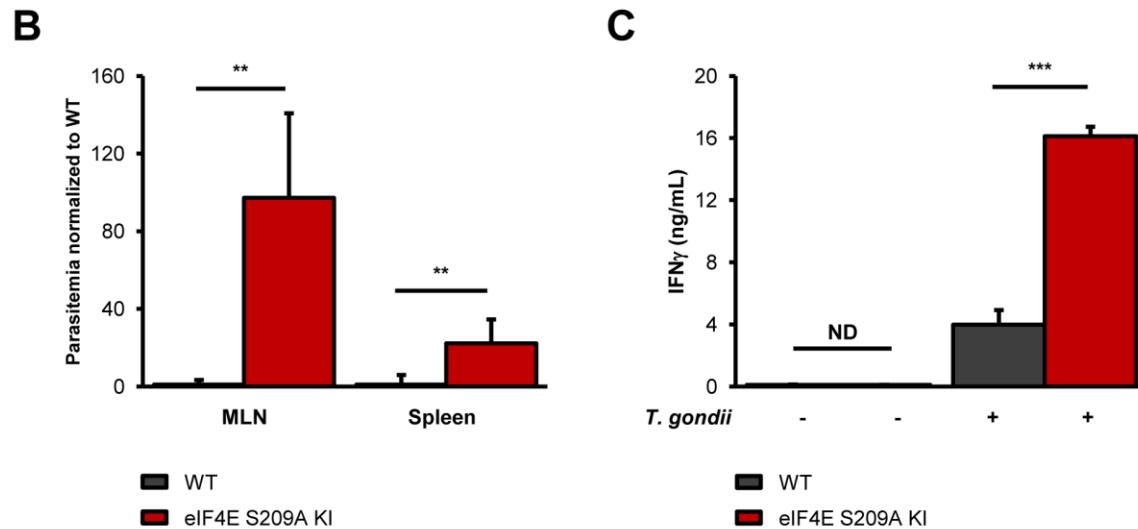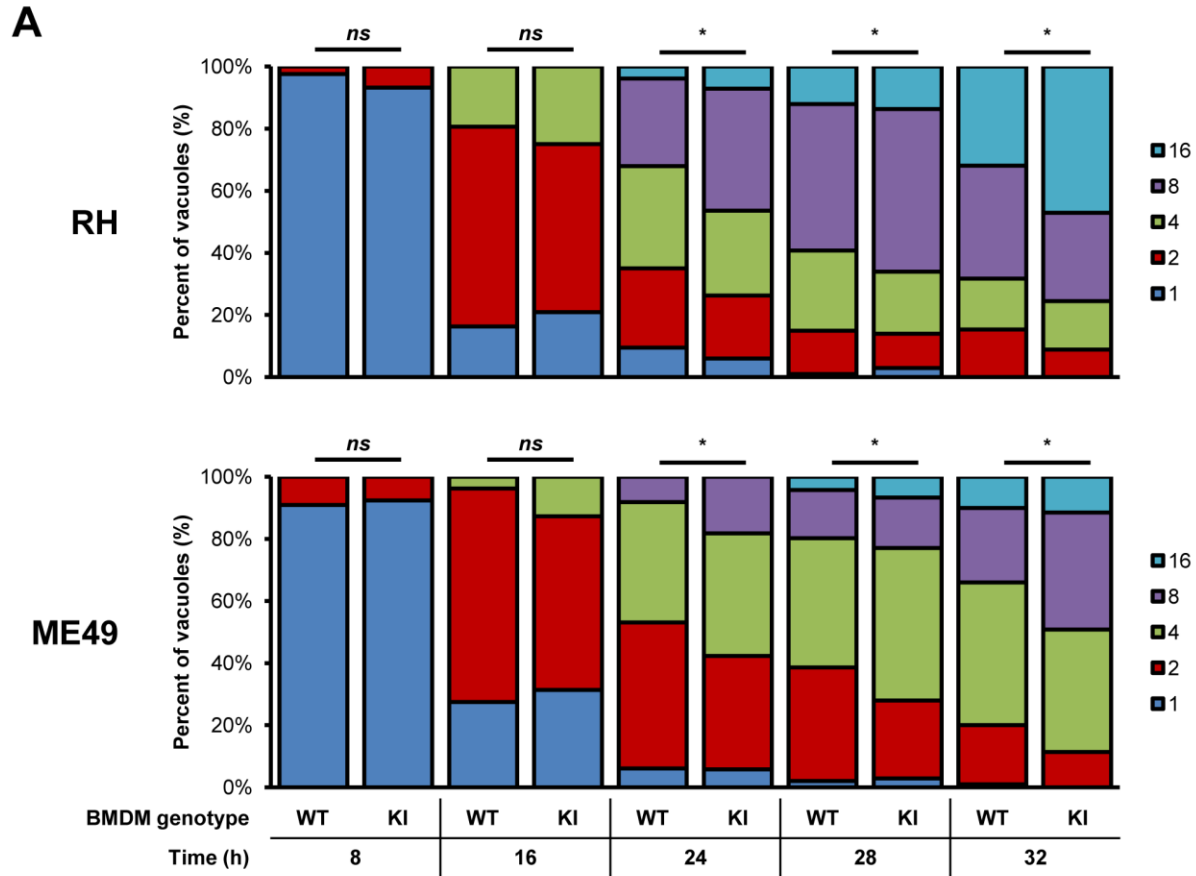
Figure 3: Genetic inhibition of eIF4E phosphorylation increases *in vitro* parasite replication, and exacerbates parasite burden and inflammation during experimental toxoplasmosis. (**A**) BMDMS differentiated from WT or eIF4E S209A KI mice were infected with RH tachyzoites for the indicated time, fixed, stained with DAPI, and mounted onto slides. The number of parasites in at least 50 vacuoles in

6282 different fields for each genotype and time point was counted by epifluorescence microscopy. Data are

6283 representative of two biological replicates; "*ns*" refers to "not significant". (**B-C**) WT and eIF4E S209A KI

6284 mice were inoculated intraperitoneally (IP) with 10^2 RH tachyzoites or PBS (mock) and euthanized 8 days

6285 post-infection. (**B**) Parasitemia in the MLN and spleen was determined by qPCR by amplification of the *T.*

6286 *gondii B1* gene. Ct values were normalized to the mouse *β-actin* gene, and values are expressed as fold-

6287 change compared to WT mice. (**C**) Serum IFNγ levels were measured by sandwich ELISA. Results are

6288 presented as mean [SD] calculated from values obtained from infected mice (two independent experiments;

6289 at least 5 mice per group); all samples were analyzed in technical triplicates; "ND" refers to "not detected".

6290

A

B
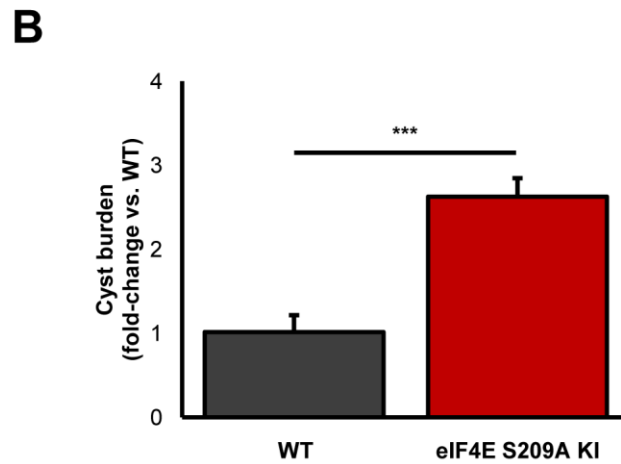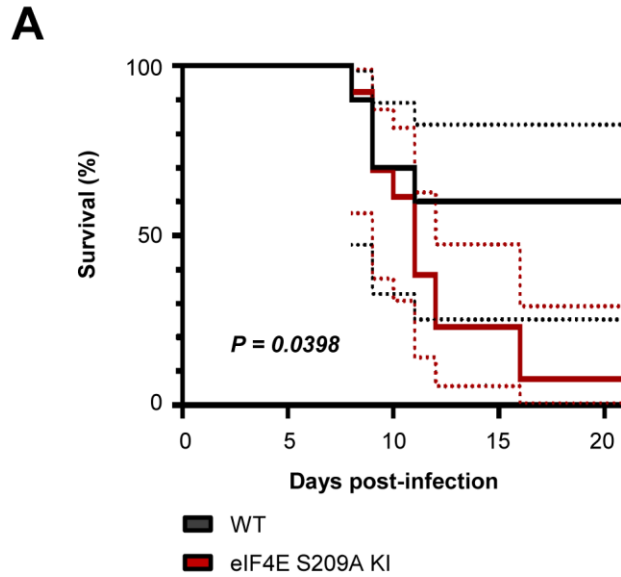
6291

6292

6293 **Figure 4: Deficiency in eIF4E phosphorylation confers higher susceptibility to experimental**

6294 **toxoplasmosis and higher brain cyst burdens**. Mice were infected IP with 10^3 ME49 tachyzoites. (**A**)

6295 Survival was monitored up to 21 days post-infection. Dashed lines represent 95% confidence intervals. (**B**)

6296 Brain cyst burden was measured by qPCR. Results are presented as mean [SD] calculated from values

6297 obtained from infected mice (two independent experiments; at least 5 mice per group; all samples were

6298 analyzed in technical triplicates.

6299
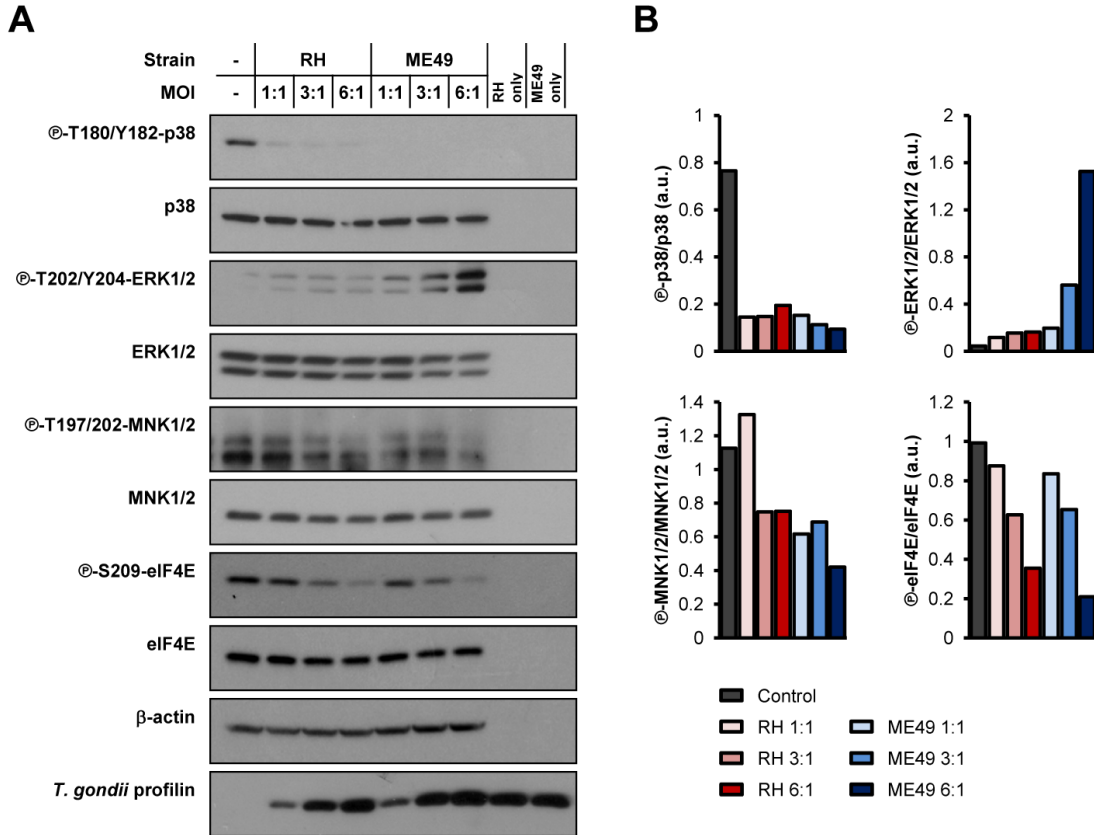
Supplementary Figure 1: Effects of different multiplicity of infection (MOI) ratios on the modulation of MNK1/2-eIF4E signaling axis in macrophages by *T. gondii*. BMDMS cultures were inoculated with either RH or ME49 at three different MOIs (1:1, 3:1, and 6:1) for 8 h. (**A**) Phosphorylation and expression levels of indicated proteins were monitored by western blotting. Total amounts of β-actin were used as a loading control and an antibody against *T. gondii* profilin-like protein was employed to assess the infection of the BMDMS cultures. Total protein extracts from extracellular tachyzoites (RH and ME49) (*Tg* only) were used to control for any cross-reactivity of the antibodies against *T. gondii* proteins. (**B**) Densitometric analysis of the phosphorylation status of indicated proteins in uninfected control and infected BMDMS cultures using FIJI. Data and data analyses are representative of two biological replicates.

A

B

RH

ME49
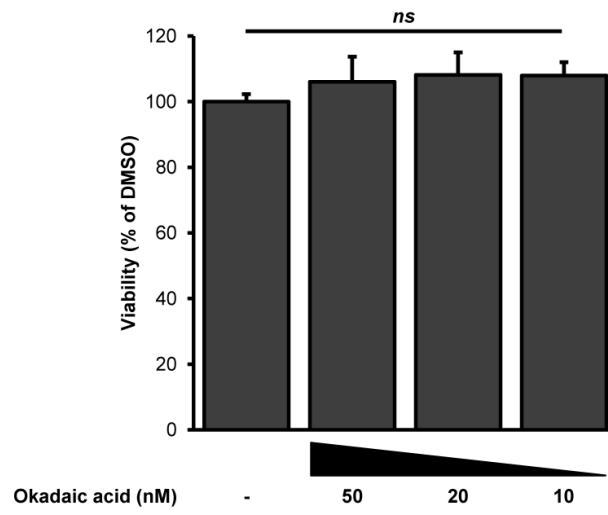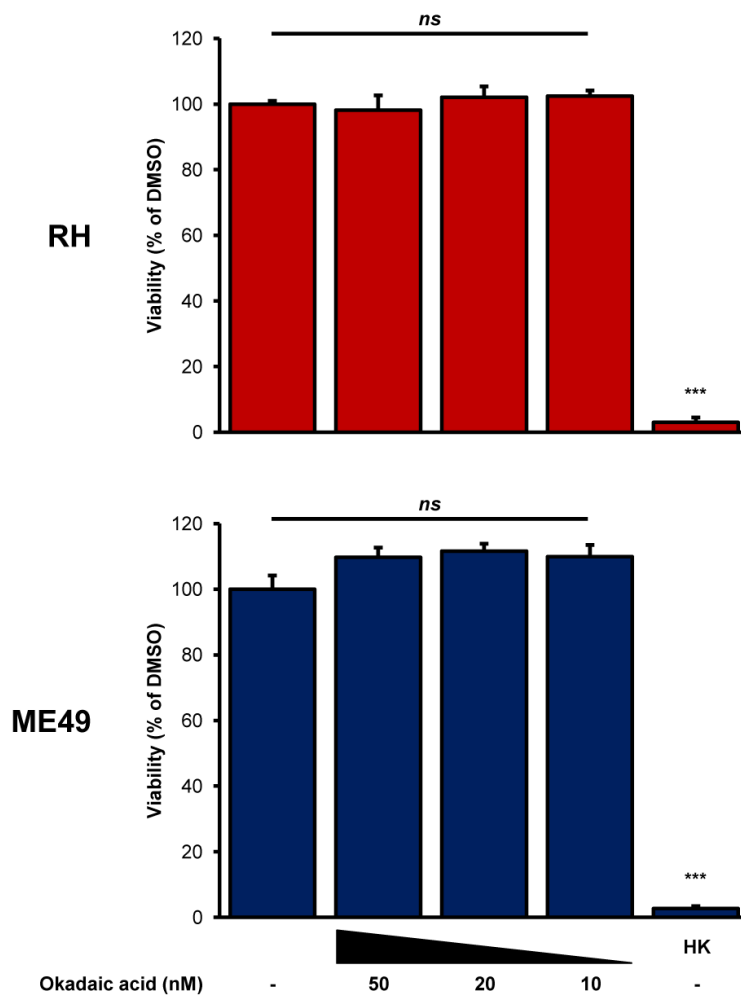
6313   **Supplementary Figure 2: Okadaic acid does not affect viability of BMDMSs and extracellular *T.***

6314   ***gondii* tachyzoites:** (**A**) BMDMS cultures and (**B**) freshly harvested tachyzoites (devoid of host cells) were

6315   treated with increasing doses of okadaic acid or DMSO (vehicle), as indicated, for 8 h at 37°C, 5% CO2.

6316   Resazurin (0.025% final) was added to the culture medium, and (**A**) BMDMS were cultured for an additional

6317   4 h while (**B**) parasites were incubated for 16 h. As a "positive kill" control, heat-killed (HK) parasites (56°C,

6318   10 min) were included. Optical density was measured at 570 and 600 nm, and values were normalized to

6319   DMSO-treated samples. Results are presented as mean [SD] and are representative of two biological

6320   replicates; all samples were performed in technical triplicates; "*ns*" refers to "not significant".

6321

A

B

| | WT | eIF4E S209A KI |

RH

ME49

C

BMDM genotype	WT	4E KI
RH	- + -	- + -
ME49	- - +	- - +

℗-T180/Y182-p38
p38
℗-T202/Y204-ERK1/2
ERK1/2
℗-T197/202-MNK1/2
MNK1/2
℗-S209-eIF4E
eIF4E
β-actin
Tg profilin

D

Control
RH
ME49
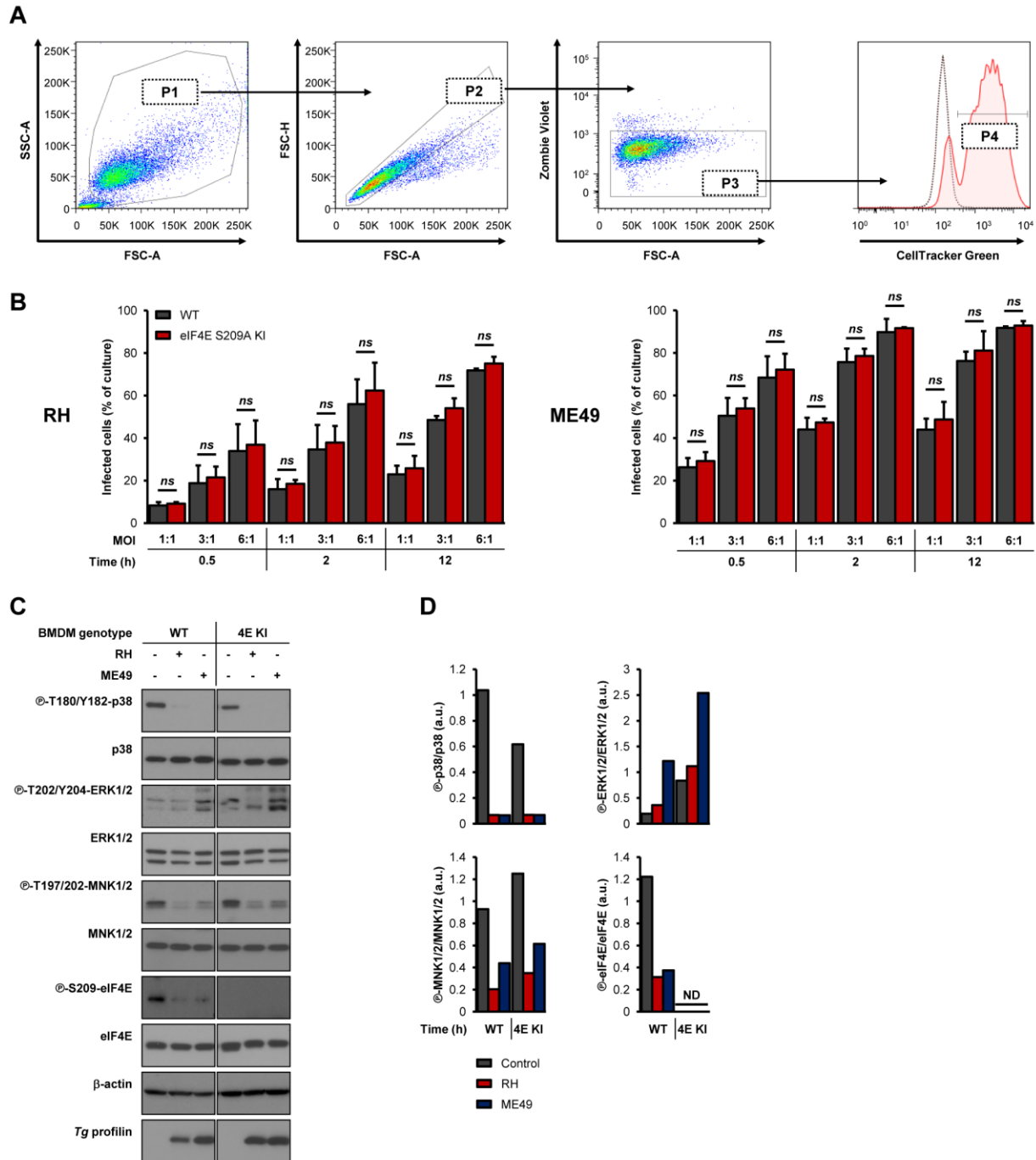
6322

Supplementary Figure 3: Infection rates and modulation of eIF4E upstream kinases by *T. gondii* do not differ between WT and eIF4E S209A KI BMDMSs: (**A-B**) WT and eIF4E S209A KI BMDMS cultures were inoculated with CellTracker Green-stained RH or ME49 parasites at three different MOIs (1:1, 3:1, and 6:1). Cultures were harvested at the indicated times, stained with the viability dye Zombie Violet (30 min, RT), then fixed with 1% PFA-PBS (15 min, on ice). Samples were analyzed by flow cytometry using a BD Fortessa. (**A**) Shown here is the gating strategy used to analyze the samples. (**B**) Results are presented

6329   as mean [SD] and are representative of two biological replicates; "*ns*" refers to "not significant". (**C-D**) WT

6330   and eIF4E S209A KI BMDMS cultures were infected with either RH or ME49 (6:1) for 8 h or left uninfected.

6331   (**C**) Phosphorylation and expression levels of indicated proteins were monitored by western blotting. Total

6332   amounts of β-actin were used as a loading control and an antibody against *T. gondii* profilin-like protein

6333   was employed to assess the infection of the BMDMS cultures. (**D**) Densitometric analysis of the

6334   phosphorylation status of indicated proteins in uninfected control and infected BMDMS cultures using FIJI.

6335   Data and data analyses are representative of two biological replicates.

References

Aguilar-Valles, A., Haji, N., De Gregorio, D., Matta-Camacho, E., Eslamizade, M.J., Popic, J., et al. (2018). Translational control of depression-like behavior via phosphorylation of eukaryotic translation initiation factor 4E. *Nat Commun* 9(1)**,** 2459. doi: 10.1038/s41467-018-04883-5.

Al-Bajalan, M.M.M., Xia, D., Armstrong, S., Randle, N., and Wastling, J.M. (2017). *Toxoplasma gondii* and *Neospora caninum* induce different host cell responses at proteome-wide phosphorylation events; a step forward for uncovering the biological differences between these closely related parasites. *Parasitol Res* 116(10)**,** 2707-2719. doi: 10.1007/s00436-017-5579-7.

Alain, T., Lun, X., Martineau, Y., Sean, P., Pulendran, B., Petroulakis, E., et al. (2010). Vesicular stomatitis virus oncolysis is potentiated by impairing mTORC1-dependent type I IFN production. *Proc Natl Acad Sci U S A* 107(4)**,** 1576-1581. doi: 10.1073/pnas.0912344107.

Amorim, I.S., Kedia, S., Kouloulia, S., Simbriger, K., Gantois, I., Jafarnejad, S.M., et al. (2018). Loss of eIF4E phosphorylation engenders depression-like behaviors via selective mRNA translation. *J Neurosci* 38(8)**,** 2118-2133. doi: 10.1523/JNEUROSCI.2673-17.2018.

Blume, M., and Seeber, F. (2018). Metabolic interactions between *Toxoplasma gondii* and its host. *F1000Res* 7. doi: 10.12688/f1000research.16021.1.

Bougdour, A., Durandau, E., Brenier-Pinchart, M.P., Ortet, P., Barakat, M., Kieffer, S., et al. (2013). Host cell subversion by Toxoplasma GRA16, an exported dense granule protein that targets the host cell nucleus and alters gene expression. *Cell Host Microbe* 13(4)**,** 489-500. doi: 10.1016/j.chom.2013.03.002.

Braun, L., Brenier-Pinchart, M.P., Yogavel, M., Curt-Varesano, A., Curt-Bertini, R.L., Hussain, T., et al. (2013). A *Toxoplasma* dense granule protein, GRA24, modulates the early immune response to infection by promoting a direct and sustained host p38 MAPK activation. *J Exp Med* 210(10)**,** 2071-2086. doi: 10.1084/jem.20130103.

6360 Buxade, M., Parra, J.L., Rousseau, S., Shpiro, N., Marquez, R., Morrice, N., et al. (2005). The Mnks are
6361   novel components in the control of TNF alpha biosynthesis and phosphorylate and regulate hnRNP
6362   A1. *Immunity* 23(2)**,** 177-189. doi: 10.1016/j.immuni.2005.06.009.

6363 Chaparro, V., Leroux, L.P., Masvidal, L., Lorent, J., Graber, T.E., Zimmermann, A., et al. (2020).
6364   Translational profiling of macrophages infected with *Leishmania donovani* identifies mTOR- and
6365   eIF4A-sensitive immune-related transcripts. *PLoS Pathog* 16(6)**,** e1008291. doi:
6366   10.1371/journal.ppat.1008291.

6367 Clough, B., and Frickel, E.M. (2017). The *Toxoplasma* parasitophorous vacuole: an evolving host-parasite
6368   frontier. *Trends Parasitol* 33(6)**,** 473-488. doi: 10.1016/j.pt.2017.02.007.

6369 Delgado Betancourt, E., Hamid, B., Fabian, B.T., Klotz, C., Hartmann, S., and Seeber, F. (2019). From
6370   entry to early dissemination-*Toxoplasma gondii*'s initial encounter with its host. *Front Cell Infect*
6371   *Microbiol* 9**,** 46. doi: 10.3389/fcimb.2019.00046.

6372 Denkers, E.Y., and Gazzinelli, R.T. (1998). Regulation and function of T-cell-mediated immunity during
6373   *Toxoplasma gondii* infection. *Clin Microbiol Rev* 11(4)**,** 569-588.

6374 Furic, L., Rong, L., Larsson, O., Koumakpayi, I.H., Yoshida, K., Brueschke, A., et al. (2010). eIF4E
6375   phosphorylation promotes tumorigenesis and is associated with prostate cancer progression. *Proc*
6376   *Natl Acad Sci U S A* 107(32)**,** 14134-14139. doi: 10.1073/pnas.1005320107.

6377 Gebauer, F., and Hentze, M.W. (2004). Molecular mechanisms of translational control. *Nat Rev Mol Cell*
6378   *Biol* 5(10)**,** 827-835. doi: 10.1038/nrm1488.

6379 Gingras, A.C., Raught, B., Gygi, S.P., Niedzwiecka, A., Miron, M., Burley, S.K., et al. (2001). Hierarchical
6380   phosphorylation of the translation inhibitor 4E-BP1. *Genes Dev* 15(21)**,** 2852-2864. doi:
6381   10.1101/gad.912401.

6382 Hakimi, M.A., Olias, P., and Sibley, L.D. (2017). *Toxoplasma* effectors targeting host signaling and
6383   transcription. *Clin Microbiol Rev* 30(3)**,** 615-645. doi: 10.1128/CMR.00005-17.

He, H., Brenier-Pinchart, M.P., Braun, L., Kraut, A., Touquet, B., Coute, Y., et al. (2018). Characterization of a *Toxoplasma* effector uncovers an alternative GSK3/beta-catenin-regulatory pathway of inflammation. *Elife* 7. doi: 10.7554/eLife.39887.

Herdy, B., Jaramillo, M., Svitkin, Y.V., Rosenfeld, A.B., Kobayashi, M., Walsh, D., et al. (2012). Translational control of the activation of transcription factor NF-kappaB and production of type I interferon by phosphorylation of the translation factor eIF4E. *Nat Immunol* 13(6)**,** 543-550. doi: 10.1038/ni.2291.

Hershey, J.W., Sonenberg, N., and Mathews, M.B. (2012). Principles of translational control: an overview. *Cold Spring Harb Perspect Biol* 4(12). doi: 10.1101/cshperspect.a011528.

Hoang, H.D., Graber, T.E., Jia, J.J., Vaidya, N., Gilchrist, V.H., Xiang, X., et al. (2019). Induction of an alternative mRNA 5' leader enhances translation of the ciliopathy gene Inpp5e and resistance to oncolytic virus Infection. *Cell Rep* 29(12)**,** 4010-4023 e4015. doi: 10.1016/j.celrep.2019.11.072.

Innes, E.A., Hamilton, C., Garcia, J.L., Chryssafidis, A., and Smith, D. (2019). A One Health approach to vaccines against *Toxoplasma gondii*. *Food Waterborne Parasitol* 15**,** e00053. doi: 10.1016/j.fawpar.2019.e00053.

Jackson, R.J., Hellen, C.U., and Pestova, T.V. (2010). The mechanism of eukaryotic translation initiation and principles of its regulation. *Nat Rev Mol Cell Biol* 11(2)**,** 113-127. doi: 10.1038/nrm2838.

Kim, L., Butcher, B.A., Lee, C.W., Uematsu, S., Akira, S., and Denkers, E.Y. (2006). "*Toxoplasma gondii* genotype determines MyD88-dependent signaling in infected macrophages", in: *J Immunol.* 2006/08/05 ed.).

Kleijn, M., Vrins, C.L., Voorma, H.O., and Thomas, A.A. (1996). Phosphorylation state of the cap-binding protein eIF4E during viral infection. *Virology* 217(2)**,** 486-494. doi: 10.1006/viro.1996.0143.

Korneeva, N.L., Song, A., Gram, H., Edens, M.A., and Rhoads, R.E. (2016). Inhibition of mitogen-activated protein kinase (MAPK)-interacting kinase (MNK) preferentially affects translation of mRNAs containing both a 5'-terminal cap and hairpin. *J Biol Chem* 291(7)**,** 3455-3467. doi: 10.1074/jbc.M115.694190.

6409   Leroux, L.P., Dasanayake, D., Rommereim, L.M., Fox, B.A., Bzik, D.J., Jardim, A., et al. (2015a). Secreted

6410   *Toxoplasma gondii* molecules interfere with expression of MHC-II in interferon gamma-activated

6411   macrophages. *Int J Parasitol* 45(5)**,** 319-332. doi: 10.1016/j.ijpara.2015.01.003.

6412   Leroux, L.P., Lorent, J., Graber, T.E., Chaparro, V., Masvidal, L., Aguirre, M., et al. (2018a). The protozoan

6413   parasite *Toxoplasma gondii* selectively reprograms the host cell translatome. *Infect Immun* 86(9).

6414   doi: 10.1128/IAI.00244-18.

6415   Leroux, L.P., Nasr, M., Valanparambil, R., Tam, M., Rosa, B.A., Siciliani, E., et al. (2018b). Analysis of the

6416   *Trichuris suis* excretory/secretory proteins as a function of life cycle stage and their

6417   immunomodulatory properties. *Sci Rep* 8(1)**,** 15921. doi: 10.1038/s41598-018-34174-4.

6418   Leroux, L.P., Nishi, M., El-Hage, S., Fox, B.A., Bzik, D.J., and Dzierszinski, F.S. (2015b). Parasite

6419   manipulation of the invariant chain and the peptide editor H2-DM affects major histocompatibility

6420   complex class II antigen presentation during *Toxoplasma gondii* infection. *Infect Immun* 83(10)**,**

6421   3865-3880. doi: 10.1128/IAI.00415-15.

6422   Li, Y., Yue, P., Deng, X., Ueda, T., Fukunaga, R., Khuri, F.R., et al. (2010). Protein phosphatase 2A

6423   negatively regulates eukaryotic initiation factor 4E phosphorylation and eIF4F assembly through

6424   direct dephosphorylation of Mnk and eIF4E. *Neoplasia* 12(10)**,** 848-855. doi: 10.1593/neo.10704.

6425   Lin, T.A., and Lawrence, J.C., Jr. (1996). Control of the translational regulators PHAS-I and PHAS-II by

6426   insulin   and   cAMP   in   3T3-L1   adipocytes.   *J   Biol   Chem*   271(47)**,**   30199-30204.   doi:

6427   10.1074/jbc.271.47.30199.

6428   Livak, K.J., and Schmittgen, T.D. (2001). Analysis of relative gene expression data using real-time

6429   quantitative   PCR   and   the   2(-Delta   Delta   C(T))   Method.   *Methods*   25(4)**,**   402-408.   doi:

6430   10.1006/meth.2001.1262.

6431   Luft, B.J., and Remington, J.S. (1992). Toxoplasmic encephalitis in AIDS. *Clin Infect Dis* 15(2)**,** 211-222.

6432   doi: 10.1093/clinids/15.2.211.

6433   Mody, P.H., Dos Santos, N.L., Barron, L.R., Price, T.J., and Burton, M.D. (2020). eIF4E phosphorylation

6434   modulates pain and neuroinflammation in the aged. *Geroscience*. doi: 10.1007/s11357-020-00220-

6435   1.

6436   Mohr, I., and Sonenberg, N. (2012). Host translation at the nexus of infection and immunity. *Cell Host*

6437   *Microbe* 12(4)**,** 470-483. doi: 10.1016/j.chom.2012.09.006.

6438   Montazeri, M., Sharif, M., Sarvi, S., Mehrzadi, S., Ahmadpour, E., and Daryani, A. (2017). A systematic

6439   review of *in vitro* and *in vivo* activities of anti-*Toxoplasma* drugs and compounds (2006-2016). *Front*

6440   *Microbiol* 8**,** 25. doi: 10.3389/fmicb.2017.00025.

6441   Montoya, J.G., and Remington, J.S. (2008). Management of *Toxoplasma gondii* infection during pregnancy.

6442   *Clin Infect Dis* 47(4)**,** 554-566. doi: 10.1086/590149.

6443   Nehdi, A., Sean, P., Linares, I., Colina, R., Jaramillo, M., and Alain, T. (2014). Deficiency in either 4E-BP1

6444   or 4E-BP2 augments innate antiviral immune responses. *PLoS One* 9(12)**,** e114854. doi:

6445   10.1371/journal.pone.0114854.

6446   Olafsson, E.B., Ten Hoeve, A.L., Li-Wang, X., Westermark, L., Varas-Godoy, M., and Barragan, A. (2020).

6447   Convergent Met and voltage-gated Ca(2+) channel signaling drives hypermigration of *Toxoplasma*-

6448   infected dendritic cells. *J Cell Sci* 134(5). doi: 10.1242/jcs.241752.

6449   Pause, A., Belsham, G.J., Gingras, A.C., Donze, O., Lin, T.A., Lawrence, J.C., Jr., et al. (1994). Insulin-

6450   dependent stimulation of protein synthesis by phosphorylation of a regulator of 5'-cap function.

6451   *Nature* 371(6500)**,** 762-767. doi: 10.1038/371762a0.

6452   Pelletier, J., Graff, J., Ruggero, D., and Sonenberg, N. (2015). Targeting the eIF4F translation initiation

6453   complex: a critical nexus for cancer development. *Cancer Res* 75(2)**,** 250-263. doi: 10.1158/0008-

6454   5472.CAN-14-2789.

6455   Piccirillo, C.A., Bjur, E., Topisirovic, I., Sonenberg, N., and Larsson, O. (2014). Translational control of

6456   immune responses: from transcripts to translatomes. *Nat Immunol* 15(6)**,** 503-511. doi:

6457   10.1038/ni.2891.

6458 Proud, C.G. (2015). Mnks, eIF4E phosphorylation and cancer. *Biochim Biophys Acta* 1849(7)**,** 766-773.

6459   doi: 10.1016/j.bbagrm.2014.10.003.

6460 Robichaud, N., del Rincon, S.V., Huor, B., Alain, T., Petruccelli, L.A., Hearnden, J., et al. (2015).

6461   Phosphorylation of eIF4E promotes EMT and metastasis via translational control of SNAIL and

6462   MMP-3. *Oncogene* 34(16)**,** 2032-2042. doi: 10.1038/onc.2014.146.

6463 Sangare, L.O., Olafsson, E.B., Wang, Y., Yang, N., Julien, L., Camejo, A., et al. (2019). *In vivo* CRISPR

6464   screen identifies TgWIP as a *Toxoplasma* modulator of dendritic cell migration. *Cell Host Microbe*

6465   26(4)**,** 478-492 e478. doi: 10.1016/j.chom.2019.09.008.

6466 Scheper, G.C., and Proud, C.G. (2002). Does phosphorylation of the cap-binding protein eIF4E play a role

6467   in translation initiation? *Eur J Biochem* 269(22)**,** 5350-5359. doi: 10.1046/j.1432-

6468   1033.2002.03291.x.

6469 Scheper, G.C., van Kollenburg, B., Hu, J., Luo, Y., Goss, D.J., and Proud, C.G. (2002). Phosphorylation of

6470   eukaryotic initiation factor 4E markedly reduces its affinity for capped mRNA. *J Biol Chem* 277(5)**,**

6471   3303-3309. doi: 10.1074/jbc.M103607200.

6472 Slepenkov, S.V., Darzynkiewicz, E., and Rhoads, R.E. (2006). Stopped-flow kinetic analysis of eIF4E and

6473   phosphorylated eIF4E binding to cap analogs and capped oligoribonucleotides: evidence for a one-

6474   step binding mechanism. *J Biol Chem* 281(21)**,** 14927-14938. doi: 10.1074/jbc.M601653200.

6475 Sonenberg, N., and Hinnebusch, A.G. (2009). Regulation of translation initiation in eukaryotes:

6476   mechanisms and biological targets. *Cell* 136(4)**,** 731-745. doi: 10.1016/j.cell.2009.01.042.

6477 Su, X., Yu, Y., Zhong, Y., Giannopoulou, E.G., Hu, X., Liu, H., et al. (2015). Interferon-gamma regulates

6478   cellular metabolism and mRNA translation to potentiate macrophage activation. *Nat Immunol* 16(8)**,**

6479   838-849. doi: 10.1038/ni.3205.

6480 Ueda, T., Watanabe-Fukunaga, R., Fukuyama, H., Nagata, S., and Fukunaga, R. (2004). Mnk2 and Mnk1

6481   are essential for constitutive and inducible phosphorylation of eukaryotic initiation factor 4E but not

6482   for cell growth or development. *Mol Cell Biol* 24(15)**,** 6539-6549. doi: 10.1128/MCB.24.15.6539-
6483   6549.2004.

6484 Volpon, L., Osborne, M.J., and Borden, K.L.B. (2019). "Biochemical and structural insights into the
6485   eukaryotic translation initiation factor eIF4E", in: *Curr Protein Pept Sci.* 2019/01/15 ed.).

6486 Walsh, D., Mathews, M.B., and Mohr, I. (2013). Tinkering with translation: protein synthesis in virus-infected
6487   cells. *Cold Spring Harb Perspect Biol* 5(1)**,** a012351. doi: 10.1101/cshperspect.a012351.

6488 Walsh, D., and Mohr, I. (2004). Phosphorylation of eIF4E by Mnk-1 enhances HSV-1 translation and
6489   replication in quiescent cells. *Genes Dev* 18(6)**,** 660-672. doi: 10.1101/gad.1185304.

6490 Wang, Y., Weiss, L.M., and Orlofsky, A. (2010). Coordinate control of host centrosome position, organelle
6491   distribution, and migratory response by *Toxoplasma gondii* via host mTORC2. *J Biol Chem* 285(20)**,**
6492   15611-15618. doi: 10.1074/jbc.M109.095778.

6493 Waskiewicz, A.J., Flynn, A., Proud, C.G., and Cooper, J.A. (1997). Mitogen-activated protein kinases
6494   activate the serine/threonine kinases Mnk1 and Mnk2. *EMBO J* 16(8)**,** 1909-1920. doi:
6495   10.1093/emboj/16.8.1909.

6496 William, M., Leroux, L.P., Chaparro, V., Graber, T.E., Alain, T., and Jaramillo, M. (2019). Translational
6497   repression of *Ccl5* and *Cxcl10* by 4E-BP1 and 4E-BP2 restrains the ability of mouse macrophages
6498   to induce migration of activated T cells. *Eur J Immunol*. doi: 10.1002/eji.201847857.

6499 Xie, J., Merrett, J.E., Jensen, K.B., and Proud, C.G. (2019). The MAP kinase-interacting kinases (MNKs)
6500   as targets in oncology. *Expert Opin Ther Targets* 23(3)**,** 187-199. doi:
6501   10.1080/14728222.2019.1571043.

6502 Xu, H., Zhu, J., Smith, S., Foldi, J., Zhao, B., Chung, A.Y., et al. (2012). Notch-RBP-J signaling regulates
6503   the transcription factor IRF8 to promote inflammatory macrophage polarization. *Nat Immunol* 13(7)**,**
6504   642-650. doi: 10.1038/ni.2304.

6505 Yang, C., and Arrizabalaga, G. (2017). The serine/threonine phosphatases of apicomplexan parasites. *Mol*
6506   *Microbiol* 106(1)**,** 1-21. doi: 10.1111/mmi.13715.

6507   Yang, Z., Hou, Y., Hao, T., Rho, H.S., Wan, J., Luan, Y., et al. (2017). A human proteome array approach

6508   to identifying key host proteins targeted by *Toxoplasma* kinase ROP18. *Mol Cell Proteomics* 16(3)**,**

6509   469-484. doi: 10.1074/mcp.M116.063602.

6510   Zakaria, C., Sean, P., Hoang, H.D., Leroux, L.P., Watson, M., Workenhe, S.T., et al. (2018). Active-site

6511   mTOR inhibitors augment HSV1-dICP0 infection in cancer cells via dysregulated eIF4E/4E-BP

6512   axis. *PLoS Pathog* 14(8)**,** e1007264. doi: 10.1371/journal.ppat.1007264.

6513   Zuberek, J., Jemielity, J., Jablonowska, A., Stepinski, J., Dadlez, M., Stolarski, R., et al. (2004). Influence

6514   of electric charge variation at residues 209 and 159 on the interaction of eIF4E with the mRNA 5'

6515   terminus. *Biochemistry* 43(18)**,** 5370-5379. doi: 10.1021/bi030266t.

6516   Zuberek, J., Wyslouch-Cieszynska, A., Niedzwiecka, A., Dadlez, M., Stepinski, J., Augustyniak, W., et al.

6517   (2003). Phosphorylation of eIF4E attenuates its interaction with mRNA 5' cap analogs by

6518   electrostatic repulsion: intein-mediated protein ligation strategy to obtain phosphorylated protein.

6519   *RNA* 9(1)**,** 52-61. doi: 10.1261/rna.2133403.

6520

6521

6522

6523

6524

Appendix 4

6525 **The protozoan parasite *Toxoplasma gondii* selectively reprograms the host cell translatome**

6526

6527 Louis-Philippe Leroux[a, b], Julie Lorent[c,¶] Tyson E. Graber[d,¶], Visnu Chaparro[a, b], Laia Masvidal[c], Maria

6528 Aguirre[e], Bruno D. Fonseca[d], Léon C. van Kempen[e, f, g], Tommy Alain[d], Ola Larsson[c], Maritza Jaramillo[a, b,#]

6529

6530 [a]Institut National de la Recherche Scientifique (INRS) - Institut Armand-Frappier (IAF), Laval, Quebec,

6531 Canada

6532 [b]Centre for Host-Parasite Interactions, INRS-IAF, Laval, Quebec, Canada

6533 [c]Department of Oncology-Pathology, Science for Life Laboratory, Karolinska Institutet, Stockholm, Sweden

6534 [d]Children's Hospital of Eastern Ontario Research Institute, Department of Biochemistry, Microbiology and

6535 Immunology, University of Ottawa, Ottawa, Ontario, Canada

6536 [e]Lady Davis Institute, Jewish General Hospital, Montreal, Quebec, Canada

6537 [f]Department of Pathology, McGill University, Montreal, Quebec, Canada

6538 [g]Department of Pathology and Medical Biology, University Medical Centre Groningen, The Netherlands

6539

6540 [¶]These authors equally contributed to this work

6541 [#]Correspondence should be addressed to: maritza.jaramillo@iaf.inrs.ca

6542 INRS - Institut Armand Frappier, 531 boul. des Prairies, Laval, Quebec, H7V 1B7, Canada

6543 Tel.: +1 (450) 687-5010 ext. 8872; fax: +1 (450) 686-5566

6544 **Running Title**: Dysregulation of host mRNA translation by *T. gondii*

6546

Abstract

6547

6548   The intracellular parasite *Toxoplasma gondii* (*T. gondii*) promotes infection by targeting multiple

6549   host cell processes; however, whether it modulates mRNA translation is currently unknown. Here, we show

6550   that infection of primary murine macrophages with type I or II *T. gondii* strains causes a profound

6551   perturbation of the host cell translatome. Notably, translation of transcripts encoding proteins involved in

6552   metabolic activity and components of the translation machinery was activated upon infection. In contrast,

6553   translational efficiency of mRNAs related to immune cell activation and cytoskeleton/cytoplasm organization

6554   was largely suppressed. Mechanistically, *T. gondii* bolstered mTOR signaling to selectively activate

6555   translation of mTOR-sensitive mRNAs, including those with a 5' terminal oligopyrimidine (5' TOP) motif and

6556   those encoding mitochondrion-related proteins. Consistent with parasite modulation of host mTOR-

6557   sensitive translation to promote infection, inhibition of mTOR activity suppressed *T. gondii* replication. Thus,

6558   selective reprogramming of host mRNA translation represents an important subversion strategy during *T.*

6559   *gondii* infection.

6560

Introduction

6561

6562   *Toxoplasma gondii* (*T. gondii*), the causative agent of toxoplasmosis, is an obligate intracellular

6563   protozoan parasite that invades virtually all nucleated cells (Dubey 2004) and infects a remarkably diverse

6564   range of vertebrate hosts, including humans and mice (Dubey, Miller et al. 1970, Frenkel, Dubey et al.

6565   1970). Although toxoplasmosis is generally asymptomatic, reactivation of encysted parasites can lead to

6566   deleterious consequences in immunosuppressed individuals (Luft and Remington 1992, Dubey 2004).

6567   Furthermore, congenital toxoplasmosis can cause spontaneous abortion or severe birth defects (Montoya

6568   and Remington 2008). To replicate, *T. gondii* hijacks host cell organelles and scavenges nutrients (Laliberte

6569   and Carruthers 2008, Hakimi, Olias et al. 2017). In addition, the parasite targets signaling pathways and

6570   affects host cell transcription to subvert immune functions, promote host cell survival, and modulate host

6571   cell processes to favor its own replication (Hunter and Sibley 2012, Hakimi and Bougdour 2015, Hakimi,

6572   Olias et al. 2017). Despite this body of evidence, how *T. gondii* modulates host cell protein synthesis

6573   remains unknown.

6574   Translational control allows cells to rapidly change their proteome to respond to external triggers

6575   or other cues without *de novo* mRNA synthesis (Gebauer and Hentze 2004, Sonenberg and Hinnebusch

6576   2009). In fact, modulation of translational efficiency represents a critical mechanism in a plethora of

6577   biological processes such as cell differentiation, metabolism, growth, and proliferation (Gebauer and

6578   Hentze 2004, Schneider 2007, Hershey, Sonenberg et al. 2012, Lasko 2012). Accordingly, dysregulation

6579   of mRNA translation is a hallmark of various types of cancer (Silvera, Formenti et al. 2010, Ruggero 2013)

6580   and other clinical disorders such as inflammatory airway pathologies (Ezegbunam and Foronjy 2018),

6581   fibrosis (Parker, Rossi et al. 2014), and neurodegenerative diseases (Roffe, Beraldo et al. 2010, Moreno,

6582   Radford et al. 2012, Ma, Trinh et al. 2013, Bellato and Hajj 2016). In eukaryotes, translation is mainly

6583   regulated at the initiation step during which ribosomes are recruited to the mRNA, a process which can be

6584   modulated via multiple mechanisms. For instance, the association of mRNAs to RNA-binding proteins

6585   (Garcia-Maurino, Rivero-Rodriguez et al. 2017), and the presence of features including the 5'-terminal

6586   oligopyrimidine motif (5' TOP) (Meyuhas and Kahan 2015) or structured sequence motifs within the 5'

6587   untranslated region (UTR) of mRNA (Hinnebusch, Ivanov et al. 2016) represent regulatory mechanisms

6588   selectively influencing translational efficiency. Notably, ribosome recruitment is facilitated by recognition of

6589   the mRNA 5'-m^{7}G-cap structure by eukaryotic initiation factor 4E (eIF4E), which, together with scaffold

6590   protein eIF4G and RNA helicase eIF4A, form the eIF4F complex (Gingras, Gygi et al. 1999). Assembly of

6591   the eIF4F complex is prevented by eIF4E-binding proteins (4E-BPs), which blocks eIF4E:eIF4G interaction

6592   and eIF4F formation (Pause, Belsham et al. 1994, Lin, Kong et al. 1995). Hyper-phosphorylation of 4E-BPs

6593   by the serine/threonine kinase mechanistic target of rapamycin (mTOR) complex 1 (mTORC1) leads to a

6594   reduction of 4E-BPs' affinity to eIF4E, which favors eIF4E:eIF4G interaction and initiation of translation

6595   (Gingras, Raught et al. 2001). Thus, signaling through the mTORC1 axis is pivotal for translational control.

6596   Regulation of mRNA translation efficiency is required for normal immune functions (Piccirillo, Bjur

6597   et al. 2014) and is altered during infection (Mohr and Sonenberg 2012, Walsh, Mathews et al. 2013).

6598   mTORC1 and its downstream targets 4E-BP1/4E-BP2 and S6K1/S6K2 are key components of the innate

6599   immune response (Kaur, Lal et al. 2007, Cao, Manicassamy et al. 2008, Costa-Mattioli and Sonenberg

6600   2008, Alain, Lun et al. 2010, Nehdi, Sean et al. 2014). Accordingly, alterations in mTORC1 signaling are

6601   linked to subversion of host mRNA translation by viruses (Spangle and Munger 2010, Clippinger, Maguire

6602   et al. 2011), bacteria (Chakrabarti, Liehl et al. 2012, Sokolova, Vieth et al. 2014), and the protozoan parasite

6603   *Leishmania major* (Jaramillo, Gomez et al. 2011).

6604   With regards to toxoplasmosis, translational control has only been assessed in the parasite

6605   (Hassan, Vasquez et al. 2017, Holmes, Augusto et al. 2017); however, how the parasite modulates host

6606   cell translation is unknown. Here, we report that *T. gondii* selectively reprograms the translational landscape

6607   of the host cell to promote its replication. Through a non-biased approach (i.e., transcriptome-wide

6608   polysome-profiling), we identified a large number of transcripts whose translation efficiency is modulated

6609   upon infection (i.e., activated or repressed). In addition, we show that selective activation of host mRNA

6610   translation by *T. gondii* is mTOR-sensitive and is associated with the presence of distinct motifs in the 5'

6611   UTR of identified transcripts. Accordingly, inhibition of mTOR activity dampens parasite replication. Overall,

6612   this study provides evidence that selective regulation of host mRNA translation contributes to *T. gondii*

6613   survival.

Results

Toxoplasma gondii increases protein synthesis in infected macrophages

During infectious diseases, translational control can act as a host defense mechanism but also be exploited by the invading pathogen as a survival strategy (Mohr and Sonenberg 2012, Walsh, Mathews et al. 2013, Piccirillo, Bjur et al. 2014). To explore these possibilities during _T. gondii_ infection, we inoculated bone marrow-derived murine macrophages (BMDMS) with RH (type I) or ME49 (type II) strains and assessed their effects on global protein synthesis by comparing the amount of monosomes (inefficient translation) and heavy polysomes (efficient translation) as observed from polysome-tracings. This approach revealed an increase in heavy polysomes with a concomitant decrease in monosomes in _T. gondii_-infected cells (**Fig 1A**, left panel). The normalized absorbance (254 nm) ratio between heavy polysomes and monosomes indicated that type I and II strains enhance host cell protein synthesis to a similar extent (RH = 1.59 [0.19] and ME49 = 1.60 [0.11] mean fold-change over uninfected control [SD]) (**Fig 1A**, right panel). These observed differences did not result from a contaminating signal originating from the parasite as polysome-tracings from _T. gondii_ tachyzoites alone were barely detected (**Fig S1A**). Thus, _T. gondii_ infection leads to increased macrophage protein synthesis.

T. gondii infection causes selective modulation of host cell translation

The increased amount of mRNA associated with heavy polysomes following parasite infection is consistent with parasite-induced mRNA-selective and/or global changes in host cell translational efficiency. To resolve selective regulation of translational efficiency, we used polysome-profiling quantified by RNA-Seq (**Fig 1B**). During polysome-profiling, both efficiently translated mRNA (herein defined as mRNA associated with > 3 ribosomes) and cytosolic mRNA (input) are isolated and quantified. As altered cytosolic mRNA levels will lead to corresponding changes in polysome-associated mRNA even without modulation of translational efficiency, differences in polysome-associated mRNA levels require adjustment for changes in cytosolic mRNA levels to identify _bona fide_ changes in translational efficiency. Here, we used the _anota_ (analysis of translational activity) algorithm for this purpose (Larsson, Sonenberg et al. 2011). Polysome-profiling coupled with _anota_ analysis from uninfected, and RH- or ME49-infected BMDMS revealed widespread selective alterations in translational efficiency upon infection with either strain (**Fig 1C**). In total, 322 and 625 mRNAs showed activated and repressed translational efficiency, respectively, in response to either strain (FDR $\leq$ 0.25; **Fig 1D** and **Table S1**). In contrast, only 51 targets showed translational efficiencies modulated differently between RH and ME49 strains (**Fig S1B** and **Table S1**). We selected 220 targets regulated via translation and 30 non-regulated genes for validation using a custom-designed nCounter codeset from Nanostring Technologies (**Table S2**). Targets were selected based on biological functions of the encoded proteins that were of particular interest (e.g. cell death, metabolism, immune response, and translation). In addition, expression level (similar numbers of low, intermediate, and high levels of polysome-associated mRNAs) and proportions for directionality of translational regulation (~1/3 up- and ~2/3 down-regulated) were also considered as selection criteria. Changes in translational efficiency

274

6651   as estimated by RNA-Seq and nCounter assays were highly correlated (RH vs. Control Spearman rank

6652   correlation ρ = 0.76; ME49 vs. Control ρ = 0.76; RH vs. ME49 ρ = 0.56) (**Fig S1C**). Accordingly, mRNAs

6653   identified as translationally activated or repressed using RNA-Seq largely showed consistent directionality

6654   of regulation. Thus, both *T. gondii* strains induce abundant and similar selective changes in host cell

6655   translational efficiency.

6656

6657   **_T. gondii_ selectively reprograms translation of mRNAs encoding proteins involved in protein**

6658   **synthesis, cell activation, and cytoskeleton/cytoplasm organization**

6659   To identify functional classes enriched for translationally-regulated host mRNAs and to predict

6660   biological processes consequently affected during *T. gondii* infection, we used Ingenuity Pathway Analysis

6661   (IPA) (Kramer, Green et al. 2014). Within the *Molecular & Cellular Functions* IPA classification, several

6662   functional networks were significantly enriched (FDR < 0.05) among proteins encoded by mRNAs whose

6663   translation was altered during *T. gondii* infection relative to background (all mRNAs detected by RNA-Seq

6664   above) (**Fig 2A** and **Table S3**). The enriched categories include mRNAs involved in translation, organization

6665   of cytoskeleton and cytoplasm, cell activation, and cell movement. Globally, translational efficiencies of

6666   targets that belong to these categories displayed a similar directionality of regulation by RH and ME49 (**Fig**

6667   **2B**). Within the *Translation* category, all mRNAs encoding ribosomal proteins were translationally-activated.

6668   Conversely, targets grouped in the *Organization of cytoplasm and cytoskeleton* were generally repressed.

6669   These transcripts encode proteins involved in membrane dynamics, microtubule-based movement,

6670   organelle formation and organization, and vesicular trafficking (e.g. dyneins *Dync1H1* and *Dync2H1*;

6671   kinesins *Kif11* and *Kif3A*; and myosins *Myh10*, *Myo6*, *Myo7A*, *Myo10*, and *Myo18A*). Within the category

6672   *Activation of cells*, translational efficiencies of some mRNAs related to cell movement and chemotaxis were

6673   activated (chemokines *Ccl5* and *Ccl9*) while others were repressed (chemokine receptors *Ccr2*, *Ccr5*,

6674   *CxcCr1*; and matrix metalloproteases *Mmp9* and *13*). Although not classified in this category by IPA, *Mmp8*,

6675   *Mmp11*, and *Mmp12* were also identified as translationally down-regulated upon infection (**Table S1**).

6676   Notably, mRNAs encoding immune cell activators were largely repressed (CD molecules *Cd2*, *Cd93*, and

6677   *Cd180*; interleukin receptors *Il2Rb1*, *Il18Rap*, and *Il6Ra*; and integrins *Itgam* and *Itgav*). In stark contrast,

6678   transcripts involved in immune suppression and negative regulation of inflammation (e.g. *Cd200* and *Il1Ra*)

6679   were more efficiently translated in infected cells (**Fig 2B**). Interestingly, translational repression of

6680   transcripts promoting cell death was concomitant with translational activation of anti-apoptotic and cell-

6681   cycle progression regulators. For instance, negative regulator of cell differentiation *Notch2* and pro-

6682   apoptotic transcription factor *Foxo3a* were decreased, whereas anti-apoptotic and positive regulators of

6683   cell-cycle progression and macrophage differentiation were enhanced (e.g. *Bcl2A1D* and *Hbegf*) (**Fig 2B**).

6684   Consistent with this, other negative regulators of cell proliferation and differentiation (*Bcl6* and *Notch 4*)

6685   were also translationally repressed (**Table S1**). Thus, *T. gondii* appears to selectively modulate translational

6686   efficiencies of host mRNAs favoring survival of infected cells while reorganizing host cell architecture and

6687   preventing deleterious immune responses.

T. gondii infection selectively activates mTOR-sensitive translation

6688

6689   We next assessed whether altered selective translation following parasite infection could be linked

6690   to distinct 5' UTR features. To this end, we first calculated 5' UTR GC content and length of non-redundant

6691   mouse 5' UTRs collected in the Refseq database (O'Leary, Wright et al. 2016). While no significant

6692   differences in GC content were observed (**Fig S2A**), mRNAs translationally activated upon parasite

6693   infection had significantly shorter 5' UTRs as compared to background (all Refseq mouse 5' UTRs) (**Fig**

6694   **3A**). Secondly, we searched for sequence motifs using MEME (Bailey, Johnson et al. 2015). This analysis

6695   identified a contiguous pyrimidine-rich (CU) motif (E = 2.6×10^{-18}) within 223 out of the 322 mRNAs showing

6696   activated translation (**Fig 3B** and **Table S4**); and a GC-rich stretch (E = 2.1×10^{-215}) in 314 out of the 625

6697   translationally suppressed transcripts (**Fig S2B** and **Table S4**). Interestingly, the CU-motif has some

6698   resemblance to the 5' TOP motif (CY_n) [$n \geq 4$], where Y represents a pyrimidine nucleoside (Levy, Avni et

6699   al. 1991). TOP-containing mRNAs encode ribosomal proteins and factors for translation initiation and

6700   elongation (eIFs and eEFs) whose translational efficiency is sensitive to mTOR activity (Miloslavski, Cohen

6701   et al. 2014, Gandin, Masvidal et al. 2016, Masvidal, Hulea et al. 2017). Indeed, translation of TOP mRNAs

6702   was selectively activated following infection with both parasite strains (RH and ME49 vs. Control p < 0.001;

6703   **Fig 3C** and **3D**, and **Table S5**). In contrast, translational efficiency of IRES-containing mRNAs was largely

6704   unaffected upon +infection (**Fig 3D** and **Table S5**). In addition to TOP mRNAs, transcripts with short 5'

6705   UTRs whose translation is also mTOR-dependent but does not require a 5' TOP motif, such as those

6706   encoding mitochondrion-related proteins (Gandin, Masvidal et al. 2016), were translationally activated in

6707   infected cells (i.e., mRNAs related to mitochondrial translation, electron transport chain, mitochondrial

6708   respiratory chain, and mitochondrial proton-transporting ATP synthase complex) (**Fig 3E** and **Table S5**).

6709   Data above indicate that increased mTOR activity underlies a substantial proportion of parasite-

6710   induced changes in the translatome. To directly assess this, we used a previously published translation

6711   signature (Larsson, Morita et al. 2012), consisting of mRNAs whose translation efficiency is suppressed

6712   following mTOR inhibition (using PP242 in the breast carcinoma cell line MCF-7). Indeed, infection with

6713   either strain was associated with selectively activated translation of such mTOR-sensitive mRNAs (RH and

6714   ME49 vs. Control p < 0.001; **Fig 3F** and **Table S5**). Altogether, these data suggest that _T. gondii_ selectively

6715   augments mTOR-sensitive translation in BMDMS.

6716

T. gondii infection increases host mTORC1 activity in BMDMS

6717

6718   Translation of mRNAs whose translational efficiency parallels mTOR activity was enhanced in _T._

6719   _gondii_-infected macrophages. Therefore, we next determined mTORC1 kinase activity by assessing

6720   phosphorylation of its downstream targets, S6K1/S6K2 and 4E-BP1/4E-BP2. Of note, parasite extracts (i.e.,

6721   devoid of any host cell; "_Tg only_") were probed in parallel to rule out the possibility that observed changes

6722   in mTORC1 signaling were due to cross-reactivity of the antibodies against parasite proteins (**Fig 4A**).

6723   Phosphorylation of S6K1 (T389) and levels of S6K2 were increased in BMDMS infected with either the RH

6724   or ME49 strains (**Fig 4A**). Accordingly, phosphorylation of the downstream target of S6K1/S6K2, ribosomal

protein (RP) S6 (S235, S236, S240, and S244), was augmented, and required active invasion without noticeable by-stander effects (**Fig S3A**). Phosphorylation of RPS6 in infected cells was completely abrogated in S6K1$^{-/-}$/S6K2$^{-/-}$ BMDMS, confirming that this cellular response is S6K1/S6K2-dependent (**Fig S3B**). In addition, the hierarchical phosphorylation of 4E-BP1/4E-BP2 (i.e., T37/46, T70, and S65) was induced in *T. gondii*-infected BMDMS with similar kinetics for the two strains (**Fig 4A**). Hyper-phosphorylation of 4E-BP1/4E-BP2 was also evident by a mobility shift on SDS-PAGE and increased amounts of the gamma (γ) form as compared to α and β forms. The hyper-phosphorylated forms of 4E-BP1/4E-BP2 have lower affinity for the mRNA 5'-m^{7}G-cap-binding protein eIF4E (Gingras, Raught et al. 2001). Consistently, m^{7}GTP pull-down assays revealed a reduced interaction between 4E-BP1/4E-BP2 and m^{7}GTP-bound eIF4E in *T. gondii*-infected BMDMSs (**Fig 4B** and **4C**). Treatment with Torin-1, an active-site TOR inhibitor (asTORi) (Thoreen, Kang et al. 2009), resulted in complete dephosphorylation of 4E-BP1/4E-BP2 and strong binding to m^{7}GTP-bound eIF4E regardless of the infection status of the host cell (**Fig 4B**). In summary, *T. gondii* activates mTORC1 signaling and promotes dissociation of 4E-BP1/4E-BP2 from cap-bound eIF4E in BMDMS.

Next, we aimed to elucidate upstream events activating mTORC1 during *T. gondii* infection. To this end, we assessed the contribution of AKT, which phosphorylates and inactivates the mTORC1 repressor TSC2 (Laplante and Sabatini 2009). Pretreatment with a pan-AKT inhibitor, MK-2206 (Hirai, Sootome et al. 2010), partially decreased phosphorylation of RPS6 and 4E-BP1 (**Fig S3C**). In light of these results, we monitored mTORC1 activity in *T. gondii*-infected BMDMS deprived of L-leucine, an amino acid whose intracellular levels regulate mTORC1 in an AKT-independent fashion (Jewell, Kim et al. 2015). Simultaneous pharmacological inhibition of AKT and L-leucine starvation abrogated RPS6 and 4E-BP1 phosphorylation in *T. gondii*-infected BMDMS (**Fig S3C**). Altogether, these data suggest that activation of mTORC1 in *T. gondii*-infected BMDMS relies on both AKT-dependent and -independent mechanisms.

Inhibition of mTOR reverses *T. gondii*-induced activation of host mRNA translation and dampens parasite replication

To further assess whether changes in translational efficiency observed in *T. gondii*-infected cells depend on mTOR, polysome-tracings were generated from BMDMS treated with rapamycin, an allosteric mTORC1 inhibitor, or Torin-1. Rapamycin induced a similar shift from heavy polysomes to monosomes in RH- and ME49-infected BMDMS (48.3% and 37.2% reduction, respectively) (**Fig 5A** and **5B**). As expected, Torin-1 exerted a more dramatic effect than rapamycin (RH = 62.2%; ME49 = 62.5%), owing to its greater potency (Thoreen, Kang et al. 2009). Of note, no differences in infection rates and no acute toxicity was observed on parasites exposed to the inhibitors (**Fig S4**). While rapamycin and Torin-1 abrogated phosphorylation of S6K1 (T389) and its downstream target RPS6 (S235, 236, 240, and 244) in *T. gondii*-infected BMDMS, only Torin-1 completely abolished 4E-BP1/4E-BP2 phosphorylation (as described previously (Dowling, Topisirovic et al. 2010)) (**Fig 5C**). To evaluate whether chemical inhibition of mTOR is sufficient to reverse the translation program induced following parasite infection, we performed polysome-

6762   profiling quantified by nCounter assays (same targets as described above, **Table S2**) in *T. gondii*-infected

6763   and uninfected BMDMSs treated with rapamycin or Torin-1. We next assessed how fold-changes in

6764   polysome-associated and cytosolic mRNA (for the subset of mRNAs translationally-activated upon infection

6765   by either RH or ME49) were affected in cells treated with rapamycin or Torin-1. This approach revealed that

6766   chemical inhibition of mTOR is sufficient to largely reverse effects on selective translation induced during

6767   parasite infection (**Fig 5D** and **Table S6**).

6768   As parasite infection appears to profoundly affect host cell properties essential for synthesis of

6769   biomolecules and growth by perverting host mTOR-sensitive mRNA translation, we hypothesized that

6770   upregulation of mTOR activity constitutes a parasite survival strategy. To test this, BMDMS were pre-treated

6771   with either rapamycin or Torin-1 and infected with either RH or ME49 *T. gondii* tachyzoites. Parasites were

6772   allowed to egress and re-infect new host cells for 72 h, after which parasite numbers were evaluated by

6773   qPCR. Rapamycin treatment had a modest effect on parasite proliferation (12.8% and 19.5% reduction for

6774   RH and ME49, respectively) while Torin-1 caused a more pronounced reduction in replication (57.1% and

6775   55.1%) compared to DMSO treatment (**Fig 5E**). These data indicate that *T. gondii* relies on augmenting

6776   mTOR activity for unhindered replication.

6777

Discussion

Translational control of gene expression is a central mechanism of host defense (Mohr and Sonenberg 2012, Walsh, Mathews et al. 2013). As such, pathogens hijack the host translation machinery to survive (Mohr and Sonenberg 2012, Walsh, Mathews et al. 2013). Using transcriptome-wide polysome-profiling, we demonstrate that the protozoan parasite *T. gondii* selectively augments mTOR-sensitive translation to favor host cell survival and parasite replication. Type I and II *T. gondii* strains regulate mTOR activity and mRNA translation in a similar fashion, suggesting that this is a core process needed for parasite propagation that does not depend on strain-specific virulence factors. Further supporting the notion that regulation of mTOR-sensitive mRNA translation constitutes a parasite survival strategy, mTOR inactivation dampened *T. gondii* replication.

Our data on activation of mTOR signaling are consistent with a recent analysis of the phospho-proteome of *T. gondii*-infected HFF showing an enrichment of phosphorylated proteins both up- and downstream of mTOR, including RPS6 and 4E-BP1 (Al-Bajalan, Xia et al. 2017). Interestingly, Wang and colleagues had previously reported that the phosphorylation of S6K1 following *T. gondii* infection was not consistently observed in different host cell lines (HFF, 3T3, HeLa) (Wang, Weiss et al. 2009, Wang, Weiss et al. 2009)-(Wang, Weiss et al. 2010). In some cases no increased or prolonged phosphorylation of S6K1was observed (Wang, Weiss et al. 2009, Wang, Weiss et al. 2009) while in others sustained and augmented phosphorylation was detected (Wang, Weiss et al. 2010). To resolve S6K-dependent phosphorylation of S6 in our experimental setting, we combined a chemical approach (i.e., mTOR inhibitors) and a genetic approach (i.e., BMDMS derived from *s6k1/s6k2* DKO mice) that confirmed the requirement for S6K1 and S6K2 activity for RPS6 phosphorylation in *T. gondii*-infected macrophages. Our results showing inducible and sustained phosphorylation of 4E-BP1 following infection are also in sharp contrast to those of Wang and colleagues, who reported the absence of this phenomenon in *T. gondii*-infected 3T3 and HeLa cells (Wang, Weiss et al. 2009, Wang, Weiss et al. 2009). This discrepancy might be related to distinct signals triggered by *T. gondii* depending on the species and/or the type of host cell, which could result in differential activation of mTOR effectors. Further characterization of mTOR outputs in immune and non-immune cell populations will shed light on this matter. The mechanism by which *T. gondii* upregulates mTOR activity appears to be multifactorial, as indicated by the requirement of both AKT-mediated signaling and AKT-independent events, such as L-leucine availability. Amino acid abundance promotes Rag-dependent translocation and activation of mTORC1 at the lysosomal surface (Sancak, Bar-Peled et al. 2010). Notably, mTOR associates to the parasitophorous vacuole (PV) in *T. gondii*-infected cells (Wang, Weiss et al. 2009). These observations, along with our data, suggest that the PV surface offers a favorable site for mTORC1 activation during *T. gondii* infection.

Chemical inhibition of mTOR allowed us to confirm its requirement for selective translational activation in *T. gondii*-infected macrophages. Consistent with this, numerous mRNAs containing a 5' TOP motif were present exclusively among translationally-activated mRNAs, including those encoding ribosomal proteins. Interestingly, several of them play a role in cell cycle progression (e.g. RPS3, RPS7, RPS15a,

6815   RPL15, and RPL36a) and regulation of apoptosis (e.g. RPS14, RPS29 and RPL7) (Xu, Xiong et al. 2016).

6816   Moreover, *T. gondii* suppressed translation of macrophage mRNAs encoding pro-apoptotic proteins such

6817   as *Foxo3a* while leading to translational activation of pro-survival factors and cell cycle regulators (e.g.

6818   *Bcl2A1D, Cdk2*, *Hbegf*, and *Id2*). *T. gondii* has the ability to inhibit apoptosis and regulate host cell cycle to

6819   promote infection (Goebel, Luder et al. 1998, Nash, Purner et al. 1998, Molestina, El-Guendy et al. 2008,

6820   Lavine and Arrizabalaga 2009). Moreover, mTOR activity is required for host cell cycle progression during

6821   *T. gondii* infection (Wang, Weiss et al. 2009). In view of these studies and our current findings, *T. gondii*

6822   appears to regulate translational efficiency of select mRNAs that favor survival of the infected cell and

6823   ultimately enhance parasite replication.

6824   Enrichment for transcripts encoding proteins related to cell activation and movement was mainly

6825   associated with translational repression by *T. gondii*. Strikingly, several of these factors are critical during

6826   toxoplasmosis. For instance, mice deficient in *Ccr2* fail to recruit Gr1^{+} inflammatory monocytes to the

6827   intestine and are susceptible to oral challenge with *T. gondii* cysts (Dunay, Damatta et al. 2008). Similarly,

6828   genetic deletion of *Ccr5* increases susceptibility to toxoplasmosis, and signaling through this receptor is

6829   required for IL-12 production by dendritic cells in response to *T. gondii* (Aliberti, Reis e Sousa et al. 2000).

6830   In stark contrast, *Cd200*, whose translational efficiency was activated in *T. gondii*-infected macrophages,

6831   has a detrimental effect during chronic toxoplasmosis. Indeed, CD200 expression downregulates microglial

6832   activation in the brain of *T. gondii*-infected mice. Accordingly, *Cd200*^{-/-} mice display an efficient local anti-

6833   parasitic response (Deckert, Sedgwick et al. 2006). These studies, along with our data, indicate that

6834   selective translational control of immune-related genes by *T. gondii* contributes to its ability to subvert

6835   protective immune responses.

6836   Numerous mRNAs pertaining to mitochondrial functions were translationally activated upon *T.*

6837   *gondii* infection, including mitoribosomal proteins, factors implicated in the electron transport chain, and

6838   ATP synthases. These data are consistent with mTOR-sensitive translation of mRNAs encoding proteins

6839   related to mitochondrial biogenesis and functions (Morita, Gravel et al. 2013, Morita, Prudent et al. 2017).

6840   With regards to *T. gondii*, it is well documented that the PV associates with the host mitochondria (de Melo,

6841   de Carvalho et al. 1992, Lindsay, Mitschler et al. 1993, Sinai and Joiner 2001). Accumulating evidence

6842   indicates that this association not only provides the parasite with nutrients such as amino acids and glucose

6843   (Sinai, Webster et al. 1997), but also leads to altered oxidative phosphorylation (OXPHOS) (Syn, Anderson

6844   et al. 2017) and impacts innate immune responses (Pernas, Adomako-Ankomah et al. 2014). Moreover,

6845   the metabolism of intracellular *T. gondii* tachyzoites appears to rely on host-derived ATP (Sorensen,

6846   Billington et al. 1997), and parasite egress is particularly sensitive to host cell ATP levels (Silverman, Qi et

6847   al. 1998). Therefore, it is plausible that translational control of select host mRNAs by *T. gondii* contributes

6848   to subversion of host mitochondrial functions, which in turn favors parasite metabolic activity and replication.

6849   Future studies should therefore aim to address these issues.

6850   Several genes related to autophagy were identified in our study as translationally repressed in *T.*

6851   *gondii*-infected cells (e.g. *Atp13a2*, *Htr2b*, *Iigp1*, *Kdr*, *Lrrk2*, *Nbr1*, *Tecpr1*, *Tpcn1*, *Trim21*, and *Wdfy3*) while

6852 others were activated (e.g. *Hspa8* and *Mefv*). Interestingly, host autophagy appears to have dual role during

6853 *T. gondii* infection since it provides macromolecules to replicating parasites (Coppens 2017), but also

6854 contributes to parasite clearance by stripping the PV membrane (Saeij and Frickel 2017). MEFV (or

6855 TRIM20) is induced by IFNγ and is involved in "precision autophagy", by specifically targeting

6856 inflammasome components NLRP3, pro-caspase 1, and NLRP1 to limit excessive inflammation (Kimura,

6857 Jain et al. 2015). Therefore, by favoring the translational efficiency of *Mefv*, it possible that the parasite

6858 aims at limiting inflammasome activation, a mechanism required for host resistance against *T. gondii*

6859 (Ewald, Chavarria-Smith et al. 2014, Gorfu, Cirelli et al. 2014). Translational repression of *Iigp1* and *Trim21*

6860 could also favor parasite persistence within the infected cell. IIGP1 (or Irga6) is targeted and inactivated by

6861 the parasite virulence factor kinase complex ROP5/ROP18/GRA7 (Hermanns, Muller et al. 2016) to prevent

6862 immune-related GTPases (IRG)-mediated destruction of the parasite (Fentress, Behnke et al. 2010,

6863 Steinfeldt, Konen-Waisman et al. 2010). Similarly, TRIM21 accumulates at the PV membrane following

6864 IFNγ stimulation to restrict parasite replication and modulate inflammatory cytokine production in *T. gondii*-

6865 infected cells (Foltz, Napolitano et al. 2017). Moreover, *Trim21*-deficient mice are more susceptible to

6866 toxoplasmosis, and display higher parasite burden and lower pro-inflammatory cytokine levels. Hence, it is

6867 tempting to suggest that modulation of translational efficiency of host mRNAs involved in autophagy

6868 constitutes an additional mechanism employed by *T. gondii* to promote infection.

6869 In addition to the identification of pyrimidine-rich (CU) motifs in the 5' UTR of mRNAs translationally

6870 activated upon *T. gondii* infection, 5' UTR analysis indicated the presence of GC-rich stretches in ~50% of

6871 the mRNAs that are translationally repressed. Of interest, this feature was absent in the mRNAs whose

6872 translation was activated upon parasite infection. GC-rich motifs in the 5' UTR are associated with formation

6873 of secondary structures that limit mRNA translation efficiency (Babendure, Babendure et al. 2006, Jenkins,

6874 Bennagi et al. 2010). Translational control is also achieved via *trans* regulatory factors such as RNA-binding

6875 proteins, microRNAs, and "specialized ribosomes" (Landry, Hertz et al. 2009, Leung and Sharp 2010, Liu

6876 and Qian 2014). A recent study by Fischer and colleagues reported that infection by *T. gondii* causes the

6877 formation of stress granules containing poly-(A) binding proteins (PABPs) in the nucleus of the host cell

6878 (Fischer, Roberts et al. 2018). PABPs regulate several steps in mRNA processing, such as export,

6879 degradation, stability, polyadenylation and deadenylation (Goss and Kleiman 2013, Smith, Blee et al. 2014).

6880 Upon stress (e.g. UV irradiation, viral infection), mRNA can be stored in nuclear stress granules through

6881 interaction with PABPs leading to translational silencing (Eliseeva, Lyabin et al. 2013). Further investigation

6882 is needed to define the role of PABPs in translational control during *T. gondii* infection. It is conceivable that

6883 numerous mechanisms act in concert during *T. gondii* infection to fine-tune selective host mRNA translation.

6884 Collectively, this study defines the translational signature of macrophages infected by *T. gondii*,

6885 and provides evidence that translational control constitutes a key mechanism of host cell subversion by the

6886 parasite. Further supporting a central role for post-transcriptional regulatory mechanisms of gene

6887 expression during toxoplasmosis, lack of correlation between transcriptomic and proteomic data was

6888 reported from human fibroblasts infected by *T. gondii* (Nelson, Jones et al. 2008). Thus, it is likely that by

6889   modulating translation efficiencies in different cell types, *T. gondii* promotes its survival and dissemination

6890   through the infected host. Future studies using *in vitro* and *in vivo* models of *T. gondii* infection will contribute

6891   to a better understanding of the impact and the mechanisms underlying regulation of mRNA translation

6892   during toxoplasmosis.

Materials and Methods

Reagents

      Culture media and supplements were purchased from Wisent and Gibco; cycloheximide was purchased from BioShop; CellTracker™ Green CMFDA dye was purchased from Molecular Probes; RNasin was provided by Promega; rapamycin (sirolimus) was bought from LC Laboratories; Torin-1 and MK-2206 were purchased from Cayman; pyrimethamine was obtained from Tocris; XTT (2,3-bis-(2-methoxy-4-nitro-5-sulfophenyl)-2H-tetrazolium-5-carboxanilide) was ordered from Biotium; [5,6-^{3}H] uracil was purchased from Perkin-Elmer; cOmplete EDTA-free protease inhibitor and PhosSTOP phosphatase inhibitor tablets were purchased from Roche; DAPI (4',6-diamidino-2-phenylindole dilactate) and CellTracker Green (CMFDA) was acquired from Invitrogen; primary and secondary antibodies for western blotting and microscopy were purchased from Cell Signaling Technologies, Santa Cruz Biotechnology, R&D Systems, Sigma-Aldrich, BioLegend and Invitrogen.

Parasite Maintenance and Harvest

      Toxoplasma gondii tachyzoite cultures (RH and ME49 strains) were maintained by serial passages in VERO cells kindly provided by Dr. Angela Pearson (INRS-Institut Armand-Frappier, Laval, QC, Canada) cells grown in DMEM culture medium supplemented with 5% heat-inactivated FBS, 2 mM L-glutamate, 1 mM sodium pyruvate, 100 U/mL penicillin, and 100 µg/mL streptomycin, and incubated at 37°C, 5% CO_2. For experimental infections, freshly egressed tachyzoites (RH and ME49 strains) were harvested from VERO cultures, pelleted by centrifugation (1,300 × g, 7 min, 4°C), resuspended in ice-cold PBS (pH 7.2-7.4), and passed through a syringe fitted with a 27 G needle. Large cellular debris and intact host cells were pelleted by low-speed centrifugation (200 × g, 3 min, 4°C), and the supernatant containing parasites was filtered with a 3 µm-polycarbonate filter (Millipore). Tachyzoites were then washed twice in PBS and finally resuspended in the appropriate culture medium, according to the experiment.

Bone Marrow-Derived Macrophage (BMDMS) Differentiation

      Bone marrow-derived macrophages (BMDMS), were obtained by differentiating precursor cells from murine bone marrow (Leroux, Nishi et al. 2015). Briefly, mice were euthanized by CO_2 asphyxiation, hind legs were collected in Hank's Balanced Salt Solution (HBSS) (100 U/mL penicillin, 100 µg/mL streptomycin, 4.2 mM sodium bicarbonate), and marrow was flushed out of bones. Red blood cells were lysed in ACK lysis buffer (150 mM NH_4Cl, 10 mM $KHCO_3$, 0.1 mM EDTA) for 7 min at RT. Precursor cells were washed in HBSS and resuspended in BMDMS culture medium (DMEM, 10% heat-inactivated FBS, 2 mM L-glutamate, 1 mM sodium pyruvate, 100 U/mL penicillin, 100 µg/mL streptomycin, 20 mM HEPES, 55 µM β-mercaptoethanol) supplemented with 15% L929 fibroblast-conditioned culture medium (LCCM), seeded in tissue culture-treated dishes, and incubated O/N at 37°C, 5% CO_2. The following day, cells that had not adhered were collected, resuspended in BMDMS culture medium supplemented with 30% LCCM, and plated in regular Petri dishes (i.e., 3 × 10^6 precursor cells per dish). Medium was changed 2 days later,

6930 and differentiated BMDMS were collected at 7 days after marrow extraction. Differentiation of precursor
6931 cells into macrophages was routinely assessed by monitoring CD11b and F4/80 co-expression by flow
6932 cytometry. Hind legs from $s6k1^{-/-}/ s6k2^{-/-}$ C57BL/6 mice were kindly provided by Dr. Nahum Sonenberg
6933 (McGill University).

6934

6935 **Ethics Statement**

6936 Experiments were carried out under a protocol approved by the Comité Institutionnel de Protection
6937 des Animaux of the INRS - Institut Armand Frappier (CIPA#1502-03). This protocol respects procedures
6938 on good animal practice provided by the Canadian Council on animal care.

6939

6940 **Infection of BMDMS**

6941 Macrophages were plated one day before infection with *T. gondii* in BMDMS culture medium
6942 without LCCM and allowed to adhere O/N at 37°C, 5% CO_2. Cultures were serum-starved for 2 h and
6943 treated with inhibitors, when applicable. BMDMS were then inoculated with parasites (RH or ME49) or left
6944 uninfected in fresh medium with 1% FBS. Any remaining extracellular parasites were rinsed away with
6945 warm PBS (pH 7.2-7.4) 1 h following inoculation, fresh medium was added with inhibitors, when applicable,
6946 and cells were incubated until the end of the experiment. Unless specified otherwise, this procedure was
6947 carried out for all *in vitro* experiments.

6948

6949 **Western Blot Analysis**

6950 Cultures were collected following infection and other treatments and lysed in ice-cold RIPA lysis
6951 buffer (25 mM Tris (pH 7.6), 150 mM NaCl, 1% Triton-X 100, 0.5% sodium deoxycholate, 0.1% SDS)
6952 supplemented with phosphatase and EDTA-free protease inhibitor cocktails (Roche, Basel, Switzerland).
6953 Insoluble material was removed by centrifugation (20,000 × g, 15 min, 4°C), and protein concentration in
6954 the supernatant was measured by the bicinchoninic acid assay (BCA), according to the manufacturer's
6955 specifications. About 20 µg of protein sample was mixed with Laemmli loading buffer and subjected to SDS-
6956 PAGE, and the resolved proteins were transferred onto PVDF membranes. Membranes were blocked for
6957 1 h at RT in TBS-0.05% Tween-20, 5% skim milk, then probed with the following primary antibodies: anti-
6958 4E-BP1, anti-phospho-4E-BP1 (T37/46), anti-phospho-4E-BP1 (T70), anti-phospho-4E-BP1 (S65), anti-
6959 4E-BP2, anti-phospho-RPS6 (S235/236), anti-phospho-RPS6 (S240/244), anti-phospho-S6K1, anti-S6K2,
6960 anti-AKT, anti-phospho-AKT (T308), anti-phospho-AKT (S473), and β-actin were obtained from Cell
6961 Signaling Technologies; anti-RPS6, and anti-S6K1 were purchased from Santa Cruz Biotechnology; anti-
6962 eIF4E was purchased from BD Biosciences, and anti-*T. gondii* profilin-like protein was purchased from R&D
6963 Systems. Membranes were then probed with either goat anti-rabbit, goat anti-mouse (Sigma-Aldrich), or
6964 rabbit anti-goat (R&D Systems) IgG horseradish peroxidase (HRP)-linked antibodies. Subsequently,
6965 proteins were visualized using the Clarity ECL Western blotting substrate (Bio-Rad) and exposing the

6966 membranes to autoradiography film (Denville Scientific, Holliston, MA) or a chemiluminescence imager
6967 (Bio-Rad).

6968

6969 **m^{7}GTP-Agarose Pull-Down Assay**

6970 BMDMS cultures were plated in 10 cm diameter plates in complete medium and allowed to adhere
6971 O/N at 37°C, 5% CO$_2$. Cultures were serum-starved for 2 h in the presence of DMSO (vehicle), 20 nM
6972 rapamycin, or 200 nM Torin-1, then inoculated with *T. gondii* tachyzoites (RH and ME49 strains) at an MOI
6973 of 6:1 or left uninfected in fresh medium with 1% heat-inactivated FBS. Any remaining extracellular
6974 parasites were rinsed away with warm PBS (pH 7.2-7.4) 1 h following inoculation, fresh medium was added,
6975 and cells were incubated for an additional 7 h. Cultures were washed with ice-cold PBS, gently scrapped,
6976 and pelleted by centrifugation (200 × *g*, 10 min, 4°C). Cells were lysed in ice-cold Buffer A (lysis buffer; 50
6977 mM MOPS pH 7.4, 100 mM NaCl, 2 mM EDTA, 2 mM EGTA, 1% IGEPAL CA-630, 1% sodium
6978 deoxycholate, 7 mM β-mercaptoethanol) supplemented with phosphatase and EDTA-free protease inhibitor
6979 cocktails (Roche). Samples were incubated 15 min on ice and regularly mixed gently, and the crude lysates
6980 were cleared by centrifugation (16,000 × *g*, 10 min, 4°C). The supernatant was transferred to new tubes,
6981 and protein concentration was measured by the Bradford assay (Bio-Rad), according to the manufacturer's
6982 specifications. About 0.5-0.75 mg of proteins of each sample were mixed with 50% slurry of 2'/3'-EDA-
6983 m^{7}GTP immobilized on agarose beads (Jena Bioscience) and diluted up to 1 mL with Buffer B (wash buffer;
6984 50 mM MOPS pH 7.4, 100 mM NaCl, 0.5 mM EDTA, 0.5 mM EGTA, 7 mM β-mercaptoethanol, 0.1 mM
6985 GTP) supplemented with phosphatase and EDTA-free protease inhibitor cocktails (Roche). Samples were
6986 mixed for 1 h at 4°C with end-over-end (EOE) rotation. Beads were pelleted by centrifugation (500 × *g*, 1
6987 min, 4°C). The supernatants (i.e., flow-through, FT) were kept, while the beads were washed twice in Buffer
6988 B and finally resuspended in Laemmli loading buffer for further analysis by western blotting.

6989

6990 **Polysome-Tracing Analysis**

6991 BMDMS cultures were plated in 15 cm diameter plates O/N, serum-starved for 2 h in the presence
6992 or absence of vehicle (DMSO), 20 nM rapamycin, or 200 nM Torin-1, then inoculated with *T. gondii*
6993 tachyzoites (RH and ME49 strains) at an MOI of 3:1 or left uninfected in fresh medium with 1% heat-
6994 inactivated FBS. After 8 h of infection, cycloheximide (CHX) was added to cultures to a final concentration
6995 of 100 μg/mL and plates were incubated 5 min at 37°C, 5% CO$_2$. Cells were then rinsed with cold PBS
6996 containing 100 μg/mL CHX, scraped, and pelleted by centrifugation (200 × *g*, 10 min, 4°C). Pellets were
6997 lysed in hypotonic lysis buffer (5 mM Tris (pH 7.5), 2.5 mM MgCl$_2$, 1.5 mM KCl, 2 mM DTT, 0.5% Triton X-
6998 100, 0.5% sodium deoxycholate, 100 μg/mL CHX, and 200 U RNAsin ribonuclease inhibitor (Promega,
6999 Madison, WI), and lysates were cleared by centrifugation (20,000 × *g*, 2 min, 4°C). Lysates were loaded
7000 onto 5 to 50% sucrose density gradients (20 mM HEPES (pH 7.6), 100 mM KCl, 5 mM MgCl$_2$, 100 μg/mL
7001 CHX, and 200 U RNAsin) and centrifuged in a Beckman SW41 rotor at 36,000 rpm for 2 h at 4°C. Gradients

7002 were fractionated and collected (30 s and 500 μL per fraction), and the absorbance at 254 nm was recorded

7003 continuously using a Brandel BR-188 density gradient fractionation system.

7004

Purification of RNA

7006 Efficiently translated mRNA (associated with ≥ 3 ribosomes) and the input material (total

7007 cytoplasmic mRNA) were extracted with TRIzol (Invitrogen) and chloroform followed by isopropanol

7008 precipitation. In brief, polysome fractions and input material were diluted up to 1 mL with RNase-free H_2O,

7009 then 500 μL of TRIzol and 150 μL of chloroform was added. Samples were vortexed vigorously for 5 sec,

7010 incubated 3 min at RT, and centrifuged (18,000 × g, 15 min, 4°C). The aqueous phase of each sample was

7011 mixed with an equal volume (~750 μL) of ice-cold isopropanol and 1 μL of GlycoBlue (Thermo Fisher), then

7012 the RNA was precipitated O/N at -20°C then pelleted by centrifugation (18,000 × g, 10 min, 4°C). The RNA

7013 pellet was washed twice with 500 μL of 75% ice-cold ethanol. Samples were air-dried and resuspended in

7014 RNase-free H_2O and polysome fractions of corresponding treatment were pooled. RNA was further cleaned

7015 using an RNeasy MinElute Cleanup Kit (Qiagen), according to the manufacturer's specifications. Finally,

7016 approximate concentration, purity, and integrity of the purified RNA was assessed spectrophometrically

7017 using a NanoDrop 1000 (Thermo Fisher) and a Bioanalyzer 2100 with a Eukaryote Total RNA Nano chip

7018 (Agilent Technologies). Samples were aliquoted and stored at -80°C until further analyses.

7019

RNA-Seq Data Processing

7021 Library preparation and sequencing were carried out at SciLifeLab (Stockholm, Sweden). RNA-

7022 Seq libraries were generated using the strand specific TruSeq protocol and sequenced using Illumina

7023 HiSeq2500 (Illumina) with a 1×51 setup for both total cytosolic and polysome-associated mRNA (mRNA

7024 associated with > 3 ribosomes) from three independent biological replicates. RNA-Seq reads from infected

7025 samples were first aligned to *T. gondii* reference genomes GT1 (type I) and ME49 (type II) (the genome of

7026 the RH strain is not completely annotated, but it was estimated that among *T. gondii* RH gene families,

7027 97.8% have orthologs in the GT1 strain (Lau, Lee et al. 2016)). Reads from infected samples which did not

7028 map to the *T. gondii* genomes as well as all reads from uninfected samples were aligned to the mouse

7029 genome mm10. HISAT2 was used for all alignments with default settings (Kim, Langmead et al. 2015).

7030 Alignments to *T. gondii* and *Mus musculus* resulted in 4.4% and 93.7% mapping on average, respectively.

7031 Gene expression was quantified using the RPKMforgenes.py script

7032 (http://sandberg.cmb.ki.se/media/data/rnaseq/rpkmforgenes.py) (Ramskold, Wang et al. 2009) with options

7033 -fulltranscript -readcount -onlycoding from which raw per gene RNA-Seq counts were obtained (version last

7034 modified 07.02.2014). Annotation of genes was done using RefSeq. Genes that had 0 counts in all samples

7035 were removed. One replicate of the uninfected control condition was excluded from downstream analysis

7036 based on outlier behavior in principal component analyses.

7037

7038

RNA-Seq Analysis of Empirical Data Set Using *anota*

The limma::voom R function was used to compute $\log_2$ counts per million (Ritchie, Phipson et al. 2015). To identify changes in translational efficiency leading to altered protein levels, *anota* (Larsson, Sonenberg et al. 2010, Larsson, Sonenberg et al. 2011) was used with parameters minSlope = -0.5 and maxSlope = 1.5. Replicate was included as a batch effect in the models. The following criteria were considered for significant changes in translational efficiency: false discovery rate (FDR) < 0.25, translational efficiency *(apvEff)* > $\log_2(1.5)$, log ratio of polysome-associated mRNA data by cytosolic mRNA data (deltaPT) > $\log_2(1.25)$, polysome-associated mRNA log fold-change (deltaP) > $\log_2(1.5)$. Genes that overlap, resulting in that RNA sequencing reads cannot be associated with only one gene, were excluded from downstream analyzes. Similar FDR and fold-change thresholds were used when selecting differential expression of polysome-associated mRNA. For further analysis, we used a published list of TOP- and IRES-containing mRNAs (Thoreen, Chantranupong et al. 2012); mitochondrion-related function genes included in the Gene Ontology (GO) (Gene Ontology, 2015) terms indicated in **S5 Table**; and a signature for mTOR-sensitive translation (Larsson, Morita et al. 2012); gene symbols were converted from human to mouse and are listed in **S5 Table**. The difference in $\log_2$ fold-change of translational efficiency between the signatures and the background was assessed using Wilcoxon-Mann-Whitney tests.

nCounter™ Analysis

For nCounter analysis (Nanostring Technologies), a subset of 250 genes were selected according to RNA-Seq data. Sequences for the probes in the custom-designed nCounter codeset are listed in **S2 Table**. Infected and uninfected cells were treated with rapamycin or Torin-1 followed by isolation of efficiently translated mRNA and cytosolic mRNA from three independent biological replicates (as described above). The positive spike-in RNA hybridization controls for each lane were used to normalize Nanostring counts as implemented in the posCtrlNorm function of the Bioconductor package NanoStringQCPro (Nickles, Sandmann et al. 2017) (with parameter summaryFunction = "sum"). Targets with less than half of the samples above the background level (7 [$\log_2$ scale]) were excluded. The quality of the normalization was assessed using 30 non-regulated genes selected from the RNA-Seq data analysis to verify that their expression levels remained stable in the DMSO samples. Spearman rank correlation coefficients were calculated between fold-changes obtained from the RNA-Seq data and the nCounter data. Analysis of translational control was performed with *anota* to select targets which were translationally up-regulated upon infection with each *T. gondii* strain. Genes with FDR < 0.25 were considered significant and the following parameters were used: minSlope = -1, maxSlope = 2, selDeltaPT = $\log_2(1.2)$. For these targets, Empirical Cumulative Distribution Function (ECDF) curves were used to visualize the distribution of their $\log_2$ fold-change (both for cytosolic and polysome-associated mRNA) upon treatment with rapamycin or Torin-1. Distribution differences were evaluated using Wilcoxon-Mann-Whitney tests.

287

Functional Classification of Gene Lists

Enrichment of translationally-regulated genes in specific functional networks was determined using Ingenuity Pathway Analysis (IPA; Qiagen) by comparing *anota*-regulated genesets against the entire sequenced datasets (Kramer, Green et al. 2014). Within the IPA application, statistical significance was calculated using a right-tailed Fisher Exact test and p-values were adjusted for multiple hypothesis testing using the Benjamini-Hochberg method to arrive at a FDR.

RNA Sequence Motif Analyses

For 5' UTR sequence analysis, non-redundant RefSeq 5' UTRs were retrieved from genome build mm10 using the UCSC Table Browser (https://genome.ucsc.edu/cgi-bin/hgTables). Length and GC content of the UTRs were computed using a custom script. To minimize the bias associated with analyzing GC content and sequence motifs of very short sequences, 5' UTRs of less than 20 nucleotides were omitted from further analyses. Novel RNA sequence motifs were detected in the 5' UTRs using MEME (Multiple Em for Motif Elicitation) (Bailey, Johnson et al. 2015). To accurately estimate the probability of a candidate motif appearing by chance (E-value) and to improve the sensitivity of the motif search, a custom background model was employed. Briefly, the "fasta-get-markov" utility included in the program was used to compute a background Markov model of order 1 using all Refseq mouse 5' UTRs. Sequence logos were generated using the ggseq*Logo* package in R. CAGE-Seq data were retrieved from FANTOM5 (http://fantom.gsc.riken.jp/5/) and sequences mapped to the mm9 build using the UCSC genome browser.

XTT and [5,6-³H] Uracil Incorporation Viability Assays

To test for acute toxicity of the inhibitors against extracellular tachyzoites, parasite viability was measured using the tetrazolium reduction-based XTT assay (Dzitko, Dudzinska et al. 2010). Briefly, freshly egressed tachyzoites (RH and ME49 strains) were resuspended in culture medium (without FBS) and transferred to 96-well plates (2×10^6 tachyzoites per well). Parasites were treated with 20 nm rapamycin, 200 nM Torin-1 or an equal volume of vehicle (DMSO), and incubated for 2 h at 37°C, 5% CO_2. As a negative control, heat-killed (HK) parasites incubated at 56°C for 10 minutes were included in the assay. Then, the XTT reagents were prepared according to the manufacturer's specifications (Biotium) and added to the parasites. Tachyzoite cultures were incubated for 20 h. Absorbance was measured using Multiskan GO 1510 plate reader (Thermo Fisher) at 470 nm from which absorbance at 660 nm was subtracted.

To test for acute toxicity of the inhibitors on intracellular tachyzoites, the incorporation of [5,6-³H] radiolabeled-uracil by the parasite was measured as an assessment of viability (Weiss and Kim 2007). Briefly, BMDMS were plated in 24-well plates O/N, serum-starved for 2 h, treated with either 20 nM rapamycin, 200 nM Torin-1 or an equal volume of vehicle (DMSO), and inoculated with *T. gondii* tachyzoites (RH and ME49 strains) at an MOI of 3:1 in fresh medium with 1% heat-inactivated dialyzed FBS. Cultures were incubated O/N, then 5 µCi of [5,6-³H]-uracil (Perkin-Elmer) were added to each well, and cultures were incubated for another 2 h at 37°C, 5% CO_2. Plates were chilled at -20°C for 2 min, an equal volume

7113 of ice-cold 0.6 N TCA was added to each well, and cells were fixed on ice for 1 h. Wells were rinsed with

7114 PBS, then with deionized H_2O. Plates were air-dried, and the precipitated material was resolubilized in 500

7115 μL of 0.1 N NaOH for 1 h. Half of the material was thoroughly mixed with an equal volume of OptiPhase

7116 Supermix Scintillation Cocktail (Perkin-Elmer), and radioactivity was measured (counts per minute; CPM)

7117 with a MicroBeta TriLux Scintillation Counter (Perkin-Elmer). Uninfected cells were included to measure

7118 background incorporation of uracil by host cells, and treatment with 10 μM pyrimethamine was included as

7119 a positive control for chemical toxicity against *T. gondii* parasites.

7120

Immunofluorescence Microscopy

7122 BMDMS were seeded onto glass coverslips in 24-well plates O/N, serum-starved for 2 h, then

7123 inoculated with *T. gondii* tachyzoites (RH and ME49 strains), previously stained with 20 μM CellTracker

7124 Green™ CMFDA dye (Molecular Probes) for 20 min, at an MOI of 3:1 or left uninfected. After 8 h of infection,

7125 cells were rinsed with PBS thrice, then fixed with 3.7% PFA (in PBS) for 15 min at RT. Cell membranes

7126 were permeabilized with 0.2% Triton X-100 (in PBS) for 5 min at RT. Fc receptors and non-specific binding

7127 sites were blocked by incubating samples with 5 μg/mL anti-CD16/32 (BioLegend) diluted in PBS

7128 supplemented with 10 mg/mL BSA. Primary antibody against phospho-RPS6 (S240/244) (CST) was diluted

7129 in PBS with 10 mg/mL BSA and incubated with samples for 1 h at RT. A goat anti-rabbit IgG (H+L)

7130 secondary antibody conjugated to Alexa Fluor 594 (Invitrogen) was incubated with the samples for 1 h at

7131 RT. Nuclei were stained with 300 nM DAPI (4',6-diamidino-2-phenylindole dilactate) (Invitrogen) for 5 min

7132 at RT. Coverslips were mounted onto slides with Fluoromount G (Southern Biotech). Samples were

7133 visualized using a Leica microscope, and image processing was performed with Fiji (Schindelin, Arganda-

7134 Carreras et al. 2012).

7135

Measurement of Parasite Replication by qPCR

7137 Parasite replication *in vitro* was assessed by extracting genomic DNA followed by measuring the

7138 amplification of the *T. gondii* B1 gene by qPCR, as previously described (Leroux, Nishi et al. 2015). Briefly,

7139 BMDMS cultures were plated in 12-well plates O/N, serum-starved for 2 h in the presence of DMSO

7140 (vehicle), 20 nM rapamycin, or 200 nM Torin-1, then inoculated with *T. gondii* tachyzoites (RH and ME49

7141 strains) at an MOI of 1:20. Parasites were allowed to replicate, egress, and re-infect cells for 72 h. Culture

7142 supernatants were collected (for extracellular parasites), while remaining adherent cells (containing

7143 intracellular parasites) were detached by adding ice-cold PBS with 5 mM EDTA for 15 min at 4°C followed

7144 by vigorous pipetting, then were pooled to culture supernatants. Tachyzoites and host cells were pelleted

7145 by centrifugation (16,000 × *g*, 10 min, 4°C), then resuspended in 200 μL PBS. Genomic DNA (gDNA) was

7146 extracted using Roche High Pure PCR Template Preparation Kit, according to the manufacturer's

7147 specifications. To measure parasite replication, the 35-fold repetitive *T. gondii* B1 gene was amplified by

7148 qPCR using the PowerUP SYBR Green PCR Master Mix (Applied Biosystems) with $MgCl_2$ concentration

7149 adjusted to 3.5 μM, 10 ng of template gDNA, and 0.5 μM of forward primer (5'-

7150   TCCCCTCTGCTGGCGAAAAGT-3') and reverse primer (5'-AGCGTTCGTGGTCAACTATCGATTG-3')

7151   (Integrated DNA Technologies) in a 20 µl reaction volume. Reaction was carried out in a QuantStudio 3

7152   Real-Time PCR System (Applied Biosciences) with the following program: 10 min initial denaturation at

7153   95°C, followed by 45 cycles of 15 sec of denaturation at 95°C, 30 sec of annealing at 58°C, and 30 sec of

7154   extension at 72°C. Cycle threshold (Ct) values were normalized using the mouse β-actin gene (0.2 µM of

7155   forward   (5'-CACCCACACTGTGCCCATCTACGA-3')   and   reverse   (5'-   CAGCGGAACCG-

7156   CTCATTGCCAATGG-3') primers, and $MgCl_2$ concentration adjusted to 2.5 µM). Analysis was carried out

7157   by relative quantification using the Comparative CT method ($2^{-\Delta\Delta Ct}$) (Livak and Schmittgen 2001). Effect of

7158   the inhibitors on replication was calculated by normalizing to values obtained from parasite cultures treated

7159   with DMSO. Values are presented as mean [SD]; all samples performed in triplicates.

7160

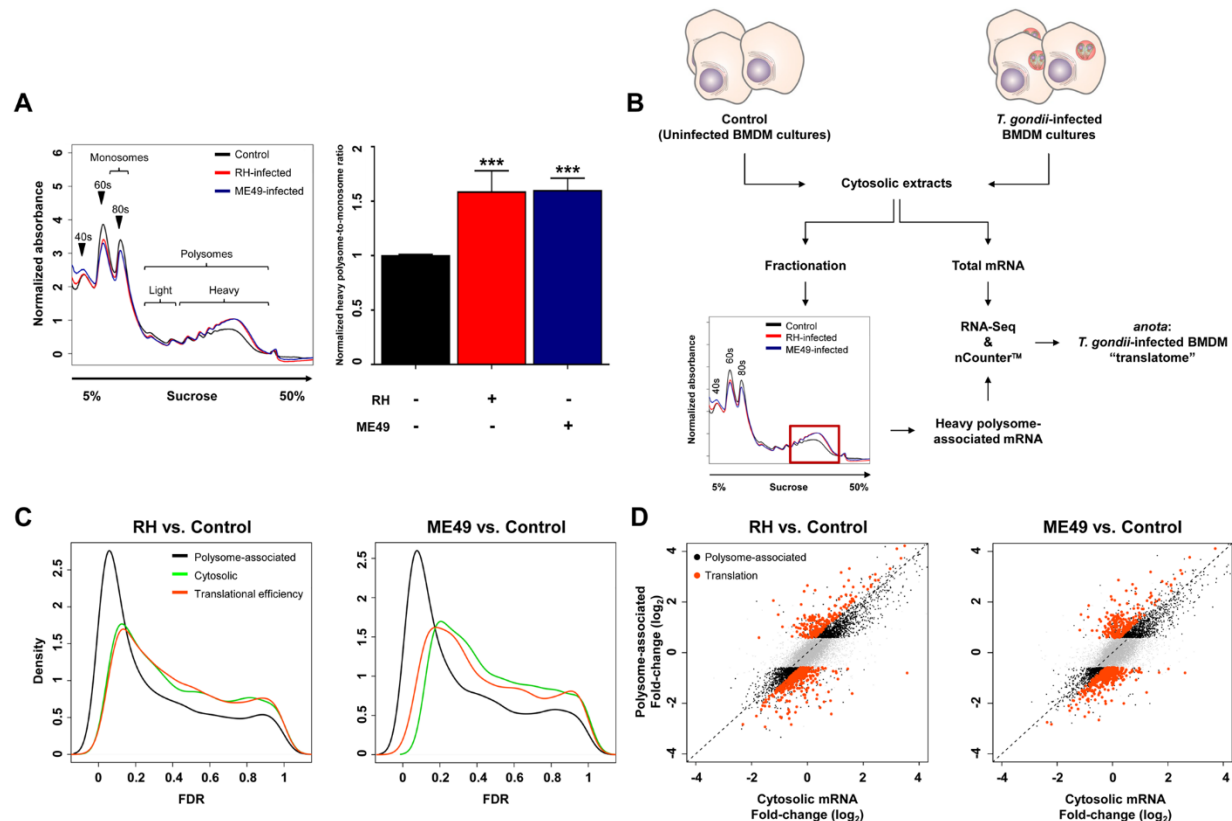7161   **Statistical Analysis**

7162   Where applicable, data are presented as mean [SD]. Statistical significance was determined using

7163   one-way ANOVA followed by Tukey post-hoc test; calculations were performed using Prism Software

7164   (GraphPad, La Jolla, CA). Differences were considered significant when * $p < 0.05$, ** $p < 0.01$, *** $p <$

7165   0.001.

Acknowledgements

7181

Figure 1. *T. gondii* infection stimulates protein synthesis and selectively modulates translational efficiencies in BMDMS. (**A**) BMDMS cultures were inoculated with either RH or ME49 *T. gondii* tachyzoites (MOI 3:1) or left uninfected (Control) for 8 h. Cell lysates were sedimented on 5 to 50% sucrose gradients. Gradients were fractionated and absorbance at 254 nm was recorded continuously; absorbance values were normalized (left panel). Arrows indicate the 40S and 60S ribosomal subunits, and 80S (monosomes). The light and heavy polysome regions were identified as fractions containing mRNA associated to 2-3 and > 3 ribosomes, respectively. Polysome tracings are representative of at least four independent experiments. The area under the curve of the monosome and heavy polysome regions was calculated, and the heavy polysome-to-monosome ratios were then normalized to uninfected BMDMS cultures (Control) (right panel; mean [SD]; biological replicates n = 4). (**B**) Workflow strategy to characterize the translatome of *T. gondii*-infected BMDMS. Cytosolic extracts from Control (uninfected) and *T. gondii*-infected (RH or ME49) BMDMS cultures were sedimented on a sucrose gradient. Heavy polysome fractions were pooled (referred to as heavy polysome-associated mRNA). Total and heavy polysome-associated mRNAs were sequenced by RNA-Seq and analyzed by anota, an R package (biological replicates n = 3). Validation of genes identified by RNA-Seq was accomplished with targeted nCounter assays (custom panel; biological replicates n = 3). (**C**) Densities of FDRs for changes in polysome-associated mRNA, cytosolic mRNA, or translational efficiency (i.e., following *anota* analysis) for each strain compared to uninfected control. (**D**) Scatter plots of log$_2$ fold-changes (for the same comparisons as in B) for polysome-associated and cytosolic mRNA. Transcripts showing altered translational efficiencies are indicated in orange while mRNAs showing

292

7201   changed polysome-association (which can be explained by altered cytosolic mRNA levels following e.g.

7202   modulated transcription) are in indicated in black. (**C** and **D**) Data analyses were performed on samples

7203   generated from three independent biological replicates.

7204
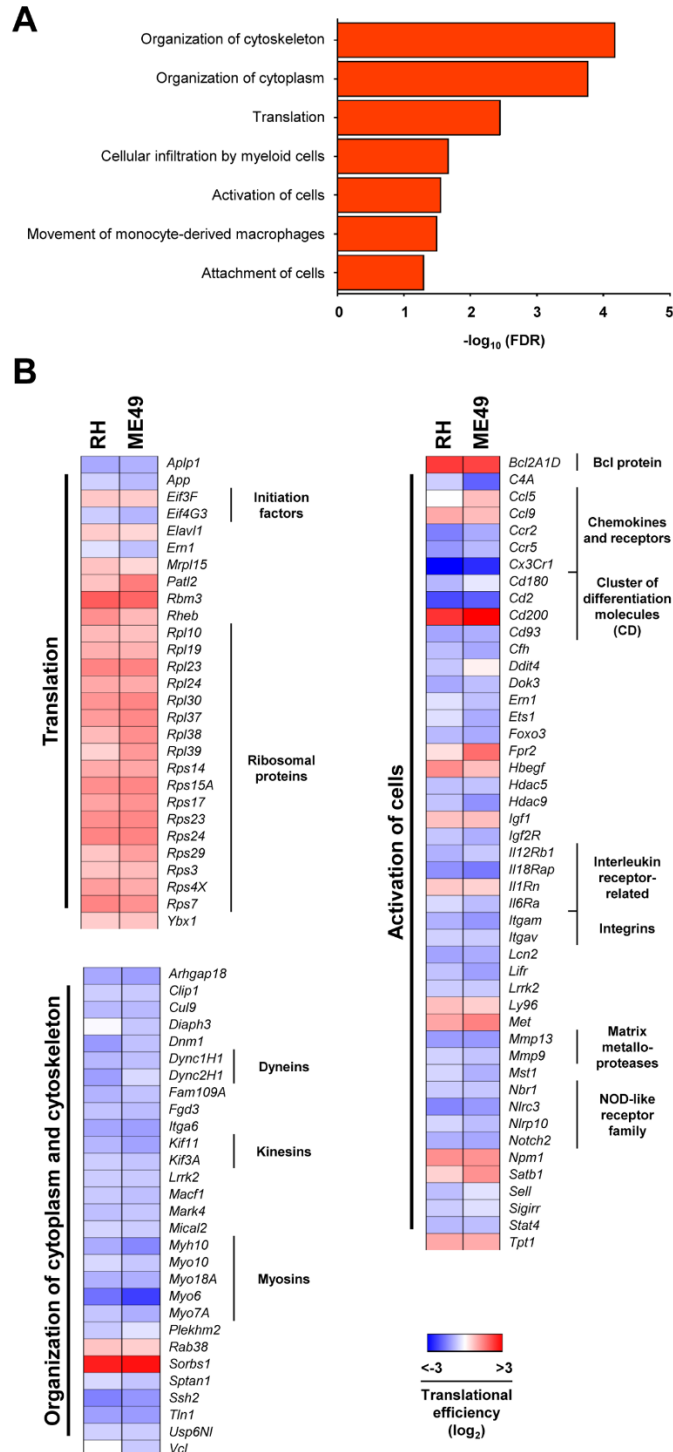
7205

Figure 2. Enriched cell processes for translationally-regulated host mRNAs upon *T. gondii* infection.
IPA was performed on translationally-regulated mRNAs by *T. gondiii* infection. (**A**) FDR values (-log$_{10}$) for
select biologically relevant IPA categories that were significantly enriched in *T. gondii*-infected cells. (**B**)
Heatmaps showing translational efficiency changes for selected genes in enriched categories were

294

7210　　　generated using Morpheus (https://software.broadinstitute.org/morpheus/index.html, Broad Institute). (**A**

7211　　　and **B**) Analyses were carried out on data generated from three independent biological replicates.

7212

296
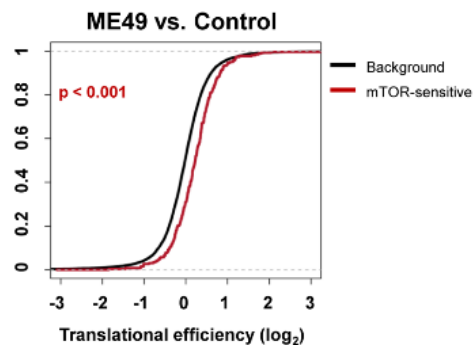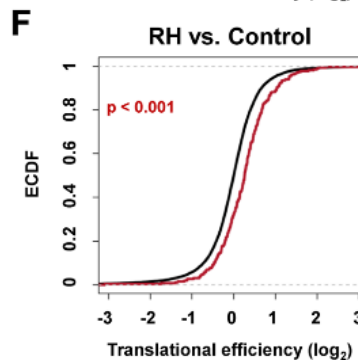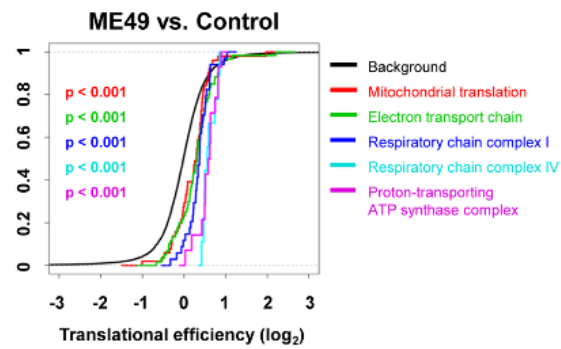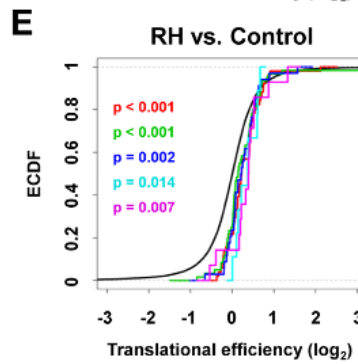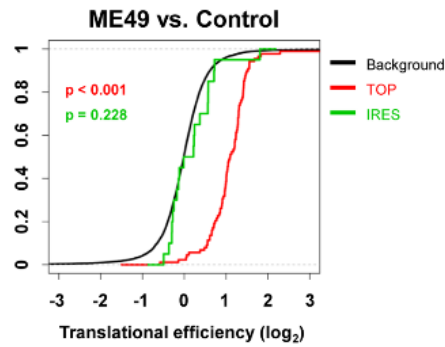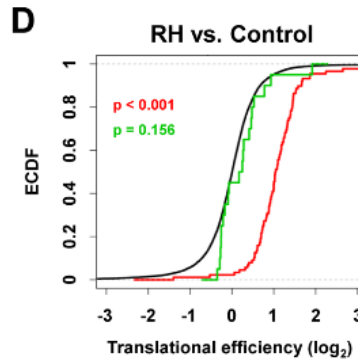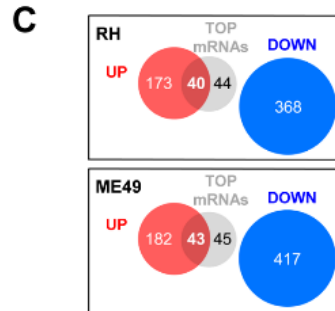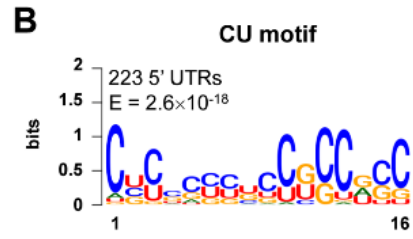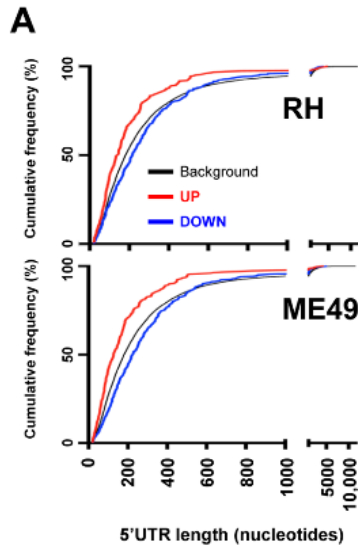
7213   **Figure 3. *T. gondii* infection selectively activates mTOR-sensitive translation.** (**A**) Cumulative

7214   frequency distributions of Refseq 5' UTR lengths across the mm10 genome (black), compared to that of

7215   the upregulated (red) and downregulated (blue) sets in RH (top) and ME49 (bottom) infections. (**B**)

7216   Sequence logo of the MEME motif found in the upregulated 5' UTR set. Nucleotide position is indicated on

7217   the x-axis. (**C**) Venn diagrams indicating the number of genes harboring a TOP motif present in the

7218   upregulated vs. downregulated genesets. (**D**) Cumulative distribution of translational efficiencies of TOP

7219   mRNAs (red), IRES-containing mRNAs (green) and the background (all transcripts; black). (**E**) Cumulative

7220   distribution of translational efficiencies of mRNAs related to mitochondrial translation (red), electron

7221   transport chain (green), mitochondrial respiratory chain complex I (dark blue), mitochondrial respiratory

7222   chain complex IV (light blue), proton-transporting ATP synthase complex (magenta), and the background

7223   (all transcripts; black). (**F**) Cumulative distribution of translational efficiencies of mRNAs whose translation

7224   was previously defined as depending on mTOR activity (red) and the background (transcripts not belonging

7225   to the gene signature; black). (**D**-**F**) Changes in translational efficiencies between RH- (left) or ME49-

7226   infected (right) BMDMS vs. uninfected cells were evaluated. Wilcoxon test p-values are indicated (tests

7227   consider genes belonging vs. not belonging to each group). ECDF = Empirical Cumulative Distribution

7228   Function. (**A** - **F**) Data analyses were conducted on samples obtained from three independent biological

7229   replicates.

A

Time	4 h			6 h			8 h			10 h			12 h			*Tg* only	
RH	-	+	-	-	+	-	-	+	-	-	+	-	-	+	-	+	-
ME49	-	-	+	-	-	+	-	-	+	-	-	+	-	-	+	-	+

B

	Input						*Tg* only		m⁷GTP pull down						Flow-through (FT)					
RH	-	+	-	-	+	-	+	-	-	+	-	-	+	-	-	+	-	-	+	-
ME49	-	-	+	-	-	+	-	+	-	-	+	-	-	+	-	-	+	-	-	+
Torin-1 (200 nM)	-	-	-	+	+	+	-	-	-	-	-	+	+	+	-	-	-	+	+	+

C

	4E-BP1			4E-BP2		
RH	-	+	-	-	+	-
ME49	-	-	+	-	-	+

7230

298
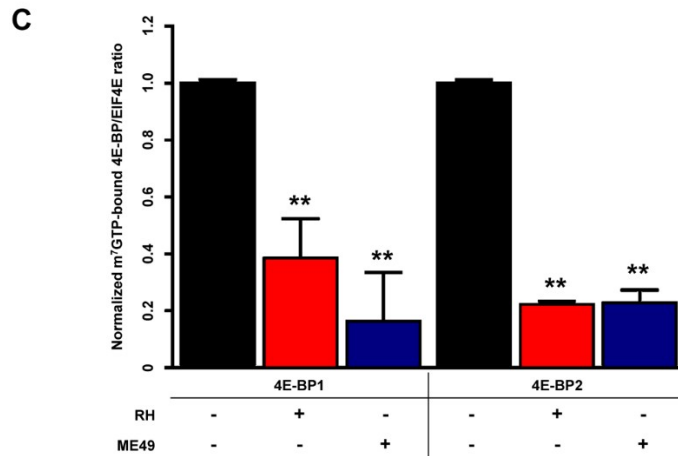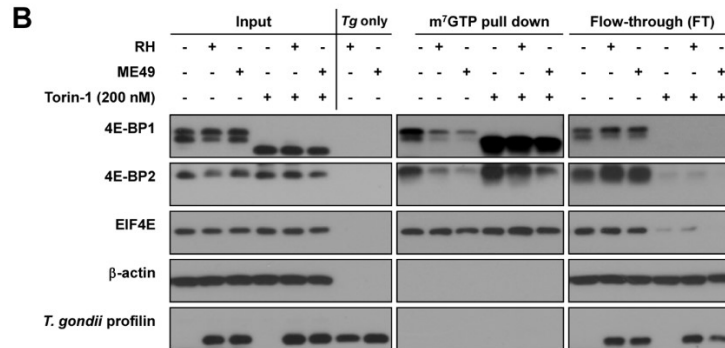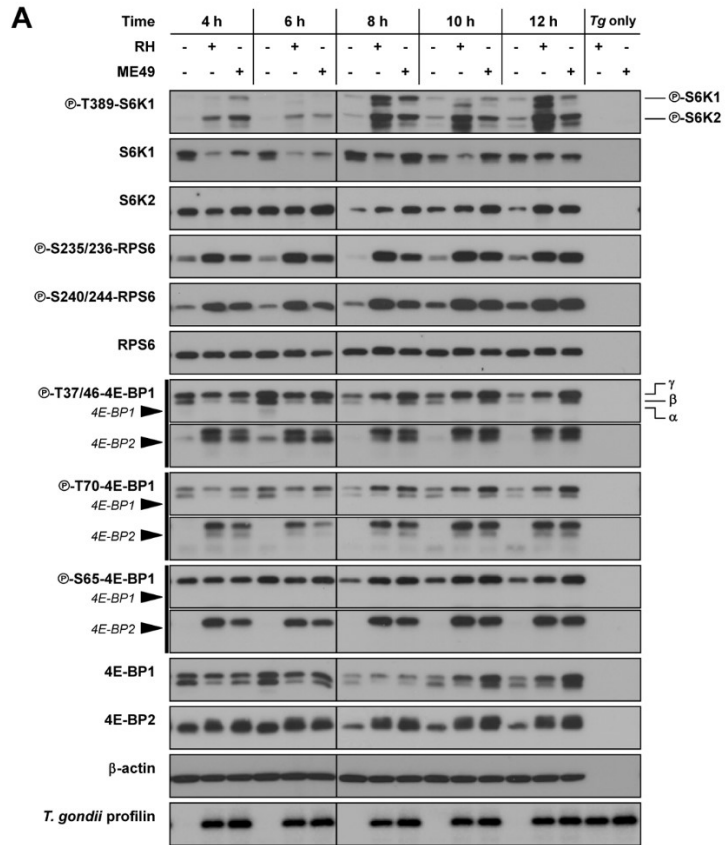
Figure 4. *T. gondii* augments mTORC1 activity and promotes 4E-BP1/4E-BP2 dissociation from cap-bound eIF4E in BMDMS. (**A**) BMDMS cultures were inoculated with either RH or ME49 *T. gondii* tachyzoites or left uninfected for the indicated time. Phosphorylation and expression levels of indicated proteins were monitored by western blotting. Total amounts of β-actin were used as a loading control and an antibody against *T. gondii* profilin-like protein was employed to assess the infection of the BMDMS cultures. Total protein extracts from extracellular tachyzoites (both RH and ME49 strains) (*Tg* only) were used to control for any cross-reactivity of the antibodies against *T. gondii* proteins. (**B**) BMDMS cultures were pre-treated with 200 nM Torin-1 or equal volume of DMSO (vehicle) for 2 h, then inoculated with either RH or ME49 *T. gondii* tachyzoites or left uninfected. Total protein extracts were collected at 8 h post-infection and were prepared for m^{7}GTP pull-down assays. Levels of indicated proteins in input (15 µg), pulled-down material (20%) and flow-through (FT) (15 µg) were determined by western blotting. (**C**) m^{7}GTP-bound 4E-BP/eIF4E ratios were calculated based on densitometric measurements of the band intensities of 4E-BP1, 4E-BP2, and eIF4E and were normalized to uninfected BMDMS control (mean [SD]; biological replicates n = 3). (**A** and **B**) Data are representative of at least three independent biological replicates.

299
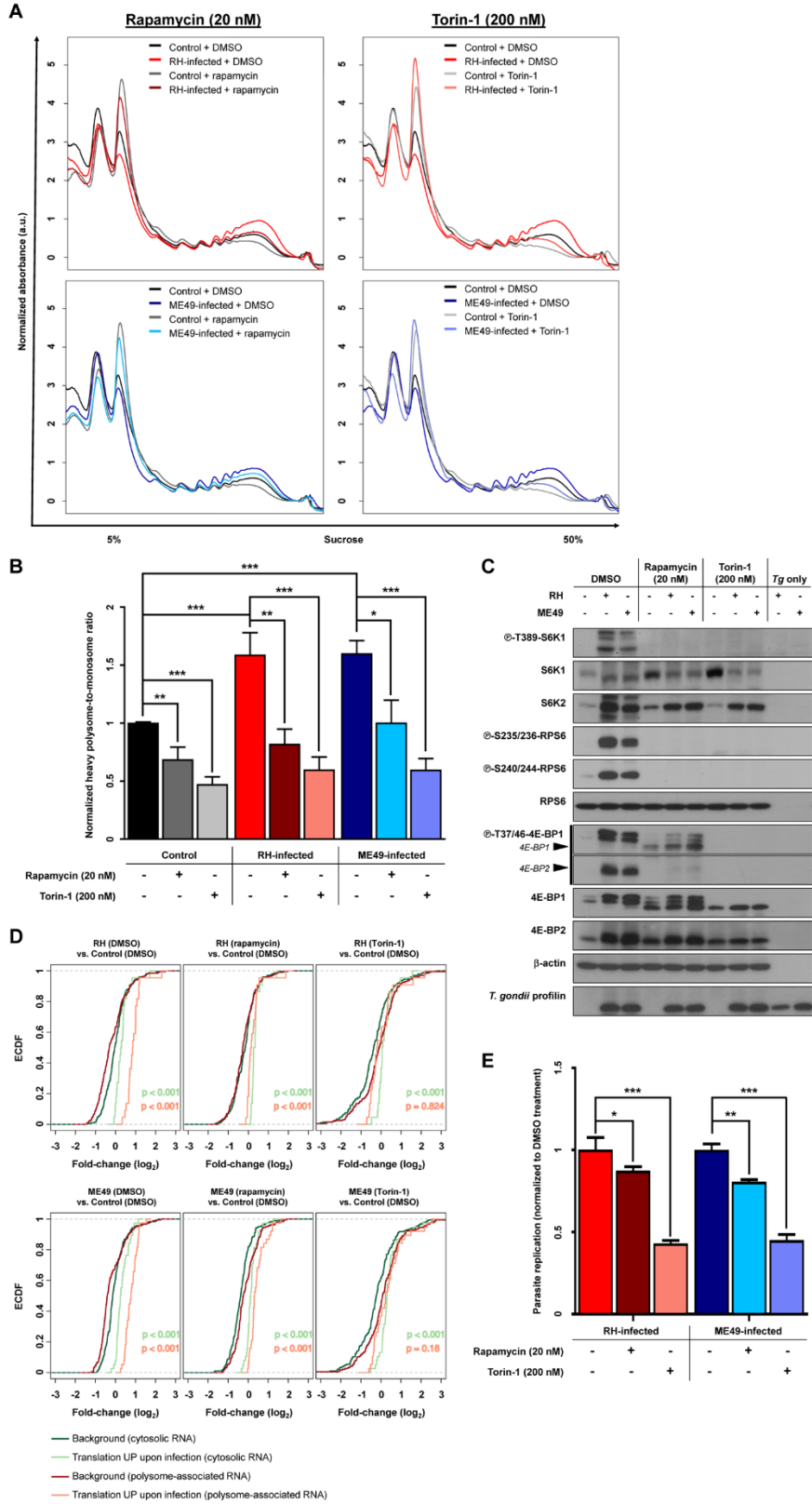
Figure 5. Inhibition of mTOR reverses *T. gondii*-induced activation of host mRNA translation and dampens parasite replication. BMDMS cultures were pre-treated with 20 nM rapamycin, 200 nM Torin-1 or equal DMSO (vehicle) volume for 2 h, then inoculated with either RH or ME49 *T. gondii* tachyzoites or left uninfected (Control) for 8 h. (**A**) Shown are polysome tracings representative of at least four independent biological replicates. (**B**) Heavy polysome-to-monosome ratios normalized to DMSO-treated uninfected BMDMS cultures (Control) (mean [SD]; biological replicates n = 4). (**C**) A fraction of the cultures utilized for polysome tracings was used to collect total protein extracts. Phosphorylation status and expression levels of indicated proteins were monitored by western blotting. Data are representative of four separate experiments. (**D**) Transcripts showing activated translational efficiencies following parasite infection were selected and their mTOR-sensitive translation was assessed using polysome-profiling coupled to nCounter assays (same treatments as in **A**). The cumulative distributions of $\log_2$ fold-changes for these targets were compared to background (all other nCounter quantified mRNAs) in infected cells with or without rapamycin or Torin-1 and compared to uninfected DMSO controls. Empirical cumulative distribution functions (ECDF) are shown for $\log_2$ fold-changes for cytosolic mRNA (light green: selected targets, dark green: background genes) and polysome-associated mRNA (orange: selected targets, red: background genes). Wilcoxon tests p-values for comparison of selected targets with their corresponding background are given. Data analyses were conducted on samples obtained from three independent biological replicates. (**E**) BMDMS were pre-treated with 20 nM rapamycin, 200 nM Torin-1 or equal DMSO (vehicle) volume for 2 h, then inoculated with either RH or ME49 *T. gondii* tachyzoites at parasite-to-BMDMS ratio of 1:20 for 72 h. Genomic DNA was extracted, and parasite replication was assessed by qPCR by amplification of the *T. gondii* gene B1. Ct values were normalized to the mouse β-actin, and effects of the inhibitors on parasite replication were calculated by normalizing to values obtained from cultures treated with DMSO for each strain. Values from one representative experiment of two independent trials are presented as mean [SD]; all samples performed in technical triplicates.

7271
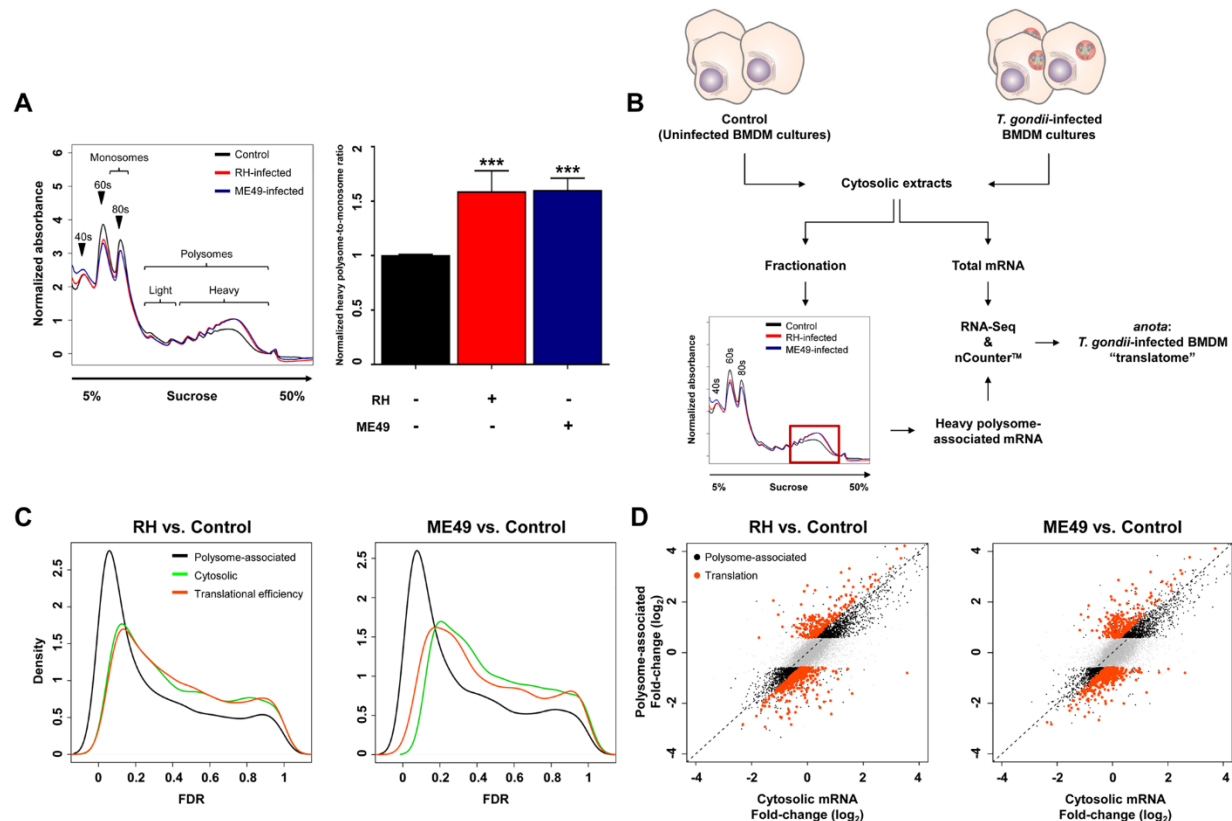
Figure S1. Polysome-tracings of parasite extracts and validation of changes in translational efficiency upon *T. gondii* infection. (**A**) Cell lysates from ~9 × 10^7 uninfected BMDMS, and ~2.7 × 10^8 tachyzoites of either RH or ME49 strains (a number corresponding to the number of parasites inoculated onto BMDMS cultures during infection trials, i.e., MOI 3:1), were sedimented on 5 to 50% sucrose gradients. Gradients were fractionated and absorbance at 254 nm was recorded continuously; shown here are raw absorbance values. Arrows indicate the 40S and 60S ribosomal subunits, and 80S (monosomes). Polysome tracings are representative of at least four independent biological replicates. (**B**) Densities of FDRs for changes in polysome-associated mRNA, cytosolic mRNA or translational efficiency (i.e., following anota analysis) (top panel) and scatter plots of log2 fold-changes in polysome-associated and cytosolic mRNA (bottom panel) for RH-infected compared to ME49-infected BMDMS cultures. (**C**) Scatter plot of translational efficiencies (anota) obtained from the two technologies (RNA-Seq and nCounter) are compared. Polysome-profiling coupled with RNA-Seq identified a set of host mRNAs whose translational efficiency was altered in each of the 3 represented comparisons (cells infected with each strain vs control and the comparison between cells infected with the two strains). These identified mRNAs are colored in orange. (**B** and **C**) Analyses were carried out on data generated from three independent biological replicates.

7288

7289

302

A

RH

ME49

— Background
— **UP**
— **DOWN**

Cumulative frequency(%)

GC content (%)

B

GC stretch

314 5' UTRs

$E = 2.1 \times 10^{-215}$

bits
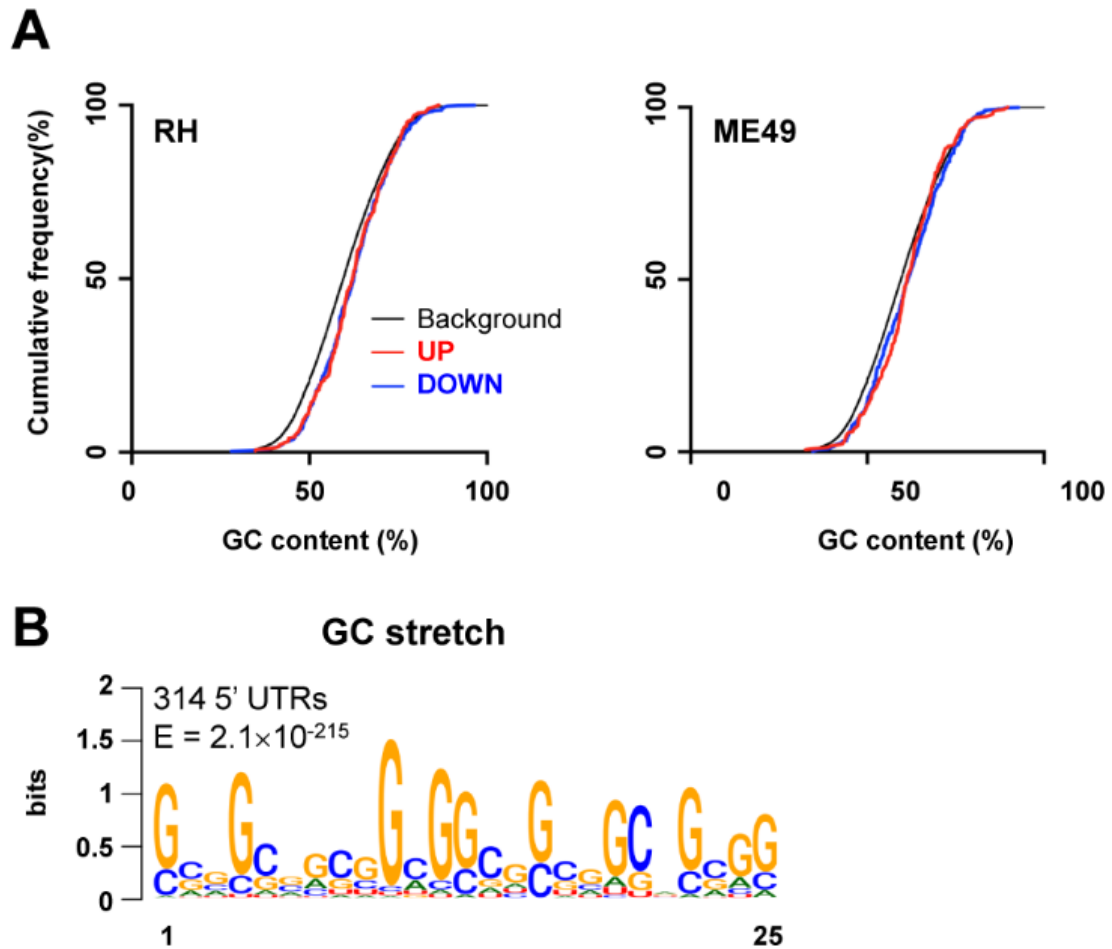
7290

Figure S2. GC content and GC-rich stretches in translationally downregulated genes. (**A**) Cumulative frequency distribution of the GC content of 5' UTRs in translationally-upregulated (red line) and -downregulated (blue line) sets were calculated and compared to background (i.e., all RefSeq mouse 5' UTRs) (black line). (**B**) Sequence logo of the MEME motif found in the downregulated 5' UTR set. (A and B) Data analyses were performed on samples generated from three independent biological replicates.
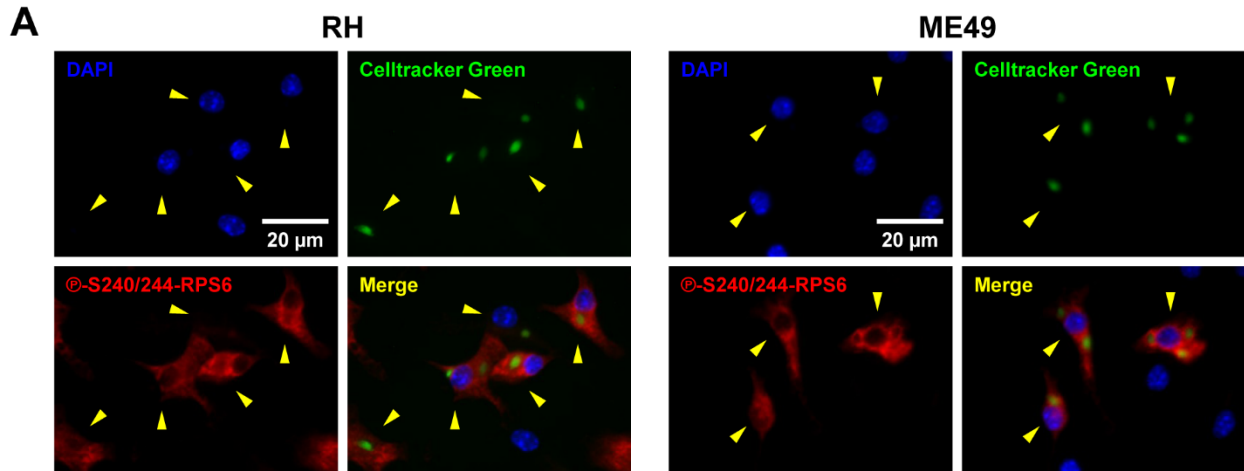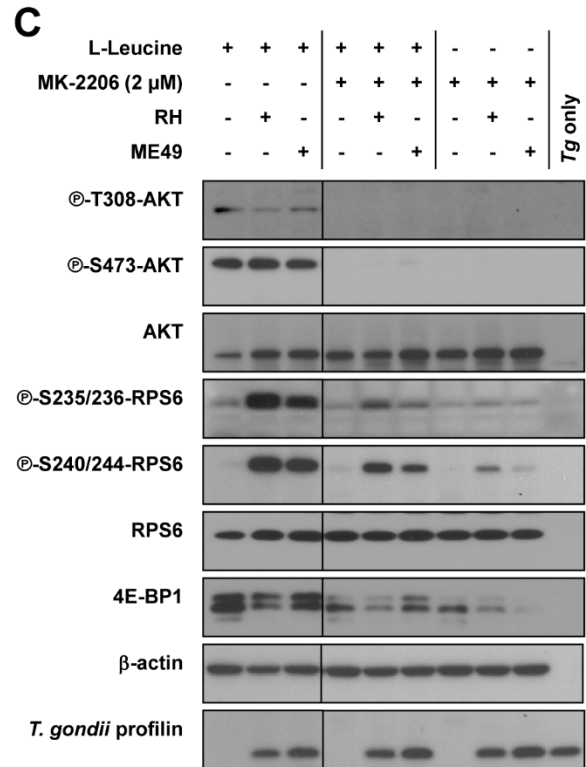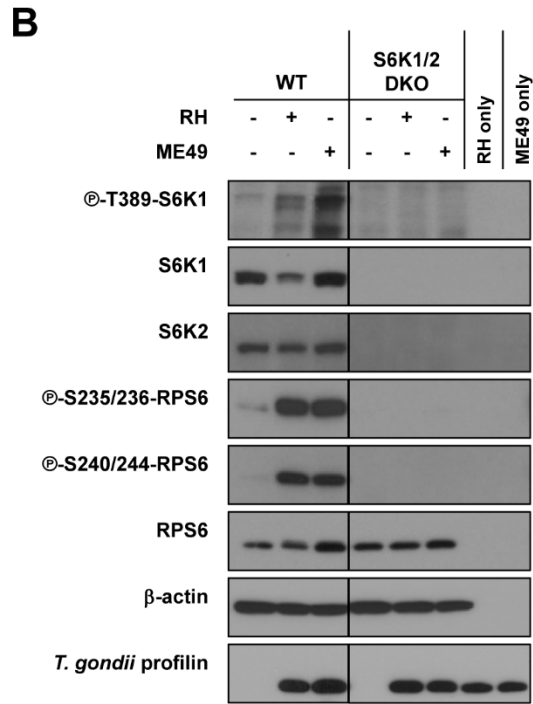
Figure S3. S6K1/S6K2-dependent RPS6 phosphorylation, and AKT-dependent and -independent mTORC1 activation in *T. gondii*-infected BMDMS. (**A**) BMDMS cultures were infected with either RH or ME49 *T. gondii* tachyzoites, previously stained with 20 µM CellTracker Green for 8 h. Cells were fixed and processed for immunofluorescence microscopy. Samples were stained for phospho-RPS6 (S240/244) (shown in red) and DAPI. Infected cells are identified by yellow arrowheads. (**B**) BMDMS cultures from WT or S6K1/S6K2 DKO mice were infected with either RH or ME49 *T. gondii* tachyzoites or left uninfected for 8 h. Activation of the S6K1/S6K2-S6 axis was monitored by western blotting. (**C**) BMDMS cultures were incubated O/N in the presence or absence of L-leucine in the culture medium. The following day, cultures

7305 were pre-treated with either 2 µM MK-2206 or equal DMSO (vehicle) volume for 2 h, then infected with *T.*

7306 *gondii* for 8 h or left uninfected. Phosphorylation status and total levels of indicated proteins were assessed

7307 by western blotting. (**B**, **C**) Total amounts of β-actin were used as a loading control, and an antibody against

7308 *T. gondii* profilin-like protein served to monitor the infection of the BMDMS cultures. Data are representative

7309 of three independent biological replicates.

7310
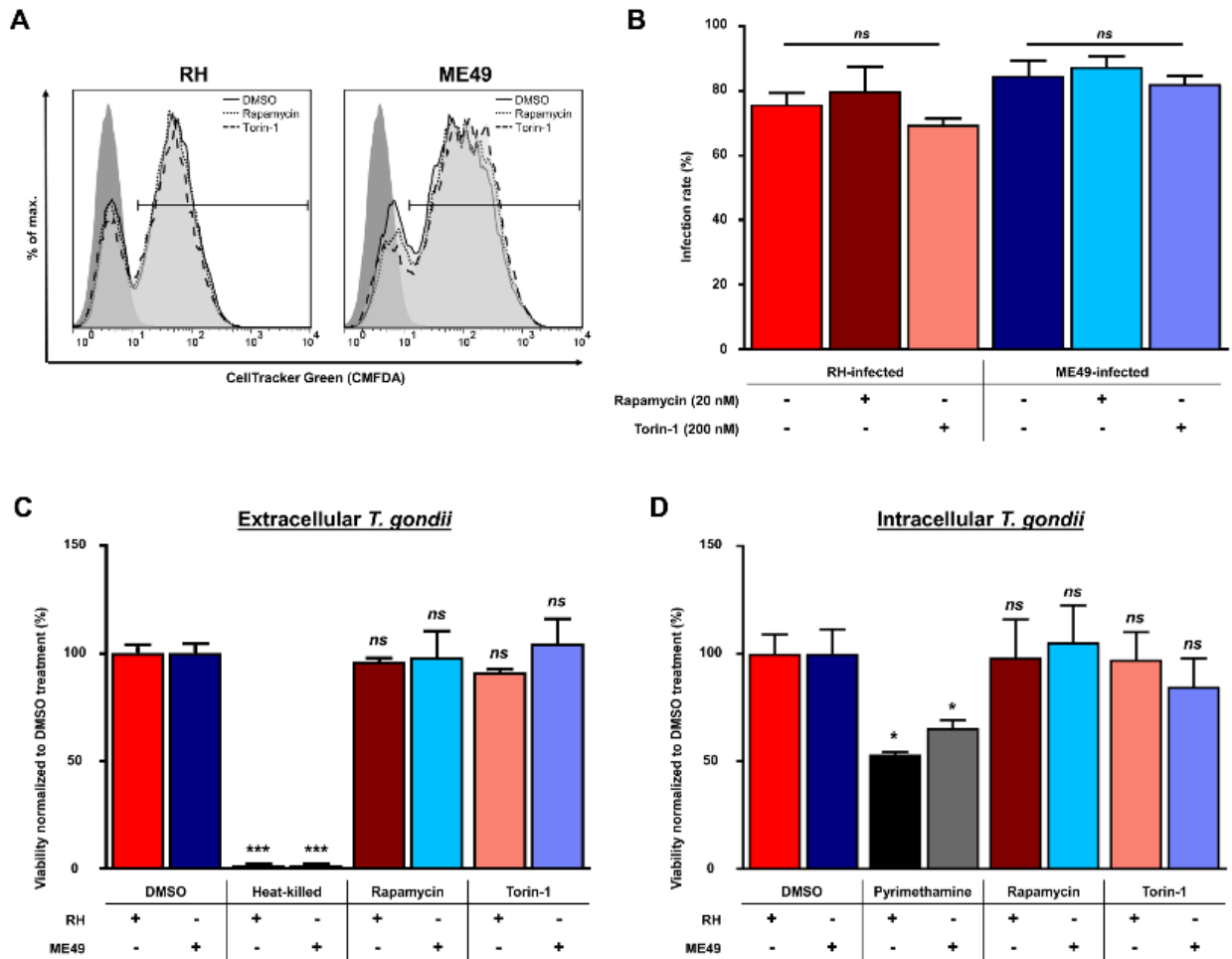
Figure S4. Measurement of acute toxicity of mTOR inhibitors on *T. gondii* tachyzoites and infection rates of inhibitor-treated BMDMS cultures. (**A-B**) Infection rates of BMDMS pre-treated with mTOR inhibitors were assessed by flow cytometry. Freshly harvested parasites were stained with 20 µM CellTracker Green (CMFDA) for 20 min at RT. BMDMS cultures pre-treated with either 20 nM rapamycin or 200 nM Torin-1, or with an equal volume of DMSO (vehicle) for 2 h were inoculated with the fluorescent parasites. Cells were harvested after 8 h of infection and analyzed by flow cytometry. (**A**) Infection rates were determined by gating on CellTracker Green-positive cells for DMSO- (solid line), rapamycin- (dotted line), and Torin-1-treated (dashed line) cultures. Uninfected cells (dark gray curve) were used to determine baseline fluorescence. Histograms are representative of at least four independent experiments. (**B**) Average infection rates from four independent biological replicates were calculated, and the error bars represent standard deviation (SD). Acute toxicity of rapamycin and Torin-1 on *T. gondii* tachyzoites was measured using (**C**) the XTT viability assay and (**D**) the radiolabeled [5,6]^{3}H-uracil incorporation assay. (**C**) Extracellular tachyzoites (RH and ME49 strains) devoid of any host cell were treated with either 20 nM

7327   rapamycin or 200 nM Torin-1, or with an equal volume of DMSO for 1 h (a maximum exposure time during

7328   which extracellular parasites were in contact with the inhibitors before invading host cells in the

7329   experimental design followed for all our experiments) at 37°C, 5% CO2. As a control, parasites were heat-

7330   killed at 56°C for 10 min. The XTT substrate was added to the cultures, and parasites were incubated for

7331   another 16 h in the presence of the inhibitors. Optical density (OD) was measured at 470 nm from which

7332   absorbance at 660 nm was subtracted. Percent viability was normalized to DMSO-treated parasites. (**D**)

7333   BMDMS cultures were treated with either 20 nm rapamycin or 200 nM Torin-1, or with an equal volume of

7334   vehicle (DMSO), and inoculated with *T. gondii* tachyzoites (RH and ME49 strains) at an MOI of 3:1 in fresh

7335   medium. Any remaining extracellular parasites were rinsed away with warm PBS 1 h following inoculation,

7336   after which fresh medium was added, and cells were incubated for 16 h. Then, 5 μCi of [5,6-^{3}H]-uracil were

7337   added to each well, and cultures were incubated for another 2 h. Viability of parasites was determined by

7338   the incorporation of radiolabeled uracil as measured by liquid scintillation. Percent viability was normalized

7339   to DMSO-treated cultures. Uninfected cells were included to measure background incorporation of uracil

7340   by host cells, and a 10 μM pyrimethamine treatment served as a positive control for chemical toxicity against

7341   T. gondii parasites. (**C** and **D**) All samples were done in technical triplicate, data were normalized to DMSO-

7342   treated cultures, and the error bars represent standard deviation (SD). Values from one representative

7343   experiment of two independent trials are shown here.

References

Al-Bajalan, M. M. M., D. Xia, S. Armstrong, N. Randle and J. M. Wastling (2017). "Toxoplasma gondii and Neospora caninum induce different host cell responses at proteome-wide phosphorylation events; a step forward for uncovering the biological differences between these closely related parasites." Parasitol Res.

Alain, T., X. Lun, Y. Martineau, P. Sean, B. Pulendran, E. Petroulakis, F. J. Zemp, C. G. Lemay, D. Roy, J. C. Bell, G. Thomas, S. C. Kozma, P. A. Forsyth, M. Costa-Mattioli and N. Sonenberg (2010). "Vesicular stomatitis virus oncolysis is potentiated by impairing mTORC1-dependent type I IFN production." Proc Natl Acad Sci U S A **107**(4): 1576-1581.

Aliberti, J., C. Reis e Sousa, M. Schito, S. Hieny, T. Wells, G. B. Huffnagle and A. Sher (2000). "CCR5 provides a signal for microbial induced production of IL-12 by CD8 alpha+ dendritic cells." Nat Immunol **1**(1): 83-87.

Babendure, J. R., J. L. Babendure, J. H. Ding and R. Y. Tsien (2006). "Control of mammalian translation by mRNA structure near caps." RNA **12**(5): 851-861.

Bailey, T. L., J. Johnson, C. E. Grant and W. S. Noble (2015). "The MEME Suite." Nucleic Acids Res **43**(W1): W39-49.

Bellato, H. M. and G. N. Hajj (2016). "Translational control by eIF2alpha in neurons: Beyond the stress response." Cytoskeleton (Hoboken) **73**(10): 551-565.

Cao, W., S. Manicassamy, H. Tang, S. P. Kasturi, A. Pirani, N. Murthy and B. Pulendran (2008). "Toll-like receptor-mediated induction of type I interferon in plasmacytoid dendritic cells requires the rapamycin-sensitive PI(3)K-mTOR-p70S6K pathway." Nat Immunol **9**(10): 1157-1164.

Chakrabarti, S., P. Liehl, N. Buchon and B. Lemaitre (2012). "Infection-induced host translational blockage inhibits immune responses and epithelial renewal in the Drosophila gut." Cell Host Microbe **12**(1): 60-70.

Clippinger, A. J., T. G. Maguire and J. C. Alwine (2011). "The changing role of mTOR kinase in the maintenance of protein synthesis during human cytomegalovirus infection." J Virol **85**(8): 3930-3939.

Coppens, I. (2017). "How Toxoplasma and malaria parasites defy first, then exploit host autophagic and endocytic pathways for growth." Curr Opin Microbiol **40**: 32-39.

Costa-Mattioli, M. and N. Sonenberg (2008). "RAPping production of type I interferon in pDCs through mTOR." Nat Immunol **9**(10): 1097-1099.

de Melo, E. J., T. U. de Carvalho and W. de Souza (1992). "Penetration of Toxoplasma gondii into host cells induces changes in the distribution of the mitochondria and the endoplasmic reticulum." Cell Structure and Function **17**(5): 311-317.

Deckert, M., J. D. Sedgwick, E. Fischer and D. Schluter (2006). "Regulation of microglial cell responses in murine Toxoplasma encephalitis by CD200/CD200 receptor interaction." Acta Neuropathologica **111**(6): 548-558.

Dowling, R. J., I. Topisirovic, T. Alain, M. Bidinosti, B. D. Fonseca, E. Petroulakis, X. Wang, O. Larsson, A. Selvaraj, Y. Liu, S. C. Kozma, G. Thomas and N. Sonenberg (2010). "mTORC1-mediated cell proliferation, but not cell growth, controlled by the 4E-BPs." Science **328**(5982): 1172-1176.

Dubey, J. P. (2004). "Toxoplasmosis - a waterborne zoonosis." Vet Parasitol **126**(1-2): 57-72.

Dubey, J. P., N. L. Miller and J. K. Frenkel (1970). "The Toxoplasma gondii oocyst from cat feces." J Exp Med **132**(4): 636-662.

Dunay, I. R., R. A. Damatta, B. Fux, R. Presti, S. Greco, M. Colonna and L. D. Sibley (2008). "Gr1(+) inflammatory monocytes are required for mucosal resistance to the pathogen Toxoplasma gondii." Immunity **29**(2): 306-317.

Dzitko, K., D. Dudzinska, M. Grzybowski and H. Dlugonska (2010). "[The utility of MTT and XTT colorimetric tests in the studies conducted in vitro with Toxoplasma gondii tachyzoites]." Wiad Parazytol **56**(2): 145-152.

Eliseeva, I. A., D. N. Lyabin and L. P. Ovchinnikov (2013). "Poly(A)-binding proteins: structure, domain organization, and activity regulation." Biochemistry (Mosc) **78**(13): 1377-1391.

Ewald, S. E., J. Chavarria-Smith and J. C. Boothroyd (2014). "NLRP1 is an inflammasome sensor for Toxoplasma gondii." Infect Immun **82**(1): 460-468.

Ezegbunam, W. and R. Foronjy (2018). "Posttranscriptional control of airway inflammation." Wiley Interdiscip Rev RNA **9**(1).

Fentress, S. J., M. S. Behnke, I. R. Dunay, M. Mashayekhi, L. M. Rommereim, B. A. Fox, D. J. Bzik, G. A. Taylor, B. E. Turk, C. F. Lichti, R. R. Townsend, W. Qiu, R. Hui, W. L. Beatty and L. D. Sibley

7400   (2010). "Phosphorylation of immunity-related GTPases by a Toxoplasma gondii-secreted kinase promotes

7401   macrophage survival and virulence." Cell Host Microbe **8**(6): 484-495.

7402   Fischer, K., M. Roberts, S. Roscoe, Y. Avci and S. Ananvoranich (2018). "<i>Toxoplasma

7403   gondii</i> infection induces the formation of host's nuclear granules containing poly (A)-binding proteins."

7404   Can J Microbiol.

7405   Foltz, C., A. Napolitano, R. Khan, B. Clough, E. M. Hirst and E. M. Frickel (2017). "TRIM21 is critical

7406   for survival of Toxoplasma gondii infection and localises to GBP-positive parasite vacuoles." Sci Rep **7**(1):

7407   5209.

7408   Frenkel, J. K., J. P. Dubey and N. L. Miller (1970). "Toxoplasma gondii in cats: fecal stages

7409   identified as coccidian oocysts." Science **167**(3919): 893-896.

7410   Gandin, V., L. Masvidal, L. Hulea, S. P. Gravel, M. Cargnello, S. McLaughlan, Y. Cai, P.

7411   Balanathan, M. Morita, A. Rajakumar, L. Furic, M. Pollak, J. A. Porco, Jr., J. St-Pierre, J. Pelletier, O.

7412   Larsson and I. Topisirovic (2016). "nanoCAGE reveals 5' UTR features that define specific modes of

7413   translation of functionally related MTOR-sensitive mRNAs." Genome Research **26**(5): 636-648.

7414   Garcia-Maurino, S. M., F. Rivero-Rodriguez, A. Velazquez-Cruz, M. Hernandez-Vellisca, A. Diaz-

7415   Quintana, M. A. De la Rosa and I. Diaz-Moreno (2017). "RNA Binding Protein Regulation and Cross-Talk

7416   in the Control of AU-rich mRNA Fate." Front Mol Biosci **4**: 71.

7417   Gebauer, F. and M. W. Hentze (2004). "Molecular mechanisms of translational control." Nat Rev

7418   Mol Cell Biol **5**(10): 827-835.

7419   Gingras, A. C., S. P. Gygi, B. Raught, R. D. Polakiewicz, R. T. Abraham, M. F. Hoekstra, R.

7420   Aebersold and N. Sonenberg (1999). "Regulation of 4E-BP1 phosphorylation: a novel two-step

7421   mechanism." Genes Dev **13**(11): 1422-1437.

7422   Gingras, A. C., B. Raught, S. P. Gygi, A. Niedzwiecka, M. Miron, S. K. Burley, R. D. Polakiewicz,

7423   A. Wyslouch-Cieszynska, R. Aebersold and N. Sonenberg (2001). "Hierarchical phosphorylation of the

7424   translation inhibitor 4E-BP1." Genes Dev **15**(21): 2852-2864.

7425   Goebel, S., C. G. Luder, R. Lugert, W. Bohne and U. Gross (1998). "Toxoplasma gondii inhibits the

7426   in vitro induced apoptosis of HL-60 cells." Tokai Journal of Experimental and Clinical Medicine **23**(6): 351-

7427   356.

7428   Gorfu, G., K. M. Cirelli, M. B. Melo, K. Mayer-Barber, D. Crown, B. H. Koller, S. Masters, A. Sher,

7429   S. H. Leppla, M. Moayeri, J. P. Saeij and M. E. Grigg (2014). "Dual role for inflammasome sensors NLRP1

7430   and NLRP3 in murine resistance to Toxoplasma gondii." MBio **5**(1).

7431   Goss, D. J. and F. E. Kleiman (2013). "Poly(A) binding proteins: are they all created equal?" Wiley

7432   Interdiscip Rev RNA **4**(2): 167-179.

7433   Hakimi, M. A. and A. Bougdour (2015). "Toxoplasma's ways of manipulating the host transcriptome

7434   via secreted effectors." Curr Opin Microbiol **26**: 24-31.

7435   Hakimi, M. A., P. Olias and L. D. Sibley (2017). "Toxoplasma Effectors Targeting Host Signaling

7436   and Transcription." Clin Microbiol Rev **30**(3): 615-645.

7437   Hassan, M. A., J. J. Vasquez, C. Guo-Liang, M. Meissner and T. Nicolai Siegel (2017).

7438   "Comparative ribosome profiling uncovers a dominant role for translational control in Toxoplasma gondii."

7439   BMC Genomics **18**(1): 961.

7440   Hermanns, T., U. B. Muller, S. Konen-Waisman, J. C. Howard and T. Steinfeldt (2016). "The

7441   Toxoplasma gondii rhoptry protein ROP18 is an Irga6-specific kinase and regulated by the dense granule

7442   protein GRA7." Cell Microbiol **18**(2): 244-259.

7443   Hershey, J. W., N. Sonenberg and M. B. Mathews (2012). "Principles of translational control: an

7444   overview." Cold Spring Harb Perspect Biol **4**(12).

7445   Hinnebusch, A. G., I. P. Ivanov and N. Sonenberg (2016). "Translational control by 5'-untranslated

7446   regions of eukaryotic mRNAs." Science **352**(6292): 1413-1416.

7447   Hirai, H., H. Sootome, Y. Nakatsuru, K. Miyama, S. Taguchi, K. Tsujioka, Y. Ueno, H. Hatch, P. K.

7448   Majumder, B. S. Pan and H. Kotani (2010). "MK-2206, an allosteric Akt inhibitor, enhances antitumor

7449   efficacy by standard chemotherapeutic agents or molecular targeted drugs in vitro and in vivo." Mol Cancer

7450   Ther **9**(7): 1956-1967.

7451   Holmes, M. J., L. D. S. Augusto, M. Zhang, R. C. Wek and W. J. Sullivan, Jr. (2017). "Translational

7452   Control in the Latency of Apicomplexan Parasites." Trends Parasitol **33**(12): 947-960.

7453   Hunter, C. A. and L. D. Sibley (2012). "Modulation of innate immunity by Toxoplasma gondii

7454   virulence effectors." Nat Rev Microbiol **10**(11): 766-778.

7455   Jaramillo, M., M. A. Gomez, O. Larsson, M. T. Shio, I. Topisirovic, I. Contreras, R. Luxenburg, A.

7456   Rosenfeld, R. Colina, R. W. McMaster, M. Olivier, M. Costa-Mattioli and N. Sonenberg (2011). "Leishmania

7457   repression of host translation through mTOR cleavage is required for parasite survival and infection." <u>Cell</u>

7458   <u>Host Microbe</u> **9**(4): 331-341.

7459   Jenkins, R. H., R. Bennagi, J. Martin, A. O. Phillips, J. E. Redman and D. J. Fraser (2010). "A

7460   conserved stem loop motif in the 5'untranslated region regulates transforming growth factor-beta(1)

7461   translation." <u>PloS One</u> **5**(8): e12283.

7462   Jewell, J. L., Y. C. Kim, R. C. Russell, F. X. Yu, H. W. Park, S. W. Plouffe, V. S. Tagliabracci and

7463   K. L. Guan (2015). "Metabolism. Differential regulation of mTORC1 by leucine and glutamine." <u>Science</u>

7464   **347**(6218): 194-198.

7465   Kaur, S., L. Lal, A. Sassano, B. Majchrzak-Kita, M. Srikanth, D. P. Baker, E. Petroulakis, N. Hay,

7466   N. Sonenberg, E. N. Fish and L. C. Platanias (2007). "Regulatory effects of mammalian target of rapamycin-

7467   activated pathways in type I and II interferon signaling." <u>J Biol Chem</u> **282**(3): 1757-1768.

7468   Kim, D., B. Langmead and S. L. Salzberg (2015). "HISAT: a fast spliced aligner with low memory

7469   requirements." <u>Nat Methods</u> **12**(4): 357-360.

7470   Kimura, T., A. Jain, S. W. Choi, M. A. Mandell, K. Schroder, T. Johansen and V. Deretic (2015).

7471   "TRIM-mediated precision autophagy targets cytoplasmic regulators of innate immunity." <u>J Cell Biol</u> **210**(6):

7472   973-989.

7473   Kramer, A., J. Green, J. Pollard, Jr. and S. Tugendreich (2014). "Causal analysis approaches in

7474   Ingenuity Pathway Analysis." <u>Bioinformatics</u> **30**(4): 523-530.

7475   Laliberte, J. and V. B. Carruthers (2008). "Host cell manipulation by the human pathogen

7476   Toxoplasma gondii." <u>Cell Mol Life Sci</u> **65**(12): 1900-1915.

7477   Landry, D. M., M. I. Hertz and S. R. Thompson (2009). "RPS25 is essential for translation initiation

7478   by the Dicistroviridae and hepatitis C viral IRESs." <u>Genes and Development</u> **23**(23): 2753-2764.

7479   Laplante, M. and D. M. Sabatini (2009). "mTOR signaling at a glance." <u>J Cell Sci</u> **122**(Pt 20): 3589-

7480   3594.

Larsson, O., M. Morita, I. Topisirovic, T. Alain, M. J. Blouin, M. Pollak and N. Sonenberg (2012). "Distinct perturbation of the translatome by the antidiabetic drug metformin." Proc Natl Acad Sci U S A **109**(23): 8977-8982.

Larsson, O., N. Sonenberg and R. Nadon (2010). "Identification of differential translation in genome wide studies." Proc Natl Acad Sci U S A **107**(50): 21487-21492.

Larsson, O., N. Sonenberg and R. Nadon (2011). "anota: Analysis of differential translation in genome-wide studies." Bioinformatics **27**(10): 1440-1441.

Lasko, P. (2012). "mRNA localization and translational control in Drosophila oogenesis." Cold Spring Harb Perspect Biol **4**(10).

Lau, Y. L., W. C. Lee, R. Gudimella, G. Zhang, X. T. Ching, R. Razali, F. Aziz, A. Anwar and M. Y. Fong (2016). "Deciphering the Draft Genome of Toxoplasma gondii RH Strain." PloS One **11**(6): e0157901.

Lavine, M. D. and G. Arrizabalaga (2009). "Induction of mitotic S-phase of host and neighboring cells by Toxoplasma gondii enhances parasite invasion." Mol Biochem Parasitol **164**(1): 95-99.

Leroux, L. P., M. Nishi, S. El-Hage, B. A. Fox, D. J. Bzik and F. S. Dzierszinski (2015). "Parasite Manipulation of the Invariant Chain and the Peptide Editor H2-DM Affects Major Histocompatibility Complex Class II Antigen Presentation during Toxoplasma gondii Infection." Infect Immun **83**(10): 3865-3880.

Leung, A. K. and P. A. Sharp (2010). "MicroRNA functions in stress responses." Molecular Cell **40**(2): 205-215.

Levy, S., D. Avni, N. Hariharan, R. P. Perry and O. Meyuhas (1991). "Oligopyrimidine tract at the 5' end of mammalian ribosomal protein mRNAs is required for their translational control." Proceedings of the National Academy of Sciences of the United States of America **88**(8): 3319-3323.

Lin, T. A., X. Kong, A. R. Saltiel, P. J. Blackshear and J. C. Lawrence, Jr. (1995). "Control of PHAS-I by insulin in 3T3-L1 adipocytes. Synthesis, degradation, and phosphorylation by a rapamycin-sensitive and mitogen-activated protein kinase-independent pathway." J Biol Chem **270**(31): 18531-18538.

Lindsay, D. S., R. R. Mitschler, M. A. Toivio-Kinnucan, S. J. Upton, J. P. Dubey and B. L. Blagburn (1993). "Association of host cell mitochondria with developing Toxoplasma gondii tissue cysts." American Journal of Veterinary Research **54**(10): 1663-1667.

7508   Liu, B. and S. B. Qian (2014). "Translational reprogramming in cellular stress response." <u>Wiley Interdiscip Rev RNA</u> **5**(3): 301-315.

7510   Livak, K. J. and T. D. Schmittgen (2001). "Analysis of relative gene expression data using real-time quantitative PCR and the 2(-Delta Delta C(T)) Method." <u>Methods</u> **25**(4): 402-408.

7512   Luft, B. J. and J. S. Remington (1992). "Toxoplasmic encephalitis in AIDS." <u>Clin Infect Dis</u> **15**(2): 211-222.

7514   Ma, T., M. A. Trinh, A. J. Wexler, C. Bourbon, E. Gatti, P. Pierre, D. R. Cavener and E. Klann (2013). "Suppression of eIF2alpha kinases alleviates Alzheimer's disease-related plasticity and memory deficits." <u>Nature Neuroscience</u> **16**(9): 1299-1305.

7517   Masvidal, L., L. Hulea, L. Furic, I. Topisirovic and O. Larsson (2017). "mTOR-sensitive translation: Cleared fog reveals more trees." <u>RNA Biology</u> **14**(10): 1299-1305.

7519   Meyuhas, O. and T. Kahan (2015). "The race to decipher the top secrets of TOP mRNAs." <u>Biochimica et Biophysica Acta</u> **1849**(7): 801-811.

7521   Miloslavski, R., E. Cohen, A. Avraham, Y. Iluz, Z. Hayouka, J. Kasir, R. Mudhasani, S. N. Jones, N. Cybulski, M. A. Ruegg, O. Larsson, V. Gandin, A. Rajakumar, I. Topisirovic and O. Meyuhas (2014). "Oxygen sufficiency controls TOP mRNA translation via the TSC-Rheb-mTOR pathway in a 4E-BP-independent manner." <u>Journal of Molecular Cell Biology</u> **6**(3): 255-266.

7525   Mohr, I. and N. Sonenberg (2012). "Host translation at the nexus of infection and immunity." <u>Cell Host Microbe</u> **12**(4): 470-483.

7527   Molestina, R. E., N. El-Guendy and A. P. Sinai (2008). "Infection with Toxoplasma gondii results in dysregulation of the host cell cycle." <u>Cell Microbiol</u> **10**(5): 1153-1165.

7529   Montoya, J. G. and J. S. Remington (2008). "Management of Toxoplasma gondii infection during pregnancy." <u>Clin Infect Dis</u> **47**(4): 554-566.

7531   Moreno, J. A., H. Radford, D. Peretti, J. R. Steinert, N. Verity, M. G. Martin, M. Halliday, J. Morgan, D. Dinsdale, C. A. Ortori, D. A. Barrett, P. Tsaytler, A. Bertolotti, A. E. Willis, M. Bushell and G. R. Mallucci (2012). "Sustained translational repression by eIF2alpha-P mediates prion neurodegeneration." <u>Nature</u> **485**(7399): 507-511.

314

7535   Morita, M., S. P. Gravel, V. Chenard, K. Sikstrom, L. Zheng, T. Alain, V. Gandin, D. Avizonis, M.

7536   Arguello, C. Zakaria, S. McLaughlan, Y. Nouet, A. Pause, M. Pollak, E. Gottlieb, O. Larsson, J. St-Pierre,

7537   I. Topisirovic and N. Sonenberg (2013). "mTORC1 controls mitochondrial activity and biogenesis through

7538   4E-BP-dependent translational regulation." Cell Metab **18**(5): 698-711.

7539   Morita, M., J. Prudent, K. Basu, V. Goyon, S. Katsumura, L. Hulea, D. Pearl, N. Siddiqui, S. Strack,

7540   S. McGuirk, J. St-Pierre, O. Larsson, I. Topisirovic, H. Vali, H. M. McBride, J. J. Bergeron and N. Sonenberg

7541   (2017). "mTOR Controls Mitochondrial Dynamics and Cell Survival via MTFP1." Molecular Cell **67**(6): 922-

7542   935 e925.

7543   Nash, P. B., M. B. Purner, R. P. Leon, P. Clarke, R. C. Duke and T. J. Curiel (1998). "Toxoplasma

7544   gondii-infected cells are resistant to multiple inducers of apoptosis." Journal of Immunology **160**(4): 1824-

7545   1830.

7546   Nehdi, A., P. Sean, I. Linares, R. Colina, M. Jaramillo and T. Alain (2014). "Deficiency in either 4E-

7547   BP1 or 4E-BP2 augments innate antiviral immune responses." PLoS One **9**(12): e114854.

7548   Nelson, M. M., A. R. Jones, J. C. Carmen, A. P. Sinai, R. Burchmore and J. M. Wastling (2008).

7549   "Modulation of the host cell proteome by the intracellular apicomplexan parasite Toxoplasma gondii."

7550   Infection and Immunity **76**(2): 828-844.

7551   Nickles, D., T. Sandmann, R. Ziman and R. Bourgon (2017). NanoStringQCPro: Quality metrics

7552   and data processing methods for NanoString mRNA gene expression data.

7553   O'Leary, N. A., M. W. Wright, J. R. Brister, S. Ciufo, D. Haddad, R. McVeigh, B. Rajput, B.

7554   Robbertse, B. Smith-White, D. Ako-Adjei, A. Astashyn, A. Badretdin, Y. Bao, O. Blinkova, V. Brover, V.

7555   Chetvernin, J. Choi, E. Cox, O. Ermolaeva, C. M. Farrell, T. Goldfarb, T. Gupta, D. Haft, E. Hatcher, W.

7556   Hlavina, V. S. Joardar, V. K. Kodali, W. Li, D. Maglott, P. Masterson, K. M. McGarvey, M. R. Murphy, K.

7557   O'Neill, S. Pujar, S. H. Rangwala, D. Rausch, L. D. Riddick, C. Schoch, A. Shkeda, S. S. Storz, H. Sun, F.

7558   Thibaud-Nissen, I. Tolstoy, R. E. Tully, A. R. Vatsan, C. Wallin, D. Webb, W. Wu, M. J. Landrum, A. Kimchi,

7559   T. Tatusova, M. DiCuccio, P. Kitts, T. D. Murphy and K. D. Pruitt (2016). "Reference sequence (RefSeq)

7560   database at NCBI: current status, taxonomic expansion, and functional annotation." Nucleic Acids Res

7561   **44**(D1): D733-745.

7562   Parker, M. W., D. Rossi, M. Peterson, K. Smith, K. Sikstrom, E. S. White, J. E. Connett, C. A.

7563   Henke, O. Larsson and P. B. Bitterman (2014). "Fibrotic extracellular matrix activates a profibrotic positive

7564   feedback loop." Journal of Clinical Investigation **124**(4): 1622-1635.

7565   Pause, A., G. J. Belsham, A. C. Gingras, O. Donze, T. A. Lin, J. C. Lawrence, Jr. and N. Sonenberg

7566   (1994). "Insulin-dependent stimulation of protein synthesis by phosphorylation of a regulator of 5'-cap

7567   function." Nature **371**(6500): 762-767.

7568   Pernas, L., Y. Adomako-Ankomah, A. J. Shastri, S. E. Ewald, M. Treeck, J. P. Boyle and J. C.

7569   Boothroyd (2014). "Toxoplasma effector MAF1 mediates recruitment of host mitochondria and impacts the

7570   host response." PLoS Biology **12**(4): e1001845.

7571   Piccirillo, C. A., E. Bjur, I. Topisirovic, N. Sonenberg and O. Larsson (2014). "Translational control

7572   of immune responses: from transcripts to translatomes." Nat Immunol **15**(6): 503-511.

7573   Ramskold, D., E. T. Wang, C. B. Burge and R. Sandberg (2009). "An abundance of ubiquitously

7574   expressed genes revealed by tissue transcriptome sequence data." PLoS Computational Biology **5**(12):

7575   e1000598.

7576   Ritchie, M. E., B. Phipson, D. Wu, Y. Hu, C. W. Law, W. Shi and G. K. Smyth (2015). "limma powers

7577   differential expression analyses for RNA-sequencing and microarray studies." Nucleic Acids Res **43**(7):

7578   e47.

7579   Roffe, M., F. H. Beraldo, R. Bester, M. Nunziante, C. Bach, G. Mancini, S. Gilch, I. Vorberg, B. A.

7580   Castilho, V. R. Martins and G. N. Hajj (2010). "Prion protein interaction with stress-inducible protein 1

7581   enhances neuronal protein synthesis via mTOR." Proceedings of the National Academy of Sciences of the

7582   United States of America **107**(29): 13147-13152.

7583   Ruggero, D. (2013). "Translational control in cancer etiology." Cold Spring Harb Perspect Biol **5**(2).

7584   Saeij, J. P. and E. M. Frickel (2017). "Exposing Toxoplasma gondii hiding inside the vacuole: a role for

7585   GBPs, autophagy and host cell death." Curr Opin Microbiol **40**: 72-80.

7586   Sancak, Y., L. Bar-Peled, R. Zoncu, A. L. Markhard, S. Nada and D. M. Sabatini (2010). "Ragulator-

7587   Rag complex targets mTORC1 to the lysosomal surface and is necessary for its activation by amino acids."

7588   Cell **141**(2): 290-303.

7589   Schindelin, J., I. Arganda-Carreras, E. Frise, V. Kaynig, M. Longair, T. Pietzsch, S. Preibisch, C.

7590   Rueden, S. Saalfeld, B. Schmid, J. Y. Tinevez, D. J. White, V. Hartenstein, K. Eliceiri, P. Tomancak and A.

7591   Cardona (2012). "Fiji: an open-source platform for biological-image analysis." Nat Methods **9**(7): 676-682.

7592   Schneider, R. J., Sonenberg, N. (2007). Translational control in cancer development and progression.

7593   Translational Control in Biology and Medicine. M. B. Mathews, Sonenberg, N., Hershey, J. W. Cold Spring

7594   Harbor New York, Cold Spring Harbor Laboratory Press**:** 401-431.

7595   Silvera, D., S. C. Formenti and R. J. Schneider (2010). "Translational control in cancer." Nat Rev

7596   Cancer **10**(4): 254-266.

7597   Silverman, J. A., H. Qi, A. Riehl, C. Beckers, V. Nakaar and K. A. Joiner (1998). "Induced activation

7598   of the Toxoplasma gondii nucleoside triphosphate hydrolase leads to depletion of host cell ATP levels and

7599   rapid exit of intracellular parasites from infected cells." J Biol Chem **273**(20): 12352-12359.

7600   Sinai, A. P. and K. A. Joiner (2001). "The Toxoplasma gondii protein ROP2 mediates host organelle

7601   association with the parasitophorous vacuole membrane." Journal of Cell Biology **154**(1): 95-108.

7602   Sinai, A. P., P. Webster and K. A. Joiner (1997). "Association of host cell endoplasmic reticulum

7603   and mitochondria with the Toxoplasma gondii parasitophorous vacuole membrane: a high affinity

7604   interaction." Journal of Cell Science **110 (Pt 17)**: 2117-2128.

7605   Smith, R. W., T. K. Blee and N. K. Gray (2014). "Poly(A)-binding proteins are required for diverse

7606   biological processes in metazoans." Biochem Soc Trans **42**(4): 1229-1237.

7607   Sokolova, O., M. Vieth, T. Gnad, P. M. Bozko and M. Naumann (2014). "Helicobacter pylori

7608   promotes eukaryotic protein translation by activating phosphatidylinositol 3 kinase/mTOR." Int J Biochem

7609   Cell Biol **55**: 157-163.

7610   Sonenberg, N. and A. G. Hinnebusch (2009). "Regulation of translation initiation in eukaryotes:

7611   mechanisms and biological targets." Cell **136**(4): 731-745.

7612   Sorensen, S. W., C. J. Billington, S. A. Norris, J. E. Briggs, M. T. Reding and G. A. Filice (1997).

7613   "Toxoplasma gondii: metabolism of intracellular tachyzoites is affected by host cell ATP production." Exp

7614   Parasitol **85**(1): 101-104.

7615   Spangle, J. M. and K. Munger (2010). "The human papillomavirus type 16 E6 oncoprotein activates

7616   mTORC1 signaling and increases protein synthesis." J Virol **84**(18): 9398-9407.

7617   Steinfeldt, T., S. Konen-Waisman, L. Tong, N. Pawlowski, T. Lamkemeyer, L. D. Sibley, J. P. Hunn

7618   and J. C. Howard (2010). "Phosphorylation of mouse immunity-related GTPase (IRG) resistance proteins

7619   is an evasion strategy for virulent Toxoplasma gondii." PLoS Biol **8**(12): e1000576.

7620   Syn, G., D. Anderson, J. M. Blackwell and S. E. Jamieson (2017). "Toxoplasma gondii Infection Is

7621   Associated with Mitochondrial Dysfunction in-Vitro." Front Cell Infect Microbiol **7**: 512.

7622   Thoreen, C. C., L. Chantranupong, H. R. Keys, T. Wang, N. S. Gray and D. M. Sabatini (2012). "A

7623   unifying model for mTORC1-mediated regulation of mRNA translation." Nature **485**(7396): 109-113.

7624   Thoreen, C. C., S. A. Kang, J. W. Chang, Q. Liu, J. Zhang, Y. Gao, L. J. Reichling, T. Sim, D. M.

7625   Sabatini and N. S. Gray (2009). "An ATP-competitive mammalian target of rapamycin inhibitor reveals

7626   rapamycin-resistant functions of mTORC1." J Biol Chem **284**(12): 8023-8032.

7627   Walsh, D., M. B. Mathews and I. Mohr (2013). "Tinkering with translation: protein synthesis in virus-

7628   infected cells." Cold Spring Harb Perspect Biol **5**(1): a012351.

7629   Wang, Y., L. M. Weiss and A. Orlofsky (2009). "Host cell autophagy is induced by Toxoplasma

7630   gondii and contributes to parasite growth." J Biol Chem **284**(3): 1694-1701.

7631   Wang, Y., L. M. Weiss and A. Orlofsky (2009). "Intracellular parasitism with Toxoplasma gondii

7632   stimulates mammalian-target-of-rapamycin-dependent host cell growth despite impaired signalling to S6K1

7633   and 4E-BP1." Cell Microbiol **11**(6): 983-1000.

7634   Wang, Y., L. M. Weiss and A. Orlofsky (2010). "Coordinate control of host centrosome position,

7635   organelle distribution, and migratory response by Toxoplasma gondii via host mTORC2." J Biol Chem

7636   **285**(20): 15611-15618.

7637   Weiss, L. M. and K. Kim (2007). Toxoplasma gondii : the model apicomplexan : perspectives and

7638   methods. Amsterdam ; Boston, Elsevier/Academic Press.

7639   Xu, X., X. Xiong and Y. Sun (2016). "The role of ribosomal proteins in the regulation of cell

7640   proliferation, tumorigenesis, and genomic integrity." Sci China Life Sci **59**(7): 656-672.

7641

Appendix 5

7643

7644

7645

Leishmania donovani lipophosphoglycan increases macrophage-dependent chemotaxis of

7646

CXCR6-expressing cells via CXCL16 induction

7647

7648

7649

Visnu Chaparro[a], Louis-Philippe Leroux[a], Aude Zimmermann[a], Armando Jardim[b], Brent Johnston[c], Albert

7650

Descoteaux[a], Maritza Jaramillo[a, #]

7651

7652

[a]Institut National de la Recherche Scientifique (INRS) - Institut Armand-Frappier, Laval, Quebec, Canada

7653

[b]Institute of Parasitology, McGill University, Sainte-Anne-de-Bellevue, Quebec, Canada

7654

[c]Departments of Microbiology and Immunology and Pediatrics, Dalhousie University, Halifax, Nova Scotia,

7655

Canada

7656

7657

[#]Correspondence should be addressed to: maritza.jaramillo@iaf.inrs.ca

7658

INRS - Institut Armand Frappier, 531 boul. des Prairies, Laval, Quebec, H7V 1B7, Canada

7659

Tel.: +1 (450) 687-5010 ext. 8872; fax: +1 (450) 686-5566

7660

7661

Running Title: Modulation of Mϕ CXCL16 production by _L. donovani_ LPG

7662

7663

7664

Abstract

CXCL16 is a multifunctional chemokine that is highly expressed by macrophages and other immune cells in response to bacterial and viral pathogens; however, little is known regarding the role of CXCL16 during parasitic infections. The protozoan parasite *Leishmania donovani (L. donovani)* is the causative agent of visceral leishmaniasis. Even though chemokine production is a host defense mechanism during infection, subversion of the host chemokine system constitutes a survival strategy adopted by the parasite. Here, we report that *L. donovani* promastigotes upregulate CXCL16 synthesis and secretion by bone marrow-derived macrophages (BMDMS). In contrast to wild-type parasites, a strain deficient in the virulence factor lipophosphoglycan (LPG) failed to induce CXCL16 production. Consistent with this, cell treatment with purified *L. donovani* LPG augmented CXCL16 expression and secretion. Notably, the ability of BMDMS to promote migration of cells expressing CXCR6, the cognate receptor of CXCL16, was augmented upon *L. donovani* infection in a CXCL16- and LPG-dependent manner. Mechanistically, CXCL16 induction by *L. donovani* required the activity of AKT and the mechanistic target of rapamycin (mTOR) but was independent of Toll-like receptor signaling. Collectively, these data provide evidence that CXCL16 is part of the inflammatory response elicited by *L. donovani* LPG *in vitro*. Further investigation using CXCL16 knockout mice is required to determine whether this chemokine contributes to the pathogenesis of visceral leishmaniasis, and to elucidate the underlying molecular mechanisms.

Introduction

7683

7684   The CXC chemokine ligand 16 (CXCL16) is mainly expressed by macrophages and dendritic cells

7685 but is also produced by B and T cells, fibroblasts, and activated endothelial cells (Shimaoka, Kume et al.

7686 2000, Shimaoka, Nakayama et al. 2004, Izquierdo, Martin-Cleary et al. 2014, Veinotte, Gebremeskel et al.

7687 2016). Along with CX3CL1/Fractalkine, CXCL16 is one of two transmembrane chemokines identified to

7688 date (Shimaoka, Nakayama et al. 2003). The protein structure of CXCL16 comprises a small C-terminal

7689 intracellular domain and an extracellular N-terminal chemokine domain bound to the transmembrane region

7690 through a heavily glycosylated mucin-like stalk (Izquierdo, Martin-Cleary et al. 2014). CXCL16 was initially

7691 described as a scavenger receptor for phosphatidylserine and oxidized low density lipoprotein (oxLDL), and

7692 therefore was named SR-PSOX (Shimaoka, Kume et al. 2000). In addition to its function as a scavenger

7693 receptor, the transmembrane form of CXCL16 mediates adhesion to cells expressing its specific receptor,

7694 CXCR6/BONZO (Shimaoka, Nakayama et al. 2004). In response to pro-inflammatory stimuli such as IFN-

7695 γ and TNF, the chemokine domain of CXCL16 is cleaved by the action of the metalloproteinase ADAM10

7696 (Abel, Hundhausen et al. 2004). Upon release into the extracellular milieu, the soluble form of CXCL16 acts

7697 as a chemoattractant for CXCR6^{+} cells such as activated NKT, NK, B cells, monocytes, and T cells

7698 (Johnston, Kim et al. 2003, Huang, Zhu et al. 2008, Izquierdo, Martin-Cleary et al. 2014). Increased CXCL16

7699 production is part of the inflammatory response elicited during bacterial and viral infections, and has been

7700 associated with either protective or harmful effects (Fahy, Townley et al. 2006, Sarkar, Chelvarajan et al.

7701 2016). For instance, CXCL16 expression in the liver and spleen is required to control bacterial burden

7702 during experimental salmonellosis (Fahy, Townley et al. 2006). Conversely, surface-bound CXCL16 acts

7703 as an entry receptor for an equine virus, and is essential for host cell permissiveness to viral infection

7704 (Sarkar, Chelvarajan et al. 2016). In regard to parasitic infections, a recent study suggested that CXCL16

7705 is dispensable for controlling *Leishmania donovani* (*L. donovani*) infection in the liver (Murray, Luster et al.

7706 2017); however, the impact of the CXCL16-CXCR6 axis was not investigated in other organs (e.g. spleen,

7707 bone marrow and lymph nodes) that also contribute to the pathogenesis of the infection.

7708   Visceral leishmaniasis is a neglected tropical disease caused by parasites of the *L. donovani* and

7709 *L. infantum* species (Wyllie, Patterson et al. 2012). The World Health Organization estimates that nearly

7710 300,000 new cases and 20,000 deaths occur annually in endemic areas inhabited by more than 600 million

7711 people at risk of infection (WHO 2017). The promastigote form of the parasite is transmitted by the sandfly

7712 vector to the mammalian host, where is rapidly internalized by phagocytic cells, including macrophages

7713 (Kaye and Scott 2011). Promastigotes subsequently differentiate into amastigotes that replicate within

7714 phagosomes, also named parasitophorous vacuoles (de Assis, Ibraim et al. 2012). To establish infection

7715 within phagocytes, *Leishmania* relies on a set of virulence factors that modulate immune and microbicidal

7716 macrophage functions (Olivier, Atayde et al. 2012, Podinovskaia and Descoteaux 2015).

7717   Lipophosphoglycan (LPG) is one of the major surface glycoconjugates of *Leishmania*

7718 promastigotes, which forms a dense glycocalyx covering the entire surface of the parasite and the flagellum

7719 (de Assis, Ibraim et al. 2012). In addition, LPG can be released from promastigotes into the extracellular

milieu (King, Chang et al. 1987). The structure of LPG consists of a polymer of repeating Gal(β1,4)Man(α1)-PO$_4$ units bound to the membrane via a core glycan structure attached to a glycosyl phosphatidylinositol (GPI) anchor (Descoteaux and Turco 1999). The lipid anchor and the glycan core of LPG are conserved but the sugar composition and sequence of branching sugars attached to or capping the repeat units vary among *Leishmania* species (de Assis, Ibraim et al. 2012). LPG is a multifaceted molecule that plays a crucial role in the establishment of the infection (de Assis, Ibraim et al. 2012, Olivier, Atayde et al. 2012, Podinovskaia and Descoteaux 2015). Notably, LPG prevents phagosome maturation (Desjardins and Descoteaux 1997), inhibits phagosomal acidification and oxidative burst (Lodge, Diallo et al. 2006, Vinet, Fukuda et al. 2009), reduces the phagocytic capacity of host macrophages (Vinet, Jananji et al. 2011), and hampers the lytic action of the complement system (Puentes, Da Silva et al. 1990). In addition to its inhibitory effects, extensive work supports the notion that LPG alters macrophage signaling and contributes to the inflammatory response triggered during *Leishmania* infection (de Veer, Curtis et al. 2003, Balaraman, Singh et al. 2005, Ibraim, de Assis et al. 2013, Rojas-Bernabe, Garcia-Hernandez et al. 2014, Lima, Araujo-Santos et al. 2017). For example, *L. mexicana* LPG stimulates the synthesis of TNF, IL-1β IL-12, and nitric oxide (NO) through the activation of ERK1/2 and p38 MAPK signaling (Rojas-Bernabe, Garcia-Hernandez et al. 2014). Moreover, *L. major* LPG interacts with Toll-like receptor 2 (TLR2) and induces the secretion of IL-12 and TNF in a MyD88-dependent manner (de Veer, Curtis et al. 2003). Similarly, *L. amazonensis* and *L. braziliensis* LPG up-regulate NO and TNF production via TLR2- and TLR4-mediated mechanisms (Ibraim, de Assis et al. 2013). More recently, it was shown that *L. infantum* LPG interacts with TLR1/2, activates ERK1/2 and JNK signaling, and induces the release of prostaglandin E$_2$, NO, TNF,IL-6, IL-12, and CCL2 (Lima, Araujo-Santos et al. 2017). Although less investigated than other *Leishmania* spp., purified *L. donovani* LPG also modulates pro-inflammatory mediator production, as evidenced by the up-regulation of the nuclear translocation of the transcription factor AP-1 and the synthesis of NO in a macrophage cell line (Balaraman, Singh et al. 2005). Interestingly, LPG has the opposite effect during infection of primary macrophages with *L. donovani* promastigotes (Prive and Descoteaux 2000). Extending these findings, here we report that the ability of *L. donovani* promastigotes to induce the synthesis of CXCL16 in infected macrophages is largely dependent on the presence of LPG. Accordingly, the ability of macrophages to induce migration of cells expressing CXCR6, the cognate receptor of CXCL16, is enhanced upon treatment with *L. donovani* LPG, or infection with wild-type (WT) but not with LPG-deficient *L. donovani* promastigotes.

Results

Leishmania donovani induces CXCL16 expression in macrophages

CXCL16 is induced during bacterial and viral infections (Fahy, Townley et al. 2006, Sarkar, Chelvarajan et al. 2016), and is highly expressed by activated macrophages (Shimaoka, Kume et al. 2000). Notably, *L. donovani* promotes the synthesis of a number of chemokines *in vitro* and *in vivo* (E.J., R. et al. 1999, Matte and Olivier 2002, Dasgupta, Roychoudhury et al. 2003, Gregory, Godbout et al. 2008, Oghumu, Lezama-Davila et al. 2010). These findings prompted us to investigate whether the expression of CXCL16 was modulated during *L. donovani* infection. To begin addressing this issue, we incubated bone marrow-derived murine macrophages (BMDMS) with or without *L. donovani* 1S promastigotes and measured levels of CXCL16 in the culture supernatant by ELISA. Infected BMDMS secreted higher amounts of CXCL16 than uninfected cultures (**Fig. 1A**). Interestingly, CXCL16 secretion in response to *L. donovani* was similar to that induced by IFN-γ stimulation. The expression of CXCL16 is regulated at the transcriptional level (Abel, Hundhausen et al. 2004). Thus, we next assessed whether enhanced CXCL16 production resulted from changes in mRNA expression. RT-qPCR experiments revealed an increasing accumulation of *Cxcl16* mRNA in *L. donovani*-infected BMDMS as compared to uninfected controls that was detectable as early as 4 h post-infection, and was maximal after 24 h (**Fig. 1B**). CXCL16 is synthesized as an intracellular precursor form that is glycosylated before being translocated to the cell membrane (Izquierdo, Martin-Cleary et al. 2014). Accordingly, western blot analyses showed that *L. donovani* rapidly induces the expression of a ~50 kDa migrating form of CXCL16 that corresponds to the size of the glycosylated protein (Gough, Garton et al. 2004) (**Fig. 1C**). We next examined whether the increase in total CXCL16 levels correlated with the up-regulation of the transmembrane from of the protein. In contrast to LPS, which served as positive control, no changes in the cell surface expression of CXCL16 were detected upon *L. donovani* infection (**Fig. 1D**, left). These data are consistent with a greater induction of CXCL16 in response to LPS than to *L. donovani* infection, as monitored by western blotting (**Fig. 1D**, right). Thus, *L. donovani* promotes the synthesis and subsequent secretion of CXCL16 by macrophages.

Induction of CXCL16 by *L. donovani* is dependent on the virulence factor LPG

LPG is the one of the major surface glycoconjugates of *Leishmania* promastigotes and plays a central role in the establishment of infection (Podinovskaia and Descoteaux 2015). Importantly, macrophages secrete several immune mediators following exposure to purified LPG (de Veer, Curtis et al. 2003, Ibraim, de Assis et al. 2013, Rojas-Bernabe, Garcia-Hernandez et al. 2014, Lima, Araujo-Santos et al. 2017). Therefore, we hypothesized that this virulence factor could be implicated in the up-regulation of CXCL16 in *L. donovani*-infected macrophages. To test this, we initially treated BMDMS with increasing concentrations of LPG purified from promastigote cultures of *L. donovani* 1S. We observed a dose-dependent effect of LPG on the induction of CXCL16, as monitored by western blotting (**Fig. 2A**). Of note, LPG concentrations as low as 250 ng/mL augmented CXCL16 protein levels to the same extent as live parasites (**Fig. 2A**); thus, subsequent cell treatments were carried out using this experimental condition.

324

7788   Additionally, time course experiments revealed that CXCL16 protein expression augments in response to
7789   LPG following a similar kinetics to that observed in *L. donovani*-infected BMDMS (**Fig. 2B**). To further
7790   investigate the role of LPG in the modulation of CXCL16 during *Leishmania* infection, we employed an
7791   LPG-defective strain of *L. donovani* 1S (Sudan), (i.e., *lpg1- knockout* [*KO*]), and an *lpg1-KO* add-back strain
7792   (i.e., *lpg1-KO+LPG1*) (Prive and Descoteaux 2000). In contrast to WT parasites, *L. donovani lpg1-KO*
7793   promastigotes failed to up-regulate the expression of CXCL16 in BMDMS (**Fig. 2C**). Remarkably, genetic
7794   rescue of the *lpg1* gene restored the ability of the parasite to augment CXCL16 production. Moreover, heat-
7795   killed or formalin-fixed *L. donovani* promastigotes retained their capacity to increase CXCL16 levels (**Fig.
7796   2C**), an indication that the observed effect does not require metabolically active parasites. In addition to *L.
7797   donovani* 1S, CXCL16 was also up-regulated upon infection with the Ethiopian strain *L. donovani* LV9
7798   (promastigotes and amastigotes) and with a different *Old World* species, *L. major* Seidman A2 (Senegal)
7799   (**Fig. 2C**). Notably, genetic deletion of GP63, another potent leishmanial virulence factor (Olivier, Atayde et
7800   al. 2012, Arango Duque and Descoteaux 2015), did not prevent CXCL16 induction by *L. major*
7801   promastigotes. Moreover, *New World* strains *L. infantum* Ba262 (Brazil) and *L. mexicana* M379 (Belize)
7802   were also able to enhance CXCL16 expression in BMDMS (**Fig. 2D**). Thus, the effect of *Leishmania* on
7803   CXCL16 does not appear to be stage-, species- or strain-specific, and does not depend on GP63. Further
7804   supporting the notion that LPG is required for CXCL16 induction by *L. donovani*, BMDMS infected with
7805   *lpg1-KO* promastigotes did not secrete CXCL16 above basal levels (**Fig. 2E**). In stark contrast, *L. donovani*
7806   WT and *lpg1-KO+LPG1* strains markedly increased the release of CXCL16 by infected cells as compared
7807   to uninfected controls (2.65 ± 0.05 and 2.79 ± 0.18 fold-change, respectively) (**Fig. 2E**). Similarly, treatment
7808   of BMDMS cultures with purified LPG significantly augmented CXCL16 secretion by BMDMS (5.05 ± 0.23
7809   fold-change). In agreement with our western blot and ELISA data, RT-qPCR experiments showed a marked
7810   accumulation of *Cxcl16* mRNA in BMDMS infected with either WT or *lpg1-KO+LPG1* parasites, or incubated
7811   with purified LPG (2.11 ± 0.05, 2.08 ± 0.03, and 2.45 ± 0.07 fold-change, respectively) (**Fig. 2F**). Conversely,
7812   infection with the *lpg1-KO* strain only led to a modest yet significant increase in *Cxcl16* mRNA levels as
7813   compared to control cultures (1.33 ± 0.04 fold-change). Collectively, this set of experiments indicates that
7814   up-regulation of CXCL16 expression following *L. donovani* infection is largely dependent on the virulence
7815   factor LPG.

7816

7817   ***L. donovani* induces the expression of CXCL16 in macrophages via AKT/mTOR-dependent but TLR-**
7818   **independent mechanisms**

7819   CXCL16 is induced via surface and endosomal TLR stimulation (Steffen, Abraham et al. 2018),
7820   and LPG triggers TLR-mediated signaling (de Veer, Curtis et al. 2003, S., P. et al. 2013, Rojas-Bernabe,
7821   Garcia-Hernandez et al. 2014, Lima, Araujo-Santos et al. 2017). Therefore, we postulated that the up-
7822   regulation of CXCL16 in macrophages incubated with *L. donovani* promastigotes could be dependent on
7823   TLR activation by LPG. To test this, we employed BMDMS isolated from mice deficient either in MyD88 or
7824   UNC93B, the two main adaptor proteins required for TLR-mediated cell responses (Kawai and Akira 2011).

As shown in **Fig. 3A**, MyD88 KO and UNC93B KO BMDMS produced similar levels of CXCL16 as WT cells following incubation with either *L. donovani* promastigotes or purified LPG. Similarly, *E. coli* LPS, a TLR4 ligand, augmented the expression of CXCL16 in a MyD88-independent manner (**Fig. 3B**, left). Interestingly, unlike *L. donovani* and LPG, up-regulation of CXCL16 in response to the TLR3 ligand Poly (I:C) was abrogated in the absence of UNC93B (**Fig. 3B**, right). Thus, the regulatory mechanisms of CXCL16 expression in macrophages appear to be stimulus-specific. In addition to TLRs, the induction of CXCL16 involves PI3K-AKT signaling (Chandrasekar, Mummidi et al. 2005). Interestingly, it was recently reported that the activity of AKT is sustained during *L. donovani* infection, which appears to be mediated by phosphoinositides present in the parasitophorous vacuole membrane (Zhang, Prasad et al. 2018). Consistent with this, we observed that AKT remained phosphorylated in cells infected with WT and *lpg1-KO+LPG1* parasites but was substantially reduced upon infection with the *lpg1-KO* promastigotes (**Fig. 3C**). Signaling through the kinase mechanistic target of rapamycin (mTOR) is a major output of AKT activity (Roux and Topisirovic 2018). Notably, increased mTOR signaling has been observed in *L. donovani*-infected macrophages (Cheekatla, Aggarwal et al. 2012). In line with our data on AKT, sustained phosphorylation of the ribosomal protein (rp) S6, a downstream target of mTOR, was also LPG-dependent (**Fig. 3C**). Accordingly, up-regulation of CXCL16 in response to *L. donovani* infection was affected when the activity of AKT or mTOR was blocked by the chemical inhibitors MK-2206 or Torin-1, respectively (**Fig. 3D**). Note that these compounds do not exert toxic effects on BMDMS up to 24 h, as we previously described (Leroux, Lorent et al. 2018). Thus, these data provide evidence that *L. donovani* induces the expression of CXCL16 in macrophages via AKT/mTOR-dependent and TLR-independent mechanisms.

CXCL16 secretion by *L. donovani*-infected macrophages promotes the migration of CXCR6-expressing cells

In response to pro-inflammatory cytokines, the N-terminal chemokine domain of CXCL16 is cleaved by the metalloprotease ADAM10 (Abel, Hundhausen et al. 2004) and released into the extracellular milieu to promote the migration of CXCR6-expressing cells (e.g. monocytes, neutrophils, NKT, B, T and dendritic cells) (Johnston, Kim et al. 2003, Huang, Zhu et al. 2008, Izquierdo, Martin-Cleary et al. 2014). Thus, we hypothesized that elevated CXCL16 secretion by *L. donovani*-infected macrophages would enhance chemotactic migration of CXCR6^{+} cells. Initially, CXCR6 was over-expressed in RAW 264.7 cells by transient transfection, and increased surface expression of the receptor was confirmed by flow cytometric analysis (**Fig. S1**). CXCR6^{+} RAW 264.7 cells were then used as effector cells in chemotaxis assays performed in the presence of conditioned medium (CM) from *L. donovani*-infected or uninfected BMDMS (**Figs. 4A**). A greater number of CXCR6^{+} cells migrated towards CM from BMDMS infected with WT than *lpg1-KO L. donovani* promastigotes (30.03 ± 7.53 and 9.01 ± 0.74 fold-change, respectively, over CM from uninfected BMDMS) (**Fig. 4B**). Consistent with this, CXCR6^{+} cell migration was induced in presence of CM from LPG-treated BMDMS (**Fig. S2**). Conversely, LPG added directly during migration assays failed to attract CXCR6^{+} cells (**Fig. S2**). Notably, CXCR6^{+} cell migration in response to recombinant CXCL16 or CM

7862   from *L. donovani*-infected BMDMS was dramatically reduced in the presence of a neutralizing antibody

7863   against CXCL16 (**Fig. 4B**). Accordingly, CM from *L. donovani*-infected CXCL16 KO BMDMS was a much

7864   less potent chemoattractant for CXCR6$^+$ cells than CM from *L. donovani*-infected WT BMDMS (~75%

7865   reduction in migration of CXCR6$^+$ cells) (**Fig. 4C**). Note that similar infection rates were observed in WT

7866   and CXCL16 KO BMDMS up to 24 h (**Fig. S3**), ruling out the possibility that differences in chemotactic

7867   activity between CM from *L. donovani*-infected WT and CXCL16 KO BMDMS were caused by changes in

7868   the percentage of infected cells. Thus, *L. donovani*–infected BMDMS promote migration of CXCR6$^+$ cells

7869   via LPG-inducible CXCL16 secretion.

7870

Discussion

7871

7872   The multifaceted chemokine CXCL16 displays a number of functions including lipid scavenging,

7873   cell-to-cell adhesion, and chemoattraction (Shimaoka, Kume et al. 2000, Johnston, Kim et al. 2003,

7874   Shimaoka, Nakayama et al. 2004, Huang, Zhu et al. 2008, Izquierdo, Martin-Cleary et al. 2014). Here, we

7875   demonstrate that the intracellular protozoan parasite *L. donovani* modulates the expression of CXCL16 in

7876   infected macrophages both at the mRNA and soluble protein levels, thereby influencing their ability to

7877   mediate chemotaxis of CXCR6^{+} cells. Using an LPG-deficient parasite mutant and purified LPG, we show

7878   that the induction of CXCL16 is dependent on this potent virulence factor.

7879

7880   Accumulating evidence supports the notion that different *Leishmania* spp. modulate the host

7881   chemokine system to attract cells that represent their natural niche for replication (Oghumu, Lezama-Davila

7882   et al. 2010, Hurrell, Beaumann et al. 2017). This becomes particularly relevant since we observed that

7883   CXCL16 up-regulation is not exclusive to *L. donovani*, and is not limited to species causing visceral

7884   leishmaniasis. Indeed, we detected a similar phenotype in macrophages infected with *Leishmania* spp. of

7885   different geographical origins (i.e., *Old World* and *New World* species) including two that cause cutaneous

7886   leishmaniasis (i.e., *L. major* and *L. mexicana*). Importantly, CXCR6, the cognate receptor of CXCL16 is

7887   expressed by subsets of monocytes/macrophages (Huang, Zhu et al. 2008, Linke, Meyer Dos Santos et al.

7888   2017) and neutrophils (Steffen, Abraham et al. 2018); therefore, it is tempting to speculate that CXCL16

7889   induced by *Leishmania* spp. helps attract immune cells that are subsequently infected to promote pathogen

7890   dissemination. Of note, we did not detect any changes in the membrane-bound form of CXCL16 in

7891   macrophages upon infection with *L. donovani*. Despite this observation, the ability of the parasite to infect

7892   other immune cells (Oghumu, Lezama-Davila et al. 2010, Hurrell, Beaumann et al. 2017) and the potential

7893   effect of extracellular LPG (King, Chang et al. 1987) in uninfected bystander cells could influence the

7894   expression of membrane-bound CXCL16 during *L. donovani* infection *in vivo*.

7895   In a recent report, Murray and colleagues (Murray, Luster et al. 2017) used *cxcr6* KO mice as

7896   surrogates to explore the role of CXCL16 during experimental visceral leishmaniasis. The authors

7897   concluded that the CXCL16-CXCR6 axis was dispensable for the control of *L. donovani* infection since

7898   granuloma formation and parasite clearance in the liver were not affected by the absence of CXCR6.

7899   However, the pathology of visceral leishmaniasis spans throughout different tissues and organs (Kumar

7900   and Nylen 2012). For instance, disruption of spleen microarchitecture is associated with local TNF

7901   production during visceral leishmaniasis (Engwerda, Ato et al. 2002). Notably, CXCL16 expression is up-

7902   regulated by pro-inflammatory cytokines such as TNF and IFN-γ (Abel, Hundhausen et al. 2004). Hence,

7903   recruitment of TNF and IFN-γ-producing cells could contribute to an inflammatory loop in the spleen

7904   involving CXCL16.

7905

7906   The contribution of LPG to host cell inflammatory responses has been extensively described in

7907   different *Leishmania* spp. (de Veer, Curtis et al. 2003, Ibraim, de Assis et al. 2013, Rojas-Bernabe, Garcia-

7908   Hernandez et al. 2014, Lima, Araujo-Santos et al. 2017) but is understudied in *L. donovani* (Balaraman,
7909   Singh et al. 2005); an important consideration given the species-specific chemical structures of LPG
7910   molecules (de Assis, Ibraim et al. 2012, Olivier, Atayde et al. 2012, Podinovskaia and Descoteaux 2015).
7911   By genetic and biochemical approaches (i.e., *lpg1-KO* mutant and purified LPG, respectively), our work
7912   uncovered a novel function for *L. donovani* LPG via the induction of CXCL16. Interestingly, we observed
7913   that amastigotes of *L. donovani* are also able to augment the expression of CXCL16 in infected
7914   macrophages although to a lesser extent than promastigotes. Given that differentiation of *L. donovani*
7915   promastigotes into amastigotes leads to a drastic reduction in LPG levels (Bahr, Stierhof et al. 1993), our
7916   data suggest that CXCL16 induction by the amastigote stage is likely to be LPG-independent. Note that
7917   despite the drastic reduction in LPG, amastigotes retain a glycocalyx of glycosylinositol phospholipids
7918   (Naderer and McConville 2008) that could account, at least in part, for the induction of CXCL16. Further *in*
7919   *vitro* and *vivo* studies are required to elucidate the mechanism of CXCL16 up-regulation by *L. donovani*
7920   amastigotes and to define its role during visceral leishmaniasis.
7921
7922   LPG molecules from other *Leishmania* spp. were reported to interact with several surface TLRs
7923   (i.e., TLR1, 2, and 4) (de Veer, Curtis et al. 2003, Ibraim, de Assis et al. 2013, Lima, Araujo-Santos et al.
7924   2017). Unexpectedly, we observed that *L. donovani* LPG-mediated upregulation of CXCL16 was
7925   independent of TLR signaling, as indicated by our data using MyD88 KO and UNC93B KO macrophages.
7926   The presence of the lipid anchor in *L. major* LPG was shown to be required for cytokine induction in
7927   macrophages (de Veer, Curtis et al. 2003). In contrast, intact *L. infantum* LPG, but not its glycan and lipid
7928   moieties, exhibited pro-inflammatory activity (Lima, Araujo-Santos et al. 2017). Structure-function studies
7929   of *L. donovani* LPG will shed light on the molecular components necessary to enhance CXCL16 production
7930   in macrophages.
7931
7932   Although the exact signaling events linked to *L. donovani*-driven CXCL16 induction remain to be
7933   established, our results indicate that this event relies on AKT/mTOR signaling, an important node in the
7934   regulation of macrophage immune functions (Katholnig, Linke et al. 2013). Indeed, within the upstream
7935   region of the *cxcl16* promoter, binding sites for several transcription factors have been predicted, including
7936   sites for CREB, SMAD, GATA, IRF, NF-κB, and AP-1, the latter being the main driver of IL-18-induced
7937   CXCL16 expression in aortic smooth muscles cells (Chandrasekar, Mummidi et al. 2005). LPG from *L.*
7938   *donovani* was shown to activate DNA binding of AP-1 in macrophages (Balaraman, Singh et al. 2005).
7939   Moreover, *L. major* LPG was able to induce an NF-κB activity in 293T cells (de Veer, Curtis et al. 2003).
7940   Thus, it is conceivable that *L. donovani* LPG promotes *Cxcl16* mRNA expression via AP-1 and/or NF-κB-
7941   dependent transcriptional activity in macrophages. Interestingly, our data indicate that the increase in
7942   CXCL16 protein expression occurs more rapidly than the accumulation of *Cxcl16* mRNA in *L. donovani*-
7943   infected macrophages. These data suggest that in addition to transcription, *L. donovani* might enhance the
7944   stability and/or the translation efficiency of *Cxcl16* mRNA. Of note, we recently demonstrated that another

7945   protozoan parasite, *Toxoplasma gondii*, selectively regulates translation of immune-related transcripts in

7946   macrophages via mTOR complex 1 (mTORC1), including chemokines (Leroux, Lorent et al. 2018).

7947   Therefore, sustained mTOR activity during *L. donovani* infection might be required to up-regulate CXCL16

7948   expression through both transcriptional and post-transcriptional mechanisms. In addition to a direct effect

7949   on *Cxcl16* mRNA metabolism, we cannot rule out the possibility that increased production of CXCL16 during

7950   *L. donovani* infection is at least in part dependent on the secretion of an LPG-inducible factor acting in an

7951   autocrine and/or paracrine fashion. Finally, given the importance of LPG in the establishment of *Leishmania*

7952   *spp*. infection (de Assis, Ibraim et al. 2012, Olivier, Atayde et al. 2012, Podinovskaia and Descoteaux 2015),

7953   the inability of LPG-deficient parasites to enhance CXCL16 synthesis and secretion may also be related to

7954   reduced fitness within macrophages.

7955

7956   The immune response to *L. donovani* integrates a complex network of pro- and anti-inflammatory

7957   modulators, the balance of which determines the outcome of the infection (Kumar and Nylen 2012). Our

7958   study identifies an additional immune mediator, the chemokine CXCL16 as part of macrophage responses

7959   to *L. donovani* promastigotes. Importantly, this phenotype is associated with the virulence factor LPG.

7960   Further *in vivo* and *in vitro* studies are required to assess the impact of CXCL16 in the development of

7961   visceral leishmaniasis. Ultimately, CXCL16 might emerge as a useful biomarker for disease severity and

7962   perhaps as a promising target for therapeutic intervention.

7963

Materials and Methods

Reagents

7966   Dulbecco's Modified Eagle Medium (DMEM), fetal bovine serum (FBS), Hank's Balanced Salt

7967 Solution (HBSS), 0.05% EDTA-Trypsin, penicillin and streptomycin were acquired from Wisent Inc. Zeocin

7968 was purchased from Gibco. Medium 199, HEPES, hemine, hypoxanthine, biotine, 6-biopterin,

7969 lipopolysaccharide (LPS, *Escherichia coli* serotype 0111:B4), and 10-phenanthroline monohydrate were

7970 acquired from Sigma-Aldrich. Recombinant mouse interferon gamma (IFNγ) was purchased from

7971 Cederlane Laboratories. RNasin was provided by Promega. Torin-1 and MK-2206 were acquired from

7972 Cayman Chemical. Complete EDTA-free protease inhibitor and PhosSTOP phosphatase inhibitor tablets

7973 were purchased from Roche.

7974

7975 **Mice**

7976   Animal procedures were conducted in accordance with the guidelines and policies of the Canadian

7977 Council on Animal Care, and all animal work was approved by the Comité institutionnel de protection des

7978 animaux (CIPA) of INRS - Institut Armand-Frappier (CIPA #1710-02). Four to 6-week old C57BL/6J and

7979 DBA/2J mice were purchased from The Jackson Laboratory and maintained in the Centre National de

7980 Biologie Expérimentale (CNBE) at INRS - Institut Armand-Frappier. *cxcl16* KO mice were generated, as

7981 previously described (Veinotte, Gebremeskel et al. 2016) and housed within the Carleton Animal Care

7982 Facility at Dalhousie University. Hind legs from *unc93b* KO mice were provided by Dr. Simona Stäger (INRS

7983 - Institut Armand-Frappier). Hind legs from *myd88* KO mice were a gift from Dr. Alain Lamarre (INRS -

7984 Institut Armand-Frappier).

7985

7986 **Differentiation of bone marrow-derived macrophages**

7987   Bone marrow precursor cells were obtained from femurs and tibias of commercial C57BL/6J (The

7988 Jackson Laboratory), *cxcl16* KO, *unc93b* KO and *myd88* KO mice, and differentiated into bone marrow-

7989 derived macrophages (BMDMS) as previously described (Leroux, Lorent et al. 2018). Briefly, bone marrow

7990 precursor cells were flushed from femurs and tibias maintained in HBSS (100 U/mL penicillin, 100 µg/mL

7991 streptomycin, 4.2 mM sodium bicarbonate) at 4°C. Red blood cells were lysed in ACK lysis buffer (150 mM

7992 NH_4Cl, 10 mM $KHCO_3$, 0.1 mM EDTA) for 7 min at room temperature. Precursors cells were then

7993 resuspended in BMDMS culture medium (DMEM, 10% heat-inactivated FBS, 2 mM L-glutamate, 1 mM

7994 sodium pyruvate, 100 U/mL penicillin, 100 µg/mL streptomycin) supplemented with 15% L929 fibroblast-

7995 conditioned culture medium (LCCM). Cells were seeded in 10 cm-diameter tissue culture-treated dishes,

7996 and incubated overnight at 37°C, 5% CO_2. The following day, non-adherent cells were collected,

7997 resuspended in BMDMS culture medium supplemented with 30% LCCM, and plated in 10 cm-diameter

7998 non-treated Petri dishes ($5×10^6$ cells per dish). Medium was replenished two days later and differentiated

7999 BMDMS were collected 7 days after marrow extraction. Differentiation of precursor cells into macrophages

8000 was routinely assessed by monitoring for CD11b and F4/80 co-expression by flow cytometry using APC

8001 anti-mouse/human CD11b antibody #101211 and PE anti-mouse F4/80 antibody # 123109 (Biolegend), as
8002 previously described (Leroux, Dasanayake et al. 2015).

8003

8004 **Parasites**

8005 *Leishmania donovani* (1S and LV9 strains), *L. major* (SA2 strain), *L. mexicana* (M379 strain), and
8006 *L. infantum* (Ba262 strain) promastigotes were cultured at 26°C in M199 medium supplemented with 10%
8007 heat-inactivated FBS, 100 µM hypoxanthine, 5 µM hemin, 3 µM biopterin, 1 µM biotin, 50 U/ml penicillin,
8008 and 50 µg/mL streptomycin. The isogenic *L. donovani* LPG-defective mutant *lpg1-KO* and *lpg1-KO+LPG1*
8009 *add back* (i.e., rescue) were described previously (Prive and Descoteaux 2000). The *lpg1-KO* mutant
8010 secretes repeating Gal(β1,4)Man(α1)-PO$_4$-containing molecules, but lacks the ability to assemble a
8011 functional LPG glycan core (Huang and Turco 1993), precluding synthesis and expression of LPG. The *L.*
8012 *donovani lpg1-KO+LPG1* add-back strain was cultured in the presence of 100 µg/mL Zeocin. Stationary
8013 phase promastigotes were used for macrophage infections. *L. donovani* amastigotes (LV9 strain) were
8014 isolated from the spleen of infected female Golden Syrian hamsters (The Jackson Laboratory, Bar Harbor,
8015 ME, USA), as previously described (Matte and Descoteaux 2010).

8016

8017 **LPG purification**

8018 LPG from *L. donovani* promastigotes (1S strain) was purified by chromatography as previously
8019 described (Turco, Wilkerson et al. 1984). Briefly, 10^9 exponentially growing parasites were centrifuged at
8020 1,900 *x g* for 10 min at room temperature and washed with 5 mL of PBS. Cells were delipidated by
8021 sequential extraction at 4°C with 3 x 25 mL of chloroform/methanol/water (3:2:1), 3 x 25 mL
8022 chloroform/methanol/water (1:1:0.3), and 3 x 25 ml 4 mM MgCl. LPG was extracted from the resulting
8023 delipidated residue fraction by four extractions at 4°C with 25 mL of the following solvent:
8024 water/ethanol/diethyl ether/pyridine/concentrated NH$_4$OH (15:15:5:1:0.017). Solvent supernatant was taken
8025 to dryness under reduced pressure. The residue was resuspended in 5 ml of 40 mM NH$_4$OH, 1 mM EDTA,
8026 and the insoluble material was removed by centrifugation at 15,000 x *g* for 10 min. The supernatant was
8027 applied to a Sephadex G-150 column (1×40 cm) equilibrated with the same buffer. Samples containing
8028 LPG were pooled and lyophilized. The sample was resuspended in 40 mM NH$_4$OH, desalted on a Sephadex
8029 G-25 column (1×5 cm) equilibrated in 40 mM NH$_4$OH and lyophilized. LPG was resuspended in 10 mL of
8030 water/ethanol/diethyl ether/pyridine/concentrated NH$_4$OH (15:15:5:1:0.017) and precipitated at -20°C for 18
8031 h with the addition of 10 mL of methanol. Precipitated LPG was resuspended in sterile PBS, and endotoxin
8032 levels were measured with the *Limulus* amebocyte lysate (LAL) chromogenic endotoxin quantitation kit
8033 (Pierce), according to manufacturer's specifications

8034

8035 **BMDMS infection**

8036 *L. donovani* promastigotes were opsonized with 10% serum from DBA/2J mice, which are naturally
8037 deficient in complement component 5 (C5) (Howell, Soto et al. 2013), for 20 minutes at 37°C, 5% CO$_2$.

8038   Adherent BMDMSs (2×10^5 cells per cm^2) were inoculated with opsonized promastigotes of the different

8039   *Leishmania* species and strains at a multiplicity of infection (MOI) of 10:1. Non-internalized parasites were

8040   removed after 6 h, and cells were incubated in BMDMS culture media O/N at 37°C, 5% CO_2. The

8041   percentage of infected cells was assessed by microscopic examination using the PROTOCOL™ Hema3™

8042   manual staining system (Thermo Fisher Scientific).

8043

8044   **RNA extraction and quantitative RT-PCR**

8045   Total BMDMS RNA was isolated using QIAzol (Qiagen), according to the manufacturer's protocol.

8046   One μg of RNA was reverse transcribed using the Superscript IV VILO Master Mix (Invitrogen). Quantitative

8047   PCR was performed with PowerUp™ SYBR® Green Master Mix (Applied Biosystems), according to the

8048   manufacturer's instructions using a QuantStudio 3 Real-Time PCR System (Applied Biosciences). Analysis

8049   was carried out by relative quantification using the Comparative CT method ($\Delta\Delta$Ct) (Taylor, Wakem et al.

8050   2010). Experiments were performed in independent biological replicates (n=3), whereby every sample was

8051   analysed in a technical triplicate. Relative mRNA amounts were normalized to *actinb*. Primers were

8052   designed using NCBI Primer-BLAST (http://www.ncbi.nlm.nih.gov/tools/primer-blast/) for mouse *cxcl16*

8053   gene forward (5' -AGACCAGTGGGTCCGTGAAC-3') and reverse (5' -ACTATGTGCAGGGGTGCTCG-3'),

8054   and for mouse *actinb* gene forward (5' -ACTGTCGAGTCGCGTCCA-3') and reverse (5'-

8055   ATGGCTACGTACATGGCTCG-3').

8056

8057   **Western blot analysis**

8058   Following infection and other treatments, BMDMS cultures were collected in ice-cold PBS pH 7.4

8059   by scrapping, centrifuged, and lysed in ice-cold RIPA buffer (25 mM Tris-HCl pH 7.6, 150 mM NaCl, 1%

8060   Triton X-100, 0.5% sodium deoxycholate, 0.1% SDS , cOmplete™ EDTA-free protease inhibitor cocktail,

8061   PhosStop™ phosphatase inhibitor, and 10 mM 10-phenathroline). Cell debris was removed by

8062   centrifugation (15,000 × *g* for 15 min at 4°C), and protein content was estimated using the BCA Protein

8063   Assay kit (Pierce). Protein extracts were subjected to SDS-PAGE, and the resolved proteins were

8064   transferred onto PVDF membranes (Bio-Rad). Membranes were blocked for 1 h in 5% skim milk TBS with

8065   0.1% Tween 20 and probed with the following primary antibodies overnight at 4°C: anti-CXCL16 (no.

8066   AF503) from R&D Systems; anti-phospho-AKT (T308) (no. 2965), anti-β-actin (no. 3700), anti-COX-2 (no.

8067   4842), and anti-phospho S6 (S235/236 (no. 2211) from Cell Signaling Technologies; anti-*Leishmania* GP63

8068   was a gift from Dr. Robert McMaster (University of British Columbia, Vancouver, Canada); and anti-

8069   *Leishmania* inosine 5'-monophosphate dehydrogenase (IMPDH) was previously described (Fulwiler, Soysa

8070   et al. 2011). Membranes were then incubated with the following IgG horseradish peroxidase-linked

8071   antibodies: goat anti-rabbit IgG (no. A0545) and goat anti-mouse IgG (no. A4416) from Sigma-Aldrich;

8072   donkey anti-goat IgG (no. HAF109) and goat anti-guinea pig IgG (no. CLAS10-653) from R&D Systems.

8073   Proteins were then detected by chemiluminescence using Clarity Western ECL substrate (Bio-Rad) and

8074   exposing membranes to autoradiography film (Denville Scientific).

ELISA

Soluble CXCL16 in the supernatants from infected, treated, and control BMDMS cultures were assessed using the ELISA Capture mouse CXCL16 antibody (no. MAB503) and ELISA Detection mouse CXCL16 biotinylated antibody (no. BAF503) from R&D systems. Concentrations were calculated from standard curves generated using linear regression analysis of data obtained from serial dilutions using recombinant murine CXCL16 chemokine domain (no. 503-CX/CF).

Macrophage cell line transfection

The RAW 264.7 mouse macrophage cell line was maintained in DMEM supplemented with 10% FBS, 100 U/mL penicillin, 100 µg/mL streptomycin and 2 mM L-glutamine at 37°C, 5% CO2. Cell transfection with the BONZO/CXCR6 ORF pCMV3 expression plasmid (Sino Biological) was carried out using Lipofectamine 2000 (Invitrogen), according to the manufacturer's specifications. Transfection efficiency was monitored by flow cytometry.

Flow cytometry staining

BMDMS and CXCR6-overexpressing RAW 264.7 cultures were harvested, washed, and resuspended in FACS buffer (PBS [pH 7.2-7.4] with 0.1% BSA). Fc receptors were blocked with anti-mouse CD16/32 (Fcγ III/II) (clone 93; #101302) (BioLegend), then probed with the following antibodies for 30 min: goat anti-mouse CXCL16 (R&D Systems) or FITC-anti-CXCR6 (CD186) (clone SA051D1; #151108) (BioLegend). When required, samples were then stained with a chicken anti-goat IgG coupled to Alexa Fluor 488 (Invitrogen). Isotype-matched FITC-coupled rat IgG2b,κ (clone RTK4530; #400605) (BioLegend) or AF488-coupled chicken anti-goat IgG only were included to control for non-specific staining. After staining, cells were fixed in PBS with 1% PFA for 15 min on ice. The fixative was quenched with PBS with 0.1 M glycine, and cells were washed twice in FACS buffer. Samples were acquired using either a BD FACSCalibur, and data were analyzed using Flowing Software (Turku, Finland).

Chemotactic migration assays

Chemotactic migration of CXCR6-overexpressing RAW264.7 macrophages was monitored by Transwell™ assays using 8-µm pore size membrane inserts (Corning). Conditioned medium from untreated, *L. donovani*-infected and LPG-treated WT and CXCL16 KO BMDMS were added to the lower chambers of Transwell™ plates. CXCR6-overexpressing RAW264.7 macrophages (5×10^5 / well) were added to Transwell™ inserts and were incubated at 37°C, 5% CO_2 for 4 h. Cell migration was quantified by manual staining of the insert membranes with the PROTOCOL™ Hema3™ system, remaining cells in the upper chamber were removed after the last wash using a cotton swab.

Statistical analysis

Statistical significance was determined using the Student's T test for simple comparisons and one-way ANOVA followed by Bonferroni post-hoc test for multiple comparisons. Calculations were performed using Prism software (GraphPad Software, La Jolla CA). Differences were considered significant when * P < 0.05, ** P < 0.01, *** P < 0.001, **** P < 0.0001.

Author Contributions

Conceived and designed the experiments: VC, LPL, AZ, MJ. Performed the experiments: VC, LPL, AZ. Analyzed the data: VC, LPL, AZ, MJ. Contributed reagents and materials: AJ, BJ, AD. Wrote the manuscript: VC, LPL, MJ.

Declaration of Interests

The authors declare no competing interests.

8138
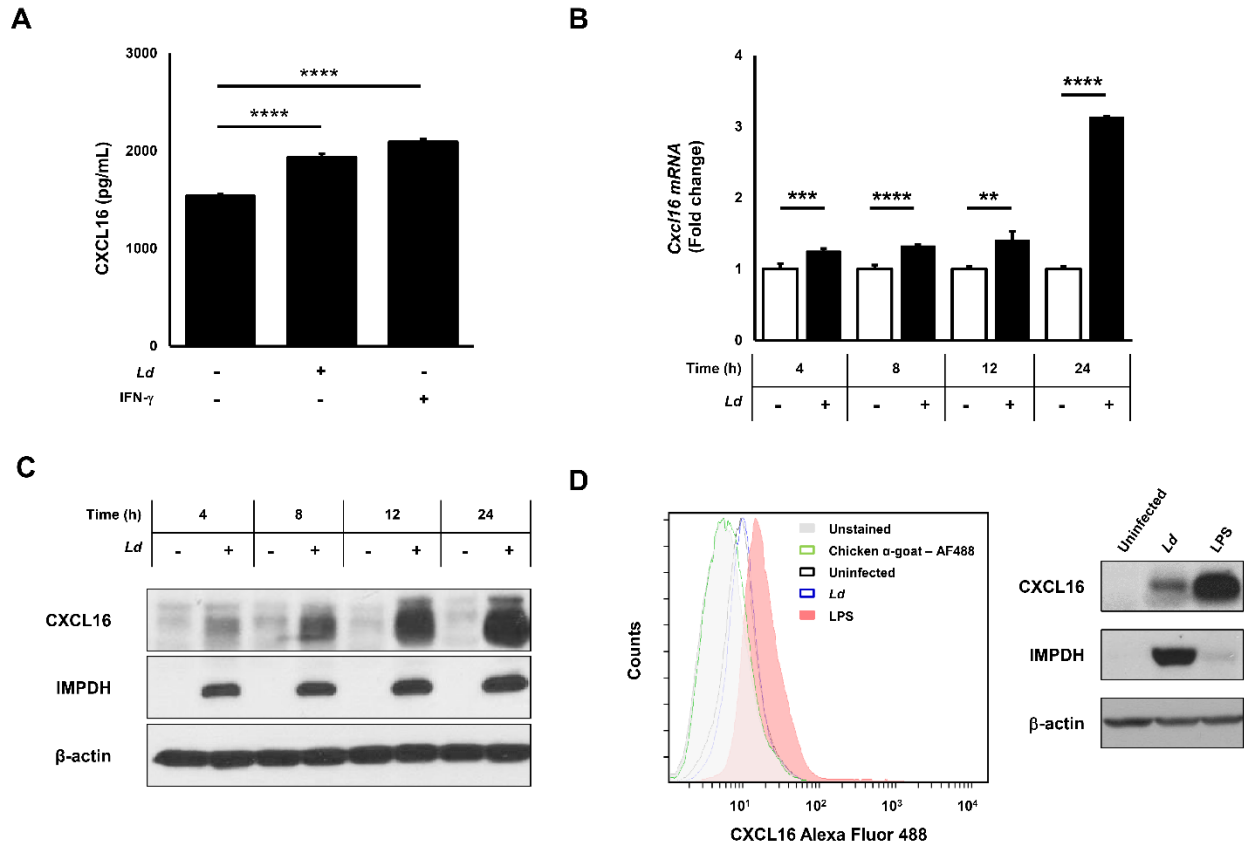
Figure 1. *Leishmania donovani* augments CXCL16 production in macrophages. BMDMS cultures were inoculated with *L. donovani* (*Ld*) promastigotes (MOI 10:1), treated with 100 U/mL IFN-γ or 100 ng/mL LPS, or left untreated/uninfected (control) for 24 h (**A, D**) or the indicated time (**B-C**). (**A**) Secreted CXCL16 was measured by sandwich ELISA. (**B**) *Cxcl16* mRNA amounts were quantified by RT-qPCR (normalized to *β-actin*); data are expressed as fold-increase in infected over control samples. (**C**) Total CXCL16 protein levels were monitored by western blotting; total amounts of β-actin were used as a loading control. (**D**) Expression of the transmembrane form of CXCL16 was examined by flow cytometry (left). Total CXCL16 protein levels were monitored by western blotting as indicated in (C) (right). (**A-B**) Results are presented as mean ± SD (biological replicates n = 3). *** $P < 0.001$, **** $P < 0.0001$ compared to uninfected. (**C-D**) Data are representative of three independent experiments.

8149

336

A

LPG (ng/mL)

0   250   500   1000   *Ld* WT

CXCL16

β-actin

B

Time (h)	4		8		12		24	
LPG	−	+	−	+	−	+	−	+

CXCL16

β-actin

C

Ld 1S   *Ld* LV9   *Lmj* SA2

Uninfected / WT / *lpg1*-KO / *lpg1*-KO+LPG1 / WT heat-killed / WT formalin-fixed / Promastigotes / Amastigotes / WT / *gp63* KO

CXCL16

IMPDH

GP63

β-actin

D

Uninfected / *L. infantum chagasi* Ba262 / Uninfected / *L. mexicana* M379

CXCL16

β-actin

E

CXCL16 (pg/mL)

Uninfected / *Ld* WT / *Ld lpg1*-KO / *Ld lpg1*-KO+*LPG1* / LPG

ns   ***   ***   ****

F

Cxcl16 mRNA (Fold-change)

Uninfected / *Ld* WT / *Ld lpg1*-KO / *Ld lpg1*-KO+*LPG1* / LPG

****   ***   ****   ****

8150

8151

337

Figure 2. Induction of macrophage CXCL16 by *L. donovani* is dependent on the virulence factor LPG. BMDMS cultures were treated with increasing concentrations of *Ld* LPG for 24 h (**A**) or with 250 ng/mL LPG for the indicated time (**B**), and the expression of CXCL16 was monitored by western blotting. β-actin was used as a loading control. (**C-D**) BMDMS cultures were infected at MOI 10:1 with different *L. donovani* strains and stages (*L. donovani* 1S promastigotes: WT, *lpg1-KO*, *lpg1-KO+LPG1*, WT heat-killed [hk], WT formalin-fixed [ff]; *L. donovani* LV9 promastigotes and amastigotes), promastigotes of other *Leishmania* spp. (*L. major* SA2 WT or *gp63*-KO, *L. infantum* Ba262, *L. mexicana* M379), or left uninfected for 24 h. CXCL16 protein levels were examined as in (A). Parasite infection was monitored by probing for *Leishmania* IMPDH. Efficient KO of *gp63* in *L. major* was verified by probing with an anti-*Leishmania* GP63 antibody. (**E-F**) Cells were infected as in (C) or treated with 250 ng/mL LPG as indicated in (A). (**E**) Secreted CXCL16 was measured by sandwich ELISA. (**F**) Fold-change in *Cxcl16* mRNA expression (normalized to *β-actin*) in *L. donovani*-infected or LPG-treated over control samples was determined by RT-qPCR. (**A-D**) Results are representative of three independent biological replicates. (**E-F**) Data are presented as mean ± SD (biological replicates n = 3). *** $P < 0.001$; **** $P < 0.0001$ compared to uninfected/untreated; *ns* = not significant.

A

	WT			MyD88 KO			UNC93B KO		

Ld   − + −   − + −   − + −
LPG   − − +   − − +   − − +

CXCL16

IMPDH

β-actin

B

	WT		MyD88 KO	

LPS   − +   − +

CXCL16

COX-2

β-actin

	WT		UNC93B KO	

Poly (I:C)   − +   − +

CXCL16

β-actin

C

Ld 1S

Uninfected   WT   *lpg1*-KO   *lpg1*-KO+*LPG1*

CXCL16

Ⓟ-Thr308-AKT

AKT

Ⓟ-Ser235/236-rpS6

rpS6

IMPDH

β-actin

D

Ld 1S

Uninfected   DMSO   MK-2206   Torin-1

CXCL16

Ⓟ-Thr308-AKT

AKT

Ⓟ-Ser235/236-rpS6

rpS6

IMPDH

β-actin

8168

339
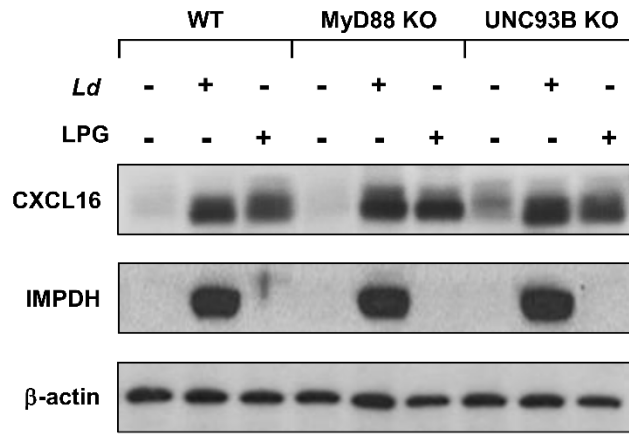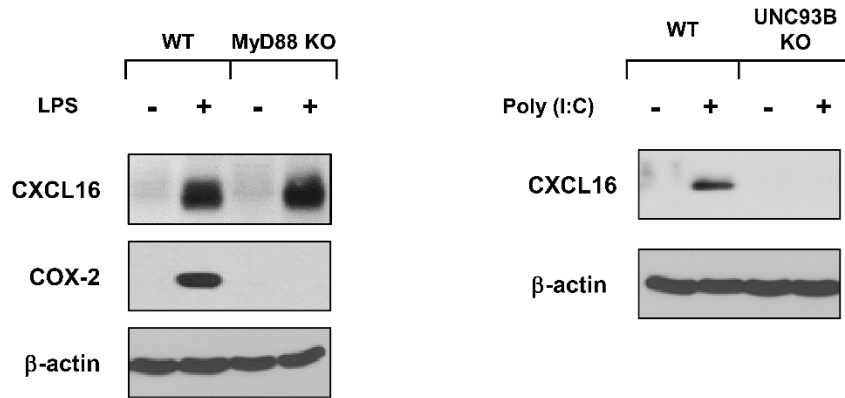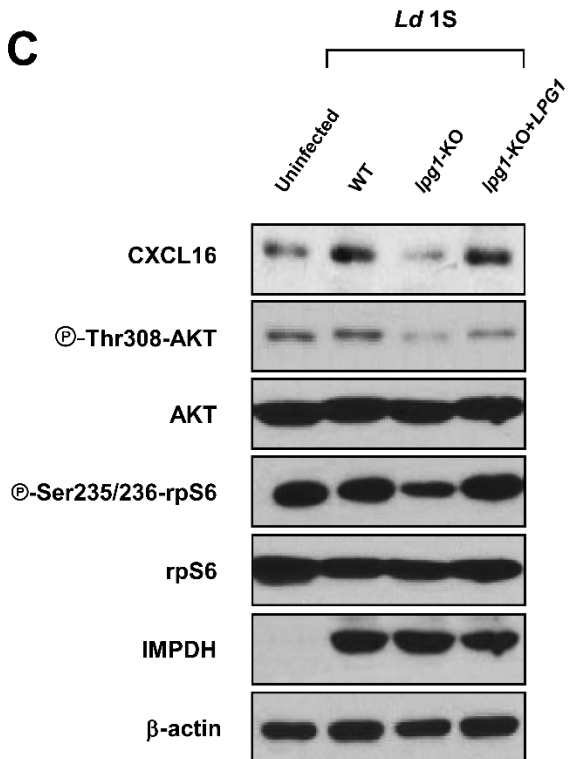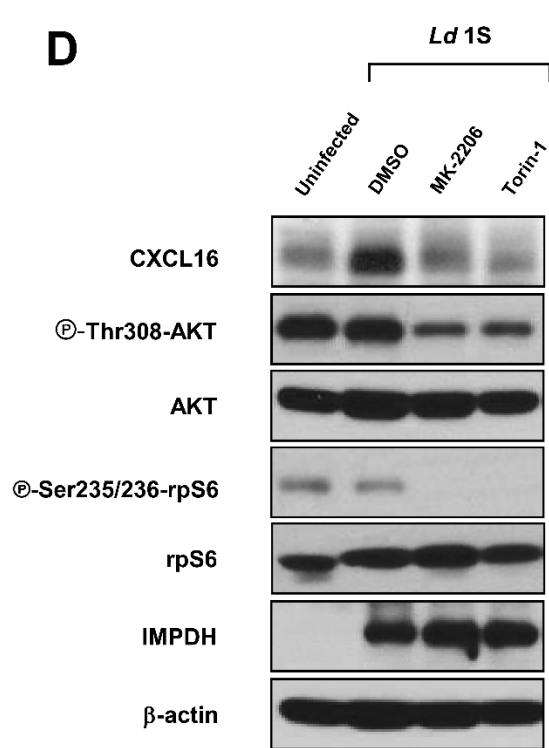
8169 **Figure 3. CXCL16 induction in *L. donovani*-infected macrophages is AKT/mTOR-dependent but TLR-**

8170 **independent.** (**A-B**) WT, MyD88 KO and UNC93B KO BMDMS cultures were inoculated with *Ld,* treated

8171 with 250 ng/mL LPG, 100 ng/mL LPS, or 250 ng/mL poly (I:C) or left uninfected/untreated for 24 h. CXCL16

8172 protein expression was assessed by western blotting. β-actin was used as a loading control. Parasite

8173 infection was monitored by probing for *Leishmania* IMPDH. Induction of COX-2 served as surrogate for

8174 disrupted TLR signaling in MyD88 KO cells. **(C)** BMDMS cultures were inoculated with *L. donovani* WT,

8175 *lpg1-KO* or *lpg1-KO+LPG1* or left uninfected for 24 h, and the activity of AKT/mTOR signaling was

8176 monitored by western blotting using phospho-specific and total antibodies against AKT and S6,

8177 respectively. CXCL16 expression and efficacy of infection were examined as in (A). **(D)** BMDMS cultures

8178 were pre-treated with 2 µM MK-2206, 200 nM Torin-1, or an equal volume of DMSO (vehicle) for 1 h, then

8179 infected with *Ld* promastigotes for 24 h. Phosphorylation status and total levels of AKT and S6 were

8180 assessed as in (C). Results are representative of at least two independent biological replicates.

8181

8182
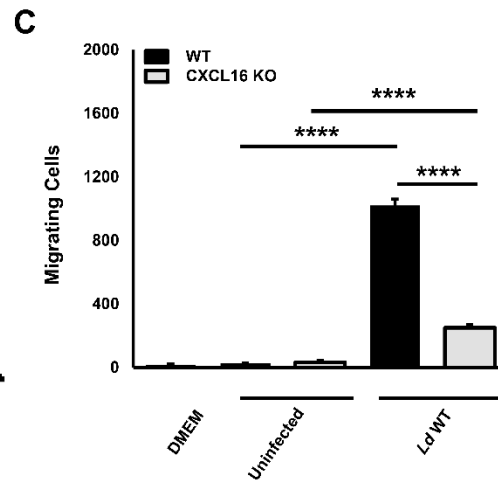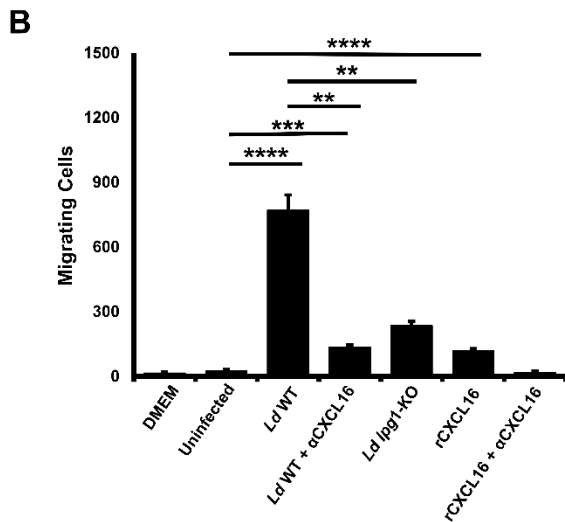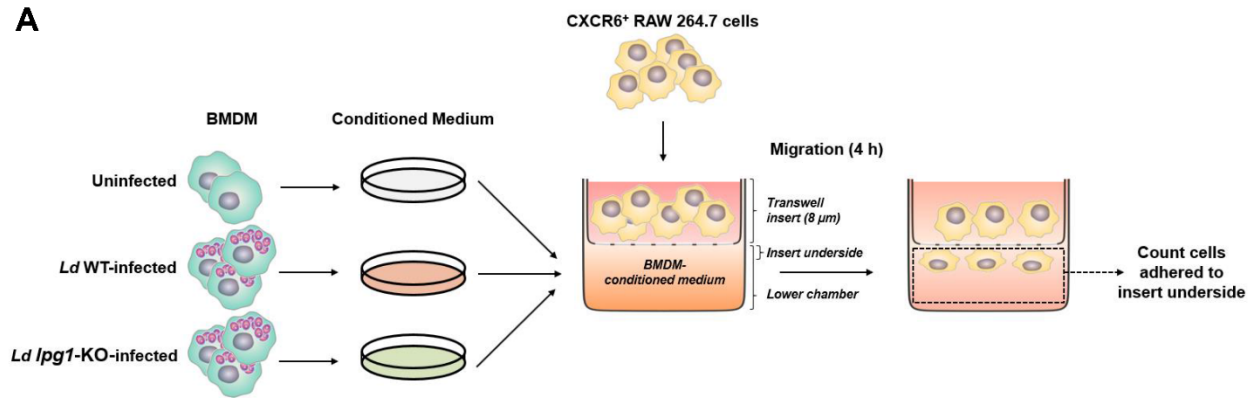
Figure 4. *L. donovani* **promotes macrophage-mediated chemotaxis of CXCR6^{+} cells via LPG-dependent CXCL16 production.** (**A**) Experimental design to assess chemotactic activity of secreted CXCL16. Conditioned-medium from infected or uninfected BMDMS cultures was collected after 24 h and added to the lower chamber of Transwell™ plates. CXCR6-transfected RAW 264.7 cells were added to the upper Transwell™ insert (8 μm pore-size) and allowed to migrate for 4 h. Migrated cells adhering to the insert underside were counted by microscopy. **(B-C)** Conditioned medium from WT or CXCL16 KO BMDMS cultures infected with *Ld* WT or *Ld lpg1-KO*, or left uninfected for 24 h were tested for chemotactic activity. Fresh medium (DMEM; non-conditioned) was included to monitor basal migration activity. As a positive control, murine recombinant CXCL16 (rCXCL16) was added (500 pg/mL) to the lower chamber. A CXCL16 neutralizing antibody was added (250 ng/mL) to specifically block CXCL16-mediated chemotactic activity. Data are presented as mean ± SD (biological replicates n = 3). ** $P < 0.01$, **** $P < 0.0001$ for indicated comparisons.
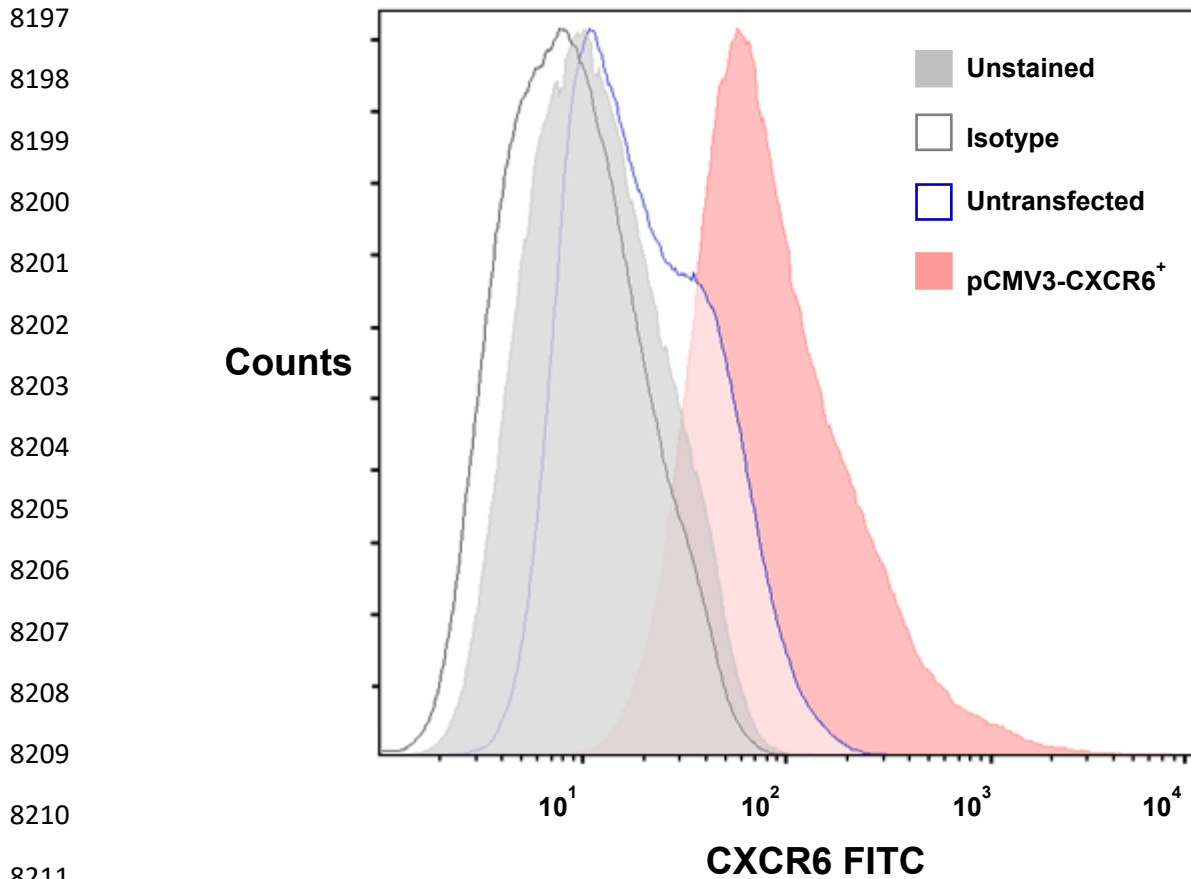
Figure S1. CXCR6 expression in pCMV3-CXCR6-transfected RAW 264.7 cells. RAW 264.7 cells were transfected with a BONZO/CXCR6 ORF pCMV3 expression plasmid using Lipofectamine 2000. Transfected cells were cultured 24 h, stained with a FITC-conjugated anti-mouse CXCR6 antibody (pink shaded curve) and analyzed by flow cytometry. Unstained cells (gray shaded curve) were included to adjust baseline fluorescence parameters. A FITC-conjugated isotype-matched antibody was used as a staining control (gray solid line curve). Untransfected RAW 264.7 cells (blue solid line) were included as a comparison to show CXCR6-overexpression in the transfected cells. Results are representative of at least three independent experiments.
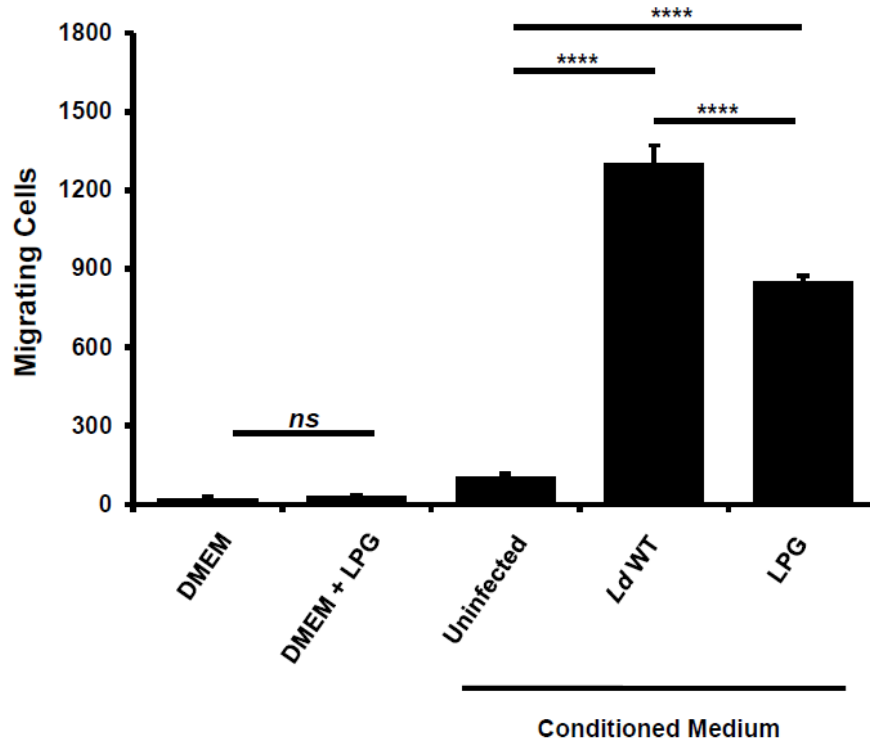
8223

8224

8225 **Figure S2.** *L. donovani* **LPG promotes macrophage-mediated chemotaxis of CXCR6^{+} cells**.

8226 Conditioned medium from WT BMDMS cultures infected with *Ld* WT, treated with *Ld* LPG or left uninfected

8227 for 24 h were tested for chemotactic activity. Fresh medium (DMEM; non-conditioned) was included to

8228 monitor basal migration activity. Purified LPG was added to fresh medium to rule out a possible direct

8229 chemotactic effect of LPG. Data are presented as mean ± SD (biological replicates n = 3). **** $P < 0.0001$

8230 for indicated comparisons. *ns = non significant*

8231
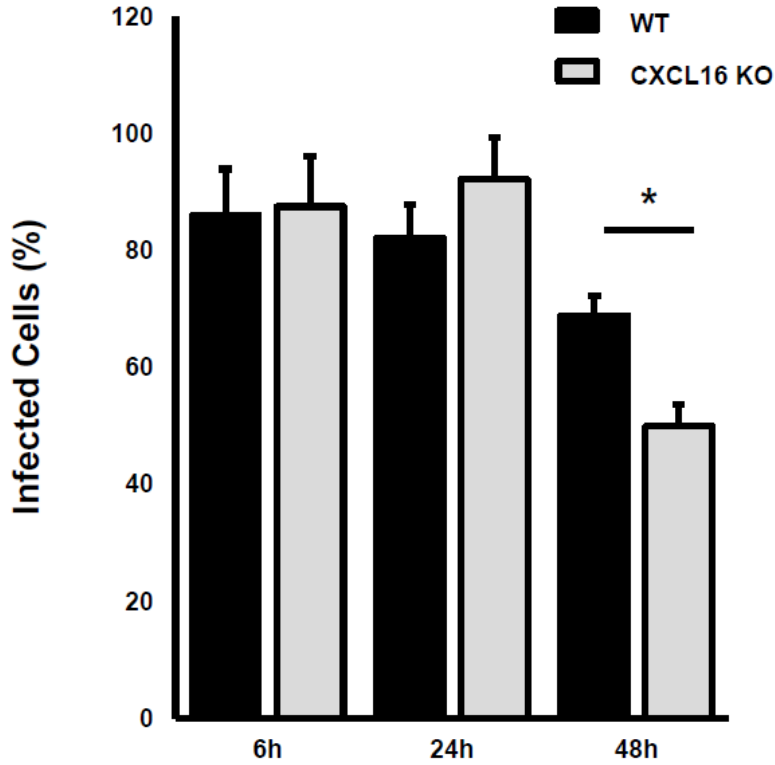
8232

8233

8234 **Fig. S3. Infection rates in WT and CXCL16 KO BMDMS**. WT and CXCL16 KO BMDMS cultures were

8235 infected with *L. donovani* promastigotes (MOI 10:1). Cells were collected, fixed and stained at the indicated

8236 time points and the number of infected cells was calculated by light microscopy. Results are presented as

8237 percentage of infected cells ± SD (two independent biological replicates, each consisting of a triplicate).

8238

8239

References

Abel, S., C. Hundhausen, R. Mentlein, A. Schulte, T. A. Berkhout, N. Broadway, D. Hartmann, R. Sedlacek, S. Dietrich, B. Muetze, B. Schuster, K. J. Kallen, P. Saftig, S. Rose-John and A. Ludwig (2004). "The transmembrane CXC-chemokine ligand 16 is induced by IFN-gamma and TNF-alpha and shed by the activity of the disintegrin-like metalloproteinase ADAM10." J Immunol **172**(10): 6362-6372.

Arango Duque, G. and A. Descoteaux (2015). "Leishmania survival in the macrophage: where the ends justify the means." Current Opinion in Microbiology **26**: 32-40.

Bahr, V., Y.-D. Stierhof, T. Ilg, M. Demar, M. Quinten and P. Overath (1993). "Expression of lipophosphoglycan, high-molecular weight phosphoglycan and glycoprotein 63 in promastigotes and amastigotes of Leishmania mexicana." Molecular and Biochemical Parasitology **58**(1): 107-121.

Balaraman, S., V. K. Singh, P. Tewary and R. Madhubala (2005). "Leishmania lipophosphoglycan activates the transcription factor activating protein 1 in J774A.1 macrophages through the extracellular signal-related kinase (ERK) and p38 mitogen-activated protein kinase." Mol Biochem Parasitol **139**(1): 117-127.

Chandrasekar, B., S. Mummidi, A. J. Valente, D. N. Patel, S. R. Bailey, G. L. Freeman, M. Hatano, T. Tokuhisa and L. E. Jensen (2005). "The pro-atherogenic cytokine interleukin-18 induces CXCL16 expression in rat aortic smooth muscle cells via MyD88, interleukin-1 receptor-associated kinase, tumor necrosis factor receptor-associated factor 6, c-Src, phosphatidylinositol 3-kinase, Akt, c-Jun N-terminal kinase, and activator protein-1 signaling." J Biol Chem **280**(28): 26263-26277.

Cheekatla, S. S., A. Aggarwal and S. Naik (2012). "mTOR signaling pathway regulates the IL-12/IL-10 axis in Leishmania donovani infection." Med Microbiol Immunol **201**(1): 37-46.

Dasgupta, B., K. Roychoudhury, S. Ganguly, M. A. Akbar, P. Das and S. Roy (2003). "Infection of human mononuclear phagocytes and macrophage-like THP1 cells with Leishmania donovani results in modulation of expression of a subset of chemokines and a chemokine receptor." Scand J Immunol **57**(4): 366-374.

de Assis, R. R., I. C. Ibraim, P. M. Nogueira, R. P. Soares and S. J. Turco (2012). "Glycoconjugates in New World species of Leishmania: polymorphisms in lipophosphoglycan and glycoinositolphospholipids and interaction with hosts." Biochim Biophys Acta **1820**(9): 1354-1365.

8268   de Veer, M. J., J. M. Curtis, T. M. Baldwin, J. A. DiDonato, A. Sexton, M. J. McConville, E. Handman

8269   and L. Schofield (2003). "MyD88 is essential for clearance of Leishmania major: possible role for

8270   lipophosphoglycan and Toll-like receptor 2 signaling." Eur J Immunol **33**(10): 2822-2831.

8271   Descoteaux, A. and S. J. Turco (1999). "Glycoconjugates in Leishmania infectivity." Biochim Biophys Acta

8272   **1455**(2-3): 341-352.

8273   Desjardins, M. and A. Descoteaux (1997). "Inhibition of phagolysosomal biogenesis by the

8274   Leishmania lipophosphoglycan." J Exp Med **185**(12): 2061-2068.

8275   E.J., C. S., E. C. R. and K. P. M. (1999). "Leishmania donovani infection initiates T cell-independent

8276   chemokine responses, which are subsequently amplified in a T cell-dependent manner." European Journal

8277   of Immunology **29**(1): 203-214.

8278   Engwerda, C. R., M. Ato, S. E. Cotterell, T. L. Mynott, A. Tschannerl, P. M. Gorak-Stolinska and P.

8279   M. Kaye (2002). "A role for tumor necrosis factor-alpha in remodeling the splenic marginal zone during

8280   Leishmania donovani infection." Am J Pathol **161**(2): 429-437.

8281   Fahy, O. L., S. L. Townley and S. R. McColl (2006). "CXCL16 regulates cell-mediated immunity to

8282   Salmonella enterica serovar Enteritidis via promotion of gamma interferon production." Infect Immun

8283   **74**(12): 6885-6894.

8284   Fulwiler, A. L., D. R. Soysa, B. Ullman and P. A. Yates (2011). "A rapid, efficient and economical

8285   method for generating leishmanial gene targeting constructs." Mol Biochem Parasitol **175**(2): 209-212.

8286   Gough, P. J., K. J. Garton, P. T. Wille, M. Rychlewski, P. J. Dempsey and E. W. Raines (2004). "A

8287   Disintegrin and Metalloproteinase 10-Mediated Cleavage and Shedding Regulates the Cell Surface

8288   Expression of CXC Chemokine Ligand 16." The Journal of Immunology **172**(6): 3678-3685.

8289   Gregory, D. J., M. Godbout, I. Contreras, G. Forget and M. Olivier (2008). "A novel form of NF-

8290   kappaB is induced by Leishmania infection: involvement in macrophage gene expression." Eur J Immunol

8291   **38**(4): 1071-1081.

8292   Howell, G. R., I. Soto, M. Ryan, L. C. Graham, R. S. Smith and S. W. John (2013). "Deficiency of

8293   complement component 5 ameliorates glaucoma in DBA/2J mice." J Neuroinflammation **10**: 76.

8294   Huang, C. and S. J. Turco (1993). "Defective galactofuranose addition in lipophosphoglycan

8295   biosynthesis in a mutant of Leishmania donovani." J Biol Chem **268**(32): 24060-24066.

8296   Huang, Y., X. Y. Zhu, M. R. Du and D. J. Li (2008). "Human trophoblasts recruited T lymphocytes

8297   and monocytes into decidua by secretion of chemokine CXCL16 and interaction with CXCR6 in the first-

8298   trimester pregnancy." J Immunol **180**(4): 2367-2375.

8299   Hurrell, B. P., M. Beaumann, S. Heyde, I. B. Regli, A. J. Muller and F. Tacchini-Cottier (2017).

8300   "Frontline Science: Leishmania mexicana amastigotes can replicate within neutrophils." J Leukoc Biol

8301   **102**(5): 1187-1198.

8302   Ibraim, I. C., R. R. de Assis, N. L. Pessoa, M. A. Campos, M. N. Melo, S. J. Turco and R. P. Soares

8303   (2013). "Two biochemically distinct lipophosphoglycans from Leishmania braziliensis and Leishmania

8304   infantum trigger different innate immune responses in murine macrophages." Parasites & Vectors **6**(1): 54.

8305   Izquierdo, M. C., C. Martin-Cleary, B. Fernandez-Fernandez, U. Elewa, M. D. Sanchez-Nino, J. J.

8306   Carrero and A. Ortiz (2014). "CXCL16 in kidney and cardiovascular injury." Cytokine Growth Factor Rev

8307   **25**(3): 317-325.

8308   Johnston, B., C. H. Kim, D. Soler, M. Emoto and E. C. Butcher (2003). "Differential Chemokine

8309   Responses and Homing Patterns of Murine TCRαβ NKT Cell Subsets." The Journal of Immunology **171**(6):

8310   2960-2969.

8311   Katholnig, K., M. Linke, H. Pham, M. Hengstschlager and T. Weichhart (2013). "Immune responses

8312   of macrophages and dendritic cells regulated by mTOR signalling." Biochem Soc Trans **41**(4): 927-933.

8313   Kawai, T. and S. Akira (2011). "Toll-like Receptors and Their Crosstalk with Other Innate Receptors

8314   in Infection and Immunity." Immunity **34**(5): 637-650.

8315   Kaye, P. and P. Scott (2011). "Leishmaniasis: complexity at the host-pathogen interface." Nat Rev

8316   Microbiol **9**(8): 604-615.

8317   King, D. L., Y. D. Chang and S. J. Turco (1987). "Cell surface lipophosphoglycan of Leishmania

8318   donovani." Mol Biochem Parasitol **24**(1): 47-53.

8319   Kumar, R. and S. Nylen (2012). "Immunobiology of visceral leishmaniasis." Front Immunol **3**: 251.

8320   Leroux, L. P., D. Dasanayake, L. M. Rommereim, B. A. Fox, D. J. Bzik, A. Jardim and F. S.

8321   Dzierszinski (2015). "Secreted Toxoplasma gondii molecules interfere with expression of MHC-II in

8322   interferon gamma-activated macrophages." Int J Parasitol **45**(5): 319-332.

8323   Leroux, L. P., J. Lorent, T. E. Graber, V. Chaparro, L. Masvidal, M. Aguirre, B. D. Fonseca, L. C.

8324   van Kempen, T. Alain, O. Larsson and M. Jaramillo (2018). "The protozoan parasite Toxoplasma gondii

8325   selectively reprograms the host cell translatome." Infect Immun.

8326   Lima, J. B., T. Araujo-Santos, M. Lazaro-Souza, A. B. Carneiro, I. C. Ibraim, F. H. Jesus-Santos,

8327   N. F. Luz, S. M. Pontes, P. F. Entringer, A. Descoteaux, P. T. Bozza, R. P. Soares and V. M. Borges (2017).

8328   "Leishmania infantum lipophosphoglycan induced-Prostaglandin E2 production in association with PPAR-

8329   gamma expression via activation of Toll like receptors-1 and 2." Sci Rep **7**(1): 14321.

8330   Linke, B., S. Meyer Dos Santos, B. Picard-Willems, M. Keese, S. Harder, G. Geisslinger and K.

8331   Scholich (2017). "CXCL16/CXCR6-mediated adhesion of human peripheral blood mononuclear cells to

8332   inflamed endothelium." Cytokine.

8333   Lodge, R., T. O. Diallo and A. Descoteaux (2006). "Leishmania donovani lipophosphoglycan blocks

8334   NADPH oxidase assembly at the phagosome membrane." Cell Microbiol **8**(12): 1922-1931.

8335   Matte, C. and A. Descoteaux (2010). "Leishmania donovani amastigotes impair gamma interferon-

8336   induced STAT1alpha nuclear translocation by blocking the interaction between STAT1alpha and importin-

8337   alpha5." Infect Immun **78**(9): 3736-3743.

8338   Matte, C. and M. Olivier (2002). "Leishmania-induced cellular recruitment during the early

8339   inflammatory response: modulation of proinflammatory mediators." J Infect Dis **185**(5): 673-681.

8340   Murray, H. W., A. D. Luster, H. Zheng and X. Ma (2017). "Gamma Interferon-Regulated

8341   Chemokines in Leishmania donovani Infection in the Liver." Infect Immun **85**(1).

8342   Naderer, T. and M. J. McConville (2008). "The Leishmania-macrophage interaction: a metabolic

8343   perspective." Cell Microbiol **10**(2): 301-308.

8344   Oghumu, S., C. M. Lezama-Davila, A. P. Isaac-Marquez and A. R. Satoskar (2010). "Role of

8345   chemokines in regulation of immunity against leishmaniasis." Exp Parasitol **126**(3): 389-396.

8346   Olivier, M., V. D. Atayde, A. Isnard, K. Hassani and M. T. Shio (2012). "Leishmania virulence

8347   factors: focus on the metalloprotease GP63." Microbes and Infection **14**(15): 1377-1389.

8348   Podinovskaia, M. and A. Descoteaux (2015). "Leishmania and the macrophage: a multifaceted

8349   interaction." Future Microbiol **10**(1): 111-129.

8350   Prive, C. and A. Descoteaux (2000). "Leishmania donovani promastigotes evade the activation of mitogen-activated protein kinases p38, c-Jun N-terminal kinase, and extracellular signal-regulated kinase-1/2 during infection of naive macrophages." Eur J Immunol **30**(8): 2235-2244.

8353   Puentes, S. M., R. P. Da Silva, D. L. Sacks, C. H. Hammer and K. A. Joiner (1990). "Serum resistance of metacyclic stage Leishmania major promastigotes is due to release of C5b-9." J Immunol **145**(12): 4311-4316.

8356   Rojas-Bernabe, A., O. Garcia-Hernandez, C. Maldonado-Bernal, J. Delegado-Dominguez, E. Ortega, L. Gutierrez-Kobeh, I. Becker and M. Aguirre-Garcia (2014). "Leishmania mexicana lipophosphoglycan activates ERK and p38 MAP kinase and induces production of proinflammatory cytokines in human macrophages through TLR2 and TLR4." Parasitology **141**(6): 788-800.

8360   Roux, P. P. and I. Topisirovic (2018). "Signaling pathways involved in the regulation of mRNA translation." Mol Cell Biol.

8362   S., S., P. S. P., J. M. K., C. H. S. and S. B. (2013). "Leishmania expressed lipophosphoglycan interacts with Toll-like receptor (TLR)-2 to decrease TLR-9 expression and reduce anti-leishmanial responses." Clinical & Experimental Immunology **172**(3): 403-409.

8365   Sarkar, S., L. Chelvarajan, Y. Y. Go, F. Cook, S. Artiushin, S. Mondal, K. Anderson, J. Eberth, P. J. Timoney, T. S. Kalbfleisch, E. Bailey and U. B. Balasuriya (2016). "Equine Arteritis Virus Uses Equine CXCL16 as an Entry Receptor." J Virol **90**(7): 3366-3384.

8368   Shimaoka, T., N. Kume, M. Minami, K. Hayashida, H. Kataoka, T. Kita and S. Yonehara (2000). "Molecular cloning of a novel scavenger receptor for oxidized low density lipoprotein, SR-PSOX, on macrophages." J Biol Chem **275**(52): 40663-40666.

8371   Shimaoka, T., T. Nakayama, N. Fukumoto, N. Kume, S. Takahashi, J. Yamaguchi, M. Minami, K. Hayashida, T. Kita, J. Ohsumi, O. Yoshie and S. Yonehara (2004). "Cell surface-anchored SR-PSOX/CXC chemokine ligand 16 mediates firm adhesion of CXC chemokine receptor 6-expressing cells." J Leukoc Biol **75**(2): 267-274.

8375   Shimaoka, T., T. Nakayama, N. Kume, S. Takahashi, J. Yamaguchi, M. Minami, K. Hayashida, T. Kita, J. Ohsumi, O. Yoshie and S. Yonehara (2003). "Cutting edge: SR-PSOX/CXC chemokine ligand 16 mediates bacterial phagocytosis by APCs through its chemokine domain." J Immunol **171**(4): 1647-1651.

8378   Steffen, S., S. Abraham, M. Herbig, F. Schmidt, K. Blau, S. Meisterfeld, S. Beissert, J. Guck and

8379   C. Gunther (2018). "Toll-Like Receptor-Mediated Upregulation of CXCL16 in Psoriasis Orchestrates

8380   Neutrophil Activation." J Invest Dermatol **138**(2): 344-354.

8381   Taylor, S., M. Wakem, G. Dijkman, M. Alsarraj and M. Nguyen (2010). "A practical approach to RT-

8382   qPCR-Publishing data that conform to the MIQE guidelines." Methods **50**(4): S1-5.

8383   Turco, S. J., M. A. Wilkerson and D. R. Clawson (1984). "Expression of an unusual acidic

8384   glycoconjugate in Leishmania donovani." J Biol Chem **259**(6): 3883-3889.

8385   Veinotte, L., S. Gebremeskel and B. Johnston (2016). "CXCL16-positive dendritic cells enhance

8386   invariant natural killer T cell-dependent IFNgamma production and tumor control." Oncoimmunology **5**(6):

8387   e1160979.

8388   Vinet, A. F., M. Fukuda, S. J. Turco and A. Descoteaux (2009). "The Leishmania donovani

8389   lipophosphoglycan excludes the vesicular proton-ATPase from phagosomes by impairing the recruitment

8390   of synaptotagmin V." PLoS Pathog **5**(10): e1000628.

8391   Vinet, A. F., S. Jananji, S. J. Turco, M. Fukuda and A. Descoteaux (2011). "Exclusion of

8392   synaptotagmin V at the phagocytic cup by Leishmania donovani lipophosphoglycan results in decreased

8393   promastigote internalization." Microbiology **157**(Pt 9): 2619-2628.

8394   WHO (2017). "Global leishmaniasis update, 2006-2015: a turning point in leishmaniasis

8395   surveillance." Wkly Epidemiol Rec **92**(38): 557-565.

8396   Wyllie, S., S. Patterson, L. Stojanovski, F. R. Simeons, S. Norval, R. Kime, K. D. Read and A. H.

8397   Fairlamb (2012). "The anti-trypanosome drug fexinidazole shows potential for treating visceral

8398   leishmaniasis." Sci Transl Med **4**(119): 119re111.

8399   Zhang, N., S. Prasad, C. E. Huyghues Despointes, J. Young and P. E. Kima (2018). "Leishmania

8400   parasitophorous vacuole membranes display phosphoinositides that create conditions for continuous Akt

8401   activation and a target for miltefosine in Leishmania infections." Cell Microbiol: e12889.

8402

Appendix 6

8404

8405

8406

Exploitation of the *Leishmania* exosomal pathway by *Leishmania* RNA virus 1

8408

8409

8410

Vanessa Diniz Atayde[1, 2], Alonso da Silva Lira Filho[1,2], Visnu Chaparro[3], Aude Zimmermann[3], Caroline Martel[1,2], Maritza Jaramillo[3] and Martin Olivier[1, 2]*

8413

8414

8415

8416

[1] Department of Medicine, Microbiology and Immunology, McGill University, 3775 University Street, Montréal, QC, Canada, H3A 2B4; [2] Infectious Diseases and Immunity in Global Heath Program, Research Institute of the McGill University Health Centre, 1001 Boulevard Décarie, Montréal, QC, Canada, H4A 3J1; [3] Institut National de la Recherche Scientifique (INRS) - Institut Armand Frappier, 531 Boulevard des Prairies, Laval, QC, Canada, H7V 1B7

* Correspondence to: Martin Olivier, Department of Medicine, Microbiology and Immunology, Research Institute of the McGill University Health Centre, 1001 Boulevard Décarie, Montréal, QC, Canada, H4A 3J1, Phone: (+1)514-934-1934, Ext. 76356, E-mail: martin.olivier@mcgill.ca

8425

8433

8434 **Abstract**

8435   *Leishmania* are ancient eukaryotes that have retained the exosome pathway through evolution.
8436 Leishmania RNA virus 1 (LRV1)-infected *Leishmania* species are associated with a particularly aggressive
8437 mucocutaneous disease triggered in response to the double-stranded RNA (dsRNA) virus. However, it is
8438 unclear how LRV1 is exposed to the mammalian host cells. In higher eukaryotes, some viruses are known
8439 to utilize the host exosome pathway for their formation and cell-to-cell spread. As a result, exosomes
8440 derived from infected cells contain viral material or particles. Herein, we investigated whether LRV1 exploits
8441 the *Leishmania* exosome pathway to reach the extracellular environment. Biochemical and electron
8442 microscopy analyses of exosomes derived from LRV1-infected Leishmania revealed that most dsRNA
8443 LRV1 co-fractionated with exosomes, and that a portion of viral particles was surrounded by these vesicles.
8444 Transfer assays of LRV1-containing exosome preparations showed that a significant amount of parasites
8445 were rapidly and transiently infected by LRV1. Remarkably, these freshly infected parasites generated more
8446 severe lesions in mice than non-infected ones. Moreover, mice co-infected with parasites and LRV1-
8447 containing exosomes also developed a more severe disease. Overall, this work provides evidence that
8448 *Leishmania* exosomes function as viral envelopes, thereby facilitating LRV1 transmission and increasing
8449 infectivity in the mammalian host.

8450

8451

8452

8453

8454

8455

8456

8457

8458   **Introduction**

8459

8460   *Leishmania* are ancient eukaryotic parasites with a complex life cycle that involves many
8461   developmental forms, occurring either in the midgut of the sand fly vector or in mammalian host
8462   macrophages. They are transmitted by the sand fly during a blood meal, and a successful infection develops
8463   into the disease termed leishmaniasis. This disease is represented by three main clinical forms: visceral,
8464   mucocutaneous and cutaneous. Our work focuses on depicting the last of these, which was reported to
8465   affect about a million of individuals throughout the world from 2008 to 2013 (Pigott et al. 2014). *Leishmania*
8466   species that cause cutaneous leishmaniasis are divided in subgenera *Leishmania* and *Viannia. L. Viannia*
8467   species are present exclusively in the New World and are known to cause an aggressive form of the
8468   disease, namely mucocutaneous, in 5-10% of the cases. This disease is characterized by the appearance
8469   of secondary nasopharyngeal metastatic lesions, disfiguring if left untreated. In hamster models, *L. Viannia*
8470   species develop tail and foot secondary lesions (Martinez et al. 2000; Hartley et al. 2012).

8471   Some species belonging to the subgenus *Viannia (*for example, *L.V. guyanensis)* are commonly
8472   infected with *Leishmania* RNA Virus 1 (LRV1), which belongs to the Totiviridae family, along with other
8473   protozoan and fungal-infecting viruses (Janssen et al. 2015). LRV1 is non-enveloped and encompasses a
8474   double-stranded RNA (dsRNA) genome that codes for the capsid protein and for an active RNA-dependent
8475   RNA polymerase (Widmer et al. 1989; Stuart et al. 1992). Phylogenetic analysis suggested that *Leishmania*
8476   infection with LRV1 predates the divergence of the parasite into different lineages (Widmer and Dooley
8477   1995). So far, it has been proposed that LRV1 is transmitted among *Leishmania* during cell
8478   division(Martinez et al. 2000).

8479   LRV1 seems to be a key factor for the development of some cases of mucocutaneous
8480   leishmaniasis. Ives and colleagues (Ives et al. 2011) observed that the LRV1 viral genome is recognized
8481   by endosomal TLR3 receptors, triggering a hyperinflammatory response that results in an increased
8482   pathological condition. Although it was proposed that LRV1is released from dead parasites that could not
8483   survive within the phagolysosome, the precise mechanism responsible for exposing the viral genome to
8484   host receptors still remains unclear (Ives et al. 2011; Olivier 2011).

8485   Some viruses such as human immunodeficiency virus and Epstein-Barr virus are known to exploit
8486   different aspects of the host exosome/extracellular vesicle machinery for their formation, spread,
8487   intercellular communication and modulation of immune responses (Alenquer and Amorim 2015; Chahar,
8488   Bao, and Casola 2015). Vesicles derived from infected cells may contain viral proteins, DNA and RNA, and
8489   trigger specific effects on target cells that lead to symptomatic infection (Schwab et al. 2015). Interestingly,
8490   recent works with hepatitis C and hepatitis A viruses, among others, demonstrated that vesicles derived
8491   from infected mammalian cells may also contain viral particles, and that this coating protects virions from
8492   neutralizing antibodies, an immune evasion mechanism (Ramakrishnaiah et al. 2013; Feng et al. 2013).

8493   *Leishmania* has retained the exosome pathway through evolution. Recently, our group made the

8494   discovery that *Leishmania* secretes exosomes within the sandfly midgut, which are co-egested with the

8495   parasite during the sand fly blood meal. Exosomes exacerbate disease by creating an opportune

8496   environment for parasite replication (Atayde et al. 2015). Leishmania exosomes are described to be

8497   secreted from multivesicular bodies (MVBs) and from the flagellar pocket

8498   (Atayde et al. 2016). Herein, we provide evidence that LRV1 exploits the *Leishmania* exosomal pathway to

8499   reach the extracellular environment. This research explores mechanisms whereby LRV1 could hijack the

8500   *Leishmania* exosomal pathway to promote its propagation and infectivity towards its host, leading to

8501   development of severe leishmaniasis.

8502

Results

L. guyanensis clone 21 secretes LRV1 through the exosome pathway

Numerous viruses have been reported to hijack the exosome machinery to guarantee successful host infection (Alenquer and Amorim 2015); we hypothesized that this could also be the case for LRV1 (Olivier 2011). As previously shown for other *Leishmania* species (Hassani et al. 2011; Silverman et al. 2010), *L. guyanensis* clone 21 (Lg21+) promastigotes had an increase in vesicle secretion after heat-shock from 25 to 37°C, observed by scanning electron microscopy (Fig. 1a). Lg21+ parasites, alongside all other species in this experiment, were tested for the presence of the argonaute gene (unique to the *Viannia*) and LRV1 RNA and were revealed to be free of contaminants and homogeneous in size (Fig. 1b and Supplementary Figs. 1a-f and 2a). Investigation for the presence of viral material in Lg21+ exosomes (Lg21+Exo) by western blot and semi-quantitative PCR (RT-PCR) revealed that, in contrast to exosomes derived from *L. V. panamensis* (Lpa) and *L. mexicana* (Lmex) parasites, Lg21+Exo contained LRV1 proteins and RNA (Fig. 1c). These *Leishmania* species were selected because they belong to the subgenera *Viannia* (same as Lg21+) and *Leishmania*, respectively (Supplementary Fig. 1a-f). Strikingly, viral proteins and RNA co-sedimented with *Leishmania* exosome markers such as GP63 (Fig. 1d) when Lg21+ extracellular vesicle preparations (Lg21+EV) were layered onto linear sucrose density gradients. Conversely, gradients of Lg21+ cell lysates contained LRV1 RNA both in exosome fractions (4-6) and in more dense fractions (8-10) (Fig. 1d), suggesting that intracellular viral genomic material is found in two types of particle with distinct biophysical properties.

We then hypothesized that the two different observed particles were representing LRV1 surrounded by an exosome envelope and naked LRV1. To confirm this, we analyzed the presence of mature viral particles, which contain the LRV1 RNA minus (-) strand, in intact or disrupted Lg21+Exo density gradients. By RT-PCR, we observed that LRV1 (-) strand was shifted to bottom gradient fractions (7-10) only in disrupted preparations, and western blot indicated that this shift was not accompanied by exosome markers (Fig. 1e). Gradient fractions were also analyzed by nanoparticle tracking analysis (NTA), which corroborated the RT-PCR results by showing a significant increase in 30-80nm particle size in fractions 7-10 in disrupted exosome preparations (Fig.1f).

Intact exosome gradient fractions were then analyzed by transmission electron microscopy (TEM; Supplementary Fig. 2a). Fractions 4-6 presented exosomes surrounding one or more LRV1-like particles (Fig. 2a and Supplementary Fig. 2c). To rule out that LRV1-containing vesicles were an artifact from the multiple centrifugation steps or sucrose gradient, we examined Lg21+EV inputs before ultracentrifugation, and also found LRV1-like particles surrounded by membranes (Supplementary Fig. 2b), undetected in other *Leishmania* species' exosome preparation (Supplementary Fig. 2e). Lg21+EV inputs also contained naked LRV1 (Supplementary Fig. 2b), which migrated to fractions 8-10 in sucrose gradients (Fig. 2a and Supplementary Fig. 2d). Intact Lg21+Exo treated with increasing concentrations of Triton X-100 and analyzed by TEM exposed detergent-resistant LRV1-like particles (Fig. 2b). Lg21+Exo quantification of Fig.

8539   2b revealed that ~30% contained LRV1-like particles (Fig. 2c). RNA protection assays also revealed that

8540   exosome coating protects the viral dsRNA genome from degradation by RNAse III, an effect unobserved

8541   with naked LRV1 (Fig. 2d).

8542   Lastly, we wanted to establish whether LRV1 packaging is intracellular in compartments reported

8543   to contain *Leishmania* exosomes, MVB and flagellar pockets (Atayde et al. 2015), by TEM of whole

8544   parasites (Supplementary Fig. 3a). We observed frequent accumulation of one or more LRV1-like particles

8545   in parasite intracellular MVB-like compartments and flagellar pockets (Fig 2f, Supplementary Fig. 3b-i) and

8546   enveloped LRV1-like particles actively secreted by promastigotes (Fig. 2e, Supplementary Fig. 3j-m).

8547   Naked LRV1 was found more frequently in flagellar pockets (Fig. 2f, Supplementary Fig. 3e-i). Other

8548   *Leishmania* species did not present LRV1-like structures intracellularly (Supplementary Fig. 4a,b).

8549   Collectively, this set of experiments confirmed that LRV1 particles are present in intracellular

8550   Lg21$^+$Exo and are subsequently secreted into the extracellular environment. Importantly, a proteomic

8551   analysis of Lg21$^+$ exosome content altered by LRV1 infection has been performed (see Fig. 3,

8552   Supplementary Notes, Supplementary Figs 1, 5 and 6, Supplementary Tables 1-5 and Supplementary Data

8553   files 1-7)

8554   **A subset of messenger RNAs is not efficiently translate in *L. guyanensis* clone 21$^+$**

8555   Exosomes are known to mirror the cell physiological state from which they are derived. To further

8556   clarify the consequences of LRV1 infection, we compared the total protein profiles of the promastigote

8557   samples. By analyzing the mass spectrometry (MS) data from the three species, using the *L. braziliensis*

8558   database as a reference, a total of 1,512 proteins were identified. From those, 953 were shared among the

8559   three species and 295 were unique to the *Viannia* subgenus (Fig. 4a, purple, and Supplementary Data file

8560   3). Next, we compared the exponentially modified protein abundance index (emPAI) values (Ishihama et

8561   al. 2005) for all proteins Data analysis revealed that 786 proteins were equally abundant in the three

8562   species, while 142 were increased in Lmex alone, 153 in Lg21$^+$ and 224 in Lpa (Fig. 4a, yellow, Fig. 4b and

8563   Supplementary Data file 4). There were 144 proteins that were commonly increased in the *Viannia*

8564   subgenus (Fig. 4a, yellow, and Supplementary Data file 4). Proteins uniquely increased in LRV1-infected

8565   Lg21$^+$ promastigotes included cyclophilin A, cyclophilin 11 and kinetoplast-associated proteins

8566   (Supplementary Data file 4). A substantial part of Lpa and Lmex enriched proteins was involved in ribosome,

8567   proteasome and metabolic pathways (Supplementary Data file 4). Figure 4c illustrates the different protein

8568   profiles among *Leishmania* species and the accord between exosome protein profiles and their respective

8569   promastigote protein profiles.

8570   We next hypothesized that the differences observed in the proteome of LRV1-containing exosomes

8571   and parasites could be explained by a specific effect of the virus on parasite mRNA translation. To

8572   investigate, we compared total mRNA levels of *HSP83*, *HSP70*, *cyclophilin A*, *GP63* and *α-tubulin* among

8573   parasites. We found that all transcripts, with the exception of α-tubulin, were more abundant in Lg21$^+$

8574 compared to Lmex and, to a lesser extent, Lpa RNA samples (Fig. 4d and Supplementary Fig. 7a). Lpa and

8575 Lmex mRNA levels were similar, except for *HSP83* (Supplementary Fig. 7b). Lack of positive correlation

8576 between mRNA accumulation and protein levels of HSP83, HSP70 and GP63 in Lg21+ suggested a defect

8577 in translation later assessed by monitoring differences in translation initiation rates among the three species

8578 through quantification of monosomes (inefficient translation) and polysomes (efficient translation) in

8579 polysome-tracings(Masvidal et al. 2017). Translation initiation rates were lower in Lg21$^+$ promastigotes than

8580 in other species, as evidenced by a lower polysome/monosome ratio in the Lg21$^+$ polysome-tracings

8581 compared to those of Lmex and Lpa (Fig. 4e,f).

8582 The distribution of LRV1 RNA present in Lg21$^+$ showed an accumulation in the fractions containing

8583 efficiently translated mRNAs (that is, bound to three or more ribosomes, fractions 9–13) (Supplementary

8584 Fig. 7c). Comparative quantitative PCR (qRT-PCR) analyses of monosomal and polysomal fractions

8585 revealed that *Gp63*, *Hsp70* and *Hsp83* mRNAs are translated less efficiently in Lg21$^+$ than in other

8586 promastigotes, confirmed at the protein level by western blotting (Fig. 4g). In contrast, *cyclophilin A* alone

8587 appeared to be efficiently translated in Lg21$^+$ promastigotes, further suggesting its role in the LRV1 life

8588 cycle. Translation of *Gp63*, *Hsp70* and *Hsp83* mRNAs was reduced in Lpa compared to Lmex, but was

8589 higher than in Lg21$^+$ (Fig. 4g).

8590 **LRV1 is transferred among Leishmania species via exosomes**

8591 We next assessed the biological roles of LRV1-containing exosomes. Even though LRV1 is known

8592 to be transmitted among parasites during cellular division (Martinez et al. 2000), we explored the possibility

8593 that viral particles could also be transferred among Leishmania species via exosomes.

8594 First, we performed Transwell migration experiments with Lg21$^+$ promastigotes as exosome donor

8595 cells and Lpa or Lmex were recipient cells (Fig. 5a). Increased concentrations of either recipient or donor

8596 cells resulted in dose-dependent incorporation of LRV1 by both *Leishmania* species after a 48-h incubation;

8597 however, LRV1 was sustained only in Lpa promastigotes (Fig. 5b). After removing and cultivating Lpa

8598 recipient cells for up to two weeks, RT-PCR and qRT-PCR demonstrated that LRV1 levels decrease with

8599 time (Fig. 5b and Supplementary Fig. 8a,b).

8600 To determine whether exosome viral coating was essential for transfer among *Leishmania* species,

8601 we added Lg21$^+$-derived exosomes containing either coated or naked LRV1 to Lpa and Lmex cultures. To

8602 monitor the kinetics of exosome uptake by *Leishmania* species, we generated GFP-expressing Lg21$^+$ cells,

8603 which secrete GFP- and LRV1-containing exosomes. Interestingly, Lg21^{+GFP} exosomes were promptly and

8604 transiently incorporated by both Lpa and Lmex cells at 25°C (Supplementary Fig. 8c), a pattern that differed

8605 at 4°C, suggesting dependence on membrane fluidity and/or parasite metabolism (Supplementary Fig. 8c).

8606 Uptake of exosome-coated LRV1 by both Lmex and Lpa occurred within the first 15–30min, but was

8607 sustained only in Lpa cells. The latter presented detectable viral levels even two weeks post-transfer,

8608 supporting Transwell experiment findings (Fig. 5d and Supplementary Fig. 8c–e). In contrast, naked LRV1

8609 uptake was lower, delayed and transient in both species (Fig. 5d). At 4°C, LRV1 was detected at later time

8610 points, suggesting viral elimination dependent on parasite metabolism (Fig. 5d).

8611 Next, we investigated the fate of LRV1 in the early hours after Lpa promastigote uptake. Transfer

8612 experiments indicated reproducible uptake of LRV1 via Lg21$^+$ exosomes by parasites, as evidenced by

8613 LRV1 RNA quantification (Supplementary Fig. 8d). Importantly, LRV1 RNA levels rapidly decreased after

8614 culture dilution (Supplementary Fig. 8e). To determine whether LRV1 negatively impacted Lpa mRNA

8615 translation as detected in Lg21$^+$ parasites (Fig. 4e–g), Lpa promastigotes were infected overnight with

8616 Lg21$^+$Exo (Supplementary Fig. 8f) and changes in translation efficiency of parasite and viral mRNAs were

8617 monitored by polysome profiling (Fig. 5f,g and Supplementary Fig. 7e–g). LRV1 RNA mainly accumulated

8618 in the 9–13 heavy polysome fractions, indicating efficient translation in recipient Lpa parasites (Fig. 5f).

8619 qRT-PCR on monosomal and polysomal fractions revealed decreased translation efficiency for *Hsp83*,

8620 *Hsp70*, *Gp63* and *cyclophilin A*, but not *α-tubulin* mRNAs, in LRV1-infected Lpa as compared to wild-type

8621 Lpa (Fig. 5g and Supplementary Fig. 7g). Accordingly, expression of the encoded proteins was reduced in

8622 LRV1-infected Lpa promastigotes (Fig. 5g). In contrast, total mRNA levels were not affected in LRV1-

8623 infected Lpa (Fig. 5e).

8624 **Exosome-enveloped LRV1 is responsible for exacerbated cutaneous leishmaniasis**

8625 Finally, we assessed the biological significance of exosome-coated *in vivo* in two different contexts.

8626 Since Lg21$^+$ parasites alone generate extremely severe lesions in mice (Fig. 6a, Supplementary Fig. 9a,b),

8627 we co-inoculated mouse footpads with Lmex or Lpa promastigotes (which display a more controlled type

8628 of infection) (Fig. 6a), combined with their respective exosomes, Lg21$^+$ exosomes or naked LRV1. With

8629 both *Leishmania* species, co-inoculation with exosomes increased lesion size, and effect further

8630 exacerbated by Lg21$^+$Exo (Fig. 6b,c) (Atayde et al. 2015). In contrast, naked LRV1 did not exacerbate

8631 lesions, underlining the importance of the exosome coating in *in vivo* infections (Fig. 6b,c). We also used

8632 Lpa infected with LRV1 via exosomes overnight (Supp. Fig. 8a) to inoculate mouse footpads. Importantly,

8633 Lpa-LRV1 significantly increased lesion size compared to Lpa wild-type (Fig. 6d)

8634

8635

Discussion

Double-stranded RNA viruses belonging to the *Totiviridae* family naturally infect rudimentary eukaryotic single cell organisms, such as protozoans. In the case of *Leishmania*, phylogenetic analysis suggested that *Leishmania* infection with LRV1 predates the divergence of the parasite into the different lineages (Widmer and Dooley 1995). This could suggest that the advent of viral infection during evolution preceded the appearance of multicellular organisms. In this context, our main interest was to better understand what appears to be a complex relationship between LRV1 and its hosts, *Leishmania* species belonging to the New World *Viannia* subgenus. LRV1 has been implicated in resistance to treatment as well as in the development of a rather disfiguring type of mucocutaneous disease (Bourreau et al. 2016).

The first question that we addressed was precisely how the LRV1 genome is exposed to the host. Viruses are ancient human pathogens who engage a number of mechanisms for successful infections (Dreux et al. 2012). One mechanism that has been the topic of many studies in the past few years is the use of the host exosome/extracellular vesicle machinery for their biogenesis, spread and microenvironment manipulation (Alenquer and Amorim 2015; Chahar, Bao, and Casola 2015). Most relevant for this work, viruses such as hepatitis C virus are found within host secreted vesicles, an efficient immune evasion mechanism (Ramakrishnaiah et al. 2013; Feng et al. 2013). Of note, exosomes have many characteristics in common with enveloped viruses, including biophysical properties, biogenesis and mechanisms of uptake by cells (Meckes and Raab-Traub 2011). This may explain the viral dependence for the host intraluminal vesicle machinery (Alenquer and Amorim 2015).

Our most striking evidence of the LRV1 exosome enveloping was revealed by sucrose density gradients of Lg21+EV preparations. They contained two populations of LRV1 dsRNA-containing particles: one at a lower density that co-sedimented with *Leishmania* exosomes, representing enveloped LRV1, and the second one at a higher density that represented the naked virus. In a recent work, it has been shown that supernatant of cells infected with hepatitis A virus also contains two populations of viral particles, one being coated with cellular membranes that facilitates viral escape from neutralizing antibodies (Feng et al. 2013). TEM analyses confirmed our findings and demonstrated that the LRV1 packaging within exosomes occurs intracellularly followed by secretion to the extracellular milieu. Collectively, these data established that LRV1 is enveloped within *Leishmania* intracellular compartments through the exploitation of the exosome pathway, instead of being simply surrounded by parasite plasma membrane. In addition, we found that the exosome coating protects LRV1 from RNAse III, which suggests that this mechanism may have evolved to protect the pathogen from extracellular perils, such as degrading enzymes or the host immune system.

Several studies have compiled *Leishmania* exosome content by relative quantitative proteomic analyses followed by Western blot validation (Atayde et al. 2015; Silverman et al. 2010; Hassani et al. 2011). The genomes of *Leishmania* species from the subgenus *Leishmania*, such as *L. mexicana*, and species from the subgenus *Viannia,* are similarly organized comprising around 8000 genes each. However,

360

8672 the latter possesses striking differences such as the presence of transposable elements and the RNA-
8673 mediated interference machinery. Despite an estimate 20-100 million years of separation between *Viannia*
8674 and *Leishmania* subgenera, more than 99% of their genes are syntenic. Conservation within coding
8675 sequences is also high; *L. braziliensis* genome versus *L. infantum* and *L. major* genomes have around 77%
8676 amino acid identity and 82% nucleotide identity. (Llanes et al. 2015; Peacock et al. 2007). This is the
8677 reason why we decided to use the *L. braziliensis* predicted proteins as the reference to compare the three
8678 species used in this work. However, we did not ignore the fact that there is some divergence in orthologue
8679 genes between the subgenera *Viannia* and *Leishmania*.

8680   Fundamentally, many proteins involved in the endosomal sorting complex required for transport
8681 (ESCRT) machinery and endosome-associated small GTPases were found in our proteomics data, further
8682 endorsing the origin of purified exosome vesicles. In addition, relative quantitation provided by emPAI ratio
8683 analyses showed that the presence of LRV1 has a major impact in the parasite's exosome content, possibly
8684 due to its involvement in the exosome pathway. One interesting example is cyclophilin A, which is found
8685 increased in Lg21$^+$ exosomes and was described as a key factor in viral replication, with a potential for anti-
8686 viral therapies (Dawar et al. 2017). Supporting this, polysome profile analyses revealed that in contrast to
8687 *Gp63*, *Hsp70* and *Hsp83*, *cyclophilin A* mRNA was efficiently translated in Lg21$^+$ parasites, further
8688 suggesting its role in LRV1 life cycle. Proteins such as cyclophilin A could provide insight into the
8689 mechanisms of replication of LRV1 and how it can be targeted. STRING interaction networks of exosome-
8690 enriched proteins highlighted Lg21$^+$Exo peculiarities, as the presence of the mitochondria oxidative
8691 phosphorylation cluster, which could be a LRV1-induced feature since viral infection may affect
8692 mitochondria dynamics to benefit the infectious process (Khan et al. 2015). Furthermore, the generation of
8693 mitochondria-derived vesicles has been recently demonstrated, and these vesicles were shown to fuse with
8694 MVBs (Sugiura et al. 2014).

8695   The patterns of protein expression appear to be related as well to the subgenus studied. *L. Viannia*
8696 parasites, Lpa and Lg21$^+$, presented many similarities despite LRV1 infection, and we believe that this may
8697 be a main factor making these parasites more suitable for viral infection and persistence. This is partially
8698 confirmed by our transfer experiments, where Lpa parasites were more apt to be infected by LRV1 and to
8699 hold infection for a few days to weeks, contrarily to Lmex that supported LRV1 replication for only a few
8700 hours after infection. Previous attempts to reinfect *L. Viannia* with LRV1 were performed by electroporation
8701 of viruses purified from intracellular compartments and the infection not sustained for more than four days
8702 (Armstrong et al. 1993). Thus far, LRV1 was believed to maintain its infectious status by simple distribution
8703 during parasite mitosis.

8704   A number of viruses affect host mRNA translation to favor their own protein synthesis and
8705 replication (Walsh and Mohr 2011). We investigated this possibility by proteomic analysis combined with
8706 polysome-profiling of Lg21$^+$, Lpa and Lmex parasites, which showed that translation initiation rates and
8707 translation efficiency of select mRNAs were reduced in infected species. Remarkably, infection of Lpa

8708   parasites with the virus via Lg21+ exosomes leads to viral RNA association with heavy polysome fractions,

8709   which suggests active viral translation. In addition, viral infection of Lpa affects its translation, as observed

8710   for *HSP83, HSP70, GP63, cyclophilin A* mRNAs.

8711   Recently, we demonstrated that exosomes that are secreted by *Leishmania major* within the sand

8712   fly gut are in fact inoculated by the vector alongside the parasite, exacerbating the disease (Atayde et al.

8713   2015). We used mouse models to co-inoculate Lg21+Exo with non-infected parasites, and virus-containing

8714   exosomes further exacerbated lesion development. Importantly, naked LRV1 did not induce lesion

8715   exacerbation, highlighting the importance of the exosome envelope possibly for LRV1 recognition by the

8716   host cell. Remarkably, Lpa infected with LRV1 via exosomes also produced significantly larger lesions,

8717   which further evidences that LRV1 exerts an additional inflammatory effect on lesion development.

8718   Collectively, findings stemming from our study described a novel mechanism whereby *Leishmania*

8719   LRV1 reaches the extracellular environment, either to invade other parasites and maintain its infection, or

8720   to increase their infectivity in the mammalian host. Of utmost importance, our study further reveals that

8721   exploitation of exosomal pathway by a non-enveloped virus to gain an envelope -therefore maximizing its

8722   infectivity- could have occurred very early during the course of evolution.

8723

8724

8725

Methods

Leishmania parasites

Leishmania species used in the experiments were: the metastatic clone 21 (LRV1 high) and clone 3 (LRV1 low) of *L. V. guyanensis* strain WHI/BR/78/M5313, isolated from *Lutzomyia whitmani* in Para State, northern Brazil (Martinez et al. 2000; Lainson et al. 1981); the Colombian *L. V. panamensis* strain MHOM/87/CO/UA140, isolated from a patient with cutaneous leishmaniasis; the WHO reference *Leishmania mexicana* strain MNYC/BZ/62/M379, originally isolated from *Nyctomys sumichrasti* (rat) in Belize, 1962; the *L. V. braziliensis* (MHOM/BR/1975/M2904) strain that we have had for years in the laboratory was also used in some experiments. Promastigotes were cultured at 26°C in Schneider's Drosophila Medium (Gibco-BRL) supplemented with 10% heat-inactivated fetal bovine serum, 2 mM L-glutamine, 100 U ml^{-1} penicillin, and 100 µl ml^{-1} streptomycin. For mouse infections, promastigotes were cultured in supplemented Schneider's Medium at 26°C, until reached stationary phase (infective forms).

Purification of *Leishmania* exosomes

Leishmania late log phase parasites were washed twice with PBS, resuspended in RPMI 1640 medium (Life Technologies) without FBS and phenol red at a concentration of 10^8 promastigotes ml^{-1} and incubated for 4h at 37°C for the release of exosomes in the culture medium. Parasite viability was measured by propidium iodide staining before and after the incubation at 37°C. At the end of a 4-h incubation, the sample was centrifuged at 2,555g to clear out parasites, at 8,500g to clear out debris, and filtered through 0.45 µm followed by 0.20 µm syringe filters. Next, exosomes were pelleted by a 1-h centrifugation at 100,000g and resuspended in exosome buffer (137mM NaCl, 20mM Hepes, pH 7.5). For further purification, exosomes were layered in a linear sucrose gradient (0 to 2 M sucrose) and centrifuged at 100,000g for 1.5h. Ten fractions of 1 ml were collected and exosomes or their protein contents were detected by TEM or western blot, respectively, in fractions 4, 5 and 6, corresponding to the concentrations of 0.8 to 1.2 M of sucrose and densities of 1.10 to 1.15 g ml^{-1}. Exosome-containing fractions were combined, pelleted, resuspended in endotoxin-free PBS and dosed for inoculation of mice.

NTA

Leishmania exosome preparations were analyzed by NTA using a LM-10 Nanosight Machine in the laboratory of J. Rak (Research Institute of the McGill University Health Centre). For the determination of particle size and number, 5 sequential 30-second videos were acquired, using the default settings of the instrument. Exosome buffer was used as the negative control.

Mouse Infections

All experiments with mice were carried out in pathogen-free housing and in accordance with the regulations of the Canadian Council of Animal Care Guidelines, Institutional Animal Care and Use

8761 Committees at the McGill University under ethics protocol number 7791. Female BALB/c mice (6 to 8 weeks

8762 old) were infected in the right hind footpad with 5×10^6 stationary phase *Leishmania* promastigotes with or

8763 without 1μg of *in vitro* purified exosomes or 0.25μg of naked LRV1. Disease progression was monitored by

8764 measuring footpad swelling weekly with a metric caliper, up to 10 weeks post-infection. At the end of each

8765 experiment, footpads were photographed and processed for determination of the parasite burden.

8766 **Determination of footpad parasite loads by the limiting dilution assay**

8767 Footpads were surface-sterilized with a chlorine dioxide-based disinfectant followed by ethanol

8768 70% for 5 minutes. After washes in PBS, footpads were sliced, transferred to a glass tissue homogenizer

8769 containing 6 ml of PBS, and manually homogenized until complete tissue disruption was achieved. The

8770 final homogenate was then centrifuged at 3,000 x g for 5 minutes, resuspended in 20 ml of Schneider's

8771 Medium and 100 μl were added in duplicates to 96-well plates containing 100 μl of complete medium in

8772 each well (24 two-fold dilutions for each duplicate). Plates were kept at 28°C until examination after 7-10

8773 days, when the highest dilutions at which promastigotes were observed were recorded. Parasite loads were

8774 expressed as number of parasites per footpad.

8775

8776 **Scanning Electron Microscopy**

8777 Parasites were processed as previously described (Hassani et al. 2011). Briefly, promastigotes

8778 were fixed in 2.5% glutaraldehyde solution overnight at 4°C. Samples were then added to poly-L-lysine-

8779 coated slides and dehydrated in ethanol, followed by amyl acetate and supercritical CO_2. Dehydrated

8780 samples were coated with Au-Pd and visualized using a Hitachi S-4700 Cold Field Emission Gun scanning

8781 electron microscope (Facility for Electron Microscopy Research, McGill University).

8782 **TEM**

8783 For negative staining, nanoparticle preparations were coated directly on formvar carbon grids, fixed

8784 with 1% glutaraldehyde in 0.1 M sodium cacodylate buffer for 1 minute and stained with 1% uranyl acetate

8785 for 1 minute. For ultrastructure analysis, parasite pellets were fixed with 2.5% glutaraldehyde in 0.1 M

8786 sodium cacodylate buffer overnight at 4°C. After washes in the same buffer, samples were included in 1%

8787 ultrapure agarose, post-fixed with osmium tetroxide and dehydrated in a graded acetone series before the

8788 embedding in epoxy resin. Ultrathin sections (70-80 nm) were cut from resin blocks using a Reichert-Jung

8789 Ultracut E Ultramicrotome. Formvar grids covered with isolated vesicles or with ultrathin sections were

8790 visualized in the FEI Tecnai 12 120 kV transmission electron microscope. Images were taken with the AMT

8791 XR-80C CCD Camera System (Facility for Electron Microscopy Research, McGill University).

8792 **RNAse Protection Assay**

8793 Exosomes (20 μg) or naked LRV1 (5 μg) was used in the following conditions: no treatment,

8794 treatment with 10μg ml^{-1} of RNAse A (Sigma) and/or treatment with 1 μl of RNAse III (Ambion; 1 U μl^{-1}), in

8795 the presence or not of 0.1% Triton X-100. All reactions were performed in 1x RNAse III buffer (Ambion), at

8796   37°C for 20 minutes and immediately processed for RT-PCR.

Liquid Chromatography-MS/MS

8798   Liquid chromatography-MS/MS was performed at the Institute de Recherches Cliniques de
8799   Montréal (IRCM, University of Montreal, Canada). Proteins derived from purified *Leishmania* exosomes
8800   were precipitated with 15% trichloroacetic acid/acetone and processed for liquid chromatography-MS/MS
8801   analysis. After precipitation, in solution digestion was performed by the addition of trypsin at a ratio of 1:25
8802   protease/protein. After an overnight incubation at 37°C, the reactions were quenched by the addition of
8803   formic acid to a final concentration of 0.2% and cleaned with C18 Zip Tip pipette tips (Millipore), before MS
8804   analysis. Extracted peptides were injected onto a Zorbax Extended-C18 desalting column (Agilent) and
8805   subsequently chromatographically separated on a Biobasic 18 Integrafrit capillary column (Thermo
8806   Scientific) on a Nano High-Performance liquid chromatography system (1100 series unit; Agilent). Eluted
8807   peptides were electrosprayed as they exited the capillary column and were analyzed on a QTRAP 4000
8808   linear ion trap mass spectrometer (SCIEX/ABI).

Protein database search

8810   Individual sample MS/MS spectra were peak listed using the Distiller version 2.1.0.0 software
8811   (www.matrixscience.com/distiller) with peak-picking parameters set at 1 for signal-noise ratio and at 0.3 for
8812   correlation threshold. The peak-listed data was then searched against the NCBI database with the Mascot
8813   software version 2.3.02 (Matrix Science). Mascot was set up to search the *L. braziliensis* database
8814   (txid5660, 17,148 proteins) or the *L. mexicana* database (txid5665, 16,744 proteins) with a fragment ion
8815   mass tolerance of 0.50 Da and a parent ion tolerance of 1.5 Da. Carbamidomethyl was specified in both
8816   search engines as a fixed modification. Oxidation of methionine residues was specified in Mascot as a
8817   variable modification. Scaffold software version 4.0.6.1 (Proteome Software Inc.) was used to validate
8818   MS/MS peptide and protein identifications. Identification of peptides was accepted if it could be established
8819   at greater than 95.0% probability. Identification of proteins was accepted if it could be established at greater
8820   than 95.0% probability and contained at least 2 identified peptides. Proteins that contained similar peptides
8821   and could not be differentiated using MS/MS analysis alone were grouped to satisfy the principles of
8822   parsimony. The final number of peptides per protein was represented by the average of the biological
8823   replicas after normalization to the total number of peptides.

Bioinformatic analyses

8825   The initial Blastp step was performed against NCBI non-redundant database and high-scoring top
8826   blast hits were retrieved and used for annotation with Blast2GO default parameters. Signal peptide
8827   predictions were performed using SignalP 4.1 (Petersen et al. 2011). Prediction of unconventionally
8828   secreted proteins was performed using SecretomeP 2.0 server (Bendtsen et al. 2004). Exosome interacting
8829   protein networks were mapped based on gene ontology annotations (orthologues in the human database)
8830   using STRING version 10.5 (string-db.org).

8831 **Western blots**

8832   Parasite or exosome preparations were dosed with the Micro BCA Protein Assay Kit (Thermo
8833 Scientific) or with the Bradford Protein Assay Kit (Bio-Rad) and resuspended directly in SDS sample buffer
8834 containing bromophenol blue and β-mercapto-ethanol. Proteins were subjected to SDS-polyacrylamide gel
8835 electrophoresis (PAGE) and transferred to polyvinylidene difluoride membranes (Perkin Elmer). After
8836 blocking for 1-h in TBS-0.05% Tween 20 (TBST) containing 5% fat-free milk, membranes were incubated
8837 with the following specific antibodies against: *Leishmania* HSP83 (Greg Matlashewski, McGill University,
8838 Canada), *Leishmania* GP63 (Robert W. McMaster, University of British Columbia, Vancouver, Canada),
8839 *Leishmania* HGPRT (Armando Jardim, McGill University, Canada), *Leishmania* HSP70 (Jose M. Requena,
8840 CSIC-UAM, Spain), mouse/human α-tubulin (Abcam), mouse/human Sti1 (R&D Systems), mouse/human
8841 Cyclophilin a (Abcam), mouse/human Rab1 (Santa Cruz), mouse/human Calmodulin 2 (Thermo Fisher
8842 Scientific) and LRV1 RNA-dependent RNA Polymerase (custom-made, Thermo Scientific). This last
8843 antibody against LRV1 RNA polymerase was generated by Thermo Fisher Scientific from LRV1 peptide
8844 and was tested against other virus RNA polymerases to monitor its specificity. Proteins were detected with
8845 specific IgG horseradish peroxidase-conjugated antibodies (GE Healthcare) and subsequently visualized
8846 by the ECL Western Blot Detection System (GE Healthcare).

8847 **Transfer Assays**

8848   For exosome transwell migration assays, donor parasites were added to the 0.4 μm pore-size
8849 inside chamber (Corning), while recipient parasites were added to the wells. For transfer assays, particle
8850 preparations (10 μg of exosomes or 2.5 μg of naked LRV1) were added to recipient parasite cultures.
8851 Uptake of exosome content or naked LRV1 over time was measured by RT-PCR or by flow cytometry at
8852 the Flow Cytometry and Sorting Facility, McGill University.

8853 **RT-PCR and qRT-PCR**

8854   Total RNA from parasites or lymph nodes was extracted with TRIzol reagent (Life Technologies),
8855 treated with RQ1 DNase (Promega) for clearance of DNA contaminants and purified using the RNeasy Mini
8856 Kit (Qiagen). DNA-free RNA (2 μg) was reverse transcribed using Superscript III Reverse Transcriptase
8857 and random hexamers (Invitrogen). Standardized amounts of cDNA and custom designed primers were
8858 used for PCRs or mixed with SYBR Green Supermix (Bio-Rad) and the PCRs were performed in a CFX96
8859 Touch Real-Time PCR Detection System (Bio-Rad) according to manufacturer's protocol. Results were
8860 analyzed by the ΔΔCt method.

8861 **Statistical analysis.**

8862   Statistical analyses were performed using the unpaired Student's t-test (one- or two-tailed) or one-
8863 way analysis of variance. Error bars represent s.e.m. *$P \leq 0.05$, **$P \leq 0.01$, ***$P \leq 0.001$. The data were
8864 analyzed using GraphPad Prism software.

Reporting Summary.

Further information on research design is available in the Nature Research Reporting Summary linked to this article.

Data availability

The data that support the findings of this study are all reported in this paper and are available upon request. All data files containing proteomic analysis are provided in the Supplementary Information with protein names, accession numbers and statistical analysis.

Author contributions

M.O. designed and supervised the study. V.D.A. contributed to the development and the design of the study. V.D.A. performed all experiments. M.O., C.M. A.d.S.L.F. and V.D.A. analysed data. A.Z., V.C. and M.J. performed and analysed data from polysome experiments. A.d.S.L.F. and C.M. contributed to the organization of proteomic data files and submission of the manuscript. All authors read and approved the final manuscript.

Competing interests

The authors declare no competing interests.

a

25 °C

1 μm

37 °C

1 μm

b

500 nm

c

M_r (K)

Lmex-Exo Lpa-Exo Lg21$^+$Exo

150
100
75

50

Rd/Cp

Anti-LRV1

LRV1 ORF3

d

Sucrose gradient (top to bottom)

1 2 3 4 5 6 7 8 9 10

Anti-HSP83

Anti-GP63

Anti-LRV1

LRV1 ORF3

LRV1 ORF3 – Lg21$^+$Lysate

Lg21$^+$EV

e

Lg21$^+$EV fractions

I   1,2 3,4 5,6 7,8 9,10

I

D

LRV1
(−) ORF3

I

D

Anti-GP63

I

D

Anti-HSP83

f

Percentage of particles per fraction

80

60

40

20

0

1,2   3,4   5,6   7,8   9,10

Lg21$^+$EV fractions - NTA

□ I
■ D

Particles ml^{-1} (×10^8)

3

2

1

0

0   200   400   600

Lg21$^+$EV particle size (nm)

— I 7–10
— D 7–10

Fractions 7–10

$P = 0.02404$

30–80 nm particles ml^{-1} (×10^6)

8
6
4
2
0

I   D

Lg21$^+$EV

8884

8885

8886

8887

8888

8889

8890

8891

8892

368

Fig. 1 | *L. guyanensis* clone 21 (Lg21+) releases LRV1 RNA and proteins within exosomes. a, Lg21$^+$ promastigotes were processed for scanning electron microscopy before and after 37 °C heat-shock for 4 h. **b**, Exosomes derived from Lg21$^+$ promastigotes (Lg21$^+$Exo) were prepared for TEM by negative staining. **c**, Lg21$^+$Exo contain LRV1 proteins, as shown by western blot with an antibody against LRV1 (top), and LRV1 RNA, as shown by RT-PCR for LRV1 (bottom). Rd/Cp, RNA-dependent RNA polymerase/capsid protein. **d**, Lg21$^+$EV or Lg21$^+$ cell lysate was layered on a linear sucrose gradient and fractions were analysed by western blot with the indicated antibodies, and by RT-PCR for LRV1. **e**, Intact Lg21$^+$EV (I) or a disrupted preparation after 3 freezing– thawing cycles (D) was layered on sucrose gradients. Fractions were analysed by RT-PCR (LRV1 ORF3 negative strand), and by western blot with the indicated antibodies. **f**, Gradient fractions from **e** were submitted to NTA. The distribution of particles among fractions is shown. In **a–f**, the results are representative of three independent experiments. The difference between I and D (right panel, $n = 10$) was significant ($P = 0.02404$, one-tailed unpaired t-test with Welch's correction). Data are mean + s.e.m.
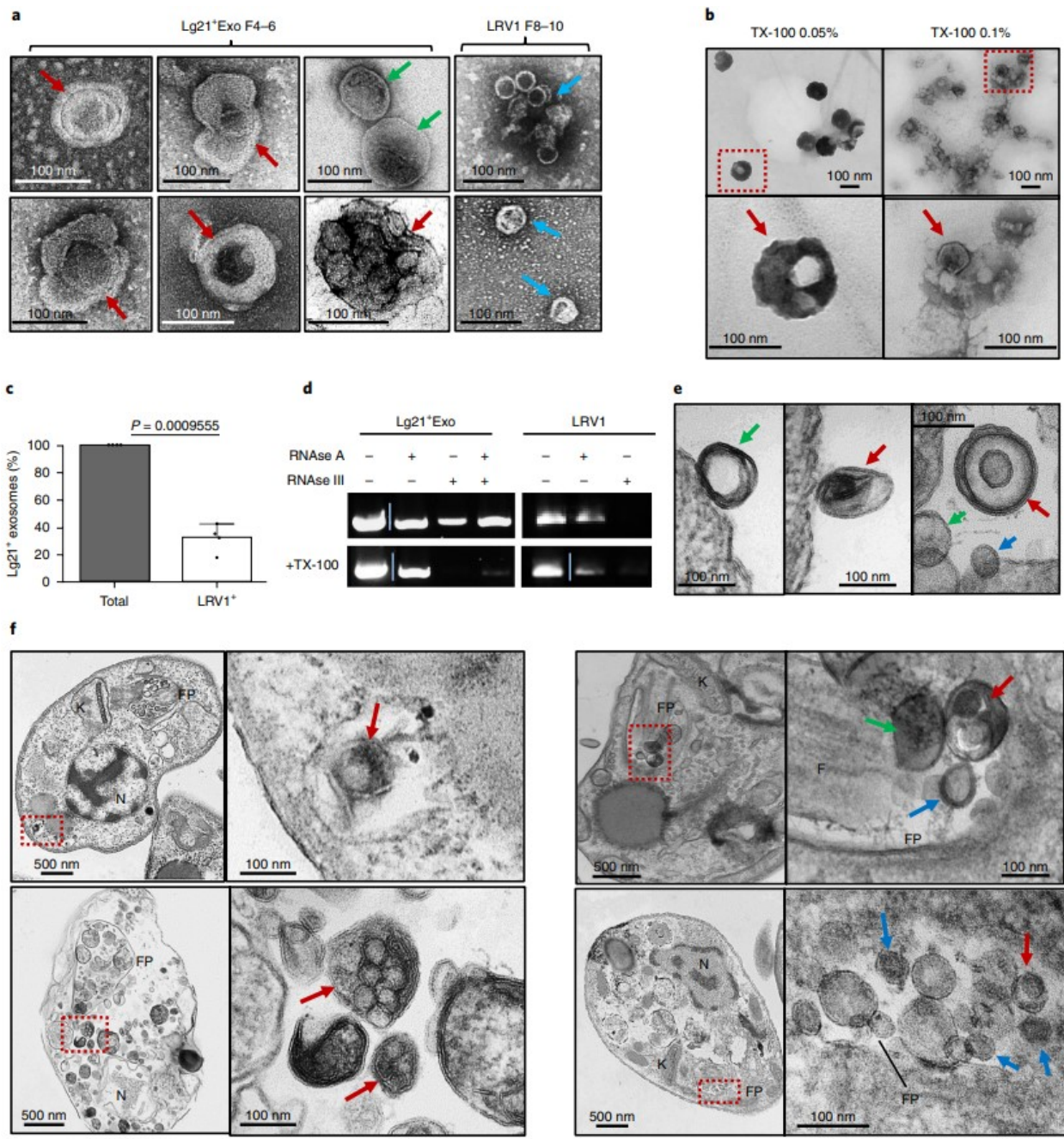
Fig. 2 | Lg21⁺ exosomes surround LRV1-like particles and protect the viral genome from enzymatic degradation. a, Lg21⁺EV gradient fractions were prepared for TEM by negative staining. LRV1-like particles are shown enveloped by membranes in exosome fractions F4–6, or naked in fractions 8–10. **b**, Lg21⁺Exo were treated with Triton X-100 and prepared for TEM by negative staining. **c**, Quantification of LRV1-containing exosomes in four independent experiments, observed by TEM. The difference between Total and LRV1⁺ was significant (P= 0.00095, n= 4, one-tailed unpaired t-test with Welch's correction). Data are mean + s.e.m. d, Lg21⁺Exo and naked LRV1 were treated with RNAse A or III in the presence or absence of Triton X-100, and processed for LRV1 ORF3 minus-strand detection by RT-PCR. **e,f**, Lg21⁺ promastigotes were processed for TEM. **e**, Promastigotes secreting exosome-like vesicles with or without LRV1-like particles in their content are shown. **f**, LRV1-like particles are shown enveloped by membrane compartments in the parasite cytoplasm (left panel) or in the flagellar pocket (FP, right panel). Red arrows, membrane-enveloped LRV1-like particles. Green arrows, LRV1- free vesicles. Blue arrows, naked LRV1-like particles. K, kinetoplast, N, nucleus. The dashed red squares indicate zoomed regions. In **a–f**, the results are representative of at least three independent experiments with similar data.
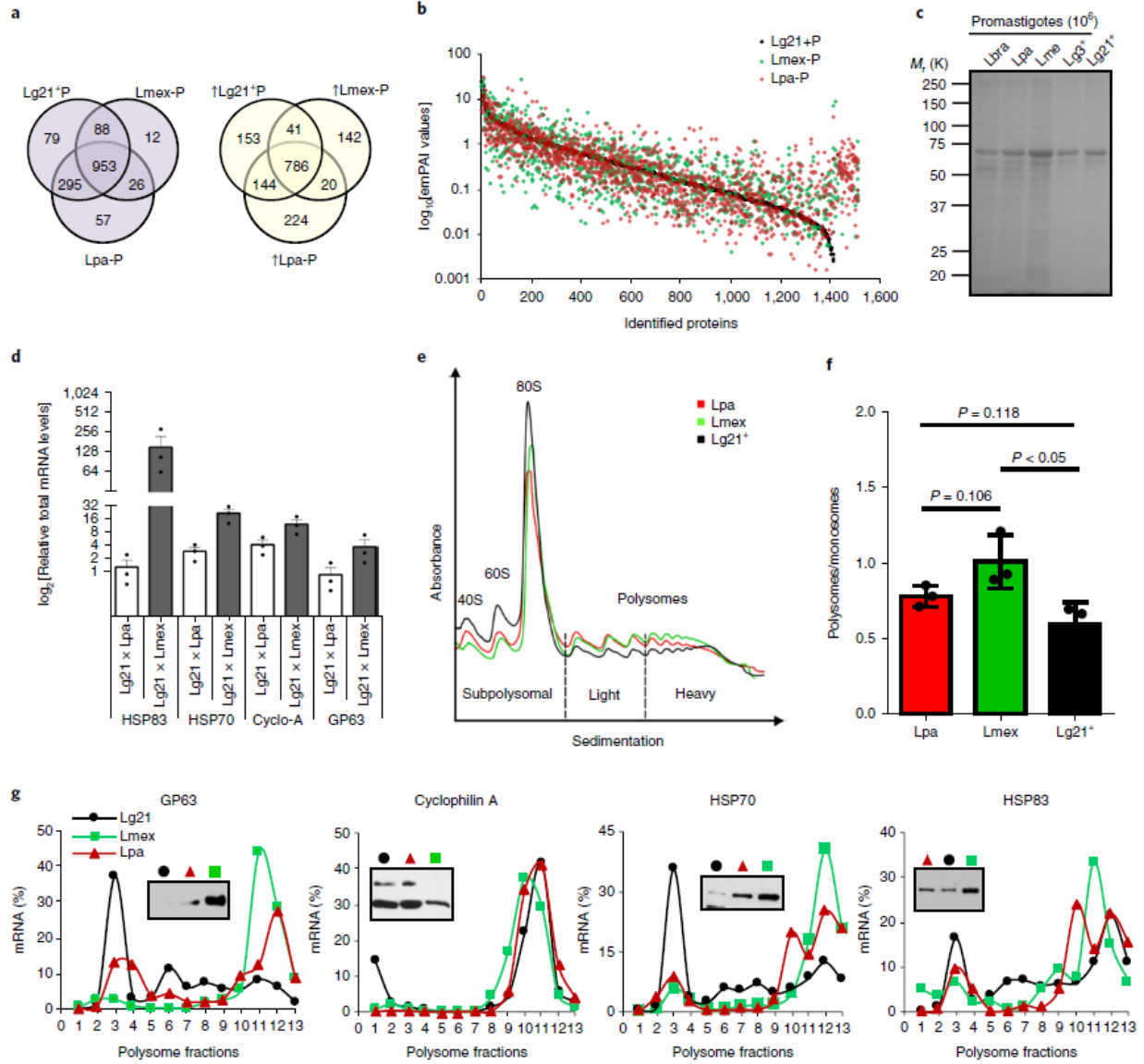
371
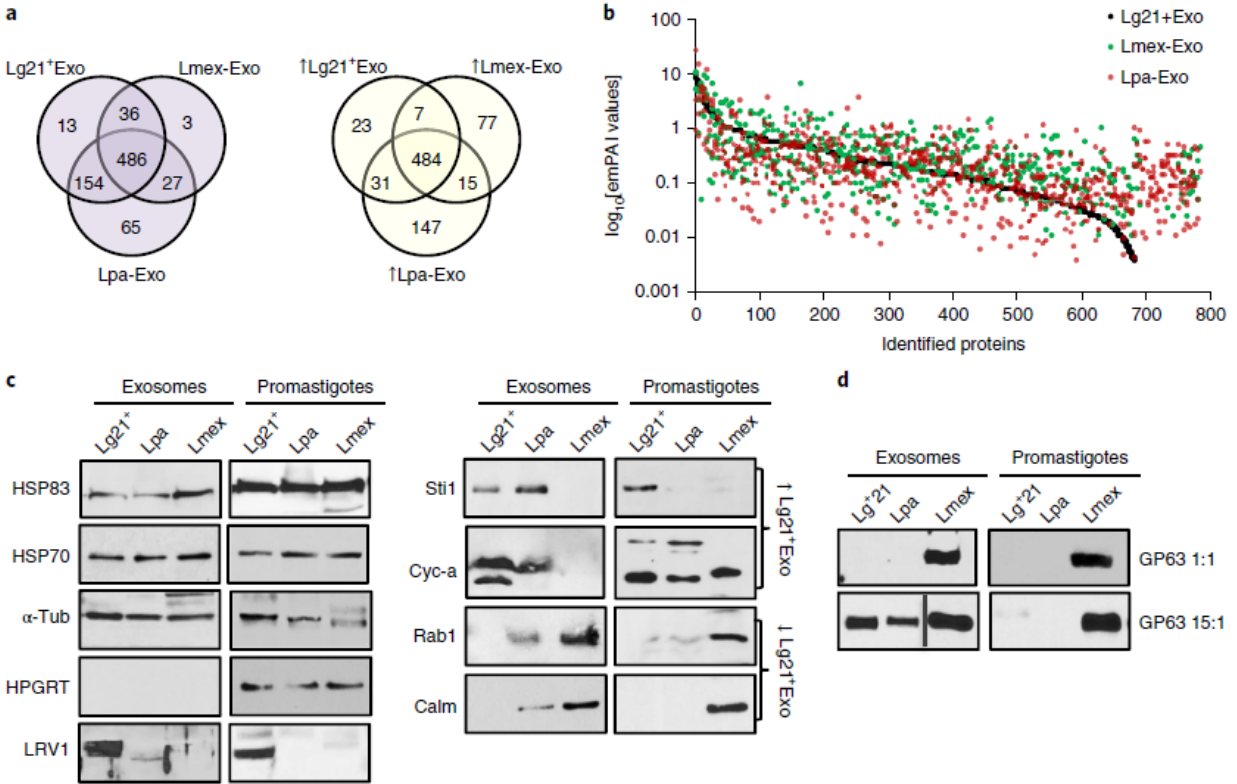
8932

8933

8934   **Fig. 3 | The proteome of Lg21⁺Exo is altered.** The protein content of exosomes derived from Lg21⁺, Lpa

8935   and Lmex promastigotes was catalogued by MS. **a**, The distribution of the identified proteins by their

8936   presence/absence (purple) and by their quantitative profiles (yellow, n = 3 for each group analyzed, see

8937   Supplementary Tables 2 and 3 and Supplementary Data files), using the *L. braziliensis* database. **b**, The

8938   distribution of the identified exosome proteins by their emPAI values. **c**, Western blot validation of selected

8939   proteins. **d**, GP63 enrichment in exosomes shown by western blot. In **c**,**d**, the results are representative of

8940   at least three independent experiments.

8941

a

Lg21⁺P, Lmex-P, Lpa-P Venn diagram: 79, 88, 12, 295, 953, 26, 57

↑Lg21⁺P, ↑Lmex-P, ↑Lpa-P Venn diagram: 153, 41, 142, 144, 786, 20, 224

b

Legend: Lg21+P, Lmex-P, Lpa-P

x-axis: Identified proteins (0–1,600)
y-axis: $\log_{10}$[emPAI values]

c

Promastigotes (10⁶)

M_r (K): 250, 150, 100, 75, 50, 37, 25, 20

Lanes: Lbra, Lpa, Lme, Lg3⁺, Lg21⁺

d

y-axis: $\log_2$[Relative total mRNA levels] (1 – 1,024)

Groups: HSP83, HSP70, Cyclo-A, GP63
(Lg21 × Lpa, Lg21 × Lmex for each)

e

y-axis: Absorbance
x-axis: Sedimentation

Peaks: 40S, 60S, 80S, Polysomes

Legend: Lpa, Lmex, Lg21⁺

Subpolysomal, Light, Heavy

f

y-axis: Polysomes/monosomes (0.0–2.0)

$P = 0.118$
$P < 0.05$
$P = 0.106$

Bars: Lpa, Lmex, Lg21⁺

g

GP63, Cyclophilin A, HSP70, HSP83

Legend: Lg21, Lmex, Lpa

x-axis: Polysome fractions (0–13)
y-axis: mRNA (%)

8942

373

8943   **Fig. 4 | The proteome of Lg21$^+$ promastigotes is altered due to altered mRNA translation**

8944   **efficiency.** The protein content of Lg21$^+$, Lpa or Lmex promastigotes was catalogued by MS (*L. braziliensis*

8945   database). **a**, The distribution of the identified proteins by their presence/absence (purple) and by their

8946   quantitative profiles (yellow). (Only proteins that appeared in 2 out of 3 triplicates (*n* = 3) from each species

8947   were included in the final list.) **b**, The distribution of the identified exosome proteins by their emPAI values

8948   (*n* = 3). **c**, LRV1-infected parasites (Lg3$^+$ and Lg21$^+$) display different protein patterns in silver-stained SDS–

8949   PAGE, compared to Lpa, Lbra and Lmex (*n* = 1). **d**, Relative mRNA levels in Lg21$^+$ versus Lpa or Lmex,

8950   analysed by qRT-PCR. Data are mean + s.e.m., *n* = 3. **e**, Polysome-tracings of Lg21$^+$, Lpa and Lmex

8951   promastigotes were generated by recording the ultraviolet absorbance at 254 nm. Shown are the

8952   subpolysomal fractions (40S, 60S and 80S) followed by the light polysome and heavy polysome fractions,

8953   which contain mRNA associated with 2–3 ribosomes and 3 ribosomes, respectively. **f**, Lg21$^+$, Lpa and Lmex

8954   promastigote polysome/monosome ratios. The difference was found to be significant ($P \leq 0.05$, one-tailed

8955   unpaired *t*-test with Welch's correction). Data are mean ± s.e.m., *n* = 3. **g**, The distribution of *GP63*,

8956   *cyclophilin A*, *Hsp70* and *Hsp83* mRNAs in polysome profiles of Lg21$^+$, Lpa and Lmex promastigotes was

8957   determined by qRT-PCR. Total extracts were used for the analysis of the respective proteins, by western

8958   blot. In **a**–**e** and **g**, the results are representative of at least three independent experiments with similar

8959   data.

8960
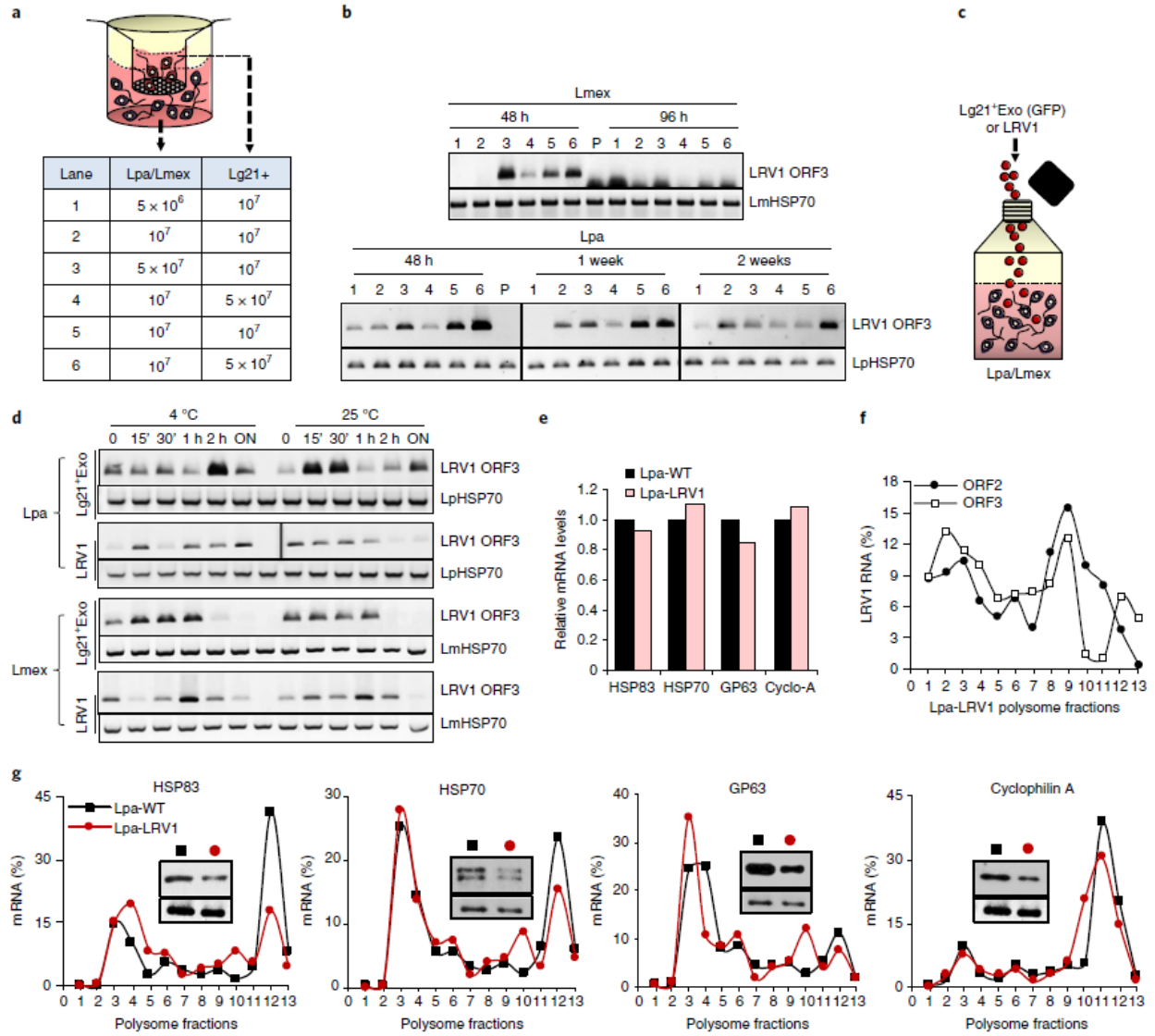
8962 **Fig. 5 | LRV1 is favourably transferred from Lg21⁺ parasites to non-infected _L. Viannia_ parasites**
8963 **when surrounded by exosomes. a**, Exosome Transwell migration settings. Lg21⁺ promastigotes were
8964 added to the 0.4 μ m pore-size chamber, while Lpa or Lmex were added to the wells. **b**, LRV1 uptake over
8965 time, measured by RT-PCR. **c**, In transfer assays, Lg21⁺GFPExo or naked LRV1 was added to Lpa or
8966 Lmex cultures. **d**, Lg21⁺GFPExo uptake over time, measured by RT-PCR. **e**, Lpa promastigotes were
8967 infected overnight with LRV1 via Lg21⁺Exo (Lpa-LRV1) and viral levels were measured by qRT-PCR 24 h
8968 post-infection. WT, wild-type. **f**, Lpa-LRV1 polysome fractions were analysed by qRT-PCR for LRV1 RNA.
8969 **g**, Polysome fractions were analysed for selected mRNAs, by qRT-PCR, and extracts were used for the
8970 analysis of the respective proteins, by western blots. The bottom western blots are HSP70 antibody cross-
8971 reacting bands that served as the experimental loading control. In **a**–**g**, the results are representative of at
8972 least three independent experiments with similar data.
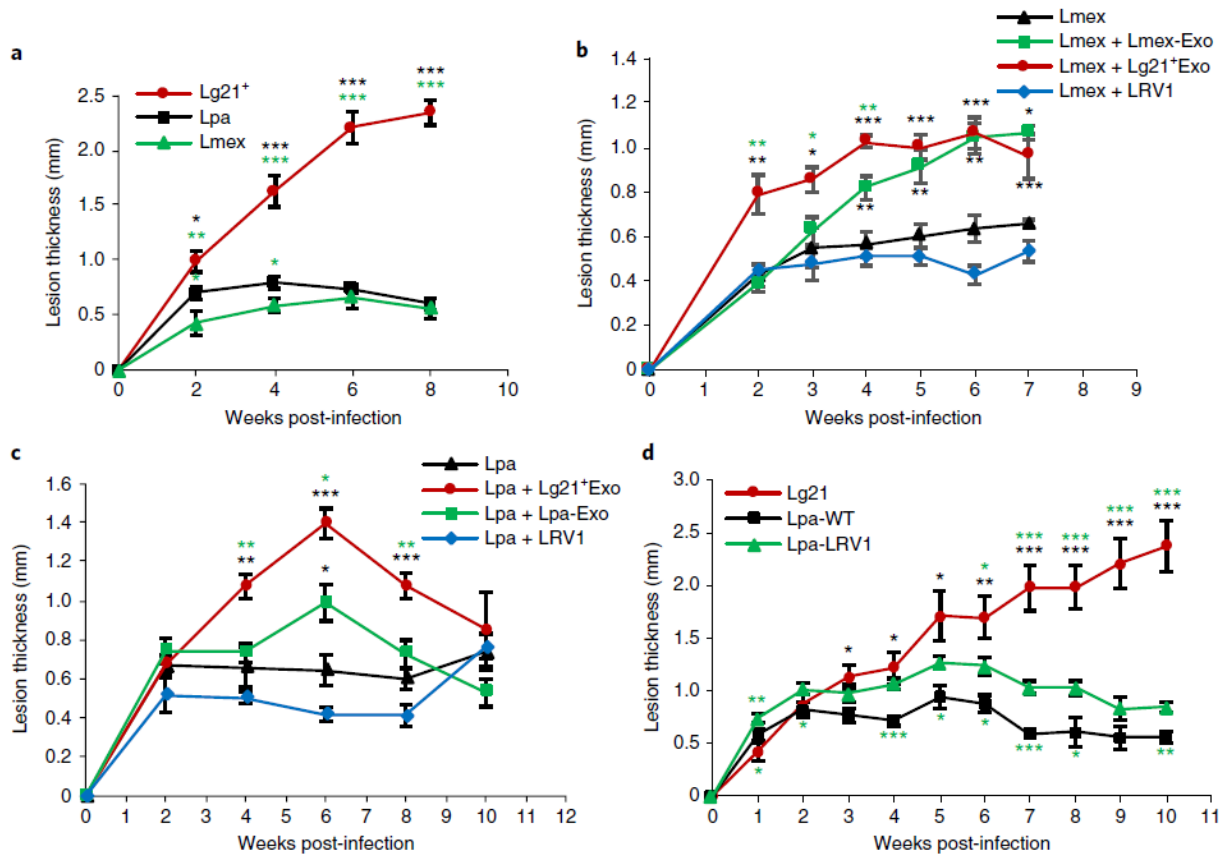
Fig. 6 | Lg21+ exosomes induce exacerbated cutaneous leishmaniasis. a, Lg21+, Lpa or Lmex promastigotes were injected into mice footpads and lesion thickness was monitored up to eight weeks post-infection. **b**,**c**, Lmex or Lpa promastigotes were co-injected into mice footpads along with their respective exosomes, Lg21+Exo or naked LRV1, and lesion thickness was monitored up to ten weeks post-infection. **d**, Lpa promastigotes were infected overnight with LRV1 via Lg21+Exo and injected into mice footpads. Lesion thickness was compared to infections with Lpa-WT and Lg21+ promastigotes, up to ten weeks post-infection. Each data point represents the average ± s.e.m., n = 6 mice per group. The differences were found to be significant using one-way analysis of variance with Holm–Sidak's multiple-comparison test. *P ≤ 0.05, **P ≤ 0.01, ***P ≤ 0.001.

377

References

Alenquer, M., and M. J. Amorim. 2015. 'Exosome Biogenesis, Regulation, and Function in Viral Infection', *Viruses*, 7: 5066-83.

Armstrong, T. C., M. C. Keenan, G. Widmer, and J. L. Patterson. 1993. 'Successful transient introduction of Leishmania RNA virus into a virally infected and an uninfected strain of Leishmania', *Proc Natl Acad Sci U S A*, 90: 1736-40.

Atayde, V. D., H. Aslan, S. Townsend, K. Hassani, S. Kamhawi, and M. Olivier. 2015. 'Exosome Secretion by the Parasitic Protozoan Leishmania within the Sand Fly Midgut', *Cell Rep*, 13: 957-67.

Atayde, V. D., K. Hassani, A. da Silva Lira Filho, A. R. Borges, A. Adhikari, C. Martel, and M. Olivier. 2016. 'Leishmania exosomes and other virulence factors: Impact on innate immune response and macrophage functions', *Cell Immunol*, 309: 7-18.

Bendtsen, J. D., Jensen, L. J., Blom, N., Von Heijne, G. & Brunak, S. 2004. Feature-based prediction of non-classical and leaderless protein secretion. Protein Eng. Des. Sel. 17, 349–356.

Bourreau, E., M. Ginouves, G. Prevot, M. A. Hartley, J. P. Gangneux, F. Robert-Gangneux, J. Dufour, D. Sainte-Marie, A. Bertolotti, F. Pratlong, R. Martin, F. Schutz, P. Couppie, N. Fasel, and C. Ronet. 2016. 'Presence of Leishmania RNA Virus 1 in Leishmania guyanensis Increases the Risk of First-Line Treatment Failure and Symptomatic Relapse', *J Infect Dis*, 213: 105-11.

Chahar, H. S., X. Bao, and A. Casola. 2015. 'Exosomes and Their Role in the Life Cycle and Pathogenesis of RNA Viruses', *Viruses*, 7: 3204-25.

Dawar, F. U., J. Tu, M. N. Khattak, J. Mei, and L. Lin. 2017. 'Cyclophilin A: A Key Factor in Virus Replication and Potential Target for Anti-viral Therapy', *Curr Issues Mol Biol*, 21: 1-20.

Dreux, M., U. Garaigorta, B. Boyd, E. Decembre, J. Chung, C. Whitten-Bauer, S. Wieland, and F. V. Chisari. 2012. 'Short-range exosomal transfer of viral RNA from infected cells to plasmacytoid dendritic cells triggers innate immunity', *Cell Host Microbe*, 12: 558-70.

Feng, Z., L. Hensley, K. L. McKnight, F. Hu, V. Madden, L. Ping, S. H. Jeong, C. Walker, R. E. Lanford, and S. M. Lemon. 2013. 'A pathogenic picornavirus acquires an envelope by hijacking cellular membranes', *Nature*, 496: 367-71.

Hartley, M. A., C. Ronet, H. Zangger, S. M. Beverley, and N. Fasel. 2012. 'Leishmania RNA virus: when the host pays the toll', *Front Cell Infect Microbiol*, 2: 99.

Hassani, K., E. Antoniak, A. Jardim, and M. Olivier. 2011. 'Temperature-induced protein secretion by Leishmania mexicana modulates macrophage signalling and function', *PLoS One*, 6: e18724.

Ishihama, Y., Y. Oda, T. Tabata, T. Sato, T. Nagasu, J. Rappsilber, and M. Mann. 2005. 'Exponentially modified protein abundance index (emPAI) for estimation of absolute protein amount in proteomics by the number of sequenced peptides per protein', *Mol Cell Proteomics*, 4: 1265-72.

Ives, A., C. Ronet, F. Prevel, G. Ruzzante, S. Fuertes-Marraco, F. Schutz, H. Zangger, M. Revaz-Breton, L. F. Lye, S. M. Hickerson, S. M. Beverley, H. Acha-Orbea, P. Launois, N. Fasel, and S. Masina.

2011. 'Leishmania RNA virus controls the severity of mucocutaneous leishmaniasis', *Science*, 331: 775-8.

Janssen, M. E., Y. Takagi, K. N. Parent, G. Cardone, M. L. Nibert, and T. S. Baker. 2015. 'Three-dimensional structure of a protozoal double-stranded RNA virus that infects the enteric pathogen Giardia lamblia', *J Virol*, 89: 1182-94.

Khan, M., G. H. Syed, S. J. Kim, and A. Siddiqui. 2015. 'Mitochondrial dynamics and viral infections: A close nexus', *Biochim Biophys Acta*, 1853: 2822-33.

Lainson, R., Shaw, J. J., Ready, P. D., Miles, M. A. & Povoa, M. 1981. Leishmaniasis in Brazil: XVI. Isolation and identifcation of *Leishmania* species from sandfies, wild mammals and man in north Para State, with particular reference to *L. braziliensis* guyanensis causative agent of "pian-bois". *Trans. R. Soc. Trop. Med. Hyg*. 75, 530–536.

Llanes, A., C. M. Restrepo, G. Del Vecchio, F. J. Anguizola, and R. Lleonart. 2015. 'The genome of Leishmania panamensis: insights into genomics of the L. (Viannia) subgenus', *Sci Rep*, 5: 8550.

Martinez, J. E., L. Valderrama, V. Gama, D. A. Leiby, and N. G. Saravia. 2000. 'Clonal diversity in the expression and stability of the metastatic capability of Leishmania guyanensis in the golden hamster', *J Parasitol*, 86: 792-9.

Masvidal, L., L. Hulea, L. Furic, I. Topisirovic, and O. Larsson. 2017. 'mTOR-sensitive translation: Cleared fog reveals more trees', *RNA Biol*: 1-7.

Meckes, D. G., Jr., and N. Raab-Traub. 2011. 'Microvesicles and viral infection', *J Virol*, 85: 12844-54.

Olivier, M. 2011. 'Host-pathogen interaction: Culprit within a culprit', *Nature*, 471: 173-4.

Peacock, C. S., K. Seeger, D. Harris, L. Murphy, J. C. Ruiz, M. A. Quail, N. Peters, E. Adlem, A. Tivey, M. Aslett, A. Kerhornou, A. Ivens, A. Fraser, M. A. Rajandream, T. Carver, H. Norbertczak, T. Chillingworth, Z. Hance, K. Jagels, S. Moule, D. Ormond, S. Rutter, R. Squares, S. Whitehead, E. Rabbinowitsch, C. Arrowsmith, B. White, S. Thurston, F. Bringaud, S. L. Baldauf, A. Faulconbridge, D. Jeffares, D. P. Depledge, S. O. Oyola, J. D. Hilley, L. O. Brito, L. R. Tosi, B. Barrell, A. K. Cruz, J. C. Mottram, D. F. Smith, and M. Berriman. 2007. 'Comparative genomic analysis of three Leishmania species that cause diverse human disease', *Nat Genet*, 39: 839-47.

Petersen, T. N., Brunak, S., von Heijne, G. & Nielsen, H. 2011. SignalP 4.0: discriminating signal peptides from transmembrane regions. Nat. Methods 8, 785–786.

Pigott, D. M., S. Bhatt, N. Golding, K. A. Duda, K. E. Battle, O. J. Brady, J. P. Messina, Y. Balard, P. Bastien, F. Pratlong, J. S. Brownstein, C. C. Freifeld, S. R. Mekaru, P. W. Gething, D. B. George, M. F. Myers, R. Reithinger, S. I. Hay. 2014. 'Global distribution maps of the leishmaniases'. *Elife*. 3, e02851.

Ramakrishnaiah, V., C. Thumann, I. Fofana, F. Habersetzer, Q. Pan, P. E. de Ruiter, R. Willemsen, J. A. Demmers, V. Stalin Raj, G. Jenster, J. Kwekkeboom, H. W. Tilanus, B. L. Haagmans, T. F. Baumert, and L. J. van der Laan. 2013. 'Exosome-mediated transmission of hepatitis C virus between human hepatoma Huh7.5 cells', *Proc Natl Acad Sci U S A*, 110: 13109-13.

9056 Schwab, A., S. S. Meyering, B. Lepene, S. Iordanskiy, M. L. van Hoek, R. M. Hakami, and F. Kashanchi.
9057   2015. 'Extracellular vesicles from infected cells: potential for direct pathogenesis', *Front Microbiol*,
9058   6: 1132.
9059 Silverman, J. M., J. Clos, C. C. de'Oliveira, O. Shirvani, Y. Fang, C. Wang, L. J. Foster, and N. E. Reiner.
9060   2010. 'An exosome-based secretion pathway is responsible for protein export from Leishmania and
9061   communication with macrophages', *J Cell Sci*, 123: 842-52.
9062 Stuart, K. D., R. Weeks, L. Guilbride, and P. J. Myler. 1992. 'Molecular organization of Leishmania RNA
9063   virus 1', *Proc Natl Acad Sci U S A*, 89: 8596-600.
9064 Sugiura, A., G. L. McLelland, E. A. Fon, and H. M. McBride. 2014. 'A new pathway for mitochondrial quality
9065   control: mitochondrial-derived vesicles', *EMBO J*, 33: 2142-56.
9066 Walsh, D., and I. Mohr. 2011. 'Viral subversion of the host protein synthesis machinery', *Nat Rev Microbiol*,
9067   9: 860-75.
9068 Widmer, G., A. M. Comeau, D. B. Furlong, D. F. Wirth, and J. L. Patterson. 1989. 'Characterization of a
9069   RNA virus from the parasite Leishmania', *Proc Natl Acad Sci U S A*, 86: 5979-82.
9070 Widmer, G., and S. Dooley. 1995. 'Phylogenetic analysis of Leishmania RNA virus and Leishmania
9071   suggests ancient virus-parasite association', *Nucleic Acids Res*, 23: 2300-4.
9072
9073
9074
9075
9076